Rock magnetic and structural investigation
of the Moss Lake stock and local area:
western Shebandowan belt

Kenneth Robert Kukkee ©

A thesis submitted in partial
fulfillment for the degree of
Master of Science

Department of Geology
Faculty of Arts and Science
Lakehead University
February, 1995

Lakehead University
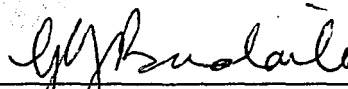## OFFICE OF GRADUATE STUDIES & RESEARCH

TITLE OF THESIS: Rock Magnetic and Structural Investigation of the Moss Lake Stock and Local Area: Western Shebandowan Belt

NAME OF STUDENT: Kenneth Kukkee

DEGREE AWARDED: Master of Science

* * * * * * * * * * * * * * * * *

This thesis has been prepared
under my supervision
and the candidate has complied
with the Master's regulations.

_____
Signature of Supervisor

March 7, 1995
Date

Abstract

The thesis area is located 120 km west of the City of Thunder Bay, Ontario, straddling the contact of the Quetico and Wawa subprovinces of the Archean Superior Province.

Metasedimentary rocks of the Quetico Subprovince with basic and granitic intrusions occupy the northwestern portion of the study area and are in contact to the southeast with metamorphosed mafic and felsic metavolcanic rocks of the Wawa Subprovince.

Tectonic compression has shortened the metasedimentary rock layers a minimum of 80%. Bedding dips steeply to the northwest and a later cleavage, developed by transpression, is sub-parallel to bedding. Graded beds young predominantly to the northwest. Some graded beds young to the southeast and may represent pre-cleavage folding. No large-scale folds are present. Metamorphic grade increases northwest from greenschist to amphibolite facies over a distance of about 10 km.

Magnetite is the predominant magnetic component of the Moss Lake stock; hematite is present in trace amounts. Magnetic susceptibility of the stock is high (12,000 $X10^{-6}$ SI), making the intrusion amenable to anisotropy of magnetic susceptibility (AMS) work.

AMS study of the Moss Lake stock shows that individual directions of maximum susceptibility have been reoriented, in most cases sub-parallel to the local planar fabric strike of the Quetico Subprovince. Magnetic fabric parameters show that the rock magnetic fabric of the intrusion is deformed. Vestiges of original magmatic fabric are evidenced by prolate (constricted) magnetic fabric associated with the central long axis of the stock but magnetic fabric parameters confirm that the intrusion margin is more deformed than the interior. The predominant oblate (flattened) magnetic fabric of the Moss Lake stock is the product of northwest-southeast tectonic compression.

Alternating field and thermal demagnetization of oriented rock specimens confirm that the Moss Lake stock is deformed by tectonic compression. Separation of magnetite and hematite magnetic contributions, by blocking temperature, reveals that primary natural remanent magnetization (NRM) orientations from hematite are parallel to the local planar fabric strike of the Quetico Subprovince. Minor preservation of primary magmatic fabric is indicated by the mean principal component analysis (PCA) orientation for magnetite which corresponds closely in trend to the mean paleomagnetic orientation for the region, obtained by previous investigators. Original Moss Lake stock magnetic fabric is overprinted by compression and shearing.

Comparison of magnetic studies (AMS and NRM) of the Moss Lake stock to structural data of country rocks argues in favor of a common tectonic control.

Acknowledgements

Foreword

The author has accumulated a vast amount of knowledge of the local geology of the thesis area through mineral exploration of Moss Township, funded through the Ontario Prospector's Assistance Program. Exploration consisted of both traditional prospecting methods and geophysical techniques followed by diamond drilling of promising targets.

TABLE OF CONTENTS

TABLE OF CONTENTS (con't)

TABLE OF CONTENTS (con't)

I. Introduction

1.1 Purpose

The main objective of this thesis is to investigate the structural relationship between a plutonic igneous intrusion and the adjacent country rock to explore the possibility that regional-scale tectonics have affected both rock units contemporaneously. Precursory surfacial field geology shows that original fabric (geometrical elements) of rock units near the stock is structurally deformed; however, field observations of the intrusion provide no evidence of rock fabric structural deformation.

The relative age relationship between the stock and planar fabric development in adjacent rocks is presently unknown and is also investigated herein by comparing magnetic data from the pluton to structural data from country rocks. If regional-scale tectonics have deformed both the stock and adjacent rock units at the same time, there may be a correlation between structural fabric of country rocks and magnetic fabric of the igneous intrusion.

This thesis is restricted to arguments relating data collected on magnetic properties of the stock to symmetry of structural data from country rocks.

1.2 Methods

Methods of data collection used to determine structural relationships between the stock and adjacent rocks include standard structural mapping techniques in conjunction with magnetic methods of AMS (anisotropy of magnetic susceptibility) and NRM (natural remanent magnetization). Introductory information regarding AMS and NRM is presented in the proceeding sections (1.2.1 and 1.2.2, respectively). Detailed theory and application of magnetism in AMS as related to plutonic rocks is located in Appendix A, Appendix B and Section IV. Refer to Section III for further information pertaining to NRM as it relates to the intrusion in question.

To interpret AMS and NRM data, magnetic mineralogy of the pluton must be precisely determined. Osmani (1993) states that magnetite content of the intrusion is variable, up to 3%. Curie balance experiments confirmed identity of predominant magnetic components. Further confirmation of magnetic mineralogy is obtained from IRM (isothermal remanent magnetization) experiments. Isothermal remanent magnetization is produced when a strong applied magnetic field produces an irreversible change in a material's remanence. More information regarding IRM is in Section II.2.

AARM (anisotropy of anhysteretic remanent magnetization) is produced when a small direct field is applied to a specimen during alternating field demagnetization (Butler, 1992). This overcomes the disadvantage of AMS, in which the contributions of ferromagnetic and paramagnetic minerals (refer to Appendix A) to the low field susceptibilities cannot be isolated (magnetic

susceptibility is explained in Appendix A). Samples of the Moss Lake stock were tested to determine their suitability for AARM. For further information regarding AARM as it pertains to the Moss Lake stock, refer to Section II.3.

1.2.1 Introduction to AMS (anisotropy of magnetic susceptibility)

Anisotropy of magnetic susceptibility (induced magnetization directional variability) provides a non-destructive analytical method useful in structural interpretation of most rock types. AMS techniques quantify the average magnetic fabric anisotropy of a rock sample by totalling all contributions of each of the magnetically-susceptible minerals in a sample (Borradaile, 1988). Changes in shape or lattice orientation of magnetically-susceptible minerals in response to tectonic deformation reflect the kinematic history of a rock fabric (Borradaile, 1988). The high magnetic anisotropy of deformed rocks makes them especially useful in AMS studies (Graham, 1954). The direction of magnetization in an anisotropic medium is deflected from that of the ambient magnetic field due to anisotropy of the medium. Therefore, magnetic anisotropy is important in paleomagnetic studies, as it is needed to correct paleomagnetic directions of remanent magnetization. Theory and application of AMS principals and techniques directly applicable to the igneous plutonic intrusion in question are located in Appendix A, Appendix B and Section IV.

1.2.2 Introduction to NRM (natural remanent magnetization)

Remanent magnetization in a rock sample, as it lies _in situ_, is termed natural remanent magnetization (NRM). NRM is commonly composed of more than one component (primary and secondary in nature) and is directly dependent upon the geological history of the specimen (Butler, 1992). Total natural remanent magnetization is the vector sum of all primary and secondary components. The primary component is usually of most interest in paleomagnetic studies and must be isolated from secondary components. Isolation of primary magnetic components from secondary magnetic components is attained by various demagnetization techniques. Refer to Section III for the NRM study of the pluton. NRM techniques are utilized in this thesis as they are anticipated to reveal part of the geologic history encountered by representative specimens of the rock body studied.

1.2.3 Instrumentation used for AMS measurements

Measurements of bulk (whole; total) magnetic susceptibility may be made directly in the field with a hand-held susceptibility meter or in the laboratory with various instruments. In this study, an SI2 induction coil system was used, operating at 750 Hertz and 0.6 Oersteds (RMS field). Data analysis was performed using the computer programs Nuspin (Borradaile and Molyneux, 1994) and Si2x (Borradaile and Stupavsky, 1994).

1.2.4 Instrumentation used for NRM measurements

Partial erasure of secondary magnetic components of rock specimens by alternating field (a.f.) demagnetization was accomplished by Sapphire Instrument's demagnetizer, from 0-200 mT. Further erasure of more-resistant secondary magnetic components was attained by heating specimens (up to 700 degrees C) in a furnace specially designed to shield samples from effects of Earth's magnetic field. For further information regarding alternating field demagnetization, refer to Section III.

1.3 Location

The thesis study area forms part of the western Shebandowan belt (Wawa Subprovince) and the Quetico Subprovince of the Archean Superior structural province (Figs. 1.1 and 1.2). It is located about 120 km west of Thunder Bay, Ontario. A simplified introductory geological map (Fig. 1.2) shows the approximate thesis study location (black star on Fig. 1.2) relative to local geology. Detailed geological maps of the thesis area, map inserts A and B, are located in the back map pocket. Detailed field mapping by the author is shown on map insert B.

Location of the igneous plutonic intrusion forming the basis of this magnetic and structural study, the Moss Lake stock, is labelled on Figure 1.2 (also refer to map inserts A and B).

1.4 General geology

The thesis study area (Figs. 1.1, 1.2 and map inserts A and B) is underlain by Archean rocks of the Wawa and Quetico subprovinces and intruded by Proterozoic diabase dikes (map A insert). The southeastern portion of the study area is composed of rocks of the western Shebandowan greenstone belt of the Wawa Subprovince. The northwestern portion of the study area is composed of metasedimentary rocks of the Quetico Subprovince. The Moss Lake stock (Fig. 1.2 and map inserts A and B) intrudes rocks of the Shebandowan greenstone belt near the sheared contact with the Quetico Subprovince (map insert A).

The Quetico Subprovince is composed of metamorphosed wacke,
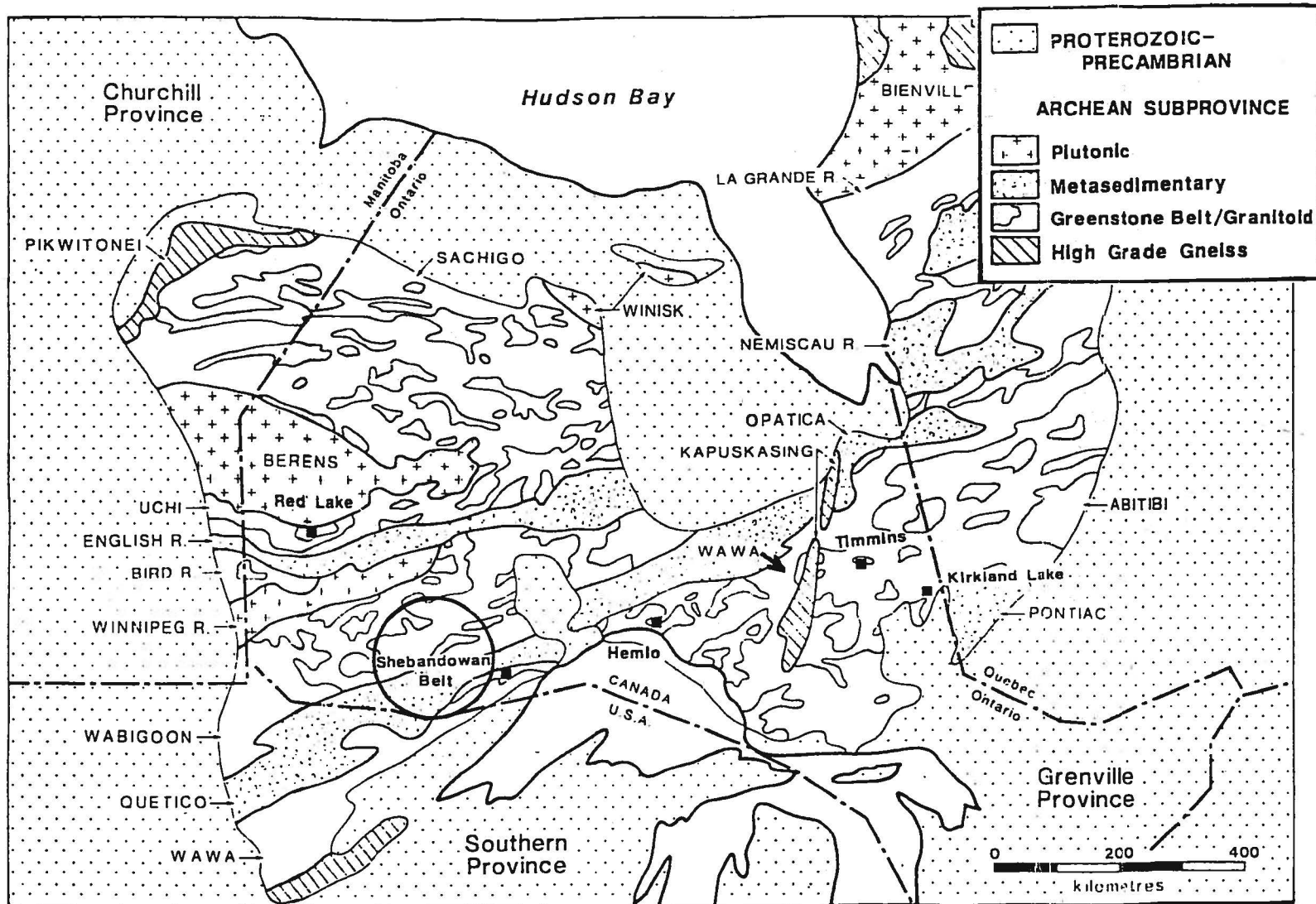
Figure 1.1. Location and general geology of the Shebandowan Belt with respect to the Superior Province and subprovinces.

(Colvine, 1989)
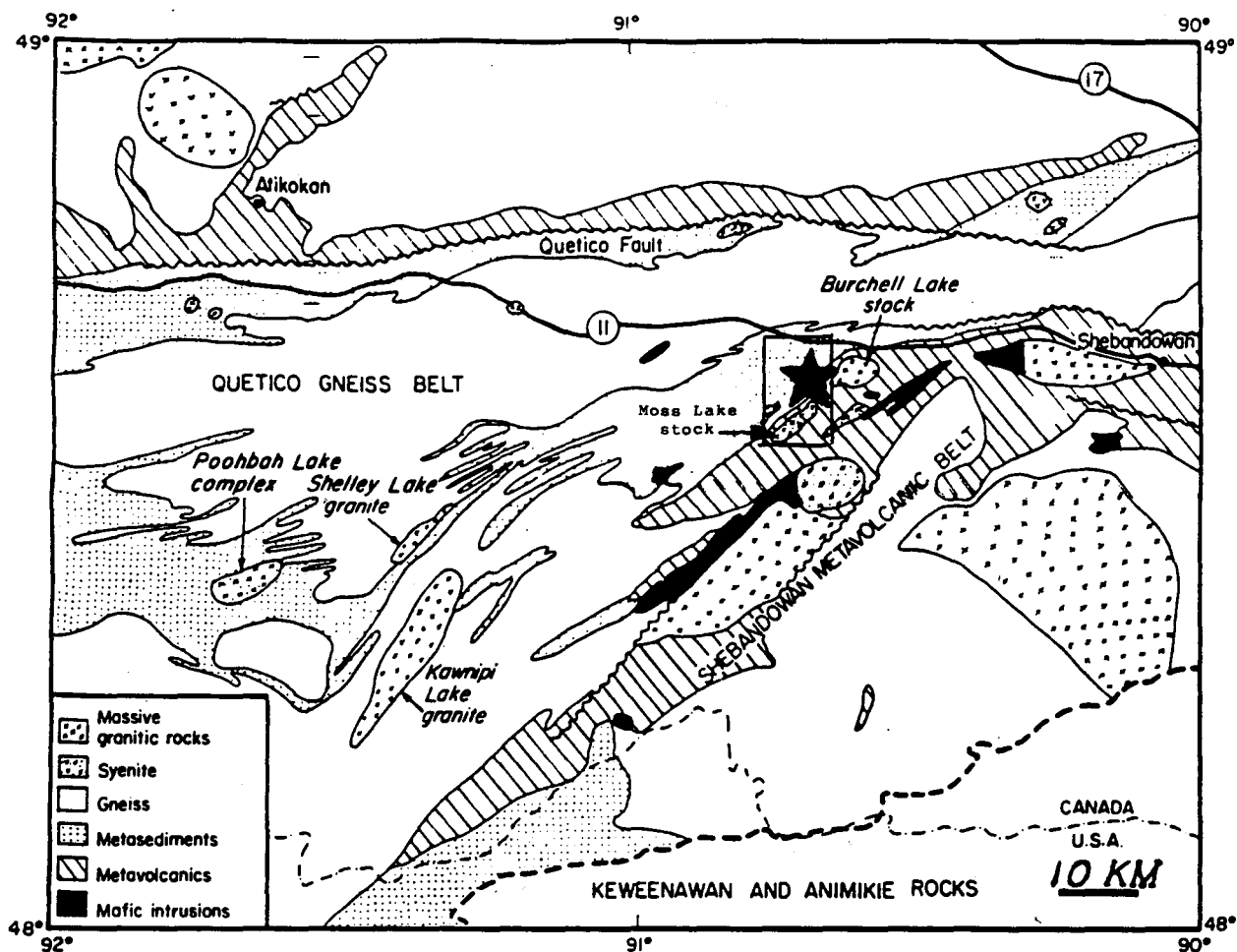
Figure 1.2. Location and general geology of the Shebandowan greenstone belt in the Superior structural province in northwestern Ontario (after Dunlop, 1984). General location of the thesis study area is shown by the black star at the northern tip of the Moss Lake stock. For detailed geology and precise location of the thesis study area, refer to maps A and B in the back map pocket.

siltstone and mudstone. A narrow zone of mafic intrusions strikes NE and is concordant to bedding (map insert A). The Shebandowan greenstone belt in the study area predominantly consists of mafic to felsic metavolcanic rocks and chlorite schist. Igneous granitoid plutons intrude both the Quetico Subprovince and the Shebandowan greenstone belt.

1.5 Structural geology

1.5.1 Faults

The Snodgrass Lake fault (map inserts A and B) sinistrally offsets blocks of the Moss Lake stock by more than 1 km. Two other minor faults (map insert B), within the confines of the Moss Lake stock, are noted by Osmani (1993).

The Moss Lake stock, where transected by the Snodgrass Lake fault, is fragmented by networks of veinlets (as seen in drill core extracted by the author) adjacent to fault gouge. Drill core taken from the Snodgrass Lake fault shows that metavolcanic units adjacent to the pluton are extensively sheared in a brittle-ductile zone about 200 meters wide.

1.5.2 Bedding and foliation

Bedding (S_o) (Figs. 1.3A,B) and cleavage (S_1) (Figs. 1.3C,D; refer to Appendix C for structural geology field measurements) have relatively consistent orientations throughout the study area but are deflected near the contact with the Moss Lake stock (map inserts A and B).
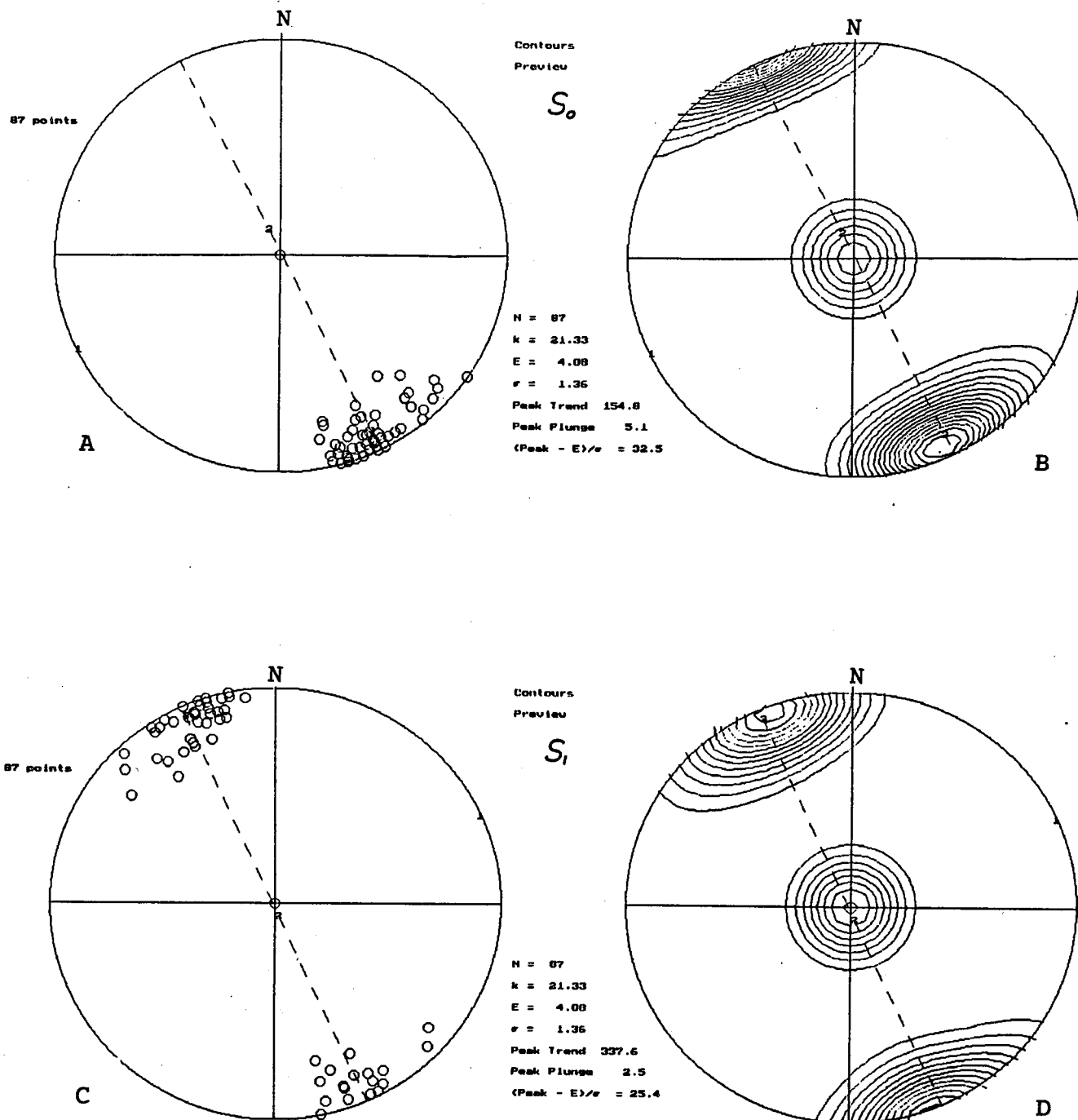
Figure 1.3A. Lower hemisphere stereographic projection of poles to bedding (S$_o$) measurements from the Quetico Subprovince. Figure 1.3B shows bedding data contoured. Figure 1.3C shows poles to cleavage (S$_1$) measurements from the Quetico Subprovince. Figure 1.3D shows cleavage data contoured. Bedding and cleavage are subparallel and are plotted on the large-scale map insert B. Refer to Appendix C for structural geology field measurements.

Bedding dips steeply northwest. The predominant younging direction, obtained from graded beds, is also northwest. Several locations with southeast-younging sedimentary layers were noted (for example, Fig. 1.4 (photograph 4); refer to map insert B for the photograph location). Regional reversals of younging direction may yield evidence of pre-cleavage folding.

In the northern portion of the study area, cleavage dips steeply to the southeast. Near the Moss Lake stock, cleavage dips steeply towards the northwest. Extensive shearing is evident in the central portion of the study area. Near the shear zones, cleavage is subvertical, as evidenced by chlorite schist (Fig. 1.5 (photograph 3), refer to map insert B for photograph location) near the contact of the Quetico Subprovince with the Shebandowan greenstone belt. A map view of the same chlorite schist unit is presented in Figure 1.6 (photograph 2 on map insert B). Well-developed S-C fabric is evident in map view, also reflecting intense shearing (Fig. 1.6). C-bands of the S-C fabric (Fig. 1.6) are oriented along the regional geology trend. Sense of shear within the chlorite schist (Fig. 1.6) is difficult to determine. Metasedimentary rocks (Fig. 1.7 (photograph 1 on map insert B)) adjacent to the sheared chlorite contain small quartz augen (eyes).

South of the chlorite schist is a metasedimentary sequence which exhibits isoclinal folding, with sub-horizontal fold hinge lines trending parallel to regional geology.

"Fish-mouth" boudins (Fig. 1.8 (photograph 6), refer to map insert B for photograph location) and boudinaged chlorite blocks
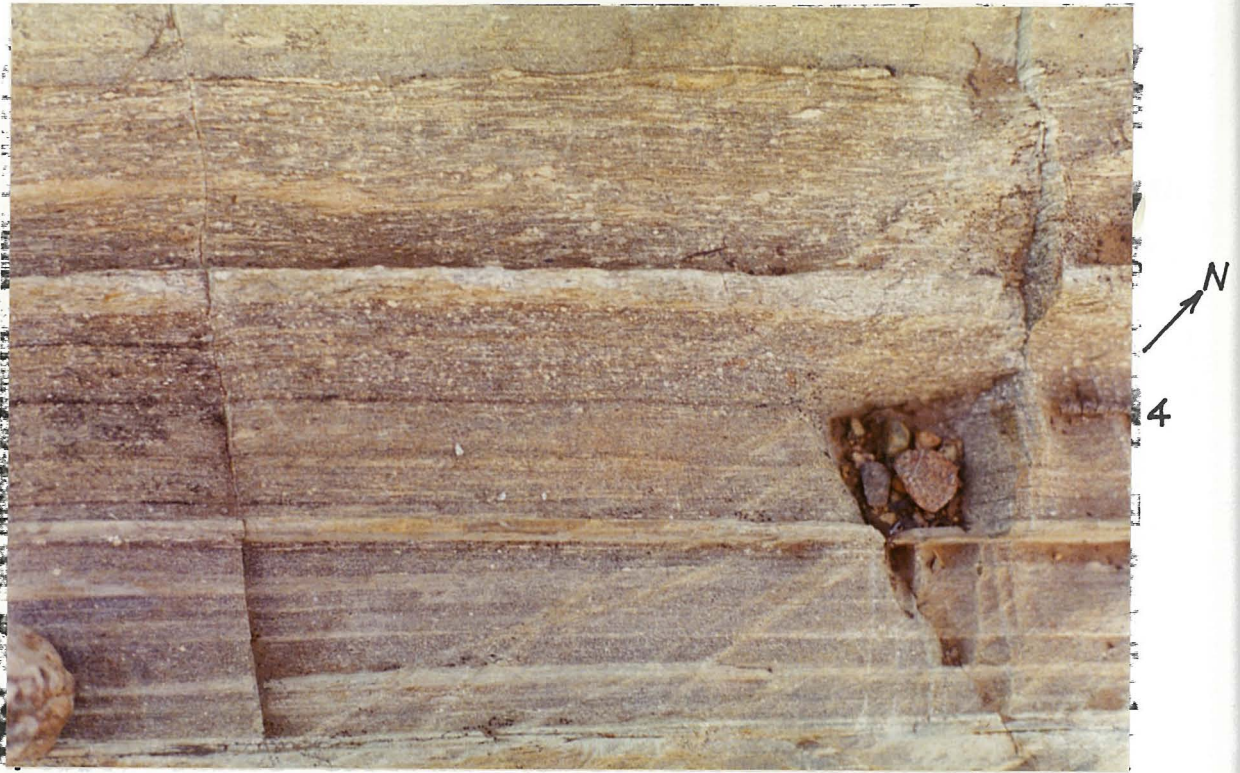
Figure 1.4. Graded sedimentary beds in the Quetico Subprovince show **minor** younging direction reversals to the southeast. The photo field of view is approximately 1m; see insert map B for location.

Figure 1.5. Chlorite schist in the central portion of the study area (refer to insert map B for photograph location). Metasedimentary rocks are found both northwest and southeast.
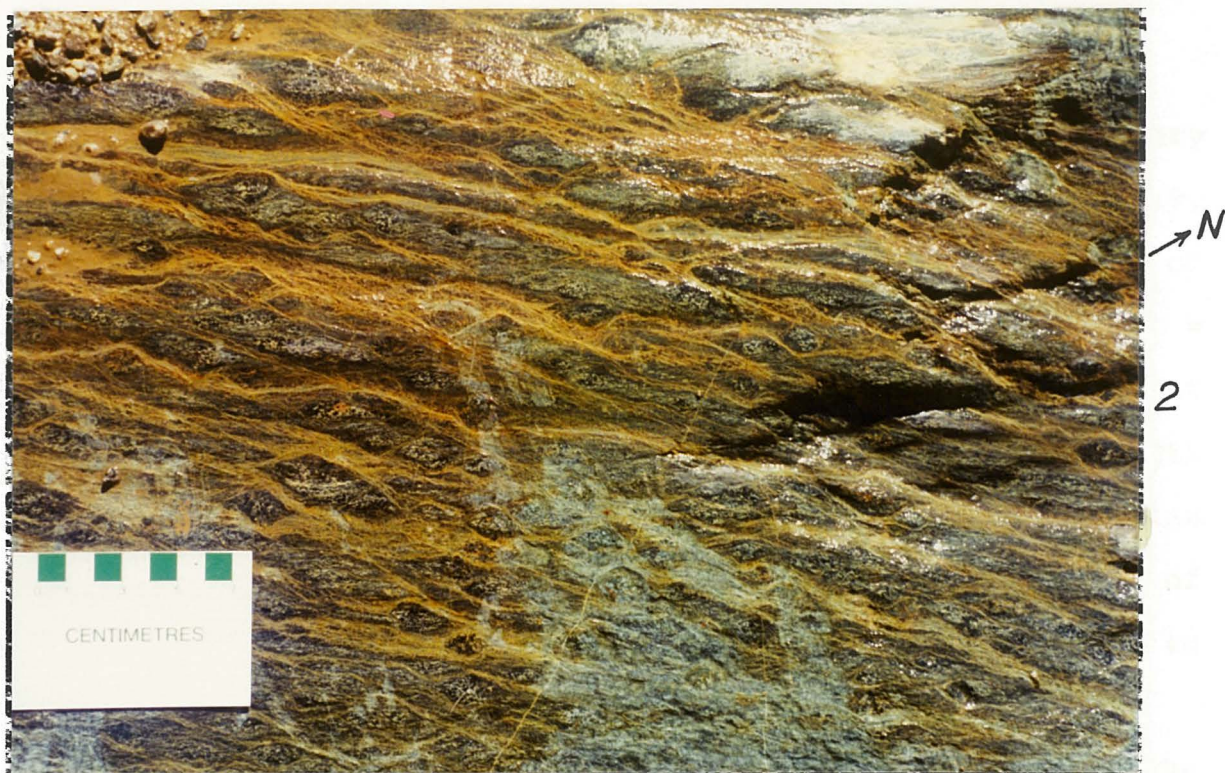
Figure 1.6. A map view of chlorite schist shows good development of S-C fabric, indicative of shearing. Refer to insert map B for photograph location.
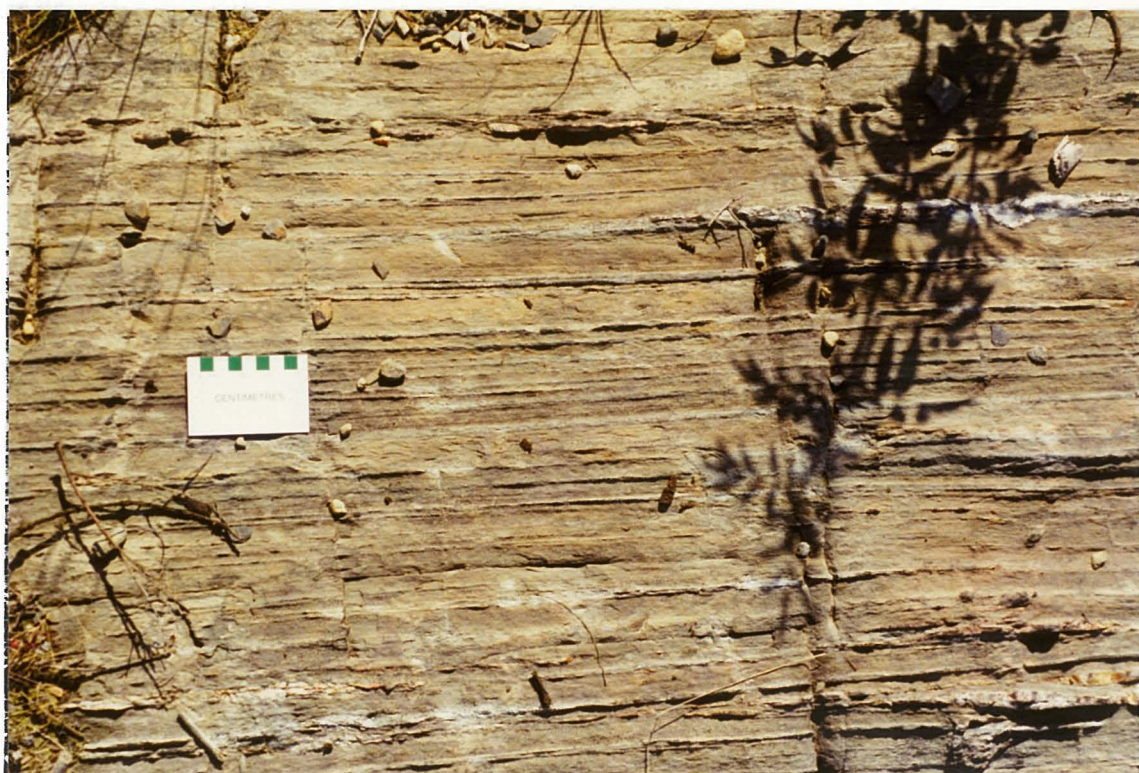
Figure 1.7. Quartz veins and bedding-parallel cleavage are apparent in metasedimentary rocks adjacent to sheared chlorite of Figure 1.6. Refer to map insert B for photograph location.

Figure 1.8. "Fish-mouth" boudins are well developed and common in the Quetico Subprovince. Refer to insert map B for photograph location.
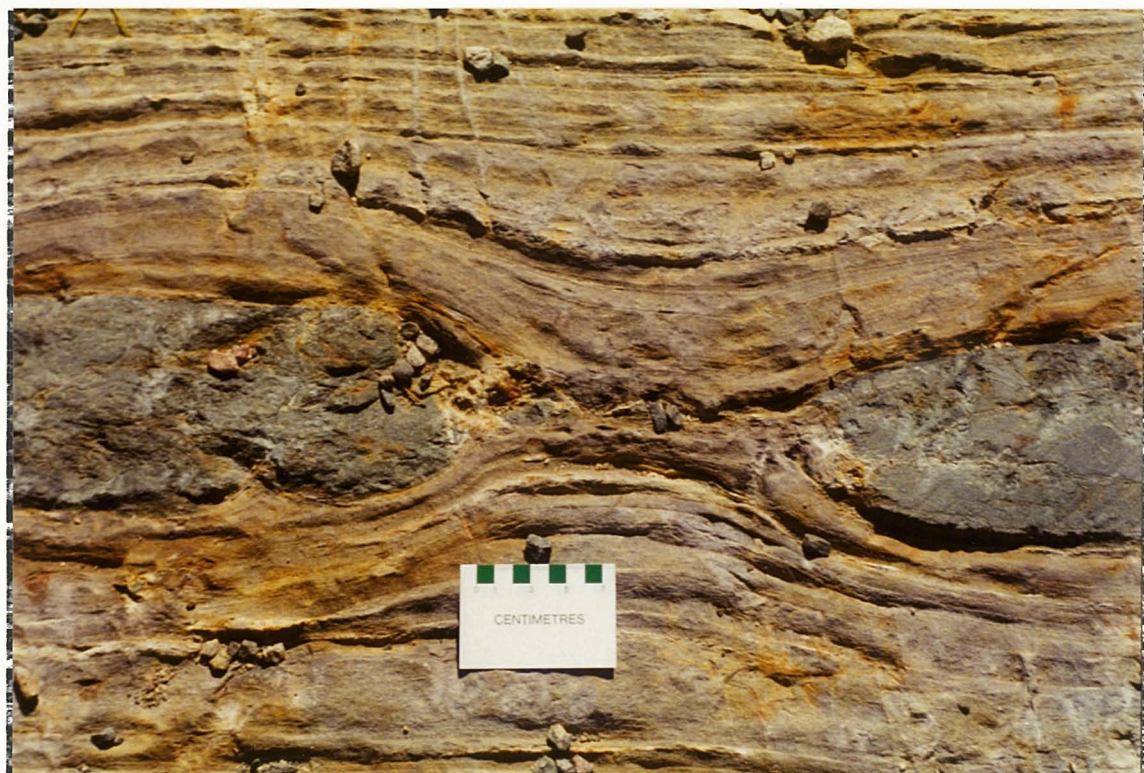
Figure 1.9. In the northern part of the study area of the Quetico Subprovince, boudinaged chlorite blocks within metasedimentary rocks record bedding-parallel extension. Refer to insert map B.

(Fig. 1.9 (photograph 5 on map insert B)) show that metasedimentary rocks have been subjected to tectonic compression. On Figure 1.9, bedding is parallel to the extension direction. An estimate of tectonic shortening may be derived from the equation $1 - l_o / l_o$ = extension, where $[l_o]$ represents original length of a competent unit (ie., the chlorite unit on Fig. 1.9) and $[l]$ represents length of the same competent unit after extension. Assuming constant area and no homogeneous strain in the competent unit, the amount of tectonic shortening required to produce this amount of extension is a minimum of 80%.

Mafic to felsic metavolcanic rocks occur south of the metasedimentary rocks (map insert A). Felsic metavolcanic rocks are typically massive and structureless except where sheared and near the pluton, where schistosity strike follows curvature of the stock, dipping steeply away from it. Brittle-ductile deformation of metavolcanic rocks is noted in many outcrops (Fig. 1.10 (photograph 7) and Fig. 1.11 (photograph 8), refer to map insert B for photograph locations).

1.6 Metamorphic grade

Metamorphic grade of the study area ranges from greenschist facies to amphibolite facies, near the Moss Lake stock (Osmani, 1993). The regional metamorphic gradient increases towards the gneissic terrain northwest of the study area (over a distance of about ten kilometers). Localized zones of higher-grade rocks accompany shear zone boundaries in both the Quetico Subprovince and

7
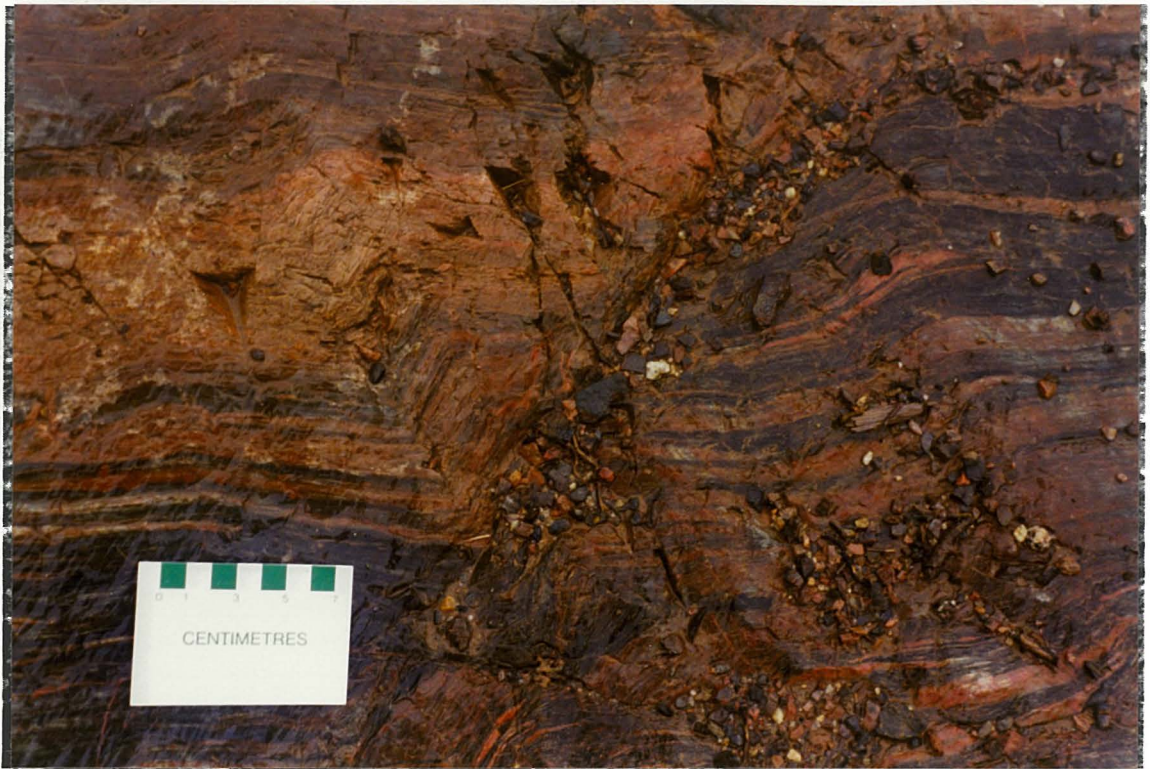
Figure 1.10. Brittle-ductile deformation is extensive in the Shebandowan metavolcanic rocks. This photo was taken from an outcrop near the sheared contact with the Quetico Subprovince.

8

Figure 1.11. This photo is from the same location. Note the early tension gash. Red-orange colouration of the material surrounding the tension gash is from hematite.

Shebandowan greenstone belt.

Minerals characteristic of greenschist facies of the Quetico Subprovince are quartz, chlorite and albite. The presence of biotite and garnet near the igneous intrusion reflects amphibolite facies metamorphism (Osmani, 1993). Reverse metamorphic grading produced by staurolite crystals is evident in the Quetico metasedimentary rocks, northwest of the study area.

In the metavolcanic rocks, greenschist facies minerals are characterized by quartz, chlorite, albite and epidote.

1.7 Mineralogy

1.7.1 Mineralogy of the Quetico Subprovince

The Quetico Subprovince is composed of metamorphosed wackes, siltstones and mudstones. The metawackes are medium to dark grey and have a sandy texture. Thin section analyses reveal the approximate modal composition to be: 45-75% plagioclase, 10-20% quartz, 5-10% lithic fragments and 10-25% biotite and muscovite (Osmani, 1993). Near shear zones and stocks of the study area, metasedimentary rocks contain garnet; a garnet isograd (refer to map insert B) is traceable across the northern portion of the study area near Highway #11. Garnet appears in metawacke northwest of the garnet isograd.

1.7.2 Mineralogy of the metavolcanic belt

Composition of metavolcanic rocks ranges from mafic to felsic. They are very fine-grained and vary in colour from dark grey to light green. Osmani (1993) describes intermediate to felsic rocks of the metavolcanic belt as very fine-grained porphyritic flows composed of plagioclase $\pm$ quartz. Sheared felsic metavolcanic rocks contain quartz, feldspar, chlorite, sericite, epidote, apatite, and arsenopyrite. Feldspars are highly altered and fractured, but twinning is still apparent. Calcite occurs mostly as anhedral masses. Scanning electron microscope analyses of sheared felsic metavolcanic rocks indicate trace quantities of barite, chalcopyrite, Pb arsenide, MoSAs and gold.

1.7.3 Mineralogy of the Moss Lake stock

The Moss Lake stock (Fig. 1.2; map inserts A and B) is hosted within metavolcanic rocks of the western Shebandowan belt. The stock is located in the southern portion of the thesis study area (refer to map inserts A and B). The approximate outcrop area of this igneous plutonic intrusion is about 28 km^2.

Granite, syenite, quartz syenite and quartz monzonite are lithologic varieties comprising the intrusion. Porphyritic phases are common. Syenite samples from the stock contain up to 30% mafic mineral content (Osmani, 1993). Average modal composition of a typical Moss Lake stock syenite sample is 78% microcline, 9% albite, 10% ferromagnesian minerals and 3% accessory minerals including apatite, zircon, sphene and magnetite. Quartz veins are common within fractures of the pluton (Figs. 1.11 (photograph 9) and 1.12 (photograph 10); refer to map insert B for photograph locations). Magnetite content of the stock is variable, up to 3 percent modally (Osmani, 1993). High magnetite content of this intrusion makes it especially amenable to magnetic studies.
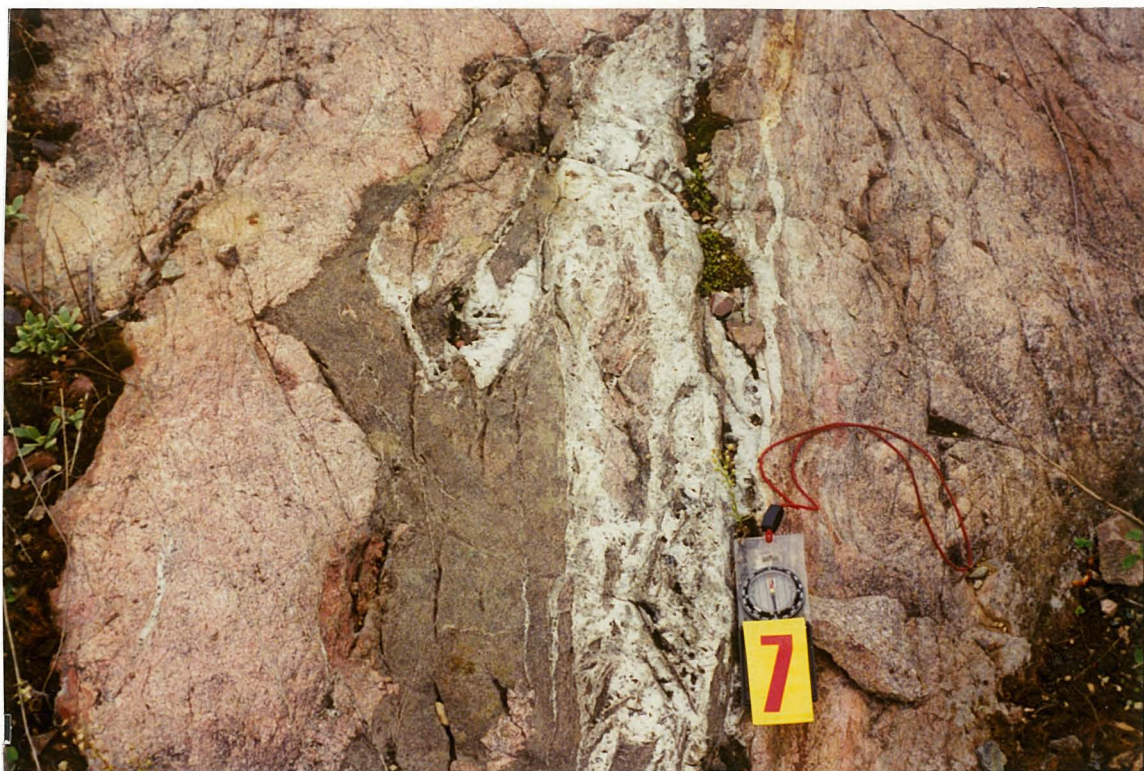
Figure 1.11. The Moss Lake stock at the Snodgrass Lake fault contains cataclastic breccia with quartz infilling. Refer to insert map B for photograph location.

Figure 1.12. This subparallel network of quartz veins represents the western shear zone boundary of the Snodgrass Lake fault. The orientation of the quartz veins is north-south.

II. Verification of magnetic mineralogy of the Moss Lake stock

2.1 Curie balance experiments

Ferromagnetic minerals may be identified by several techniques, including (1) microscopy (2) coercivity spectrum analyses and (3) determination of ferromagnetic component(s) by measurement of the Curie point(s) using thermomagnetic analyses (Butler, 1992). In the latter, saturation magnetization (maximum magnetization for a given ferromagnetic mineral) decreases to zero at the Curie temperature [Tc]. Above the Curie point, ferromagnetic materials become paramagnetic. Ferromagnetic minerals have characteristic Curie temperatures (approximately 580 C for magnetite and 680 C for hematite, Fig. 2.1), hence determination of this critical temperature is diagnostic of the ferromagnetic mineralogy, revealing information about the bulk magnetic behaviour of a sample.

One determines the Curie temperature of a rock specimen with a magnetic balance to measure the saturation magnetization [Js] as a function of temperature (Irving, 1964). Using Sapphire Instruments' Curie balance, about 0.01 gram of the magnetic fraction is placed into a fused silica tube suspended horizontally in a small furnace. This is drawn toward a neodymium permanent magnet (=650 mT field). As the temperature increases, [Js] decreases, and the glass tube swings away from the magnet. Movement is registered as a voltage change via a linear displacement transducer. This change in voltage is proportional to change in magnetization of the specimen.

	Curie temp or Neel temp	Saturation magnetization, emu/g
Ferrimagnetic		
Magnetite (Fe_3O_4)	580°C	92
Maghemite (γ Fe_2O_3)	545 to 675°C	83.5
Ilmenite-hematite solid solution: $(x)FeTiO_3$ - $(1 - x)Fe_2O_3$ $0.5 < x < 0.8$	50 to 300°C	21 (max)
Pyrrhotite $(FeS)_{1+x}$ $0 < x < \frac{1}{7}$	320°C	19.5 (max at Fe_7S_8)
Jacobsite ($MnFe_2O_4$)	300°C	84
Cubanite ($CuFe_2S_3$)	Unknown due to polymorphic transition at 270°C	0.87
Magnesioferrite ($MgFe_2O_4$)	440°C	24.5
Trevorite ($NiFe_2O_4$)	585°C	51 (very rare)
Franklinite ($ZnFe_2O_4$)	60°C	
Chromite ($FeCr_2O_4$)	88°K	
Antiferromagnetic		
Hematite (α Fe_2O_3):		
antiferromagnetism	680°C (Neel temp)	
parasitic ferromagnetism	680°C (Curie temp)	0.5 (approx)
Ilmenite ($FeTiO_3$)	57°K	
Ulvospinel (Fe_2TiO_4)	120°K	
Pyrolusite (MnO_2)	84°K	
Goethite (α $FeOOH$)	120°C	
Akaganeite (β $FeOOH$)	77°K < Tn < 295°K	
Alabandite (MnS)	165°K	
Chalcopyrite ($CuFeS_2$) (high-temperature cubic phase is magnetic)	300°K	
Siderite ($FeCO_3$)	40°K	
Rhodochrosite ($MnCO_3$)	31.5°K	
Fayalite (Fe_2SiO_4)	126°K	
Troilite (FeS)	320°C	
Pyroxene ($FeSiO_3$)	40°K	

Figure 2.1. Curie temperatures of specific minerals (Strangway, 1970).

Magnetic intensity of the specimen is plotted against temperature. One or more Curie points may be identified from inflection points on the graph.

Invariably, heating of the specimen produces changes in the ferromagnetic mineral properties, ie. magnetite-->hematite. This may be detected by the differences between heating and cooling paths on the graph. Irreversible chemical or complex ferromagnetic mineral changes cause a deviation of the cooling path from the heating path.

Four samples from the Moss Lake stock were tested by thermomagnetic analysis to determine the ferromagnetic minerals present. The two most-magnetic fractions of samples sy7, sy23, sy2 and hd1 have Curie temperatures of 580 degrees C, characteristic for magnetite (Figs. 2.2-2.9). The least-magnetic fractions of each sample are composed of tan to dark orange microcline. Colouration is due to the presence of hematite in the matrix, as shown by the Curie temperature near 680 C (Figs. 2.10-2.13). For both fractions, deviation of the cooling path from the heating path shows the production of a new mineral (mostly hematite) with a slightly lower saturation magnetization during the experiment.

M/Mo

sy2a1   n(heat)= 199 n(cool)= 234
b:\sy2a1.cb 03-17-1994 11:31

1.0

heating curve

cooling curve

0

0   100   200   300   400   500   600
Temperature degrees C

cursor at T=   573.9 M/Mo=   0.004

heat CT=   567.4   cool CT=   573.9

Figure 2.2. Curie balance graph (normalized intensity) for sample
sy2 (most-magnetic fraction) composed of magnetite grains. The
Curie temperature is the inflection point.

M/Mo

sy2b1   n(heat)= 198 n(cool)= 234
b:\sy2b1.cb 03-17-1994 12:29

1.0

heating curve

cooling curve

0

0   100   200   300   400   500   600
Temperature degrees C

cursor at T=   576.1 M/Mo=   0.013

heat CT=   567.4   cool CT=   576.1

Figure 2.3. Curie balance graph (normalized intensity) for sample
sy2 magnetic fraction composed of magnetite grains and grains with
magnetic inclusions.

M/Mo

sy7a3   n(heat)= 197 n(cool)= 232
b:\sy7a3.cb 03-17-1994 09:04

1.0

heating curve

cooling curve

0

0   100   200   300   400   500   600
Temperature degrees C

cursor at T=   550.0 M/Mo=   0.029
            heat CT=   569.6   cool CT=   550.0

Figure 2.4. Curie balance graph (normalized intensity) for sample sy7 (most-magnetic fraction) composed of magnetite grains. The Curie temperature is the inflection point.

M/Mo

sy7b1   n(heat)= 202 n(cool)= 235
b:\sy7b1.cb 03-17-1994 09:47

1.0

heating curve

cooling curve

0

0   100   200   300   400   500   600
Temperature degrees C

cursor at T=   578.3 M/Mo=   0.004
            heat CT=   567.4   cool CT=   578.3

Figure 2.5. Curie balance graph (normalized intensity) for sample sy7 magnetic fraction composed of magnetite grains and grains with magnetic inclusions.

cursor at T=   576.1 M/Mo=   0.013

heat CT=   563.0   cool CT=   576.1

Figure 2.6. Curie balance graph (normalized intensity) for sample sy23 (most-magnetic fraction) composed of magnetite grains. The Curie temperature is the inflection point.

cursor at T=   578.3 M/Mo=   0.004

heat CT=   569.6   cool CT=   578.3

Figure 2.7. Curie balance graph (normalized intensity) for sample sy23 magnetic fraction composed of magnetite grains and grains with magnetic inclusions.
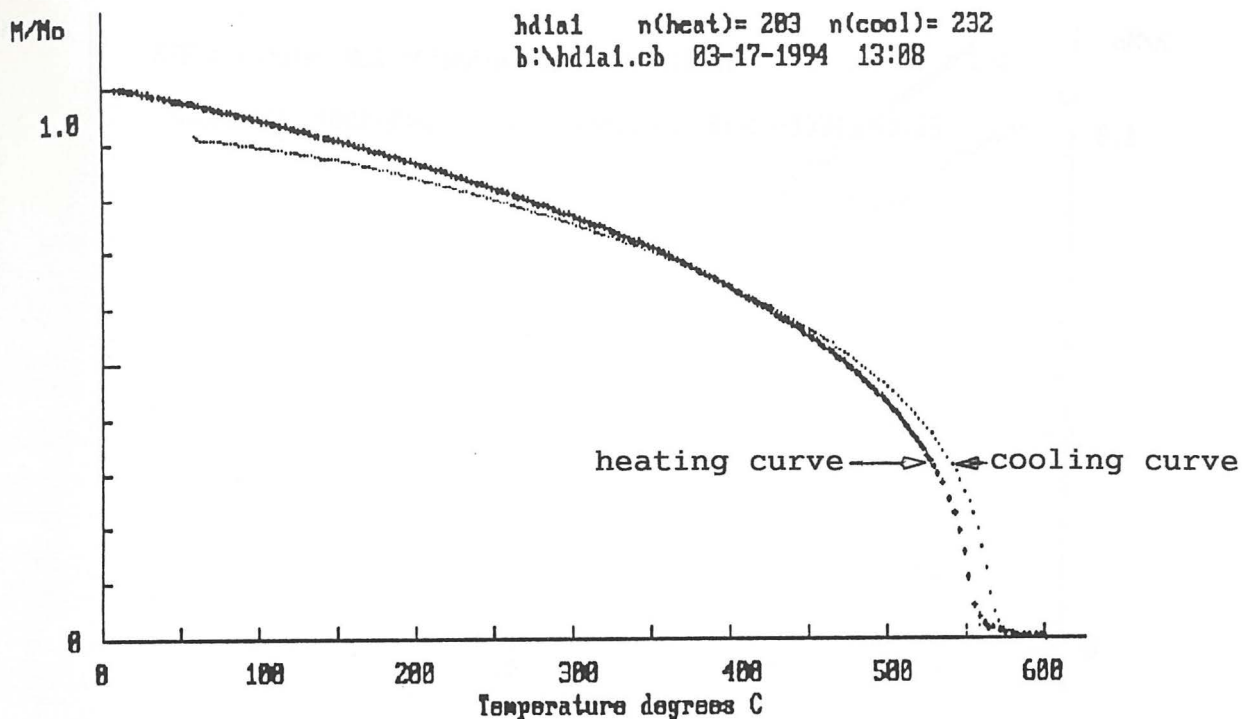
cursor at T=   573.9   M/Mo=   0.013
heat CT=   558.7   cool CT=   573.9

Figure 2.8. Curie balance graph (normalized intensity) for sample hd1 (most-magnetic fraction) composed of magnetite grains. The Curie temperature is the inflection point.
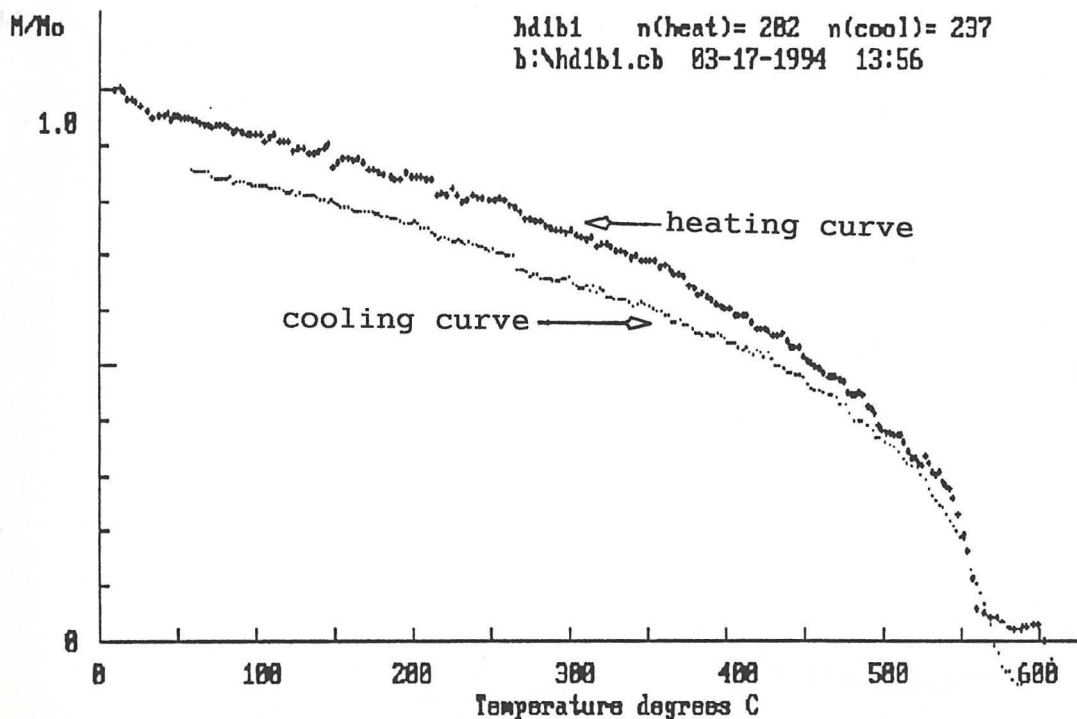
cursor at T=   589.1   M/Mo=   0.029
heat CT=   563.0   cool CT=   589.1

Figure 2.9. Curie balance graph (normalized intensity) for sample hd1 magnetic fraction composed of magnetite grains and grains with magnetic inclusions.
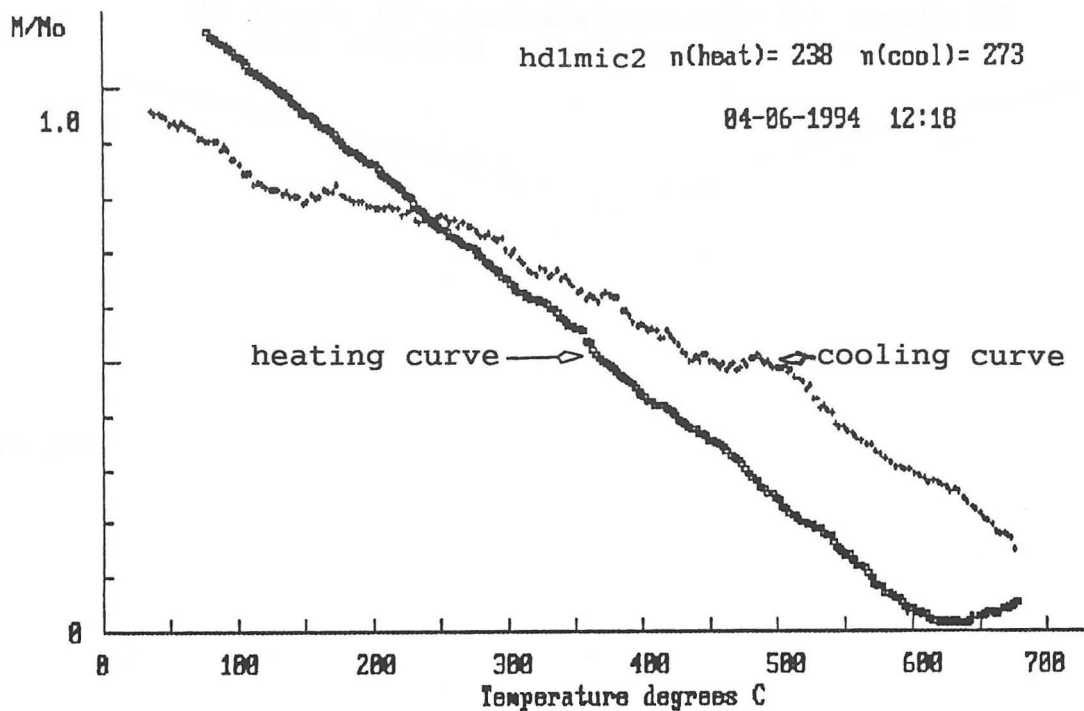
Figure 2.10. Curie balance graph (normalized intensity) for sample hd1 (least-magnetic fraction) composed of microcline grains. The Curie temperature is the inflection point.
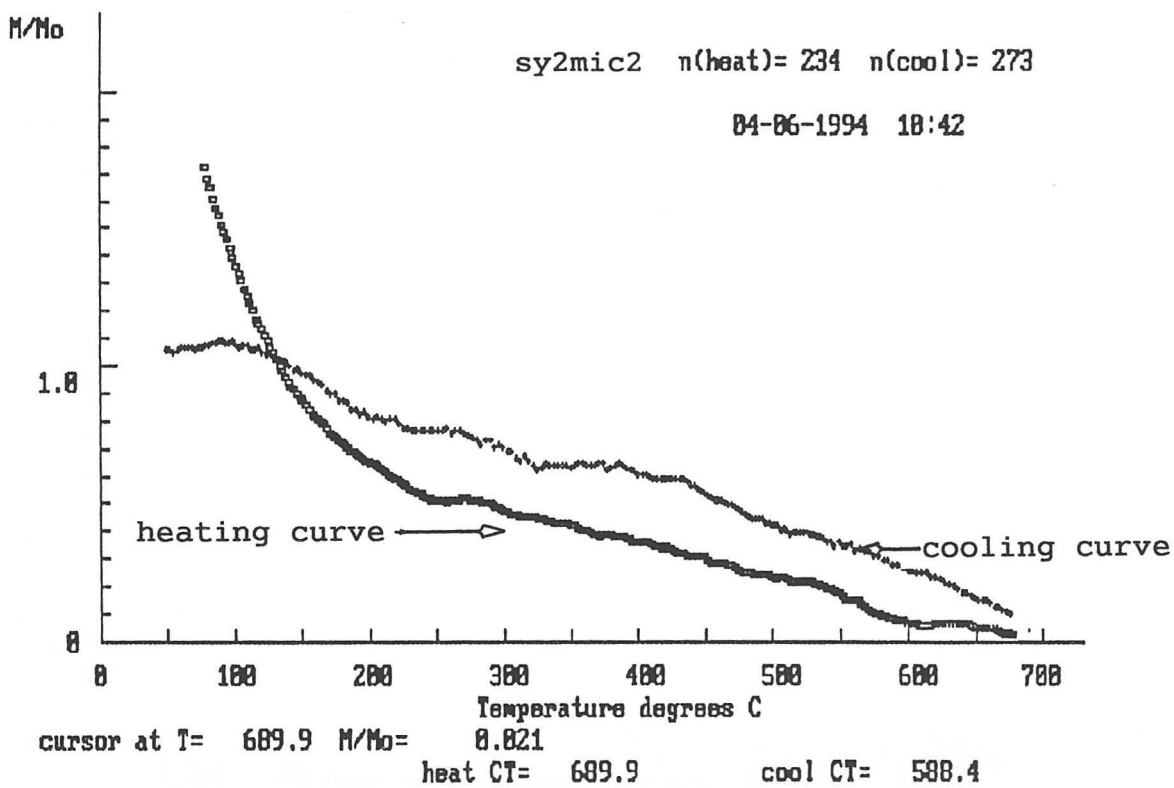
Figure 2.11. Curie balance graph (normalized intensity) for sample sy2 magnetic fraction composed of microcline grains with hematite.
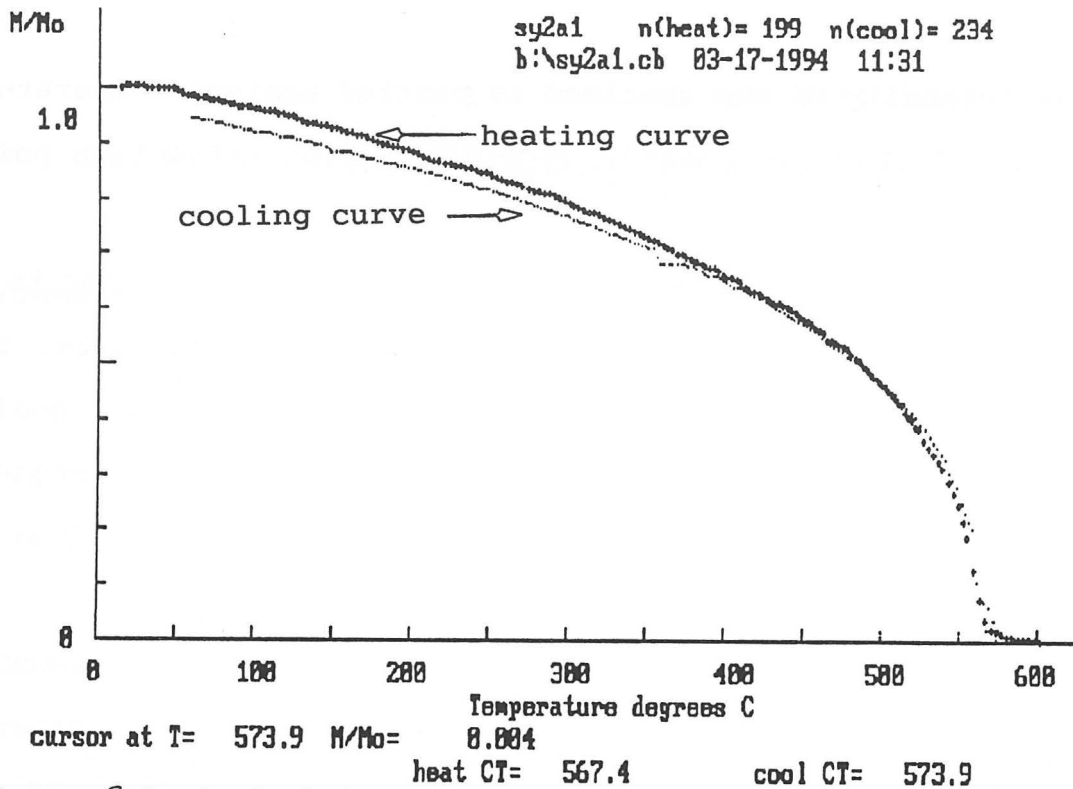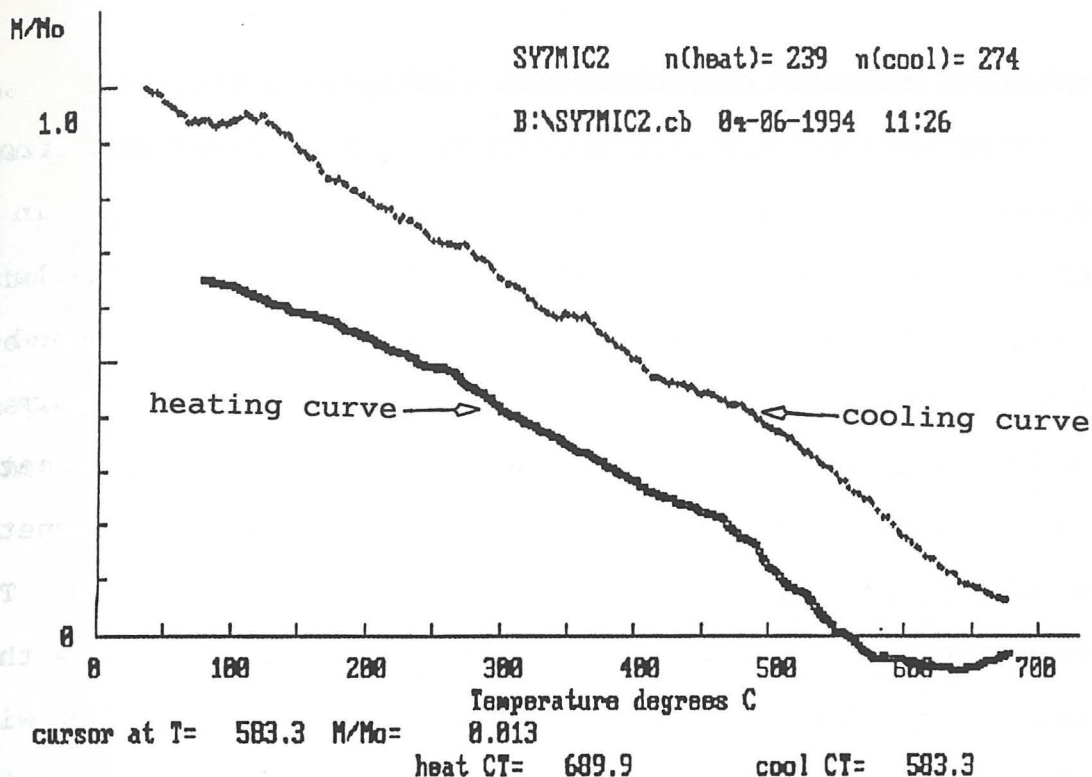
Figure 2.12. Curie balance graph (normalized intensity) for sample sy7 (least-magnetic fraction) composed of microcline grains. The Curie temperature is the inflection point.
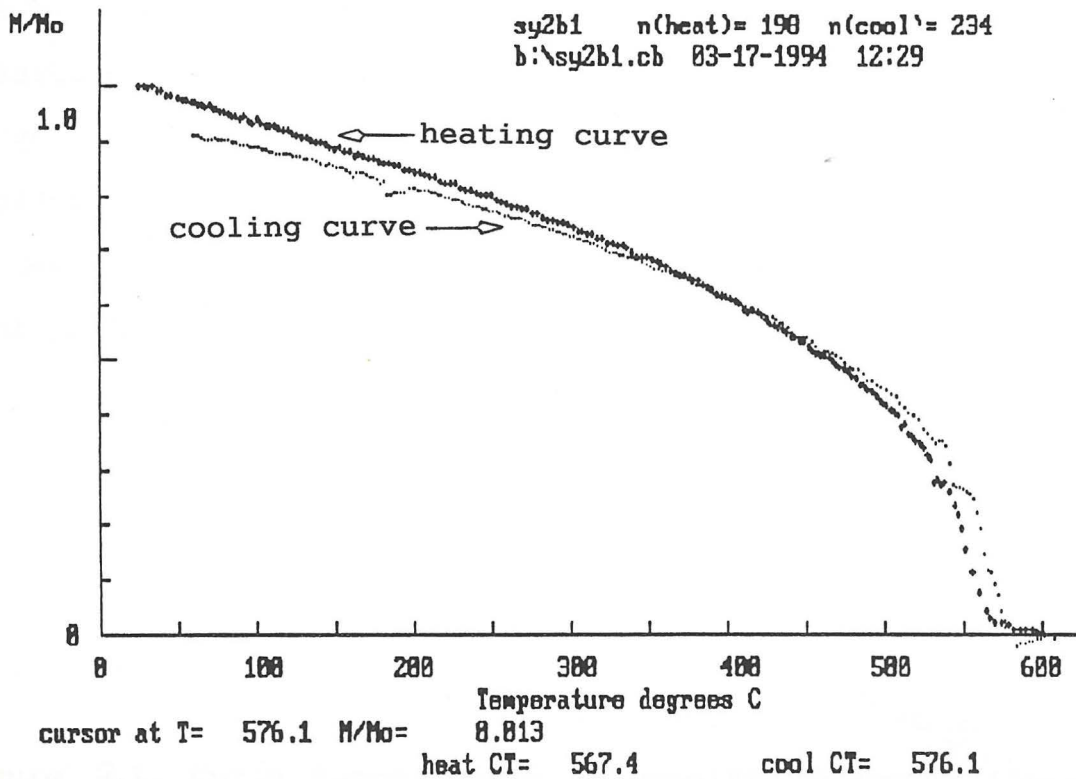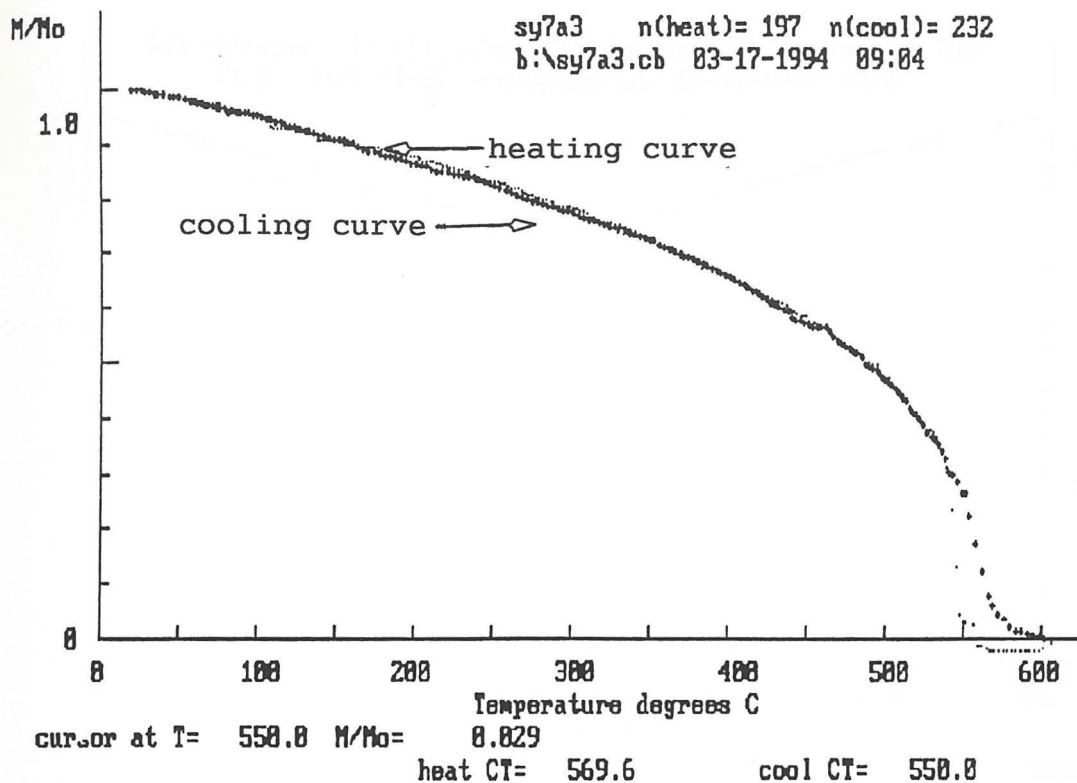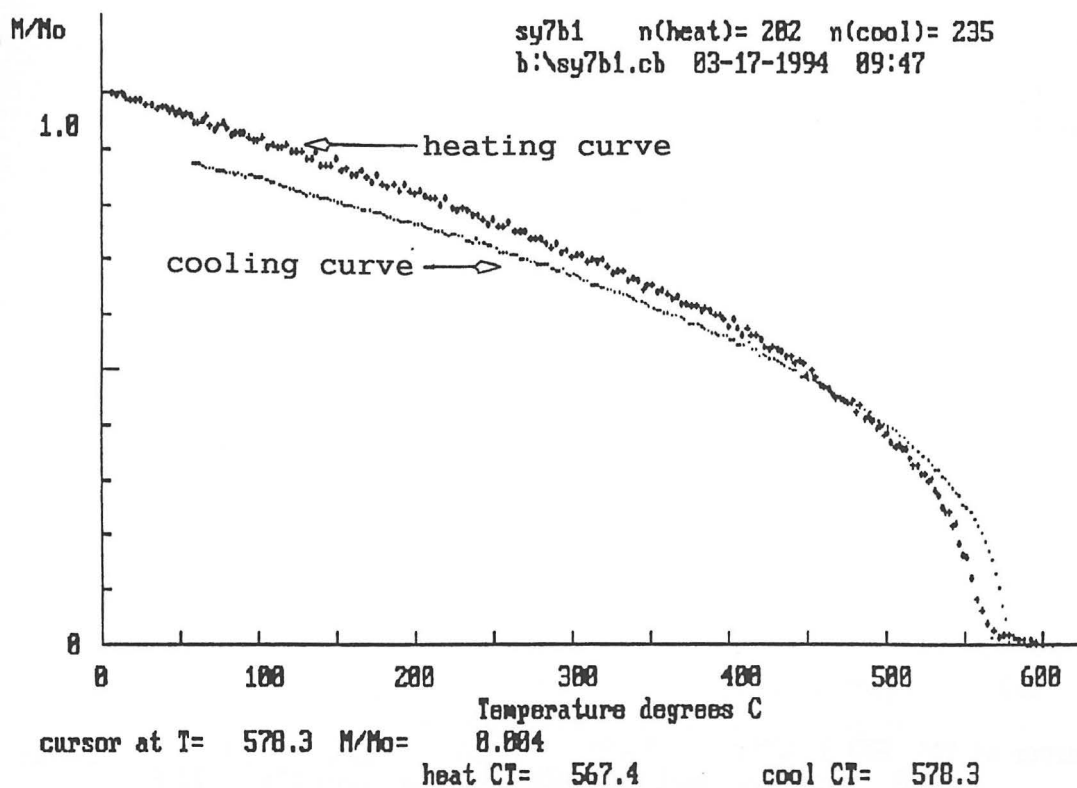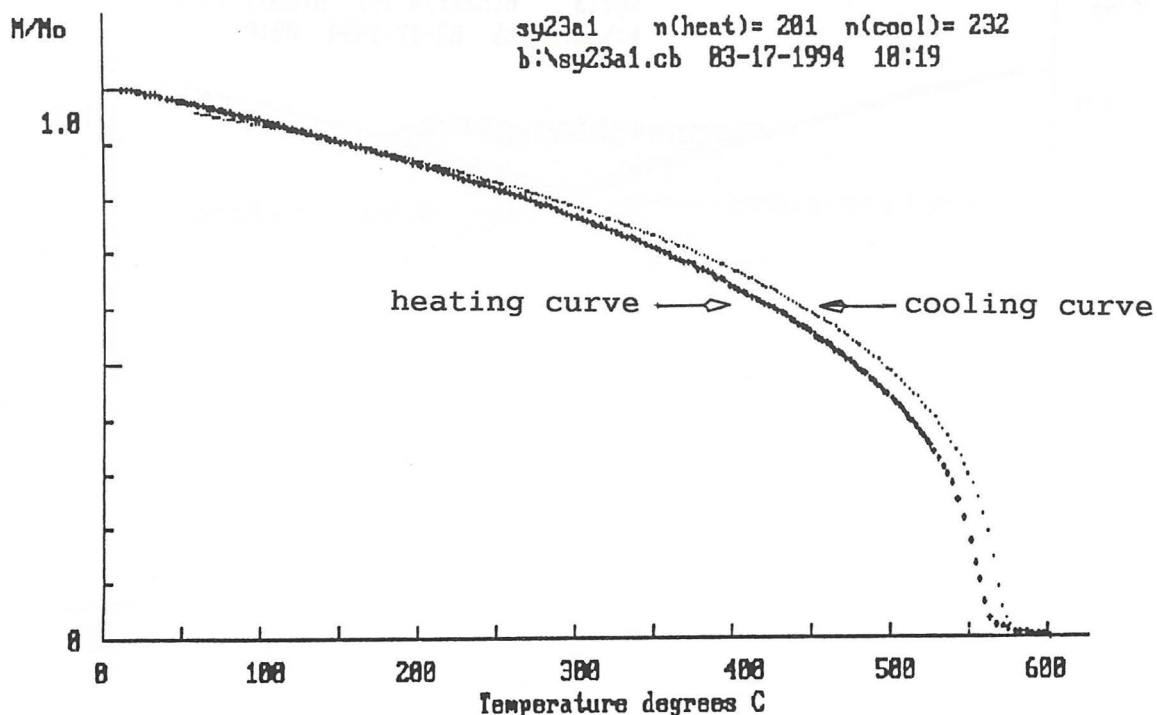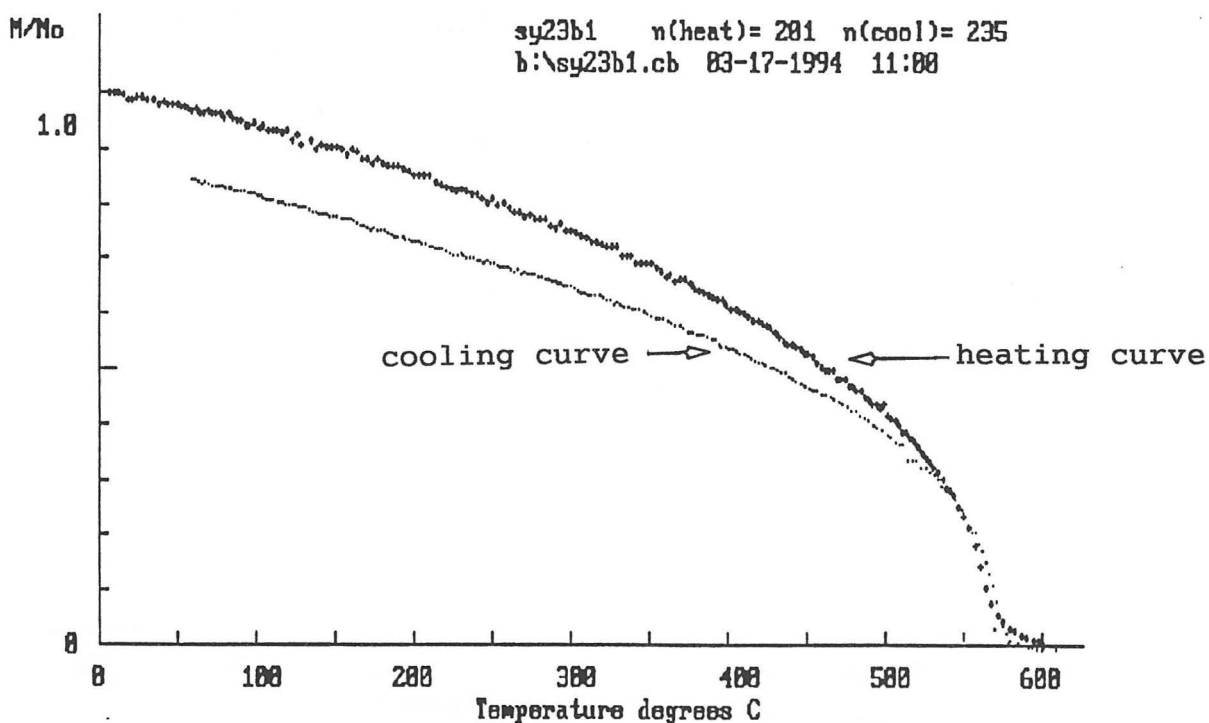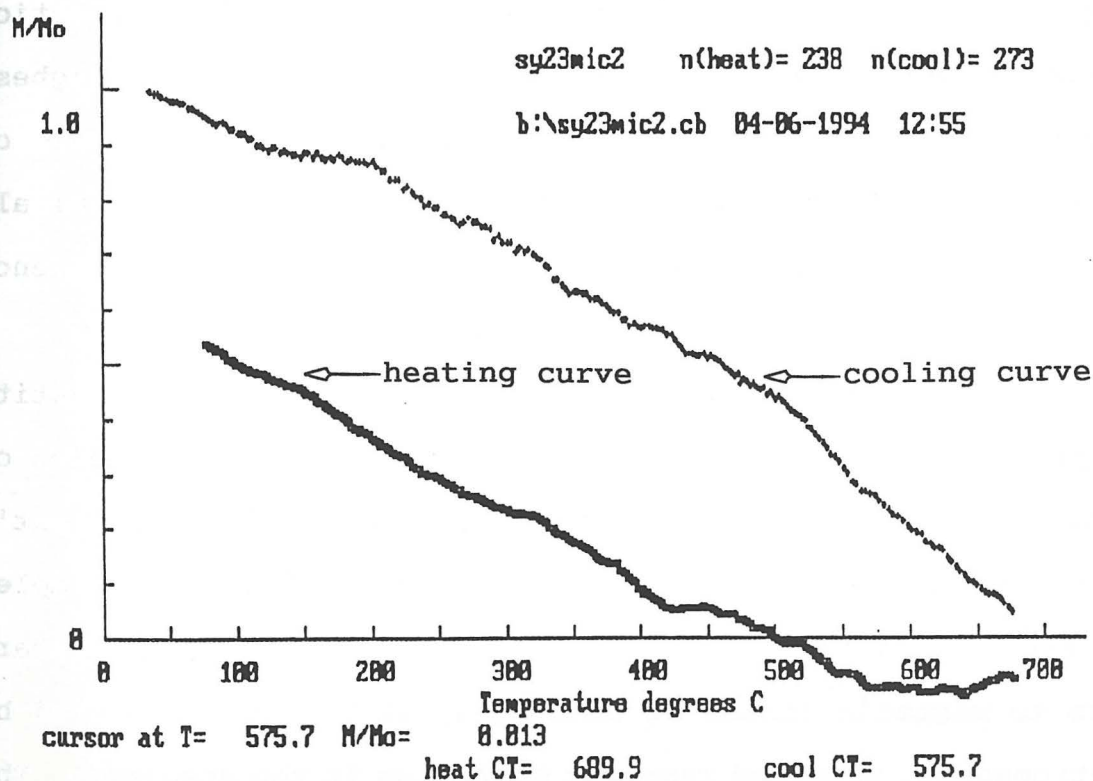

Figure 2.13. Curie balance graph (normalized intensity) for sample sy23 magnetic fraction composed of microcline grains with hematite.

2.2 Isothermal remanent magnetization (IRM)

Isothermal remanent magnetization is produced when a strong applied magnetic field produces an irreversible change in a material's remanence. In most rocks, this is due to domain walls in magnetite moving through crystal lattice energy barriers (caused by impurities or defects). If the domain walls are unable to return to their original positions after removal of the applied magnetic field, the new configuration preserves an IRM. The new magnetic moments align with the magnetic field that was applied. The coercive of remanence is the reverse field required to reduce this magnetization to zero (Strangway, 1970). Some partial IRM will always be produced if the lowest coercive force represented in the sample of the ferromagnetic minerals in the sample is smaller than the applied magnetic field (Cox and Doell, 1960). Saturation magnetization occurs when the applied field exceeds the highest coercivity of remanence in the sample and, in the case of magnetite, when all possible domain walls have moved across all energy barriers (Tarling, 1971). In nature, saturation remanence occurs rarely, for example at lightning strikes.

The purpose of this IRM experiment was to confirm the identity of the predominant magnetic component in representative samples of the Moss Lake stock. In the current study, Sapphire Instrument's pulse magnetizer was used to magnetically saturate two samples (sy4b, sy6b, orientation 180-0) at room temperature. Momentary exposure to magnetic fields of increasing strengths, generated by an electromagnet, produced remanent magnetism in the specimens. The

magnetic field strength was measured after exposure to successively larger magnetic fields in increments of 100 mT to 1200 mT.

IRM acquisition tests of the samples (sy4b, sy6b, Fig. 2.14) show an increase in magnetic intensity by factors of 5.5 and 3.16, respectively, at 1200 mT. The resulting graph of the applied magnetic field strength (mT) versus the (normalized) magnetic intensity is characteristic of magnetite.
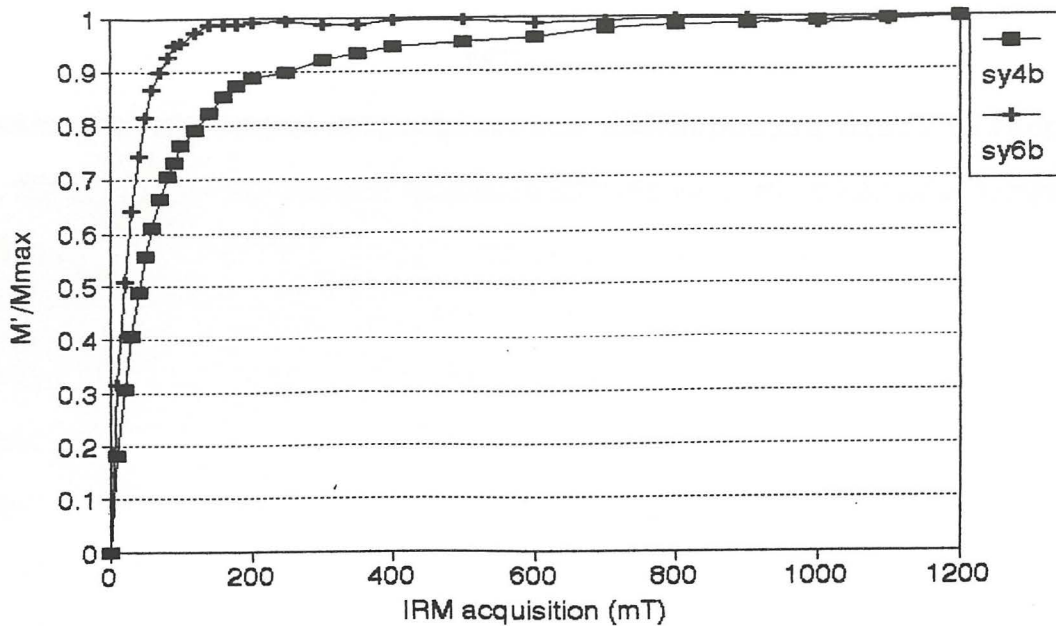
Figure 2.14. Isothermal remanent magnetization (IRM) graphical data for Moss Lake stock samples sy4b and sy6b.
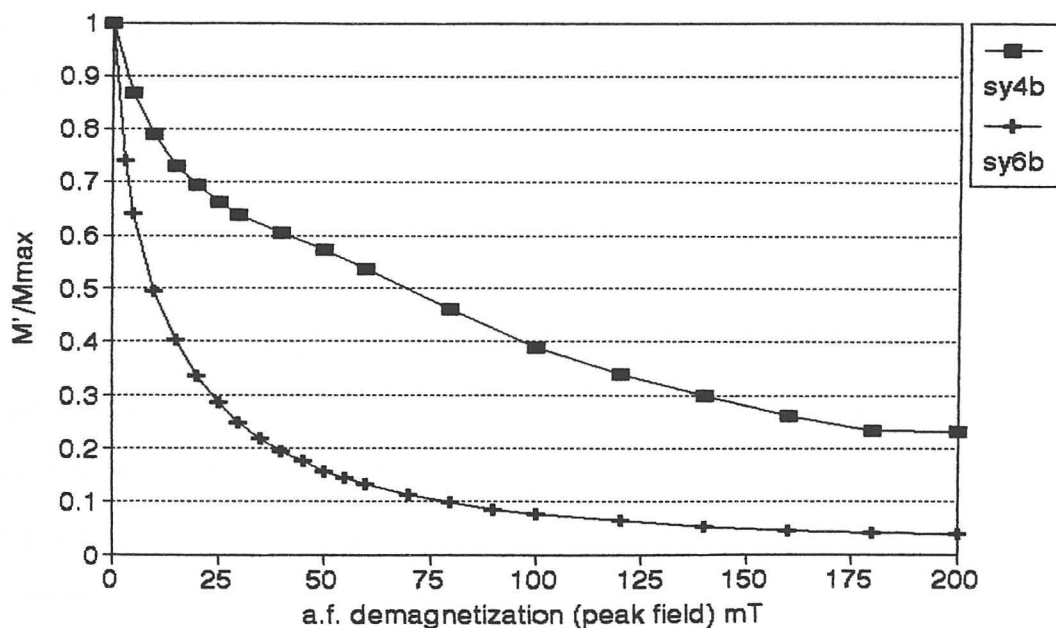
Figure 2.15. Alternating field demagnetization of an ARM produced by a 0.01mT direct field imposed during preceding alternating field demagnetization from 140mT down to 1 mT.

2.3 ARM demagnetization

Anhysteretic remanent magnetization (ARM) is produced when a small direct field is applied to a specimen during alternating field demagnetization (Butler, 1992). Ferromagnetic particles with coercive forces up to the maximum amplitude of the applied alternating magnetic field carry at least a partial ARM (Butler, 1992). Fabric of the carriers of ARM may be investigated by applying ARM in various directions in the rock sample.

Anisotropy (directional variability) of ARM (AARM) provides information relating to remanent magnetism of the ferromagnetic fabric. This overcomes the disadvantage of AMS, in which contributions of ferromagnetic and paramagnetic minerals to low field susceptibilities cannot be isolated.

The Moss Lake stock samples are unsuitable for AARM study as the samples cannot be fully demagnetized (Fig. 2.15) to determine directional variability of anhysteretic remanent magnetization. This is because of the presence of hematite which has a very high coercivity.

III. Natural remanent magnetization (NRM)

NRM is measured in this study to gain information regarding the deformational history of Moss Lake stock by determining the paleomagnetic field orientation of representative rock specimens.

Remanent magnetization in a rock sample, as it lies in situ, is termed natural remanent magnetization (NRM). NRM is commonly composed of more than one component (primary and secondary in nature) and is directly dependent upon the geological history of the specimen (Butler, 1992). Total natural remanent magnetization is the vector sum of all primary and secondary components. The primary component is usually of most interest in paleomagnetic studies and must be isolated from secondary components.

Butler (1992) outlines the three classes of NRM as: (1) thermoremanent magnetization, acquired by cooling from a high temperature, (2) chemical remanent magnetization, formed as ferromagnetic particles grown below the Curie temperature and (3) detrital remanent magnetization, formed by the alignment of detrital ferromagnetic sedimentary grains.

In nature, secondary NRM components may be added by changes in ferromagnetic minerals due to subsequent heating, metamorphism, groundwater alteration, weathering, or lightning strikes (Butler, 1992). Accidental exposure to magnetic fields can also cause such changes.

Isolation of primary NRM components may be attained by partial demagnetization techniques that erase part or all of the secondary NRM components. Secondary components are often low-stability

components and are easily removed. They usually have low coercivities and low unblocking temperatures. In contrast, primary components are usually of high-stability with high coercivity or high unblocking temperature that are more resistant to demagnetization procedures. The most stable natural remanent magnetization (NRM) component is usually the characteristic remanent magnetization component (ChRM). This characterizes the initial or oldest magnetic field direction experienced by the sample. Demagnetization will generally isolate the ChRM direction but further information may be required to confirm that the characteristic remanent magnetization is a primary natural remanent magnetization (Butler, 1992).

NRM measurements are used in this study to determine orientation of the characteristic remanent magnetization (Chrm). A comparison of changes between the paleomagnetic field orientation and the present magnetic field orientation may yield information about the deformational history of Moss Lake stock.

3.2 Alternating field (a.f.) demagnetization

Alternating field (a.f.) demagnetization erases most secondary natural remanent magnetization (NRM) components. Exposing rock samples to alternating magnetic fields of various strengths randomizes and hence erases remanences in portions of the sample in which the coercive force is exceeded by the applied alternating magnetic field. As the alternating field strength is increased, various parts of the remanence have the coercive force surpassed, thus leaving only the most stable NRM components (Strangway, 1970). Each sample has a range of coercive forces called the coercivity spectrum. Demagnetization by alternating field techniques may be carried out from 0-200 mT using the Sapphire Instrument's demagnetizer.

3.2.1 Alternating field (a.f.) demagnetization summary

Data analysis was performed using the computer programs <u>Nuspin</u> (Borradaile and Molyneux, 1994) and <u>Si2x</u> (Borradaile and Stupavsky, 1994).

Results of alternating field demagnetization of 15 selected Moss Lake stock samples are summarized in Figures 3.1 and 3.2 (a.f. demagnetization data, stereographic projections and principal component analyses (PCA) are in Appendix D). PCA is performed using the algorithm of Diggle and Fisher (1985). In Figure 3.1, the principal component analysis magnetic vectors (black symbols) of the most orientation-consistent samples point from northeast to northwest. Colour distinction is made (Fig. 3.1) between the easy

Lwr.Hem.Equal Area Net
circle=DOWN square=UP
:\nrm\afdpcas.SR2
n = 23
08-18-1994

mean inclination/declination   alpha95

☆ 69.6/31.7   56.4

☆ 58.7/32.9   53.0

★ 334.5/41.7   54.1
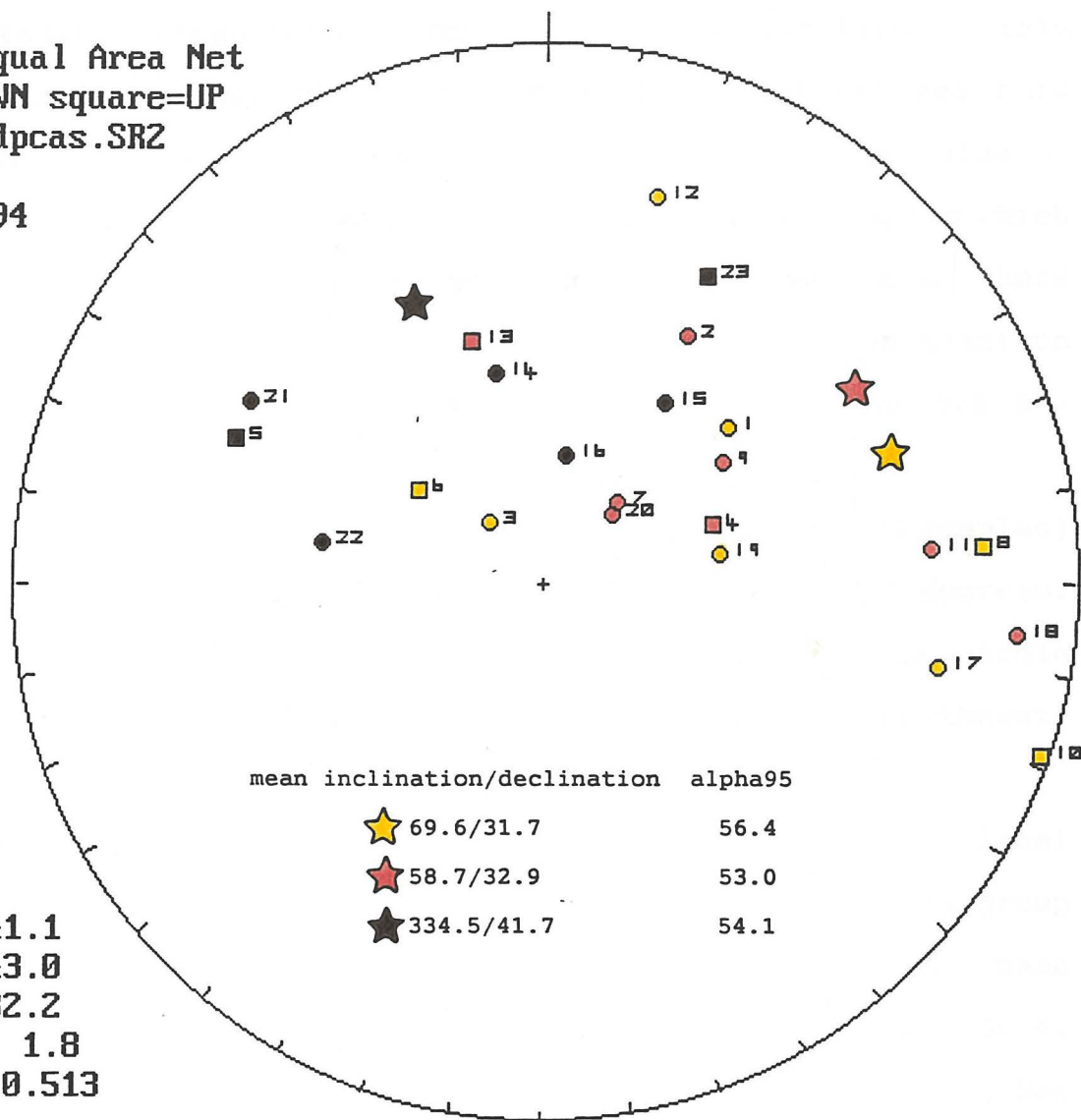
m.dec.= 41.1
m.inc.= 43.0
alpha95= 32.2
Fish. k=   1.8
sp.var.= 0.513

Figure 3.1. Summary of alternating field demagnetization of Moss Lake stock samples, lower hemisphere stereographic projection. Red=high stability component (5-200 mT), yellow=low stability component (0-5 mT) and black=consistent principal component analysis orientation (0-200 mT). Refer to Figure 3.2 (table) for sample number cross reference with stereographic projection number.

data#	MLS sample	PCA declination	PCA inclination	range of demag. (mT)	PCA data points
1	sy1bnel	50.1	53.1	0.8-5.0	3 to 8
2	sy1bneh	30.6	46.4	10.0-80.0	9 to 16
3	sy2bnel	318.2	77.6	0-10.0	1 to 9
4	sy2bneh	71.3	-62.7	20.0-50.0	10 to 13
5	sy3bnea	294.5	-36.1	0.8-70.0	3 to 16
6	sy8bnel	306.1	-66.4	0-5.0	1 to 8
7	sy8bneh	42.5	73.6	10.0-60.0	9 to 15
8	sy9bnel	85.2	-18.5	0-5.0	1 to 8
9	sy9bneh	56.5	57	10.0-80.0	9 to 17
10	sy10bne	108.7	-1.8	0.8-4.0	3 to 7
11	sy10bne	84.9	28.1	4.0-70.0	7 to 16
12	sy15bne	16.3	27.3	0-5.0	1 to 8
13	sy15bne	342.9	-51.8	10.0-40.0	9 to 13
14	sy16bne	346.9	57.4	0-80.0	1 to 17
15	sy19bne	33.9	57.1	0-15.0	1 to 10
16	sy20bne	10.2	70.7	0-30.0	1 to 11
17	sy21bne	101.6	25.5	0.5-5.0	2 to 8
18	sy21bne	96	12	5.0-50.0	8 to 14
19	sy22bne	80.4	62.6	0.8-5.0	3 to 8
20	sy22bne	46.3	75.3	5.0--160.0	8 to 22
21	sy23bne	301.2	35.5	0.8-80.0	3 to 17
22	sy26bne	280.7	55	0.5-80.0	2 to 15
23	sy27bne	28.5	-36.2	0-90.0	1 to 18

Figure 3.2. Data table for stereographic projection of Figure 3.1.
Data numbers refer to stereographic projection symbol numbers (Fig.
3.1). Principal component analysis data points refer to Appendix D
alternating field principal component analyses (PCAs).

(least-stable components removed by alternating field demagnetization values of 0.0-0.5 mT =yellow symbols) and hard (most-stable components removed by a.f. demagnetization value of 0.5-200.0 mT =red symbols) magnetic components of the samples which show transitional principal component analysis orientations. There appears to be a shift of characteristic remanent magnetization toward the northwest as the easy magnetic component vectors are removed.

The mean principal component analysis declination (all samples) is azimuth 041.1 degrees and the mean inclination is 43.0 degrees. The alpha95 value is 32.2. A best-fit line through the girdle distribution (Fig. 3.1) has an orientation parallel to a northwest-southeast fault set in northwestern Moss Township.

Dividing the sample group into consistent versus transitional principal component analysis orientations, the low-stability group (yellow symbols=0-5.0 mT on Fig. 3.1) has a mean inclination/declination of 069.6/31.7 and an alpha95 value of 56.4. The high-stability group (red symbols=5.0-200.0 mT on Fig. 3.1) has a mean inclination/ declination of 058.7/32.9 and an alpha95 value of 53.0. The most-stable PCA orientations (black symbols=0-200.0 mT in Fig. 3.1) have a mean declination/inclination of 334.5/41.7 and an alpha95 value of 54.1.

The spread of principal component analysis data on the stereographic projection (Fig. 3.1) is inconsistent with that expected of an undeformed syenite/granitoid stock. If the pluton was undeformed, a better-defined cluster of data would be expected.

A magma body cooled in an ambient magnetic field should reflect the same orientation of the ambient magnetic field in all parts. The alternating field demagnetization data suggest that the Moss Lake stock samples are deformed, therefore they have possibly acquired secondary (natural) magnetic components probably during post magmatic, tectonic deformation.

Further demagnetization is required to remove the secondary magnetic components. This was accomplished by thermal demagnetization at high temperatures.

3.3 Thermal demagnetization

Nineteen Moss Lake stock samples were incrementally heated to 700 degrees C. At each temperature increment, after cooling to room temperature in a magnetic field of less than 1 nT, each sample was measured in a JR5a automatic spinner magnetometer to determine the magnetic vector declination [azimuth], inclination [dip], intensity [mA/m] and error [%]. The sensitivity of the spinner magnetometer is 0.02 mA/m.

For hematite-bearing rocks, secondary natural remanent magnetization components are not usually completely removed by alternating field demagnetization (Butler, 1992). However, thermal demagnetization is successful because the maximum blocking temperature is the Curie temperature of 670 degrees C; this is easily reached in the thermal demagnetizer. Thermal demagnetization erases NRM of magnetic grains as all grains which have blocking temperatures [Tb] lower than the increment temperature [Tb<Tdemag]

acquire a thermoremanent magnetization in [H=0] (Butler, 1992).

The progressive method of thermal demagnetization has drawbacks in that it is impossible to produce zero magnetic field, hence the samples may acquire a slight magnetic field upon cooling to room temperature [where Tb<Tdemag]. Although the samples are well-shielded during cooling, inside the furnace, they are handled in the Earth's magnetic field during measurement. In some cases they acquire a metastable viscous remanent magnetization (VRM) during handling, perhaps because of metastable transdomain remanence. If there were magnetic minerals present with blocking temperatures greater than the incremental temperature, an erased partial remanence is not attained (Creer, 1972). Thermal demagnetization usually removes secondary magnetization components acquired from (natural) partial reheating of rock units (Strangway, 1970). Magnetic intensities (normalized) of ten Moss Lake stock samples are plotted against temperature (Figs. 3.3 and 3.4). In Figures 3.3 and 3.4 the predominant unblocking temperature is approximately 650 degrees C.
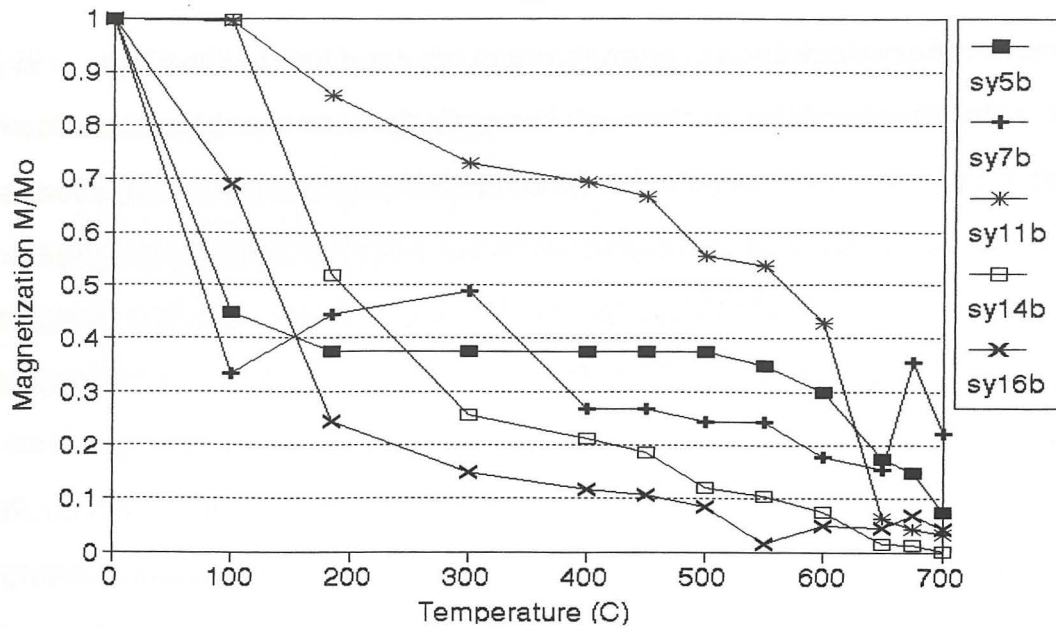
Figure 3.3. Thermal demagnetization (normalized) of Moss Lake stock samples sy5b,sy7b,sy11b,sy14b and sy16b.
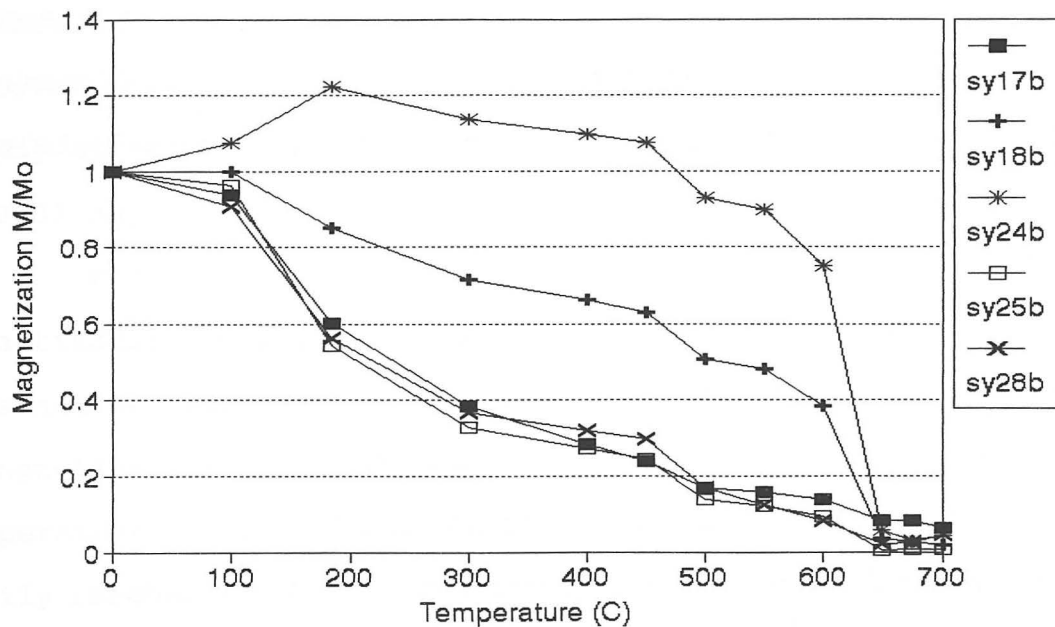
Figure 3.4. Thermal demagnetization (normalized) of Moss Lake stock samples sy17b, sy18b, sy24b, sy25b and sy28b.

3.3.1 Thermal demagnetization summary

A lower hemisphere, equal area stereographic projection (Fig. 3.5) summarizes the magnetic component data for the Moss Lake stock samples which are thermally demagnetized. In Figure 3.5 (data, Appendix E), the mean declination is azimuth 213.3 degrees and the mean inclination is 61.5 degrees. The alpha95 value is 40.6. The mean orientation of magnetic components of the Moss Lake stock syenite/granitoid samples corresponds closely to local planar fabric strike and dip of the Quetico Subprovince and the Shebandowan metavolcanic belt.

A mean vector summary of the orientations of the principal component analysis of the Moss Lake stock samples (Fig. 3.6), which are thermally demagnetized, shows a cluster of the magnetic vectors in a sub-vertical orientation. The cluster is shifted from that expected in an undeformed stock and the cluster of points is once again spread. Some scattered near-horizontal vectors (Fig. 3.6) are present but there are too few to present a meaningful interpretation.

Further analysis of the principal component analysis data is accomplished by isolating the magnetic components unblocked at different temperatures, ie., unblocking temperatures at 550 degrees C or less correspond to remanence carried mainly by magnetite, whereas unblocking temperatures greater than 550 degrees C must be attributable only to hematite. Figure 3.7 summarizes the easy magnetic components which are effectively removed at temperatures less than the Curie temperature for magnetite. The magnetic

Lwr.Hem.Equal Area Net
circle=DOWN square=UP
 rmal\rsptherm.SR2
 n =   19
 08-10-1994
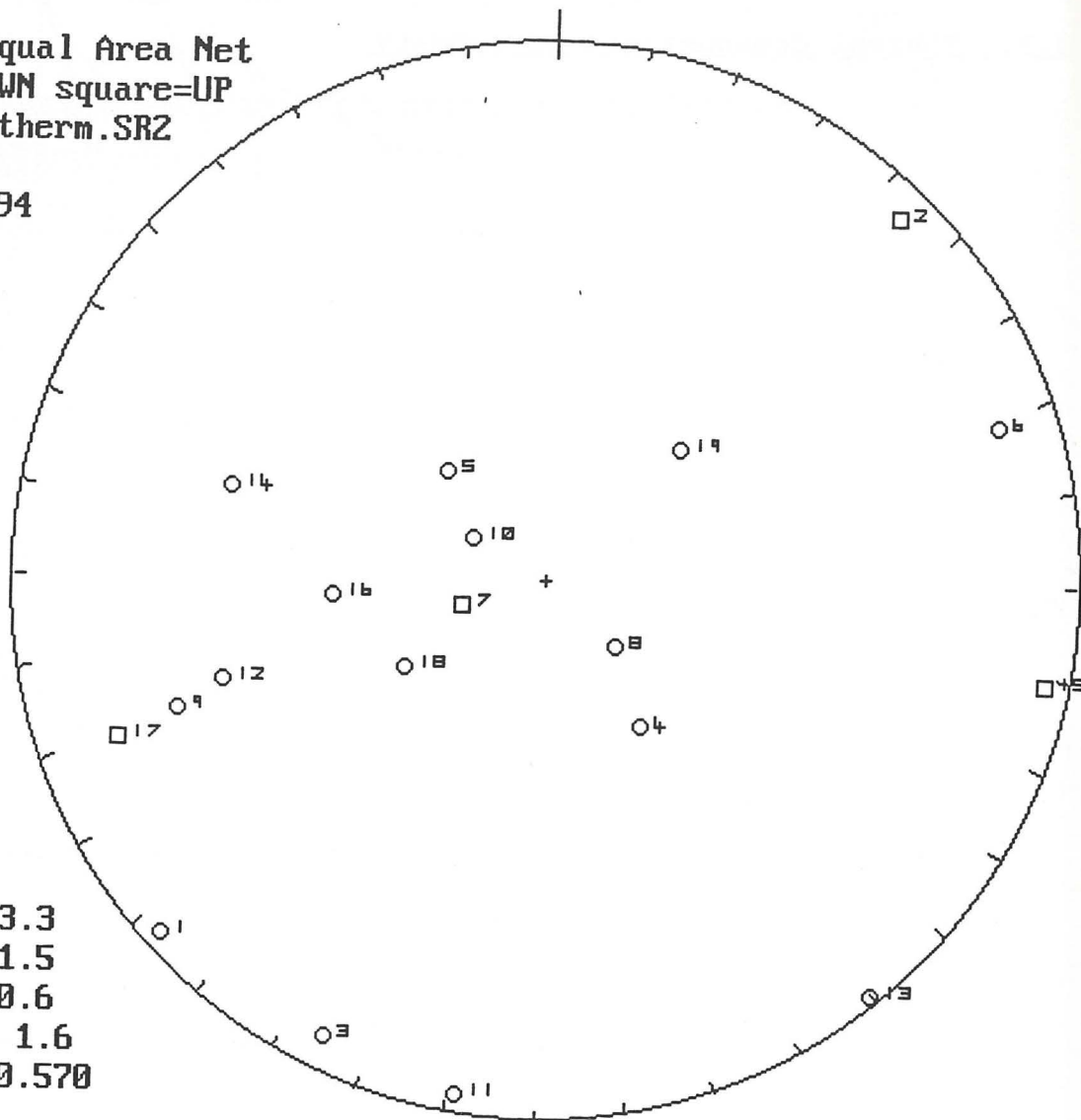
m.dec.= 213.3
m.inc.= 61.5
alpha95= 40.6
Fish. k=   1.6
sp.var.= 0.570

Figure 3.5. Lower hemisphere stereographic projection summary of thermally demagnetized Moss Lake stock sample magnetic components after exposure to an unblocking temperature of 700 degrees C but before performing the principal component analysis.

Lwr.Hem.Equal Area Net
circle=DOWN square=UP
hermal\ttpcas.SR2
n = 19
08-10-1994
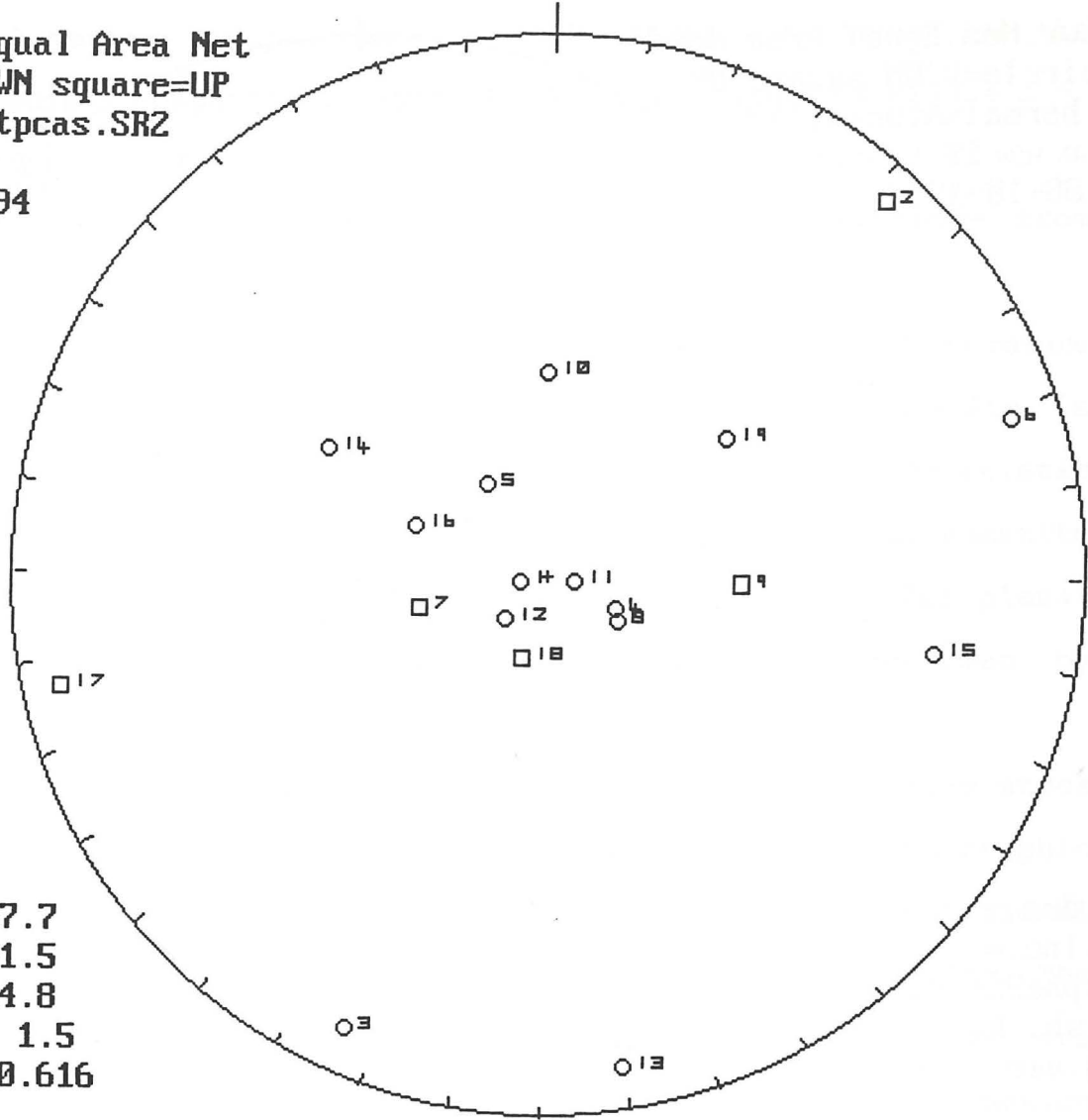
m.dec.= 107.7
m.inc.= 81.5
alpha95= 44.8
Fish. k= 1.5
sp.var.= 0.616

Figure 3.6. Lower hemisphere stereographic projection of mean thermally demagnetized principal component analyses for Moss Lake stock samples after exposure to an unblocking temperature of 700 degrees C. These orientations represent "total" thermal PCAs, ie. they have not been separated into unblocking temperatures.
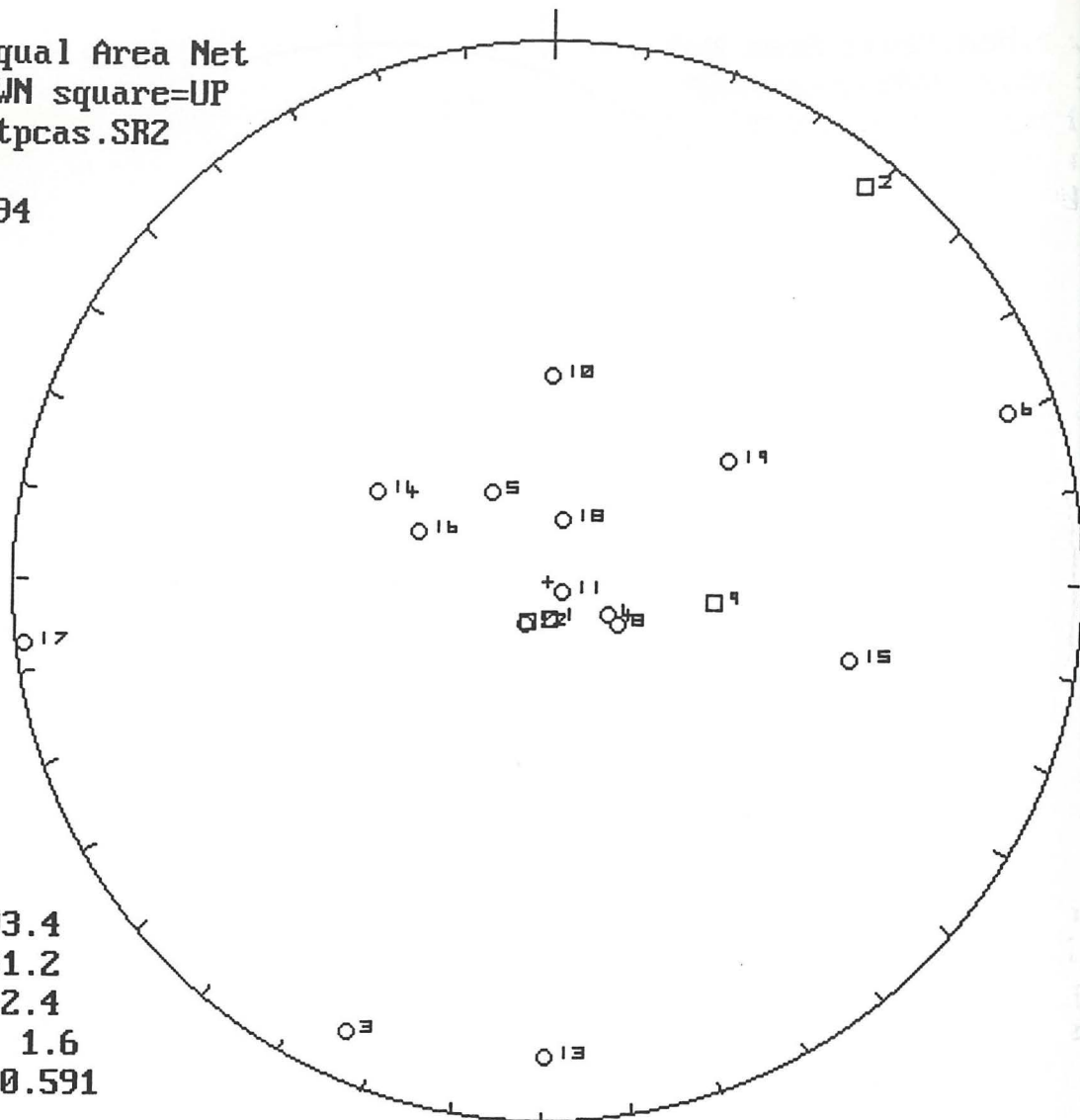
Figure 3.7. Lower hemisphere stereographic projection of principal component analysis orientations for thermally demagnetized Moss Lake stock samples after exposure to an unblocking temperature of 550 degrees C. At this temperature of thermal demagnetization, the magnetic effects of magnetite must predominate those of hematite, therefore, these PCA orientations are from magnetite.

component vector orientations are much the same as those for the mean principal component analysis (PCA) orientations of Figure 3.6. Contoured data relating to Figure 3.7 is shown in Figure 3.8, where the magnetic effects of magnetite are greater than those from hematite.

Where the unblocking temperatures exceed the Curie temperature of magnetite (for the Moss Lake stock samples), hematite is responsible for the hard magnetic component, or characteristic remanent magnetization (Chrm). The orientations of the hematite PCAs (Fig. 3.9) are distinctly translated into the local planar fabric strike of the Quetico Subprovince, as confirmed by comparison of the Eigenvectors of Figures 3.8 and 3.10.

Thermal demagnetization of five additional Moss Lake stock syenite/granitoid samples (Fig. 3.11; data, stereographic projections and principal component analyses for the transitional samples are in Appendix F) shows transitional characteristics. The higher blocking temperature components, due to hematite, are dispersed along the local planar fabric strike of the Quetico Subprovince (Fig. 1.3C,D).

component vector orientations are much the same as those for the mean principal component analysis (PCA) orientations of Figure 3.6. Contoured data relating to Figure 3.7 is shown in Figure 3.8, where the magnetic effects of magnetite are greater than those from hematite.

Where the unblocking temperatures exceed the Curie temperature of magnetite (for the Moss Lake stock samples), hematite is responsible for the hard magnetic component, or characteristic remanent magnetization (Chrm). The orientations of the hematite PCAs (Fig. 3.9) are distinctly translated into the local planar fabric strike of the Quetico Subprovince, as confirmed by comparison of the Eigenvectors of Figures 3.8 and 3.10.

Thermal demagnetization of five additional Moss Lake stock syenite/granitoid samples (Fig. 3.11; data, stereographic projections and principal component analyses for the transitional samples are in Appendix F) shows transitional characteristics. The higher blocking temperature components, due to hematite, are dispersed along the local planar fabric strike of the Quetico Subprovince (Fig. 1.3C,D).

N = 19

k = 6.22

E = 3.05

σ = 1.02

Peak Trend   0.0

Peak Plunge   85.5

(Peak - E)/σ = 7.0
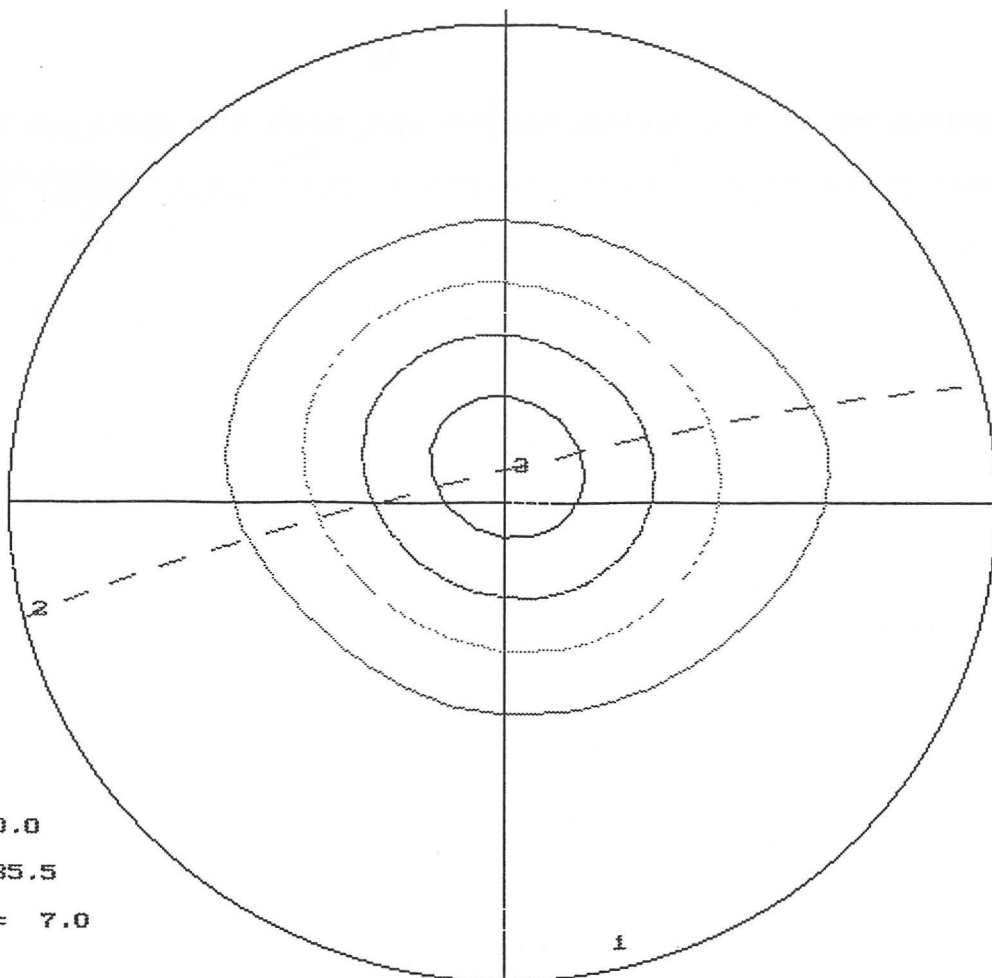
EigenVector Results   Data File : MTPCAS
                                   No. of Data: 19

Vector	Trend	Plunge	Eigenvalue	
1	165.88	5.35	2.3664 +/-	0.2392
2	256.25	3.97	4.2690 +/-	0.3420
3	22.66	83.33	12.3646 +/-	0.4073

Confidence Cones

Vector	Major	Minor	Average	Angle
1	41.80	10.89	26.35	-0.26
2	41.80	15.03	28.42	-0.21
3	15.86	9.59	12.72	14.39

Eigenvalue Ratios (after Woodcock, 1977)

K-ratio [ln(E3/E2)/ln(E2/E1)]: 1.80 +/- 0.49
C-ratio [ln(E3/E1)]   : 1.65 +/- 0.11

Pattern: Moderately developed girdle and cluster.

Figure 3.8. Contoured data with Eigenvector results for the stereographic projection of Figure 3.7. The moderately developed girdle and cluster represent the orientation of principal component analyses for magnetite.

Lwr.Hem.Equal Area Net
circle=DOWN square=UP
 hermal\htpcas.SR2
 n = 13
 08-22-1994

m.dec.= 189.0
m.inc.= -30.3
alpha95= 68.8
Fish. k= 1.3
sp.var.= 0.692
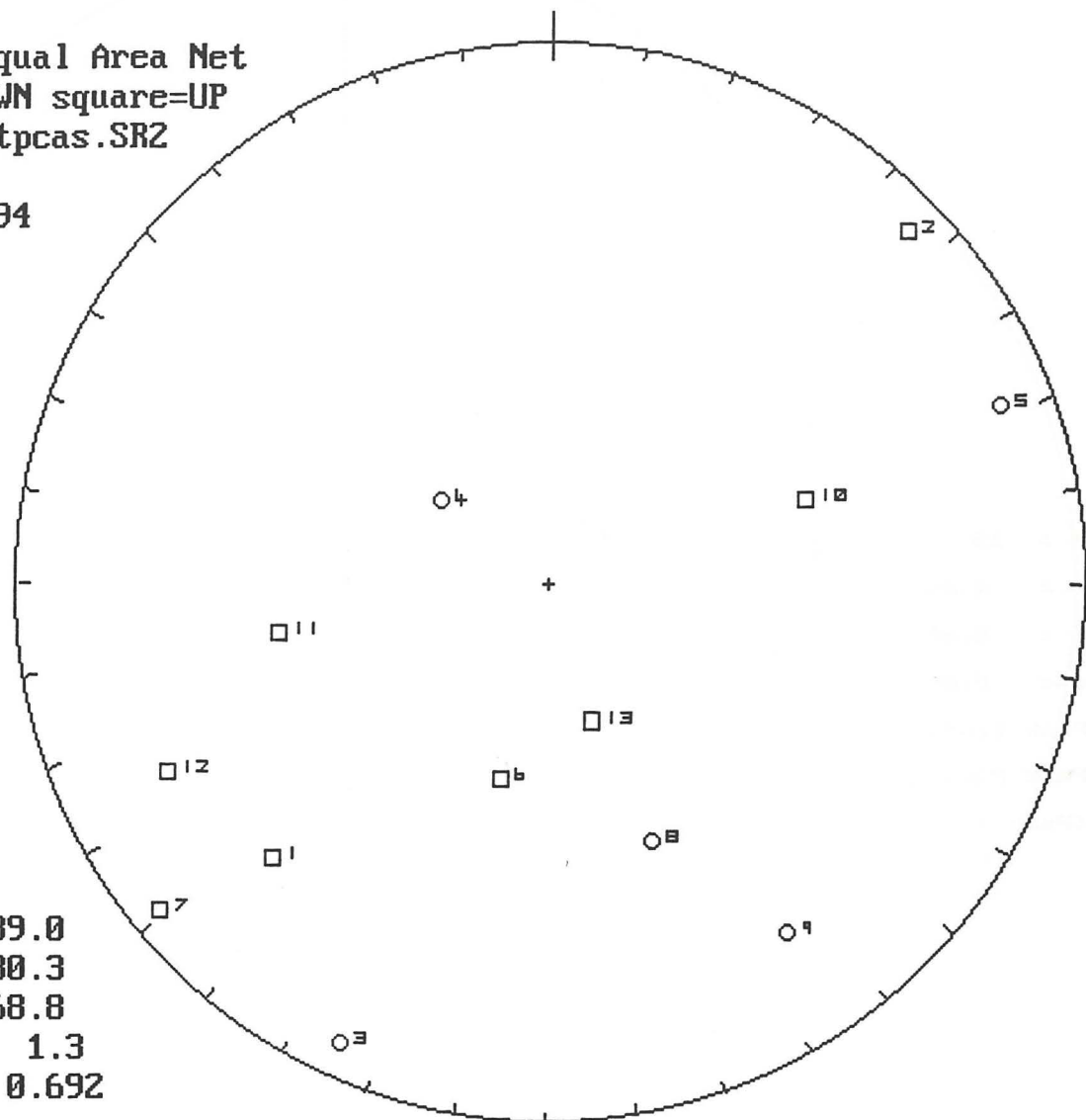
Figure 3.9. Summary of PCA vector orientations for thermally demagnetized Moss Lake stock samples after exposure to an unblocking temperature of 700 degrees C (hematite>magnetite). The data points in the stereographic projection represent the PCA orientations for the temperature range of 550 to 700 degrees C.

N = 13

k = 4.89

E = 2.66

σ = 0.89

Peak Trend 230.2

Peak Plunge 14.3

(Peak - E)/σ = 2.7
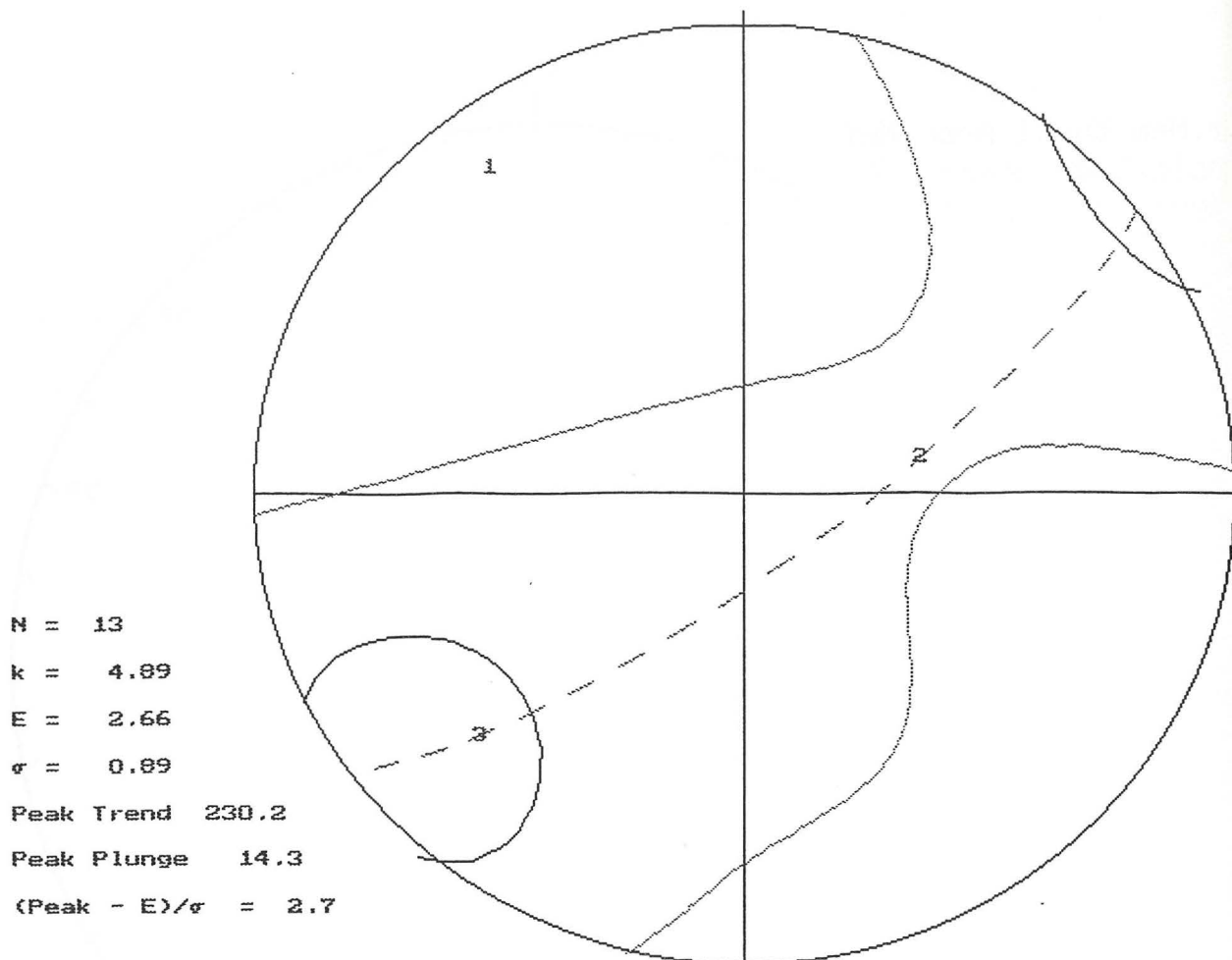
EigenVector Results

Data File : HTPCAS-
No. of Data: 13

Vector	Trend	Plunge	Eigenvalue		
1	323.23	13.79	1.8239	+/-	0.1816
2	78.24	59.86	4.4578	+/-	0.3111
3	226.29	26.22	6.7183	+/-	0.3499

Confidence Cones

Vector	Major	Minor	Average	Angle
1	37.54	18.71	28.12	10.02
2	50.86	36.42	43.64	0.45
3	50.86	21.81	36.33	0.36

Eigenvalue Ratios (after Woodcock, 1977)

K-ratio [ln(E3/E2)/ln(E2/E1)]: 0.46 +/- 0.14
C-ratio [ln(E3/E1)]   : 1.30 +/- 0.11

Pattern: Weakly developed girdle.

Figure 3.10. Contoured data with Eigenvector results for the stereographic projection of Figure 3.9.

Lwr.Hem.Equal Area Net
circle=DOWN square=UP
 rmal\trnsthrm.SR2
 n =   10
 08-10-1994

700
□2

550
○3

550
○9

550   □7
○5   +   550

700   ○1
○8   550

700
□4   700   700
         ○1 □
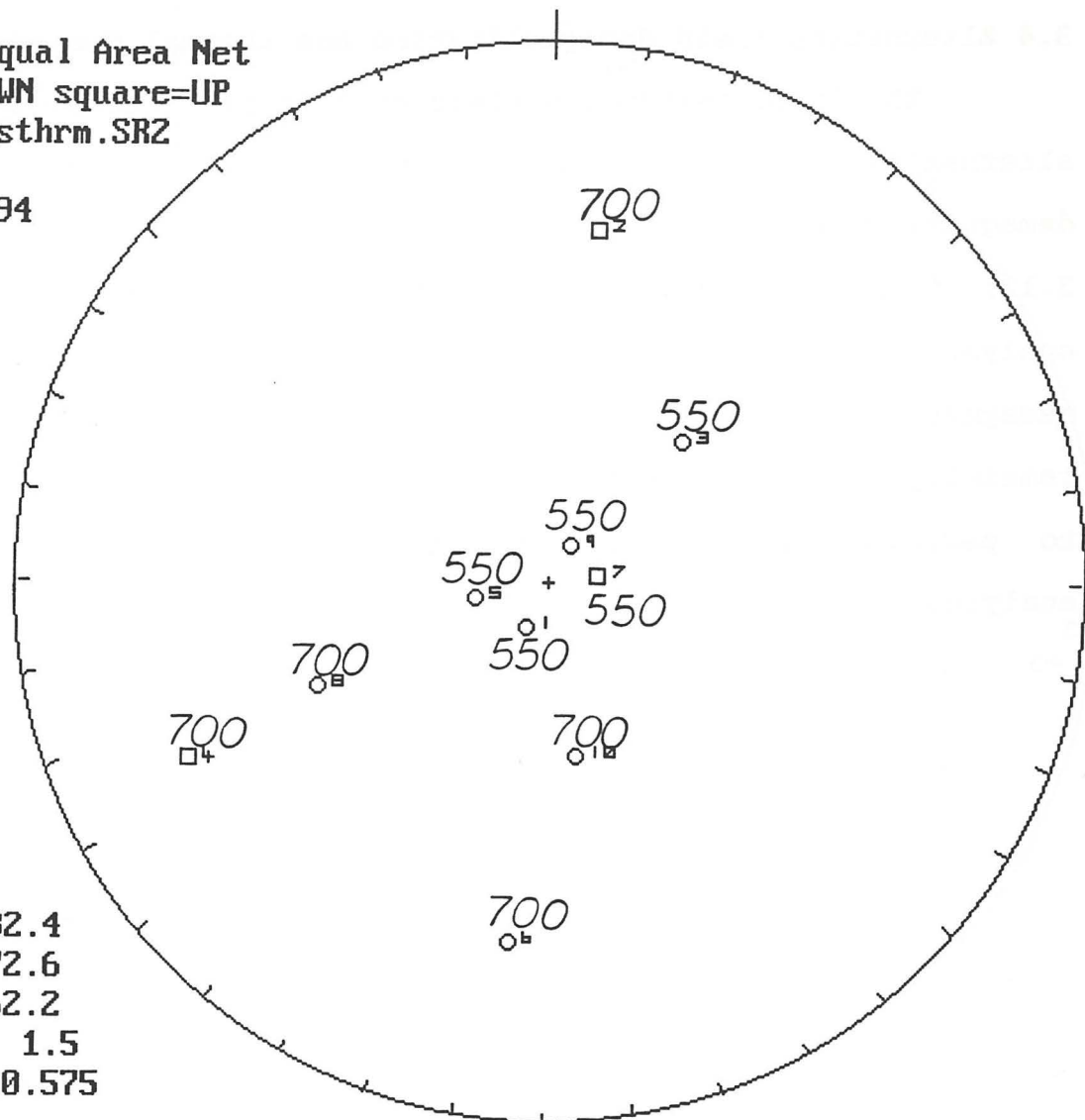
m.dec.= 232.4
m.inc.= 72.6
alpha95= 62.2
Fish. k=   1.5
sp.var.= 0.575

700
○6

Figure 3.11. Lower hemisphere stereographic projection of principal
component analysis vectors for Moss Lake stock samples which show
anomalous transitional thermal demagnetization results. The data
points represent the mean PCA vector orientations of samples
exposed to unblocking temperatures of 550 and 700 degrees C.

3.4 Alternating field demagnetization and thermal demagnetization

The lower hemisphere stereographic projection of combined alternating field demagnetization followed by thermal demagnetization generally produces uninterpretable results (Fig. 3.12; data, stereographic projections and principal component analyses are in Appendix G). During alternating field demagnetization, most of the magnetic components are erased; the remaining magnetic components are erratic and too weak upon which to perform thermal demagnetization for principal component analyses.

Lwr.Hem.Equal Area Net
circle=DOWN square=UP
 hermal\ntpcas.SR2
 n =   14
 06-02-1994
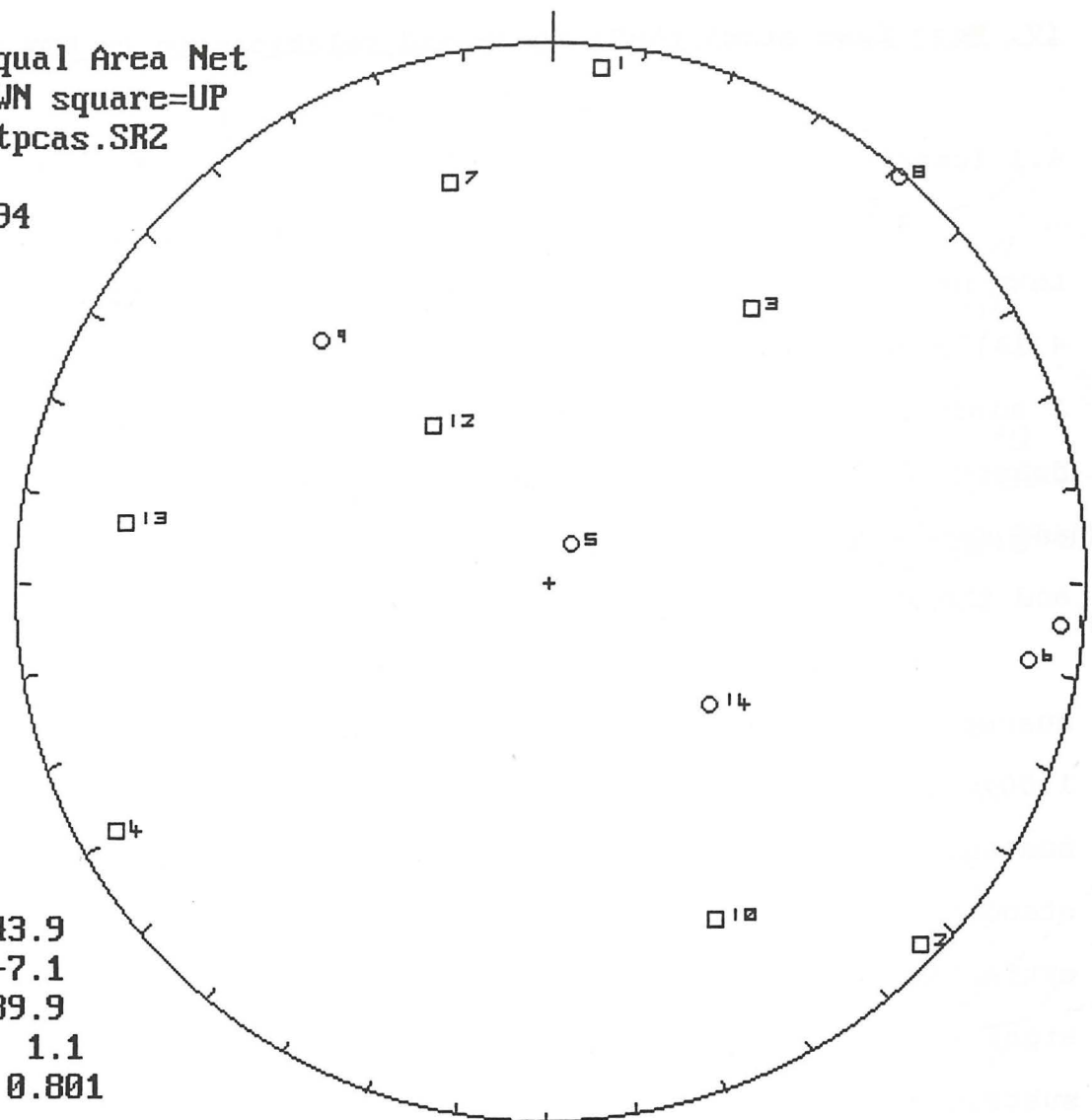
m.dec.=   43.9
m.inc.=   -7.1
alpha95= 89.9
Fish. k=   1.1
sp.var.= 0.801

Figure 3.12. Lower hemisphere stereographic projection for principal component analyses of combined alternating field demagnetization followed by thermal demagnetization of Moss Lake stock samples. The unblocking temperature for each data point is 700 degrees C.

IV. Moss Lake stock (AMS) study and relationship to NRM results

4.1 Introduction

A total of 54 oriented samples were collected from the Moss Lake stock for AMS study. Location latitudes and longitudes (Fig. 4.1A) were recorded using a GPS unit (global positioning system). A minimum of two cores per hand specimen were tested. Sampling density is two samples per square kilometer. (Refer to Appendix A and Appendix B for theory and application of AMS to plutonic rocks and the Moss Lake stock).

For the Moss Lake stock oriented samples, the mean magnetic susceptibility [kmax], [kint] and [kmin] values are 1.06 ± 0.05, 1.00 ± 0.01 and 0.93 ± 0.04, respectively. The mean bulk magnetic susceptibility of the intrusion samples is $12,219 \times 10^{-6}$ SI with a standard deviation of $13,416 \times 10^{-6}$ SI. The standard deviation is extraordinarily high therefore the mean is decreased in significance. Approximate bulk (whole; total) magnetic susceptibility values are visually illustrated on Figure 4.1B. (Refer to Appendix H for actual bulk magnetic susceptibility values.)

The magnetic foliations (kmax-kint plane) and magnetic lineations [kmax] are plotted on Figure 4.2. Strike and dip symbols represent the magnetic foliation planes and arrows represent the trend of maximum magnetic susceptibility and amount of plunge. Where orientations of magnetic foliation and magnetic lineation are within 5 degrees (for same-specimen cores), orientations are
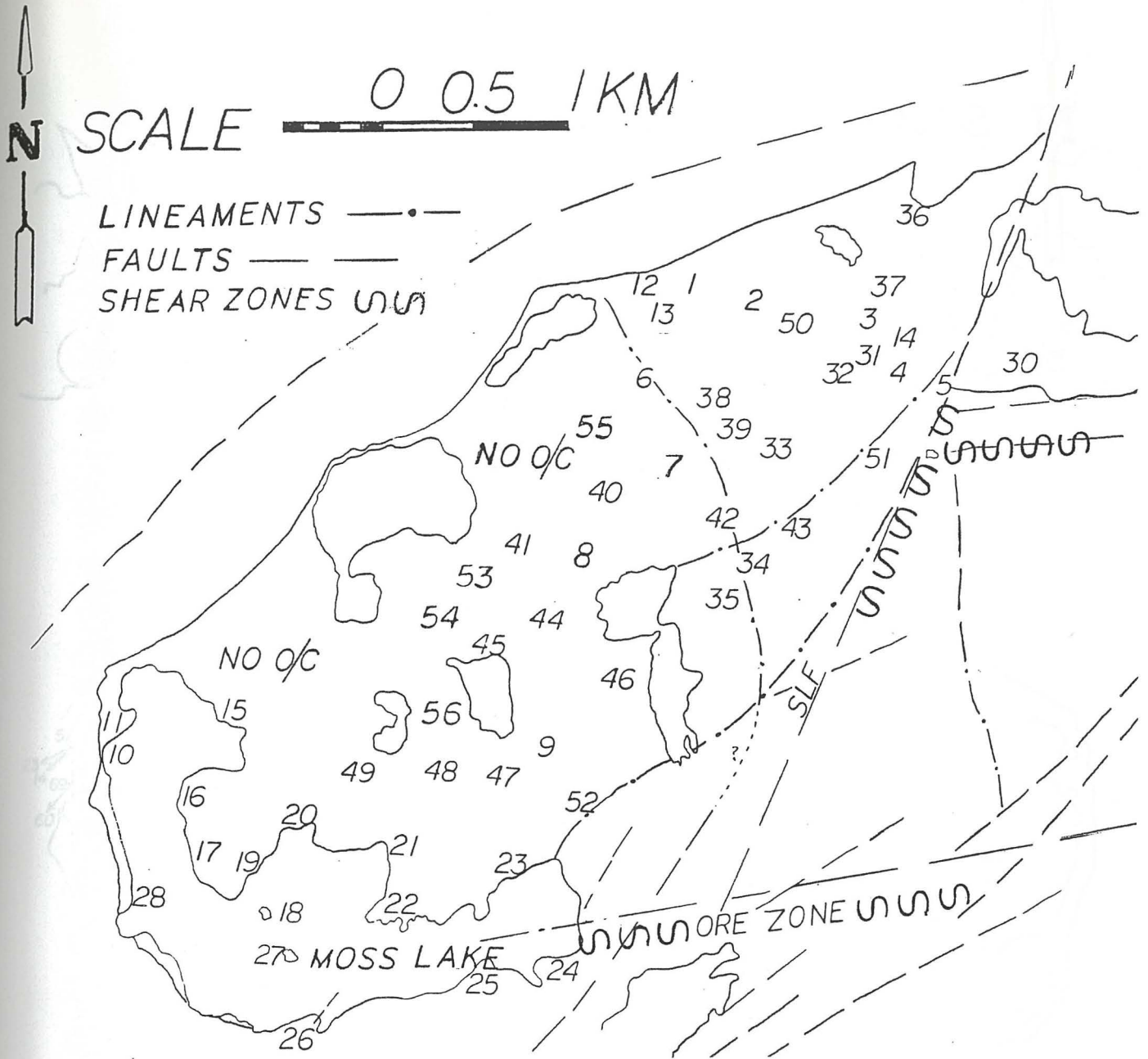
Figure 4.1A. Moss Lake stock structure and oriented sample locations. Effects from shearing along the Snodgrass Lake Fault (SLF) are noticeable more than one kilometer west of the main shear.
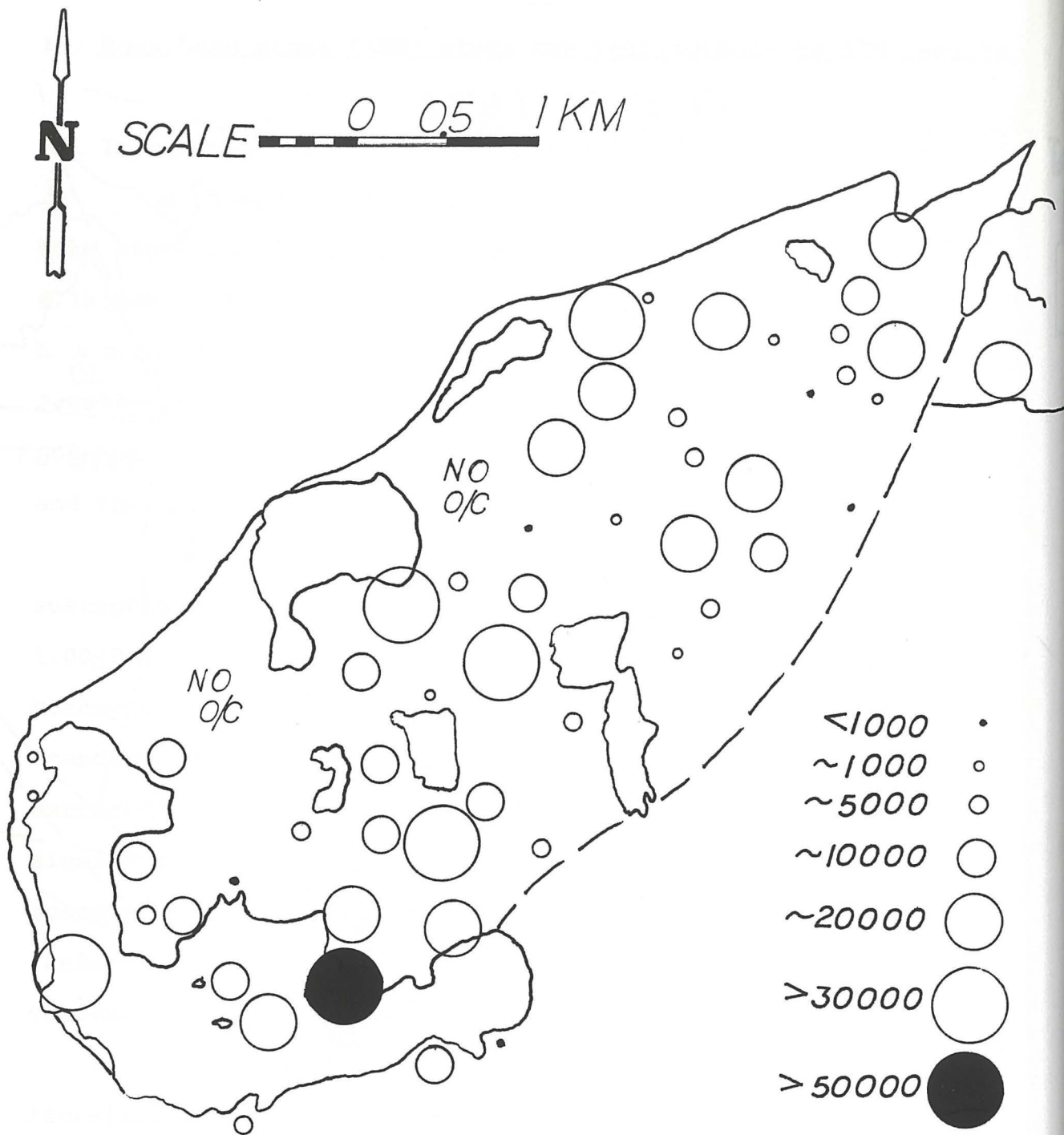
Figure 4.1B. Approximate bulk magnetic susceptibility magnitudes of Moss Lake stock oriented specimens X 10^{-6} SI shown in respective sample locations. Refer to Appendix H for exact bulk magnetic susceptibilities.
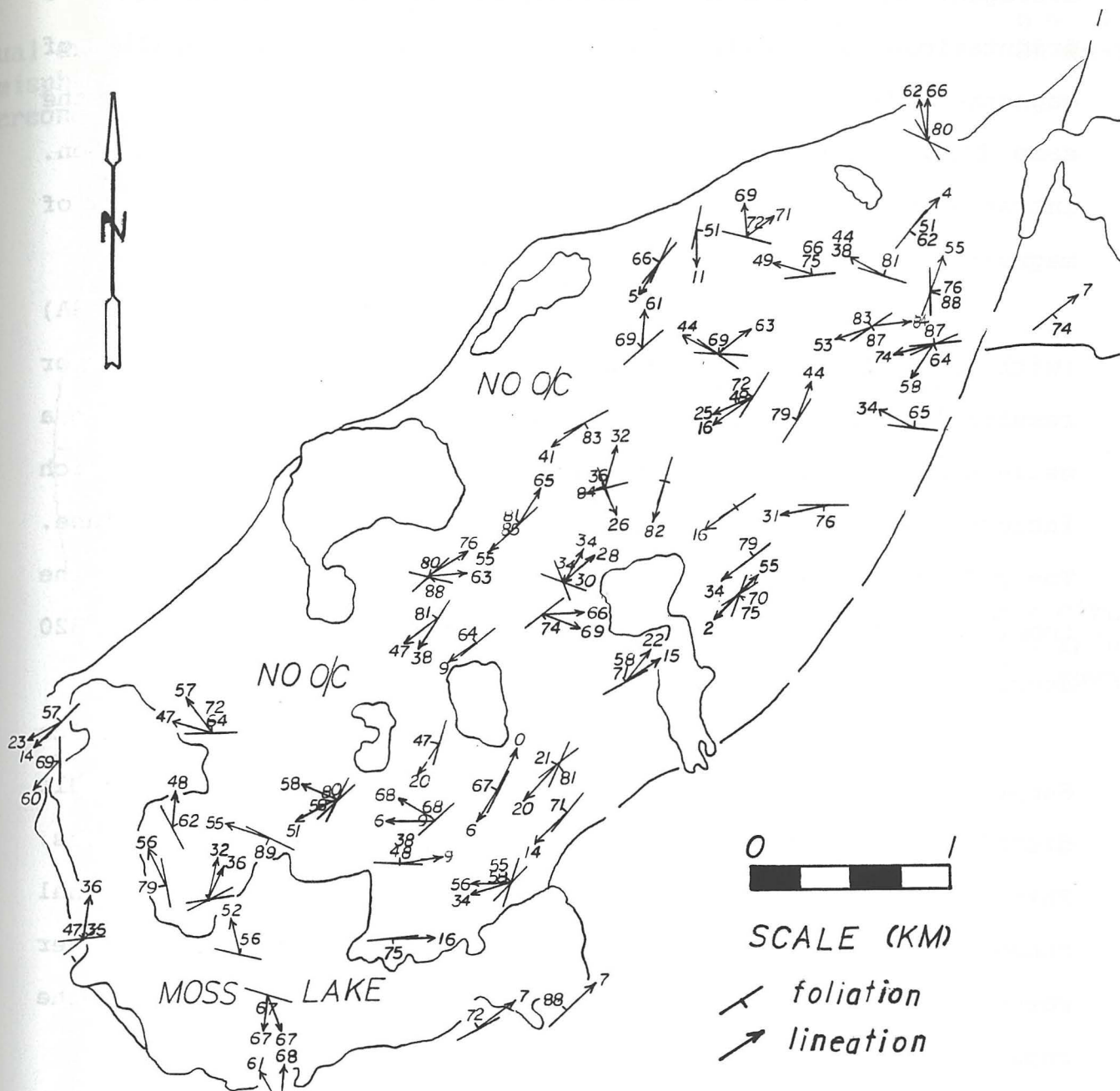
Figure 4.2. Magnetic foliation (kmax-kint plane) and lineation (kmax trend and plunge) of the Moss Lake stock oriented samples.

averaged. Where specimens exhibit directional variability, all orientations are plotted (Fig. 4.2). Variation in orientation of magnetic foliation and lineation from separate cores within the same hand specimen of the Moss Lake stock is not uncommon. Intraspecimen variability may result from incomplete development of magnetic fabric or its partial overprint by shear structures.

Figure 4.3B shows contoured [kmax] orientations (of Fig. 4.3A) (with peak trend and plunge 230-14 degrees) and EigenVector results. Maximum magnetic susceptibility values are spread along a well-developed girdle distribution (Figs. 4.3A and 4.3B) which includes two data clusters (Fig. 4.3B) contained in a common plane. The pole to the common plane containing the data clusters of the (contoured) maximum susceptibility measurements has a trend of 320 degrees.

Trend of the pole to local planar fabric strike of the Quetico Subprovince (Fig. 1.3 C,D) is 337 degrees. The pole to the girdle distribution of maximum magnetic susceptibilities is 320 degrees. This 17 degree difference in declination may represent regional change in attitude of planar fabric strike over distance. In other words, planar fabric may change slightly in orientation on the regional scale.

A diagram of maximum susceptibility orientations is shown on Figure 4.4. The [kmax] orientations appear to be more or less sub-parallel to the long axis of the stock, with some exceptions. Where the maximum susceptibility plunges are steep, their azimuth is difficult to determine with accuracy.

Equal area lower
hemisphere
stereonet
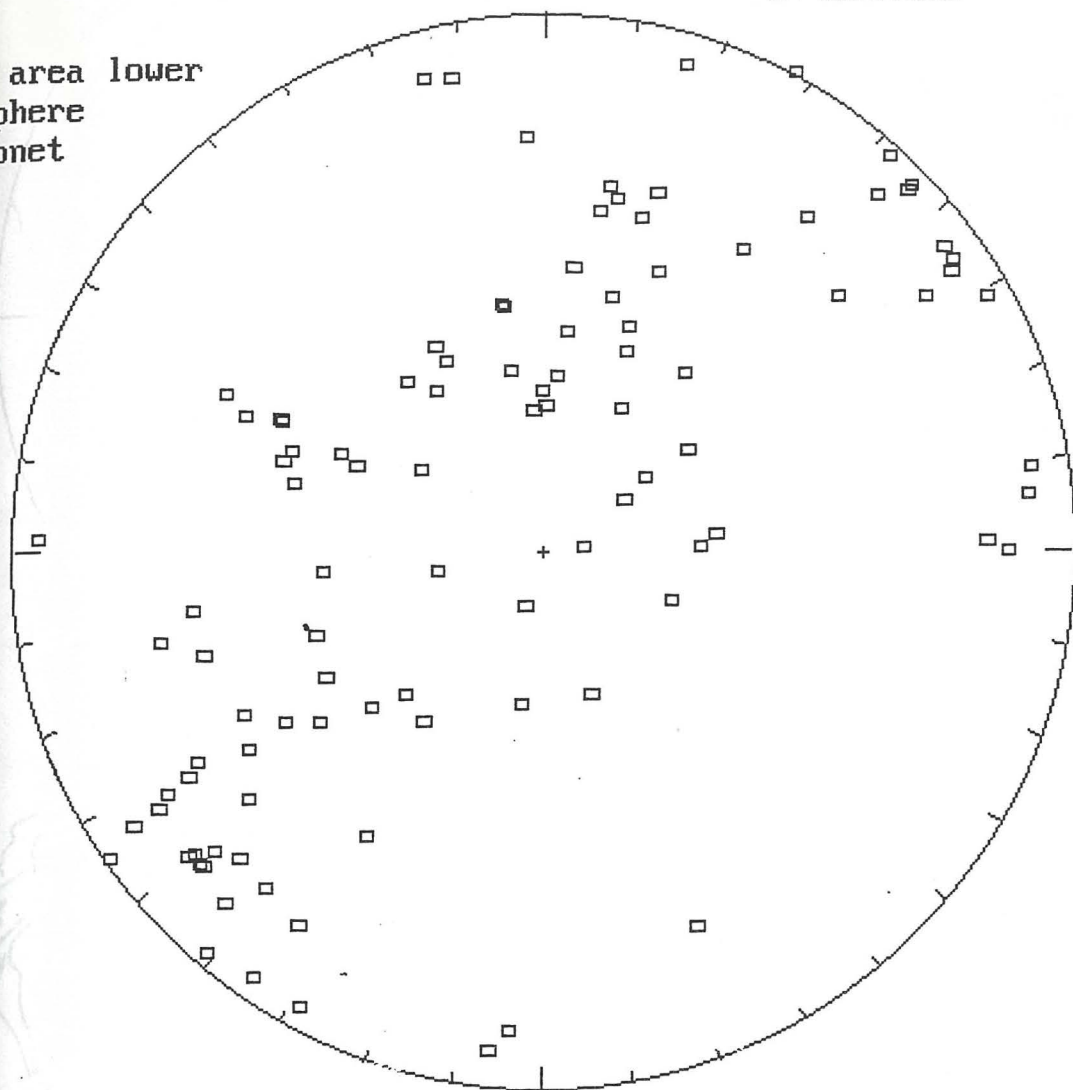
n =   104
08-24-199

MIN = circle
INT = triang
MAX = square

Figure 4.3A. Maximum susceptibility (kmax) orientations of
ferromagnetic components of the Moss Lake stock.

N = 104

k = 25.11

E = 4.14

σ = 1.38

Peak Trend 230.2

Peak Plunge 14.3

(Peak - E)/σ = 7.8
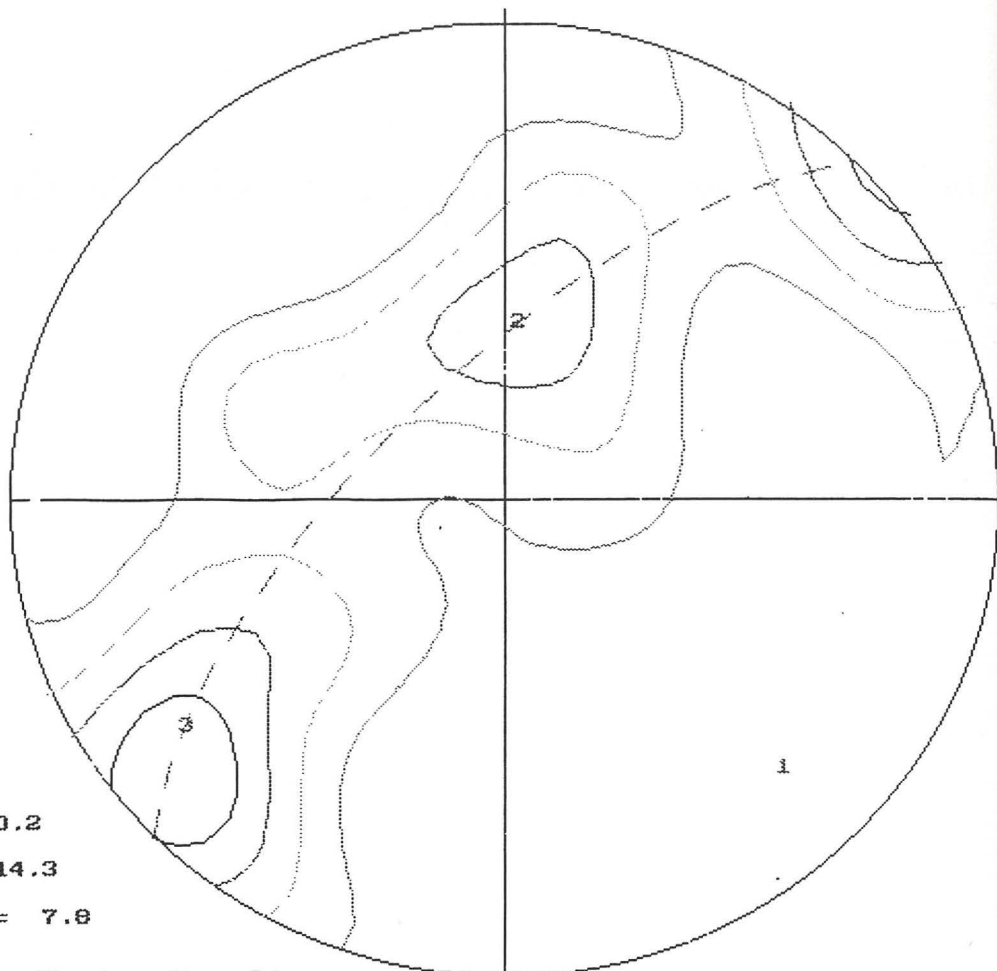
EigenVector Results

No. of Data: 104

Vector	Trend	Plunge	Eigenvalue	
1	135.11	21.27	11.0742 +/-	0.1550
2	3.80	59.47	44.4827 +/-	0.3507
3	233.63	20.83	48.4431 +/-	0.3622

Confidence Cones

Vector	Major	Minor	Average	Angle
1	8.31	7.01	7.66	-2.31
2	61.62	8.30	34.96	0.07
3	61.62	7.02	34.32	0.03

Eigenvalue Ratios (after Woodcock, 1977)

K-ratio [ln(E3/E2)/ln(E2/E1)]: 0.06 +/- 0.01
C-ratio [ln(E3/E1)] : 1.48 +/- 0.02

Pattern: Weakly developed girdle.

Figure 4.3B. Contoured maximum susceptibility (kmax) orientations of ferromagnetic components of the Moss Lake stock along with EigenVector results. The peak trend and plunge is 230-14.
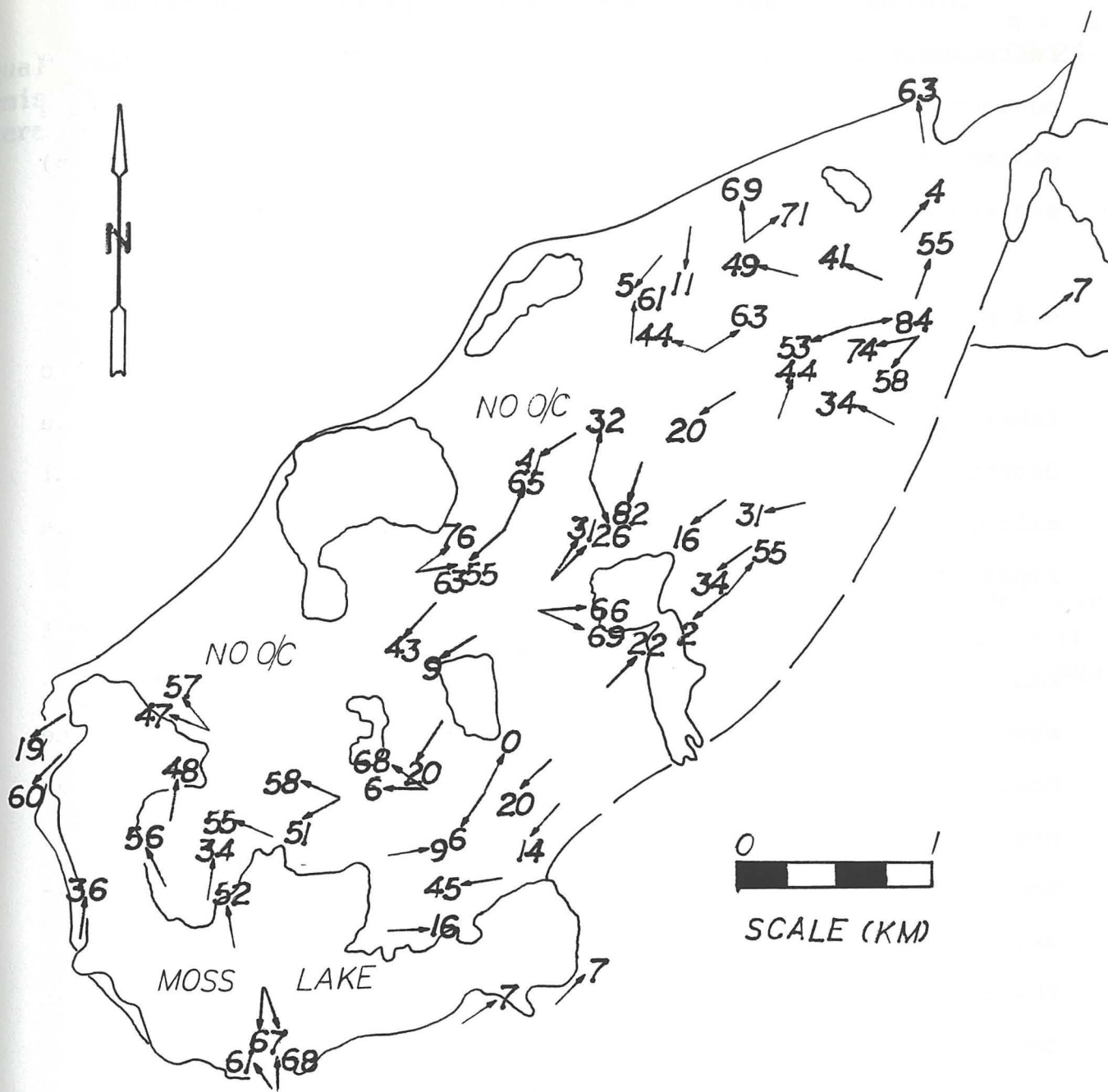
Figure 4.4. Maximum susceptibility (kmax) lineation trends of ferromagnetic components of the Moss Lake stock.

Minimum magnetic susceptibility [kmin] orientations of ferromagnetic components of the Moss Lake stock (Fig. 4.5A) are contoured with Eigenvector results in Figure 4.5B. Most of the minimum magnetic susceptibility orientations [kmin] (Figs. 4.5A,B) are sub-parallel to the pole to regional cleavage (Fig. 1.3C,D).

4.2 Moss Lake stock fabric parameters

The Flinn diagram (Fig. 4.6) of the Moss Lake stock magnetic fabric shows the oblate (flattened) nature, as revealed by AMS. The dotted line in Figure 4.6 represents the boundary of neutral ellipsoids (of "plane strain") where [a=b]. Most of the data represent oblate magnetic fabric.

The Jelinek diagram (Fig. 4.7) is a better representation of fabric shape and intensity. It reflects the trend towards disk-shaped magnetic susceptibility ellipsoids which predominate for the Moss Lake stock. The P' (intensity) values for the stock samples are plotted at each sample location and contoured in Figure 4.8. The [P'] values range from 1.04 to 1.53. The most intensely-deformed samples appear at the margins of the intrusion (Fig. 4.8). The inner portion of the stock appears to be substantially less deformed.

P' (intensity) values are plotted in their respective positions relative to [kmax] and [kmin] on Figures 4.9 and 4.10. For negative [T] values, [P'] plots on [kmax], reflecting prolate magnetic susceptibility ellipsoids (Fig. 4.9). For positive [T] values, [P'] plots on [kmin], reflecting oblate magnetic susceptibility

Equal area lower
hemisphere
stereonet
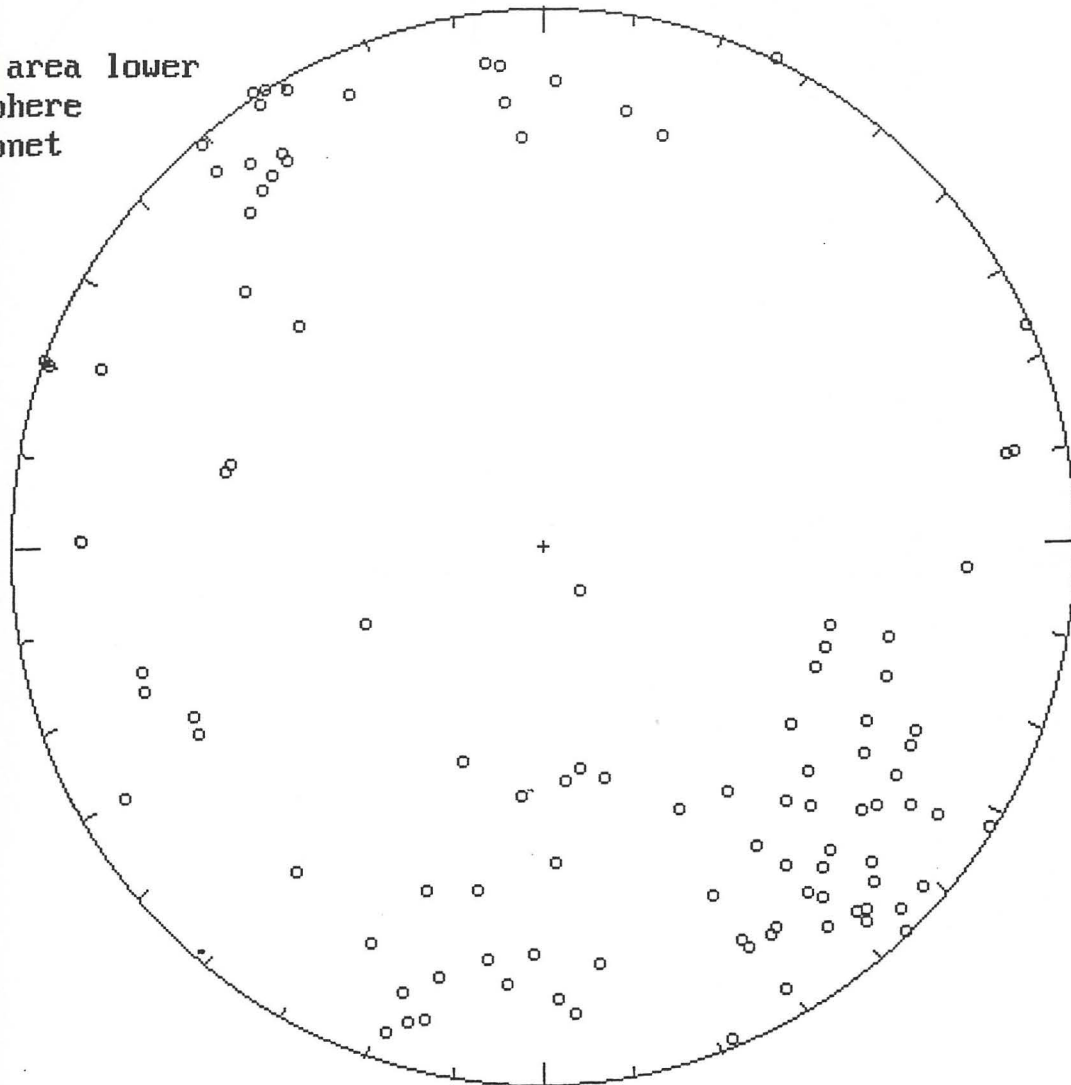
MIN = circle
INT = triang
MAX = square

Figure 4.5A. Minimum magnetic susceptibility orientations of
ferromagnetic components of the Moss Lake stock.
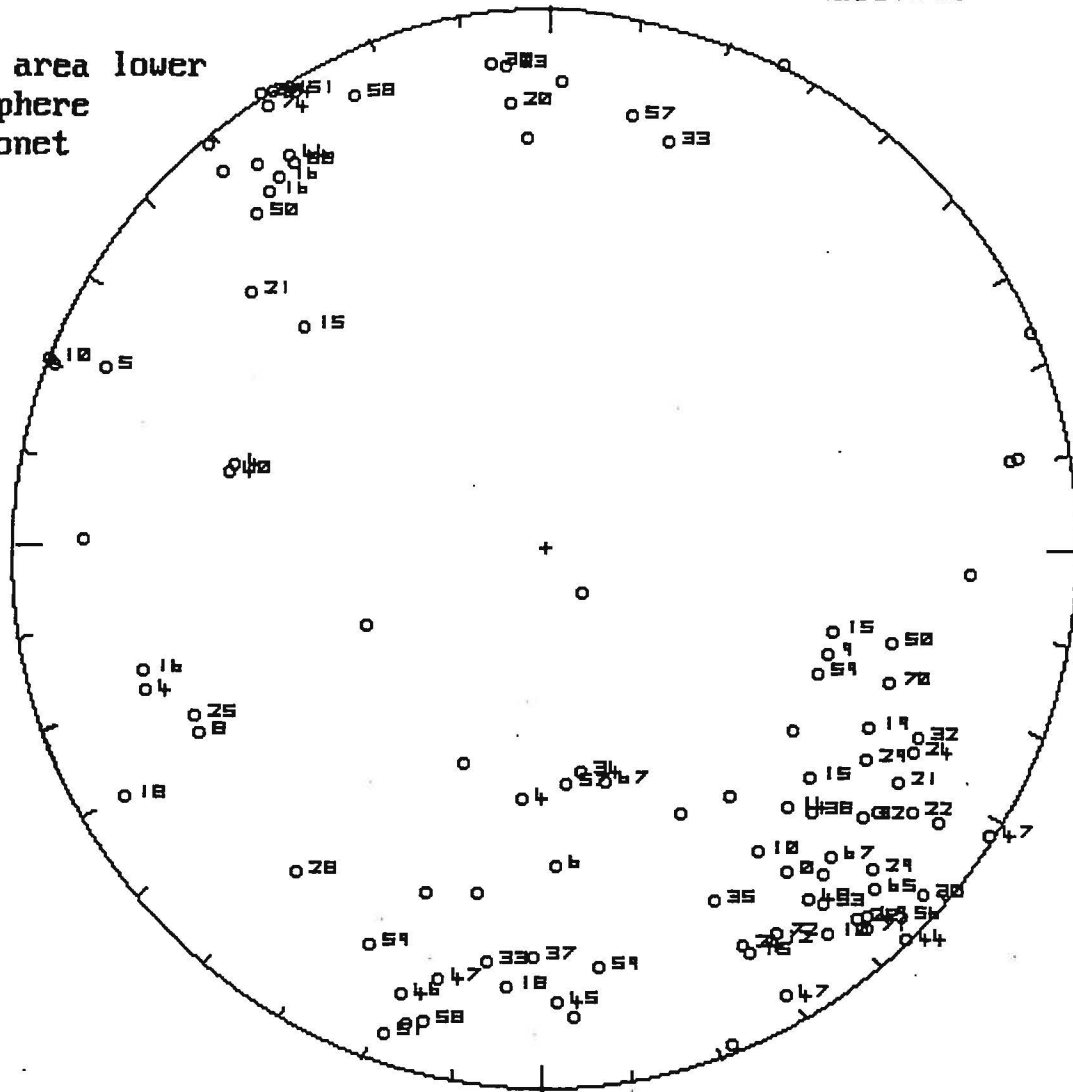
Figure 4.13. [T] values for Moss Lake stock samples, lower hemisphere projection. Positive [T] values (oblate fabric) plot on [kmin].
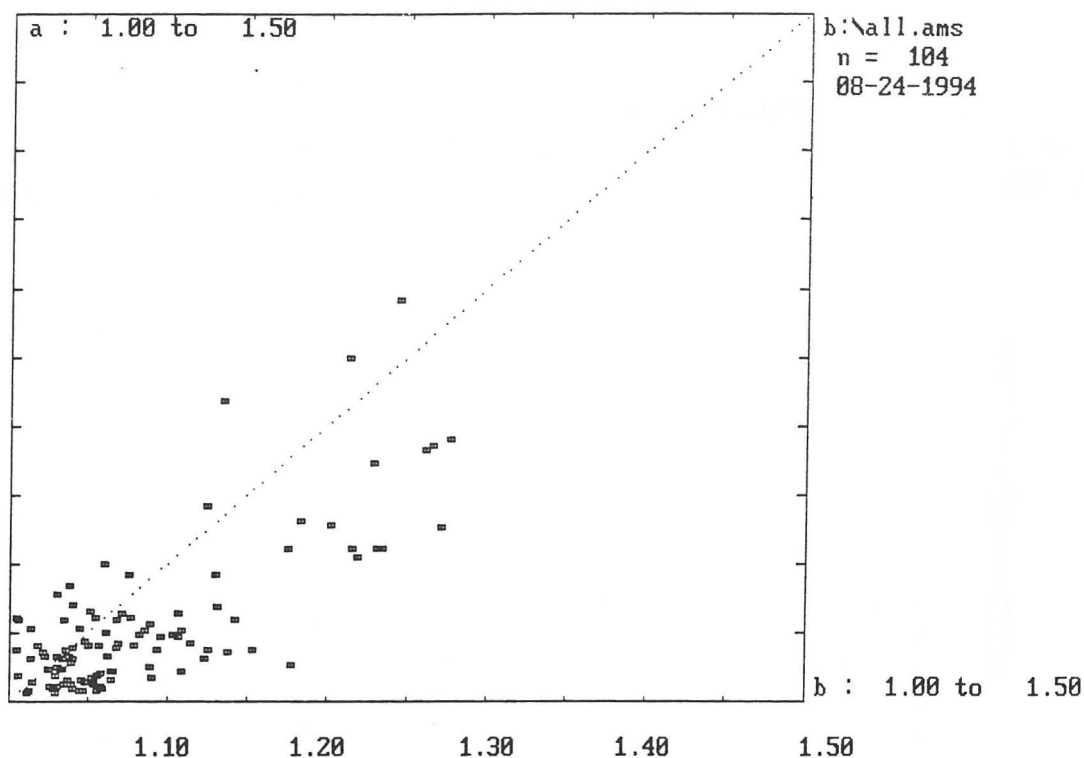
Figure 4.6. Flinn diagram of Moss Lake stock fabric parameters. The magnetic fabric, as represented by the susceptibility ellipsoid, is oblate (flattened).
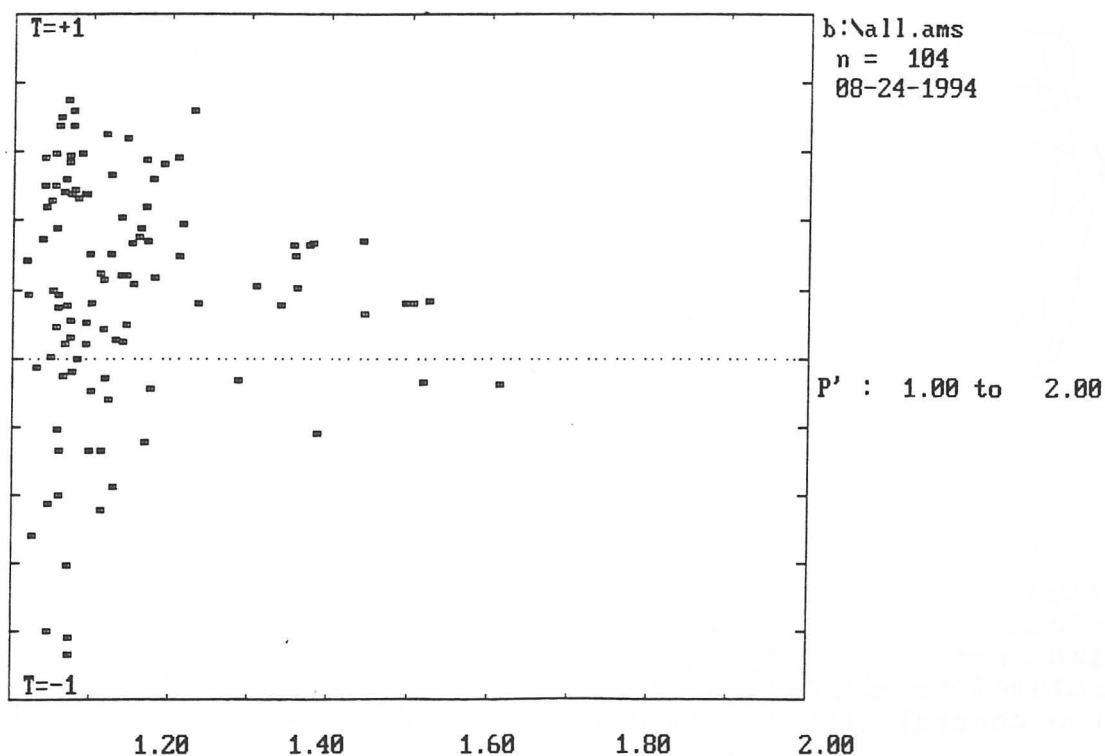
Figure 4.7. The Jelinek diagram of the Moss Lake stock fabric parameters reflects the trend towards "disk-shaped" magnetic susceptibility ellipsoids.
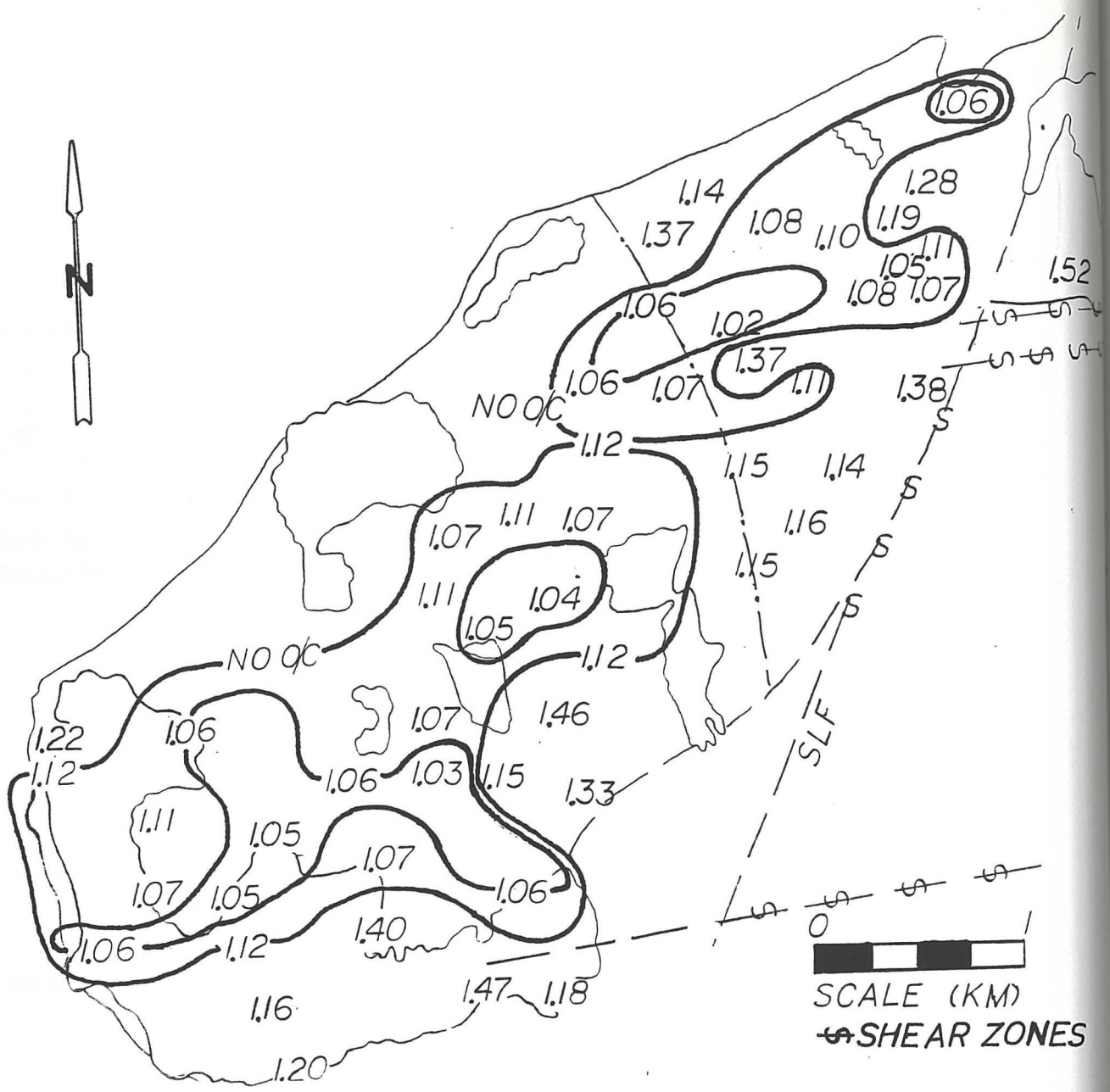
Figure 4.8. Contoured P'(intensity) values of oriented Moss Lake stock samples shown in relation to faults, shear zones and lineaments. The highest P' (intensity) values (>1.25) appear to be related to shear structures. Rock fabric is least deformed along the central axis of the intrusion.
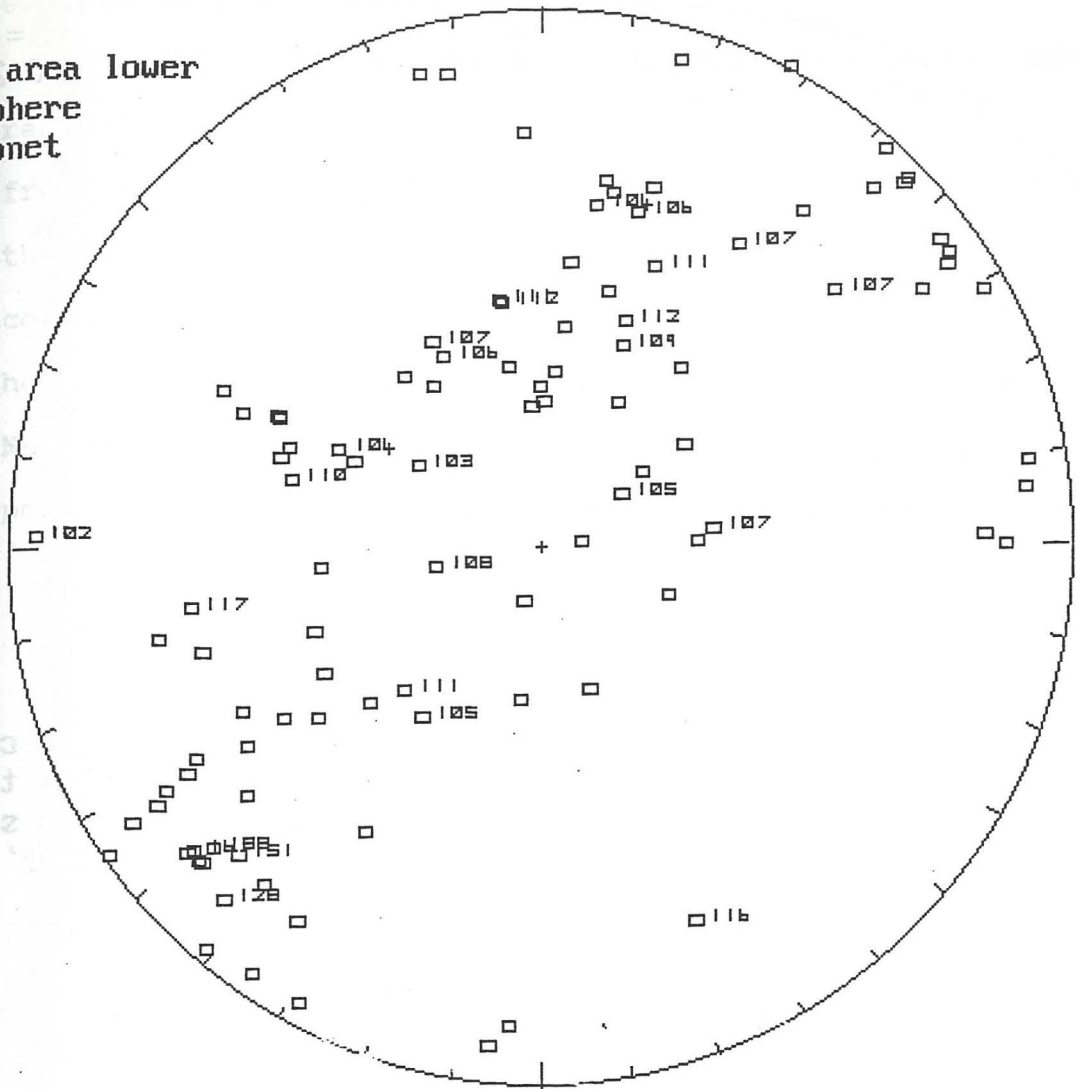
Figure 4.9. Lower hemisphere stereographic projection of P' (intensity) values for Moss Lake stock samples plotted at [kmax] positions. For negative [T] values [P'] plots on [kmax], reflecting prolate magnetic susceptibility ellipsoids.
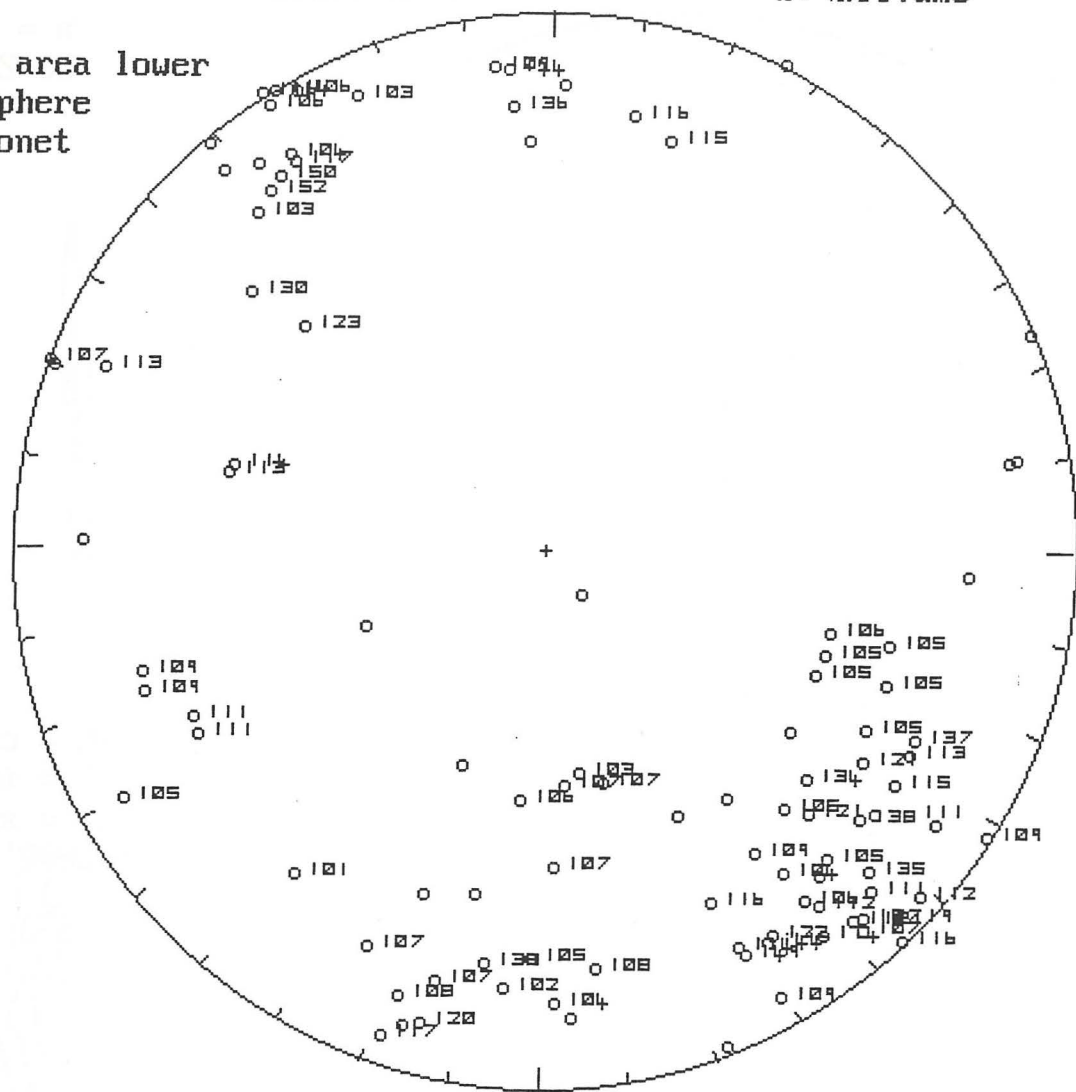
Figure 4.10. Lower hemisphere stereographic projection of P' (intensity) values for Moss Lake stock samples plotted at [kmin] positions. For positive [T] values [P'] plots on [kmin], reflecting oblate magnetic susceptibility ellipsoids.

ellipsoids (Fig. 4.10).

[T] values for each of the samples are plotted at their respective sample locations on Figure 4.11. The [T] values range from -0.87 to +0.75. Most of the negative [T] values occur along the central axis of the intrusion. [T] values are printed beside corresponding [kmax] and [kmin] orientations in the lower hemisphere stereographic projections of Figures 4.12 and 4.13. Negative [T] values (prolate fabric) plot on [kmax] (Fig. 4.12) and positive [T] values (oblate fabric) plot on [kmin] (Fig. 4.13).
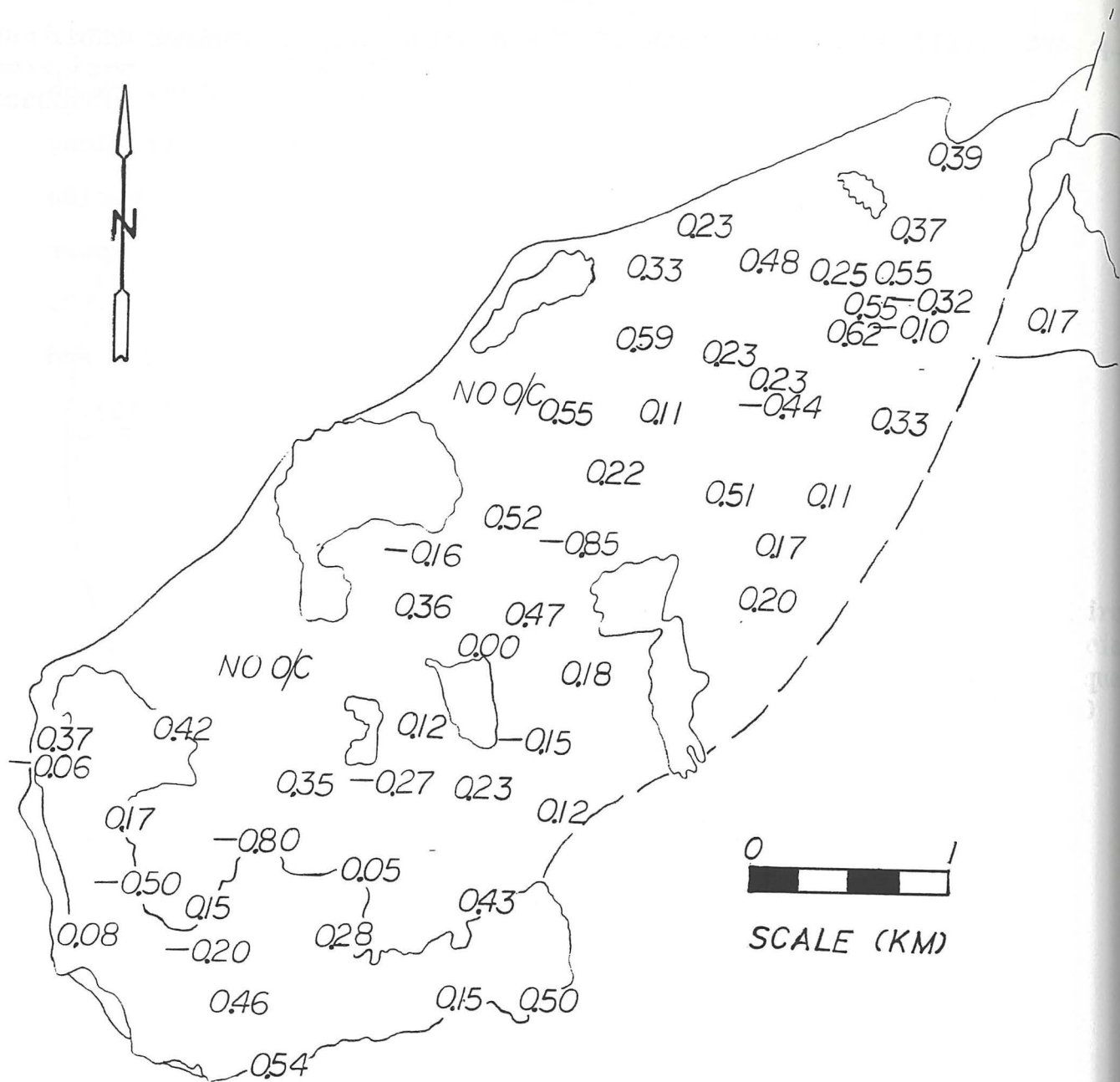
Figure 4.11. [T] values for Moss Lake stock samples shown at their respective field locations.
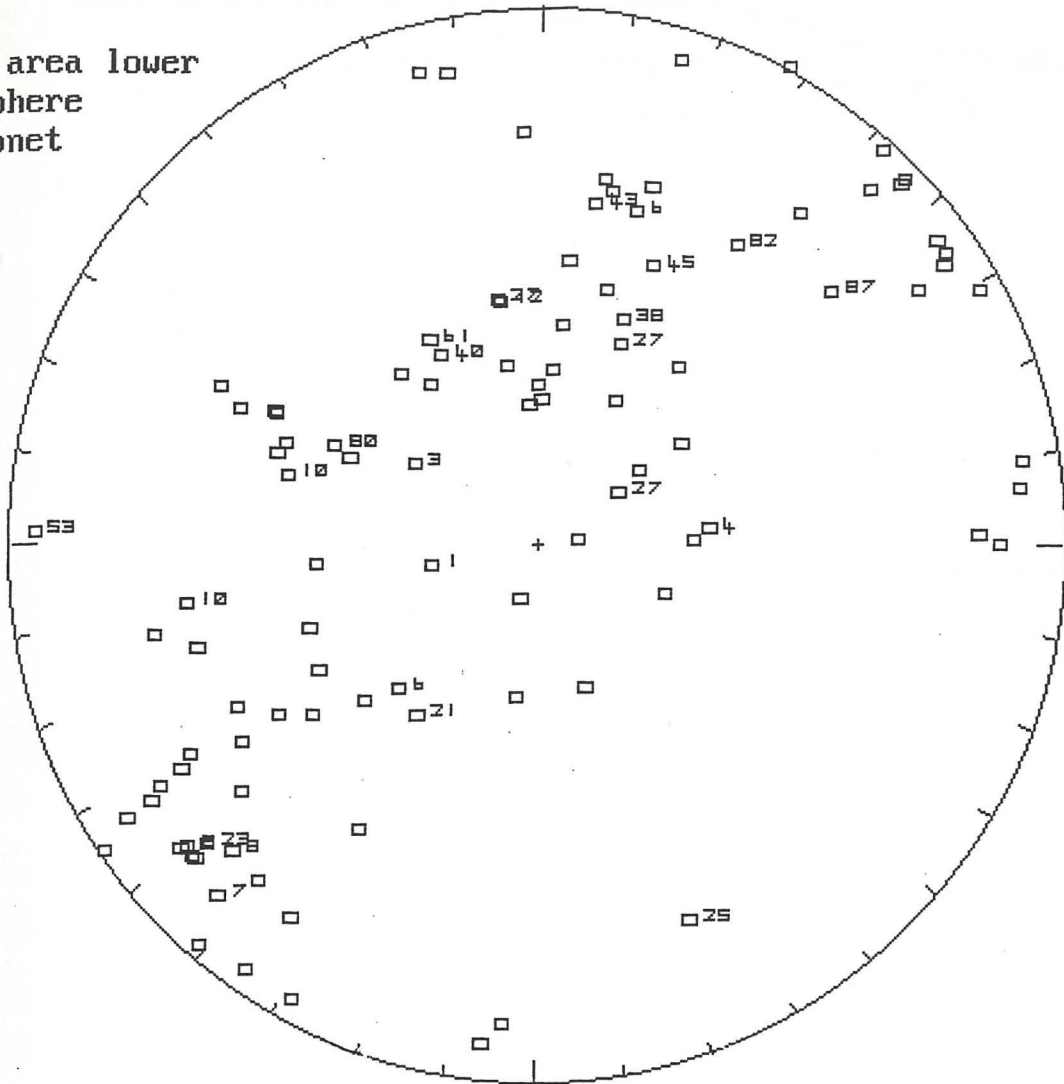
Figure 4.12. [T] values for Moss Lake stock samples, lower hemisphere stereographic projection. Negative [T] values (prolate fabric) plot on [kmax].

Equal area lower
hemisphere
stereonet
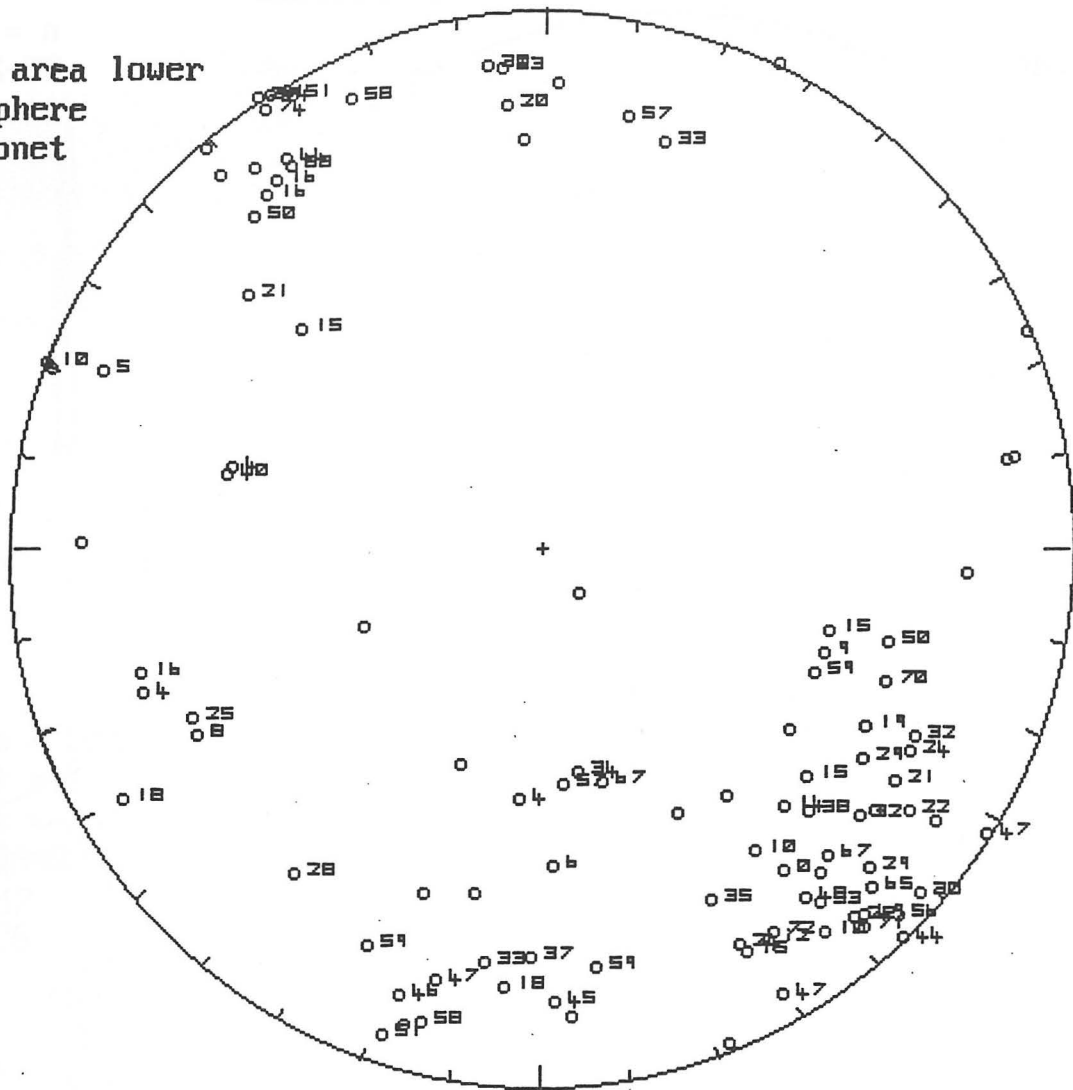
MIN = circl
INT = trian
MAX = squar
(100*ABS(T)

Figure 4.13. [T] values for Moss Lake stock samples, lower
hemisphere projection. Positive [T] values (oblate fabric) plot on
[kmin].

4.3 AMS: Structural significance

Curie balance experiments show that the predominant ferromagnetic mineral in the Moss Lake stock samples is magnetite, with traces of hematite. The plane which represents the girdle distribution of (contoured) maximum magnetic susceptibility data (Fig. 4.3B) is sub-parallel to both the local strike of planar fabric in the Quetico Subprovince (Fig. 1.3C,D) and the central long axis of the intrusion's map outline. Contoured P' (intensity) data (Fig 4.8) show that the margin of the stock (in plan view) has stronger AMS fabrics, reflecting stronger preferred orientations. This may be in response to more intense deformation or an alignment of magnetic domains within magnetite grains.

Samples with visible shear fabric taken from the stock show a coincidence between shear zone strike and local directions of maximum magnetic susceptibility. Maximum susceptibility orientations of six samples can be attributed to shear zones. The balance of the samples have maximum susceptibility orientations which when contoured produce data clusters (Fig. 4.3B) contained on a common plane sub-parallel to local planar fabric strike of the metasedimentary belt (see Fig. 1.3). Symmetry of tectonic and AMS fabrics argues in favor of a common tectonic control.

AMS studies of granitoid intrusions reported in the literature show that kinematic reconstructions are commonly possible. Unfortunately, this is not possible for the Moss Lake stock because deformation has severely obliterated primary igneous flow structures. Negative [T] values in the inner portion of the

intrusion may reflect poorly-preserved original prolate (igneous) fabric.

There are two weakly defined data clusters along the (contoured) girdle distribution of [kmax] orientations (Fig. 4.3B). One maximum represents SW-trending, sub-horizontal data which are sub-parallel to the local planar fabric of the Quetico Subprovince and clearly represent a tectonic fabric component. A second maximum is produced by N-trending, steeply plunging data lying in the foliation plane. These data may reflect a vertical magmatic flow component.

The overall magnetic fabric of the Moss Lake stock is oblate and is interpreted to be the result of a flattening strain in response to northwest-southeast compression. The NW-SE compression may be derived from the AMS data assuming that the long-term "average" maximum compressive stress was applied (horizontally) at right angles to the common plane which contains the data clusters of contoured maximum magnetic susceptibility values (Fig. 4.3B). On this basis, the (local) maximum compressive stress at the location of the Moss Lake stock was applied on azimuth 320 degrees. However, overprinting of magnetic fabric by the noncoaxial effects of shearing may require a (local) shortening direction closer to 360 degrees during the regional transpressive event.

Shear zones have overprinted the regional fabric, especially near the northeast tip of Moss Lake, where bulk magnetic susceptibility values are highest (Figs. 4.1B and 4.2). For this reason, the shear zones may be younger than the regional fabric.

4.4 Relationship of AMS data to NRM results

Comparison of the orientation of the girdle distribution of maximum magnetic susceptibility (Fig 4.3B; pole to girdle =320 degrees) and the natural remanent magnetization (NRM) principal component analysis (PCA) orientations (Fig. 3.10; pole to PCA = 320 degrees) derived from alternating field demagnetization and thermal demagnetization suggests close correlation of both to local planar fabric strike of the Quetico Subprovince (Fig. 1.3C,D; pole to S_1 = 337 degrees). Anisotropy of magnetic susceptibility data strongly suggest that the Moss Lake stock is deformed, especially along the margins.

The spread of principal component analysis data (Fig. 3.1) is inconsistent with that expected of an undeformed syenite/granitoid intrusion. In an undeformed intrusion, the paleomagnetic orientations are expected to be more uniformly preserved, ie. more consistent in orientation. Post-magmatic, tectonic deformation has imposed secondary (natural) magnetic components on the primary igneous fabric, especially along the margins of the intrusion. The mean principal component analysis for magnetite (Fig. 3.8), after removal of secondary NRM components, is plunging steeply to the north. Where unblocking temperatures are greater than the magnetite Curie temperature, characteristic remanent magnetization is attributable to hematite, in the Moss Lake stock samples. The hematite-related principal component analysis orientations are more stable and relate more closely to local geological strike than magnetite. Effects of heat produced during deformation may have

permitted magnetite magnetic domains to realign (with magnetic north) but the temperature was insufficient to produce the same effect in hematite, thus preserving the characteristic remanent magnetization orientation. The primary igneous fabric is overprinted by fabrics produced by a NW-SE regional compression and local shear zones of variable orientation.

V. Summary

5.1 Structure (summary)

Bedding (S_0) (Fig. 1.3A,B) in metasedimentary rocks of the Quetico Subprovince is consistently oriented, with mean bedding plane declination/inclination of 243-83 and cleavage (S_1) (Figs. 1.3C and 1.3D) is sub-parallel. A minimum tectonic compression of 80% (refer to section 1.5 for method) is estimated from sedimentary beds surrounding boudinaged chlorite blocks (Fig. 1.9). This minimum tectonic compression of 80% applies only to the metasedimentary rocks; this is not meant to imply that the igneous intrusion is deformed by the same amount.

Metamorphic grade ranges from greenschist to amphibolite facies, towards the northwest (refer to map insert B for location of the garnet isograd near Highway 11). In the northwestern portion of the study area, reverse metamorphic grading of sedimentary beds by the mineral staurolite is easily confused with graded bedding.

No large-scale folds are found in the study area, but two small folds (with 8-10 cm radius fold closures), with sub-horizontal hinge lines parallel to local planar fabric strike, were noted.

5.2 AMS results (summary)

Anisotropy of magnetic susceptibility (AMS) methods (refer to Appendix A, Appendix B and Section IV) are useful in structural analysis of tectonic effects.

The Moss Lake stock (Fig. 1.2 and insert maps A and B) is a 28 square kilometer plutonic igneous intrusion composed of granite, syenite, quartz syenite and quartz monzonite. High magnetic signature of the Moss Lake stock makes it especially amenable to AMS study.

Study of 54 oriented samples indicates that the stock has a tectonic AMS fabric. Oblate (flattened) magnetic fabrics predominate (Figs. 4.6 and 4.7) with high P' (intensity) values (Fig. 4.8) near the stock margin, as seen in map view. This suggests that the margin is more deformed than the central long axis of the intrusion. The presence of negative [T] values (Fig. 4.11) along the central long axis of the intrusion suggest that there is some prolate-shaped magnetic fabric which may represent original magmatic fabric.

Kinematic reconstructions of igneous intrusions are frequently possible using AMS techniques (refer to Appendix A) but in the case of the Moss Lake stock, deformation has destroyed most of the original magmatic fabric.

Orientation of the girdle distribution of maximum magnetic susceptibility measurements (Fig. 4.3A,B) of the Moss Lake stock corresponds to local planar fabric strike of the Quetico Subprovince (Figs. 1.3C,D). The greatest influence on maximum susceptibility orientations (Fig. 4.3A) in Moss Lake stock samples is attributable to the same tectonic control which has created planar fabric in the Quetico metasedimentary belt. Presumably, the common control is tectonic compression, sub-horizontally directed

NW-SE. The apparent deviation in orientation of the local planar fabric of the Quetico metasedimentary belt compared with the orientation of the girdle distribution of maximum magnetic susceptibility measurements (Fig. 4.3B) may be attributable to local change in cleavage orientation.

5.3 Paleomagnetic (NRM) results (summary)

Curie balance experiments (refer to Section II) reveal that the predominant magnetic mineral of the Moss Lake stock is magnetite and that hematite is present in trace amounts. Hematite in the rock matrix colours the Moss Lake stock samples.

AARM (anisotropy of anhysteretic remanent magnetization) studies (refer to Section II) cannot be successfully performed on the stock samples as they cannot be fully (alternating field) demagnetized because of their high coercivity and large magnetic contribution from hematite.

Separation of magnetic components of the Moss Lake stock oriented samples by blocking temperature reveals different mean principal component analysis (PCA) orientations for the minerals magnetite and hematite.

The mean PCA orientation of magnetite (for a blocking temperature of 550 degrees C, Figs. 3.7 and 3.8) corresponds in trend to other investigators' paleomagnetic north orientation of 005 for the region (Borradaile et al., 1993). The plunge of magnetite mean principal component analysis components of the Moss Lake stock is sub-vertical and corresponds closely to local planar

fabric dip of the Quetico Subprovince. Alternatively, the mean magnetite PCA plunge could be preserved from original magmatic fabric.

The mean principal component analysis for hematite (for a blocking temperature of 700 degrees C, Figs. 3.9 and 3.10) closely follows orientation of the girdle distribution of maximum magnetic susceptibility measurements (Fig. 4.3B) and the local planar fabric strike and dip of the Quetico Subprovince (Fig. 1.3).

Study of natural remanent magnetization (NRM) of the Moss Lake stock samples by both alternating field and thermal demagnetization methods indicates that samples of the intrusion are deformed (as the data set is spread) therefore they have probably acquired secondary (natural) magnetic components during post-magmatic, tectonic deformation.

Hematite occurs in granitic rocks (as an accessory mineral), in contact metamorphic deposits and in regionally metamorphosed rocks by oxidation of magnetite (Klein and Hurlbut, 1977). Heat associated with a deformation event may have transformed magnetite into hematite, contemporaneously overprinting the magnetite magnetic vector orientations, thus reorienting most of the magnetic components (including both magnetite and hematite) into the local planar fabric strike and dip of the Quetico Subprovince.

Higher concentrations of hematite are spatially associated with shear zones in Moss Township. The gold zone near the eastern tip of Moss Lake is hosted within a hematized ENE-trending shear zone (Ministry of Northern Development and Mines, Assessment Files).

Vestiges of original magmatic fabric eluded overprinting. Aside from the indication of original magnetite characteristic remanent magnetization (ChRM) preservation, most of the original magnetic fabric of magnetite has been overprinted by tectonic compression.

5.4 Conclusions

Structural mapping, natural remanent magnetization (NRM) paleomagnetic work and the AMS study lead to the conclusion that the Moss Lake stock and the Quetico metasedimentary belt have been deformed by a common tectonic control, specifically northwest-southeast directed tectonic compression. The direction of maximum compressive stress may be inferred as being perpendicular to planar fabric development, the extension direction is northeast-southwest and the intermediate stress orientation is sub-vertical.

Structural correlations between magnetic fabric of the intrusion and country rock suggest that regional-scale tectonics affected both contemporaneously. The relative timing of emplacement of the Moss Lake stock is pre-kinematic to syn-kinematic.

References

Akimoto, S., 1957. Magnetic properties of ferromagnetic oxide minerals as a basis of rock magnetism. Advances in Physics, 6: 288.

Akimoto, S. and Nagata, T., 1960. Report on the fundamental basis of rock magnetism: Report to the International Association of Geomagnetism and Aeronomy presented at Helsinki, Finland.

Balsley, J.R. and Buddington, A.F., 1958. Iron-titanium oxide minerals, rocks and aeromagnetic anomalies of the Adirondack area, New York. Econ. Geol., 53: 777.

Bhatal, R.S., 1971. Magnetic anisotropy in rocks. Earth Sci. Rev., 7: 227-253

Bateman, P.C., Dodge, F.C.W. and Kistler, R.W., 1991. Magnetic susceptibility and relation to initial $^{87}Sr/^{86}Sr$ for granitoids of the Central Sierra Nevada, California. J. Geophys. Res., 96: 19555-19568.

Benn, K., Rochette, P., Bouchez, J.L., and Hattori, K., 1992. Magnetic susceptibility, magnetic mineralogy and magnetic fabrics in a late Archean granitoid-gneiss belt. Precambrian Research, 63: 59-81.

Borradaile, G.J., and Tarling, D., 1981. The influence of deformation mechanisms on magnetic fabrics in weakly deformed rocks. Tectonophysics, 77: 151-168.

Borradaile, G.J., and Tarling, D., 1984. Strain partitioning and magnetic fabrics in particulate flow. Can. J. Earth Sci., 21: 694-697.

Borradaile, G.J. 1988 Magnetic susceptibility, petrofabrics and strain. Tectonophysics, 156: 1-20.

Borradaile, G.J. 1991. Correlation of strain with anisotropy of magnetic susceptibility (AMS). Pure and Applied Geophysics, 135: 15-29.

Borradaile, G.J. 1991. Remanent magnetism and ductile deformation in an experimentally deformed magnetite-bearing limestone. Phys. Earth Planet. Inter., 67: 362-373.

Borradaile, G.J. 1992. Deformation of remanent magnetism in a synthetic aggregate with hematite. Tectonophysics, 206: 203-218.

Borradaile, G.J. 1992. Experimental deformation of two-component IRM in magnetite-bearing limestone: a model for the behaviour of NRM during natural deformation. Phys. Earth Planet. Inter., 70: 64-77.

Borradaile, G.J., 1993. Strain and magnetic remanence. J. Struct. Geol., 15: 383-390.

Borradaile, G.J., 1993. The rotation of magnetic grains. Tectonophysics, 221: 381-384.

Borradaile, G.J. and Alford, C., 1987. Relationship between magnetic susceptibility and strain in laboratory experiments. Tectonophysics, 133: 121-135.

Borradaile, G.J. & Alford, C., 1988. Experimental shear zones and magnetic fabrics. J. Struct. Geol., 10: 895-904.

Borradaile, G.J., 1987. Anisotropy of magnetic susceptibility: rock composition versus strain. Tectonophysics, 138: 327-329.

Borradaile, G.J. and Brown, H.G., 1987. The Shebandowan Group: "Timiskaming-like" Archean rocks in northwestern Ontario. Can. J. Earth Sci., 24: 185-188.

Borradaile, G.J., Chow, N. & Werner, T., 1993. Magnetic hysteresis of limestones: facies control? Phys. Earth Planet. Inter., 76: 241-252.

Borradaile, G.J., Keeler, W., Alford, C. and Sarvas, P. 1987. Anisotropy of magnetic susceptibility of some metamorphic minerals. Phys. Earth and Planet. Inter., 48: 161-166.

Borradaile, G.B. and Molyneux, L., 1994. Computer analysis program: NUSPINX4.

Borradaile, G.B. and Stupavsky, M., 1994. Computer analysis program: SI2X.

Borradaile, G.J., Werner, T., Dehls, J.F. and Spark, R.N., 1993. Archean regional transpression and paleomagnetism in northwestern Ontario, Canada. Tectonophysics, 220: 117-125.

Bouchez, J.L., Gleizes, G., Djouadi, T. and Rochette, P., 1990. Microstructure and magnetic susceptibility applied to emplacement kinetics of granites: the example of the Foix pluton (French Pyrenees). Tectonophysics, 184: 157-171.

Bouillin, J., Bouchez, J., Lespinasse, P. and Pecher, A., 1993. Granite emplacement in an extentional setting: an AMS study of the magmatic structures of Monte Capanne (Elba, Italy). Earth Planet. Sci. Lett., 118: 263-279.

Butler, R.F., 1992. Paleomagnetism: Magnetic Domains to Geologic Terranes, 319 pp. Dept. Geol., Univer. Arizona., Blackwell Scientific Publications, Boston.

Card, K.D. and Ciesielski, A., 1986. Subdivisions of the Superior Province of the Canadian Shield, Geosci. Canada 12: 5-13.

Carmichael, R.S., 1982. Magnetic properties of minerals and rocks. In: CRC handbook of Physical Constants for Rocks, Boca Raton, Florida. 229-287.

Carmichael, R.S., 1982. CRC Handbook of Physical Properties of Rocks and Minerals, 741 pp. CRC Press, Boca Raton, Florida.

Chang, S-B.R., Kirshvink, J.L. and Stolz, J.F., 1987. Biogenic magnetite as a primary remanence carrier in limestone deposits. Phys. Earth Planet. Inter., 46: 289-303.

Clarke, D.B., 1992. Granitoid rocks, 283 pp. Department of Earth Sciences, Dalhousie University, Halifax, Canada, Chapman and Hall, London.

Cogné, J. P., and H. Perroud, 1988. Anisotropy of magnetic susceptibility as a strain gauge in the Flamanville granite, NW France, Phys. Earth Planet. Inter., 51: 264-270.

Cogné, J-P. & Perroud, H., 1988. Anisotropy of magnetic susceptibility as a strain gauge in the Flamanville granite, NW France. Phys. Earth and Planet. Inter., 51: 264-270.

Cox, A. and Doell, R. R., 1960. Review of paleomagnetism. Bull. Geol. Soc. Am., 71: 645-768.

Creer, K.M., 1967. Thermal demagnetization by the continuous method, pp. 287-295. In: Methods in Paleomagnetism, 609 pp., Elsvier Publishing Co., London.

Creer, K.M., 1972. Geomagnetic secular variation recorded in the stable remanence of recent sediments. Earth Plan. Sci. Lett., 14: 115-127.

Currie, R.G., Gromme, C.S. and Verhoogen, J., 1963. Remanent magnetization of some upper Cretaceous granitic plutons in the Sierra Nevada, California. J. Geophys. Res., 68: 2263.

Diggle, P.J. and Fisher, M.I., 1985. SPHERE: A contouring program for spherical data. Computers and Geosciences, 11: 725-766.

Dobrin, M.B., 1976. Introduction to Geophysical Prospecting, 3rd ed., McGraw-Hill, New York.

Dohr, G., 1974. Applied Geophysics, 210 pp., Halsted/John Wiley and Sons, New York.

Dunlop, D.J., 1979. A regional paleomagnetic study of Archean rocks from the Superior Geotraverse area, northwestern Ontario. Can. J. Earth Sci., 16: 1909-1919.

Dunlop, D.J., 1983. Paleomagnetism of Archean rocks from northwestern Ontario: Wabigoon gabbro, Wabigoon Subprovince. Can. J. Earth Sci., 20: 1805-1817

Dunlop, D.J., 1984a. Paleomagnetism of Archean rocks from Northwestern Ontario: II. Shelley Lake granite, Quetico Subprovince. Can. J. Earth Sci., 21: 869-878.

Dunlop, D.J., 1984b. Paleomagnetism of Archean rocks from northwestern Ontario: IV. Burchell Lake granite, Wawa-Shebandowan Subprovince. Can. J. Earth Sci., 21: 1098-1104.

Dunlop, D.J., 1985. Paleomagnetism of Archean rocks from northwestern Ontario: V. Poobah Lake alkaline complex, Quetico Subprovince. Can. J. Earth Sci., 22: 27-38.

Ellwood, B.B. and Whitney, J.A., 1980. Magnetic fabric of the Elberton Granite, Northeast Georgia. J. Geophys. Res., 85: No. B3, 1481-1486.

Gleizes, G., Nedelec, A. and Bouchez, J., 1993. Magnetic susceptibility of the Mont-Loius Andorra ilmenite-type granite (Pyrenees): A new tool for the petrographic characterization and regional mapping of zoned granite plutons. J. Geophys. Res., 98: 4317-4331.

Graham, J. W., 1954. Magnetic susceptibility anisotropy, an unexploited petrofabric element. Geol. Soc. Am. Bull., 65: 1257-1258.

Grant, F.S. and West, G.F., 1965. Interpretation Theory in Applied Geophysics, 583 pp. McGraw Hill, New York.

Guillet, P. and Bouchez, J., 1983. Anisotropy of magnetic susceptibility and magmatic structures in the Guerarde Granite Massif (France). Tectonics, 2: No.5, 419-429.

Heider, F., Dunlop, D.J. and Sugiura, N., 1987. Magnetic properties of hydrothermally recrystallized magnetite crystals. Science, 236: 1287-1290.

Heiland, C.A., 1968. Geophysical exploration, 470 pp. Hafner Publishing Company, New York.

Heller, F., 1973. Magnetic anisotropy of granitic rocks of the Bergell Massif (Switzerland). Earth Planet. Sci. Lett., 20: 180-188.

Henry, B., 1988. The magnetic fabrics of the Egletons granite (France): Separation and structural implications. Phys. Earth Planet. Inter., 51: 253-263.

Hrouda, F., 1982. Magnetic anisotropy of rocks and its application in geology and geophysics. Geophys. Surv., 5: 37-82.

Hrouda, F., Hanák, J. and Jacko, S., 1988. Parallel magnetic fabrics in metamorphic, granitoid, and sedimentary rocks of the Branisko and Cierna hora Mountains (E Slovakia) and their tectonometamorphic control. Phys. Earth Planet. Inter., 51: 271-279.

Hrouda, F. and Lanza, R., 1989. Magnetic fabric in the Biella and Traversella stocks (Periadriatic Line): implications for the mode of emplacement. Phys. Earth Plan. Int., 56: 337-348.

International Critical Tables, 1929. McGraw-Hill, New York.

Irving, E., 1964. Paleomagnetism and its Application to Geological and Geophysical Problems, 399 pp., John Wiley and Sons, Inc., New York.

Jahren, C.E., 1963. Magnetic susceptibility of bedded iron formation: Geophysics, 28: 756.

Jelínek, V., 1981. Characterization of the magnetic fabrics of rocks. Tectonophys., 79: T63-T67.

Jover, O., Rochette, P., Lorand, J.P., Maeder, M. and Bouchez, J.L., 1989. Magnetic mineralogy of some granites from the French Massif Central: Origin of their low-field susceptibility. Phys. Earth Planet. Inter., 55: 79-92.

Karlin, R., Lyle, M. and Heath, G.R., 1987. Authigenic magnetite formation in suboxic marine sediments. Nature, 326: 490-493.

Klein, C. and Hurlbut, C.S., 1977. Manual of Mineralogy (After Dana), 19th edition, 532 pp., John Wiley & Sons, New York.

Larsen, E.S., 1942. Table 1-2: Approximate mineral compositions of principal types of plutonic igneous rocks, Section 1: Composition of Igneous rocks, stony meteorites, and iron meteorites, In Handbook of Physical Constants, Birch, F., Schairer, J.F. and Spicer, H.C. eds., 325 pp., Geological Society of America Special Papers Number 36, Michigan, U.S.A.

Leblanc, D., Gleizes, G., Lespinasse, P., Olivier, Ph. and Bouchez, J.L., 1994. The Maladeta granite polydiapir, Spanish Pyrenees: a detailed magnetostructural study. J. Struct. Geol., 16: No. 2, 223-235.

Lindsley, D.H., Andreasen, G.E. and Balsley, J.R., 1966. Magnetic properties of rocks and minerals. In: Handbook of Physical Constants. Geol. Soc. Am., Memoir 97.

Mooney, H.M. and Bleifuss, R., 1953. Magnetic susceptibility measurements in Minnesota. Geophysics, 18: p. 383.

Nagata, T., 1961. Rock magnetism, 2nd ed., 350 pp., Maruzen, Tokyo.

Néel, L., 1955. Some theoretical aspects of rock magnetism. Adv. Phys., 4: 191-243.

Olivier, J., Rochette, P., Lorand, J.P., Maeder, M. and Bouchez, J.L., 1989. Magnetic mineralogy of some granites from the French Massif Central: origin of their low field susceptibility. Phys. Earth Planet. Inter., 55: 79-92

Olivier, Ph. and Archanjo, C.J., 1994. Magnetic and magmatic structures of the Emas granodiorite pluton (Cachoeirinha belt, NE Brazil). Relationships with Pan-African strike-slip fault systems. Tectonophysics, 229: 239-250.

Osmani, I.A., 1993. Geology and Mineral Potential of Moss Township, District of Thunder Bay; Ontario Geological Survey, 55 pp. Open File Report 5865.

Philpotts, A.R., 1979. Principles of Igneous and Metamorphic Petrology, 498 pp., University of Connecticut, Prentice Hall, New Jersey.

Puzicha, K., 1941. Der magnetismus der gesteine als funktion ihres magnetitgehaltes: Beitrage zur angtwewande Geophysik, 9: 158.

Rochette, P., 1987. Metamorphic control of the mineralogy of black shales in the Swiss Alps: toward the use of "magnetic isograds". Earth Planet. Sci. Lett., 84: 446-456.

Rochette, P., 1988. Relations entre deformations et metamorphisme alpins dans les schistes noir helvetiques: L'Apport de la fabrique magnetique. Geodyn. Acta, 2: 17-24.

Rochette, P., Jackson, J., and Aubourg, C., 1992. Rock magnetism and the interpretation of anisotropy of magnetic susceptibility. Rev. Geophys., 30: 209-226.

Schwerdtner, W.M., Stone, D., Osadetz, K., Morgan, J. and Stott, G.M., 1979. Granitoid complexes and the Archean tectonic record in the southern part of northwestern Ontario. Can. J. Earth Sci. 16: 1965-1977.

Shand, S.J., 1947. Eruptive Rocks. Their Genesis, Composition, Classification, and their Relation to Ore Deposits, 488 pp., 3rd edition, J. Wiley and Sons, New York.

Shandley, P.D. and Bacon, L.O., 1963. Analysis for magnetite utilizing magnetic susceptibility: Paper presented at the S.E.G. meeting, New Orleans, La.

Sharma, P.V., 1976. Geophysical Methods in Geology, 428 pp., Elsevier, Amsterdam.

Shlichter, L.B., 1929. Certain aspects of magnetic surveying. Trans. Am. Inst. Min. Metall. Pet. Eng., 81: 238.

Spark, R.N., 1990. Magnetic fabrics and boundary structure at the Quetico/Shebandowan Subprovince boundary, near Kashabowie, Ontario. M.Sc. thesis, Lakehead University, Thunder Bay, Ont. 293 pp.

Stacey, F.D., and Banerjee, S.K., 1974. The Physical Principals of Rock Magnetism. Developments in Solid Earth Geophysics, 5, 195 pp. Elsevier, Amsterdam.

Strangway, D.W., 1967. Magnetic characteristics of rocks. Society of Exploration Geophysicists' Mining Geophysics. Theory, 2: 454-462.

Strangway, D.W. 1970. History of the Earth's Magnetic Field, 168 pp. McGraw-Hill Book Co., New York.

Streikeisen, A., 1976. To each plutonic rock its proper name. Earth Sci. Rev., 12: 1-33.

Tarling, D.H., 1971. Principles and Applications of Paleomagnetism, 164 pp., Chapman and Hall, London.

Telford, W.M., Geldart, L.P., Sheriff, R.E. and Keys, D.A., 1987. Applied Geophysics, 860 pp. Cambridge University Press, Cambridge.

Tipler, P.A., 1982. Physics Vol. 2., 1062 pp. Worth Publishers Inc., Oakland University, Michigan.

Uyeda, S., Fuller, M.D., Belshe, J.C. and Girdler, R.W., 1963. Anisotropy of magnetic susceptibilty of rocks and minerals. J. Geophys. Res., 68: 279-291.

Werner, S., 1945. Determinations of the magnetic susceptibility of ores and rocks from Swedish iron ore deposits: Sveriges Geol. Unders., Arsbok 39, No. 5, S.C., No. 472, 79 pp. illus.

APPENDIX A

Magnetism and anisotropy of magnetic susceptibility (AMS)

A.1.1 Introduction

Anisotropy of magnetic susceptibility (AMS) provides a non-destructive analytical method useful in the structural interpretation of most rock types. AMS techniques quantify the average magnetic fabric anisotropy of a rock sample by totalling all contributions of each of the magnetically-susceptible minerals in a sample (Borradaile, 1988). Changes in shape or lattice orientation of magnetically-susceptible minerals in response to tectonic deformation reflect the kinematic history of a rock fabric (Borradaile, 1988). The high magnetic anisotropy (induced magnetization directional variability) of deformed rocks makes them especially useful in AMS studies (Graham, 1954). The direction of magnetization in an anisotropic medium is deflected from that of the ambient magnetic field due to the anisotropy of the medium. Therefore, magnetic anisotropy is important in palaeomagnetic studies, as it is needed to correct the palaeomagnetic directions of remanent magnetization.

Measurements of bulk (whole; total) magnetic susceptibility may be made directly in the field with a hand-held susceptibility meter or in the laboratory with various instruments. In this study, an SI2 induction coil system was used, operating at 750 Hertz and 0.6 Oersteds (RMS field).

A.1.2 How AMS may solve the thesis problem

If regional-scale tectonics have deformed both the igneous plutonic intrusion and adjacent country rocks contemporaneously, rock fabric of the Quetico metasedimentary belt may be structurally deformed in a fashion similar to deformation of magnetic fabric in rocks of the Moss Lake stock. AMS (anisotropy of magnetic susceptibility) techniques may present otherwise obscured information about the fabric of the Moss Lake stock which can then be correlated to the local planar fabric of the Quetico metasedimentary belt. If there are correlations in rock fabrics of the Moss Lake stock and the Quetico metasedimentary belt, they may have been deformed at the same time. If no correlations in rock fabric are found, this may indicate that the Moss Lake stock was emplaced after deformation of the metasedimentary rocks.

Kinematic analyses by AMS methods often reveal components of tectonic and magmatic rock fabrics not obtainable by other techniques. Kinematic reconstruction of igneous intrusions is frequently possible with information gained from AMS studies. AMS techniques permit investigation into magmatic flow patterns which relate directly to emplacement mechanisms of igneous intrusions. High magnetic susceptibility of the Moss Lake stock makes AMS of the samples easy to measure.

A.2 Magnetic susceptibility

When magnetic minerals are exposed to an applied external magnetic field (in A/m) of magnitude [H] an internal magnetization

(in A/m) of magnitude [M] is induced. The induced magnetic field produces the linear relationship [M]=[k] X [H], where the proportionality constant [k] is the dimensionless magnetic susceptibility, the response of a material to an applied magnetic field (Rochette et al., 1992).

The critical component of the anisotropy of magnetic susceptibility is the directional variability of [k]. The principal susceptibilities are [k11], [k22], [k33] (Fig. A.1) and refer to maximum, intermediate and minimum susceptibility, respectively.

At the mineral crystal scale, magnetic susceptibility [k] is represented as a tensor. The orientation of the tensor depends strictly on the orientation of the crystal lattice; the maximum crystal dimension reflects the maximum magnetic susceptibility [k1] and the minimum principal susceptibility [k3] direction is perpendicular to it. The vector sum of the contributions of all individual mineral crystal susceptibilities within a rock sample is referred to as the bulk susceptibility. Bulk susceptibility varies with rock type and is larger for mafic rocks.

The orientations of the three principal magnetic susceptibilities are accurately represented by the magnetic susceptibility ellipsoid (Fig. A.1), which reflects [k] magnitudes. The principal axes of the susceptibility ellipsoid are often oriented to reflect changes in strain or mineral orientation and may correlate well with the strain ellipsoid. Magnetic susceptibility directions change quickly during strain, especially
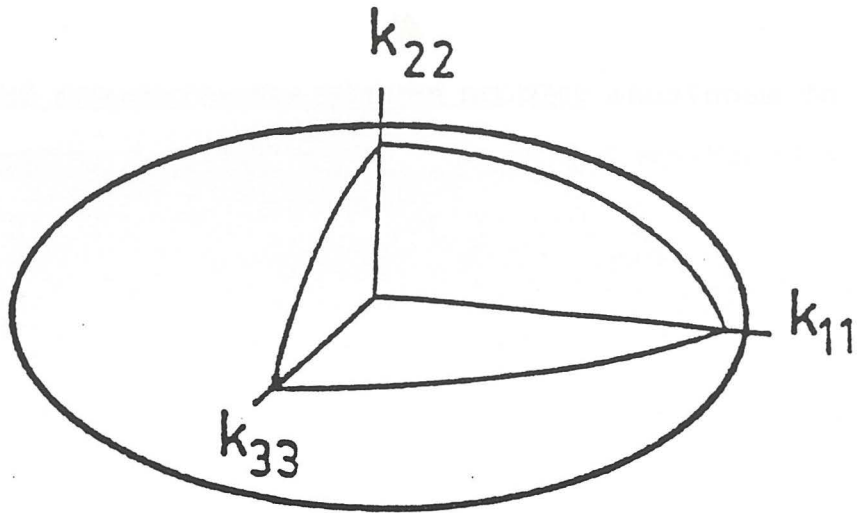
Figure A.1. Magnitude of magnetic susceptibility ellipsoid represented by the orientation of the three principal magnetic susceptibilities where: Kmax=K11, Kint=K22 and Kmin=K33. (After Spark, 1990).
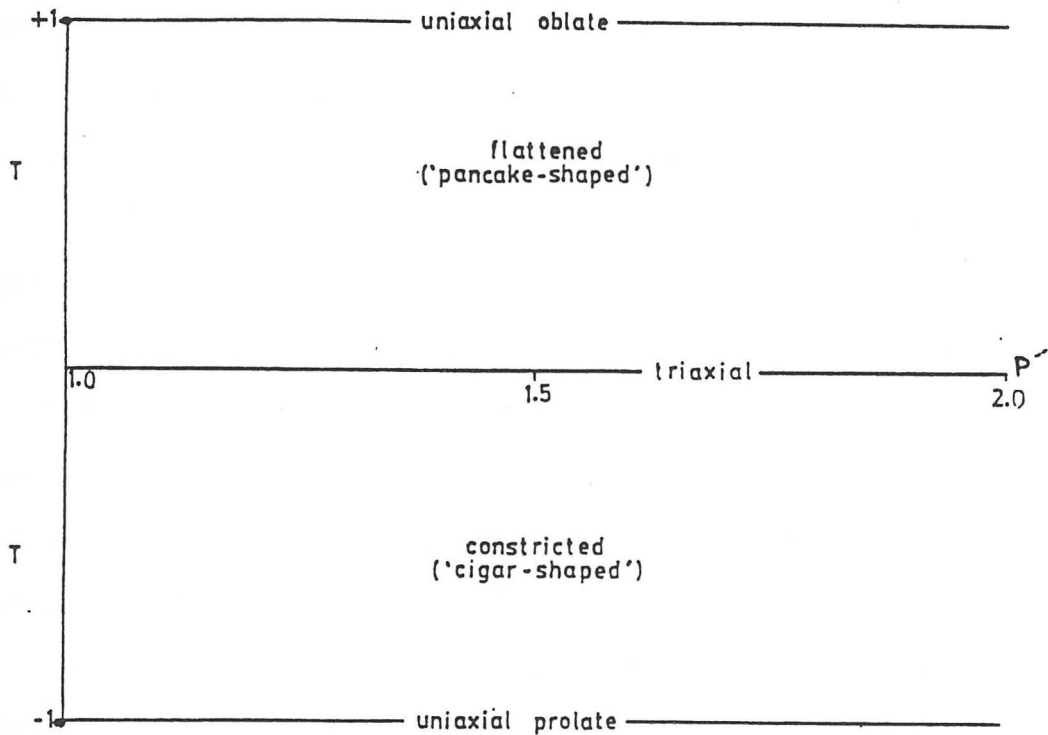
Figure A.2. Hrouda-Jelinek, or P'-T diagram equal area distribution for all susceptibility ellipsoids where they are plotted with respect to sense of anisotropy (T) versus the degree of anisotropy (P'). (After Spark, 1990).

during simple shear (Borradaile, 1988). The average bulk fabric description obtained from AMS techniques reflects fabric kinematic history and closely corresponds to structural features such as folds, shear zones and igneous flow structures (Hrouda, 1982).

A.3 Classification of magnetic materials

A.3.1 Classes

In AMS studies, the mineral sources of magnetic susceptibility should always be identified. The three classes of minerals which respond to weak applied magnetic fields are diamagnetic, paramagnetic and ferromagnetic. Most rock-forming minerals are diamagnetic or paramagnetic. Permanent magnetic dipole moments exist in molecules of paramagnetic and ferromagnetic materials (Tipler, 1982).

A.3.2 Diamagnetic materials

In diamagnetic materials, before the application of an external field, the simple dipoles generated by electrons orbiting a magnetic mineral have random orientations, producing no net magnetism. The orbiting electron motion is retarded when an external magnetic field is applied. This causes the dipoles to weaken, resulting in a small negative magnetic susceptibility (Tipler, 1982). Elements with even atomic numbers are diamagnetic and have magnetic properties dominated by orbital electron pairs. Diamagnetic minerals have negative magnetic susceptibilities. Examples of diamagnetic minerals are albite, oligoclase, quartz and

calcite.

A.3.3 Paramagnetic materials

Elements with odd atomic numbers are paramagnetic. In paramagnetic materials the unpaired dipoles are weakly interactive. Before the application of an external field, the dipoles have random orientations (Tipler, 1982). Dipoles partially align in an applied magnetic field, increasing field strength. The increase in total magnetic field strength is moderate due to random thermal orientation of molecules inhibiting alignment at moderate temperatures and moderate external fields (Tipler, 1982). Paramagnetic minerals have positive magnetic susceptibilities. Examples of paramagnetic minerals are biotite, amphibole and pyroxene.

A.3.4 Ferromagnetic materials

In ferromagnetic materials, adjacent dipoles interact strongly and readily align in weak applied magnetic fields. Ferromagnetic materials may have magnetic dipoles aligned even in the absence of an applied magnetic field (Tipler, 1982). Electron spin orientations vary for ferromagnetic, antiferromagnetic and ferrimagnetic materials (Fig. A.3). The most important members of the ferromagnetic group are magnetite (titanomagnetite series), hematite and pyrrhotite (Borradaile, 1988). These members of the ferromagnetic group have large positive susceptibilities.

(a)

(b)

(c)
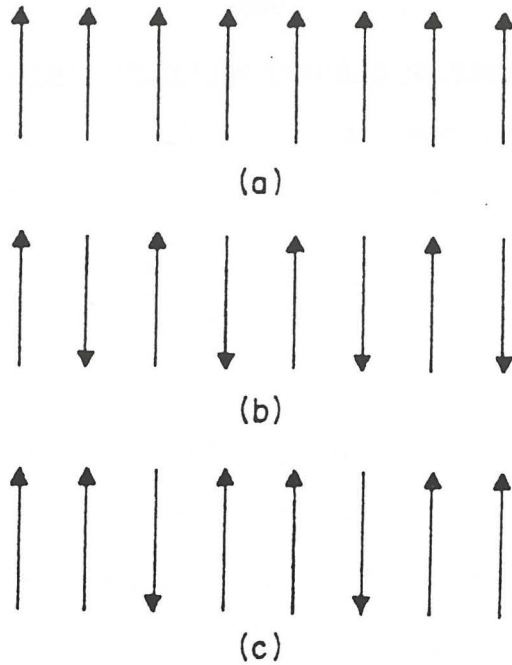
Figure A.3. Electron spin orientations in various types of strongly magnetized material. (a) Ferromagnetism - parallel spins, with a strong internal spontaneous magnetism, even in the absence of an external magnetic field. (b) Antiferromagnetism - equal numbers of electron spins in parallel and anti-parallel orientations, cancelling out the overall magnetization. (c) Ferrimagnetism - the most common magnetic condition where more spins are aligned in a parallel manner than anti-parallel. (After Strangway, 1970).
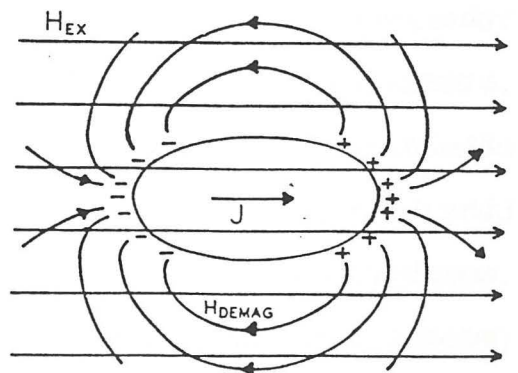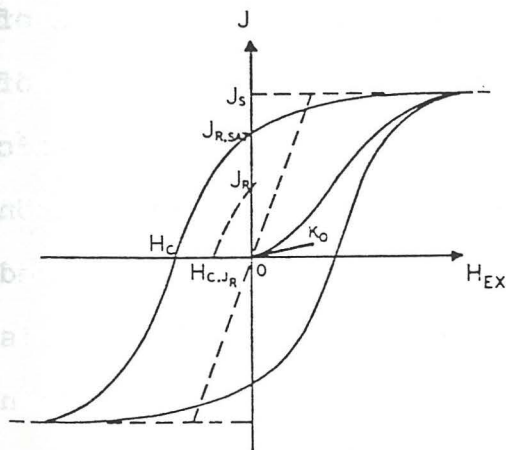
Figure A.4. (above left) General magnetic hysteresis curve showing parameters. (Carmichael, 1982). Figure A.5. (above right) Effect of demagnetizing field (Carmichael, 1982)

A.3.5 Hysteresis curve for ferromagnetic materials

Magnetic susceptibility [k] is constant in the linear relationship [M]=[k] X [H] for paramagnetic and diamagnetic materials. Carmichael (1982) shows an idealized magnetic hysteresis curve for ferromagnetic materials (Fig. A.4, note J=M) with the following parameters:

(1) the saturation magnetization [Js] depends on temperature and decreases to zero at the Curie point. By applying a sufficient magnetic field, spontaneous alignment of magnetic atomic moments occurs, aligning them in their maximum ordered configuration.

(2) When the applied field is removed, the remanent magnetization (Fig. A.4) is [Jrsat] (saturation isothermal remanence).

(3) The remanent magnetization ([Jr], Fig. A.4) is the residual magnetization resulting from a magnetization process other than IRM saturation.

(4) The coercive force ([Hc], Fig. A.4) is the field required to reduce [Jrsat] to a value of zero.

(5) The magnetic susceptibility [k] is represented by the slope of the [H] versus [J] curve. The variable [k] reflects the ability of a material to acquire magnetization in an applied external magnetic field. On the hysteresis curve (Fig. A.4), [k] varies depending on the location of [H]. Thus, magnetic susceptibility may be measured anywhere along the curve and varies with the value of [H]. For this reason, susceptibility is lower in small applied fields then increases as [H] increases but decreases near [Js].

On the hysteresis curve (Fig. A.4), the dotted line represents

the hysteresis curve for a general sample due to the demagnetizing factor or shape effect. An illustration of the effect of the demagnetizing field is shown in Figure A.5. If the magnetic energy state is not dominated by other factors, a grain (or crystal) will have predominant magnetization in the direction of the greatest dimension (Carmichael, 1982).

A.4 Relationship of magnetic susceptibility to mineralogy

A.4.1 Magnetite

The magnetic susceptibility of magnetite is large and positive, on the order of 5 SI units (vol.). Magnetite is crystallographically isotropic but has a very low magnetocrystalline anisotropy. However, its susceptibility is so high that grain shape greatly influences the orientation of the susceptibility ellipsoid (Borradaile, 1988). Detrital magnetite tends to be equidimensional. Magmatic and hydrothermal magnetites tend to have greater aspect ratios (Heider et al., 1987). Shape effects of magnetite are problematic as strings of magnetite grains can aggregate by tectonic effects, such as pressure solution, or by means of bacterial production (Karlin et al., 1987; Chang et al., 1987). Heiland (1968) explains that magnetic susceptibility is not based on the intuitive assumption that susceptibility is directly related to iron content as the Fe valence state is of extreme importance. Bivalent iron ($Fe2+$) is less magnetic than trivalent iron ($Fe3+$) (Heiland, 1968).

The susceptibility ellipsoid of a magnetite grain has axes that

tend to be parallel to the axes of the grain outline. Thus, the preferred dimensional orientation of magnetite is described by the orientation of the magnetic susceptibility ellipsoid.

A.4.2 Hematite

The magnetic susceptibility of hematite is typically on the order of 0.006 SI units (vol.) and shows an anisotropy ratio of >100:1. Hematite shows high crystallographic magnetic anisotropy for single crystals and low values for polycrystalline samples. Hematite has a magnetic fabric component controlled by anisotropic grain crystallographic alignment. The shape effects for hematite are not important as the intrinsic susceptibility is low. The AMS of hematite is crystallographically controlled, ie. by the alignment of anisotropic grains (Borradaile, 1988).

A.4.3 Pyrrhotite

Rochette (1987) and Borradaile (1988) both report that greenschist facies metamorphism may produce pyrrhotite, perhaps at the expense of pyrite. Magnetic isograds may be produced by the metamorphic production of pyrrhotite (Rochette, 1987). For pyrrhotite and hematite, only part of the symmetry is intrinsic (of or pertaining to that which is inherent). Generally, [K3] is parallel to the [c] axis but the anisotropy in the basal plane is influenced by factors such as domain state, defects and shape (Rochette et al., 1992).

A.5 Causes and control of anisotropy

Bhatal (1971) outlines the causes of magnetic anisotropy in rocks as: (1) ferromagnetic grain alignment (2) crystal magnetocrystalline anisotropy lattice alignment (3) magnetic domain alignment (4) magnetic grain stringing (5) anisotropy induced by stress and (6) exchange anisotropy. Rock anisotropy is strictly controlled by the intensity of the preferred orientation of magnetic axes if the grain anisotropy is high (Hrouda, 1982). Magnetic susceptibility anisotropic behaviour may be expressed by the magnitude ellipsoid or by the susceptibility ellipsoid. Paramagnetic mineral anisotropies are higher than anisotropies of diamagnetic minerals. The magnetic susceptibility of magnetite is very high but the anisotropy is low and controlled by grain shape. In contrast, metamorphic silicates have very high anisotropies controlled by crystallographic anisotropy and moderate susceptibilities (Borradaile, 1988). Combinations of the two produce intermediate results and variability in anisotropy will result due to compositional differences, even though strain and fabric could be identical.

A.6 Graphical representation

Graphical representation of the susceptibility ellipsoid shape is attained using magnetic anisotropy plots. The most widely-used type is introduced by Hrouda-Jelinek (1981). The [T] parameter (Fig. A.2) reflects susceptibility ellipsoid shape (the ordinate) and the P' parameter (abscissa) reflects anisotropy degree or

intensity. Hrouda (1982) describes the term "magnetic anisotropy field" as a group of susceptibility ellipsoid plots on a magnetic anisotropy plot from a particular geological unit. The horizontal line of the Jelinek plot separates oblate susceptibility ellipse shapes from prolate susceptibility ellipse shapes. These are referred to as fields of flat-shaped and rod-shaped ellipsoids in describing magnetic fabric. They may be associated with flattening and constrictive deformations, respectively, in tectonites. The magnetic anisotropy path is the curve defined as the locus of the plots of all successive susceptibility ellipsoids (Hrouda, 1982).

A high anisotropy degree, defined as $P'=k1/k3$ (Fig. A.2), reflects a strong preferred orientation of ferromagnetic minerals within a specimen (Hrouda, 1982). The lineation parameter, $L=k1/k2$ (Fig. A.2), refers to magnetic lineation showing the linear-parallel orientation intensity. Planar-parallel orientation of ferromagnetic mineral intensity is described by $F=k2/k3$ (Hrouda, 1982). Magnetic lineation is in the direction of maximum susceptibility and magnetic foliation is at right angles to the direction of minimum susceptibility (Hrouda, 1982).

A.7 Sedimentary rocks

In magnetic studies of sedimentary rocks, compaction, gravity, water currents and the Earth's geomagnetic field are the most important factors in ferromagnetic mineral alignment (Hrouda, 1982). In unmetamorphosed sediments, minimum susceptibility is usually perpendicular to bedding. Magnetite magnetic lineations may

be parallel to current directions. Hematite shows [k2] current-parallel. Thus, magnetic lineations often reveal paleocurrent directions (Hrouda, 1982). Rock magnetic anisotropy changes significantly under ductile deformation; the orientation and shape of the susceptibility ellipsoid of a sediment changes from oblate to triaxial with increased deformation.

A.8 Volcanic rocks

Lava flow patterns control magnetic susceptibility in volcanic rocks. Volcanic rock magnetic anisotropy is as low as that of sediments and depends on the orientation of titanomagnetites produced during lava flow (Hrouda, 1982), in many cases. Magnetic foliation is nearly parallel to flow planes of dikes, sills and lava flows. Magnetic lineation may be parallel or perpendicular to flow, indicating directions of lava flow currents. Magnetic anisotropy of volcanic rocks can be used to solve problems relating to flow directions and to clearly define compositionally-related but spatially-distinct volcanic/plutonic bodies.

A.9 Metamorphic and plutonic rocks

Mimetic recrystallization and ductile deformation greatly influence magnetic susceptibility in metamorphic and plutonic rocks. Plutonic rock anisotropy is highly variable due to the usually less-effective orientating mechanism of magma flow and the high anisotropy produced by ductile deformation. Flow magnetic fabric produces principal susceptibility directions which

correspond to magma flow. Where deformational magnetic fabrics are involved, the principal susceptibilities correspond to deformational fabric elements.

Low grade metamorphic rock anisotropy is substantially higher than that of sedimentary rocks, implying that magnetic grains reorient easily during low grade metamorphism as the ferromagnetic grains are rearranged, deformed or recrystallized. Low grade metamorphic rocks tend to show cleavage-parallel magnetic foliation. In higher grade metamorphic rocks (above greenschist facies), the magnetic anisotropy degree does not increase significantly. Low-field susceptibility in amphibolites is much greater than their unmetamorphosed equivalents. High grade metamorphic rocks present a problem in that some of the magnetic minerals may be recrystallized.

A.10 AMS uses

Information relating to fold genesis is revealed by magnetic anisotropy. Sense of shear movement can be determined based on the assumption that [k3] rotates similar to the minimum strain direction during deformation. In some cases, magnetic anisotropy may be used to infer something about the state of finite strain.

In the field of geophysics, a magnetic anomaly peak may be shifted with respect to the actual location of the body by a significant amount due to rock anisotropy. AMS techniques may clearly define the center of that magnetic body. Other uses of magnetic susceptibility include the classification of soil types

and structural interpretations of coal seams.

A.11 Problems

One of the greatest drawbacks of magnetic susceptibility is its tensor nature; only an average orientation of ferromagnetic minerals can be represented by the susceptibility ellipsoid. The relationship between magnetic fabric and strain is not always obvious and correlations may sometimes be local effects. The foremost problem is how to express the magnetic anisotropy of deformed rocks, putting finite strain into quantitative terms (Hrouda, 1982). Care must be taken in designing models, taking into account both sedimentary and tectonic histories, ie. the separation of depositional and deformational components to the magnetic fabric. This problem is overcome using substitutional ellipsoids. Factors such as discontinuous deformation and new mineral growth must be considered in attempting to correlate bulk strain to magnetic susceptibility.

Reproducing representative natural deformation mechanisms in the laboratory is extremely difficult. Another experimental complication may be the planar nature of magnetic fabrics whereas the mineral fabrics may be constricted or plane strain. Magnetic fabric studies are not a suitable replacement for strain analysis but do provide complementary information (Borradaile, 1988).

A.12 Origin of inverse and abnormal fabrics

Rochette et al. (1992) state that reduction in anisotropy

degree and unexpected principal directions are the most common effects associated with "inverse" minerals. An inverse mineral is one which has maximum and minimum principal susceptibility directions parallel to the minimum and maximum grain or crystal dimensions, respectively. Inverse magnetic fabrics are produced by the minerals tourmaline, goethite, cordierite, single-domain magnetite, siderite and other Fe carbonates (Rochette et al., 1992).

Rochette et al. (1992) provide details of minerals which produce inverse magnetic fabrics. Rod-shaped tourmaline crystals have [kmin] oriented parallel to the crystallographic [c] axis and [kmax] perpendicular to the [c] axis. The resulting magnetic fabric shows [kmax] perpendicular to foliation. Goethite (an antiferromagnetic oxihydroxide) commonly occurs as acicular crystals in which the [c] axis is the maximum susceptibility direction. Cordierite extracted from granite samples shows [kmin] oriented parallel to the [c] axis. Normal and inverse fabrics are known to exist in the same biotite/cordierite-bearing samples.

Multidomain magnetite, hematite and pyrrhotite produce normal fabrics. Uniaxial prolate grains of single domain magnetite have [kmin] parallel to the [c] axes and produce reverse magnetic fabrics (Rochette et al., 1992).

When combinations of normal and inverse fabrics are present, various intermediate fabrics and interchanged principal axes are evident. This may result in fabric combinations within a single sample. These intermediate fabrics may have interchanged axes in

separate samples from the same location or the [kint] orientation perpendicular to foliation (Rochette et al., 1992).

Other causes of abnormal magnetic fabric are anomalous (heterogeneous) petrofabric and secondary processes erasing flow fabric, ie. hydrothermal or cooling stresses (Rochette et al., 1992). Heiland (1968) provides evidence for negative magnetization produced by a combination of tension and torsion, an effect noted by magnetization of drill rods and drill cores.

A.13 Igneous flow fabrics

It is well documented that igneous rocks of plutonic origin with low magnetic anisotropy possess magnetic fabrics formed by movements of flowing magma (Hrouda, 1982). In rock units with flow-type magnetic fabric, the principal susceptibility directions will correlate to fabric elements intimately related to magma flow. The flow patterns indicated by magnetic fabric are tabular to orbicular in shape and provide evidence for multidiapirism. The actual vent locations may be triangulated using intersections of maximum susceptibility direction extrapolations. Some of the problems encountered in the interpretation of flow fabric data include variable mineral compositions, inverse fabrics, deformation events and accurately measuring steeply-inclined fabrics.

Correlation of magnetic fabric trajectories of the Maladeta granite polydiapir in the Spanish Pyrenees reveals petrographic zonation into four distinct genetic types. The four rock types, leucogranite, monzogranite, granodiorite and tonalite (or gabbro)

are concentrically zoned in (a minimum of) four contiguous plutons with the most mafic rock type located at the periphery of each individual pluton (LeBlanc et al., 1994). The same petrographic zonation is noted in a magnetic study of the Mont-Louis Andorra ilmenite-type granite in the Pyrenees (Gleizes et al., 1993), the Foix pluton in the French Pyrenees (Bouchez et al., 1990), the Monte Capanne, Elba Italy granite pluton (Bouillin et al., 1993) and many others. The first two studies emphasize that emplacement kinetics may be better understood from magnetic fabric investigation. The Maladeta polydiapir is thought to be emplaced in zones of crustal weakness (LeBlanc et al., 1994). In contrast, the Biella and Traversella stocks (Periadriatic Line) have magnetic fabrics which are more closely related to the stock bodies than to regional tectonics (Hrouda and Lanza, 1989; Monte Cappanne granite study by Bouillin et al., 1993). Ellwood and Whitney (1980) use magnetic fabric to determine possible tectonic rotation, flow direction and source of the Elberton granite, Northeast Georgia.

A.14 Calculating bulk magnetic susceptibility of a rock specimen

A.14.1 Factors to consider

The overall magnetic susceptibility of a rock sample may be measured by various means. Calculating the bulk susceptibility, however, presents significant complications, as bulk magnetic susceptibility is controlled by many factors. Strangway (1967) outlines the critical factors to consider for individual mineral species as (1) composition, structure and shape of minerals present

and (2) volume fraction dependence, especially in the case of ferromagnetic grains.

Various relationships have been proposed to relate magnetic susceptibility to the content of magnetite, a very important mineral in plutonic igneous rocks. Magnetite is especially important in rocks of the Moss Lake stock. Magnetic minerals have several solid solution series with corresponding variable susceptibilities (Figs. A.6 and A.7) (Akimoto, 1957; Nagata, 1961; Akimota and Nagata, 1960). Magnetic susceptibility is highly variable in igneous rocks partly due to structural and compositional variations (Strangway, 1967).

Volume fraction dependence must be considered when calculating susceptibility for very high susceptibility grains such as magnetite. Relating volume fraction to susceptibility is complex as even the smallest single grain of magnetic material has magnetic interactions with adjacent grains (Strangway, 1967), in effect reducing the bulk magnetic susceptibility of the sample. This relationship may be represented by Hint=Ho-NM where [Ho] represents the applied field, [M] the magnetization and [N] the demagnetizing factor. The variable [N] is shape-dependent (Fig. A.8) and varies from 4pi (measured through the minimum dimension) for an infinite slab to 2 pi (across the axis) for an infinite cylinder and 4pi/3 for a sphere (Strangway, 1967). Special corrections must be made for non-spherical grains to compensate for variations in applied field orientation (Strangway, 1967). The demagnetizing factor alone controls grain susceptibility in rocks with ellipsoidal to
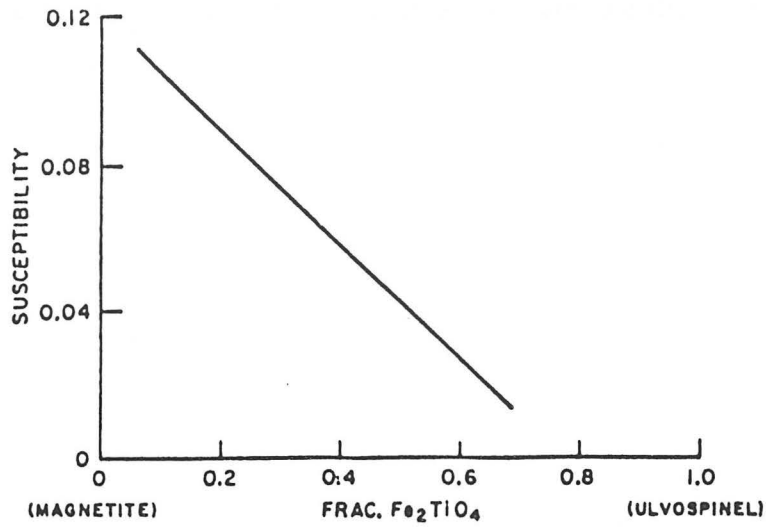
Figure A.6. Susceptibility of the magnetite-ulvospinel series (from Strangway, 1967 after Akimoto).
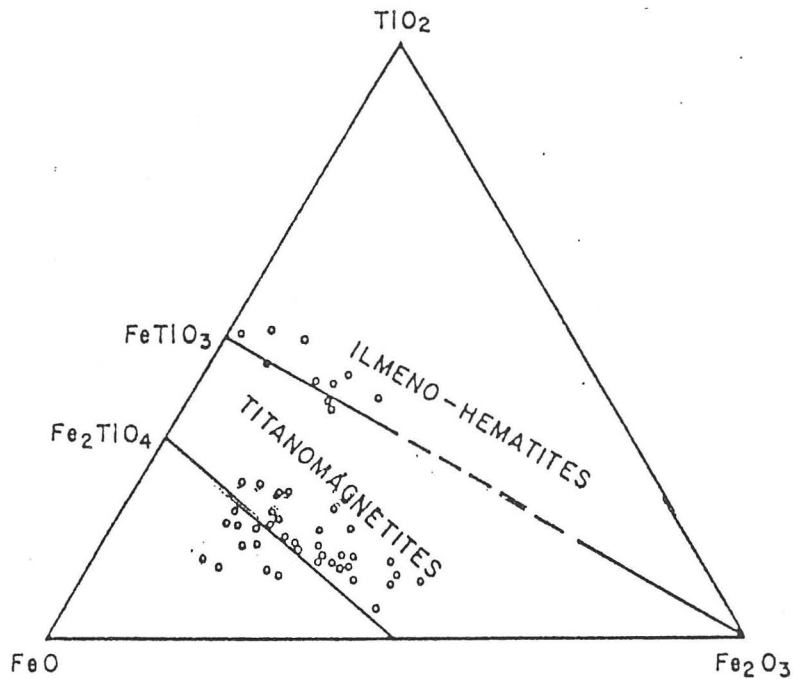
Figure A.7. Chemical composition of minerals from igneous rocks (from Strangway, 1967 after Akimoto and Nagata).

(A) prolate ellipsoid $p/q > 1$ (B) infinite cylinder (C) disc
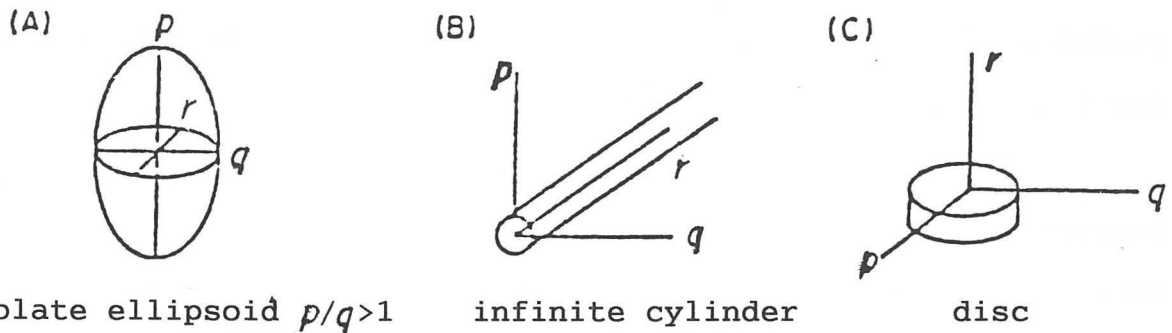
Figure A.8. Shape anisotropy for calculating N (Carmichael, 1982).

$K_M = 1.5$

$$K = \frac{K_M V}{1 + 4/3 \pi K_M (1 - V^{1/6})}$$ WERNER FORMULA

$$K = \frac{K_M V}{1 + K_M (1 - V)}$$

$$K = \frac{K_M V}{1 + 3 X_M (1 - V)}$$ PUZICHA FORMULA

$$K = \frac{K_M V}{1 + 4/3 \pi K_M (1 - V)}$$

K (c.g.s./cc)

VOLUME-PERCENT

Figure A.9. Comparison of measured magnetic susceptibilities to calculated values using various formulas based on a case study from Persberg, Sweden (Strangway, 1967).

spherical shape. A grain shape ratio of 1.5:1 for randomly-oriented grains produces an average [N] value of 3.9; this is a common value for igneous rocks (Stacey and Banerjee, 1974).

For a multi-grain sample, Strangway (1967) explains that demagnetizing factors for both individual grains and the specimen must be considered, along with volume fraction and grain interactions. Puzicha (1941) establishes a relationship for samples with few grains to eliminate the requirement of compensating for interactions:

$$k = (VKm)/(1+ NKm(1-V))$$

where [k] is the mineral susceptibility, [V] is the magnetic mineral volume fraction (the volume fraction [V] of a magnetic mineral equals 0.03 for a rock containing 3% magnetite (Carmichael, 1982)), [Km] is the true susceptibility of magnetic minerals and [N] is the demagnetizing factor 4pi/3.

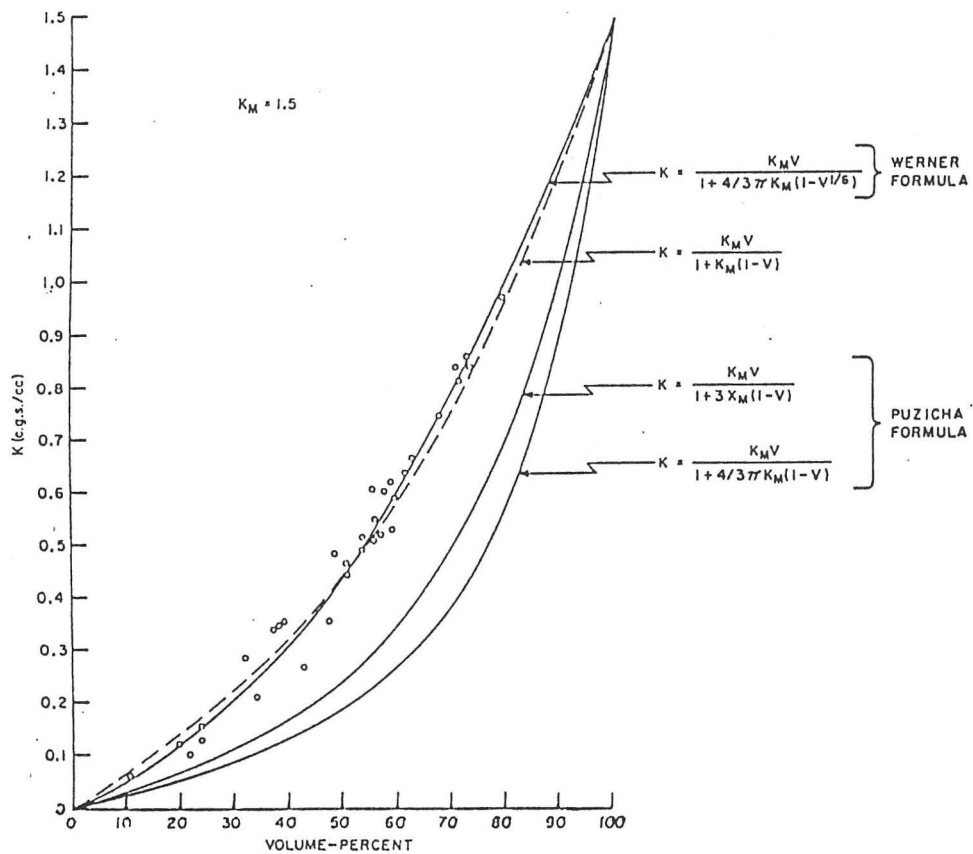Werner (1945) substitutes $V^{1/6}$ to compensate for intergranular interactions. Of the relationships shown on Figure A.9, Werner's formula fits the measured data most closely. Other authors present relationships which fit their data better (Shlichter, 1929; Jahren, 1963). The relationship between magnetite content and susceptibility is shown in Figures A.6 and A.10. Mooney and Bleifuss (1953) propose that $K=0.00289 \ V^{1.01}$ for magnetite volume fractions between 0.2 and 3.5 percent. Strangway (1967) explains that theoretical expressions appear valid for small quantities of magnetite, but depart from theoretical expressions due to less-easily predicted grain interactions as magnetite content increases.
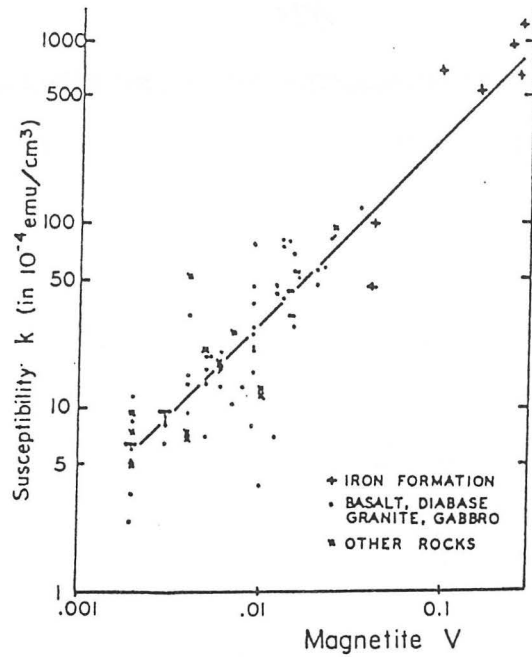
Figure A.10. Susceptibility versus magnetite content (Mooney and
Bleifuss, 1953)
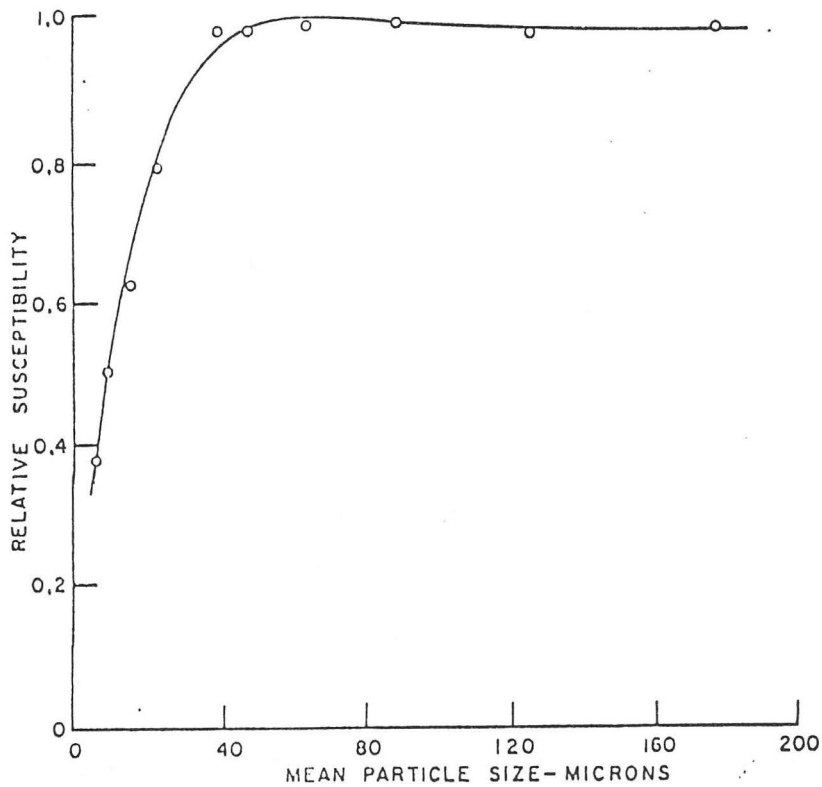
Figure A.11. The dependence of susceptibility on particle size
(from Strangway, 1967 after Shandley and Bacon).

Field strength affects magnetic susceptibility measurements and should always be reported where susceptibility has been measured in the laboratory (Strangway, 1967). A field strength value close to 0.5 Oersteds is frequently used, the value of the Earth's magnetic field and is referred to as a "low" field (hence "low field" susceptibility measurements).

Clearly, magnetic susceptibility is highly variable and depends on the state of magnetization in the case of ferromagnetic grains. Strangway (1967) notes that susceptibility usually decreases with increasing remanence (permanent magnetization or paleomagnetization). Figure A.11 shows that susceptibility is strongly dependent on grain size (Shandley and Bacon, 1963).

A.14.2 Grain size dependence

Strangway (1967) states that, in general, larger-sized ferromagnetic grains contain more domains, making the grains easier to magnetize by rearranging domain walls. Small grains thus have low susceptibility values and they are "magnetically hard", ie. more difficult to magnetize. A single-domain sized particle with a size at least the size of a domain wall (<0.5 microns for magnetite) can be represented by Neèl's (1955)
equation:

$$1/T_0 = C^{(vH_cJ_s/2kT)}$$

where [To] = relaxation time, [v] = grain volume, [Hc] = coercive, [Js] = saturation magnetization, [k] = Boltzmann's constant, [T] = absolute temperature and [C] is a constant depending on the

material elastic properties such that

$$C=(eHc/2m)*(3G\lambda+DJs^2)*(2v/3.14GkT)^{1/2}$$

where [e] = electron charge, [m] = electron mass, [G] = shear modulus, [λ] = magnetostriction coefficient and [D] = a constant with a value of approximately 3.

The following minimum estimate for magnetite is made by Strangway (1967). The [V/T] ratio controls relaxation time. Selecting 500 degrees C for the blocking temperature and particle diameter of 0.05 microns, this particle would retain its remanent magnetism for billions of years. Lattice structure imperfections or impurities should increase the expected grain size (Strangway, 1967).

Experiments performed with rock powders of various grain sizes mixed with magnetite show that fine-grained powders produce lower magnetic susceptibilities than those of coarse-grain powders. On this basis, Heiland (1968) concluded that volcanic rocks may be less magnetic than plutonic rocks, but this generalization is an oversimplification.

A.15 Other factors affecting magnetic susceptibility

Heiland (1968) outlines other factors which may influence the magnetic susceptibility of a rock unit, especially geologic history. Many factors can affect the geologic history of a rock formation. Heiland (1968) lists the thermal and mechanical physical factors as being closely related to regional metamorphism, tectonic movements, chemical and mechanical concentration, igneous

intrusions, disintegration and lightning.

Lightning strikes (usually about 20,000 amperes) produce magnetic fields that affect rock magnetism, especially near mountain and hill tops. Ferromagnetic remanent magnetism drops with temperature increase. Tectonic effects on magnetic susceptibility are complex; magnetization has a reciprocal relation to deformation (of the susceptibility ellipsoid) caused by bending (reciprocal Guillemin effect), twisting (Wertheim effect) and stretching (Villari effect) (Heiland, 1968).

Mechanical and chemical disintegration of rock materials (ie. magnetite--> limonite or hematite) reduces magnetization (also bulk magnetic susceptibility) by reducing particle size and magnetic grain spacing (Heiland, 1968). Intrusive bodies commonly have proximal concentrations of magnetic materials. Heiland's (1968) explanation is that iron in country rock is transformed into more magnetic trivalent iron by contact and dynamic-metamorphic processes.

As stated earlier, magnetite is the predominant magnetic mineral of the Moss Lake stock. Osmani (1993) states that magnetite content of the pluton varies, up to 3% modally. Investigation of magnetic properties of magnetite were essential prior to applying analytical methods of AMS and NRM. Instead of performing countless magnetic separations to determine the magnetite content of individual Moss Lake stock specimens, calculations were performed using 2% magnetite, to see if calculated bulk magnetic susceptibilities were comparable to measured bulk magnetic

susceptibilities. This calculation is performed in Appendix B for specimens of the Moss Lake stock.

Appendix B: Application of AMS to granitoid rocks and magnetic susceptibility calculation of the Moss Lake stock

B.1 Granitoid rock classification

Mafic rocks have larger magnetic susceptibilities than felsic rocks. Any discussion of AMS in granitoid rocks must be precluded by a classification of granites and their genetic relations. The IUGS classification (Fig. B.1) shows the normal field of granitoid rocks (including alkali feldspar granite, granite, granodiorite and tonalite) with 20-60% (modal) quartz as well as alkali feldspar and plagioclase between 0-100% (Philpotts, 1979).

Clarke (1992) exposes problems with characterization of granitoid rocks by acronyms, despite its usefulness in certain circumstances. In this classification, I-type granitoids have source rocks of igneous origin or infrastructure derivation, S-type granitoids have a sedimentary or supracrustal source rock, M-type granitoids have a source from the mantle or fractional crystallization of basalt and A-type granitoids are of anorogenic origin (ie. rift zones and stable cratons).

Shand's (1947) chemical classification divides granitoid rocks into peraluminous, metaluminous and peralkaline. The predominant characteristic minerals of each group are as follows:

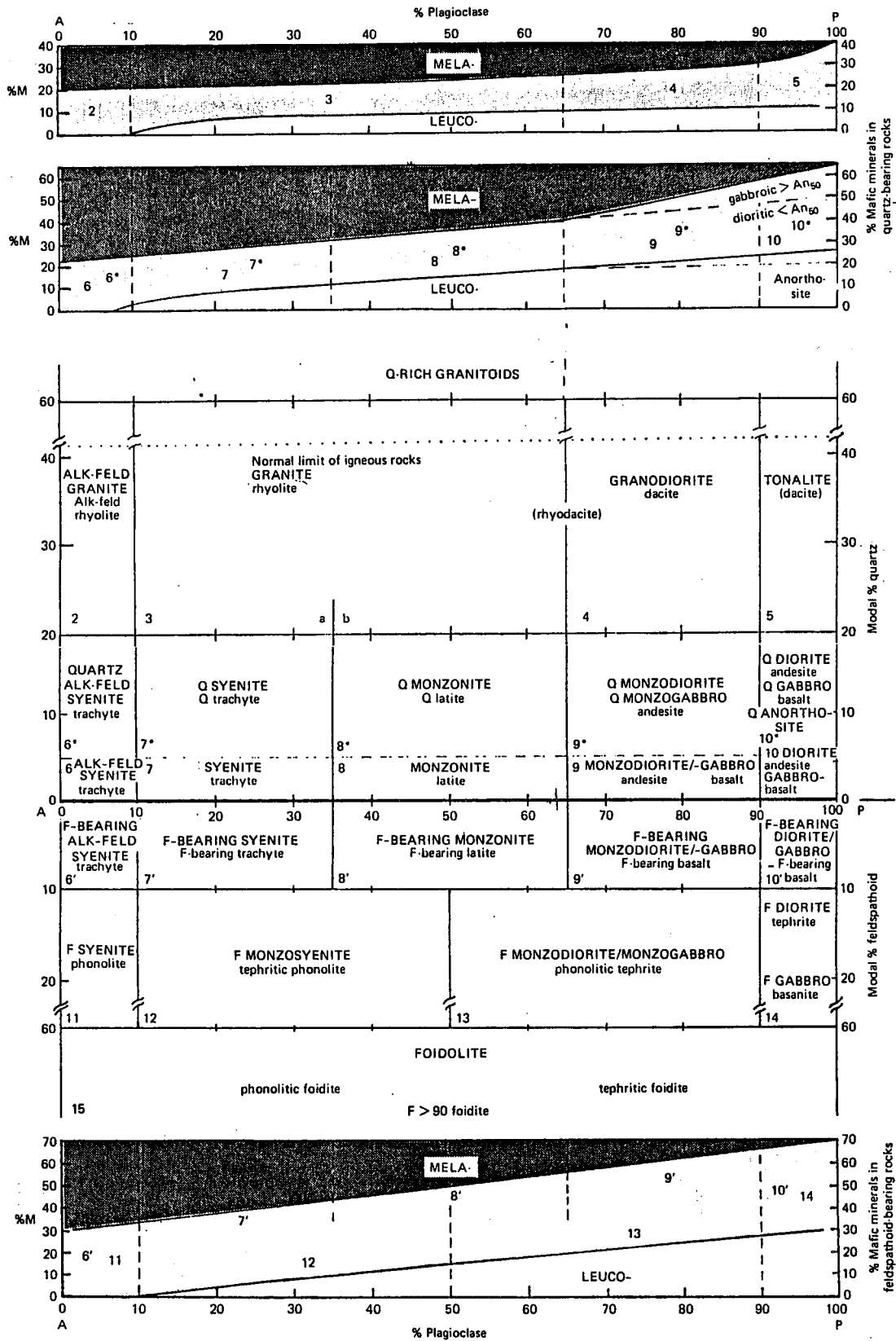| peraluminous	metaluminous	peralkaline
aluminosilicates	orthopyroxene	fayalitic olivine
cordierite, garnet	clinopyroxene	aegirine
topaz, tourmaline	cummingtonite	arfedsonite
spinel, corundum	hornblende	riebeckite
(biotite and	epidote	(minor biotite)
muscovite)	(biotite)	

Figure 8.1. IUGS classification of igneous rocks containing less than 90% mafic minerals. Plutonic rocks are given in uppercase letters and volcanic ones in lowercase letters. A=alkali feldspar + albite (<An5), and P=plagioclase (>An5) (from Philpotts, 1979).

The most important minerals in granitoid rock AMS studies are the oxide minerals ilmenite in peraluminous granitoids and magnetite in both metaluminous and peralkaline granitoids. In a typical granite, magnetite and ilmenite are the most important contributors to magnetic susceptibility with minor contributions from amphibole (hornblende) and biotite. However, the magnetic susceptibility of magnetite is much greater than that of ilmenite.

Streckeisen's (1976) QAPF double triangle plot (Fig. B.2) further divides the IUGS classification of granite into syenogranite and monzogranite. The mineral relationships among the granitoid group, syenite, diorite and gabbro are understood from their positions in the ternary diagram. The source of magnetic susceptibility for each of these rock groups is in part compositionally dependent. Presumably, each structurally and chemically-identical mineral species has a characteristic bulk magnetic susceptibility. The modal composition (volume fraction) of each rock group must first be determined, along with the true susceptibility of each mineral contained within the specimen. This information, in conjunction with Werner's (1945) formula, accurately predicts bulk magnetic susceptibility.

B.2 Case studies

In order to compare the Moss Lake stock to other plutonic intrusions, AMS data (Fig. B.3) is reported from granitoid and other rock types from around the world. For these case studies, the bulk susceptibilities range from 0 to 50,000 x 10^{-6} SI units (vol.).
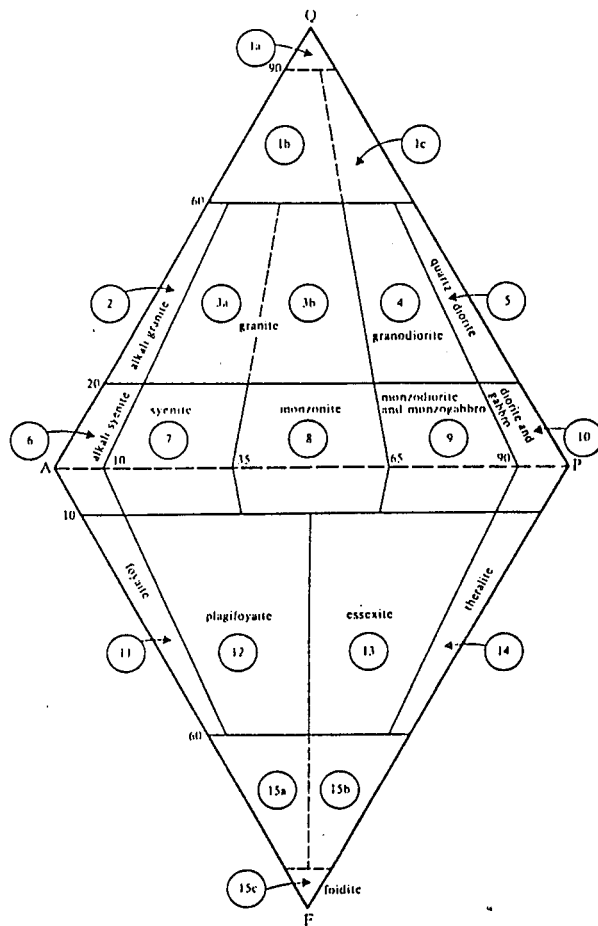
Field	Plutonic rocks	Volcanic rocks
1a	quartz rocks *sensu stricto*	—
1b	quartz–granite	—
1c	quartz–granodiorite	—
2	alkali granite	alkali rhyolite
3	granite	
3a	syenogranite	rhyolite
3b	monzogranite	rhyodacite
4	granodiorite	dacite
5	quartz–diorite	quartz–andesite
6	alkali syenite	alkali trachyte
7	syenite	trachyte
8	monzonite (≡ syenodiorite)	
9	monzodiorite and monzogabbro (≡ syenodiorite and syenogabbro)	trachyandesite and trachybasalt
10	diorite, gabbro, anorthosite[a]	andesite, basalt
11	foyaite[b]	phonolite[c]
12	plagifoyaite	tephritic phonolite
13	essexite	phonolitic tephrite
14	theralite	tephrite
15a	foyaitic foidite	phonolitic foidite
15b	theralitic foidite	tephritic foidite
15c	foidite[d] *sensu stricto*	extrusive foidite *sensu stricto*

[a]The distinction between diorite and gabbro is based on plagioclase composition (gabbro has plagioclase more calcic than An_{50}). Anorthosites have M < 10.
[b]Many plutonic rocks in fields 11 and 12 would normally be termed nepheline syenites.
[c]Most volcanic rocks in fields 11–15 have potassic equivalents (see Table 2.1).
[d]The commonest rocks in this group are the clinopyroxene–nepheline rocks, Urtite (M = 0–30), ijolite (M = 30–70) and Melteigite (M = 70–90). The approximate volcanic equivalent of ijolite is nephelinite (though most nephelinites contain appreciable normative feldspar).

The important ultramafic rocks (not shown in the QAPF diagram) are dunite (90–100% olivine), peridotite (30–90% olivine) and pyroxenite and hornblendite (0–30% olivine). The peridotites are divided into harzburgite (olivine + hypersthene), lherzolite (olivine + orthopyroxene + clinopyroxene) and wehrlite (olivine + clinopyroxene).

Figure 8.2. (Upper) QAPF double triangle plot of plutonic rock types, as classified by modal mineralogy. (Lower) Nomenclature of rocks in the Q-A-P and A-P-F triangles. (After Streckeisen, 1976)

igneous rock type	susceptibility range from	to	mean	number of samples	locality &notes	literature reference
rhyolite	251	37699				a
granite	0	50266	2513			a
granite	12566	50266			Yosemite,Calif.	c,d,e
granite	3519	25133		41	Oklahoma	d,e
granite	0	50266		31	Minnesota	f
granite			5906		same <1.4% mag.	c
granite	13	63			without mag.	c
granite	241	2930	838	126	NE Georgia	j
granite	10	200	140	74	Elba, Italy	l
granite	360	36000		6000	Sierra Nevada, Calif.	o
granite	101	352			Harz	p
granite	17844	23876			Harz	p
granite	50	362			East Slovakia	r
granitoid-gneiss	58	45654		Av87 sites	Opatica Belt.	s
leucogranite		100		145	Spanish Pyrenees	h
leucogranite	20	50		294	French Pyrenees	k
leu-mon granite		132		4	Nord-Millevaches	q
monzogranite	100	200		145	Spanish Pyrenees	h
monzogranite	110	180		294	French Pyrenees	k
biotite granite	145	232		3	Gueret (familiyll)	q
porphyritic granite			6647.626	170	Switzerland	t
anatexites	200	2500		2	Gueret (family III)	q
tonalite	300			145	Spanish Pyrenees	h
tonalite		1000			Sierra Nevada, Calif.	o
granodiorite	200	300		145	Spanish Pyrenees	h
granodiorite	158	413		73	NE Brazil	i
granodiorite	511	592		4	NE Brazil	i
granodiorite	877	3220		3	NE Brazil	i
granodiorite	180	250		294	French Pyrenees	k
quartz diorite		387		294	French Pyrenees	k
diorite			2513			g
diorite	628	125664	87965			a
diorite			591		Harz	p
augite-syenite	33929	45239				a
augite-syenite	34181	44988			Harz	p
syenite porphyry	603	1508			Harz(low-high field)	p
porphyry	251	209859	62832			a
andesite			169646			a

References

a Telford et al., 1987.

b Carmichael CRC Handbook of Phys. p.334

c Sharma, 1976

d Strangway, 1967

e Currie et al., 1963

f Mooney and Bleifuss, 1953

g Dohr, 1976

h LeBlanc et al., 1994.

i Olivier and Archanjo, 1994

j Ellwood and Whitney, 1980.

k Bouchez et al., 1990.

l Boullin et al., 1993.

n Guillet and Bouchez, 1983

o Bateman et al., 1991.

p from Puzicha but found in Heiland, 1968.

q Olivier et al., 1989

r Hrouda et al., 1988

s Benn et al., 1993

t Heller, 1973

Figure 8.3. Measured (bulk) magnetic susceptibilities for select igneous rocks X 10E-6 SI (vol.).

Leucocratic granites appear to have lower bulk magnetic susceptibilities; the reason is clearly that the light-coloured granitoids are deficient in ferromagnesian minerals. In Figure B.3, syenites have larger bulk magnetic susceptibilities than those for granitoid rocks. Figures B.4 and B.5 show susceptibilities for various rock types. Figure B.5 shows a graph of bulk magnetic susceptibility versus each rock group for Figure B.3. Note the relatively high bulk magnetic susceptibility of syenite (Fig. B.5).

B.3 Moss Lake stock magnetic susceptibility

The magnetic properties of 56 oriented samples from the Moss Lake stock have been investigated. The bulk magnetic susceptibilities of the samples (Fig. B.6) range from near zero to $56,396 \times 10^{-6}$ SI units (vol.). Individual cores ranged in bulk magnetic susceptibility up to $83,714 \times 10^{-6}$ SI. The mean is $12,219 \times 10^{-6}$ with a standard deviation of $13,416 \times 10^{-6}$. The frequency histogram (Fig. B.7) shows an approximately-Gaussian distribution. The log graph of the bulk susceptibilities (Fig. B.8) suggests the possibility of two separate populations, possibly reflecting compositionally-distinct igneous phases or zonation.

B.4 Calculation of Moss Lake stock bulk magnetic susceptibility

The direct approach of measuring magnetic content of specimens by crushing and magnetic separation is not taken due to the large number of samples required and because Osmani (1993) states that magnetite content of the stock is variable, up to 3% modally.
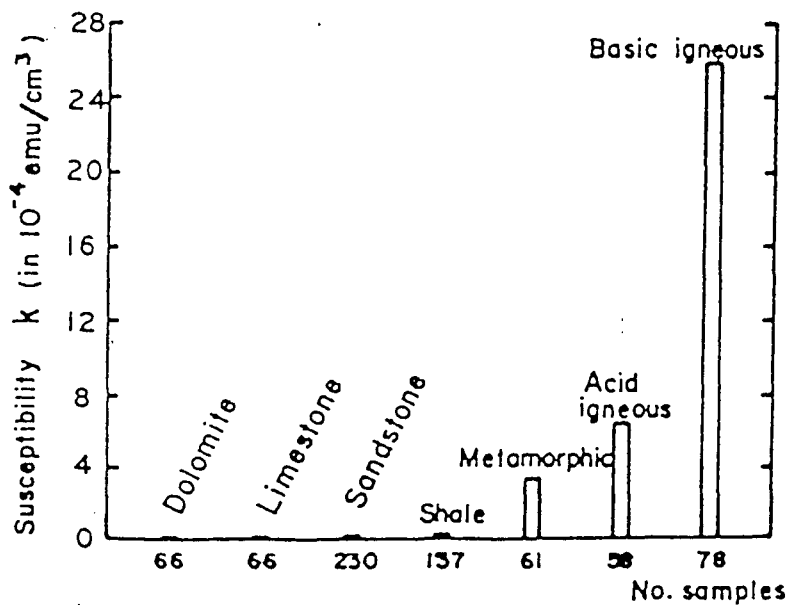
Figure B.4. Measured susceptibilities for different rock types (After Dobrin, 1976 from earlier work by J.W. Peters).
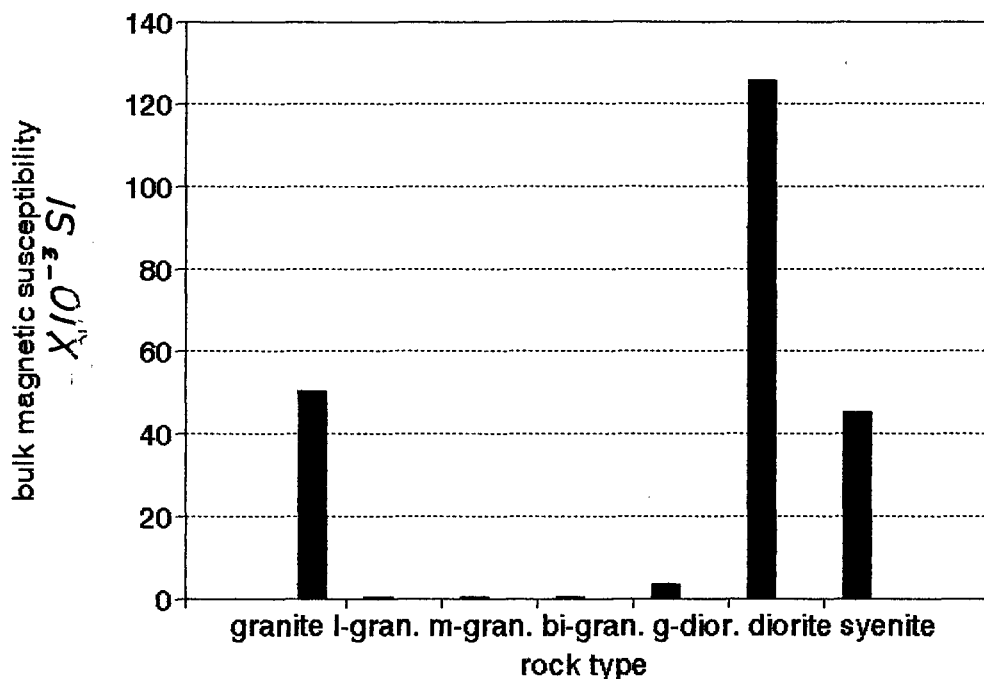

Figure B.5. Select rock group measured (bulk) magnetic susceptibilities in units of 10^{-3} SI (vol.) based on the case studies of Figure B.3. Abbreviations are l-gran=leucogranite, m-gran= monzogranite, bi-gran=biotite granite, g-dior=granodiorite.
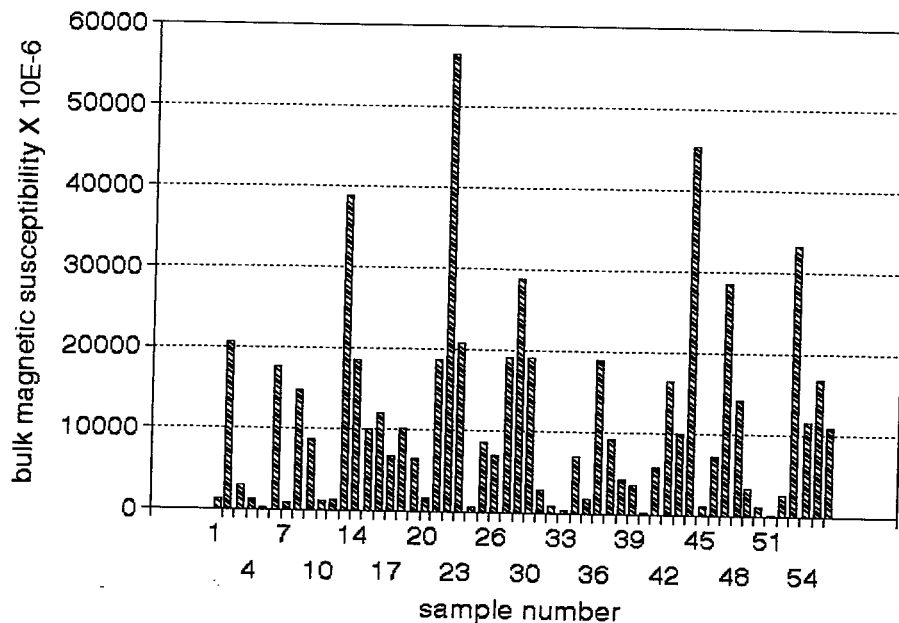
Figure 8.6. Bulk magnetic susceptibilities of Moss Lake stock oriented samples, averaged from two cores per specimen. The bulk magnetic susceptibility of individual cores ranged up to 83,714 X10E-6 SI.
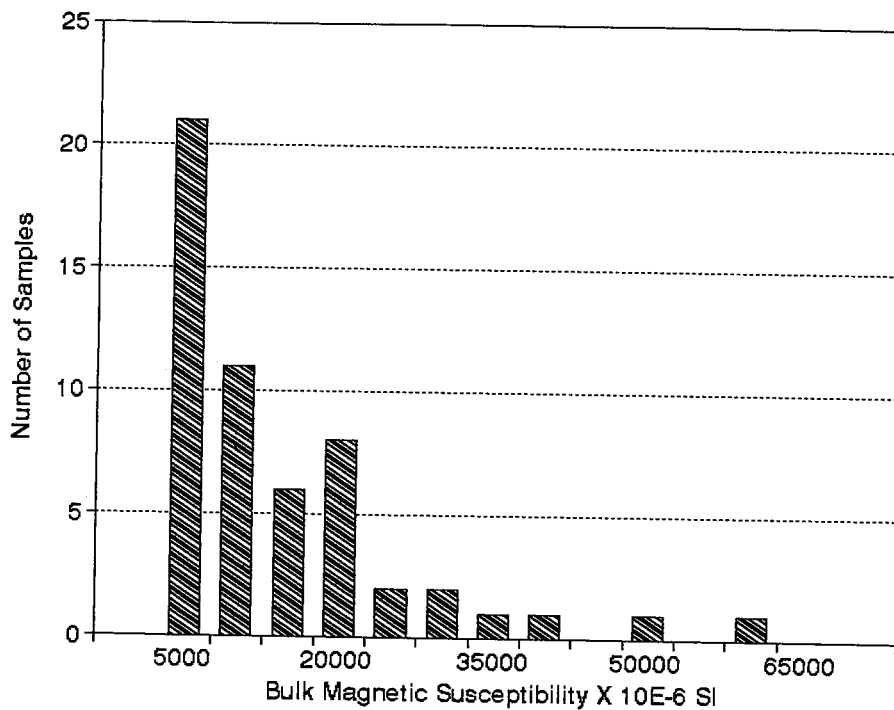

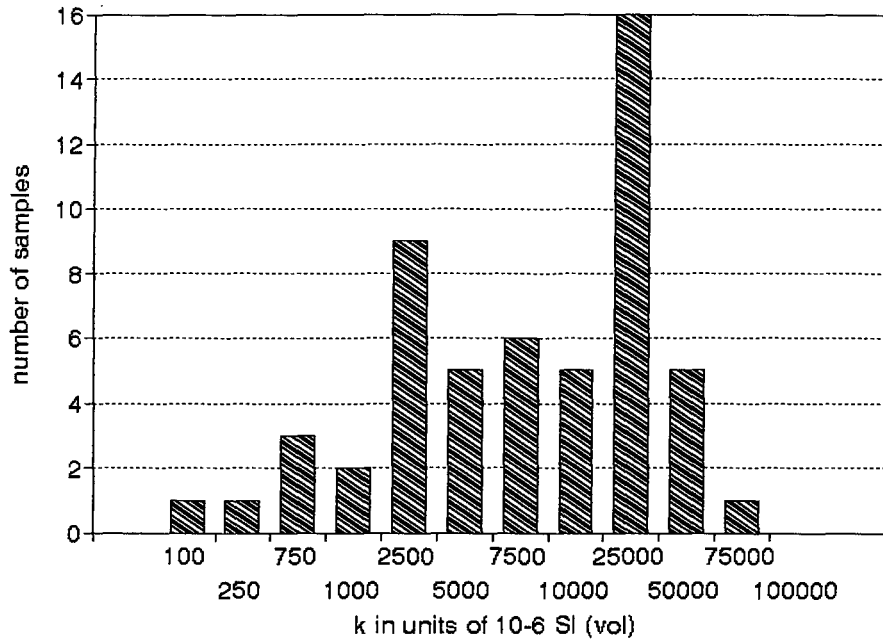Figure 8.7. Moss Lake stock oriented sample frequency histogram.

Figure 8.8. Moss Lake stock oriented sample magnetic suscep-
tibility log (bulk) magnetic susceptibility.

SUSCEPTIBILITIES OF ROCK TYPES, CALCULATED FROM THEIR
MAGNETITE AND ILMENITE CONTENT[25,39]

| | Magnetite Content and Susceptibility,* cgs units | | | | | | Ilmenite, average | |
| | Minimum | | Maximum | | Average | | | |
Material	%	k × 10⁴	%	k × 10⁶	%	k × 10⁶	%	k × 10⁴
Quartz porphyries	0.0	0	1.4	4,200	0.82	2,500	0.3	410
Rhyolites	0.2	600	1.9	5,700	1.00	3,000	0.45	610
Granites	0.2	600	1.9	5,700	0.90	2,700	0.7	1000
Trachyte-syenites	0.0	0	4.6	14,000	2.04	6,100	0.7	1000
Eruptive nephelites	0.0	0	4.9	15,000	1.51	4,530	1.24	1700
Abyssal nephelites	0.0	0	6.6	20,000	2.71	8,100	0.85	1100
Pyroxenites	0.9	3000	8.4	25,000	3.51	10,500	0.40	5400
Gabbros	0.9	3000	3.9	12,000	2.40	7,200	1.76	2400
Monzonite-latites	1.4	4200	5.6	17,000	3.58	10,700	1.60	2200
Leucite rocks	0.0	0	7.4	22,000	3.27	9,800	1.94	2600
Dacite-quartz-diorite	1.6	4800	8.0	24,000	3.48	10,400	1.94	2600
Andesites	2.6	7800	5.8	17,000	4.50	13,500	1.16	1600
Diorites	1.2	3600	7.4	22,000	3.45	10,400	2.44	4200
Peridotites	1.6	4800	7.2	22,000	4.60	13,800	1.31	1800
Basalts	2.3	6900	8.6	26,000	4.76	14,300	1.91	2600
Diabases	2.3	6900	6.3	19,000	4.35	13,100	2.70	3600

* Using k_magnetite = 0.30 emu/cm³; k_ilmenite = 0.137 emu/cm³.

Figure 8.9. Susceptibilities of rock types calculated from their
magnetite and ilmenite content (cgs units) (Dobrin, 1976; Slichter,
1929; Carmichael, 1982).

During AMS measurements the bulk magnetic susceptibility of each specimen is quantified in SI units. By predicting the bulk magnetic susceptibility of the Moss Lake stock, based on 2% magnetite content, a comparison may then be made between the calculated mean susceptibility and the measured bulk magnetic susceptibilities.

Carmichael (1982) shows calculated susceptibility values (Fig. B.9) from information by Dobrin (1976) and Shlichter (1929) of theoretical susceptibilities of various rock types based on their magnetite and ilmenite contents. The relation of magnetic susceptibility to magnetite content (Figs. B.10, B.11, B.12) is well established if other minerals are of low susceptibility.

First an attempt was made to calculate the bulk magnetic susceptibility of a typical Moss Lake stock sample based strictly on the magnetic contributions of each of the minerals present. The theoretical bulk magnetic susceptibilities for selected plutonic rocks and a representative sample from the intrusion are calculated by summing magnetic contributions of the individual minerals present (Fig. B.13), using published values for the minerals.

Figure B.13 shows the theoretical bulk magnetic susceptibility of a typical granite, granodiorite, quartz diorite, syenite and a representative sample from the Moss Lake stock. [Kmean] is given for each of the individual characteristic minerals in SI units x 10^{-6} (vol.). The volume fraction of each mineral is multiplied by the mineral's true susceptibility [Km] and normalized to 100% to reflect the theoretical susceptibility the volume fraction of that mineral would contribute to total bulk susceptibility. It is
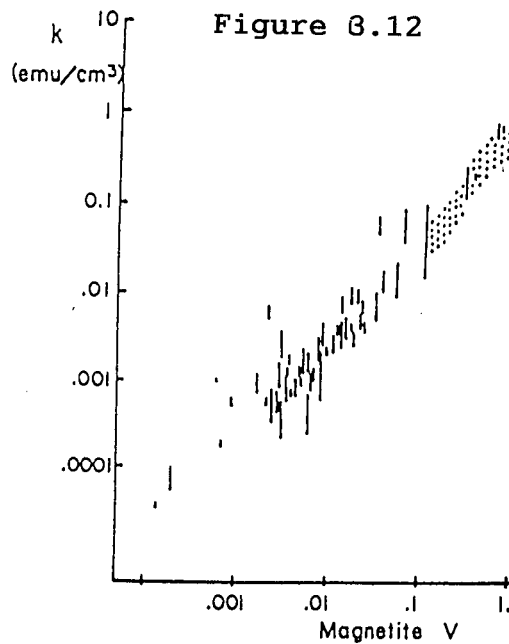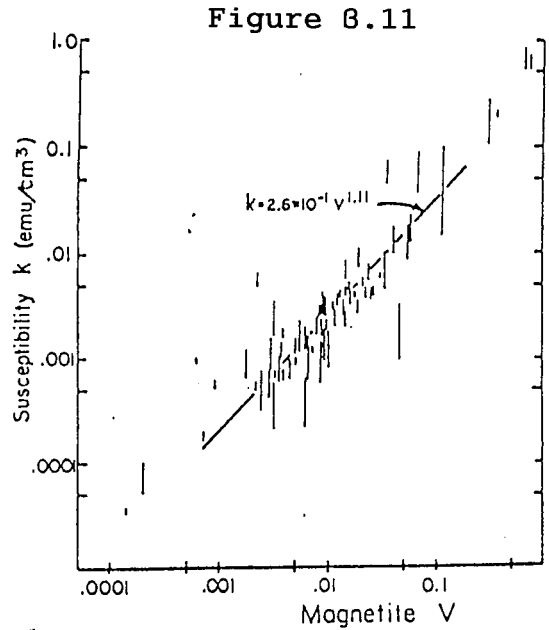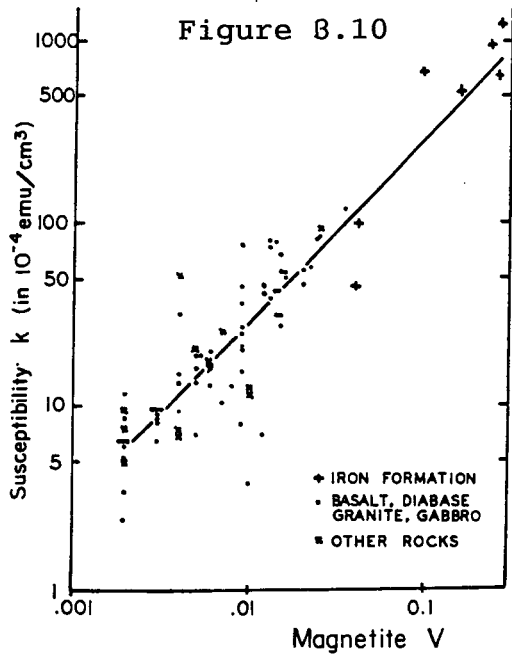
Figure β.10. Relation of susceptibility to magnetite content for some igneous and ore rocks of Minnesota (Mooney and Bleifuss, 1953).

Figure β.11. Relation of susceptibility to magnetite content for some metamorphic rocks of the Adirondacks (Grant and West, 1955; data from Balsley and Buddington, 1958).

Figure β.12. Susceptibility and magnetite content of rocks and ores (Lindsley et al., 1966; data from Balsley and Buddington, 1958 and Werner, 1945).

Mineral	Kmean in units of SI E-6	GRANITE modal %	granite theoretical susceptibility	G-DIORITE modal %	g-diorite theoretical susceptibility	Q-DIORITE modal %	q-diorite theoretical susceptibility	SYENITE modal %	syenite theoretical susceptibility	MLS modal %	MLS theoretical susceptibility
quartz (a)	-13	25	-3	21	-3	20	-3				
albite (b)	-13									7	-1
orthoclase+ microperthite (b)	-13	40	-5	15	-2	6	-1	72	-10	75	-10
oligoclase (b)	-3	26	-1					12	-0		
andesine (b)	-13			40	-5	56	-8				
biotite (b)	2500	5	125	3	75	4	100	2	50	5	125
amphibole (c)	2750	1	28	13	358	8	220	7	193	10	275
orthopyroxene (c)	2750					1	28			2	55
clinopyroxene (c)	2750					3	83	4	110		
ilmenite (d)	1800000	1	18000	1	18000			1	18000		0
hematite (d)	7000	1	70								0
magn(1) (d)	6200000	1	62000	1	62000	2	124000	2	124000	2	124000
magn(2)(Werner)	4666		4666		4666	2	10438		10438		10438
magn(3)(Wer2)	10101		10101		10101		20408		20408		20408
Whole rock(1)			80213		80422		124419		142343		124444
Whole rock(2)			22879		23088		10857		28781		10882
Whole rock(3)			28314		28523		20827		38751		20852
N value	4										

mean	12219	measured
std. dev.	13416	measured

(for 56 samples)

References:

a. Hrouda (1986)

b. Borradaile (1987-1994 and unpublished)

c. Rochette et al., (1992) variable from 500-5000

d. Carmichael (1982)

Modal compositions after Larsen (1942)

MLS modal composition after Osmani (1991)

G-diorite=granodiorite   Q-diorite=quartz diorite

MLS=Moss Lake Stock

Measured values refer to bulk magnetic susceptibilities

of MLS samples

Whole rock(1) refers to calculation based on volume fraction

Whole rock(2) refers to calculation based on Werners' formula

compensating for intergranular interactions

Whole rock(3) refers to calculation based on Werners' empirical expression

Figure 8.13. Theoretical bulk magnetic susceptibilities of some plutonic rocks calculated by magnetic contibution of individual minerals compared to the theoretical and measured bulk magnetic susceptibilities of the Moss Lake stock samples.

immediately obvious that magnetite plus ilmenite contribute >99% of the bulk magnetic susceptibility, if we use the reported mineral susceptibilities. The diamagnetic mineral contributions (negative [k] values) are deducted from the bulk susceptibility when the sums of the theoretical susceptibilities are tabulated in row "whole rock(1)" in Figure B.13. The bulk magnetic susceptibilities for the rock types derived by summing the magnetic contributions results in theoretical susceptibilities which are too large, approximately by a factor of 10.

Incorporating Werner's (2nd) empirical formula (Fig. A.9), the [kmean] value for magnetite (magnetite(3)(Wer2)) is drastically reduced from $6,200,000 \times 10^{-6}$ to 10101×10^{-6}. This results in more accurate bulk magnetic susceptibilities for the selected rocks in row "whole rock(3)" of Figure B.13. Werner's first formula (Fig. A.9), uses $V^{1/6}$ to compensate for intergranular interactions. The [kmean] of magnetite is then further reduced to 4666×10^{-6} SI units (vol.) in row "mag(2)(Werner)" (Fig. B.13). As shown in row "Whole rock (2)" of Figure B.13, the calculated theoretical bulk magnetic susceptibility, corrected for intergranular interactions, is $10,882 \times 10^{-6}$ SI units (vol.) and the actual measured mean of 56 samples is $12,219 \times 10^{-6}$. The calculated theoretical bulk magnetic susceptibility is therefore within 0.001 SI units of the measured mean bulk magnetic susceptibility using Werner's formula, assuming a demagnetizing factor of $N=4pi/3$ and 2% (modal) magnetite.

B.5 Discussion

Of all the factors which influence bulk magnetic susceptibility in the Moss Lake stock, magnetite content must be predominant. Volume fraction dependence requires an accurate estimate of modal volume proportion of magnetic mineral content. This is difficult to determine by microscopy because magnetic minerals such as magnetite are opaque and often very fine-grained.

Demagnetizing factors (shape effects) also influence susceptibility. The shape effect [N] value for a typical Moss Lake stock sample is unlikely to be 4pi/3 as this is the value applicable to a spherical grain. Fabric parameters for the tested samples show that the magnetic minerals are substantially aligned. A Flinn diagram (Fig B.14) and a Jelinek plot (Fig. B.15) are presented here to compare shape parameters; refer to Section IV for the AMS study of the Moss Lake stock. The Flinn diagram for the Moss Lake stock samples (Fig. B.14) shows oblate characteristics and the Jelinek plot (Fig. B.15) further supports oblate magnetic susceptibility ellipsoid shape. The [N] value of 3.9 may be typical for igneous rocks. Using the [N] value of 3.9 further improves the Moss Lake stock bulk magnetic susceptibility calculation, changing the theoretical mean bulk magnetic susceptibility of the intrusion from 11,800 x 10^{-6} SI units (vol.) to 11,300 x 10^{-6} SI units (vol.). The Flinn diagram and the Jelinek plot both reflect fabric shape and anisotropy intensity. The [N] value (Fig. A.8) is based on shape ratio, so that intuitively one may be able to work backwards from the fabric plots to determine the true mean value of [N] for
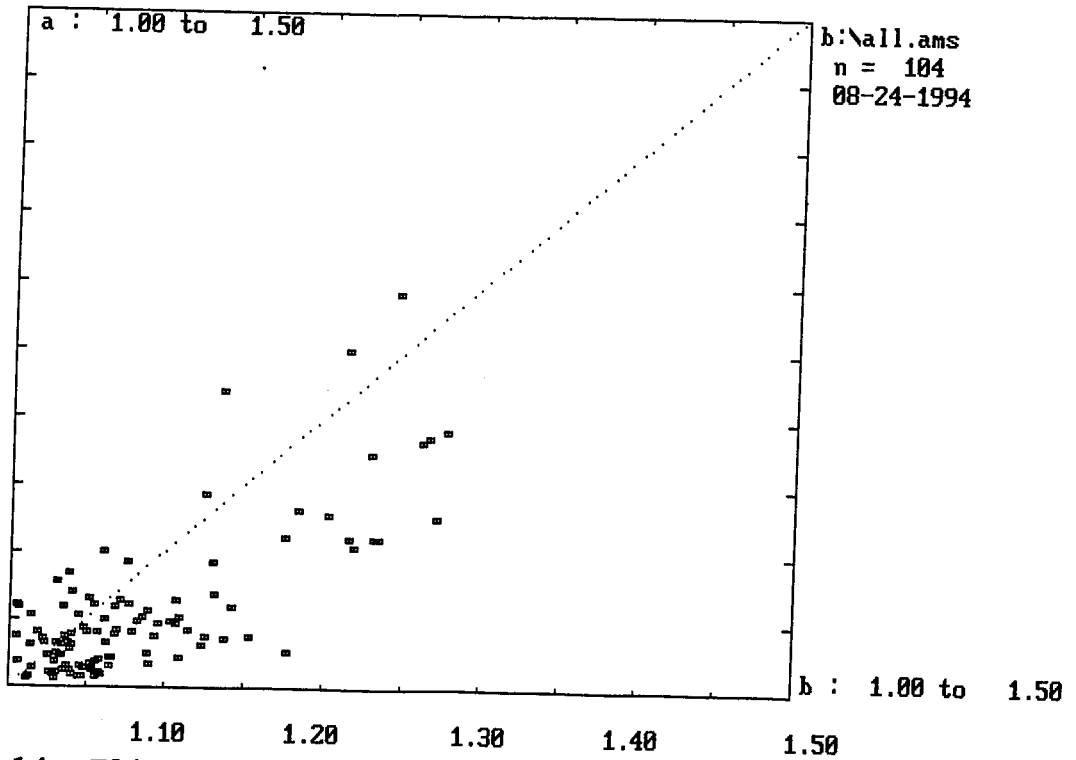
Figure 8.14. Flinn diagram of Moss Lake stock fabric parameters. The magnetic fabric, as represented by the magnetic susceptibility ellipsoid, is predominantly oblate (flattened).
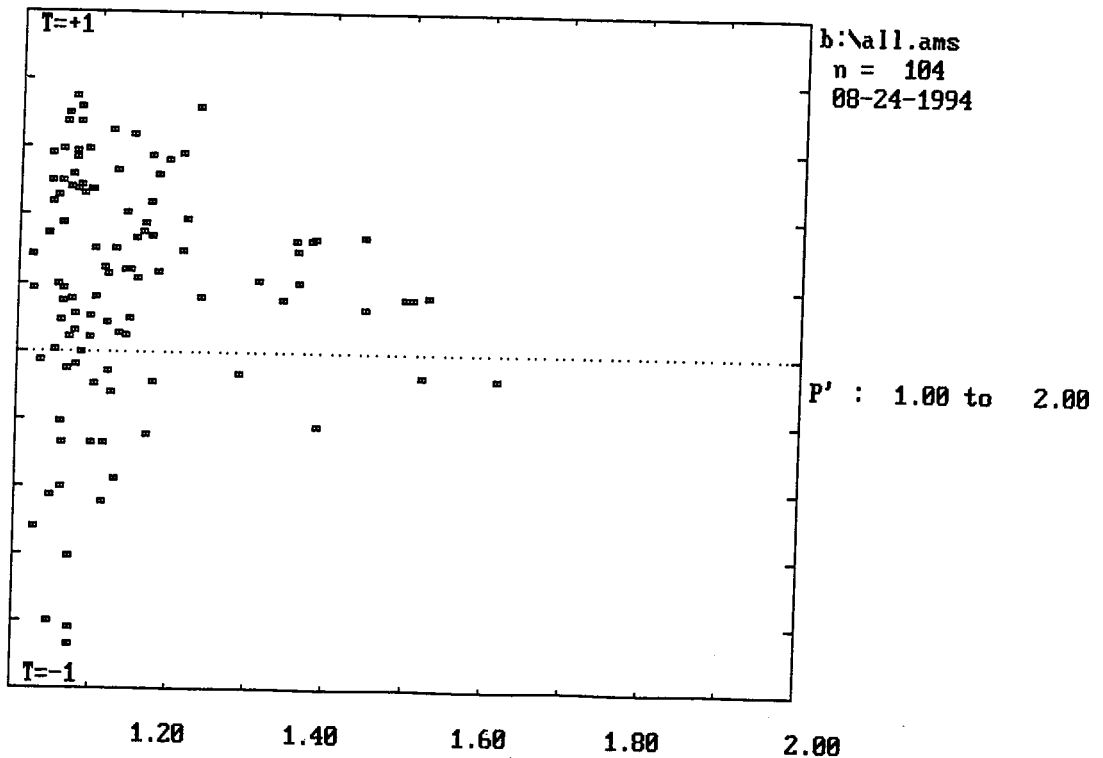

Figure 8.15. The Jelinek diagram of the Moss Lake stock fabric parameters reflects the trend towards "disk-shaped" magnetic susceptibility ellipsoids.

the stock samples. For the purposes of this study, the [N] value (Fig. A.8; a demagnetizing factor of shape effect) is of critical importance in that it allows shape comparison of the magnetic susceptibility ellipsoids of the Moss Lake stock rock fabric. Deformation, in part, involves change in shape of rock fabric. This shape comparison is made by Carmichael (1982) as the ratio [p/q] on Figure A.8.

Carmichael (1982) tabulates the relationship between the dimension ratio [p/q] (where p/q<1 represents an oblate ellipsoid, p=q=r for a sphere and p/q>1 represents a prolate ellipsoid; see Figs. A.2, A.8) and the demagnetizing factor [N] (shape effect) for an ellipsoid (Fig. B.16). Presumably, the [kmax] and [kmin] ratios accurately represent grain-shape ratios, where the maximum and minimum principal susceptibility directions are [kmax=p] and [kmin=q], respectively. Also assumed is homogenous magnetization. The values of [kmax] and [kmin] are averaged here only to produce a method of comparison, ie. to use the [p/q] ratio. The pattern of individual AMS measurements is presented in Section IV.

The mean values of [kmax] and [kmin] for the Moss Lake stock are 1.065 and 0.934, respectively. The mean kmax/kmin ratio [p/q] for the Moss Lake stock is 1.140. Since this value is greater than 1, the (mean) ellipsoid for Moss Lake stock samples is prolate in shape.

The relationship between dimension ratios [p/q] and the demagnetizing factors (shape effects) is shown in Figure B.17. The graphed line represents data from the "ellipsoid" column of

dimension ratio p/q*	ellipsoid**	cylinder***	prism****
0.01	0.9845	0.965	0.966
0.1	0.8608	0.7967	0.8051
0.2	0.7505	0.6802	0.6942
0.4	0.5882	0.5281	0.5482
0.8	0.3944	0.3619	0.3843
1	0.3333	0.3116	0.3333
2	0.1736	0.1819	0.1983
3	0.1087	0.1278	0.1404
4	0.0754	0.0984	0.1085
6	0.0432	0.0673	0.0745
8	0.0284	0.0511	0.0567
10	0.0203	0.0412	0.0457
100	0.00043	0.00423	0.00472

Figure 8.16. Demagnetizing factors, as Na/4pi, for ellipsoids, cylinders and rectangular prisms. *Dimension ratio is p/q for ellipsoid (p/q<1 for oblate ellipsoid, p=q=r for sphere, p/q>1 for prolate ellipsoid), h/dia. for cylinder of length h, and h/w for rectangular prism of length h and width w. **From Stoner, E.C., Philos. Mag., 36, 803, 1945; and Osborn, J.A., Phys. Rev., 67, 351, 1945. Ellipsoid can have uniform magnetization, and thus uniform demagnetizing field. *** From Joseph, R.I., Geophysics, 41, 1052, 1976; calculated using "magnometric" method, averaging the spatially varying demagnetizing factor over the volume of the sample. Sample assumed to be uniformly magnetized. **** Sphere (see ellipsoid column), Na=4pi/3 = 0.3333*4pi. (After Carmichael, 1982).
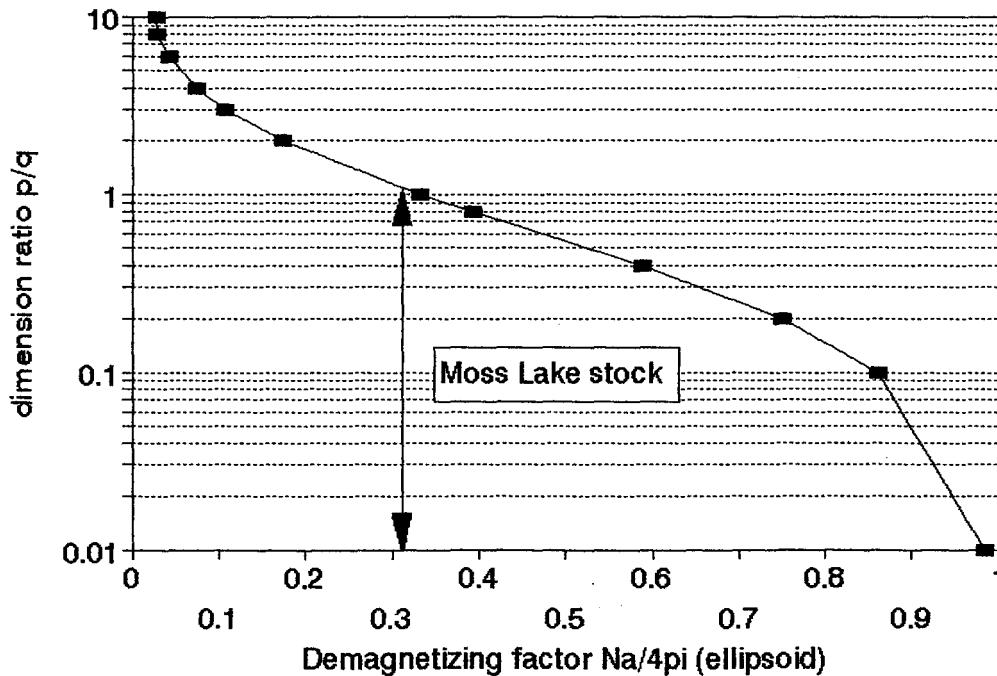
Figure 8.17. Relationship of demagnetizing factor to dimension ratio. The Moss Lake stock [p/q] ratio is 1.144 so Na/4pi=0.31; N=3.895 (using data from Fig. 8.16).

Carmichael's (1982) table (Fig. B.16), where [N], represented as Na/4pi is plotted against the dimension ratio [p/q]. The arrow (in Fig. B.17) shows that the dimension ratio [p/q] of 1.140 has a demagnetizing factor Na/4pi of approximately 0.31. Therefore, the [N] value is approximately 3.895 for the Moss Lake stock (as compared to the common [N] value of 3.9 for igneous rocks (Stacey and Banerjee, 1974)).

The fabric plots also reveal the influence of deformation mechanisms which are not compensated for in the bulk magnetic susceptibility calculation. Considering the overwhelming number and complexity of potential factors which influence magnetic susceptibility, it is encouraging that the calculation is accurate to within 0.001 SI units (2% magnetite, N=3.9). With this calculation, a crude estimate of magnetite content can be derived for each Moss Lake stock sample by comparing measured bulk magnetic susceptibilities (refer to AMS section IV) to the calculated mean.

APPENDIX C

STRUCTURAL GEOLOGY FIELD MEASUREMENTS

Moss/Ames Twp. Bedding Data (S0)
Quetico Metasedimentary Belt

outcrop	strike	dip
6	246	72
7	240	74
8	230	75
9	244	72
10	248	90
11	244	84
12	232	60
13	226	66
14	228	85
15	228	85
16	230	88
17	244	86
18	244	80
19	244	88
20	250	78
21	245	80
22	246	80
23	248	76
25	252	87
26	244	66
27	214	90
28	221	82
29	236	86
30	240	86
31	246	80
32	250	84
33	253	82
39	242	82
40	240	86
41	242	88
42	242	88
43	242	78
44	244	88

outcrop	strike	dip
45	244	84
46	224	84
47	220	78
48	228	74
49	242	90
50	238	86
51	242	85
52	230	80
53	256	88
54	258	76
55	256	85
56	254	85
57	252	87
58	252	88
60	242	90
61	244	85
62	248	85
63	248	85
64	250	90
65	250	90
70	250	90
71	246	85
72	254	90
73	254	90
74	252	90
75	244	90
76	244	90
77	252	89
78	244	86
79	246	88
84	256	68
85	256	70
86	254	80

Refer to map insert B for outcrop locations and Figures 1.3A,B for stereographic projection of these measurements. Note that dip direction = strike plus 90 degrees, ie. "right hand rule". Selected measurements are shown on map insert B.

Moss/Ames Twp. Cleavage (S1) Data
Quetico Metasedimentary Belt

outcrop	strike	dip
7	250	80
8	76	82
9	258	90
10	256	84
11	256	64
12	238	80
13	256	74
14	250	86
15	252	70
16	68	84
17	246	76
18	78	88
20	76	88
21	250	79
22	74	82
23	70	87
25	66	84
26	244	66
28	38	70
29	52	74
31	54	62
32	70	70
33	74	82
39	242	82
40	240	86
41	242	88
42	242	88
43	242	78
44	244	88
45	54	70
46	224	84

outcrop	strike	dip
47	220	78
48	43	80
49	43	80
50	58	86
51	64	70
52	56	85
53	82	86
54	70	78
55	70	70
56	72	88
57	72	88
58	72	88
60	64	72
61	64	74
62	68	85
63	68	85
64	70	90
65	66	90
70	68	80
71	72	82
72	68	85
74	72	85
75	60	70
76	62	85
77	72	90
78	60	88
79	66	90
83	74	78
84	56	88
85	78	90
86	76	78

Refer to map insert B for outcrop locations and Figures 1.3C,D for stereographic projection of these measurements. Note that dip direction = strike plus 90 degrees, ie. "right hand rule". Selected measurements are shown on map insert B.

APPENDIX D

A.F. DEMAGNETIZATION
(DATA, STEREOGRAPHIC PROJECTIONS, PCAs)

A.f. demagnetization data

sample	date	time	declination	inclination	mA/m	cm3	demag	error %
sy1bn	04-06-1994	14:51	34.87	49.4	21.2	11.15	0	0.4
sy1bn	04-06-1994	15:08	32.59	48.18	20.6	11.15	0.5	0.2
sy1bn	04-06-1994	15:10	35.52	48.2	20.6	11.15	0.8	0.2
sy1bn	04-06-1994	15:12	34.73	48.36	20.6	11.15	1	0.4
sy1bn	04-06-1994	15:14	26.63	47.44	18.8	11.15	2	0.3
sy1bn	04-06-1994	15:16	33.11	47.18	17.1	11.15	3	0.3
sy1bn	04-06-1994	15:18	29.59	46.6	16	11.15	4	0.4
sy1bn	04-06-1994	15:20	29.69	45.83	14.99	11.15	5	0.4
sy1bn	04-06-1994	15:24	27.31	42.07	11.72	11.15	10	0.3
sy1bn	04-06-1994	15:27	24.37	38.65	9.57	11.15	15	0.3
sy1bn	04-06-1994	15:29	25.66	34.08	6.36	11.15	30	0.5
sy1bn	04-06-1994	15:35	20.36	30.67	4.86	11.15	40	0.6
sy1bn	04-06-1994	15:38	16.23	24.18	4.13	11.15	50	8.3
sy1bn	04-06-1994	15:40	13.19	22.05	4.17	11.15	60	5.9
sy1bn	04-06-1994	15:45	20.7	22.71	3.77	11.15	70	8
sy1bn	04-06-1994	15:51	23.37	36.07	1.661	11.15	80	4.5
sy2bn	04-22-1994	12:10	318.88	76.27	61.556	11.15	0	0.4
sy2bn	04-22-1994	12:10	318.29	66.78	49.945	11.15	0.5	0.4
sy2bn	04-22-1994	12:10	318.17	65.56	49.315	11.15	0.8	0.2
sy2bn	04-22-1994	12:10	317.19	64.14	46.562	11.15	1	0.2
sy2bn	04-22-1994	12:10	316.07	63.38	33.78	11.15	2	0.4
sy2bn	04-22-1994	12:10	324.56	60.41	27.597	11.15	3	0.2
sy2bn	04-22-1994	12:10	318.14	56.67	23.458	11.15	4	0.5
sy2bn	04-22-1994	12:10	308.65	54.9	20.044	11.15	5	0.5
sy2bn	04-22-1994	12:10	326.4	58.74	12.47	11.15	10	0.5
sy2bn	04-22-1994	12:10	285.73	27.5	9.311	11.15	20	1.7
sy2bn	04-22-1994	12:10	312.23	27.23	6.425	11.15	30	0.7
sy2bn	04-22-1994	12:10	305.98	-24.35	6.986	11.15	40.1	1.5
sy2bn	04-22-1994	12:10	322.26	-17.54	4.747	11.15	50	2.3
sy3bn	04-06-1994	13:49	107.23	21.38	32.2	11.15	0	0.6
sy3bn	04-06-1994	13:52	106.55	19.77	31.3	11.15	0.5	0.5
sy3bn	04-06-1994	13:54	104.7	19.34	31.2	11.15	0.8	0.6
sy3bn	04-06-1994	13:56	107	19.21	30.7	11.15	1	0.5
sy3bn	04-06-1994	13:58	95.67	27.7	25.9	11.15	2	0.6
sy3bn	04-06-1994	13:59	85.87	29	20.8	11.15	3	0.6
sy3bn	04-06-1994	14:01	79.01	24.99	18.1	11.15	4	0.7

A.f. demagnetization data

sample	date	time	declination	inclination	mA/m	cm3	demag	error %
sy3bn	04-06-1994	14:04	76.15	19.84	16.8	11.15	5	1
sy3bn	04-06-1994	14:05	71.98	3.21	13.63	11.15	10	0.7
sy3bn	04-06-1994	14:10	72.25	-7.32	13.59	11.15	15	0.9
sy3bn	04-06-1994	14:12	70.67	-15.37	13.41	11.15	20	0.8
sy3bn	04-06-1994	14:14	76.42	-16.4	10.85	11.15	30	1.2
sy3bn	04-06-1994	14:16	69.49	-11.89	8.95	11.15	40	1.4
sy3bn	04-06-1994	14:18	98.86	-19.49	8.81	11.15	50	1.5
sy3bn	04-06-1994	14:21	71.81	-11.8	8.02	11.15	60	1.5
sy3bn	04-06-1994	14:24	97.38	-4.81	7.67	11.15	70	1.5
sy8bn	03-23-1994	14:50	88.53	83.59	69.936	11.15	0	0.5
sy8bn	03-23-1994	14:50	80.69	79.02	61.729	11.15	0.5	0.3
sy8bn	03-23-1994	14:50	82.14	81.5	59.452	11.15	0.8	0.3
sy8bn	03-23-1994	14:50	77	77.98	57.664	11.15	1	0.3
sy8bn	03-23-1994	14:50	48.48	80.44	49.08	11.15	2	0.3
sy8bn	03-23-1994	14:50	27.18	79.17	44.288	11.15	3	0.3
sy8bn	03-23-1994	14:50	5.87	80.18	40.087	11.15	4	0.3
sy8bn	03-23-1994	14:50	355.54	78.2	37.797	11.15	5	0.3
sy8bn	03-23-1994	14:50	336.44	73.8	30.51	11.15	10	0.4
sy8bn	03-23-1994	14:50	327.09	67.12	26.048	11.15	15	0.3
sy8bn	03-23-1994	14:50	339.96	65.47	24.62	11.15	20	0.2
sy8bn	03-23-1994	14:50	317.41	58.02	18.979	11.15	30	0.5
sy8bn	03-23-1994	14:50	306.33	59.28	13.318	11.15	40	0.9
sy8bn	03-23-1994	14:50	301.3	49.51	17.486	11.15	50	0.7
sy8bn	03-23-1994	14:50	306.99	46.16	11.949	11.15	60	0.2
sy9bn	03-29-1994	16:48	76.21	17.27	116.5	11.15	0	0.3
sy9bn	03-29-1994	16:51	76.68	16.03	112.7	11.15	0.5	0.1
sy9bn	03-29-1994	16:54	75.57	15.61	112.9	11.15	0.8	0.2
sy9bn	03-29-1994	16:56	74.58	15.27	112.5	11.15	1	0.1
sy9bn	03-29-1994	16:58	68.54	26.35	91.6	11.15	2	0.2
sy9bn	03-29-1994	17:00	64.75	37.2	79.4	11.15	3	0.3
sy9bn	03-29-1994	17:01	65.02	45.45	73.5	11.15	4	0.3
sy9bn	03-29-1994	17:03	64.3	51.16	68.2	11.15	5	0.4
sy9bn	03-29-1994	17:05	52.33	61.33	50.8	11.15	10	0.5
sy9bn	03-29-1994	17:07	50.77	63.55	39.4	11.15	15	0.6
sy9bn	03-29-1994	17:09	49.73	64.04	33.1	11.15	20	0.5
sy9bn	03-29-1994	17:11	57.21	69.36	21.9	11.15	30	0.7

A.f. demagnetization data

sample	date	time	declination	inclination	mA/m	cm3	demag	error %
sy9bn	03-29-1994	17:13	65.7	72.15	17.4	11.15	40	0.7
sy9bn	03-29-1994	17:15	6.87	79.69	10.46	11.15	50	3.3
sy9bn	03-29-1994	17:17	24.69	79.73	10.06	11.15	60	2.5
sy9bn	03-29-1994	17:20	316.17	75.32	6.44	11.15	70	3.6
sy9bn	03-29-1994	17:22	294.45	51.46	5.95	11.15	80	1.4
sy10bn	03-29-1994	11:21	102.75	11.15	48.6	11.15	0	0.3
sy10bn	03-29-1994	11:26	101.74	9.65	47.6	11.15	0.5	0.1
sy10bn	03-29-1994	11:28	103.31	9.55	47.5	11.15	0.8	0.3
sy10bn	03-29-1994	11:31	102.84	8.95	45.9	11.15	1	0.3
sy10bn	03-29-1994	11:34	99.04	9.14	38.5	11.15	2	0.2
sy10bn	03-29-1994	11:36	96.21	20.66	21.2	11.15	3	0.3
sy10bn	03-29-1994	11:38	80.19	39.15	13.85	11.15	4	0.3
sy10bn	03-29-1994	11:41	66.82	49.34	11.67	11.15	5	0.3
sy10bn	03-29-1994	11:43	15.84	55.52	8.53	11.15	10	0.3
sy10bn	03-29-1994	11:45	359.46	54.44	7.34	11.15	15	0.2
sy10bn	03-29-1994	11:48	2.63	64.76	5.31	11.15	20	8.9
sy10bn	03-29-1994	11:50	357.23	63.1	4.58	11.15	30	8.3
sy10bn	03-29-1994	11:55	349.2	73.59	3.98	11.15	40	0.5
sy10bn	03-29-1994	11:58	338.21	73.08	3.66	11.15	50	0.9
sy10bn	03-29-1994	12:00	22.79	70.93	3.52	11.15	60	1
sy10bn	03-29-1994	12:03	12.88	74.89	3.57	11.15	70	0.9
sy15bn	03-29-1994	13:42	2.63	-15.22	55.2	11.15	0	0.3
sy15bn	03-29-1994	13:46	2.31	-23.59	55.3	11.15	0.5	0.2
sy15bn	03-29-1994	13:48	4.32	-24.04	55.2	11.15	0.8	0.3
sy15bn	03-29-1994	13:50	3.27	-25.14	55	11.15	1	0.2
sy15bn	03-29-1994	13:53	2.13	-29.97	54.3	11.15	2	0.4
sy15bn	03-29-1994	13:55	356.22	-33.17	50.8	11.15	3	0.3
sy15bn	03-29-1994	13:57	0.37	-36.95	47.4	11.15	4	0.4
sy15bn	03-29-1994	13:59	354.58	-40.81	42	11.15	5	0.4
sy15bn	03-29-1994	14:02	343.02	-61.86	26.2	11.15	10	0.6
sy15bn	03-29-1994	14:04	325.06	-69.84	19.6	11.15	15	0.7
sy15bn	03-29-1994	14:07	344.32	-76.55	13.28	11.15	20	0.6
sy15bn	03-29-1994	14:09	202.69	-80.36	8.92	11.15	30	1
sy15bn	03-29-1994	14:12	321.01	-83.23	7.03	11.15	40	1.1

A.f. demagnetization data

sample	date	time	declination	inclination	mA/m	cm3	demag	error %
sy16bn	04-06-1994	10:09	342.56	56.19	187	11.15	0	0.4
sy16bn	04-06-1994	10:11	344	57.37	173	11.15	0.5	0.2
sy16bn	04-06-1994	10:13	345.95	57.39	169	11.15	0.8	0.2
sy16bn	04-06-1994	10:15	343.11	58.24	160	11.15	1	1
sy16bn	04-06-1994	10:18	344.44	58.46	145	11.15	2	0.3
sy16bn	04-06-1994	10:19	345.1	59.07	132	11.15	3	0.4
sy16bn	04-06-1994	10:21	339.9	59.19	123.2	11.15	4	0.3
sy16bn	04-06-1994	10:23	339.86	58.76	115.4	11.15	5	0.4
sy16bn	04-06-1994	10:29	340.47	58.47	87.5	11.15	10	0.2
sy16bn	04-06-1994	10:31	340.35	57.03	71.3	11.15	15	0.2
sy16bn	04-06-1994	10:33	337.4	55.25	60	11.15	20	0.2
sy16bn	04-06-1994	10:35	333.17	57.51	45.5	11.15	30	0.5
sy16bn	04-06-1994	10:37	335.51	59.07	34.7	11.15	40	0.5
sy16bn	04-06-1994	10:39	322.89	60.19	31.1	11.15	50	0.6
sy16bn	04-06-1994	10:41	323.96	56.83	25.6	11.15	60	0.5
sy16bn	04-06-1994	10:57	327.63	58.28	22.6	11.15	70	0.5
sy16bn	04-06-1994	11:00	324.83	55.06	21.2	11.15	80	0.8
sy19bn	04-05-1994	11:44	23.78	60.27	43.7	11.15	0	0.2
sy19bn	04-05-1994	11:47	20.76	61.66	40.1	11.15	0.5	0.1
sy19bn	04-05-1994	11:50	23.01	62.51	39.9	11.15	0.8	0.2
sy19bn	04-05-1994	11:52	26.2	62.5	38.4	11.15	1	0.3
sy19bn	04-05-1994	11:55	18.07	63.56	35	11.15	2	0.1
sy19bn	04-05-1994	11:57	15.66	63.08	32	11.15	3	0.1
sy19bn	04-05-1994	11:59	7.33	64.55	28.6	11.15	4	0.2
sy19bn	04-05-1994	12:01	6.22	64.75	26.7	11.15	5	0.1
sy19bn	04-05-1994	12:03	4.53	67.12	18.3	11.15	10	0.2
sy19bn	04-05-1994	12:05	2.2	65.4	13.42	11.15	15	0.2
sy20bn	04-22-1994	12:12	8	72.88	13.173	11.15	0	0.5
sy20bn	04-22-1994	12:12	8.51	72.34	12.467	11.15	0.8	0.5
sy20bn	04-22-1994	12:12	11.81	72.36	12.413	11.15	1	0.5
sy20bn	04-22-1994	12:12	4.15	74.14	11.122	11.15	2	0.5
sy20bn	04-22-1994	12:12	7.93	77.18	9.147	11.15	3	3.8
sy20bn	04-22-1994	12:12	358.72	77.23	8.151	11.15	4	2.9
sy20bn	04-22-1994	12:12	354.96	77.66	7.472	11.15	5	1.9
sy20bn	04-22-1994	12:12	353.32	77.47	5.152	11.15	10	0.8

A.f. demagnetization data

sample	date	time	declination	inclination	mA/m	cm3	demag	error %
sy20bn	04-22-1994	12:12	2.98	78.39	4.777	11.15	15	0.9
sy20bn	04-22-1994	12:12	17.55	77.1	4.606	11.15	20	1
sy20bn	04-22-1994	12:12	8.25	71.25	4.118	11.15	30	1.5
sy21bn	04-05-1994	13:16	98.6	29.13	196	11.15	0	0.2
sy21bn	04-05-1994	13:18	99.52	23.12	183	11.15	0.5	0.3
sy21bn	04-05-1994	13:20	100.29	23.1	182	11.15	0.8	0.3
sy21bn	04-05-1994	13:22	99.99	22.06	179	11.15	1	0.4
sy21bn	04-05-1994	13:24	99.48	18.41	148	11.15	2	0.4
sy21bn	04-05-1994	13:26	98.92	17.81	121.5	11.15	3	0.3
sy21bn	04-05-1994	13:28	99.11	19.35	96.3	11.15	4	0.4
sy21bn	04-05-1994	13:30	97.44	21.4	79.6	11.15	5	0.2
sy21bn	04-05-1994	13:32	94.16	34.43	39.2	11.15	10	0.5
sy21bn	04-05-1994	13:34	88.24	42.22	26.4	11.15	15	0.7
sy21bn	04-05-1994	13:36	90.12	56.31	20.7	11.15	20	0.8
sy21bn	04-05-1994	13:38	128.48	69.67	16.9	11.15	30	0.3
sy21bn	04-05-1994	13:40	115.81	59.31	13.74	11.15	40	0.8
sy21bn	04-05-1994	13:42	190.42	86.77	14.7	11.15	50	0.6
sy22an	04-06-1994	11:32	65.28	71.58	3170	11.15	0	0.3
sy22an	04-06-1994	11:47	65.73	71.32	3080	11.15	0.5	0.5
sy22an	04-06-1994	12:28	64.59	71.39	3070	11.15	0.8	0.4
sy22an	04-06-1994	12:31	62.9	71.49	3050	11.15	1	0.4
sy22an	04-06-1994	12:32	61.08	71.08	2830	11.15	2	0.5
sy22an	04-06-1994	12:35	55.36	73.09	2460	11.15	3	0.4
sy22an	04-06-1994	12:37	49.91	74.16	2160	11.15	4	0.5
sy22an	04-06-1994	12:39	47.24	75.15	1930	11.15	5	0.5
sy22an	04-06-1994	12:41	34.68	78.34	1104	11.15	10	0.3
sy22an	04-06-1994	12:43	21.01	79.77	735	11.15	15	0.3
sy22an	04-06-1994	12:45	11.08	80.86	538	11.15	20	0.4
sy22an	04-06-1994	12:47	352.8	82.39	328	11.15	30	0.4
sy22an	04-06-1994	12:49	316.22	80.31	216	11.15	40	0.6
sy22an	04-06-1994	12:53	305.2	74.91	142	11.15	50	0.9
sy22an	04-06-1994	13:08	292.17	79.15	99.3	11.15	60	0.9
sy22an	04-06-1994	13:10	292.42	70.49	71.4	11.15	70	1.1
sy22an	04-06-1994	13:13	265.26	73.43	65.8	11.15	80	1.4
sy22an	04-06-1994	13:15	280.44	53.63	48.3	11.15	90	1.5

A.f. demagnetization data

sample	date	time	declination	inclination	mA/m	cm3	demag	error %
sy22an	04-06-1994	13:18	251.36	58.49	42.8	11.15	100	1.7
sy22an	04-06-1994	13:21	261.83	43.62	32.1	11.15	120	2.4
sy22an	04-06-1994	13:24	265.03	21.45	27	11.15	140	2.8
sy22an	04-06-1994	13:27	267.81	49.98	19.7	11.15	160	4
sy23bn	04-05-1994	14:23	304.41	35.85	3250	11.15	0	0.2
sy23bn	04-05-1994	14:26	304.8	35.48	3230	11.15	0.5	0.1
sy23bn	04-05-1994	14:28	300.55	35.42	3230	11.15	0.8	0.1
sy23bn	04-05-1994	14:30	301.39	35.63	3230	11.15	1	0.2
sy23bn	04-05-1994	14:32	301.59	35.6	3160	11.15	2	0.2
sy23bn	04-05-1994	14:34	301.24	35.34	3020	11.15	3	0.1
sy23bn	04-05-1994	14:36	300.23	34.97	2890	11.15	4	0
sy23bn	04-05-1994	14:38	302.42	34.82	2740	11.15	5	0.3
sy23bn	04-05-1994	14:41	300.94	34.39	2060	11.15	10	0.1
sy23bn	04-05-1994	14:43	302.86	33.78	1521	11.15	15	0.1
sy23bn	04-05-1994	14:44	302.05	33.55	1113	11.15	20	0
sy23bn	04-05-1994	14:46	303.73	33.17	577	11.15	30	0.1
sy23bn	04-05-1994	14:48	301.12	33.05	325	11.15	40	0.3
sy23bn	04-05-1994	14:50	299.68	32.92	189	11.15	50	0.3
sy23bn	04-05-1994	14:53	300.39	33.11	119.1	11.15	60	0.2
sy23bn	04-05-1994	14:55	295.02	36.43	78.4	11.15	70	0.3
sy23bn	04-05-1994	14:57	302.74	38.25	55.7	11.15	80	0.4
sy26bn	03-28-1994	13:12	284.47	55.74	280	11.15	0	0.3
sy26bn	03-28-1994	13:15	283.81	54.79	275	11.15	0.5	0.2
sy26bn	03-28-1994	13:17	283.07	54.79	275	11.15	0.8	0.2
sy26bn	03-28-1994	13:20	280.87	55.09	273	11.15	1	0.3
sy26bn	03-28-1994	13:23	279.17	55.06	257	11.15	2	0.4
sy26bn	03-28-1994	13:26	278.38	55.7	234	11.15	3	0.3
sy26bn	03-28-1994	13:28	277.53	56.37	205	11.15	4	0.5
sy26bn	03-28-1994	13:31	277.43	56.21	180	11.15	5	0.2
sy26bn	03-28-1994	13:33	279.91	56.65	94.5	11.15	10	0.3
sy26bn	03-28-1994	13:35	284.45	56.23	60.2	11.15	15	0.2
sy26bn	03-28-1994	13:45	287.82	55.95	26.5	11.15	30	0.5
sy26bn	03-28-1994	13:48	287.82	62.97	20.5	11.15	40	0.2
sy26bn	03-28-1994	14:02	290.16	56.95	14.63	11.15	60	0.2
sy26bn	03-28-1994	14:05	266.47	55.5	11.33	11.15	70	0.2

A.f. demagnetization data

sample	date	time	declination	inclination	mA/m	cm3	demag	error %
sy26bn	03-28-1994	14:08	288.85	53.77	8.06	11.15	80	0.2
sy27bn	03-29-1994	15:32	30.79	-35.62	2490	11.15	0	0.4
sy27bn	03-29-1994	15:35	30.67	-36.02	2500	11.15	0.5	0.3
sy27bn	03-29-1994	15:38	27.25	-36.18	2510	11.15	0.8	0.2
sy27b	03-29-1994	15:40	27.88	-36.18	2510	11.15	1	0.3
sy27bn	03-29-1994	15:42	29.19	-36.52	2480	11.15	2	0.3
sy27bn	03-29-1994	15:44	27.56	-36.35	2380	11.15	3	0.4
sy27bn	03-29-1994	15:46	28.3	-35.97	2200	11.15	4	0.6
sy27bn	03-29-1994	15:48	25.93	-36.14	1960	11.15	5	0.3
sy27bn	03-29-1994	15:50	26.04	-34.99	1020	11.15	10	0.2
sy27bn	03-29-1994	15:53	29.97	-34.59	502	11.15	15	0.3
sy27bn	03-29-1994	15:55	32.03	-34.22	266	11.15	20	0.4
sy27bn	03-29-1994	15:59	32.2	-33.18	105.2	11.15	30	0.4
sy27bn	03-29-1994	16:04	37.85	-33.21	58.4	11.15	40	0.4
sy27bn	03-29-1994	16:07	39.92	-28.89	34.2	11.15	50	0.4
sy27bn	03-29-1994	16:10	35.6	-30.3	28.8	11.15	60	0.3
sy27bn	03-29-1994	16:12	39	-26.18	20.6	11.15	70	0.7
sy27bn	03-29-1994	16:15	32.24	-32.49	17.16	11.15	80	0.6
sy27bn	03-29-1994	16:18	34.71	-31.98	14.64	11.15	90	0.5

Lwr.Hem.Equal Area Net
circle=DOWN square=UP
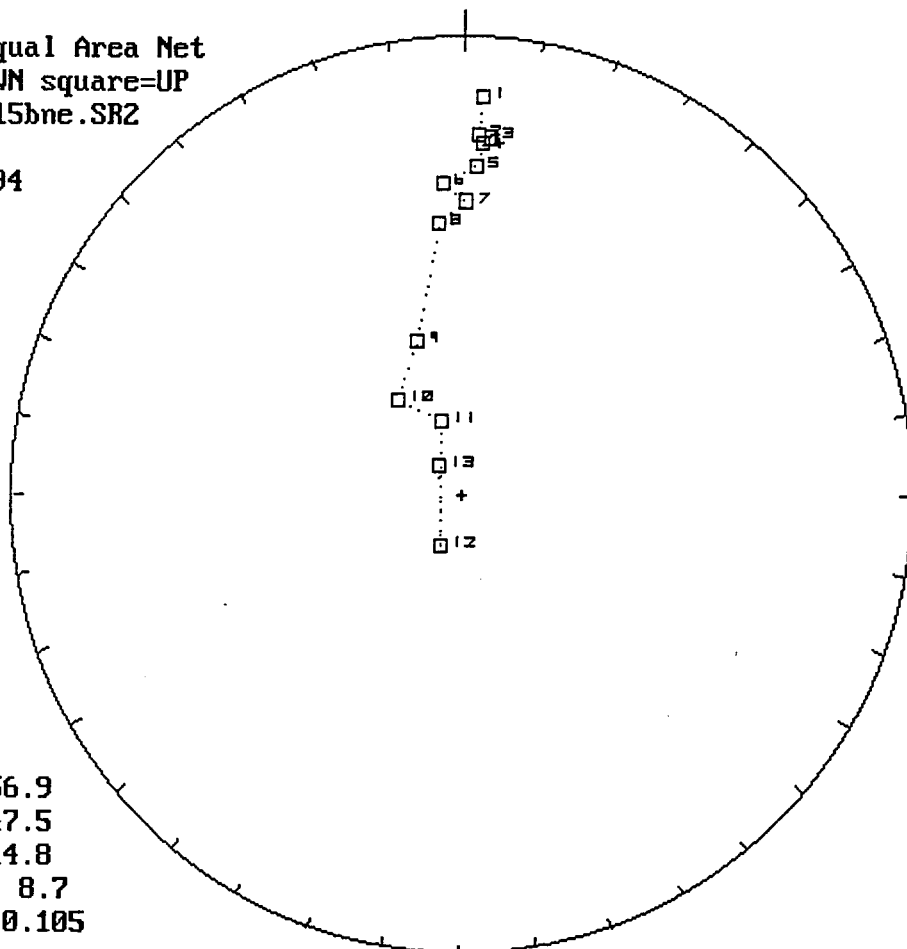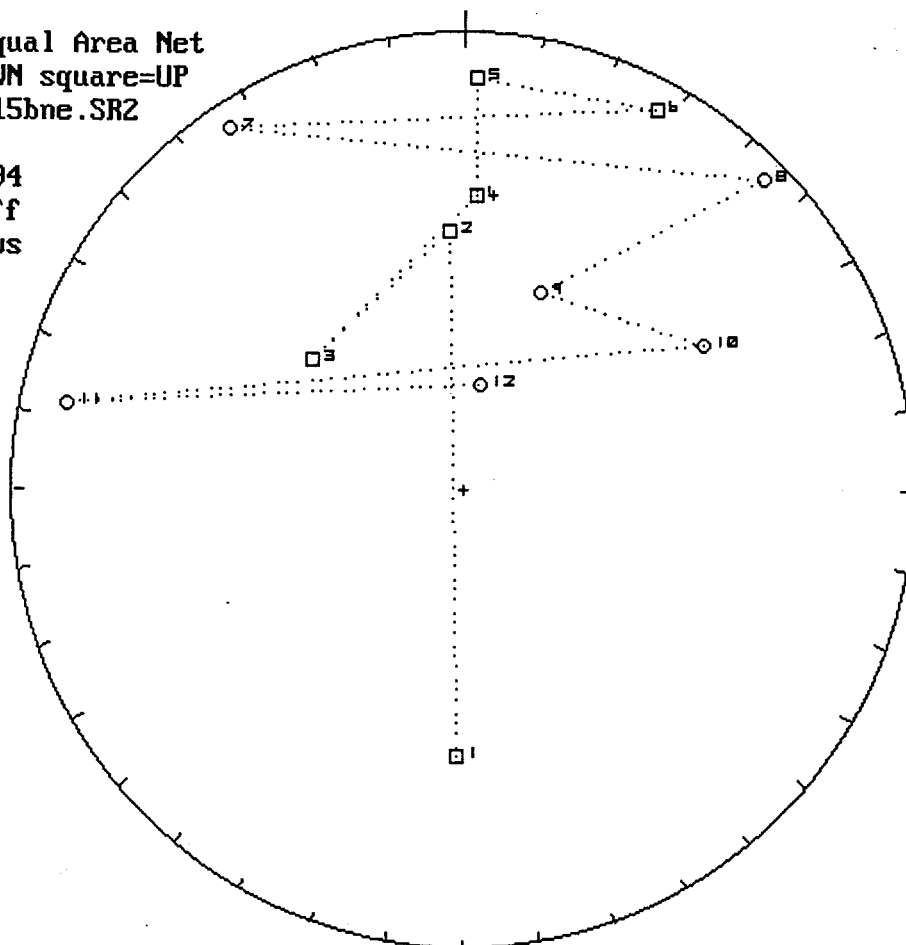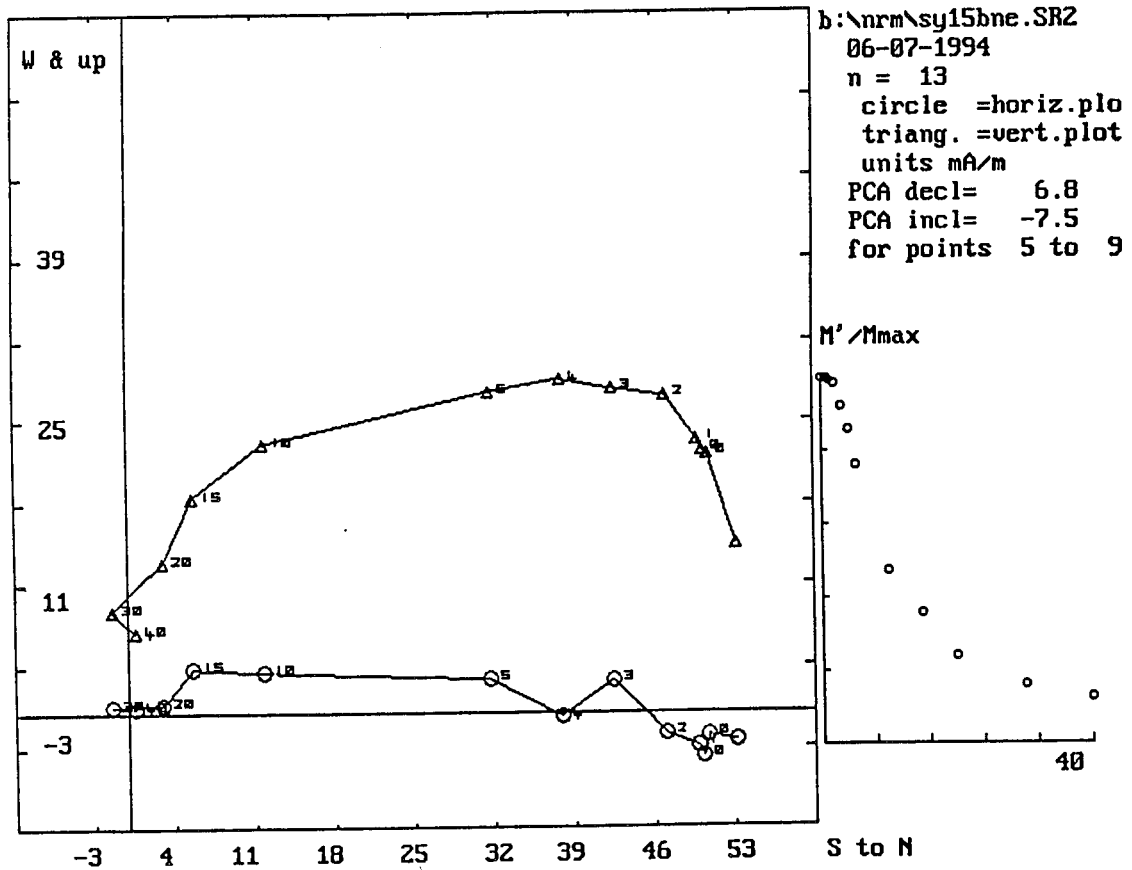 b:\nrm\sy1bne.SR2
 n = 16
 06-07-1994
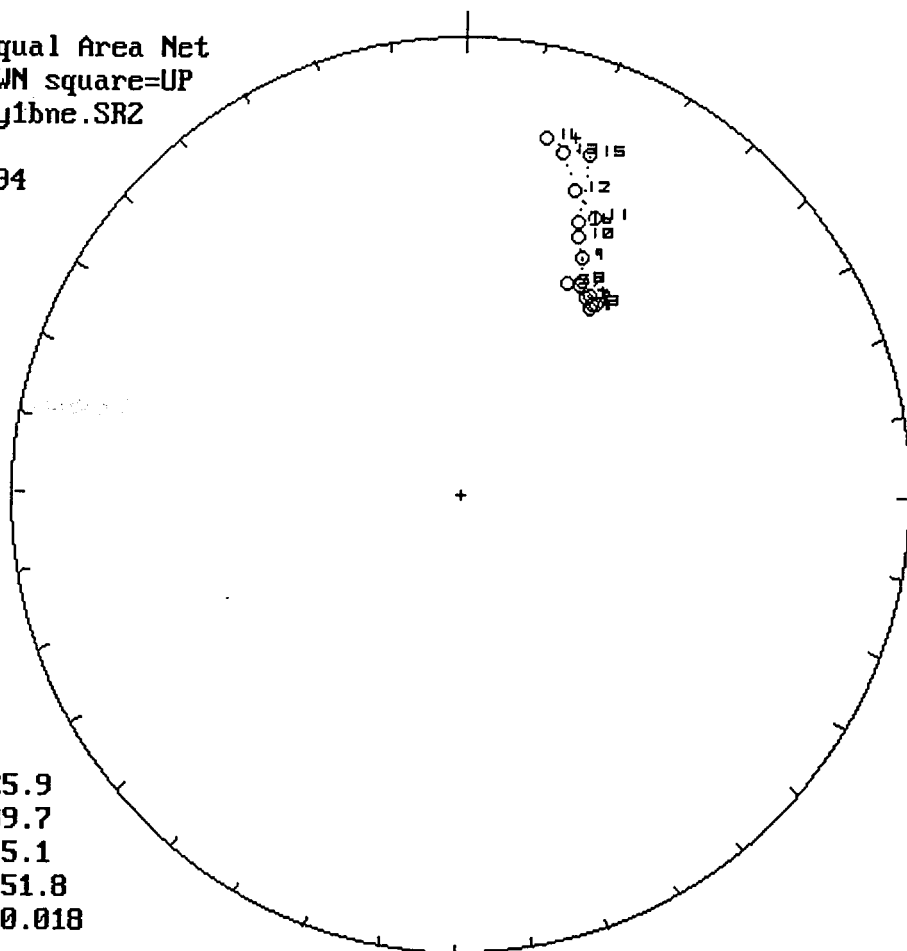
m.dec.= 25.9
m.inc.= 39.7
alpha95= 5.1
Fish. k= 51.8
sp.var.= 0.018

Lwr.Hem.Equal Area Net
circle=DOWN square=UP
 b:\nrm\sy1bne.SR2
 n = 15
 06-07-1994
Vector Diff
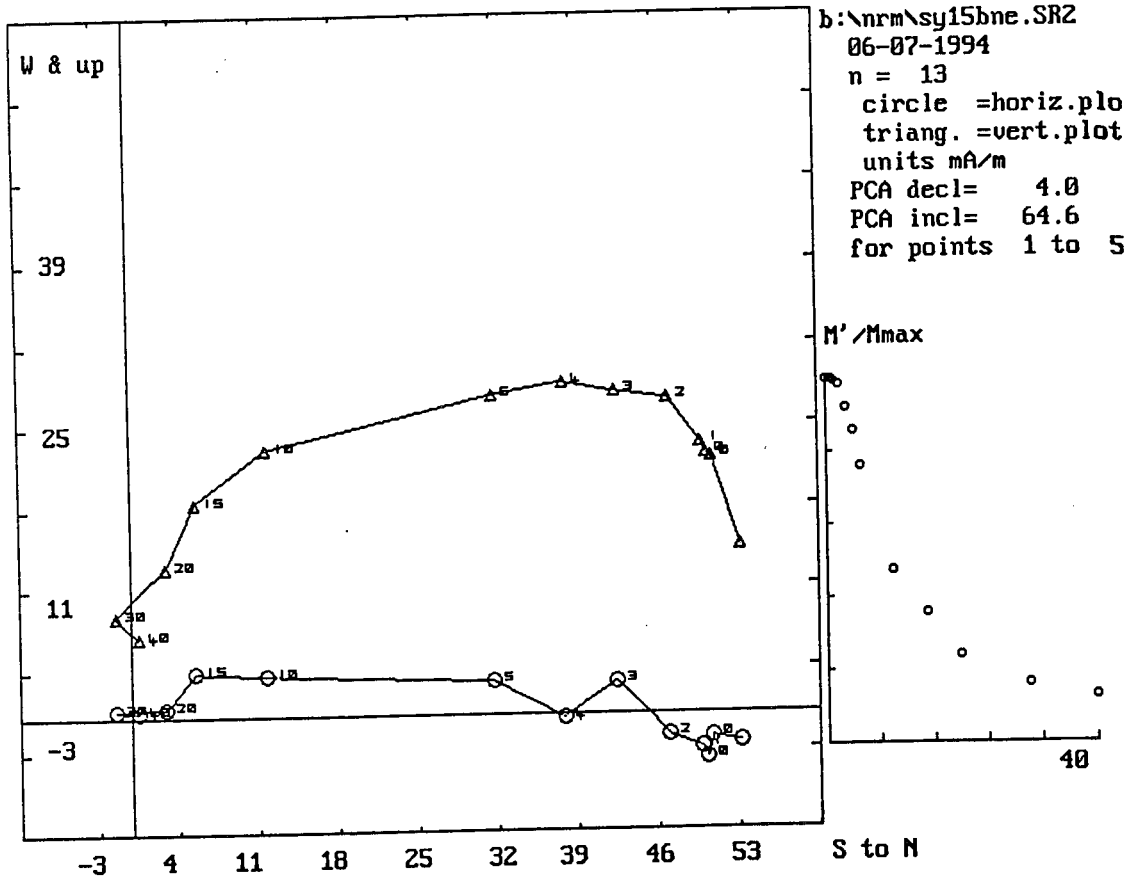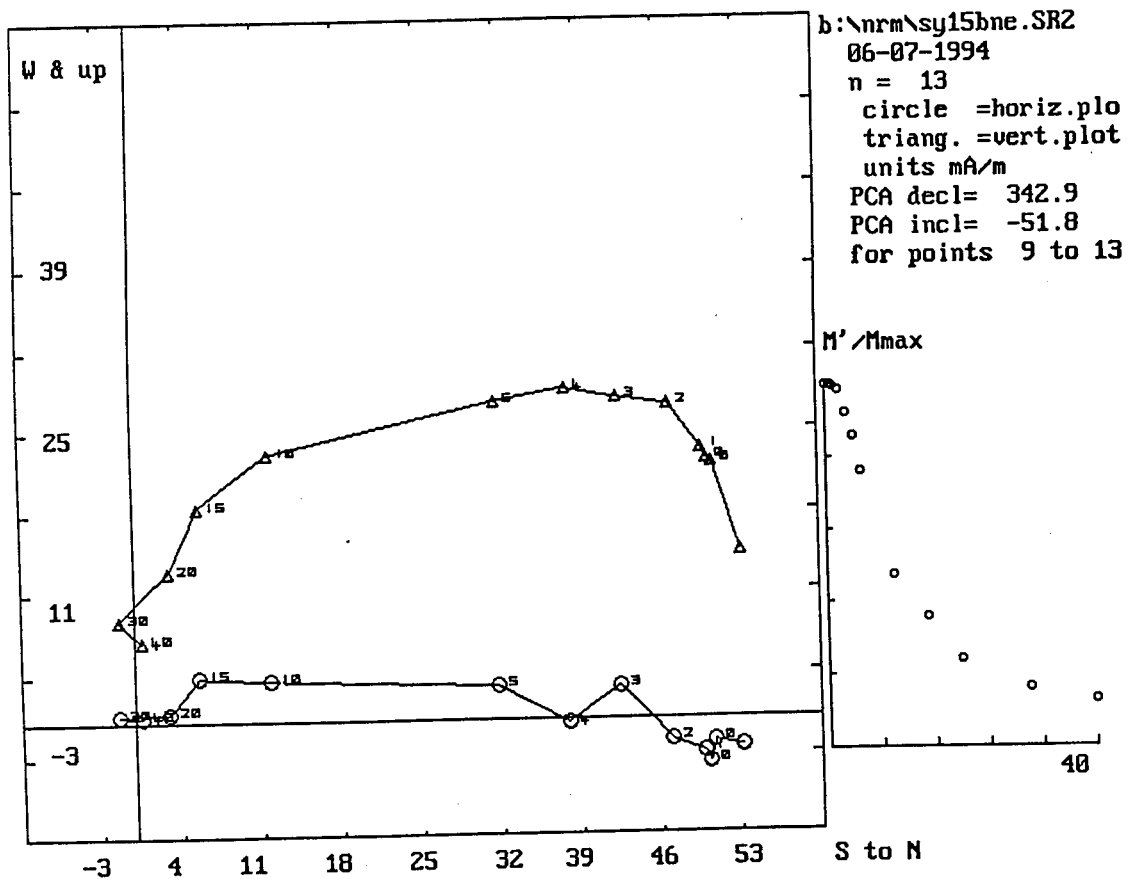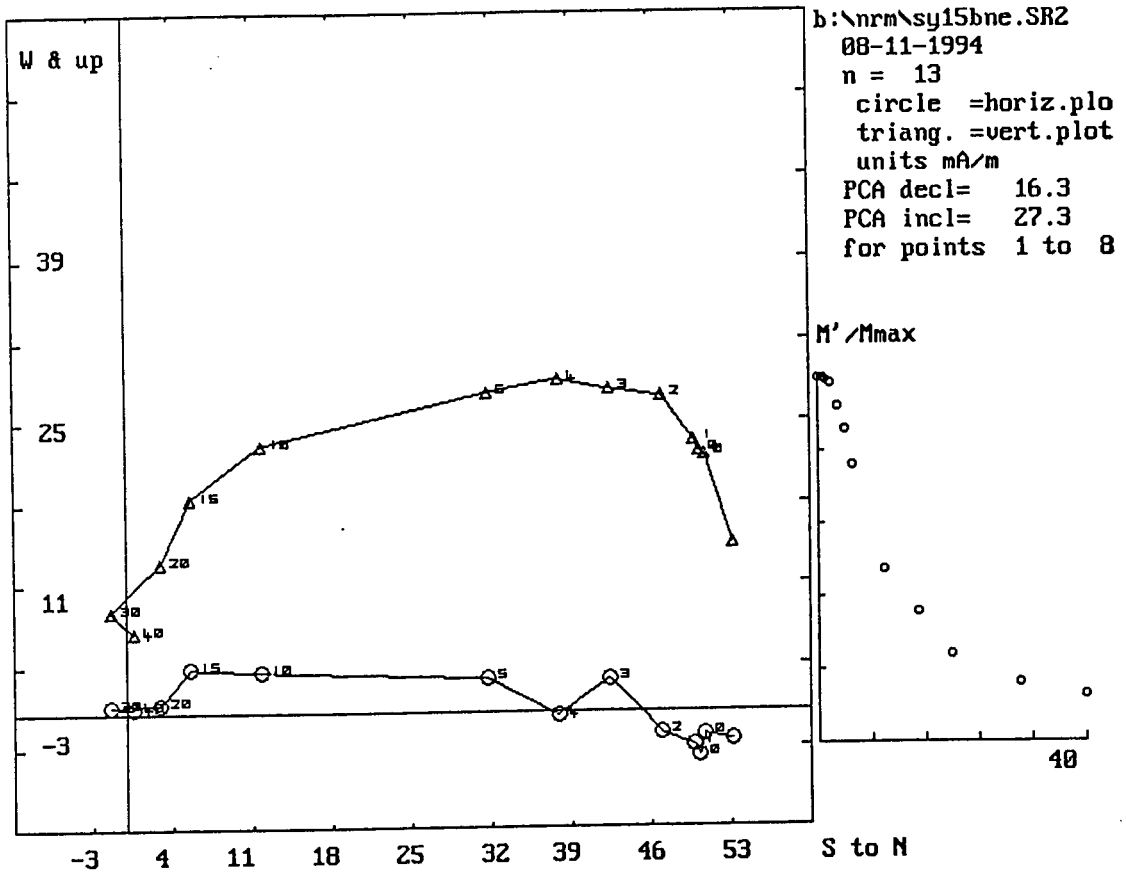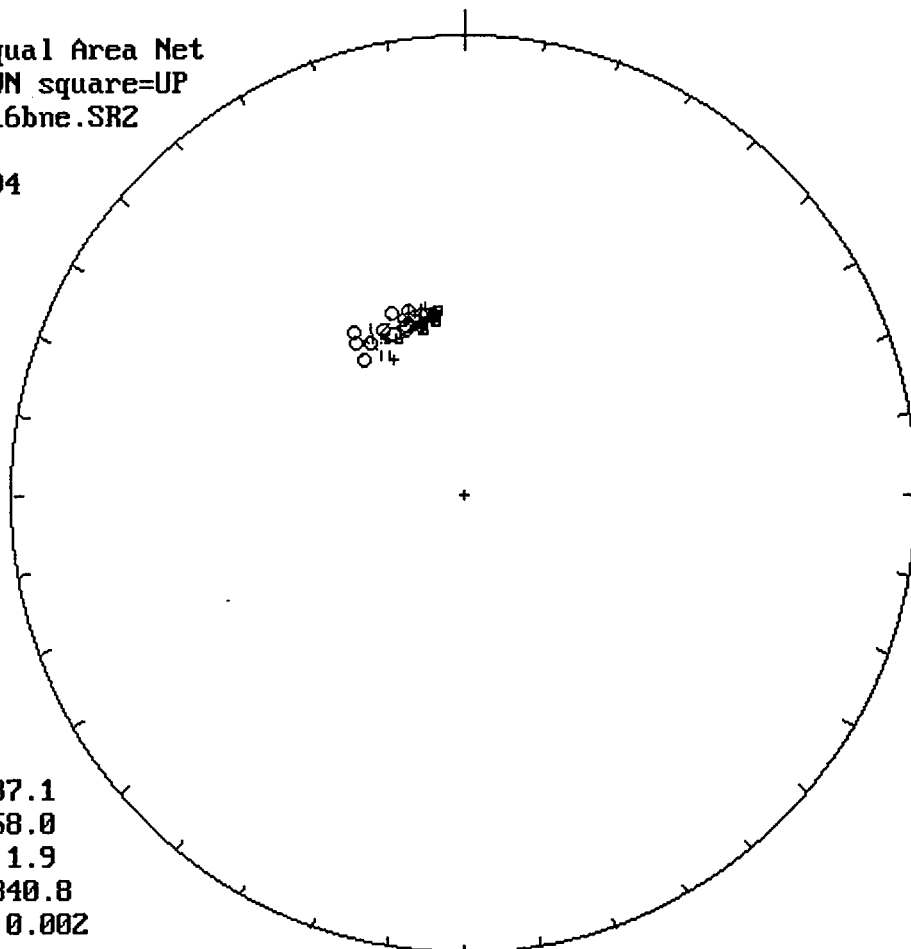Plot: shows
vectors
added in
nature
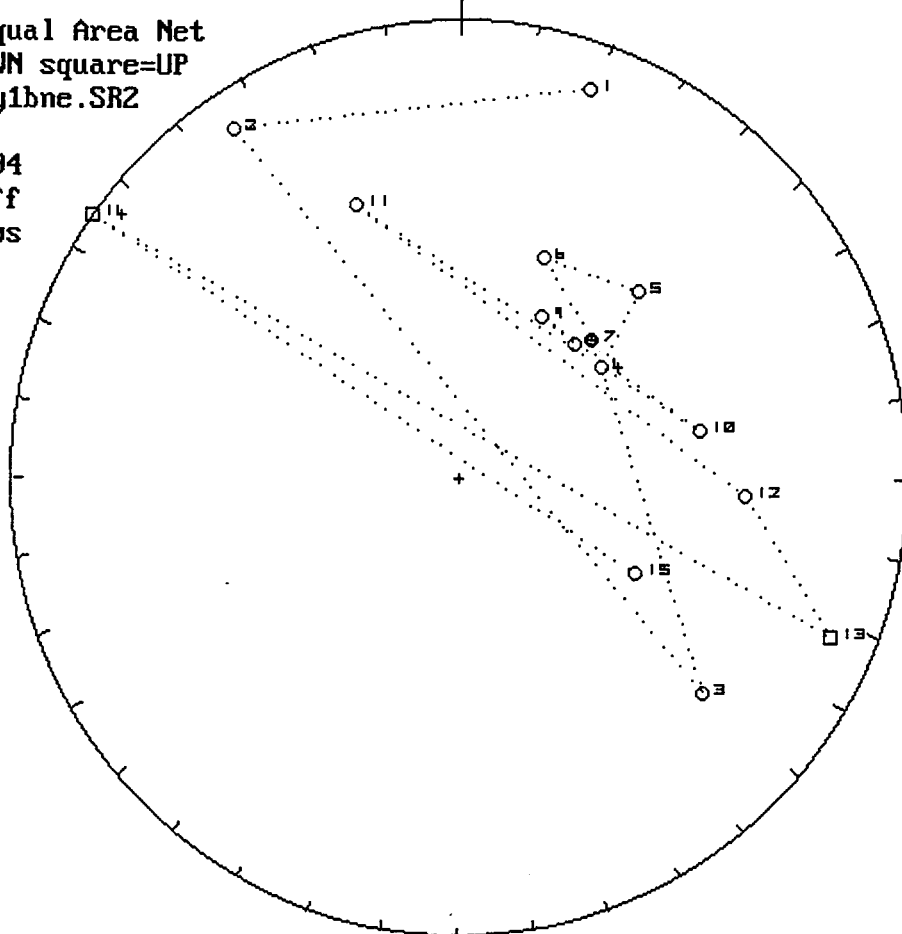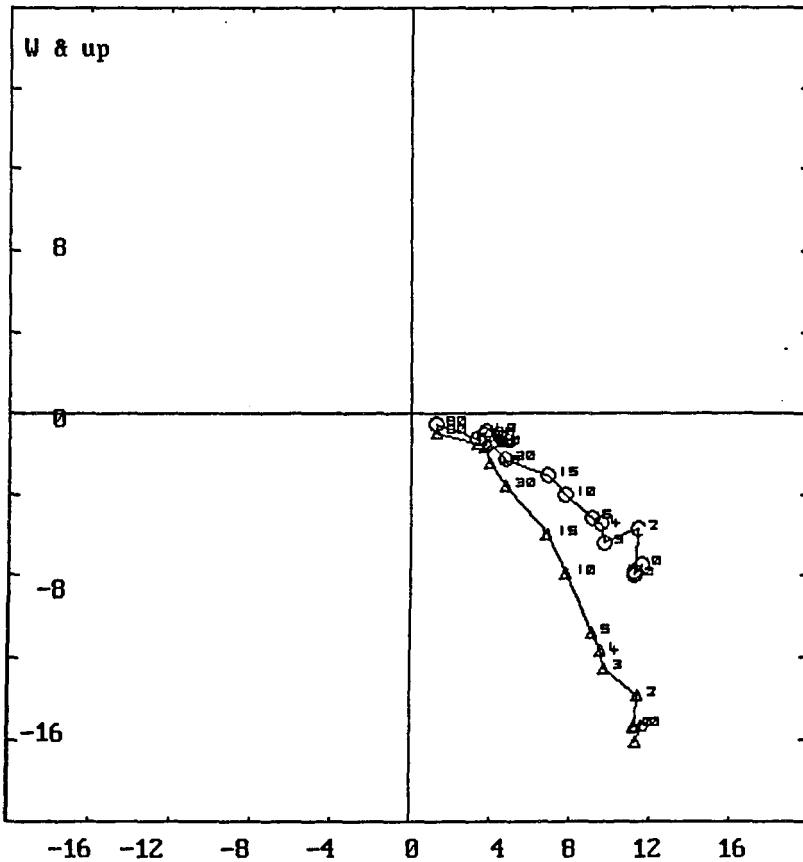
b:\nrm\sy1bne.SR2
  08-18-1994
  n =   16
   circle =horiz.plo
   triang. =vert.plot
   units mA/m
  PCA decl=   50.1
  PCA incl=   53.1
  for points 3 to 8
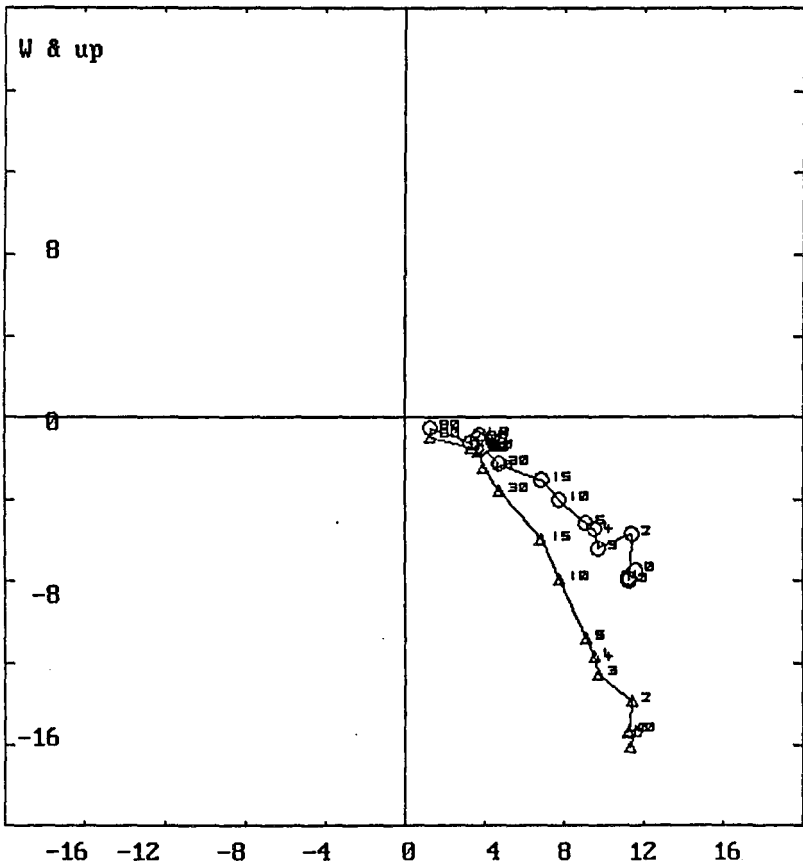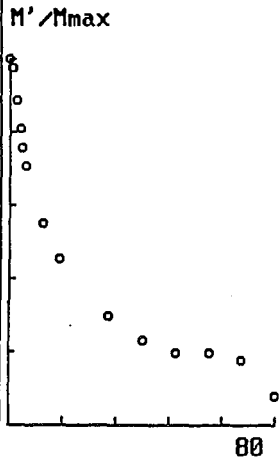
b:\nrm\sy1bne.SR2
  08-18-1994
  n =   16
   circle =horiz.plo
   triang. =vert.plot
   units mA/m
  PCA decl=   30.6
  PCA incl=   46.4
  for points 9 to 16

b:\nrm\sy1bne.SR2
06-07-1994
n = 16
 circle =horiz.plo
 triang. =vert.plot
 units mA/m
PCA decl= 37.1
PCA incl= 52.4
for points 3 to 16

W & up

M'/Mmax

S to N
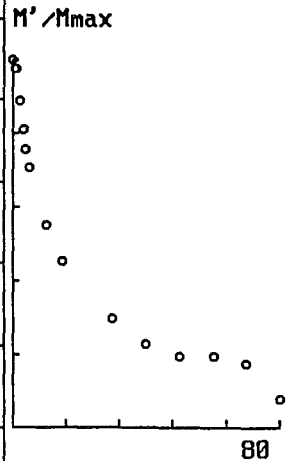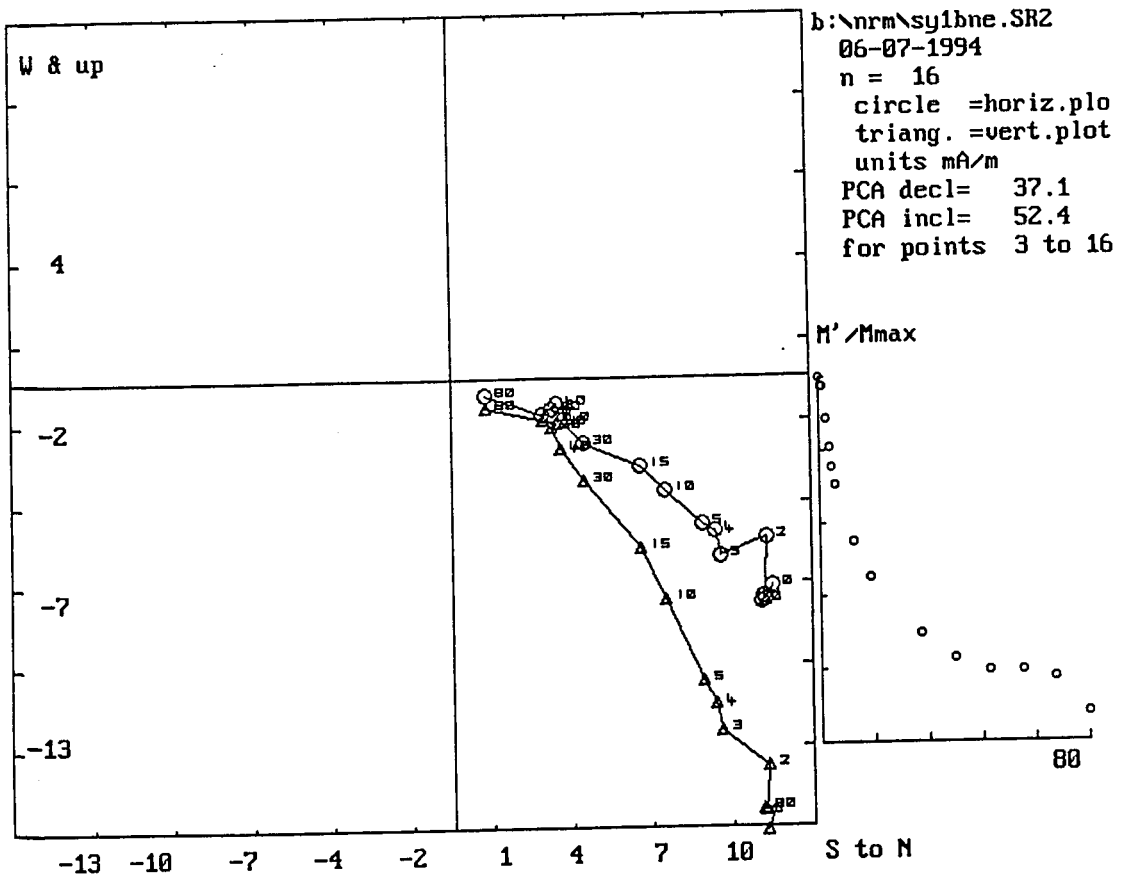
Lwr.Hem.Equal Area Net
circle=DOWN square=UP
 b:\nrm\sy2bne.SR2
 n = 13
 08-18-1994
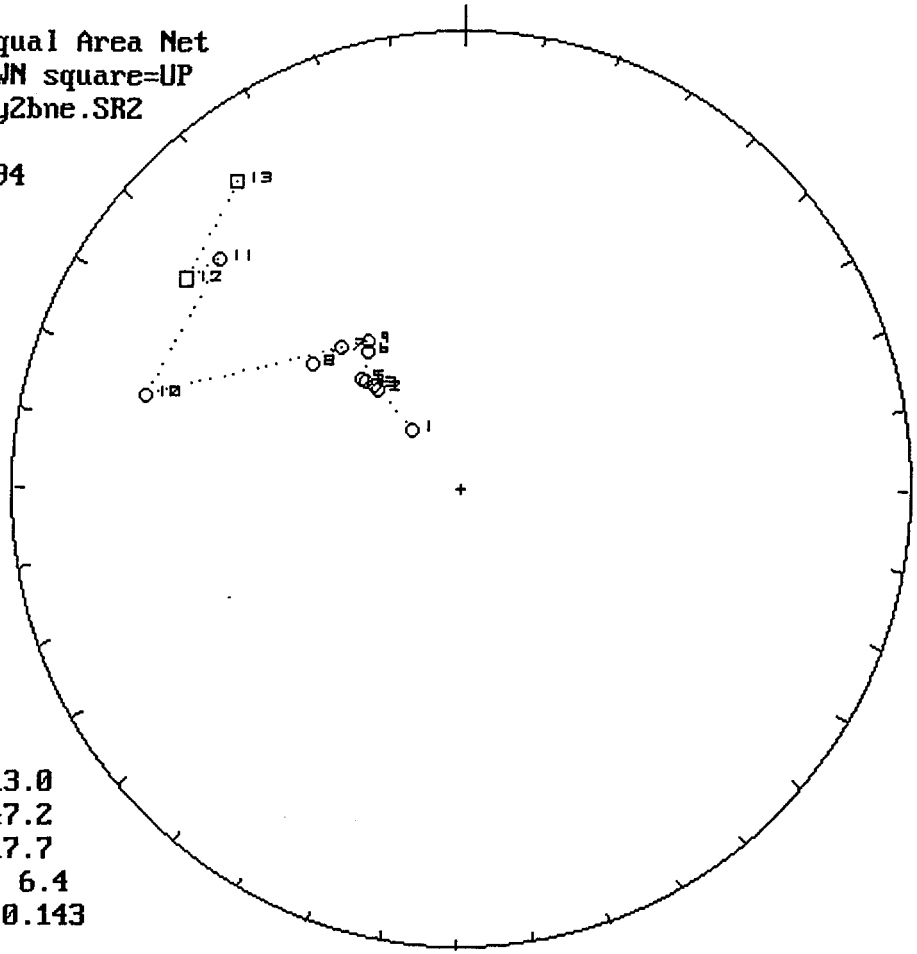
m.dec.= 313.0
m.inc.= 47.2
alpha95= 17.7
Fish. k=   6.4
sp.var.= 0.143
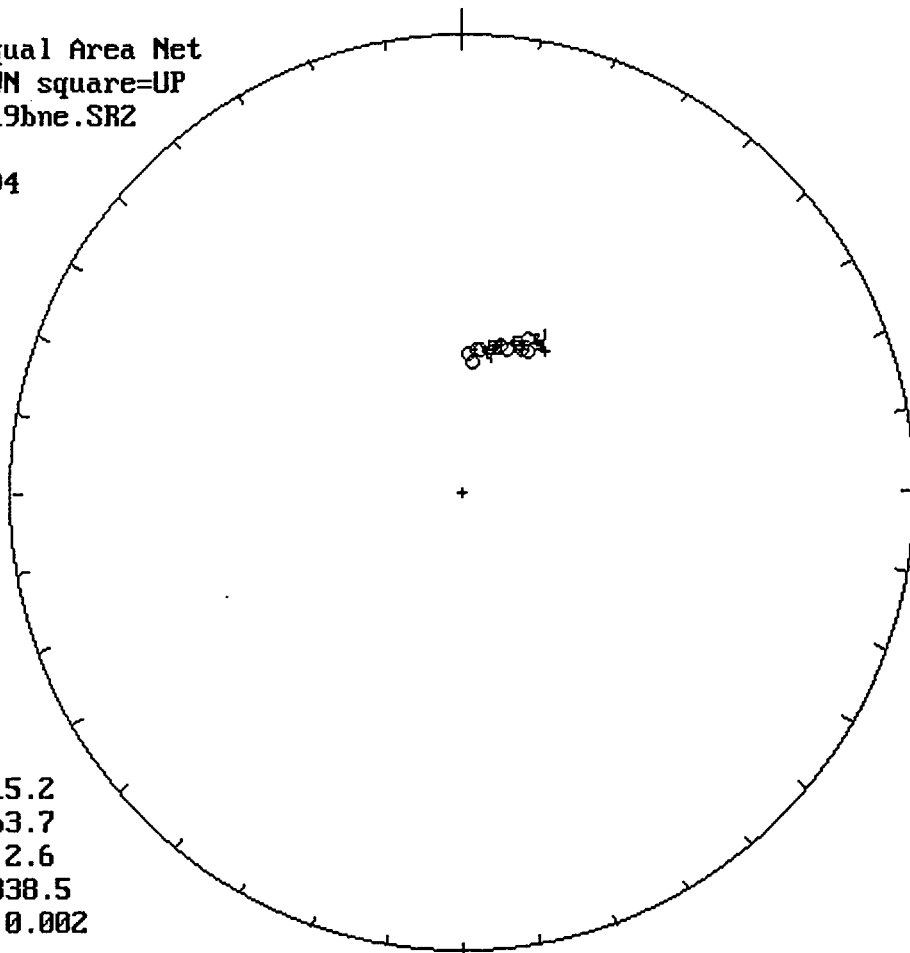
Lwr.Hem.Equal Area Net
circle=DOWN square=UP
 b:\nrm\sy2bne.SR2
 n = 12
 06-07-1994
Vector Diff
Plot: shows
vectors
added in
nature
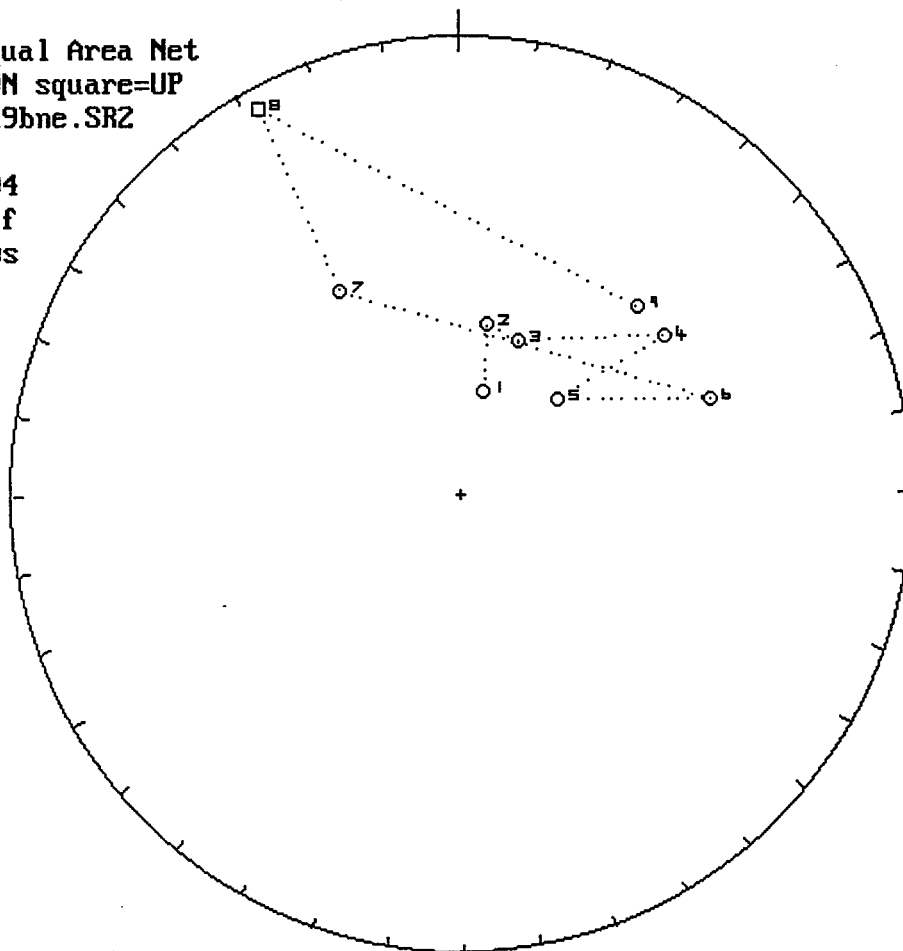
b:\nrm\sy2bne.SR2
08-18-1994
n = 13
 circle =horiz.plo
 triang. =vert.plot
 units mA/m
PCA decl= 318.2
PCA incl= 77.6
for points 1 to 9

M'/Mmax

b:\nrm\sy2bne.SR2
08-18-1994
n = 13
 circle =horiz.plo
 triang. =vert.plot
 units mA/m
PCA decl= 71.3
PCA incl= -62.7
for points 10 to 13

M'/Mmax
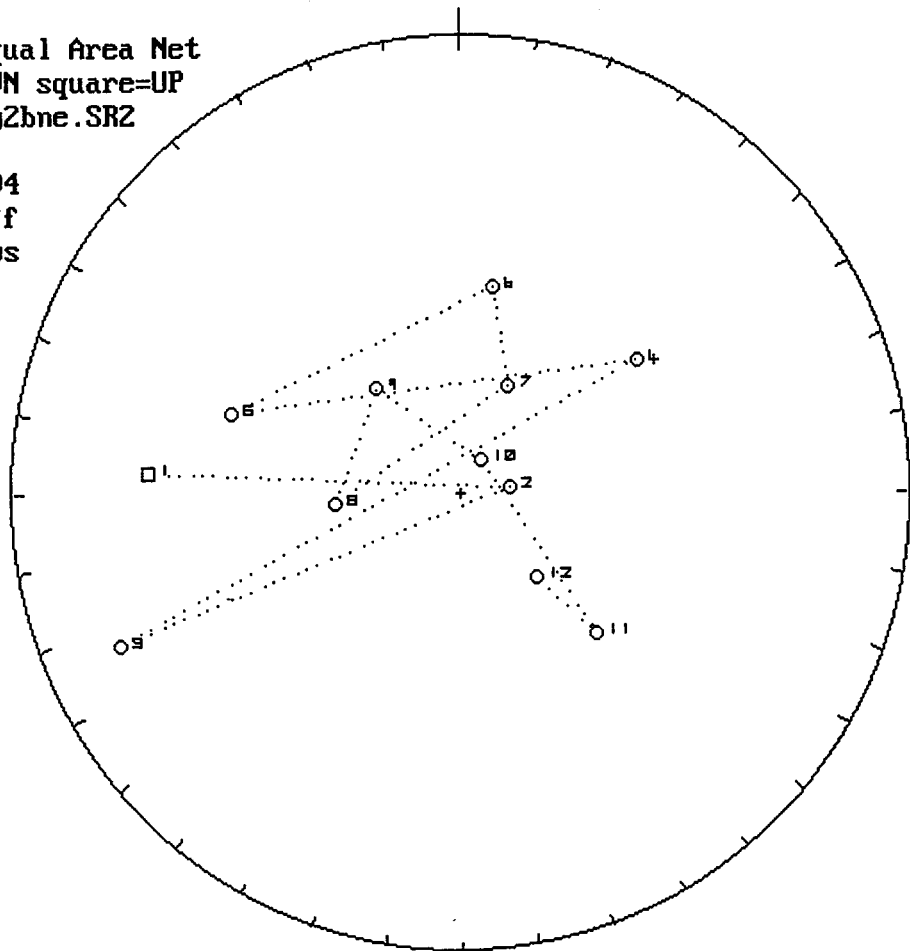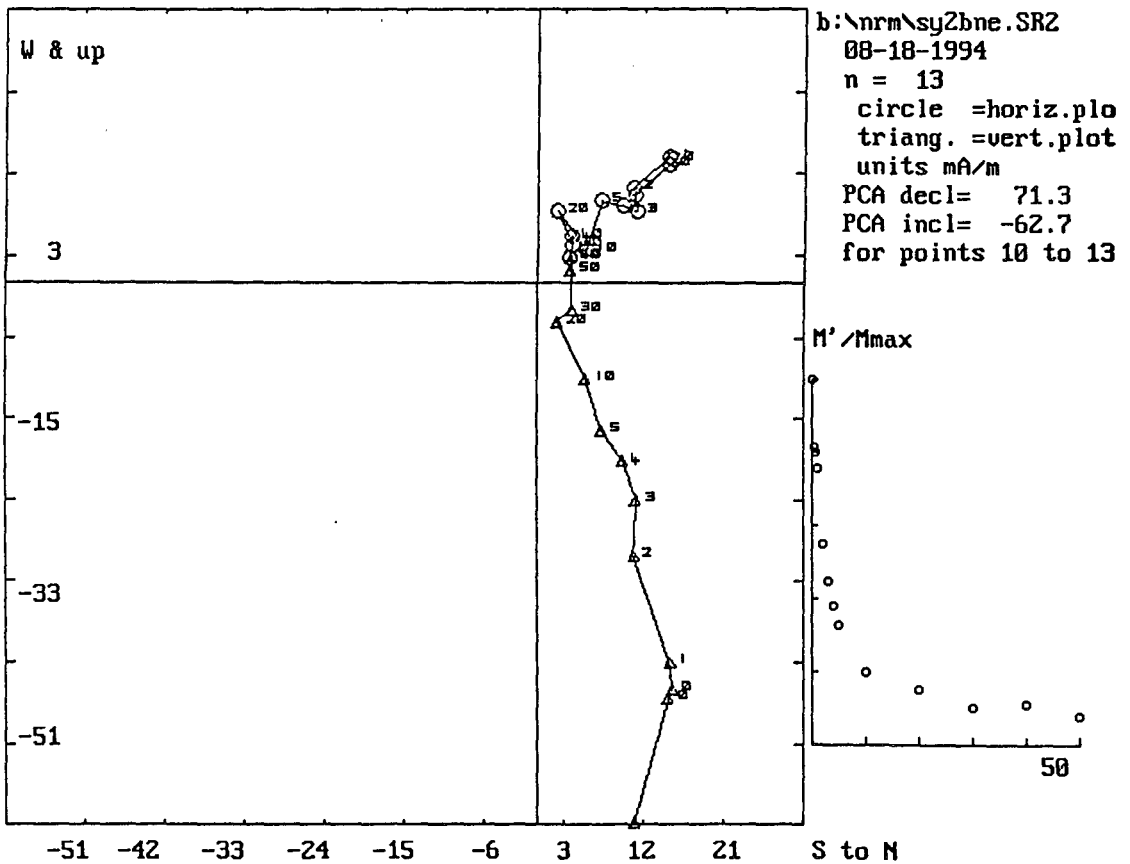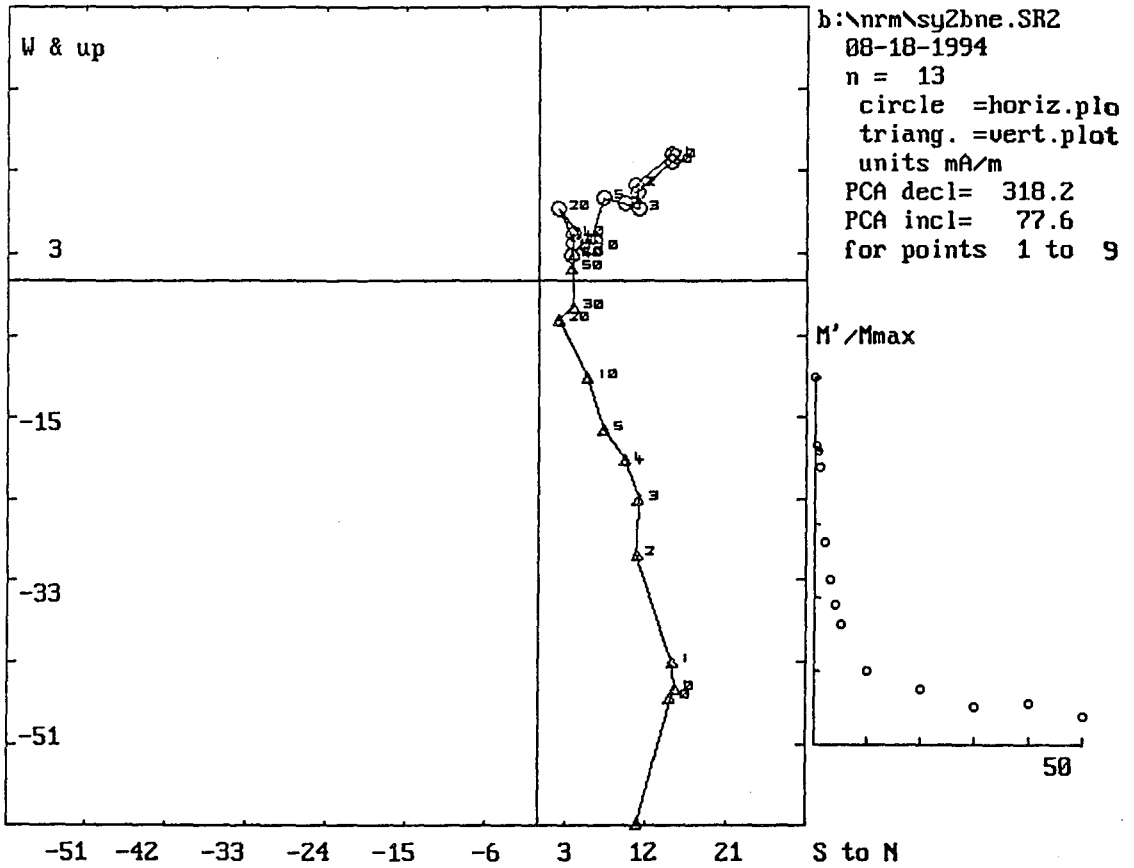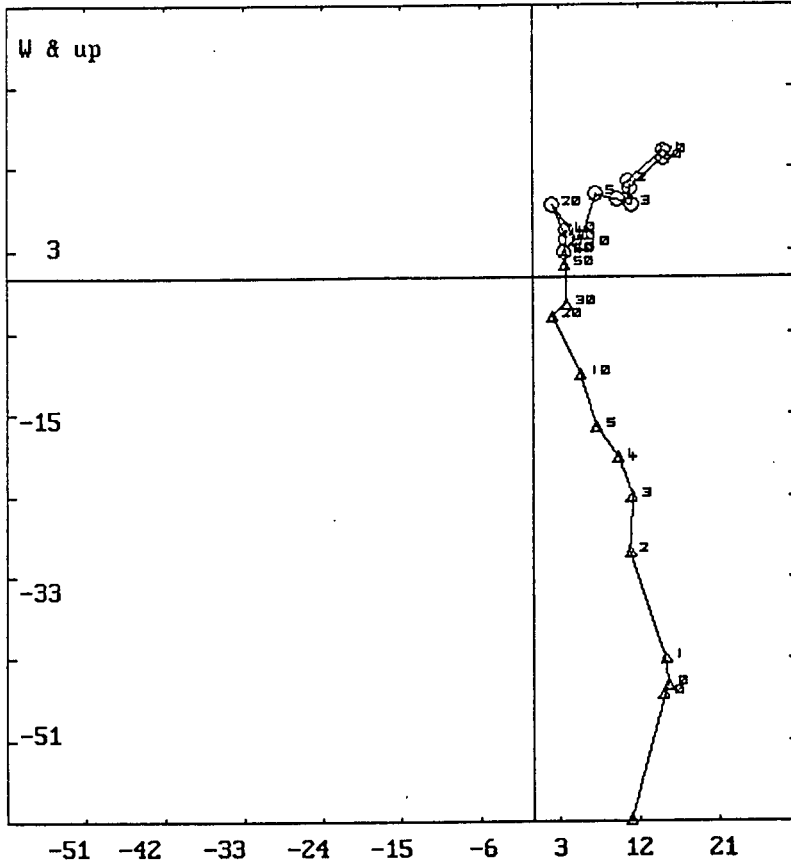
b:\nrm\sy2bne.SR2
06-07-1994
n = 13
 circle =horiz.plo
 triang. =vert.plot
 units mA/m
PCA decl= 323.2
PCA incl= 70.9
for points 4 to 13

W & up

3

-15

-33

-51

M'/Mmax

50
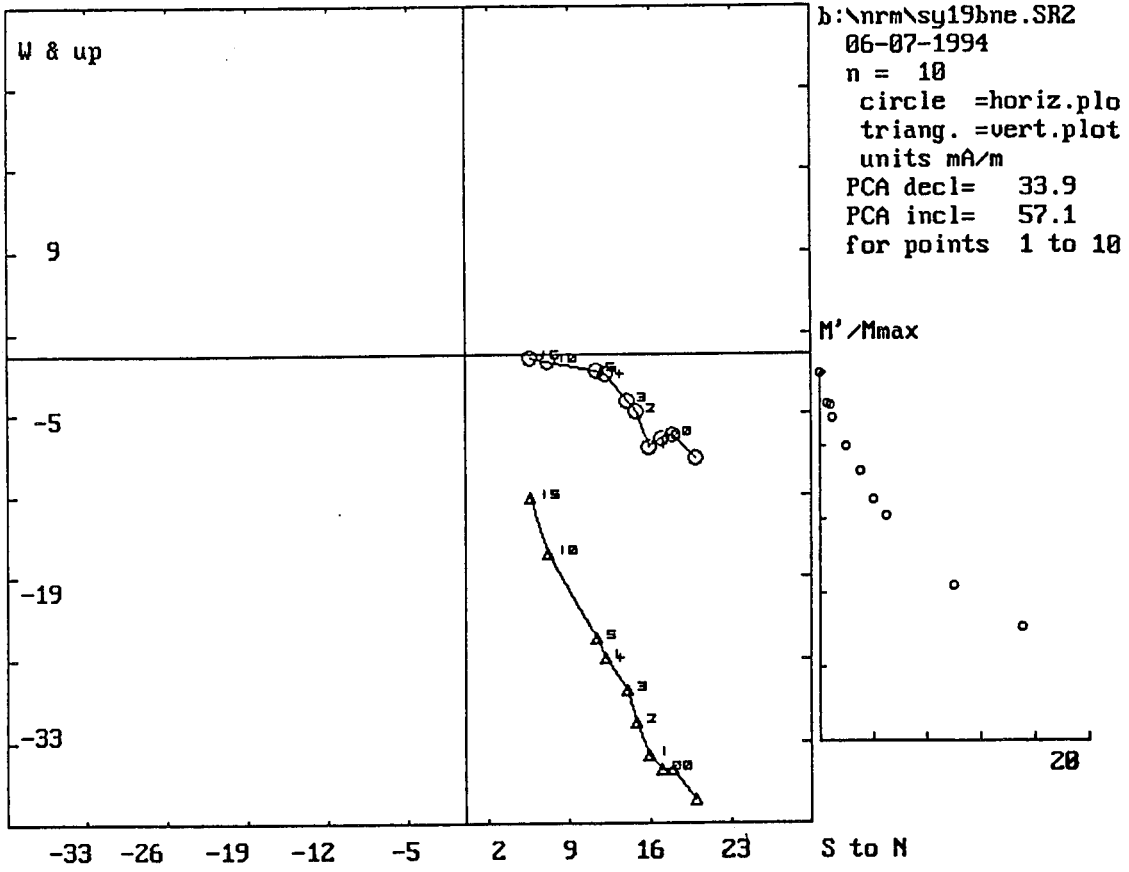
S to N

-51 -42 -33 -24 -15 -6   3   12   21
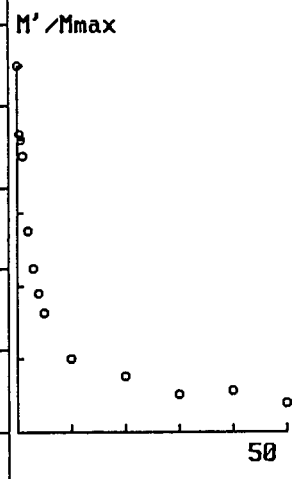
Lwr.Hem.Equal Area Net
circle=DOWN square=UP
 b:\nrm\sy3bne.SR2
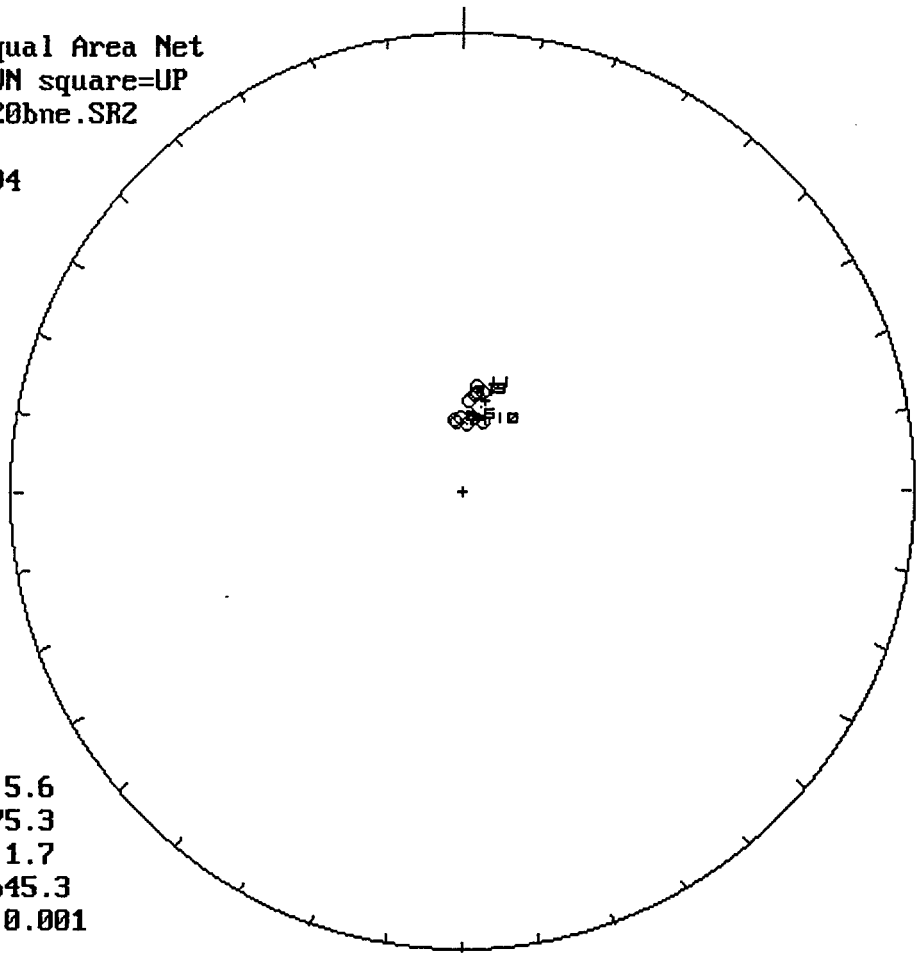 n = 16
 06-07-1994
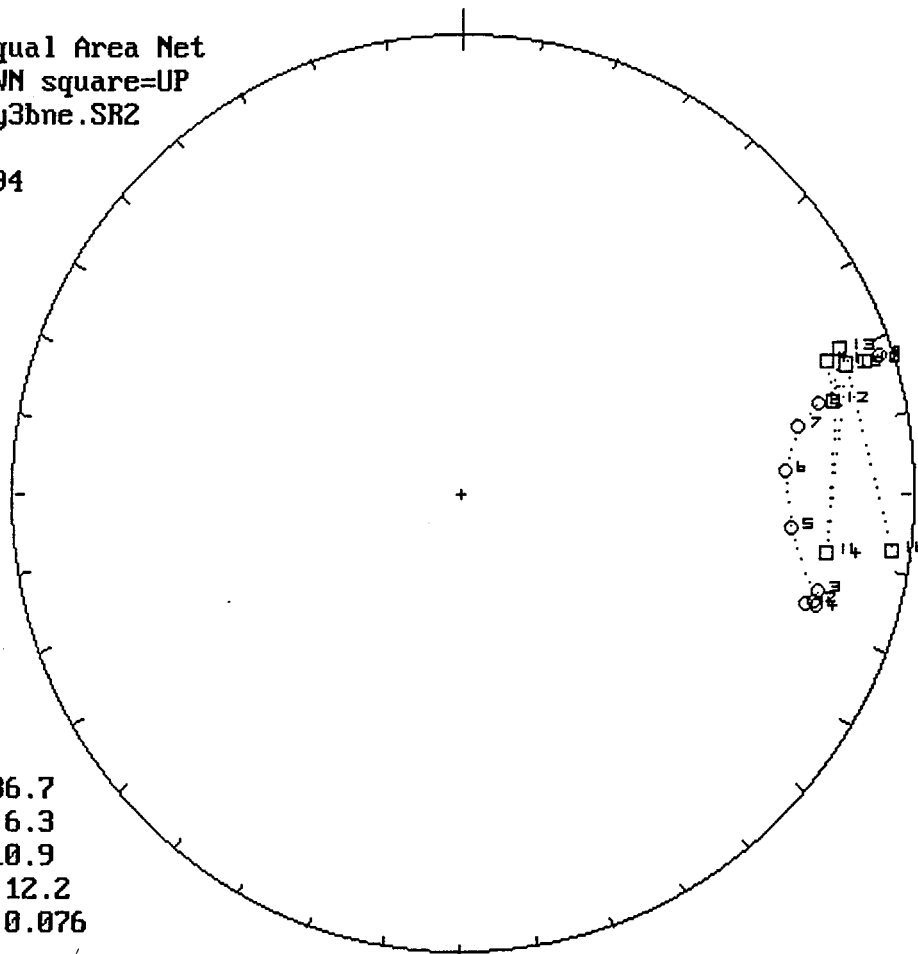
m.dec.= 86.7
m.inc.=   6.3
alpha95= 10.9
Fish. k= 12.2
sp.var.= 0.076

Lwr.Hem.Equal Area Net
circle=DOWN square=UP
 b:\nrm\sy3bne.SR2
 n = 15
 06-07-1994
Vector Diff
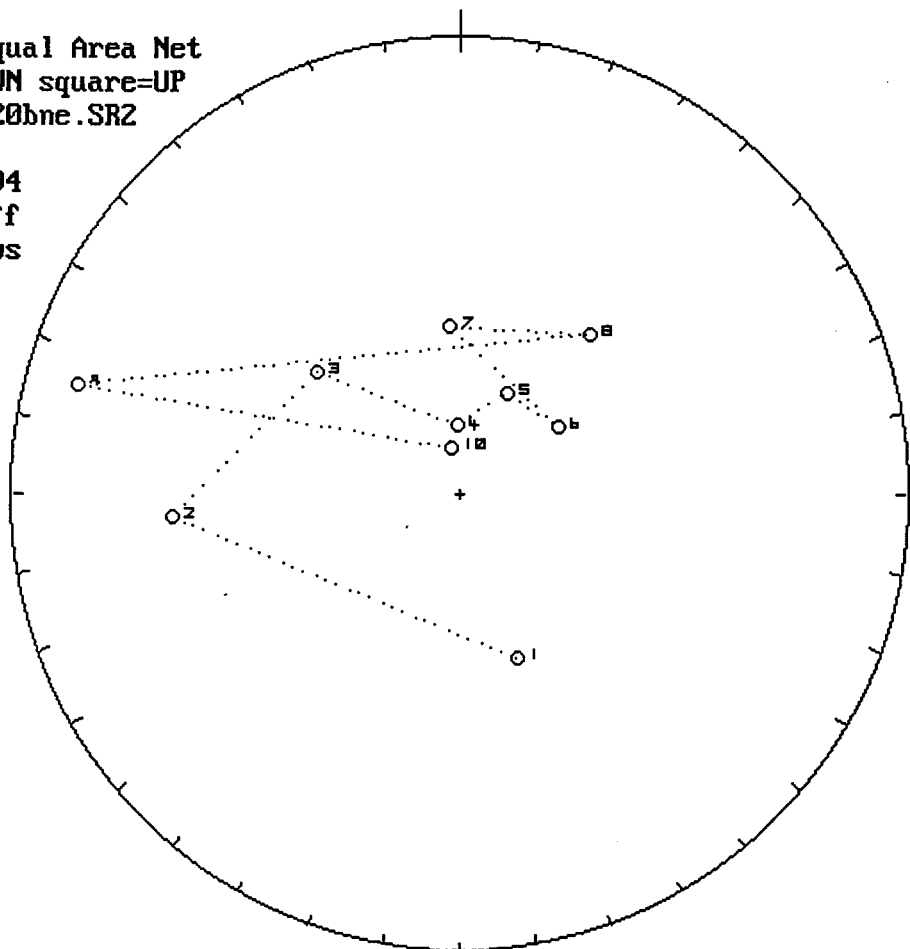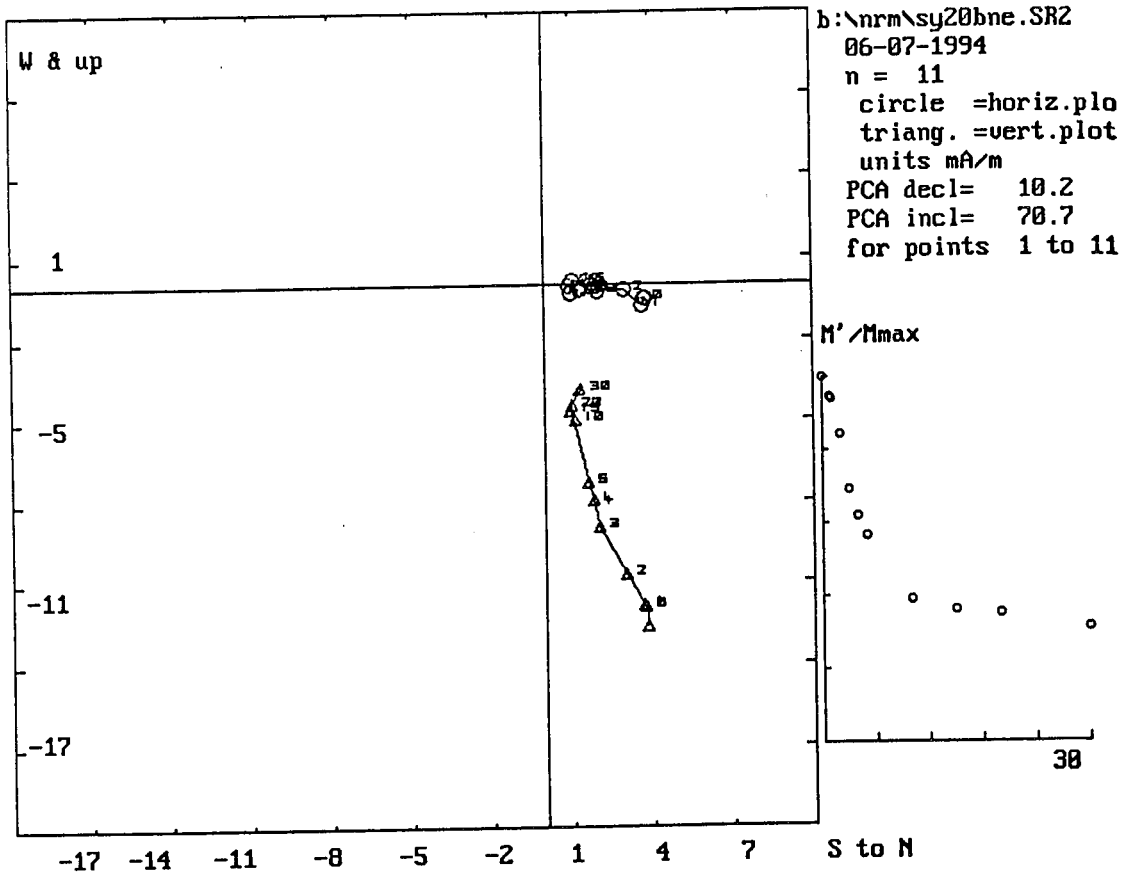Plot: shows
vectors
added in
nature

W & up

5

-5

-15

-25

-25 -20 -15 -10 -5 0 5 10 15 S to N
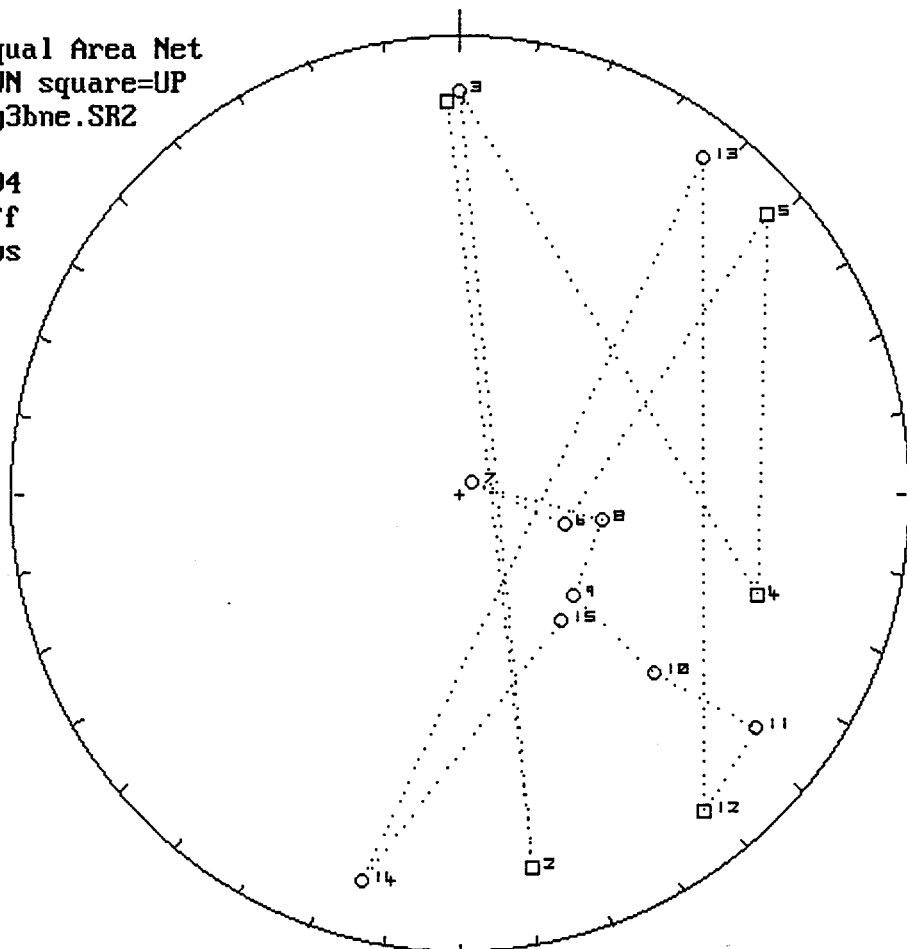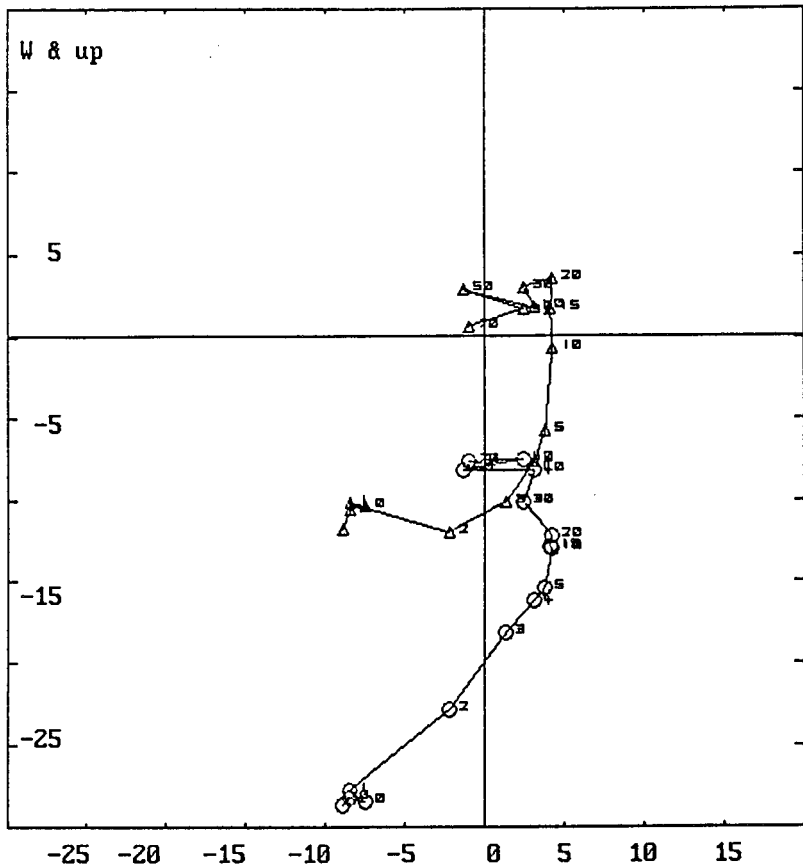
b:\nrm\sy3bne.SR2
06-07-1994
n = 16
 circle =horiz.plo
 triang. =vert.plot
 units mA/m
PCA decl= 294.5
PCA incl= -36.1
for points 3 to 16

M'/Mmax

70
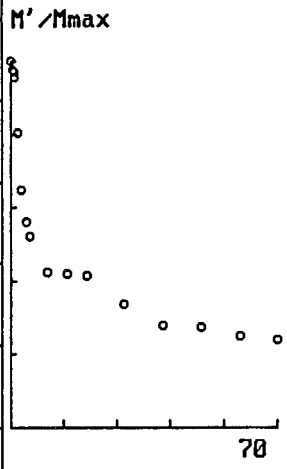
Lwr.Hem.Equal Area Net
circle=DOWN square=UP
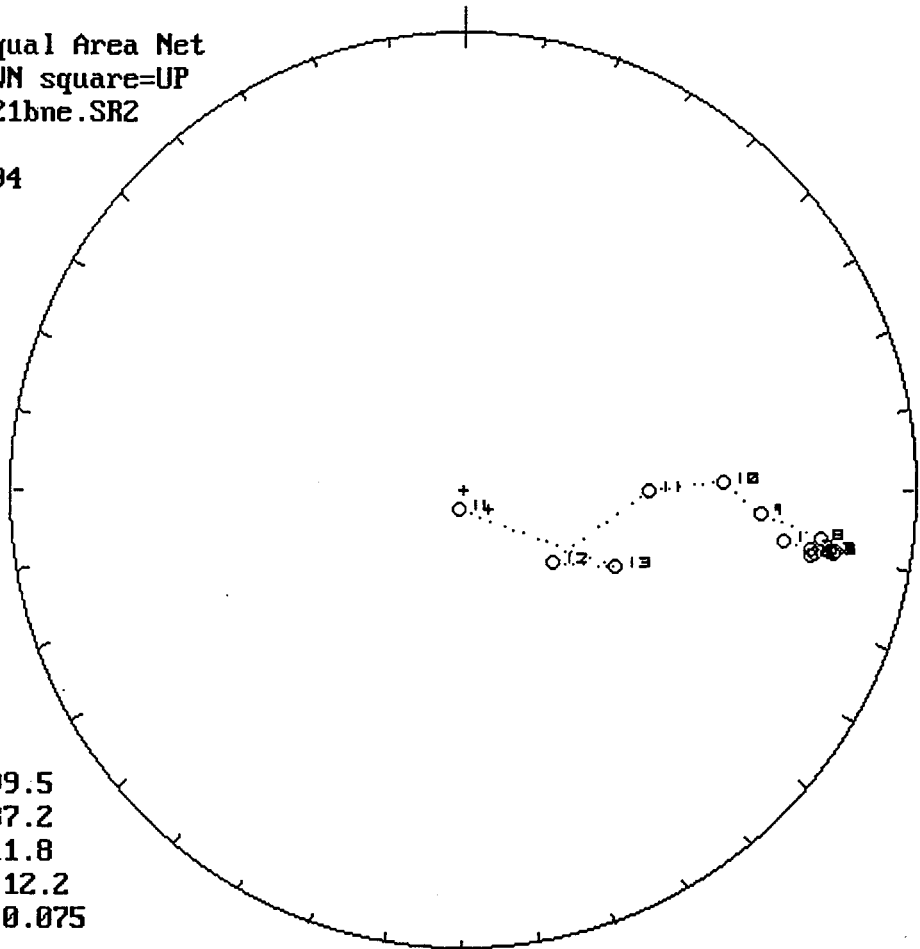 b:\nrm\sy8bne.SR2
 n = 15
 06-07-1994
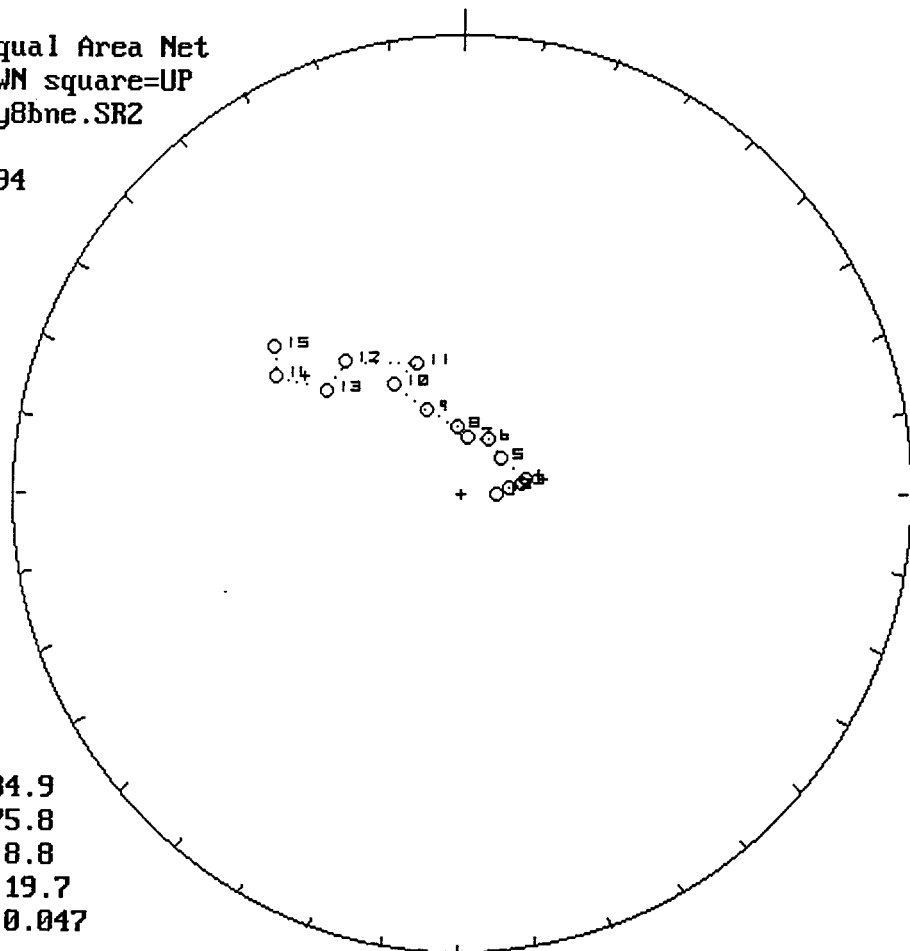
m.dec.= 334.9
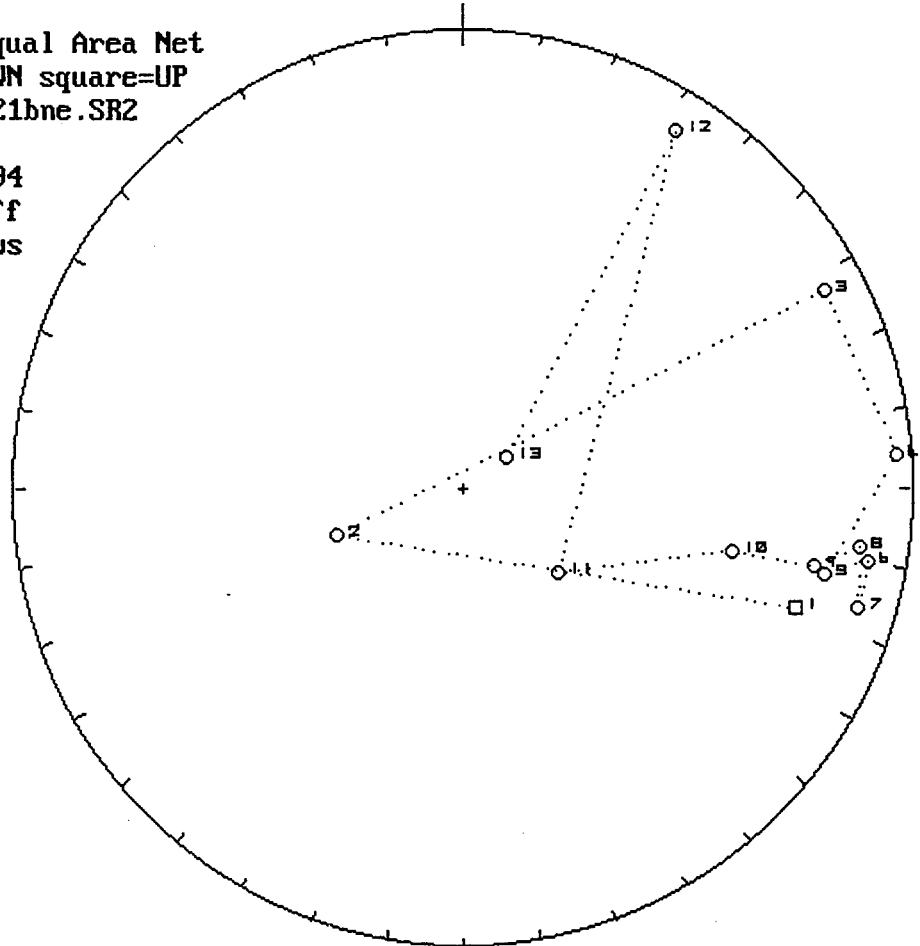m.inc.= 75.8
alpha95= 8.8
Fish. k= 19.7
sp.var.= 0.047

Lwr.Hem.Equal Area Net
circle=DOWN square=UP
 b:\nrm\sy8bne.SR2
 n = 14
 06-07-1994
Vector Diff
Plot: shows
vectors
added in
nature

b:\nrm\sy8bne.SR2
08-18-1994
n = 15
 circle =horiz.plo
 triang. =vert.plot
 units mA/m
PCA decl= 306.1
PCA incl= -66.4
for points 1 to 8

W & up

-7

-25

-43

-61

M'/Mmax

60

-61 -52 -43 -34 -25 -16 -7   2   11   S to N

b:\nrm\sy8bne.SR2
08-18-1994
n = 15
 circle =horiz.plo
 triang. =vert.plot
 units mA/m
PCA decl=   42.5
PCA incl=   73.6
for points 9 to 15

W & up

-7

-25

-43

-61

M'/Mmax

60

-61 -52 -43 -34 -25 -16 -7   2   11   S to N
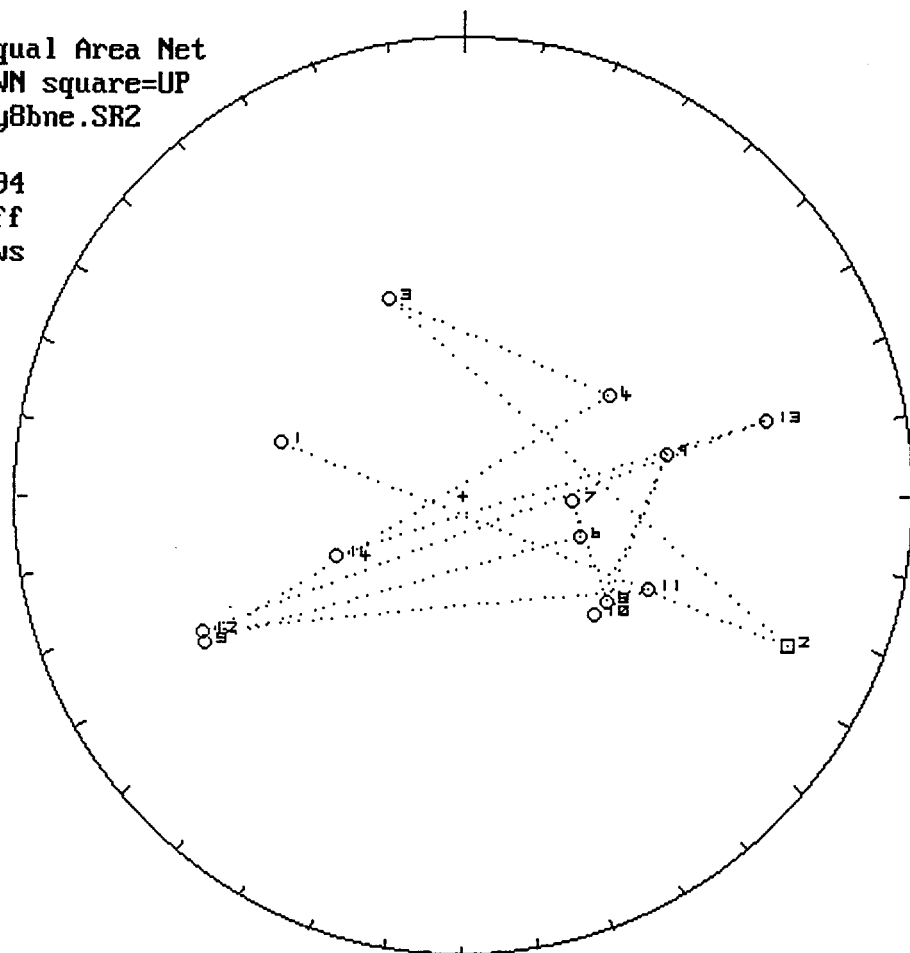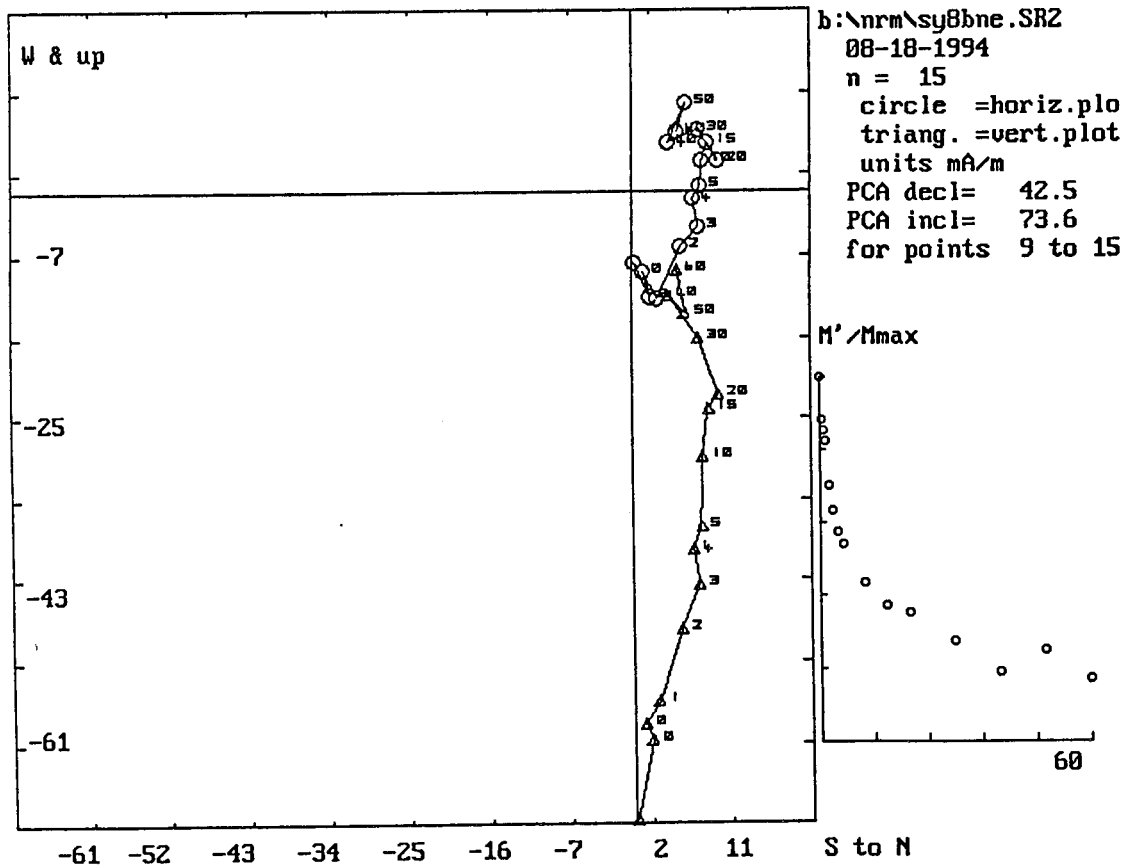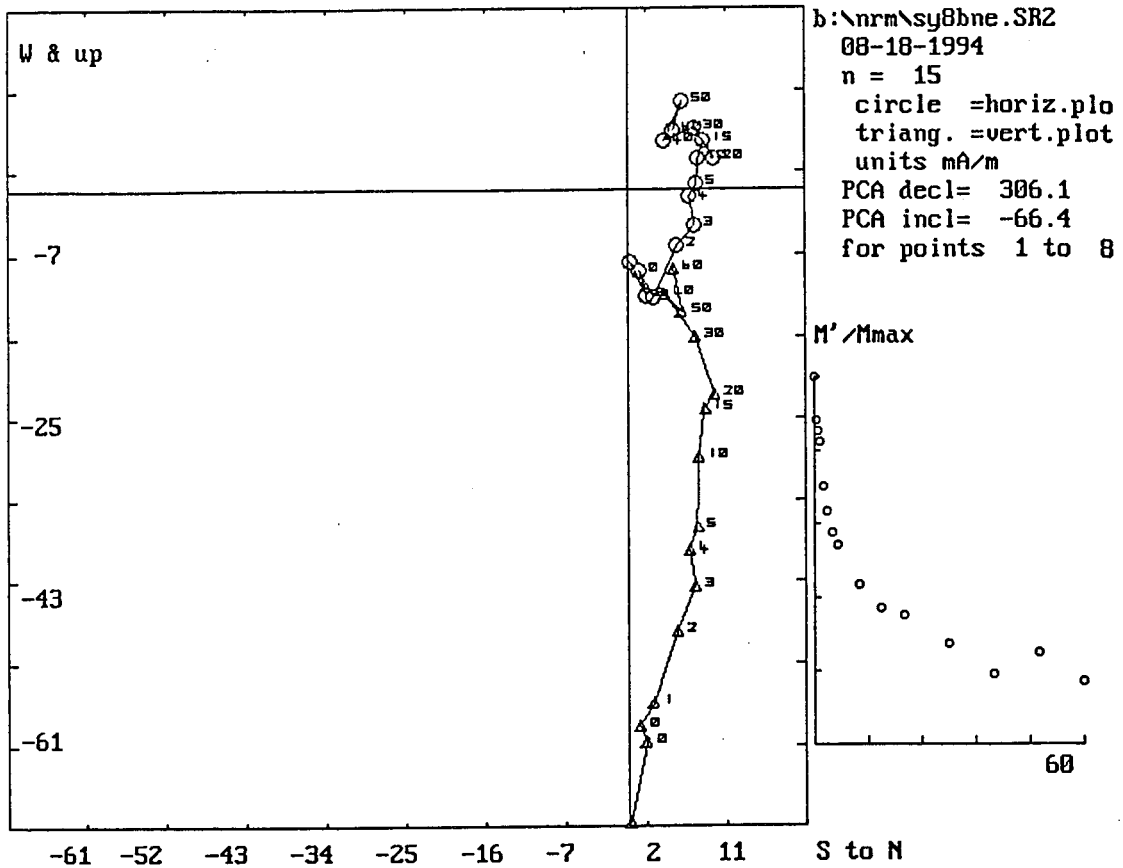
Lwr.Hem.Equal Area Net
circle=DOWN square=UP
 b:\nrm\sy9bne.SR2
 n = 17
 06-07-1994
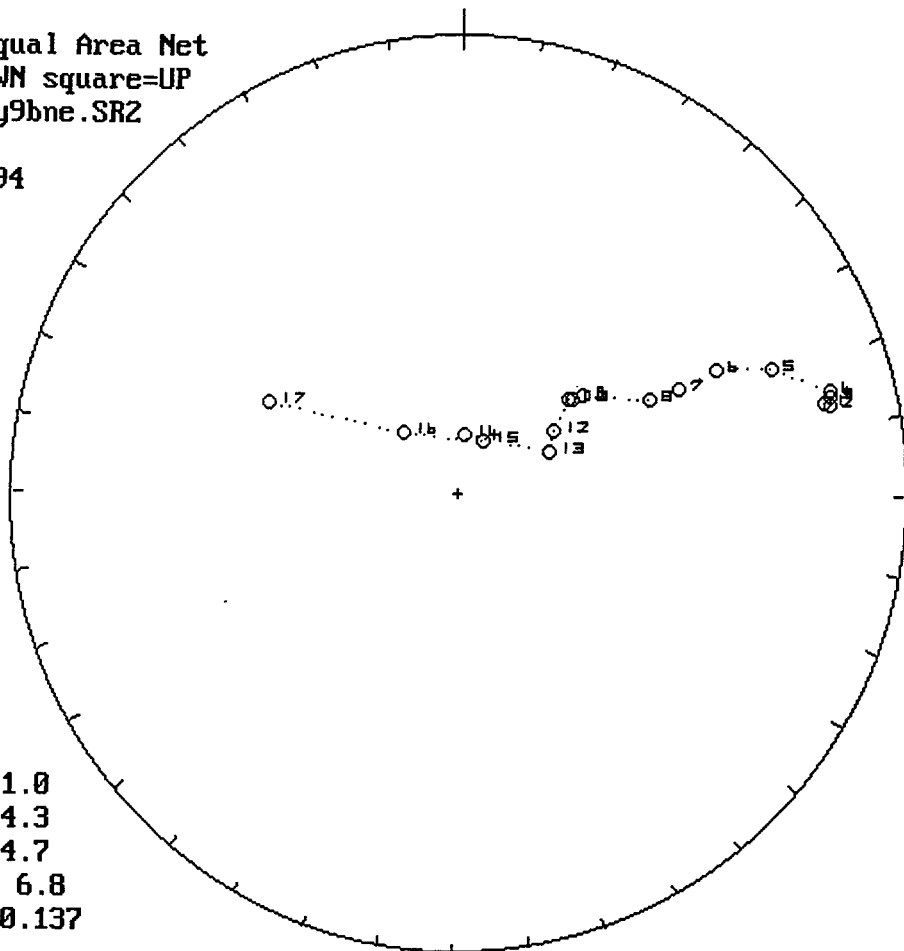
m.dec.= 61.0
m.inc.= 54.3
alpha95= 14.7
Fish. k=   6.8
sp.var.= 0.137

Lwr.Hem.Equal Area Net
circle=DOWN square=UP
 b:\nrm\sy9bne.SR2
 n = 16
 06-07-1994
Vector Diff
Plot: shows
vectors
added in
nature

b:\nrm\sy9bne.SR2
06-07-1994
n = 17
 circle =horiz.plo
 triang. =vert.plot
 units mA/m
PCA decl= 85.2
PCA incl= -18.5
for points 1 to 8

M'/Mmax

W & up

S to N

b:\nrm\sy9bne.SR2
06-07-1994
n = 17
 circle =horiz.plo
 triang. =vert.plot
 units mA/m
PCA decl= 56.5
PCA incl= 57.0
for points 9 to 17

M'/Mmax

W & up

S to N
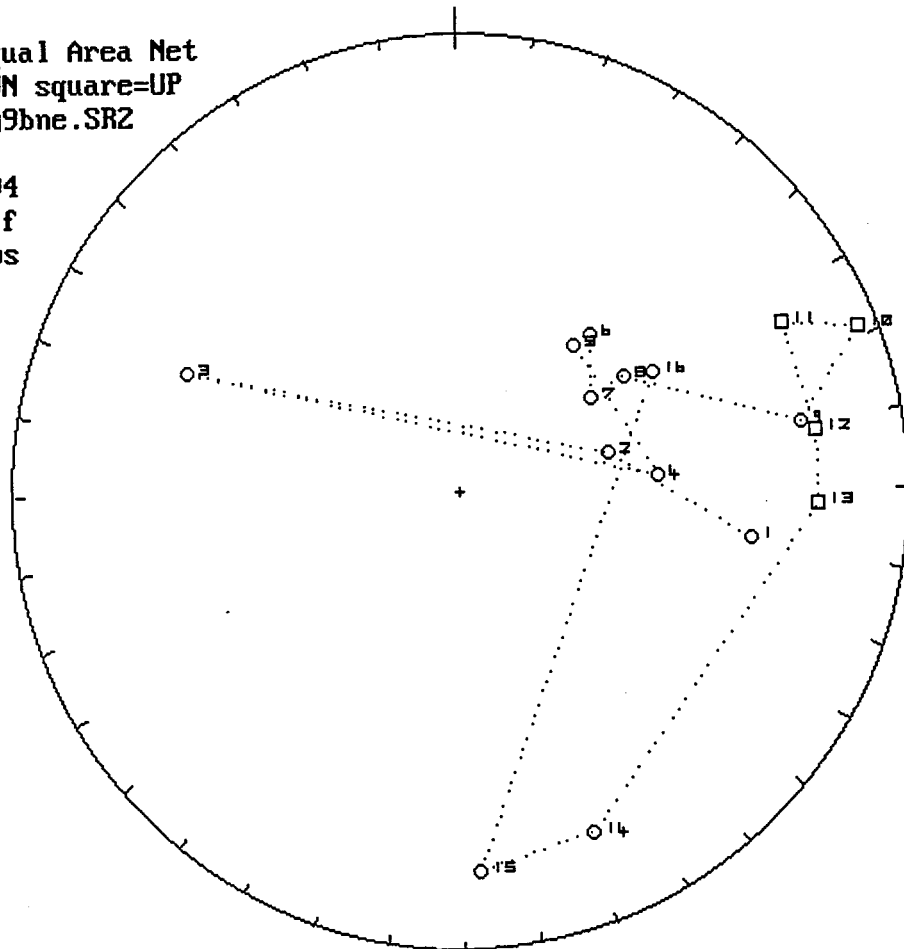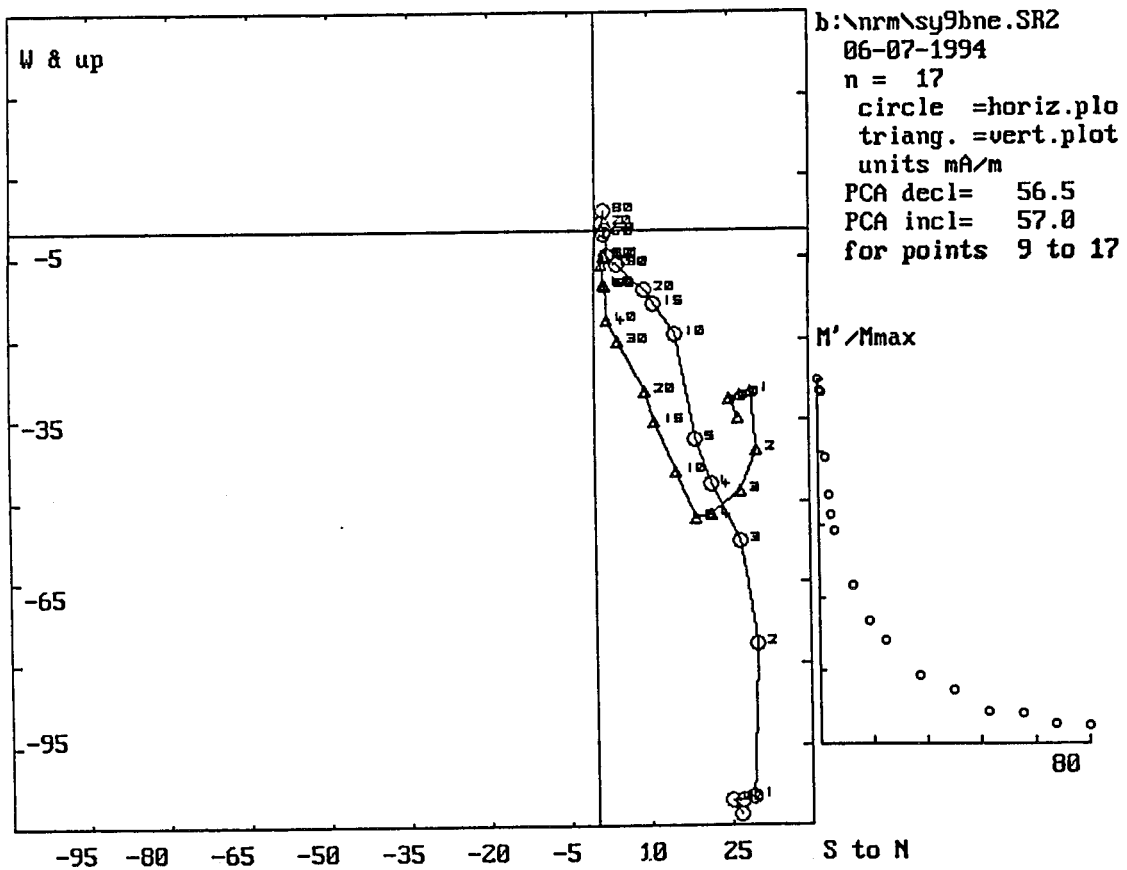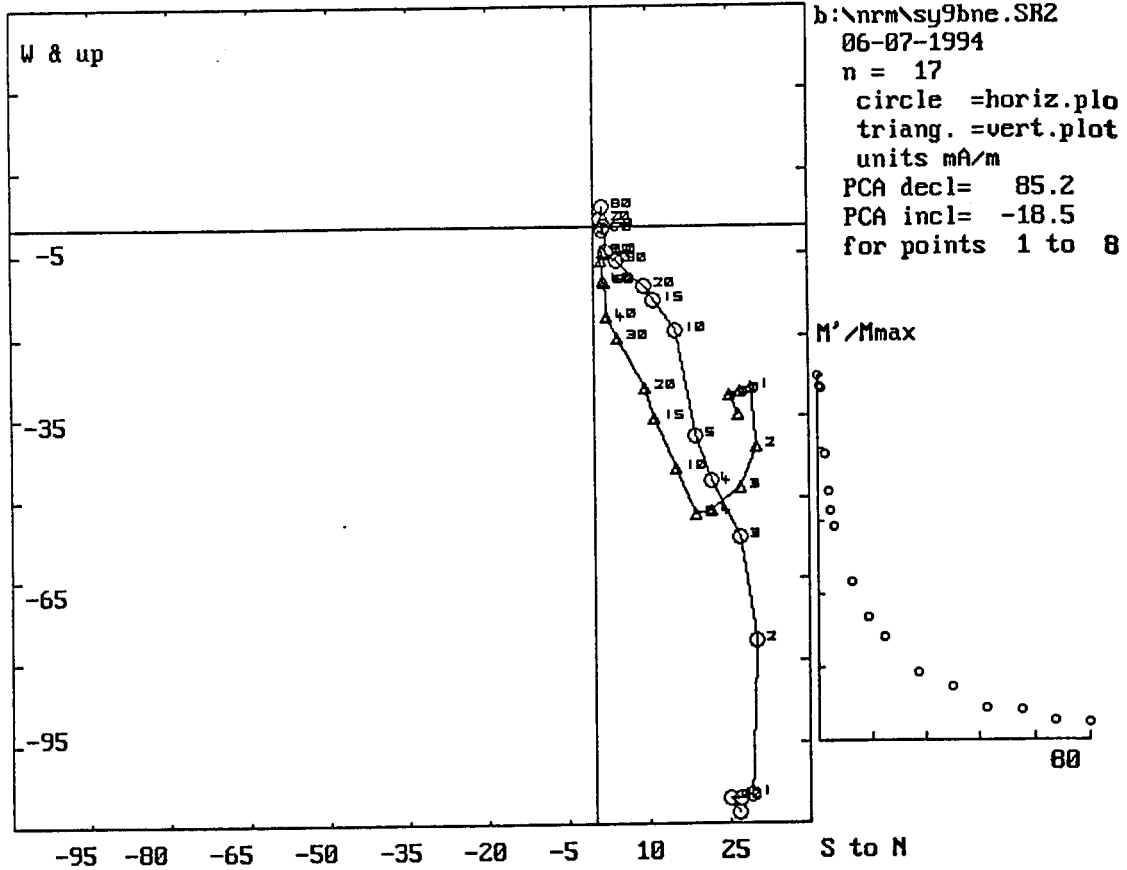
Lwr.Hem.Equal Area Net
circle=DOWN square=UP
 :\nrm\sy10bne.SR2
 n = 16
 06-07-1994
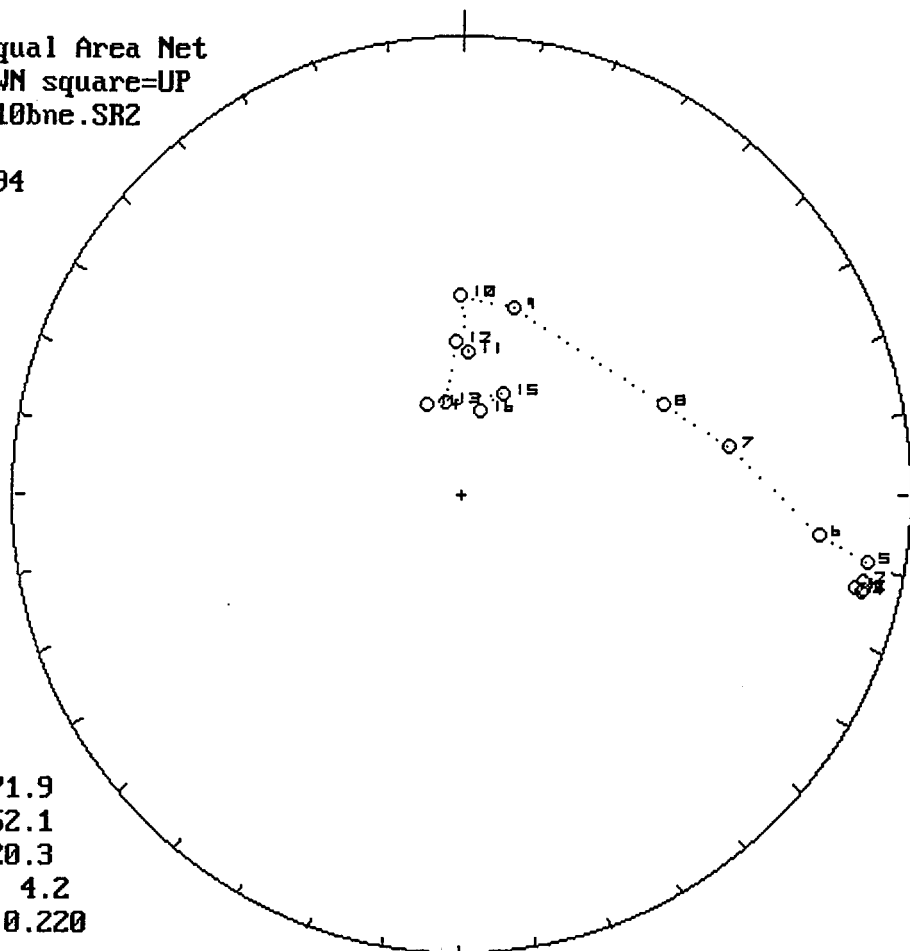
m.dec.= 71.9
m.inc.= 52.1
alpha95= 20.3
Fish. k=   4.2
sp.var.= 0.220

Lwr.Hem.Equal Area Net
circle=DOWN square=UP
 :\nrm\sy10bne.SR2
 n = 15
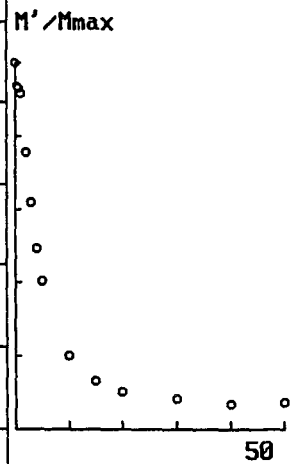 06-07-1994
Vector Diff
Plot: shows
vectors
added in
nature

b:\nrm\sy10bne.SR2
06-07-1994
n = 16
 circle =horiz.plo
 triang. =vert.plot
 units mA/m
PCA decl= 108.7
PCA incl= -1.8
for points 3 to 7

M'/Mmax

b:\nrm\sy10bne.SR2
06-07-1994
n = 16
 circle =horiz.plo
 triang. =vert.plot
 units mA/m
PCA decl= 84.9
PCA incl= 28.1
for points 7 to 16

M'/Mmax
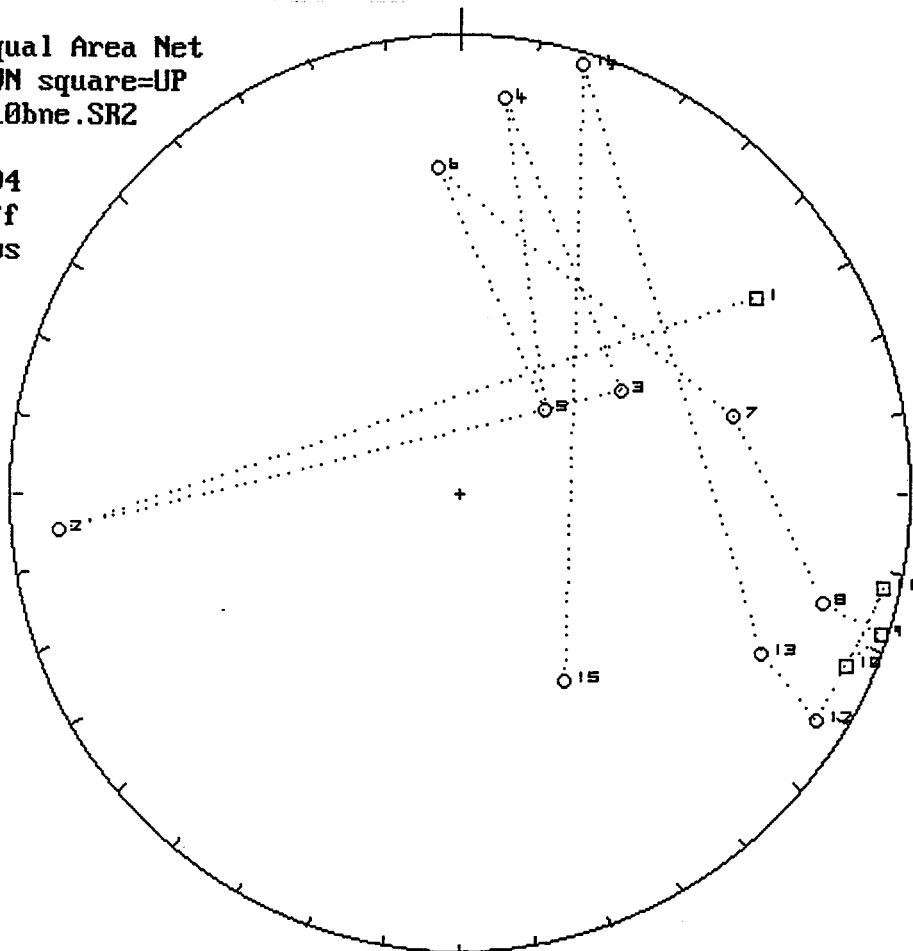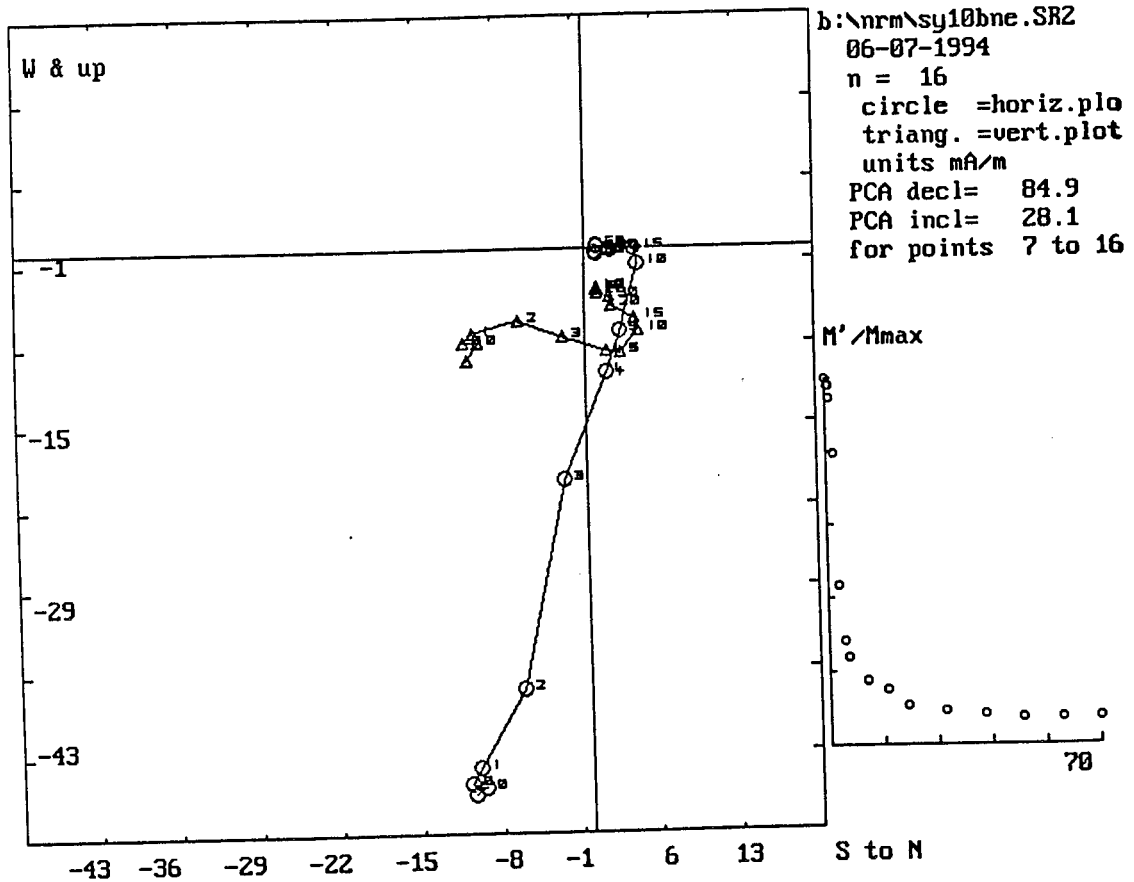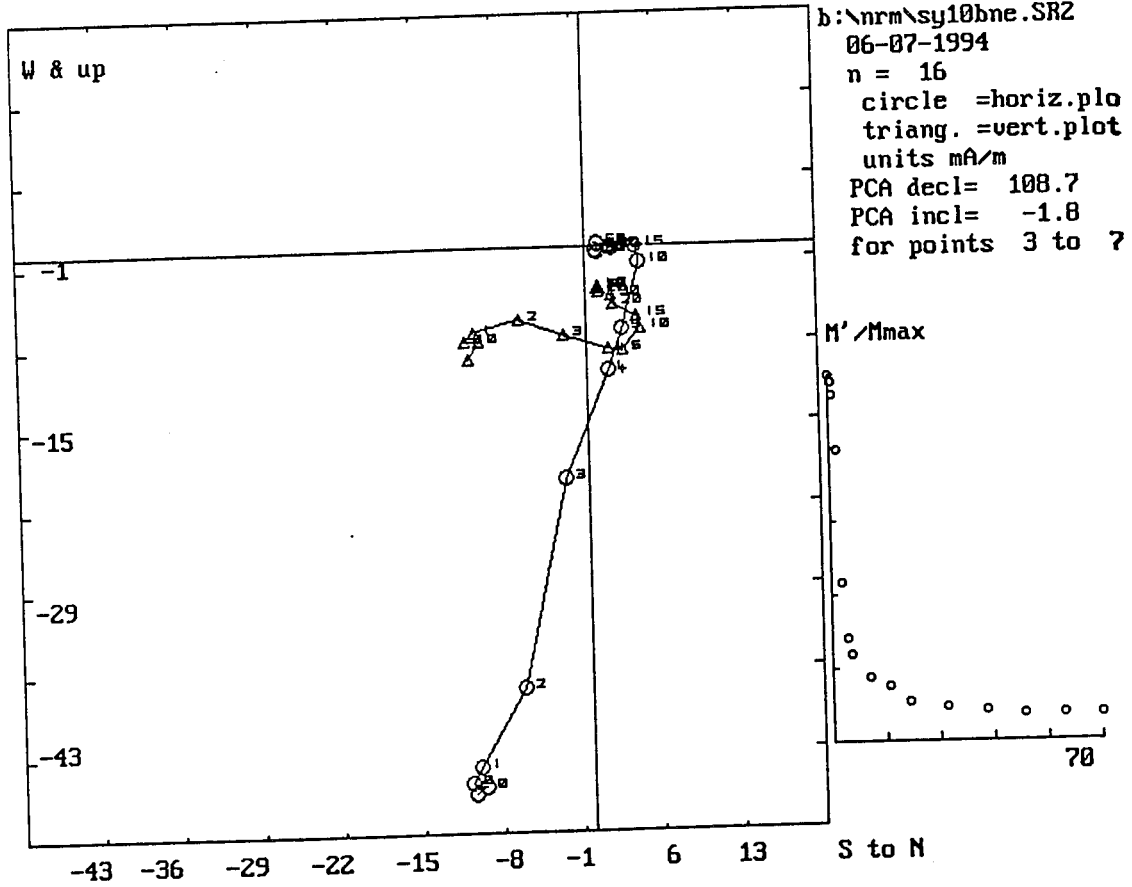
Lwr.Hem.Equal Area Net
circle=DOWN square=UP
 :\nrm\sy15bne.SR2
 n = 13
 06-07-1994

m.dec.= 356.9
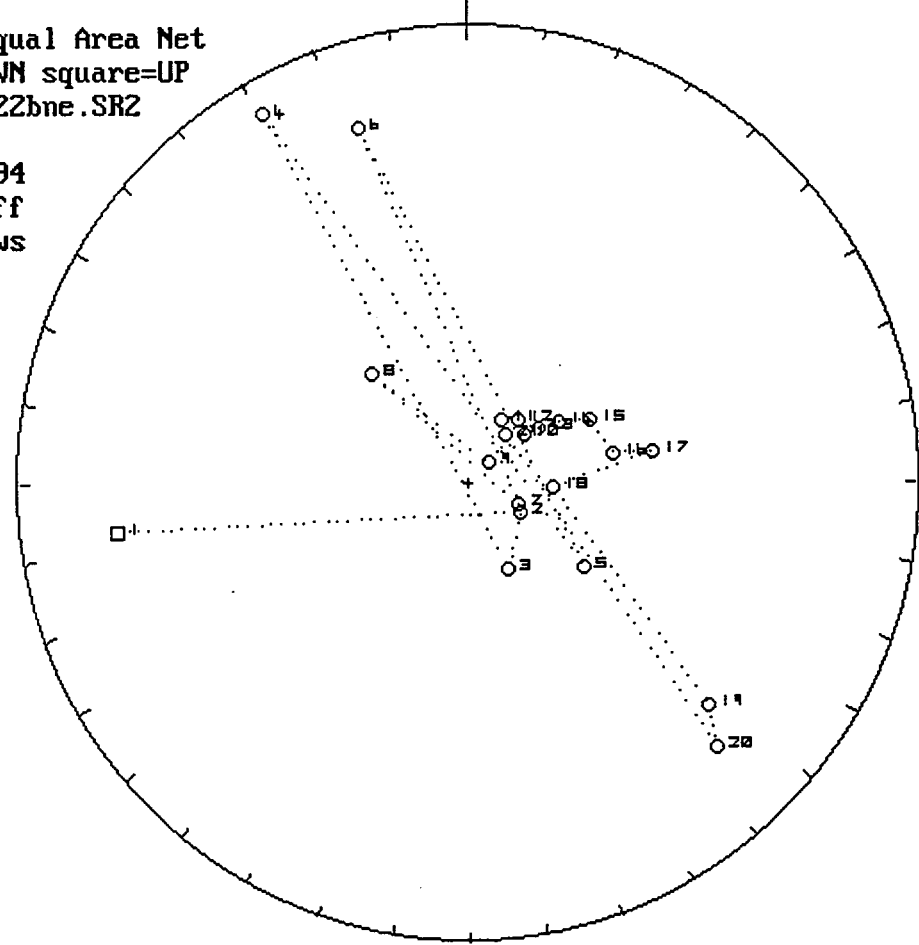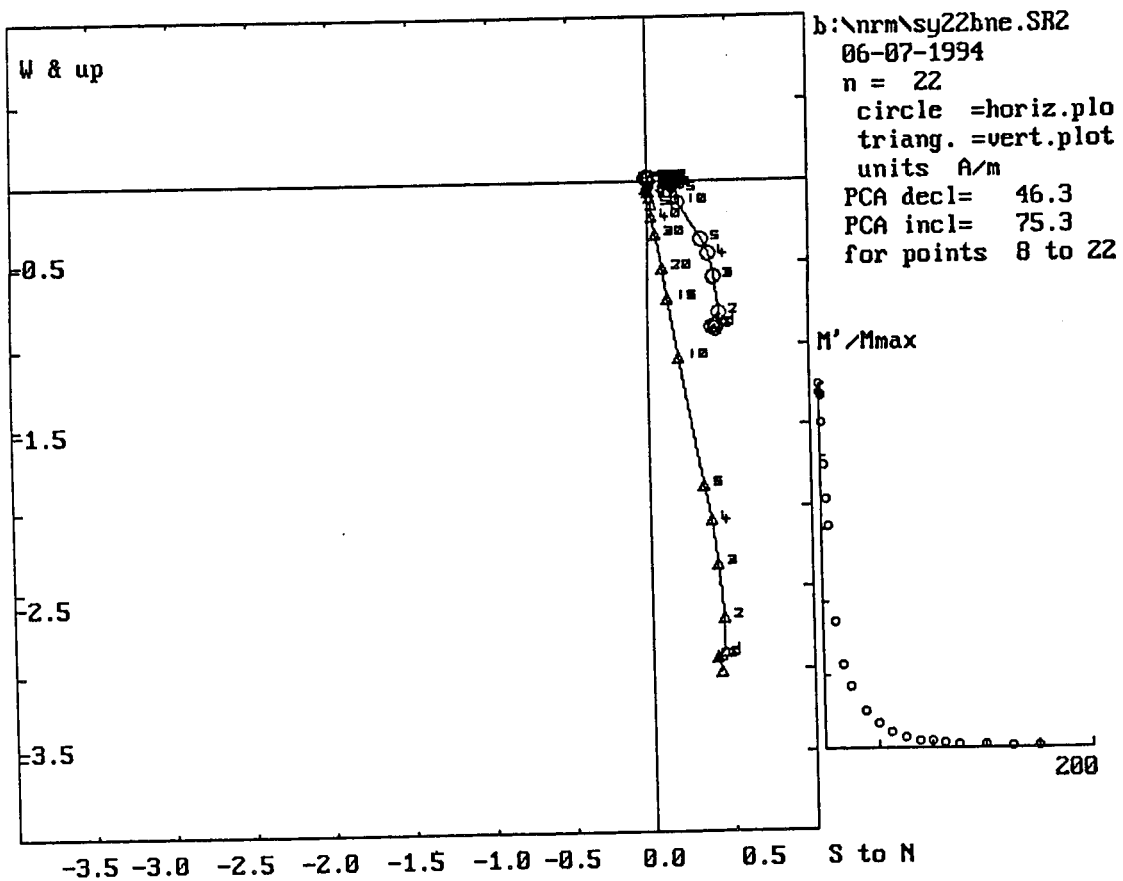m.inc.= -47.5
alpha95= 14.8
Fish. k= 8.7
sp.var.= 0.105

Lwr.Hem.Equal Area Net
circle=DOWN square=UP
 :\nrm\sy15bne.SR2
 n = 12
 06-07-1994
Vector Diff
Plot: shows
vectors
added in
nature

b:\nrm\sy15bne.SR2
06-07-1994
n = 13
 circle =horiz.plo
 triang. =vert.plot
 units mA/m
PCA decl=   4.0
PCA incl=   64.6
for points 1 to 5

M'/Mmax

S to N

b:\nrm\sy15bne.SR2
06-07-1994
 n = 13
  circle =horiz.plo
  triang. =vert.plot
  units mA/m
PCA decl=   6.8
PCA incl=   -7.5
for points 5 to 9
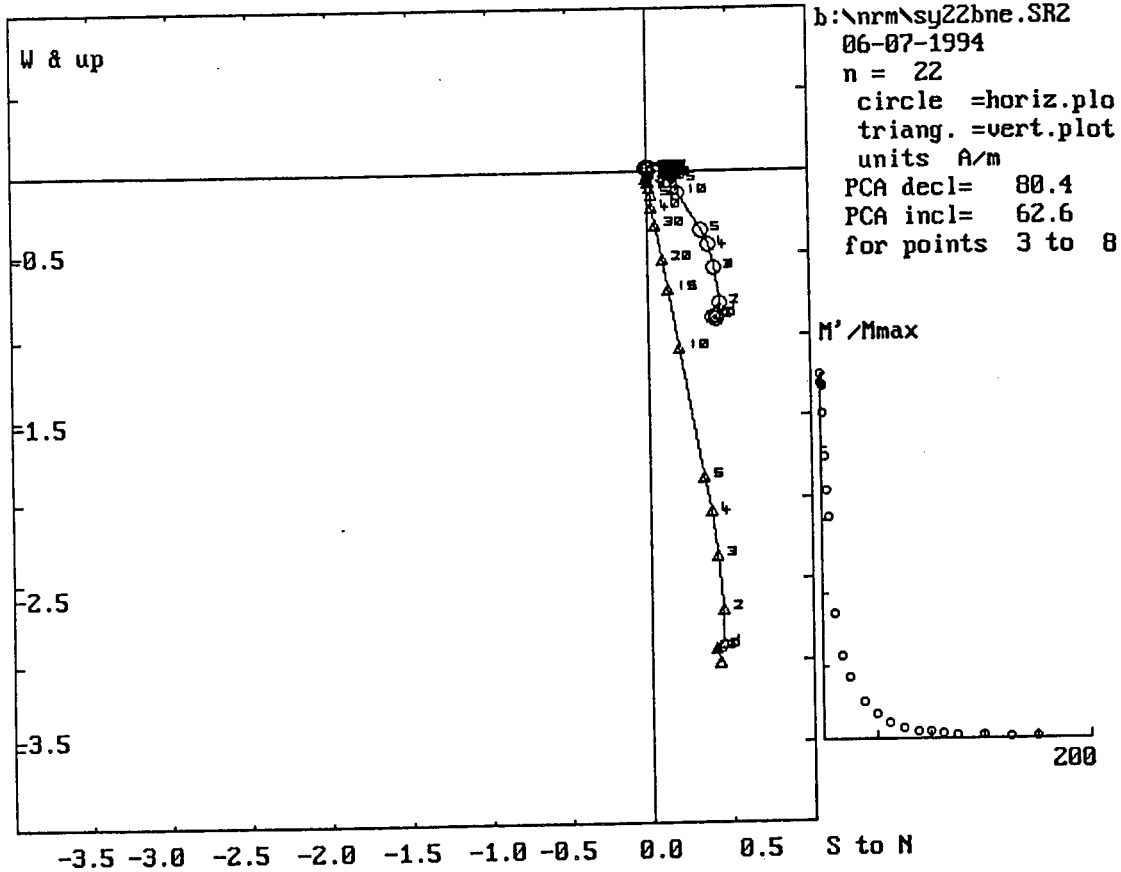
M'/Mmax

S to N

b:\nrm\sy15bne.SR2
08-11-1994
n = 13
 circle =horiz.plo
 triang. =vert.plot
 units mA/m
PCA decl= 16.3
PCA incl= 27.3
for points 1 to 8

M'/Mmax

b:\nrm\sy15bne.SR2
06-07-1994
n = 13
 circle =horiz.plo
 triang. =vert.plot
 units mA/m
PCA decl= 342.9
PCA incl= -51.8
for points 9 to 13

M'/Mmax

Lwr.Hem.Equal Area Net
circle=DOWN square=UP
 :\nrm\sy16bne.SR2
 n = 17
 06-07-1994

m.dec.= 337.1
m.inc.= 58.0
alpha95= 1.9
Fish. k= 340.8
sp.var.= 0.002

Lwr.Hem.Equal Area Net
circle=DOWN square=UP
 :\nrm\sy16bne.SR2
 n = 16
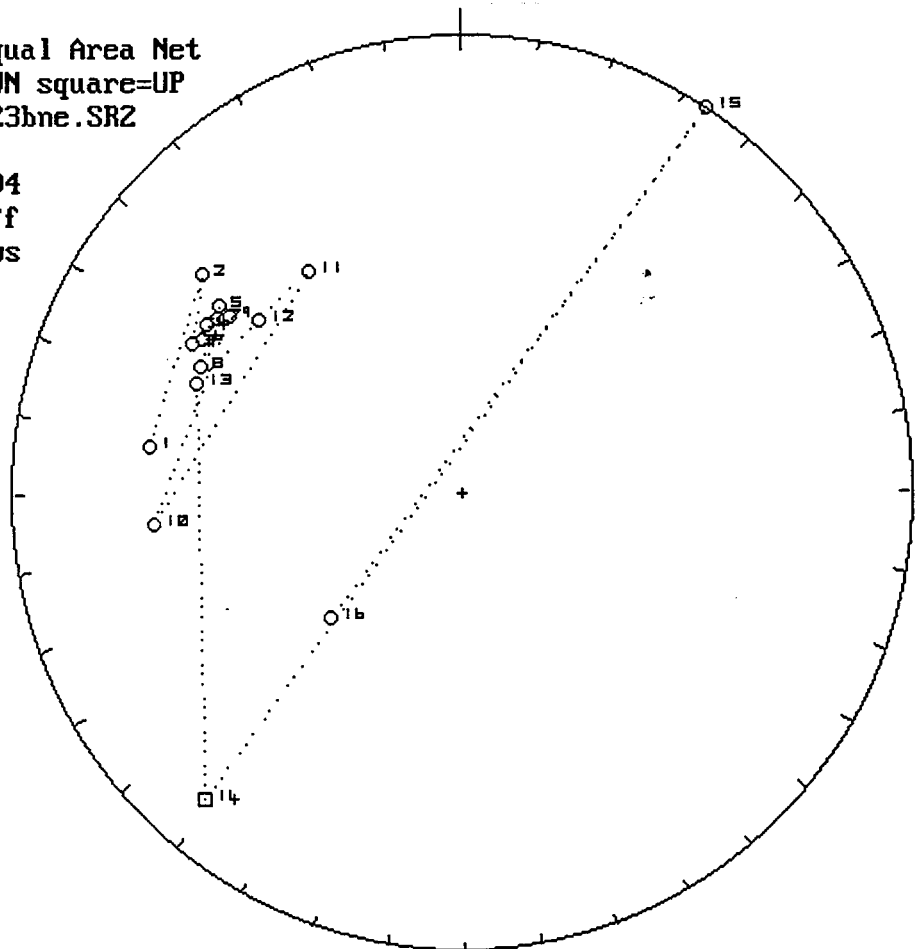 06-07-1994
Vector Diff
Plot: shows
vectors
added in
nature
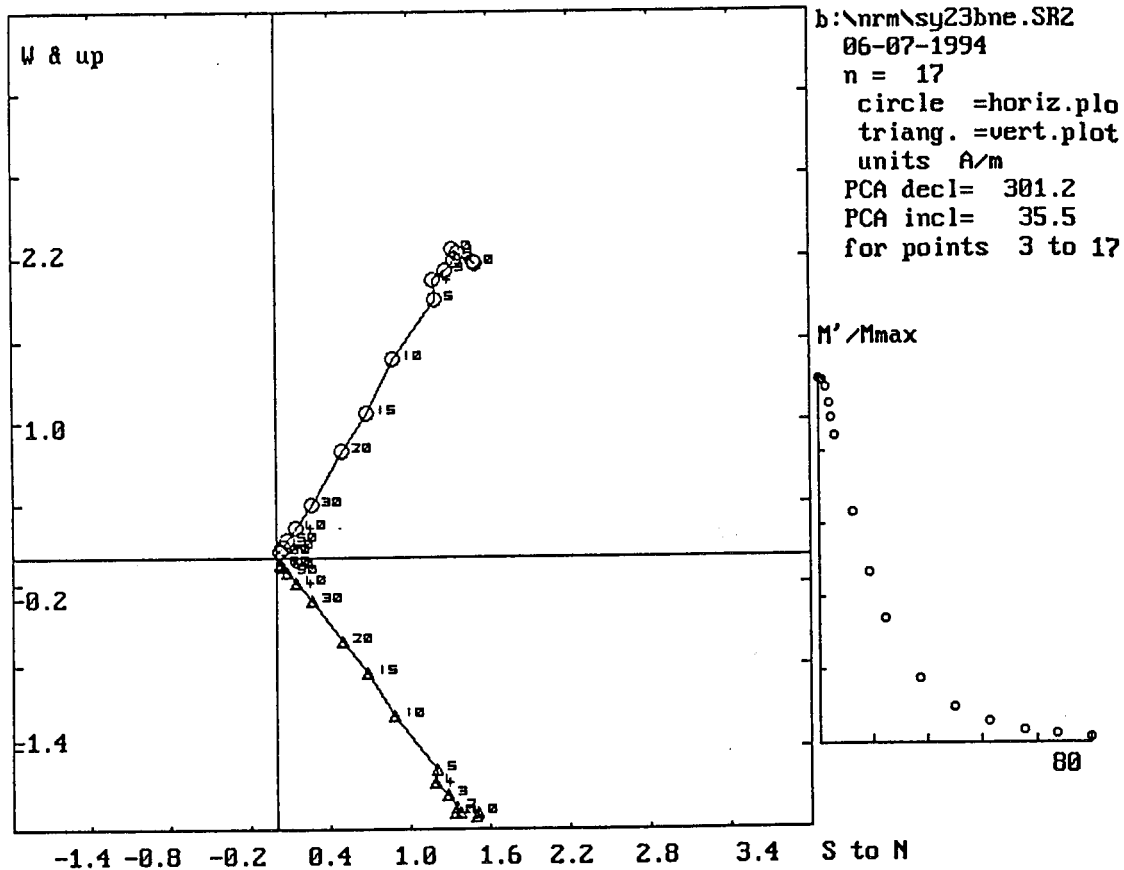
W & up
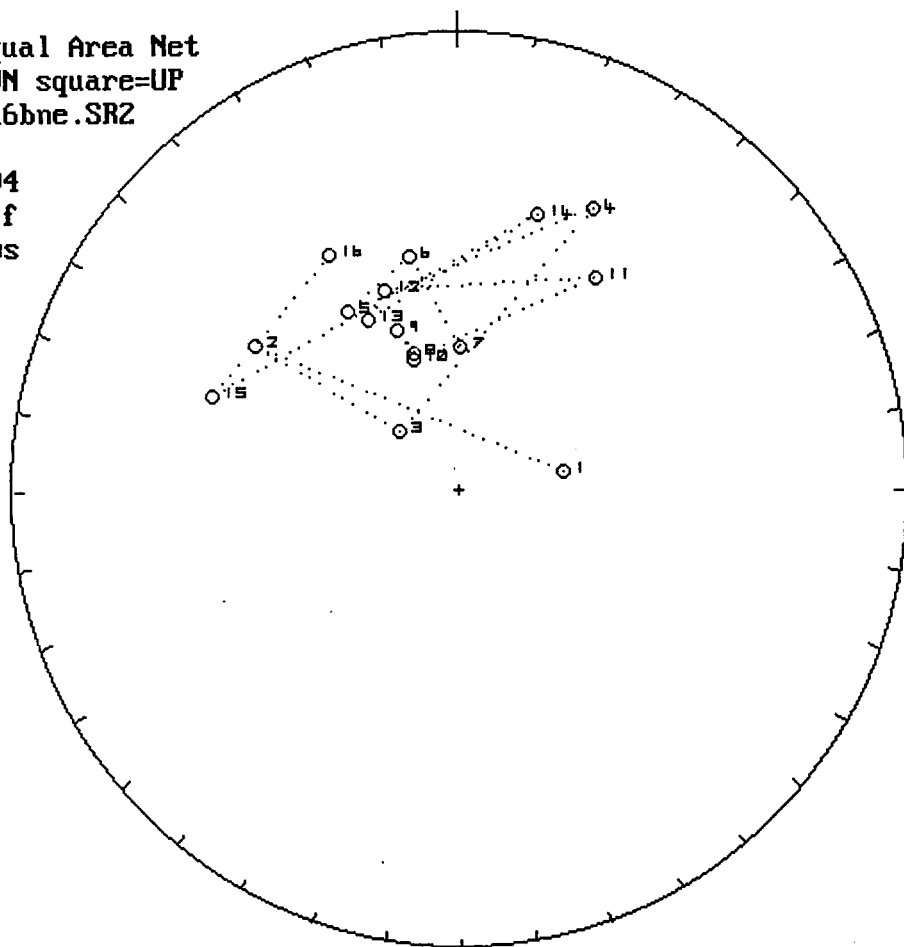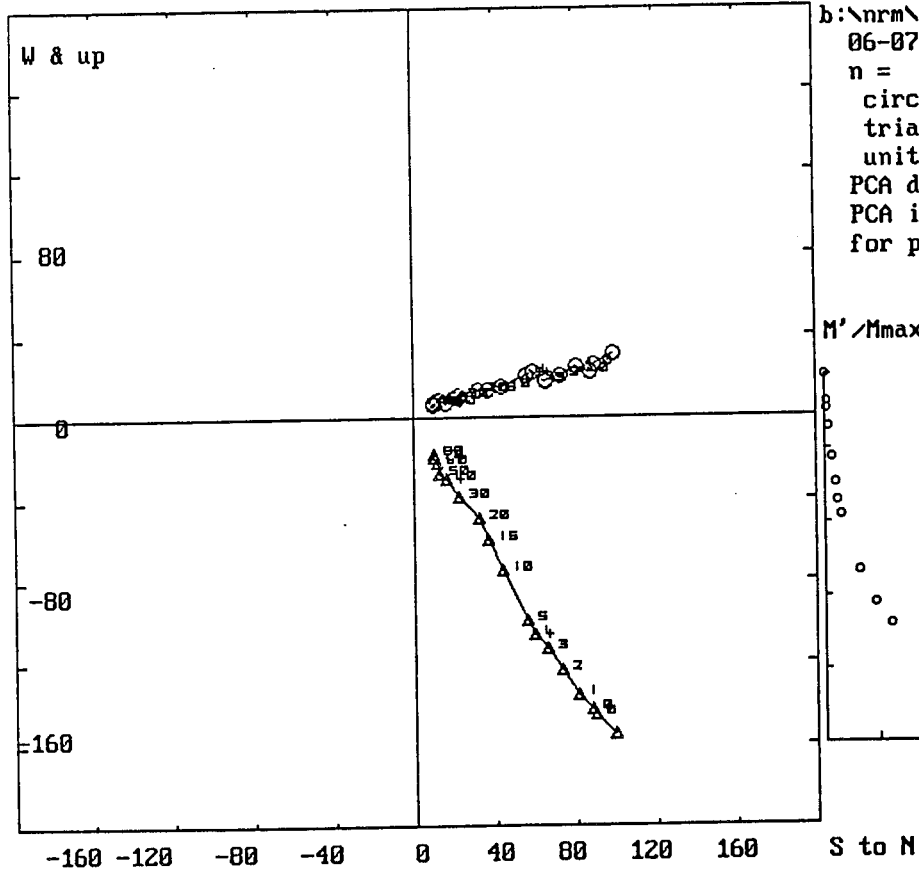
b:\nrm\sy16bne.SR2
06-07-1994
n = 17
circle =horiz.plo
triang. =vert.plot
units mA/m
PCA decl= 346.9
PCA incl= 57.4
for points 1 to 17

M'/Mmax

80

0

-80

-160

-160 -120 -80 -40   0   40   80 120 160   S to N

80

Lwr.Hem.Equal Area Net
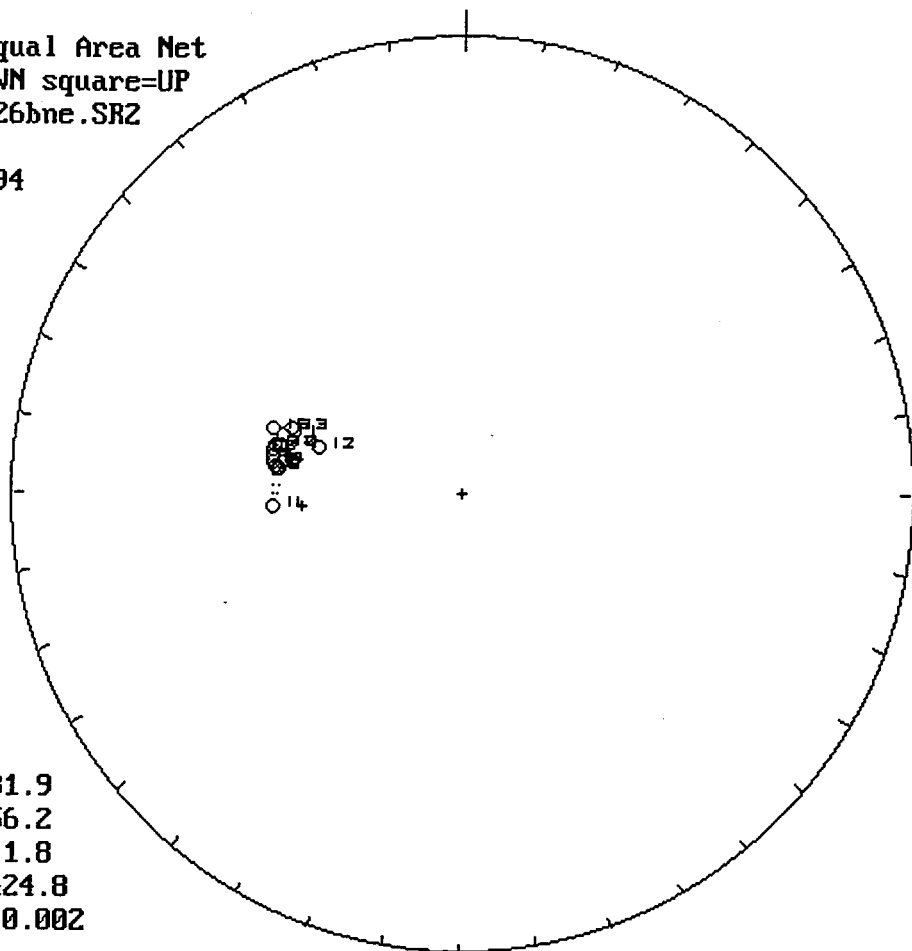circle=DOWN square=UP
 :\nrm\sy19bne.SR2
 n = 10
 06-07-1994

m.dec.= 15.2
m.inc.= 63.7
alpha95= 2.6
Fish. k= 338.5
sp.var.= 0.002

Lwr.Hem.Equal Area Net
circle=DOWN square=UP
 :\nrm\sy19bne.SR2
 n = 9
 06-07-1994
Vector Diff
Plot: shows
vectors
added in
nature
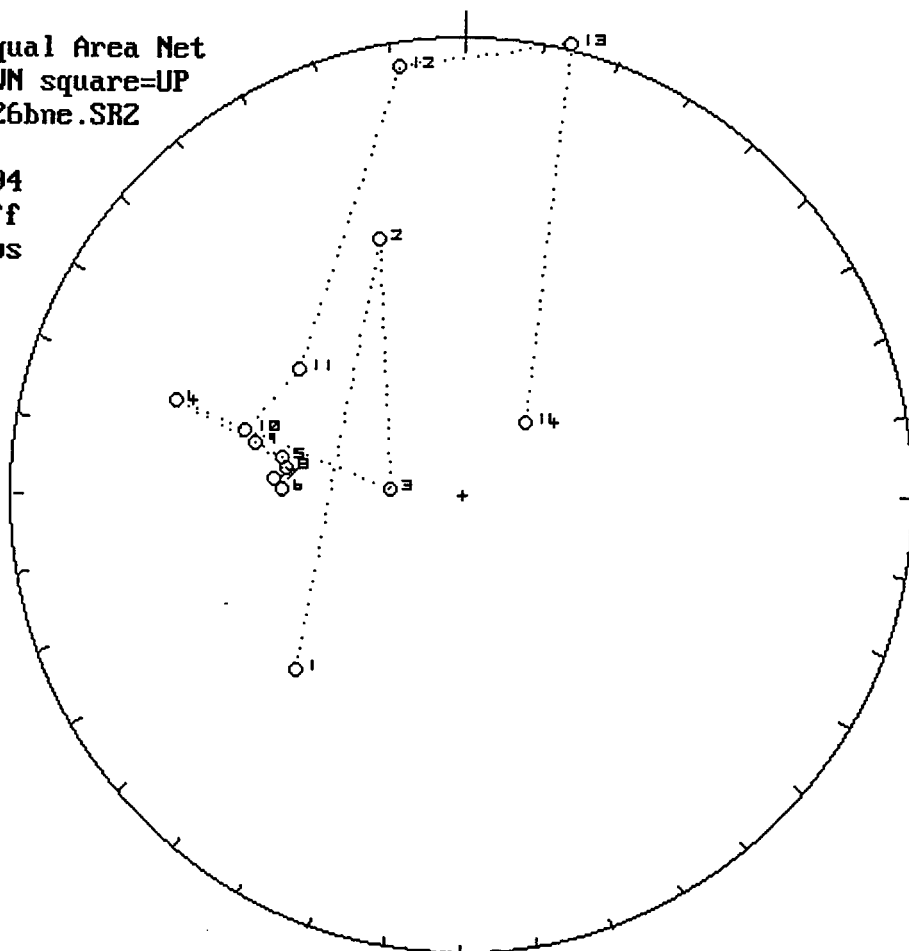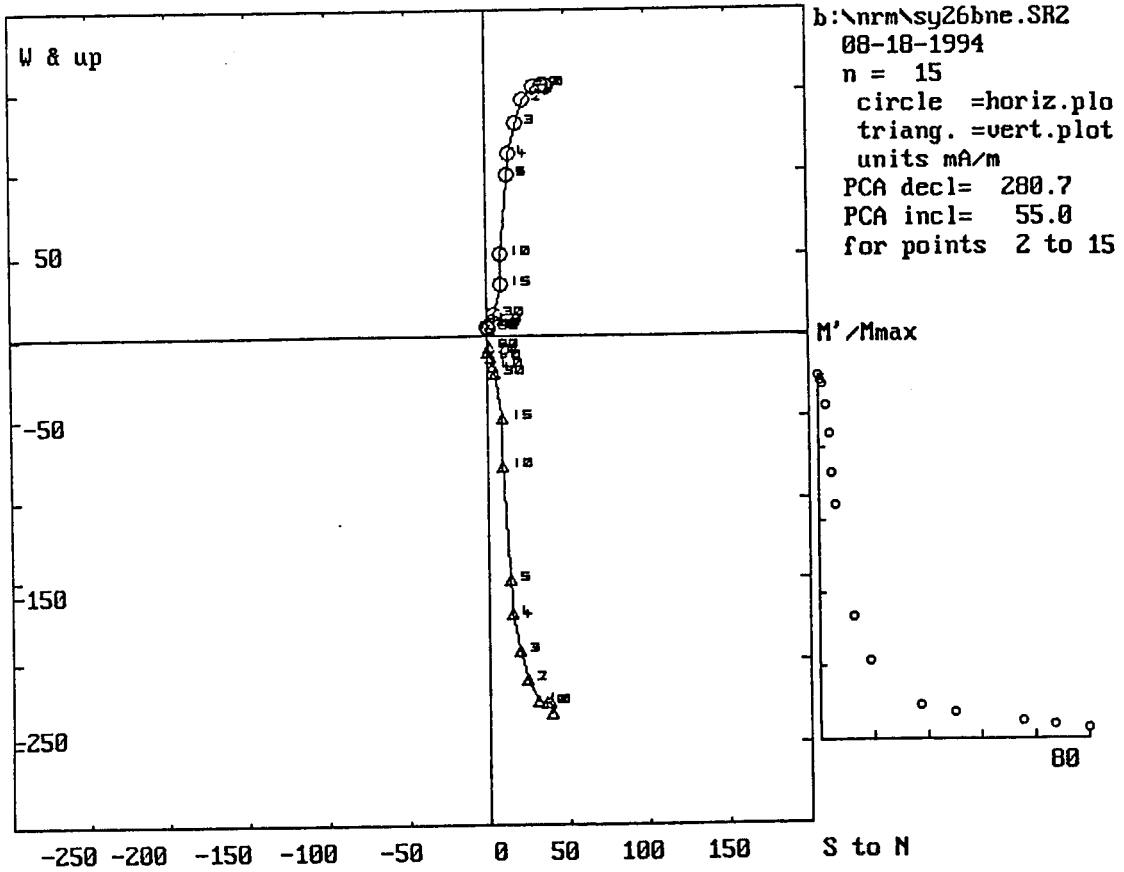
W & up

9

-5

-19

-33

-33 -26 -19 -12 -5   2   9   16   23   S to N

b:\nrm\sy19bne.SR2
  06-07-1994
  n = 10
   circle =horiz.plo
   triang. =vert.plot
   units mA/m
  PCA decl=   33.9
  PCA incl=   57.1
  for points 1 to 10

M'/Mmax

20

Lwr.Hem.Equal Area Net
circle=DOWN square=UP
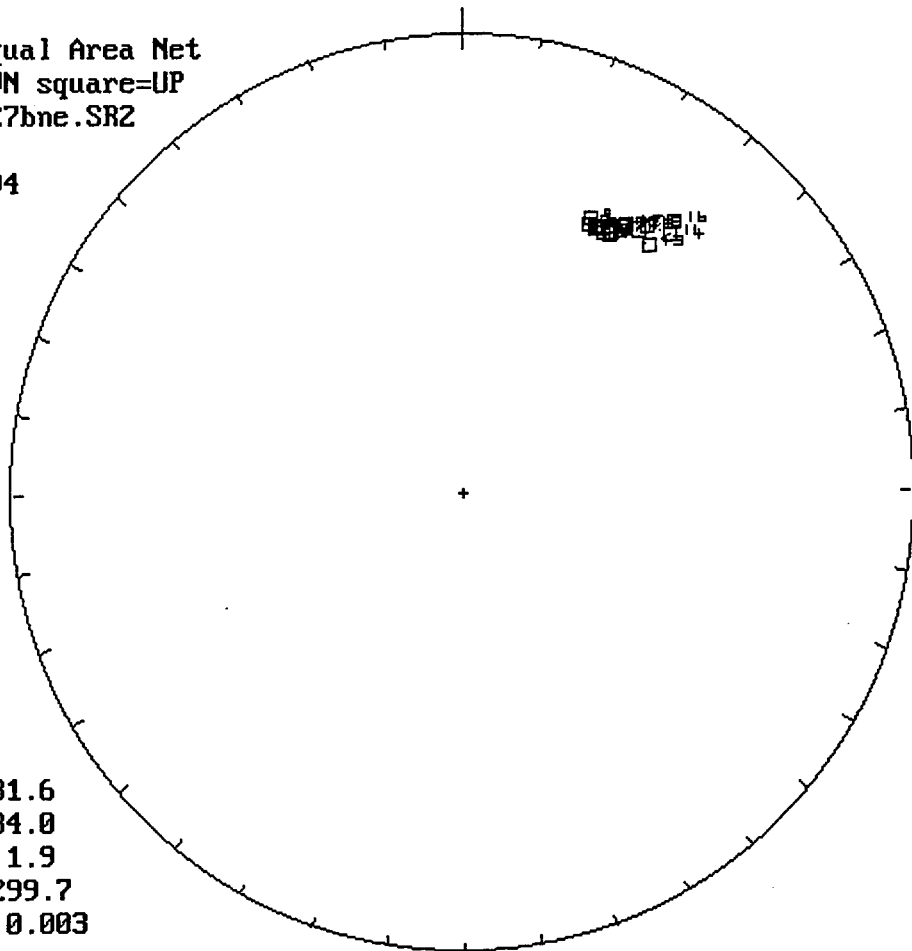 :\nrm\sy20bne.SR2
 n = 11
 06-07-1994

m.dec.=   5.6
m.inc.= 75.3
alpha95= 1.7
Fish. k= 645.3
sp.var.= 0.001

Lwr.Hem.Equal Area Net
circle=DOWN square=UP
 :\nrm\sy20bne.SR2
 n = 10
 06-07-1994
Vector Diff
Plot: shows
vectors
added in
nature

W & up

1

-5

-11

-17

-17 -14 -11 -8 -5 -2 1 4 7

S to N

b:\nrm\sy20bne.SR2
06-07-1994
n = 11
  circle =horiz.plo
  triang. =vert.plot
  units mA/m
PCA decl= 10.2
PCA incl= 70.7
for points 1 to 11

M'/Mmax

30
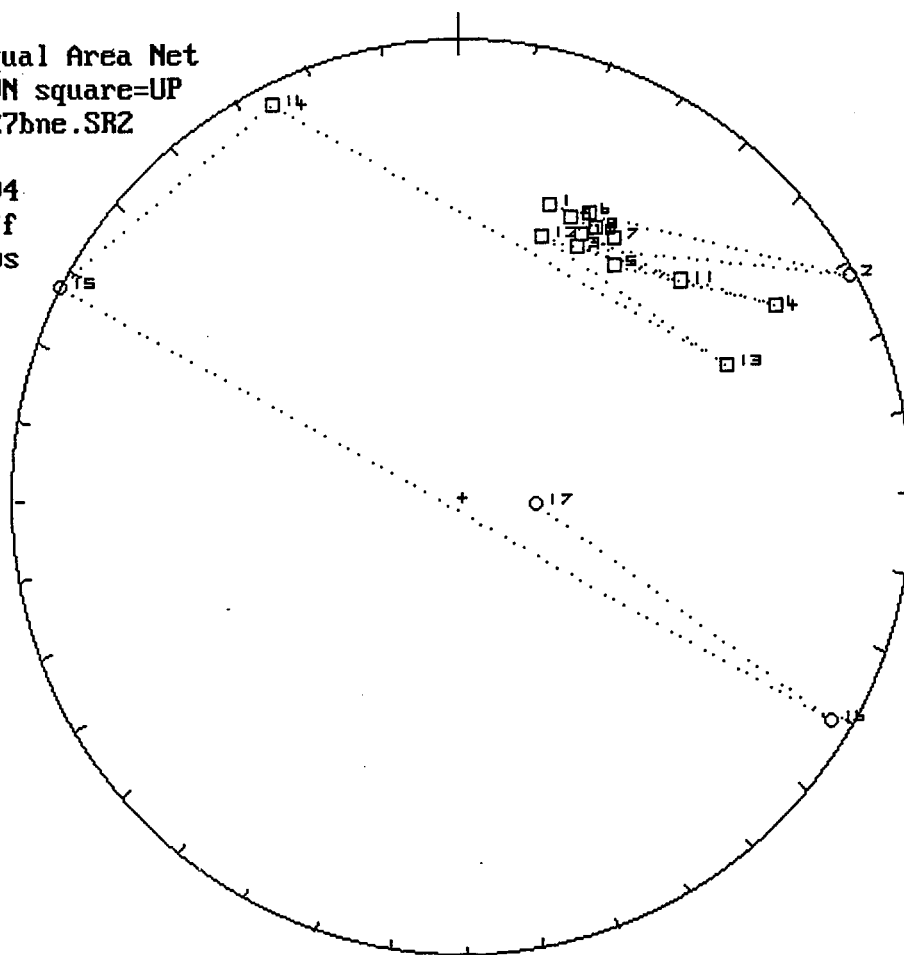
Lwr.Hem.Equal Area Net
circle=DOWN square=UP
  :\nrm\sy21bne.SR2
   n = 14
   06-07-1994

m.dec.= 99.5
m.inc.= 37.2
alpha95= 11.8
Fish. k= 12.2
sp.var.= 0.075

Lwr.Hem.Equal Area Net
circle=DOWN square=UP
  :\nrm\sy21bne.SR2
   n = 13
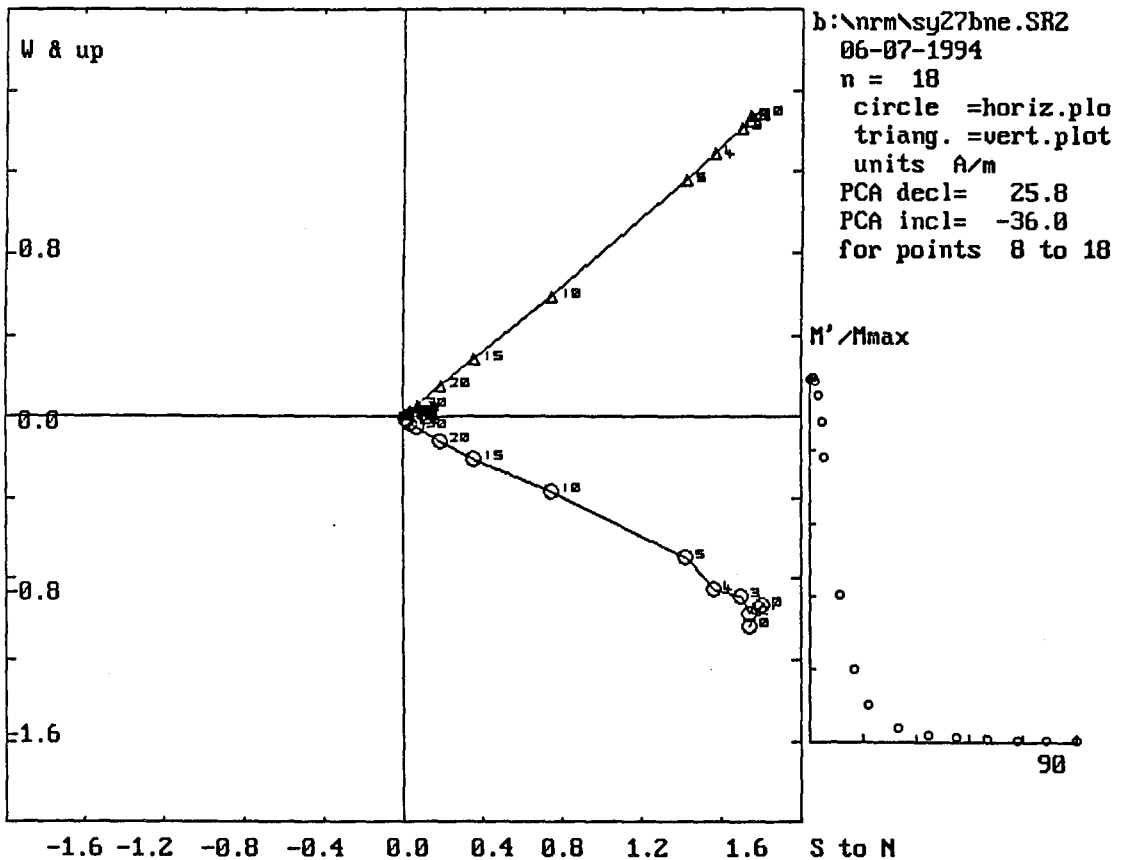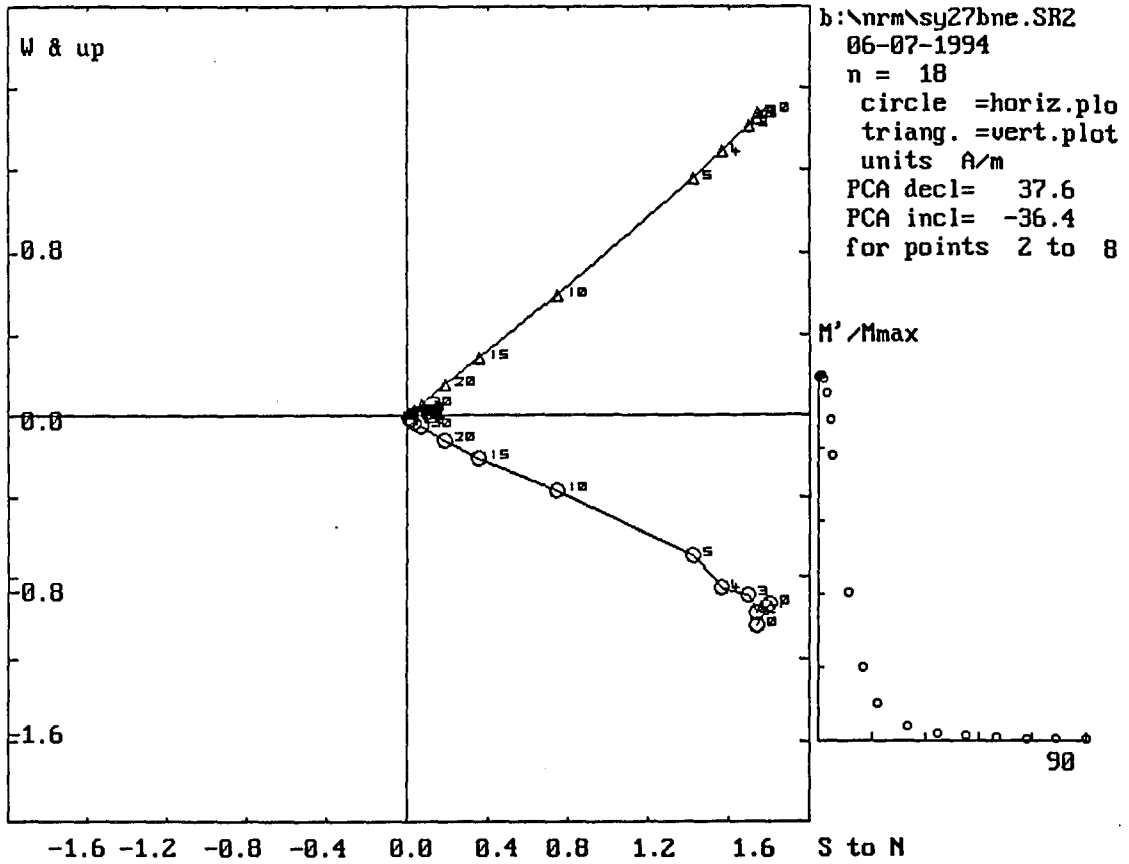   06-07-1994
Vector Diff
Plot: shows
vectors
added in
nature
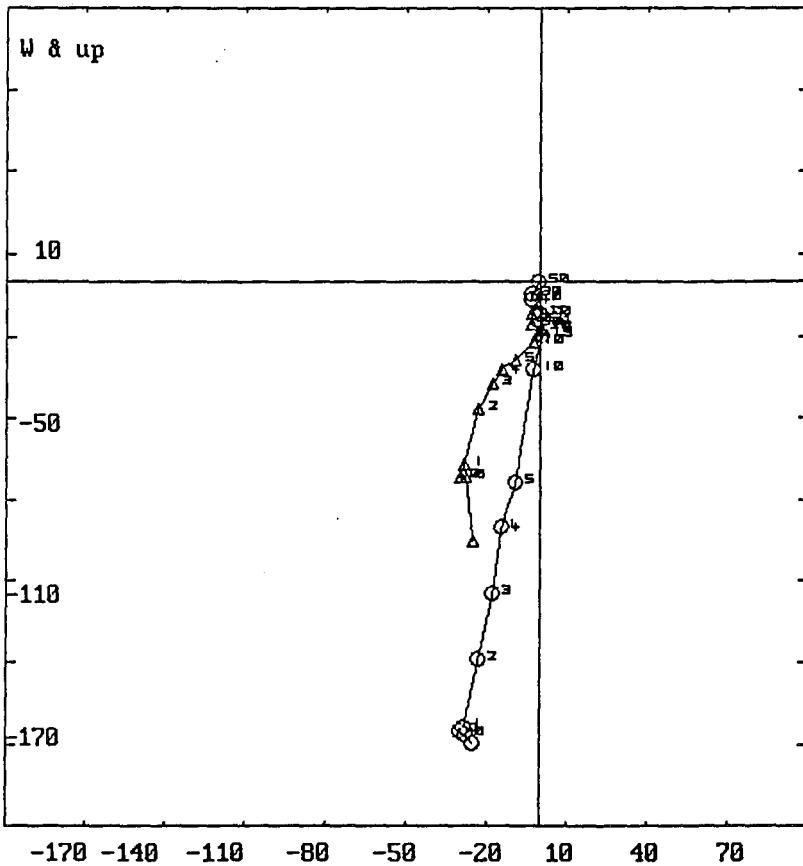
b:\nrm\sy21bne.SR2
06-07-1994
n = 14
 circle =horiz.plo
 triang. =vert.plot
 units mA/m
PCA decl= 101.6
PCA incl= 25.5
for points 2 to 8

M'/Mmax
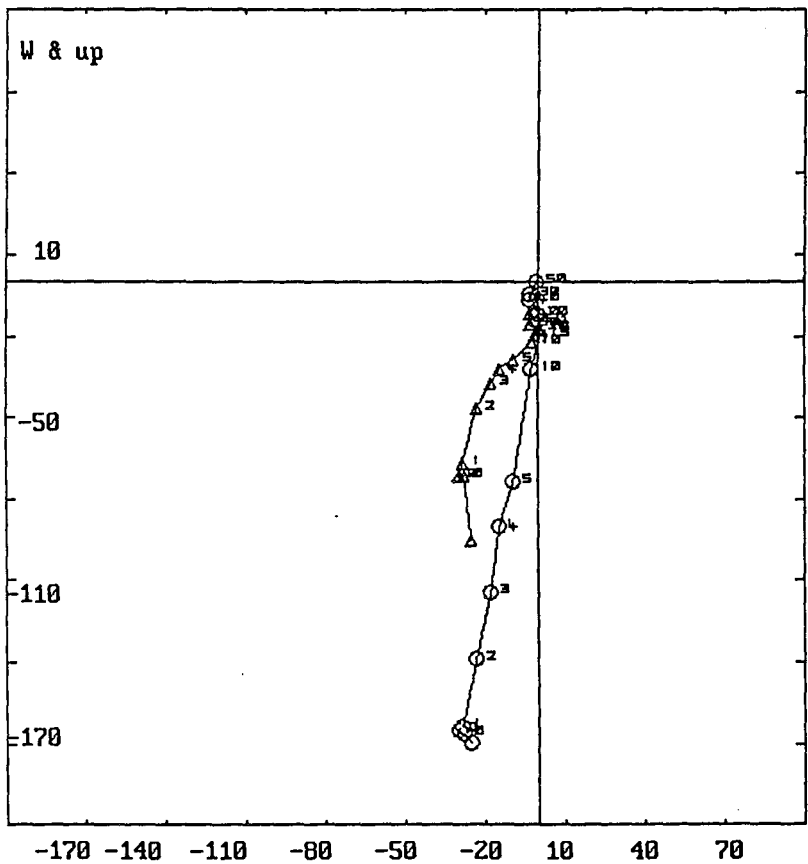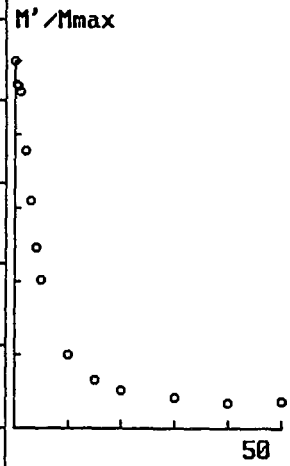
b:\nrm\sy21bne.SR2
06-07-1994
n = 14
 circle =horiz.plo
 triang. =vert.plot
 units mA/m
PCA decl= 96.0
PCA incl= 12.0
for points 8 to 14

M'/Mmax

Lwr.Hem.Equal Area Net
circle=DOWN square=UP
 :\nrm\sy22bne.SR2
 n = 22
 06-07-1994
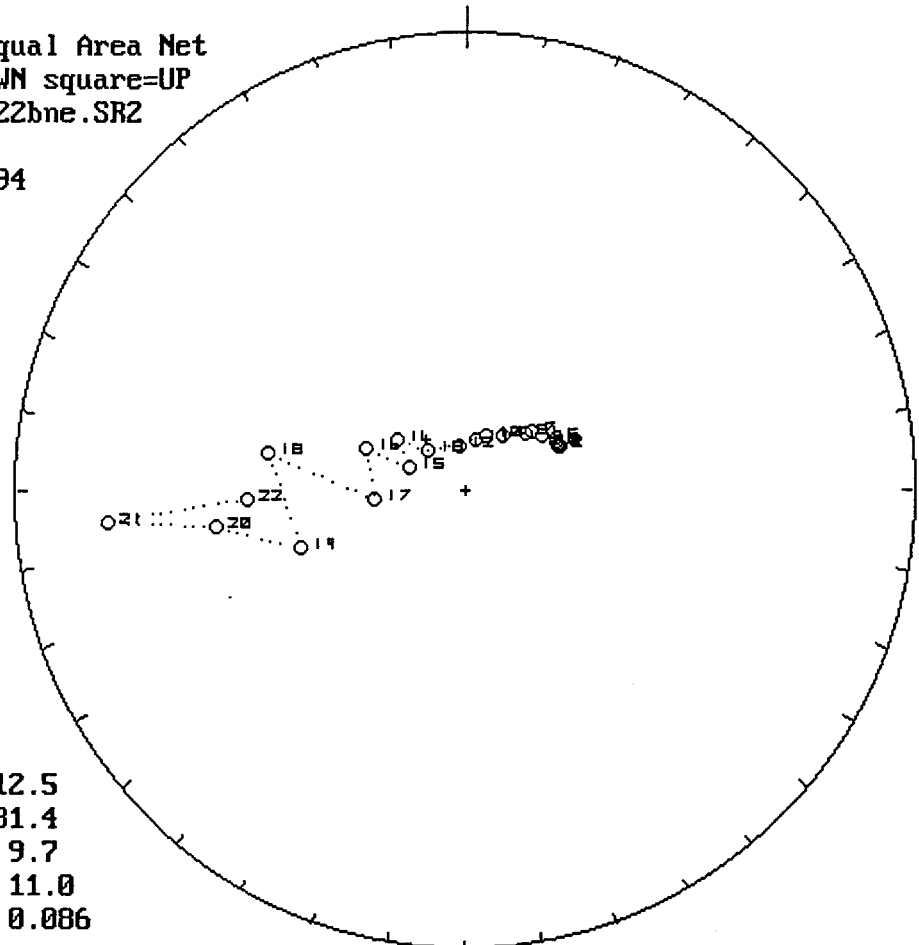
m.dec.= 312.5
m.inc.= 81.4
alpha95= 9.7
Fish. k= 11.0
sp.var.= 0.086

Lwr.Hem.Equal Area Net
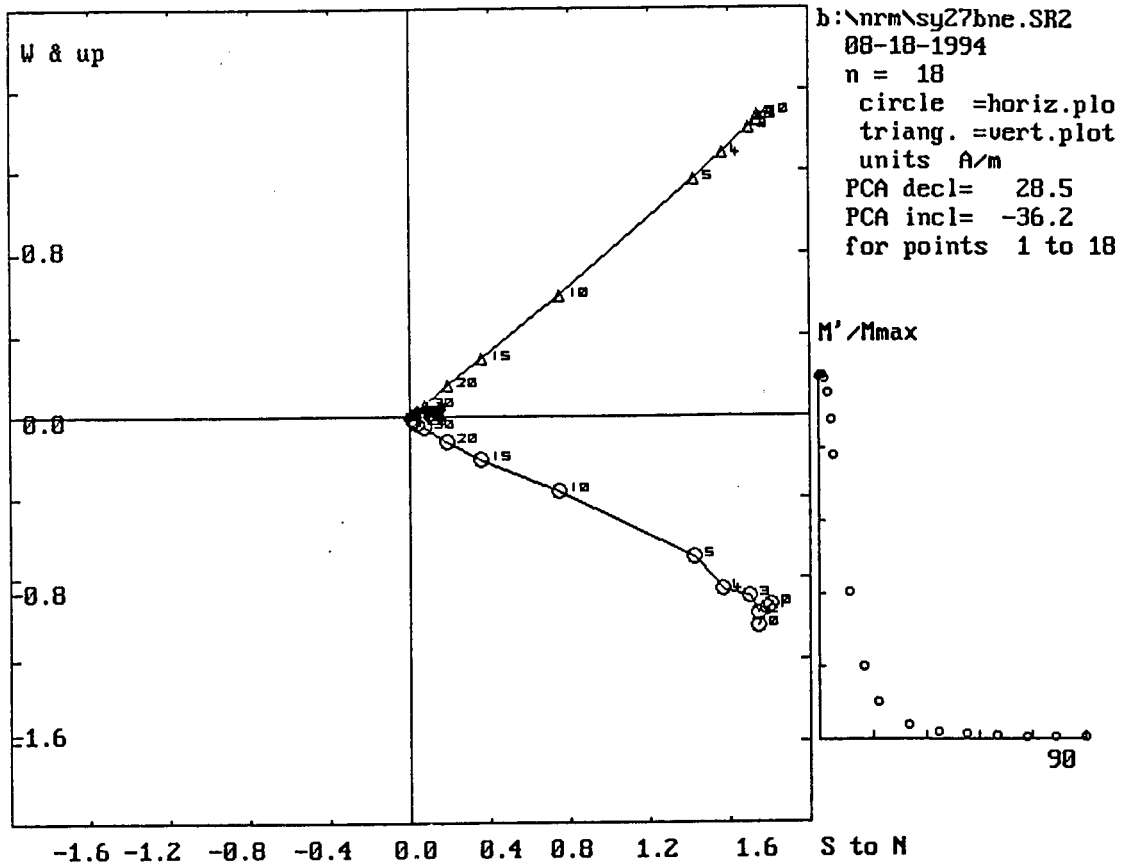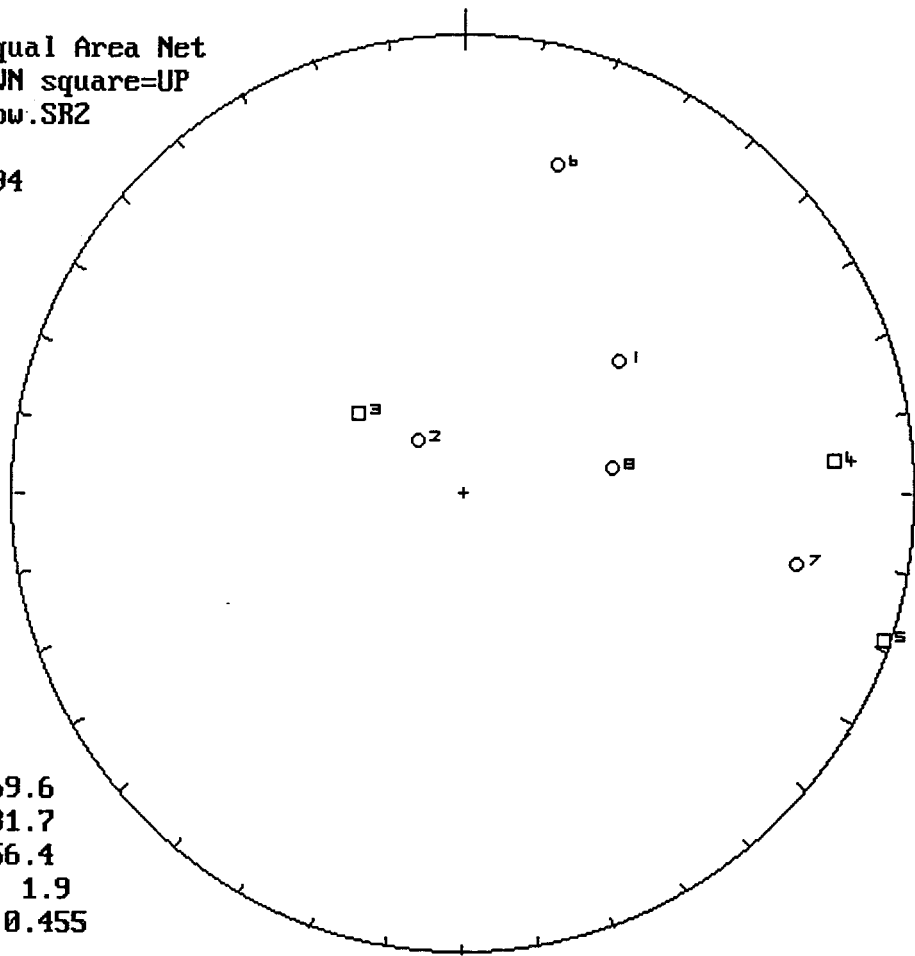circle=DOWN square=UP
 :\nrm\sy22bne.SR2
 n = 21
 06-07-1994
Vector Diff
Plot: shows
vectors
added in
nature

b:\nrm\sy22bne.SR2
06-07-1994
n = 22
 circle =horiz.plo
 triang. =vert.plot
 units A/m
PCA decl= 80.4
PCA incl= 62.6
for points 3 to 8

M'/Mmax

W & up

S to N

b:\nrm\sy22bne.SR2
06-07-1994
n = 22
 circle =horiz.plo
 triang. =vert.plot
 units A/m
PCA decl= 46.3
PCA incl= 75.3
for points 8 to 22

M'/Mmax

W & up

S to N

Lwr.Hem.Equal Area Net
circle=DOWN square=UP
 :\nrm\sy23bne.SR2
 n = 17
 06-07-1994
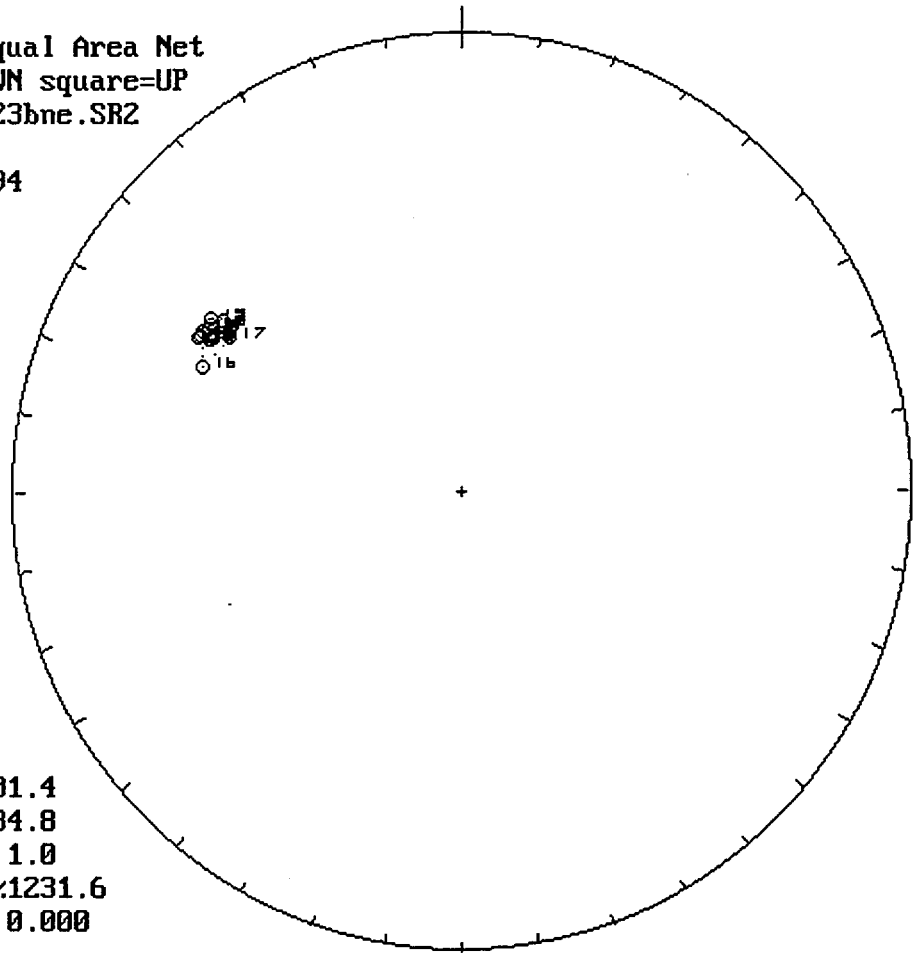
m.dec.= 301.4
m.inc.= 34.8
alpha95= 1.0
Fish. k= %1231.6
sp.var.= 0.000

Lwr.Hem.Equal Area Net
circle=DOWN square=UP
 :\nrm\sy23bne.SR2
 n = 16
 06-07-1994
Vector Diff
Plot: shows
vectors
added in
nature

b:\nrm\sy23bne.SR2
  06-07-1994
  n = 17
   circle =horiz.plo
   triang. =vert.plot
   units A/m
  PCA decl= 301.2
  PCA incl=   35.5
  for points 3 to 17

Lwr.Hem.Equal Area Net
circle=DOWN square=UP
 :\nrm\sy26bne.SR2
 n = 15
 08-18-1994

m.dec.= 281.9
m.inc.= 56.2
alpha95= 1.8
Fish. k= 424.8
sp.var.= 0.002

Lwr.Hem.Equal Area Net
circle=DOWN square=UP
 :\nrm\sy26bne.SR2
 n = 14
 08-18-1994
Vector Diff
Plot: shows
vectors
added in
nature

W & up

b:\nrm\sy26bne.SR2
08-18-1994
n = 15
circle =horiz.plo
triang. =vert.plot
units mA/m
PCA decl= 280.7
PCA incl= 55.0
for points 2 to 15

50

M'/Mmax

-50

-150

-250

-250 -200 -150 -100 -50   0   50 100 150

80

S to N

Lwr.Hem.Equal Area Net
circle=DOWN square=UP
 :\nrm\sy27bne.SR2
 n = 18
 06-07-1994

m.dec.= 31.6
m.inc.= -34.0
alpha95= 1.9
Fish. k= 299.7
sp.var.= 0.003

Lwr.Hem.Equal Area Net
circle=DOWN square=UP
 :\nrm\sy27bne.SR2
 n = 17
 06-07-1994
Vector Diff
Plot: shows
vectors
added in
nature

b:\nrm\sy27bne.SR2
06-07-1994
n = 18
  circle =horiz.plo
  triang. =vert.plot
  units A/m
PCA decl=   37.6
PCA incl= -36.4
for points 2 to 8

b:\nrm\sy27bne.SR2
06-07-1994
n = 18
  circle =horiz.plo
  triang. =vert.plot
  units A/m
PCA decl=   25.8
PCA incl= -36.0
for points 8 to 18

b:\nrm\sy27bne.SR2
08-18-1994
n = 18
 circle =horiz.plo
 triang. =vert.plot
 units A/m
PCA decl= 28.5
PCA incl= -36.2
for points 1 to 18

Lwr.Hem.Equal Area Net
circle=DOWN square=UP
 b:\nrm\low.SR2
 n = 8
 08-18-1994

m.dec.= 69.6
m.inc.= 31.7
alpha95= 56.4
Fish. k=   1.9
sp.var.= 0.455

Lwr.Hem.Equal Area Net
circle=DOWN square=UP
 b:\nrm\high.SR2
 n = 8
 08-18-1994
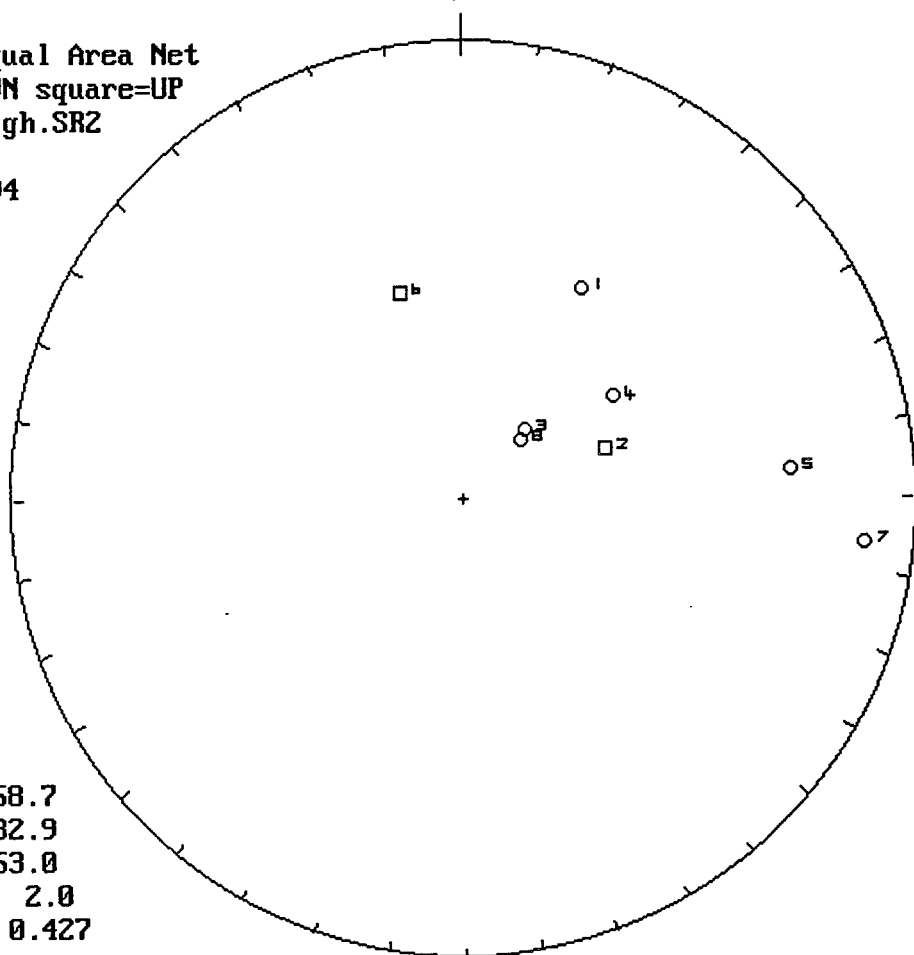
m.dec.= 58.7
m.inc.= 32.9
alpha95= 53.0
Fish. k=   2.0
sp.var.= 0.427

Lwr.Hem.Equal Area Net
circle=DOWN square=UP
 b:\nrm\lma.SR2
 n = 3
 08-18-1994

○³

○²
○¹

+
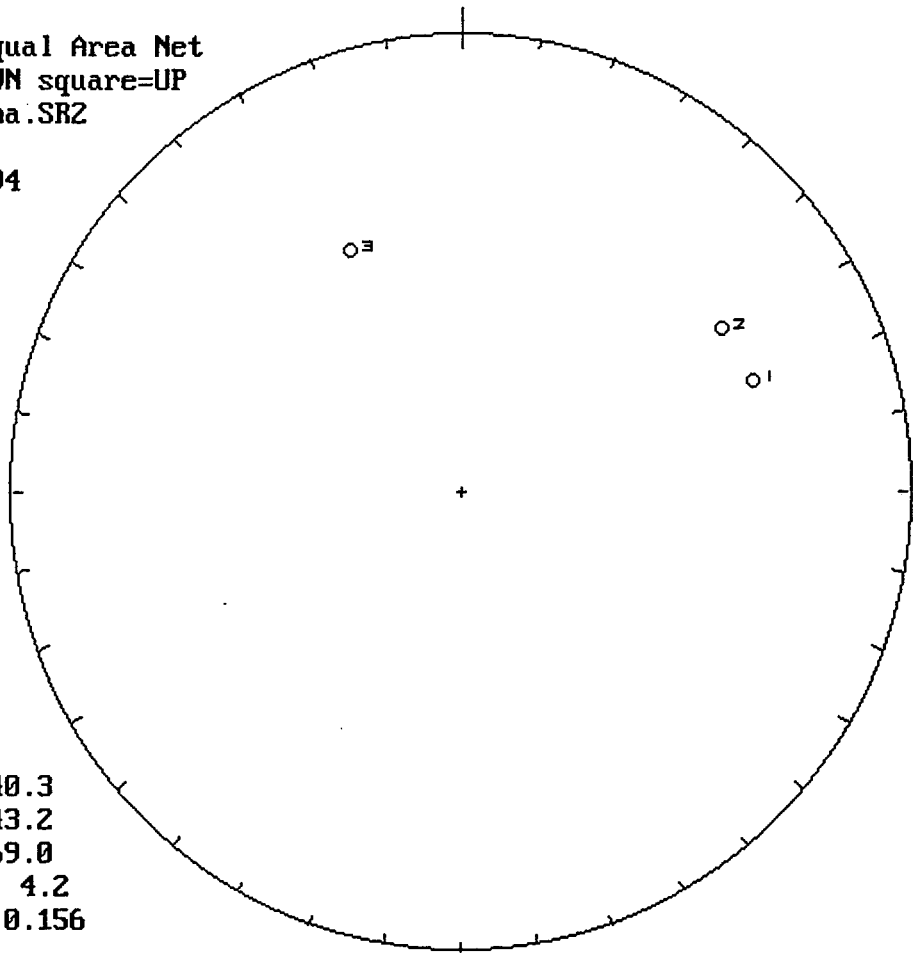
m.dec.= 40.3
m.inc.= 43.2
alpha95= 69.0
Fish. k=   4.2
sp.var.= 0.156

Lwr.Hem.Equal Area Net
circle=DOWN square=UP
 b:\nrm\all.SR2
 n = 7
 08-18-1994

□⁷

○²   ○³

○⁵   ○⁴
□¹

○⁶   +
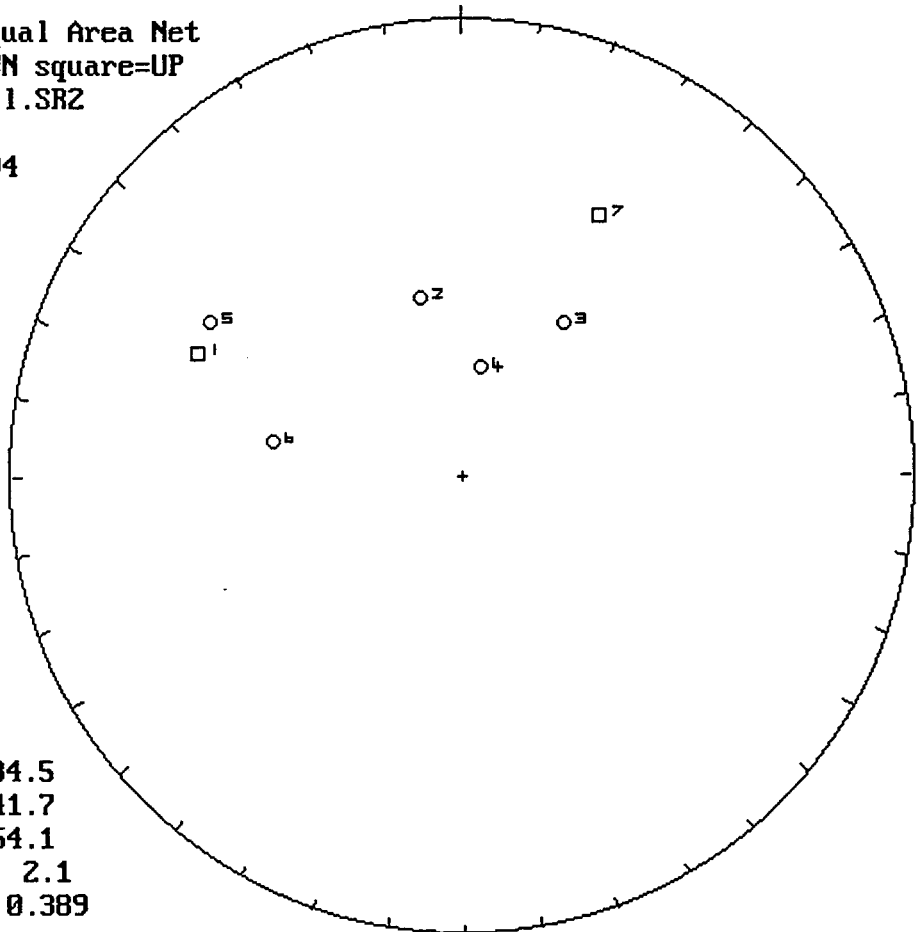
m.dec.= 334.5
m.inc.= 41.7
alpha95= 54.1
Fish. k=   2.1
sp.var.= 0.389

APPENDIX E

THERMAL DEMAGNETIZATION
(DATA, STEREOGRAPHIC PROJECTIONS, PCAs)

thermal demagnetization

sample	date	time	declination	inclination	mA/m	cm3	temp.C	error %
sy5bt	04-08-199	11:54	233.4	71.81	4.031	11.15	0	1
sy5bt	04-08-199	11:54	227.04	41.01	1.816	11.15	100	3.4
sy5bt	04-08-199	11:54	221.77	9.55	1.541	11.15	185	8.7
sy5bt	04-08-199	11:54	221.55	-11.86	1.514	11.15	300	6.4
sy5bt	04-11-199	09:07	228.23	-22.55	1.399	11.15	550	3.1
sy5bt	04-11-199	11:48	227.24	-21.42	1.17	11.15	600	1
sy5bt	04-11-199	17:30	234.89	6.33	0.552	11.15	675	4.3
sy5bt	04-12-199	10:25	229.73	-24.46	0.329	11.15	700	7.5
sy11bt	04-08-199	11:54	40.33	-7.92	2105.872	11.15	0	0.2
sy11bt	04-08-199	11:54	43.24	-7.97	2092.988	11.15	100	0.3
sy11bt	04-08-199	11:54	42.72	-8.3	1802.165	11.15	185	0.3
sy11bt	04-08-199	11:54	44.62	-8.23	1537.546	11.15	300	0.3
sy11bt	04-08-199	11:54	43.59	-8.35	1461.219	11.15	400	0.1
sy11bt	04-08-199	11:54	41.94	-8.39	1406.467	11.15	450	0.2
sy11bt	04-08-199	16:27	44.29	-7.95	1168	11.15	500	0.3
sy11bt	04-11-199	09:19	45.05	-8.53	1129	11.15	550	0.3
sy11bt	04-11-199	11:58	47.59	-6.85	905	11.15	600	1.7
sy11bt	04-11-199	14:47	43.29	-5.62	129.9	11.15	650	1.2
sy11bt	04-11-199	17:41	44.27	-5.34	93	11.15	675	1.1
sy11bt	04-12-199	10:36	48.77	-5.77	70.1	11.15	700	2
sy14bt	04-08-199	11:54	204.69	10.46	4186.12	11.15	0	0.4
sy14bt	04-08-199	11:54	203.19	9.93	4175.068	11.15	100	0.4
sy14bt	04-08-199	11:54	205.12	9.27	2171.22	11.15	185	0.4
sy14bt	04-08-199	11:54	204.74	8.91	1071.133	11.15	300	0.4
sy14bt	04-08-199	11:54	205.72	9.35	892.075	11.15	400	0.4
sy14bt	04-08-199	11:54	204.47	8.75	781.517	11.15	450	0.3
sy14bt	04-08-199	15:04	200.39	8.72	511	11.15	500	0.4
sy14bt	04-11-199	09:22	204.75	7.79	442	11.15	550	0.4
sy14bt	04-11-199	12:02	207.82	6.47	312	11.15	600	1.2
sy14bt	04-11-199	14:50	209.54	5.53	67.3	11.15	650	1.7
sy14bt	04-11-199	17:45	210.66	3.4	55.4	11.15	675	2
sy16bt	04-08-199	11:54	121.26	76.73	142.807	11.15	0	0.4
sy16bt	04-08-199	11:54	119.61	76.71	98.638	11.15	100	0.4
sy16bt	04-08-199	11:54	70.46	73.49	34.731	11.15	185	0.1

thermal demagnetization

sample	date	time	declination	inclination	mA/m	cm3	temp.C	error %
sy16bt	04-08-199	11:54	114.71	71.05	21.357	11.15	300	0.1
sy16bt	04-08-199	11:54	136.47	51.3	16.655	11.15	400	0.7
sy16bt	04-08-199	11:54	150.85	43.4	15.207	11.15	450	0.6
sy16bt	04-08-199	16:03	122.46	27.2	12.35	11.15	500	0.9
sy16bt	04-11-199	11:54	238.91	1.75	7.01	11.15	600	2.8
sy17bt	04-08-199	11:54	322.9	73.25	89.183	11.15	0	0.3
sy17bt	04-08-199	11:54	324.07	72.17	83.508	11.15	100	0.4
sy17bt	04-08-199	11:54	321.77	69.79	53.811	11.15	185	0.3
sy17bt	04-08-199	11:54	316.33	69.18	34.234	11.15	300	0.3
sy17bt	04-08-199	11:54	317.52	67.46	25.117	11.15	400	0.4
sy17bt	04-08-199	11:54	310.31	65.84	21.152	11.15	450	0.3
sy17bt	04-08-199	15:56	321.23	70.3	15.2	11.15	500	0.7
sy17bt	04-11-199	09:10	314.19	66.95	14.1	11.15	550	0.3
sy17bt	04-11-199	11:52	307.78	63.14	12.39	11.15	600	0.5
sy17bt	04-11-199	14:40	319.21	64.33	7.43	11.15	650	0.9
sy17bt	04-12-199	10:29	313.66	59.23	5.62	11.15	700	0.9
sy18bt	04-08-199	11:54	69.26	10.46	3359.925	11.15	0	0.3
sy18bt	04-08-199	11:54	72	10.3	3355.592	11.15	100	0.2
sy18bt	04-08-199	11:54	70.53	9.65	2861.747	11.15	185	0.2
sy18bt	04-08-199	11:54	72.48	10.32	2398.228	11.15	300	0.5
sy18bt	04-08-199	11:54	71.06	9.85	2221.125	11.15	400	0.2
sy18bt	04-08-199	11:54	72.61	10.37	2109.312	11.15	450	0.2
sy18bt	04-08-199	16:33	69.63	10.65	1710	11.15	500	0.1
sy18bt	04-11-199	09:20	68.85	10.52	1620	11.15	550	0.1
sy18bt	04-11-199	12:00	68.8	11.88	1291	11.15	600	1.4
sy18bt	04-11-199	14:49	70.22	16.94	127.1	11.15	650	1.4
sy18bt	04-11-199	17:43	74.57	17.8	93.3	11.15	675	1.1
sy18bt	04-12-199	10:37	69.78	17.75	62.1	11.15	700	1.3
sy24bt	04-08-199	11:54	256.24	-71.11	12.207	11.15	0	1.1
sy24bt	04-08-199	11:54	257.93	-72.17	13.12	11.15	100	0.5
sy24bt	04-08-199	11:54	251.56	-76.51	14.911	11.15	185	0.5
sy24bt	04-08-199	11:54	250.68	-78.06	13.87	11.15	300	0.7
sy24bt	04-08-199	11:54	253.23	-78.35	13.386	11.15	400	0.7
sy24bt	04-08-199	11:54	253.63	-77.69	13.142	11.15	450	0.8

thermal demagnetization

sample	date	time	declination	inclination	mA/m	cm3	temp.C	error %
sy24bt	04-08-199	15:49	254.55	-78.79	11.38	11.15	500	0.5
sy24bt	04-11-199	09:09	254.97	-77.81	10.95	11.15	550	0.4
sy24bt	04-11-199	11:50	243.92	-80.89	9.17	11.15	600	0.9
sy25bt	04-08-199	11:54	124.12	77.18	490.209	11.15	0	0.6
sy25bt	04-08-199	11:54	122.79	76.89	472.296	11.15	100	0.4
sy25bt	04-08-199	11:54	127.79	76.53	266.319	11.15	185	0.4
sy25bt	04-08-199	11:54	129.09	75.1	160.39	11.15	300	0.5
sy25bt	04-08-199	11:54	133.02	74.86	133.632	11.15	400	0.2
sy25bt	04-08-199	11:54	133.86	74.49	119.861	11.15	450	0.4
sy25bt	04-08-199	16:20	133.84	74.85	67.3	11.15	500	0.5
sy25bt	04-11-199	09:17	125.04	74.07	59.6	11.15	550	0.3
sy25bt	04-11-199	11:57	148.13	76.31	45.2	11.15	600	1.1
sy28bt	04-08-199	11:54	264.7	57.82	284.742	11.15	0	0.4
sy28bt	04-08-199	11:54	266.13	50.75	258.244	11.15	100	0.4
sy28bt	04-08-199	11:54	255.24	34.93	159.441	11.15	185	0.4
sy28bt	04-08-199	11:54	251.19	27.71	105.132	11.15	300	0.2
sy28bt	04-08-199	11:54	252.45	24.52	91.533	11.15	400	0.3
sy28bt	04-08-199	11:54	249.48	22.55	84.977	11.15	450	0.1
sy28bt	04-08-199	16:10	247.34	25.17	48.1	11.15	500	1
sy28bt	04-11-199	09:15	245.35	8.6	35.7	11.15	550	0.2
sy28bt	04-11-199	11:55	238.53	1.35	24.1	11.15	600	1.9
sy31bt	06-10-199	11:55	357.24	61.56	218	11.15	0	0.4
sy31bt	06-14-199	10:02	358.08	62.73	124.2	11.15	218	0.6
sy31bt	06-14-199	14:06	355.08	65.84	79.8	11.15	306	0.1
sy31bt	06-14-199	19:29	350.02	68.75	45.3	11.15	405	0.5
sy31bt	06-14-199	23:47	339.21	76.33	27.3	11.15	504	0.8
sy31bt	06-15-199	20:53	316.27	79.35	19.7	11.15	550	0.3
sy31bt	06-16-199	00:40	288.58	79.71	16.8	11.15	575	0.2
sy31bt	06-16-199	19:22	218.89	52.21	8.83	11.15	602	0.6
sy31bt	06-16-199	23:25	214.92	8.94	9.26	11.15	625	1
sy34bt	06-10-199	11:57	169.98	80.19	65.6	11.15	0	0.5
sy34bt	06-14-199	10:04	164.88	65.13	21.1	11.15	218	0.5
sy34bt	06-14-199	14:07	178.98	30.77	11.15	11.15	306	0.5

thermal demagnetization

sample	date	time	declination	inclination	mA/m	cm3	temp.C	error %
sy34bt	06-14-199	19:31	187.1	1.46	10.7	11.15	405	0.4
sy34bt	06-14-199	23:51	183.96	-23.84	8.93	11.15	504	1.7
sy34bt	06-15-199	20:54	198.44	-22.81	13.09	11.15	550	0.7
sy34bt	06-16-199	00:42	199.53	-27.97	13.19	11.15	575	0.7
sy34bt	06-16-199	19:23	191.22	-28.39	11.14	11.15	602	1
sy34bt	06-16-199	23:26	198.58	-2.19	5.9	11.15	625	1.3
sy37bt	06-10-199	12:00	238.62	74	38.4	11.15	0	0.7
sy37bt	06-14-199	10:07	255.16	38.99	16.5	11.15	218	0.2
sy37bt	06-14-199	14:10	259.14	33.56	10.54	11.15	306	0.4
sy37bt	06-14-199	19:34	262.19	39.82	7.09	11.15	405	0.9
sy37bt	06-14-199	23:54	248	16.21	7.91	11.15	504	0.7
sy37bt	06-15-199	20:58	248.09	33.91	6.46	11.15	550	0.6
sy37bt	06-16-199	00:45	257.2	29.17	6.3	11.15	575	1
sy37bt	06-16-199	19:26	252.18	32.57	7.23	11.15	602	0.7
sy37bt	06-16-199	23:29	246.2	38.37	6.89	11.15	625	0.5
sy38bt	06-10-199	12:01	160.93	10.92	76.2	11.15	0	0
sy38bt	06-14-199	10:09	155.19	3.84	73	11.15	218	0.1
sy38bt	06-14-199	14:13	143.98	2.1	61.1	11.15	306	0.1
sy38bt	06-14-199	19:35	139.85	0.11	48	11.15	405	0.3
sy38bt	06-14-199	23:55	135.05	1.25	34.3	11.15	504	0.5
sy38bt	06-15-199	20:59	133.38	1.9	30	11.15	550	0.3
sy38bt	06-16-199	00:47	132.28	2.45	29.1	11.15	575	0.2
sy38bt	06-16-199	19:27	131.96	0.62	27.3	11.15	602	0.6
sy38bt	06-16-199	23:30	130.93	-1.81	25.4	11.15	625	0.6
sy42bt	06-10-199	12:05	293.16	55.03	175	11.15	0	0.2
sy42bt	06-14-199	10:13	297.77	35.21	132.6	11.15	218	0.1
sy42bt	06-14-199	14:16	288.07	36.29	100.3	11.15	306	0.2
sy42bt	06-14-199	19:38	290.23	33.91	80.4	11.15	405	0.2
sy42bt	06-14-199	23:58	292.53	37.71	45.8	11.15	504	0.3
sy42bt	06-15-199	21:02	274.54	37.65	40.6	11.15	550	0.2
sy42bt	06-16-199	00:50	274.39	38.98	35.2	11.15	575	0.5
sy42bt	06-16-199	19:30	280.95	37.61	29.8	11.15	602	0.4
sy42bt	06-16-199	23:33	282.43	29.7	27.4	11.15	625	0.4

thermal demagnetization

sample	date	time	declination	inclination	mA/m	cm3	temp.C	error %
sy43bt	06-14-199	10:14	99.35	-4.59	76.2	11.15	218	0.6
sy43bt	06-14-199	14:17	93.59	-17.35	34.9	11.15	306	0.7
sy43bt	06-14-199	19:40	91.31	-34.02	28.9	11.15	405	0.7
sy43bt	06-14-199	23:59	88.36	-18.8	11.47	11.15	504	1.5
sy43bt	06-15-199	21:03	127.21	-33.19	6.08	11.15	550	1.7
sy43bt	06-16-199	00:51	92.02	4.01	5.61	11.15	575	1.9
sy43bt	06-16-199	19:31	121.36	13.49	8.37	11.15	602	2.6
sy43bt	06-16-199	23:34	97.57	10.07	9.51	11.15	625	1.4
sy48bt	06-10-199	12:11	258	-3.78	214	11.15	0	0.3
sy48bt	06-14-199	10:20	253.5	-13.28	222	11.15	218	0.3
sy48bt	06-14-199	14:22	251.58	-15.42	185	11.15	306	0.6
sy48bt	06-14-199	19:45	249.53	-18.09	143.6	11.15	405	0.7
sy48bt	06-15-199	00:05	246.33	-19.9	98.5	11.15	504	0.7
sy48bt	06-15-199	21:09	242.85	-22.44	81.2	11.15	550	0.9
sy48bt	06-16-199	00:56	246.25	-20.07	78.2	11.15	575	0.7
sy48bt	06-16-199	19:38	249.17	-16.55	68.8	11.15	602	0.7
sy48bt	06-16-199	23:41	246.62	-21.46	58.6	11.15	625	0.8
sy48bt	06-19-199	20:19	252.79	-9.53	12.78	11.15	651	0.7
sy49bt	06-10-199	12:12	335.71	84.82	19.9	11.15	0	0.4
sy49bt	06-14-199	10:22	6.55	73.74	10.48	11.15	218	0.4
sy49bt	06-14-199	14:24	299.89	75.94	5.64	11.15	306	0.5
sy49bt	06-14-199	19:47	218.4	71.25	3.03	11.15	405	1.3
sy49bt	06-15-199	00:06	237.79	56.88	3.62	11.15	504	1
sy49bt	06-15-199	21:10	233.57	36.53	2.53	11.15	550	1.8
sy49bt	06-16-199	00:58	218.03	33.48	2.89	11.15	575	1.9
sy49bt	06-16-199	23:42	235.81	46.11	3.26	11.15	625	1.7
sy52bt	06-10-199	12:13	52.81	57.97	72	11.15	0	0.6
sy52bt	06-14-199	10:24	45.97	51.77	40.3	11.15	218	0.5
sy52bt	06-14-199	14:25	39.94	52.32	25	11.15	306	0.7
sy52bt	06-14-199	19:48	38.32	57.33	17.3	11.15	405	0.4
sy52bt	06-15-199	00:08	39.19	61.87	13.04	11.15	504	0.8
sy52bt	06-15-199	21:12	53.74	69.19	7.4	11.15	550	1.3
sy52bt	06-16-199	00:59	55.39	79.67	5.2	11.15	575	1.8

thermal stereonet plot

sample			declination	inclination
sy5bt			227.4	4.3
sy11bt			44.1	-7.5
sy14bt			205.5	8
sy16bt			145.1	63.7
sy17bt			316.5	67.5
sy18bt			70.8	12.2
sy24bt			253.5	-76.9
sy25bt			130.9	75.6
sy28bt			250.8	28.3
sy31bt			299.2	77.3
sy34bt			189.1	5.3
sy37bt			252.8	37.3
sy38bt			140.3	2.4
sy42bt			285.8	38.2
sy43bt			100.9	-5.4
sy47bt			266.1	57.3
sy48bt			249.7	-16.2
sy49bt			238.7	65
sy52bt			45	61.5

total thermal PCAs

sample			declination	inclination
sy5bt			258	85.8
sy11bt			42	-8.3
sy14bt			203.9	10.3
sy16bt			114	78.5
sy17bt			325.5	73.5
sy18bt			71	9.9
sy24bt			256.2	-70.1
sy25bt			121.4	77.4
sy28bt			91.8	-60.4
sy31bt			359.6	59.6
sy34bt			102.5	85.8
sy37bt			224.8	81
sy38bt			170.2	10
sy42bt			299.1	50.9
sy43bt			100.5	27.5
sy47bt			290.1	68.6
sy48bt			257	-7.8
sy49bt			197.5	-77.4
sy52bt			52.7	55.6

magnetite PCAs

sample			declination	inclination
sy5bt			177.2	-84.6
sy11bt			38.8	-7.6
sy14bt			204	10.5
sy16bt			117.3	79.7
sy17bt			326.9	74.1
sy18bt			69.9	10.2
sy24bt			205.7	-83.4
sy25bt			119.7	77.4
sy28bt			96.8	-64.3
sy31bt			0.6	59
sy34bt			121.1	87.2
sy37bt			207	83
sy38bt			179.6	14
sy42bt			297.3	60.5
sy43bt			103.9	41.6
sy47bt			290.5	68.8
sy48bt			263.1	1.5
sy49bt			13.5	80.4
sy52bt			56.4	57.1

hematite PCAs

| sample			declination	inclination
sy5bt			225.6	-28.7
sy11bt			46	-8.2
sy14bt			204.6	8
sy17bt			307.1	69.2
sy18bt			68.7	10.6
sy31bt			193.6	-60
sy34bt			230.4	-6.8
sy37t			157.3	47.6
sy38t			144.8	23
sy42bt			71.9	-48.5
sy43bt			259.9	-47.5
sy47bt			244.3	-22
sy49bt			161.5	-68.4

Lwr.Hem.Equal Area Net
circle=DOWN square=UP
 hermal\sy5bte.SR2
 n = 8
 06-07-1994
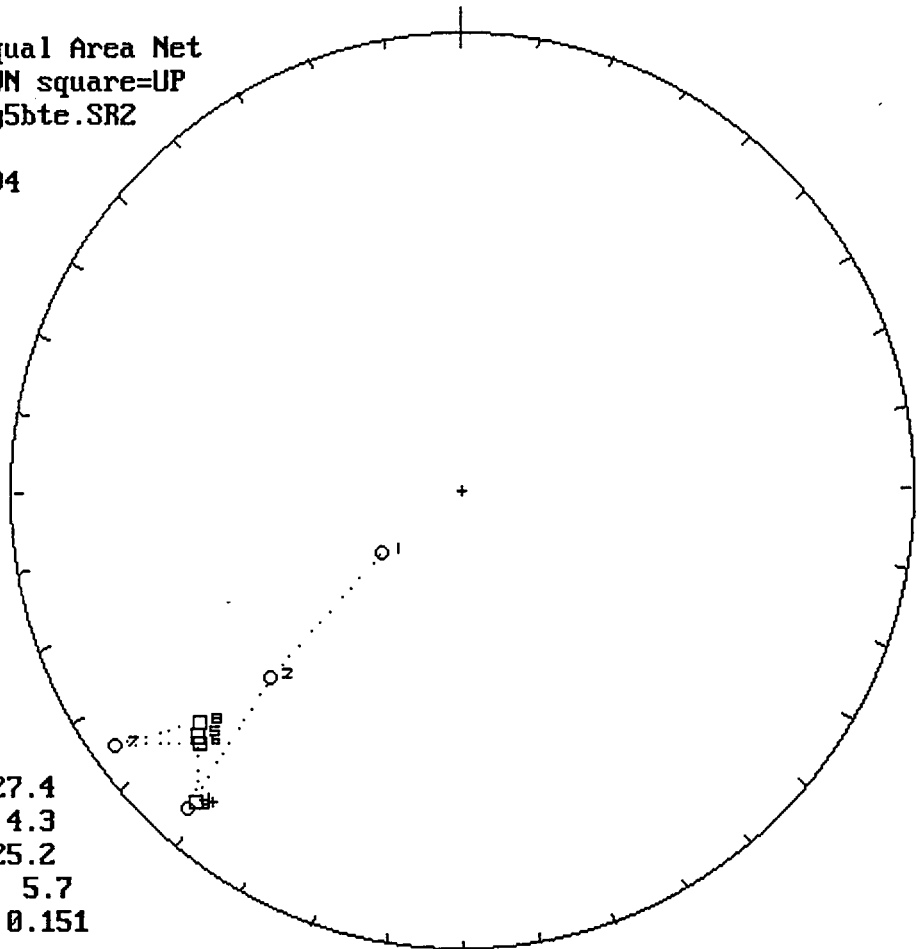
m.dec.= 227.4
m.inc.=   4.3
alpha95= 25.2
Fish. k=   5.7
sp.var.=   0.151

Lwr.Hem.Equal Area Net
circle=DOWN square=UP
 hermal\sy5bte.SR2
 n = 7
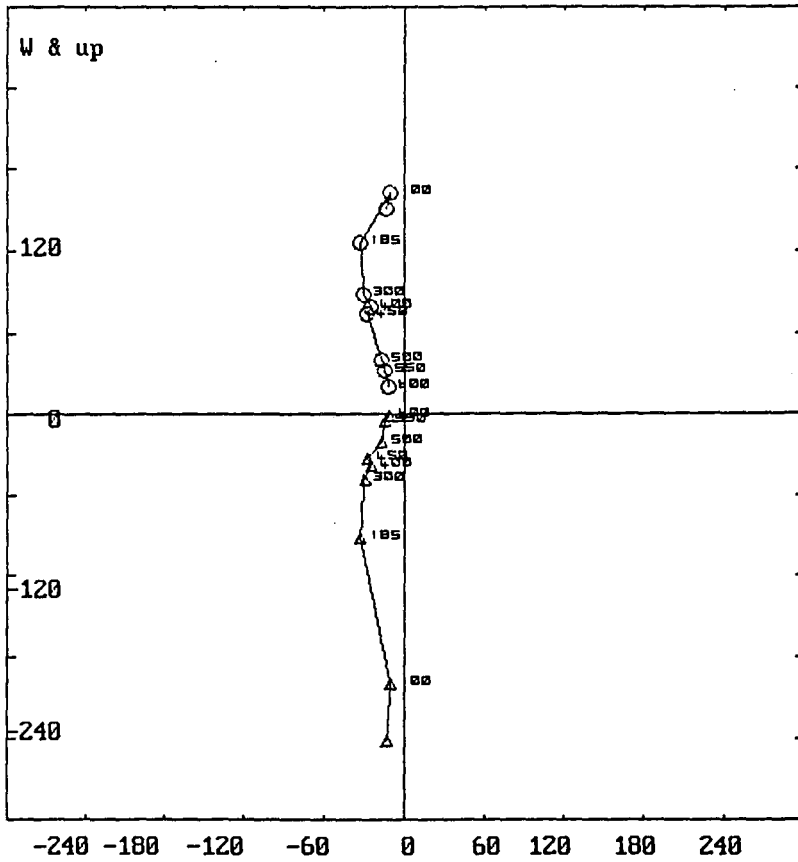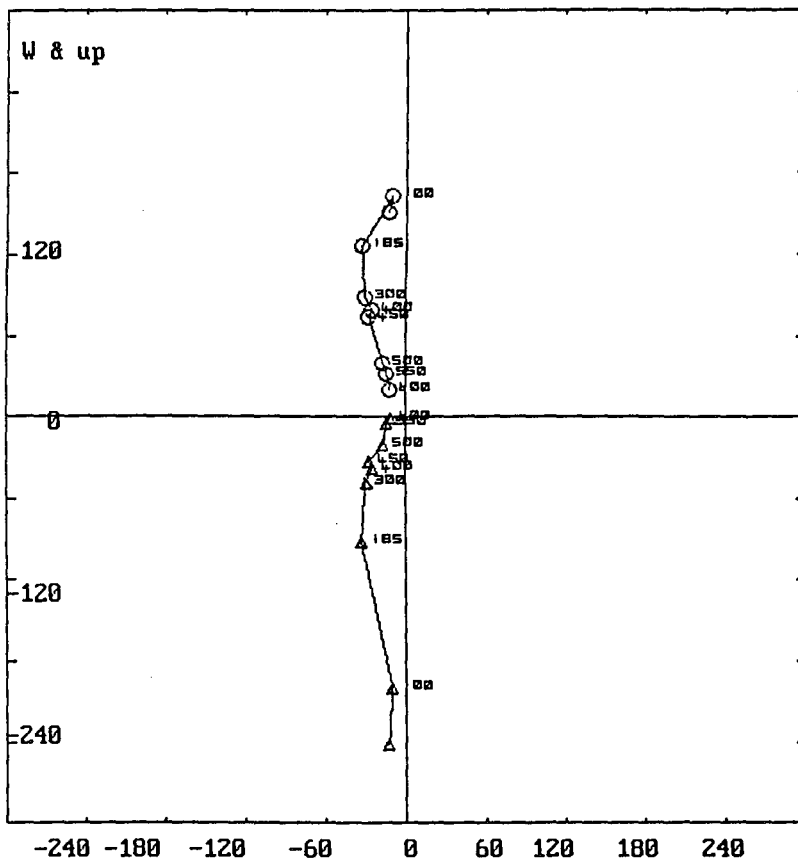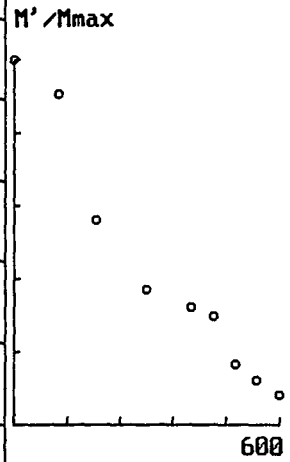 06-07-1994
Vector Diff
Plot: shows
vectors
added in
nature

:\thermal\sy5bte.SR2
06-07-1994
n = 8
 circle =horiz.plo
 triang. =vert.plot
 units mA/m
PCA decl= 177.2
PCA incl= -84.6
for points 1 to 4

M'/Mmax

700

W & up

-0.2

=1.0

=2.2

=3.4

-3.4 -2.8 -2.2 -1.6 -1.0 -0.4 0.2 0.8 1.4 S to N

:\thermal\sy5bte.SR2
06-07-1994
n = 8
 circle =horiz.plo
 triang. =vert.plot
 units mA/m
PCA decl= 221.5
PCA incl= -21.3
for points 4 to 8

M'/Mmax

700

W & up

-0.2

=1.0

=2.2

=3.4

-3.4 -2.8 -2.2 -1.6 -1.0 -0.4 0.2 0.8 1.4 S to N
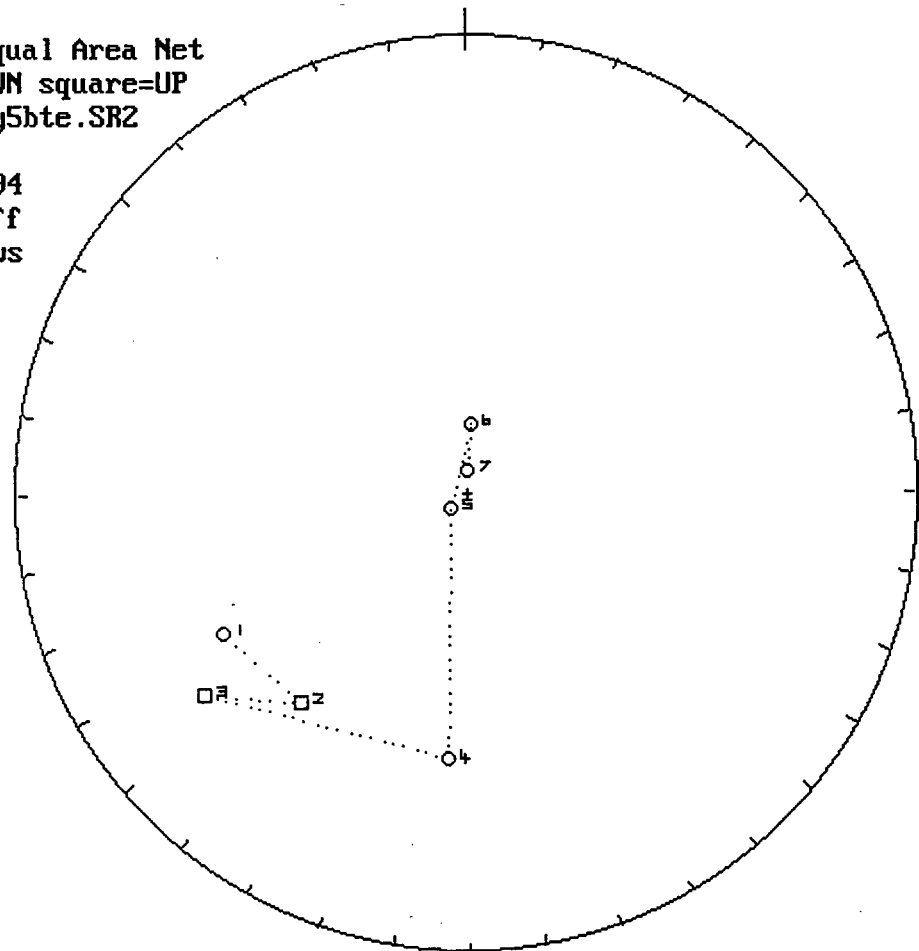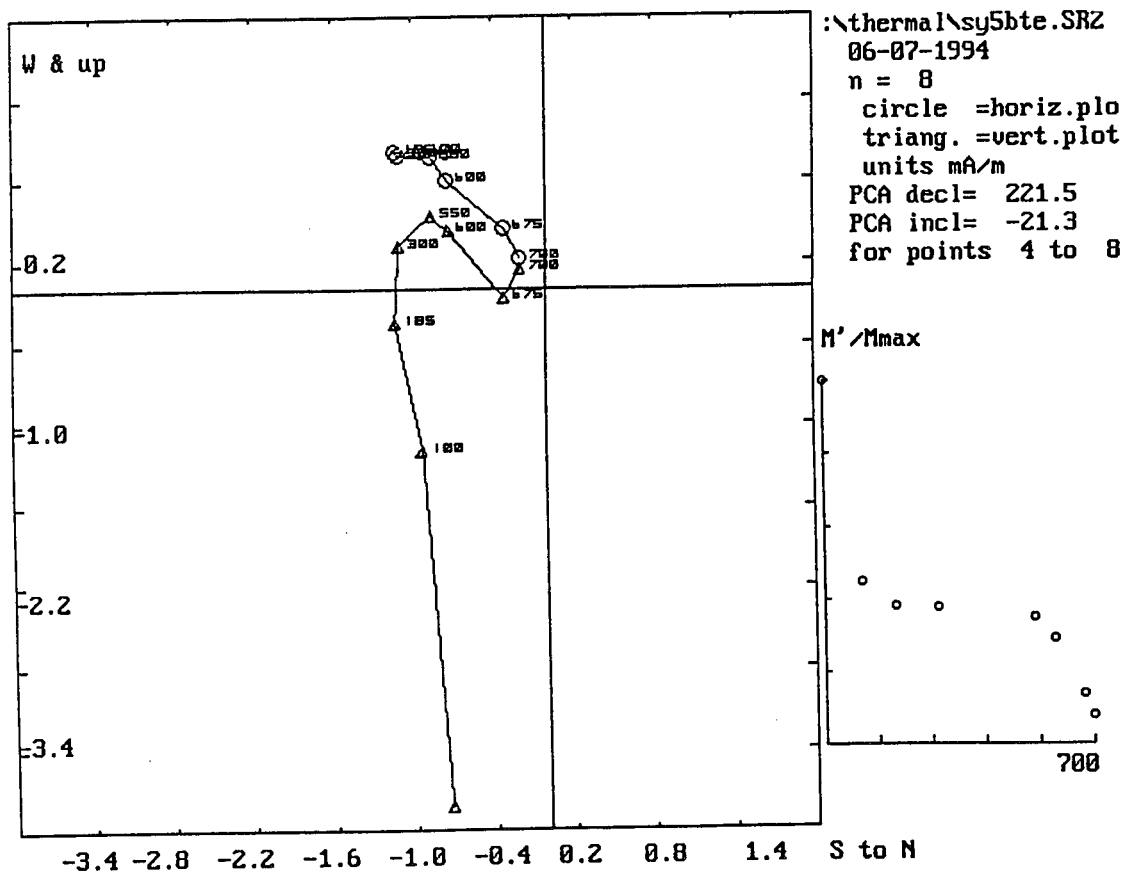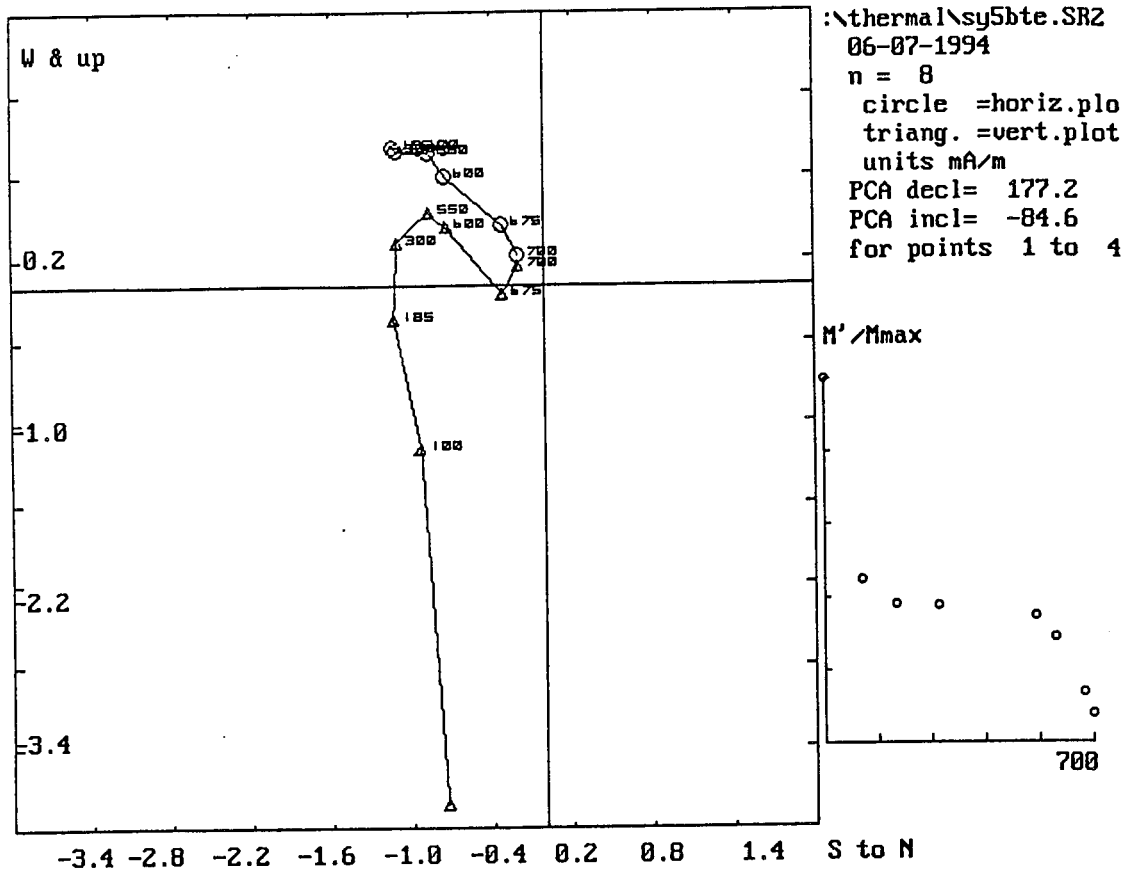
Lwr.Hem.Equal Area Net
circle=DOWN square=UP
 ermal\sy11bte.SR2
 n = 12
 06-08-1994
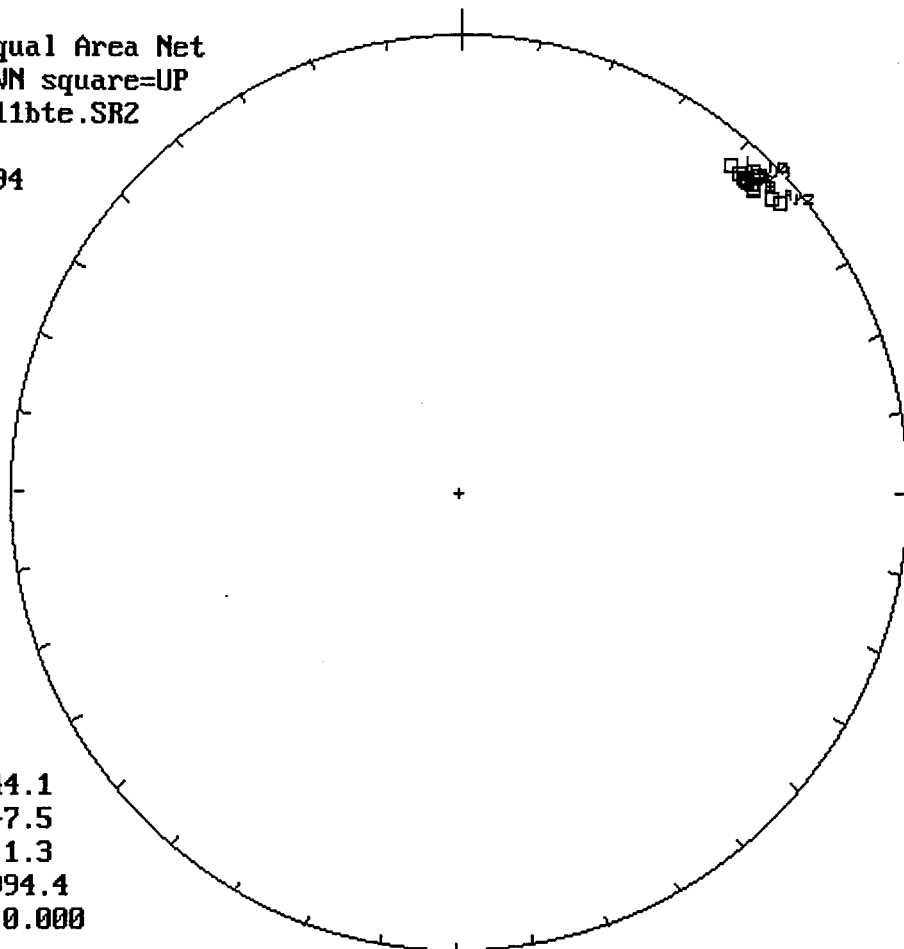
m.dec.= 44.1
m.inc.= -7.5
alpha95= 1.3
Fish. k= 994.4
sp.var.= 0.000

Lwr.Hem.Equal Area Net
circle=DOWN square=UP
 ermal\sy11bte.SR2
 n = 11
 06-08-1994
Vector Diff
Plot: shows
vectors
added in
nature

\thermal\sy11bte.SR2
06-08-1994
n = 12
 circle =horiz.plo
 triang. =vert.plot
 units A/m
PCA decl=   42.0
PCA incl=   -8.3
for points 1 to 12
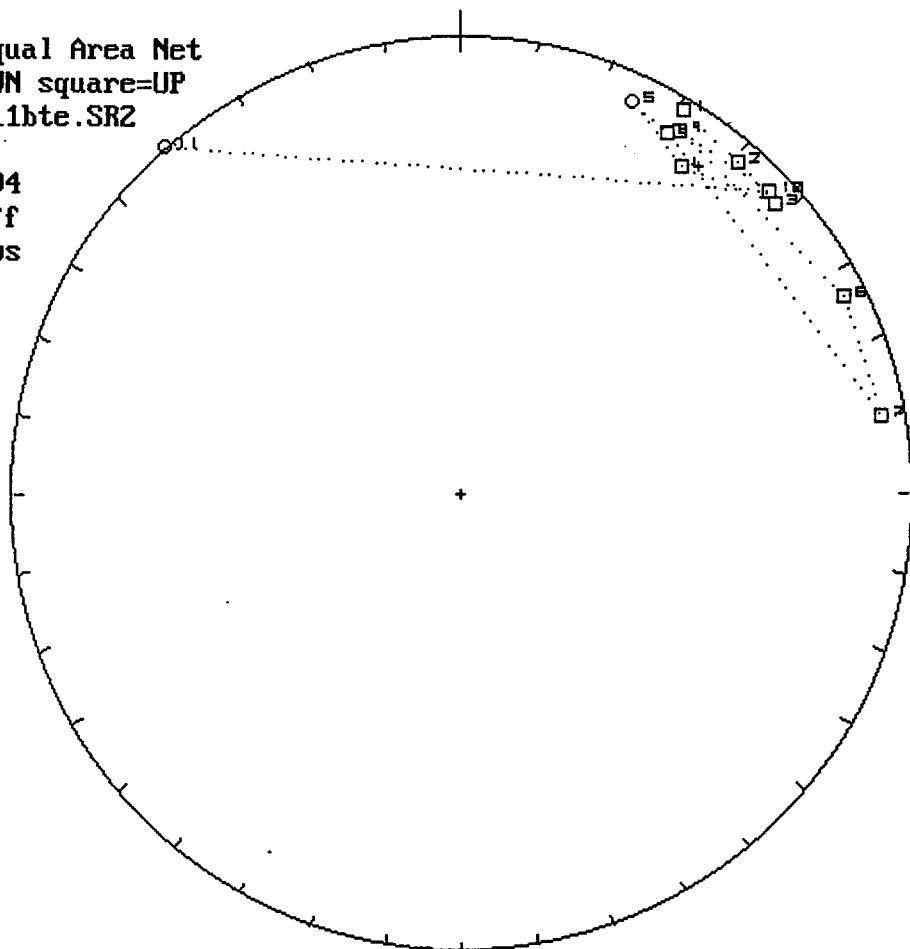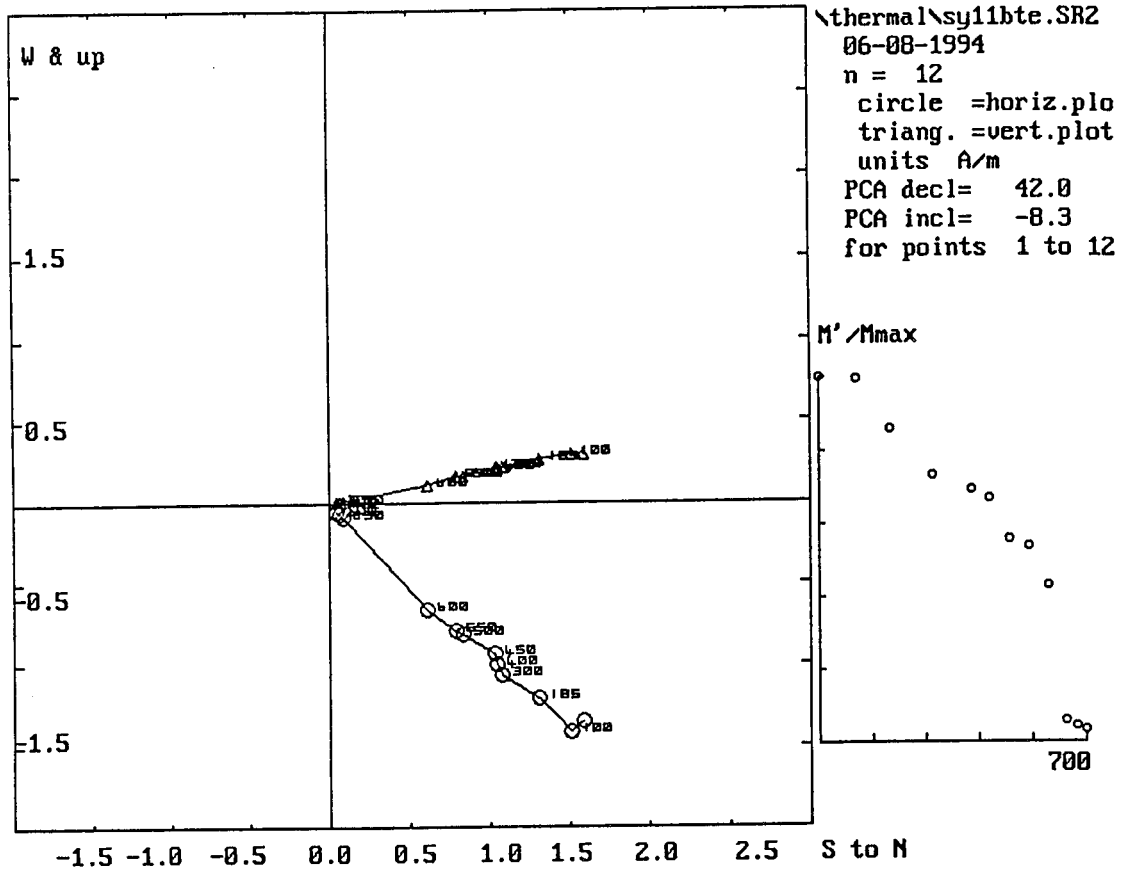
Lwr.Hem.Equal Area Net
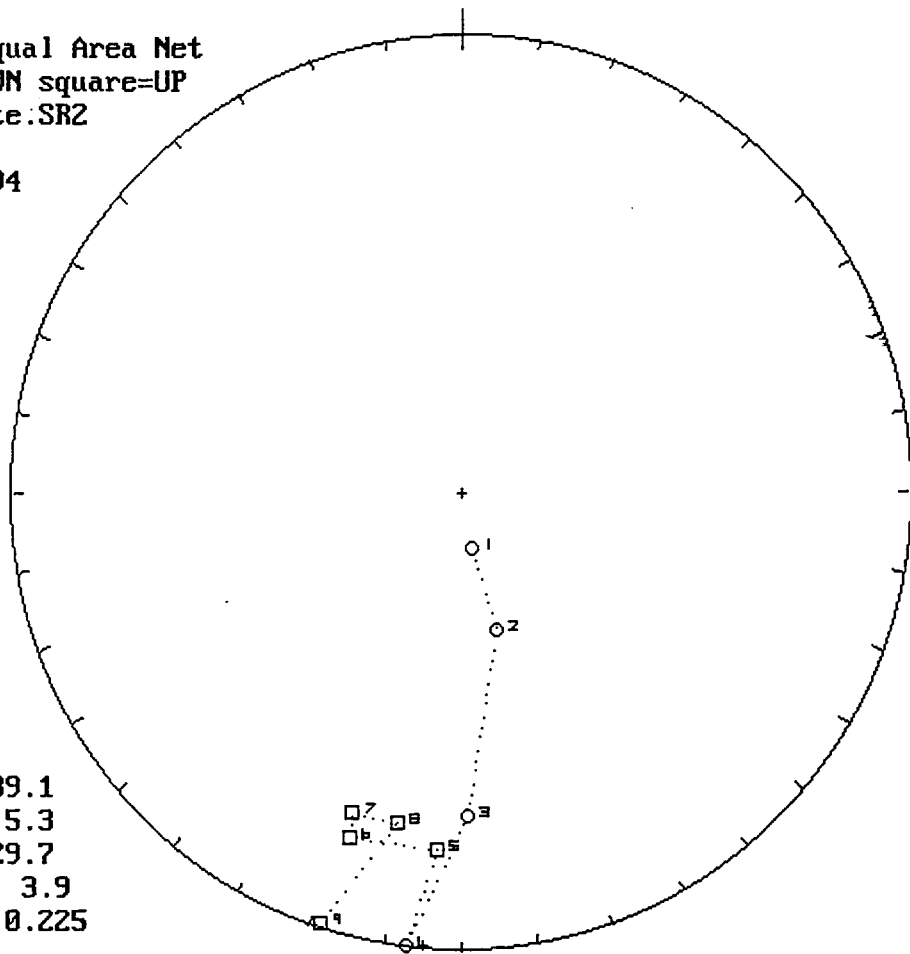circle=DOWN square=UP
 ermal\sy14bte.SR2
 n = 11
 06-08-1994
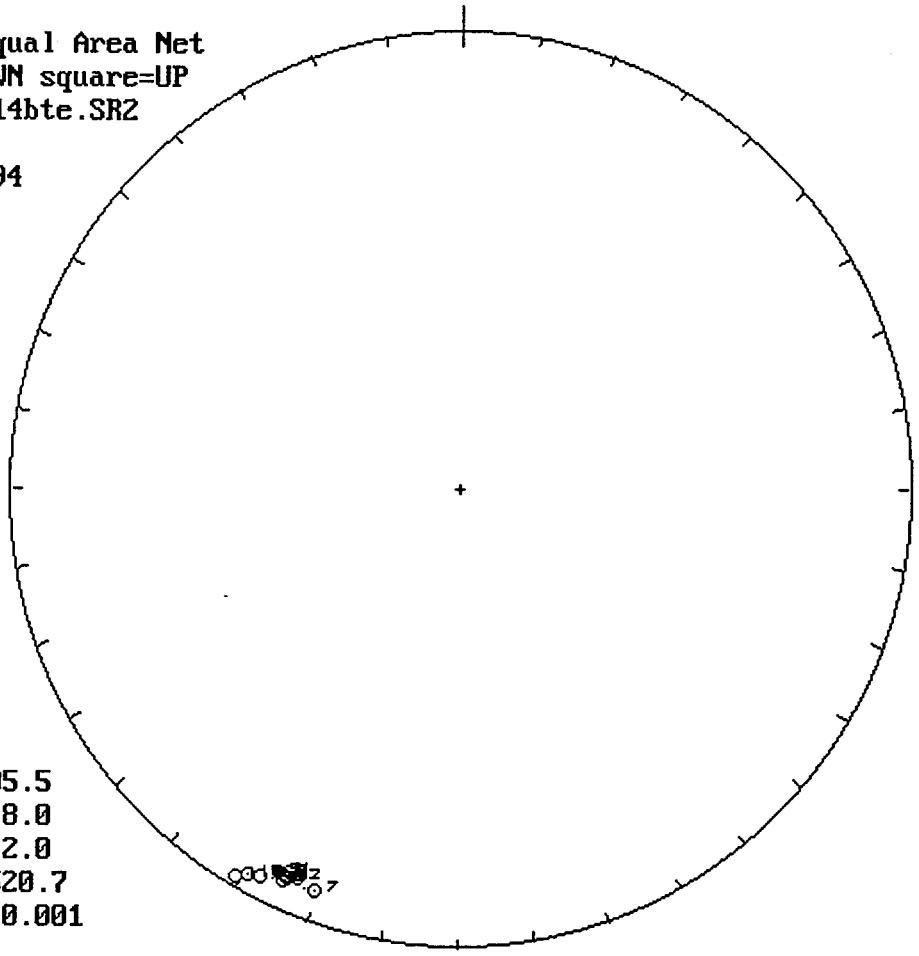
m.dec.= 205.5
m.inc.=   8.0
alpha95= 2.0
Fish. k= 520.7
sp.var.= 0.001

Lwr.Hem.Equal Area Net
circle=DOWN square=UP
 ermal\sy14bte.SR2
 n = 10
 06-08-1994
Vector Diff
Plot: shows
vectors
added in
nature
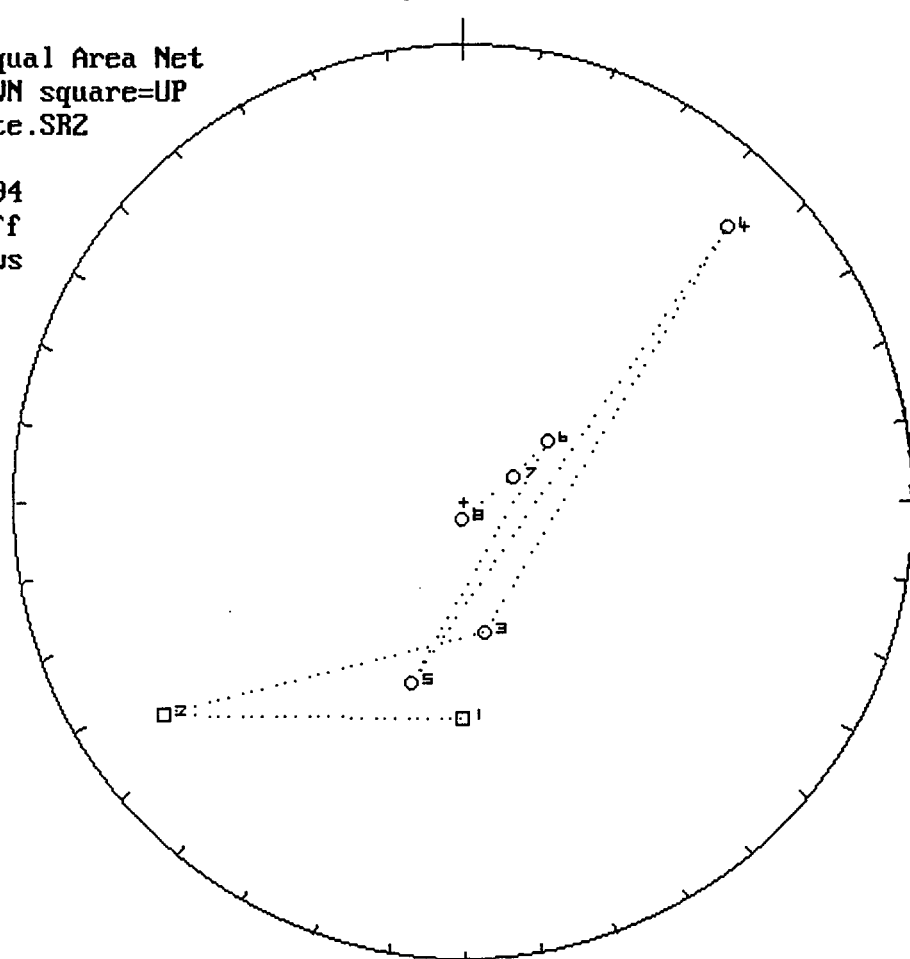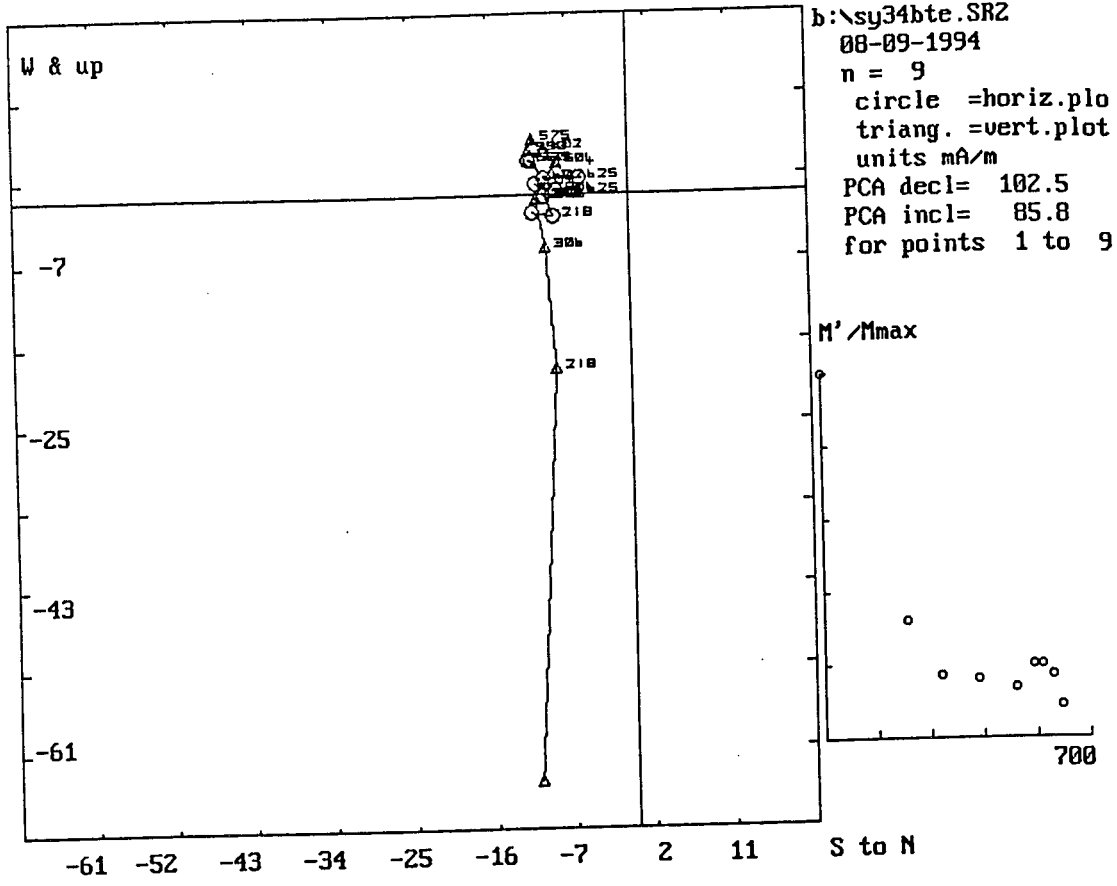
W & up

\thermal\sy14bte.SR2
  06-08-1994
  n = 11
   circle =horiz.plo
   triang. =vert.plot
   units A/m
  PCA decl= 203.9
  PCA incl=   10.3
  for points 1 to 11

M'/Mmax

700

-3.3 -2.6 -1.9 -1.2 -0.5   0.2 0.9   1.6   2.3   S to N
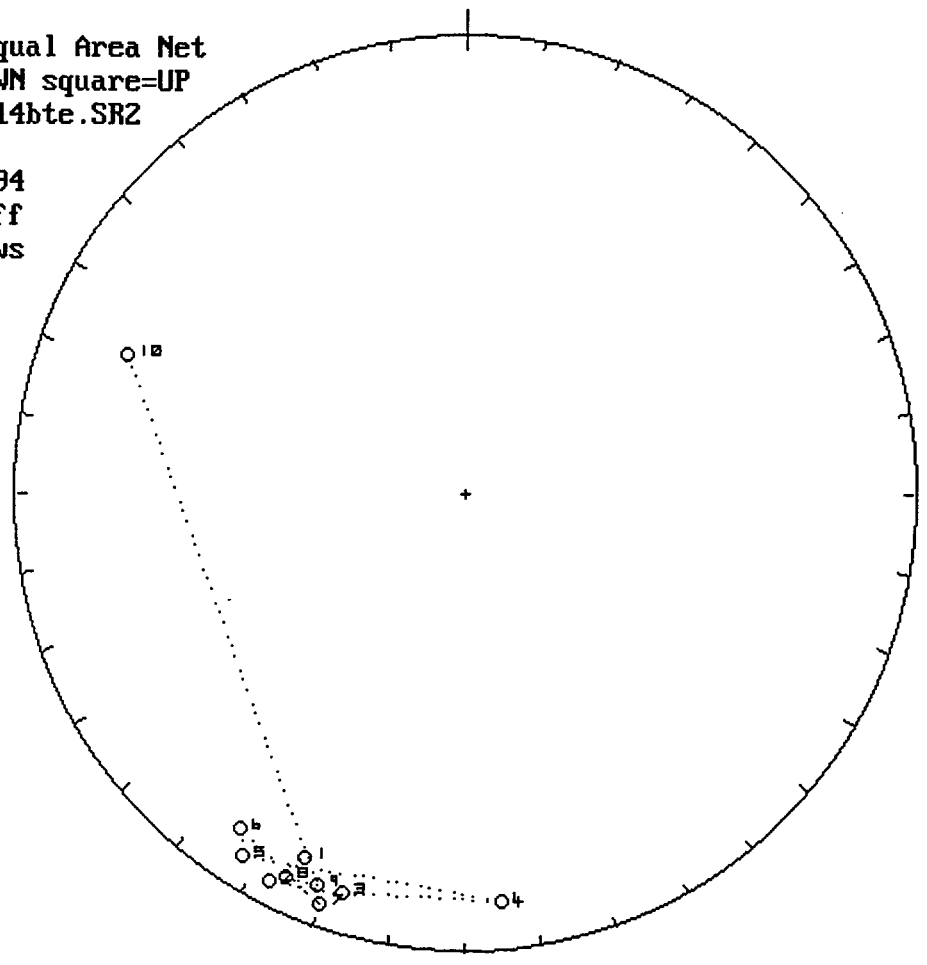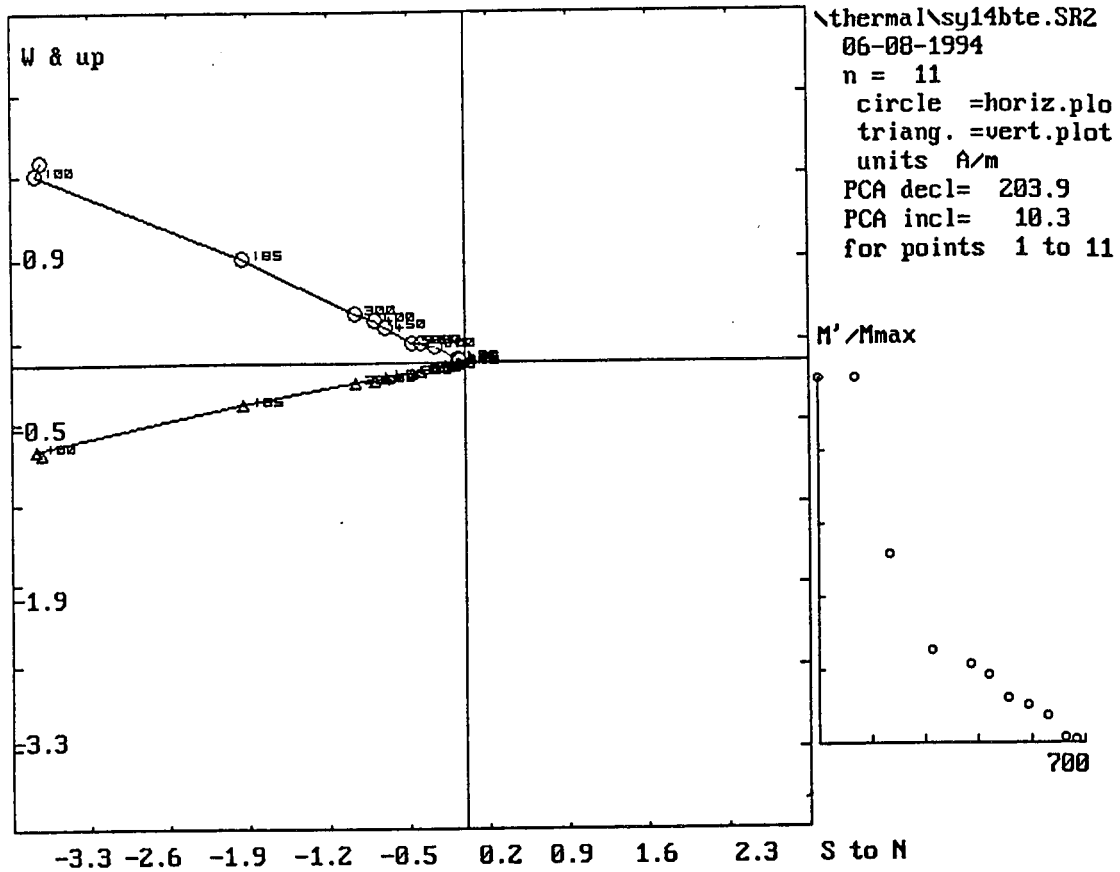
Lwr.Hem.Equal Area Net
circle=DOWN square=UP
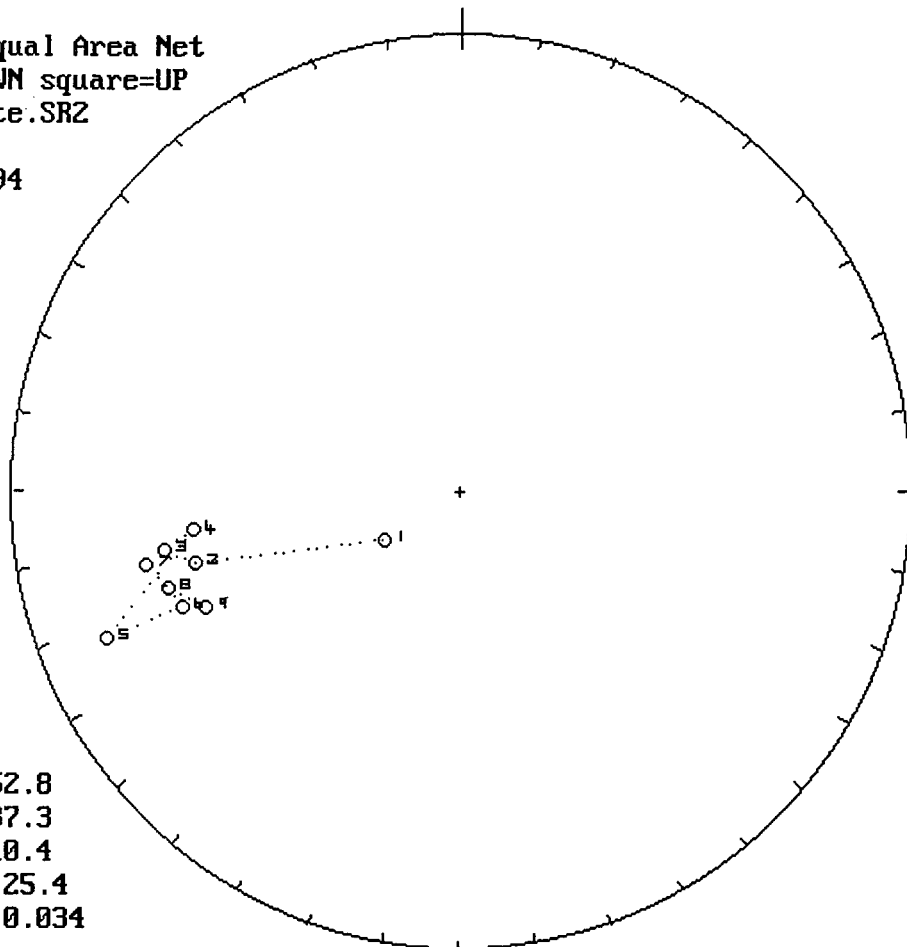 erma1\sy16bte.SR2
 n = 8
 08-10-1994
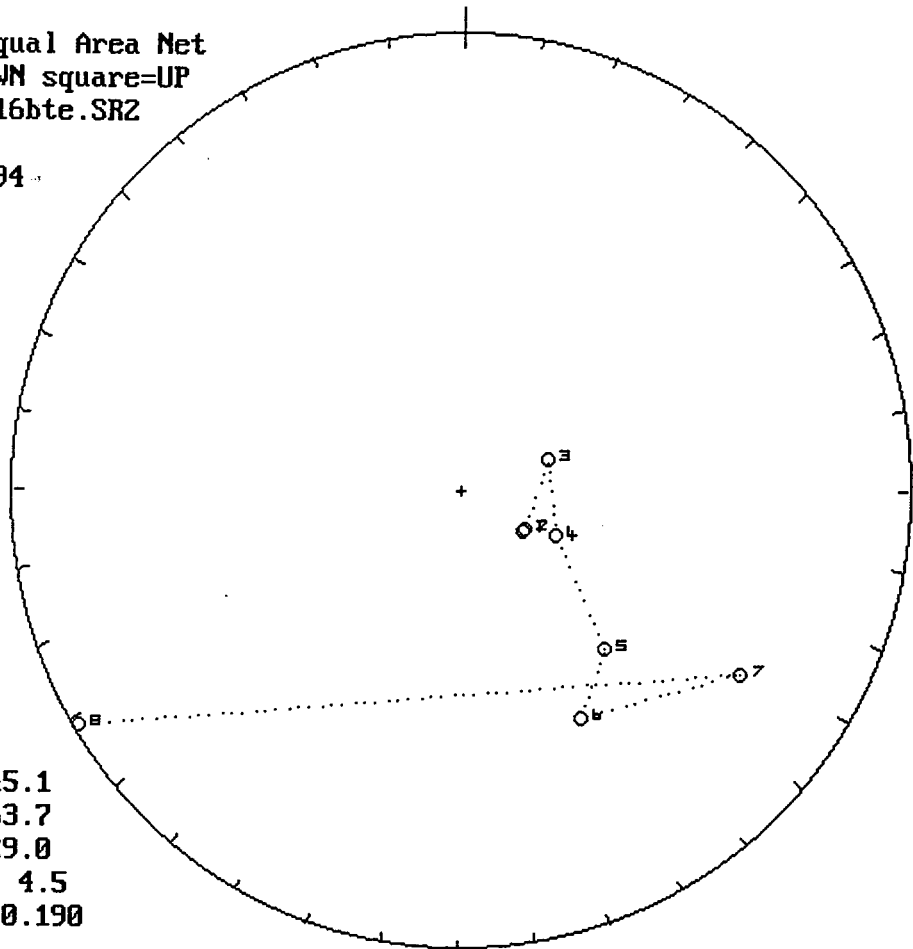
m.dec.= 145.1
m.inc.= 63.7
alpha95= 29.0
Fish. k= 4.5
sp.var.= 0.190

Lwr.Hem.Equal Area Net
circle=DOWN square=UP
 erma1\sy16bte.SR2
 n = 7
 08-10-1994
Vector Diff
Plot: shows
vectors
added in
nature

\thermal\sy16bte.SR2
08-10-1994
n = 8
 circle =horiz.plo
 triang. =vert.plot
 units mA/m
PCA decl= 114.0
PCA incl= 78.5
for points 1 to 8
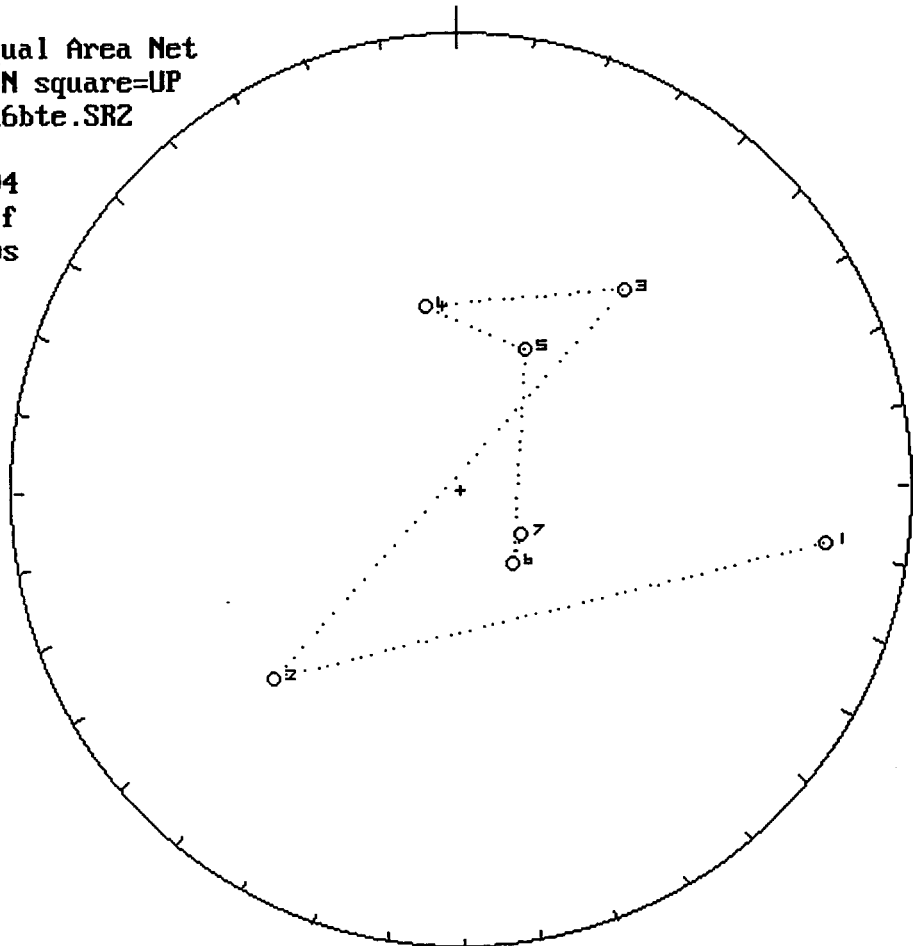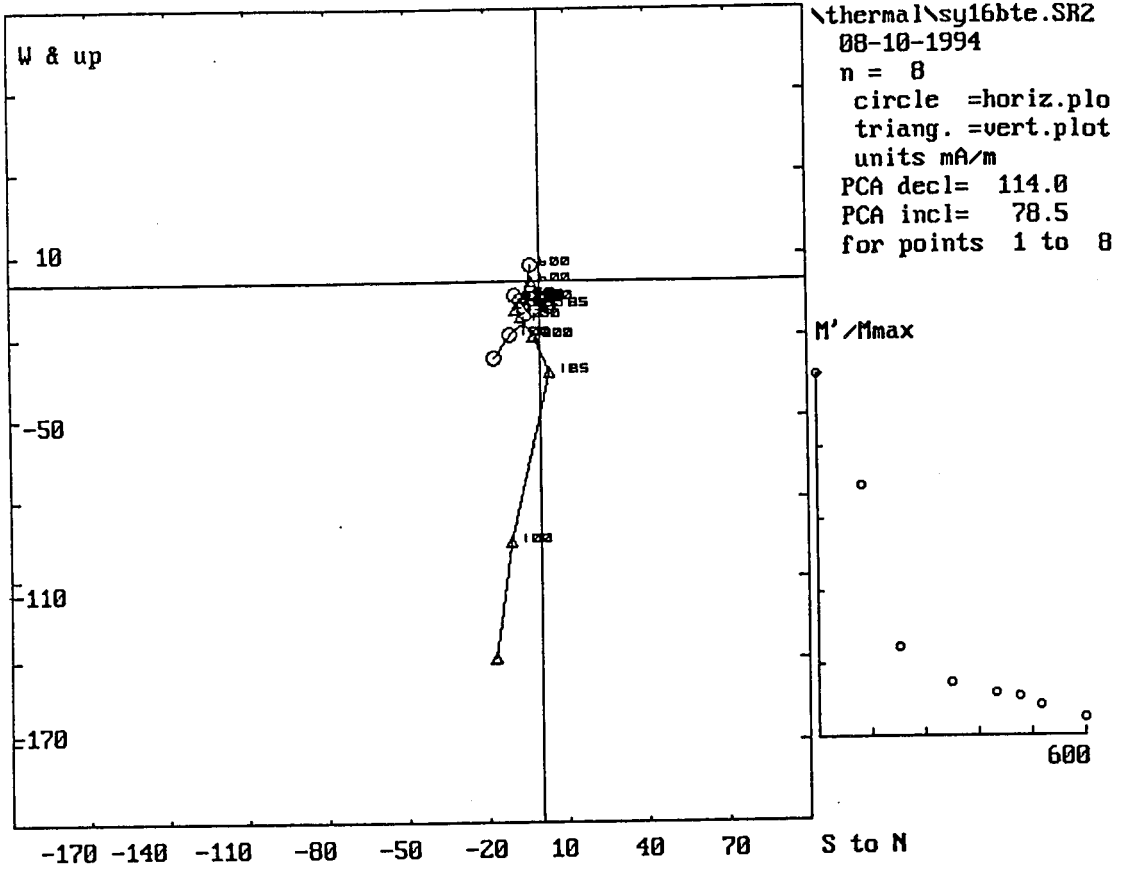
Lwr.Hem.Equal Area Net
circle=DOWN square=UP
 ermal\sy17bte.SR2
 n =   11
 06-08-1994
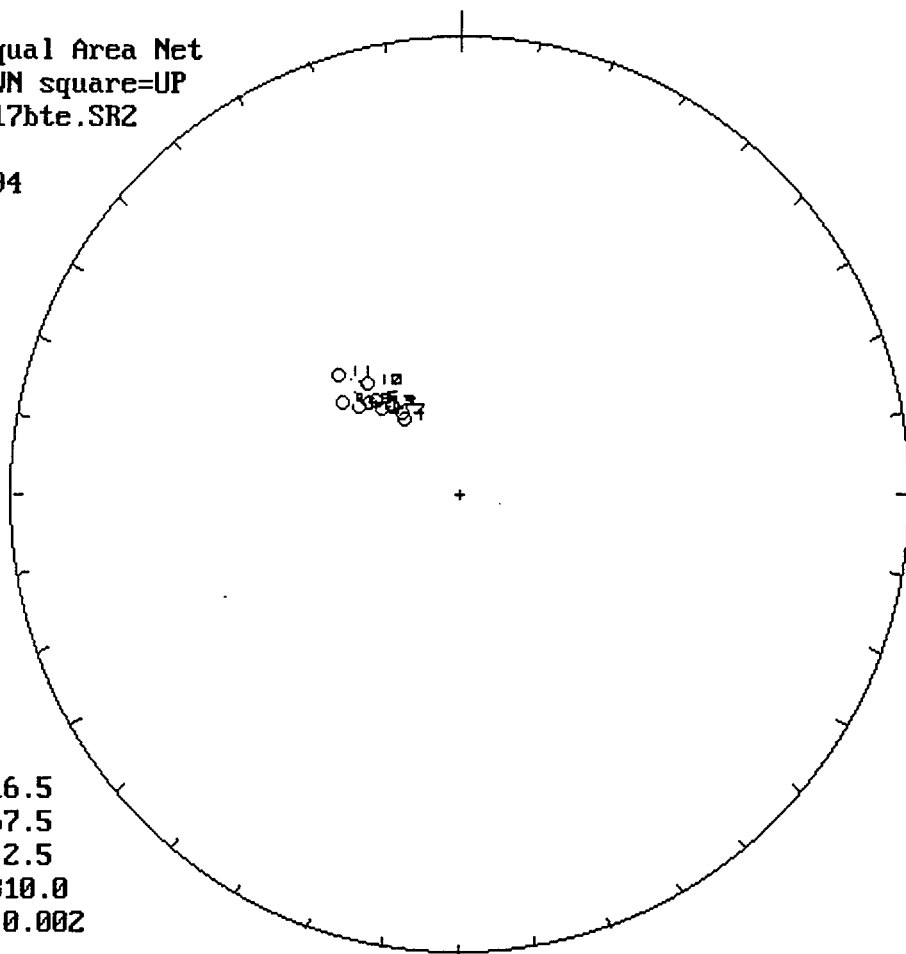
m.dec.= 316.5
m.inc.= 67.5
alpha95= 2.5
Fish. k= 310.0
sp.var.= 0.002

Lwr.Hem.Equal Area Net
circle=DOWN square=UP
 ermal\sy17bte.SR2
 n =   10
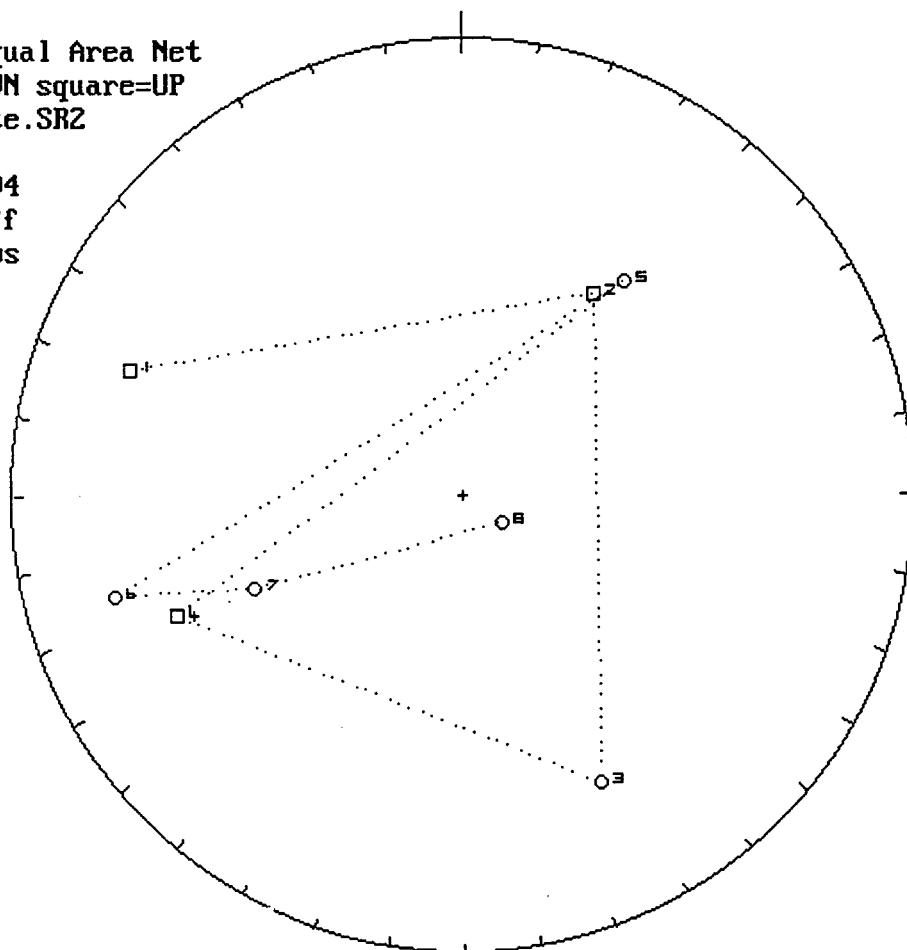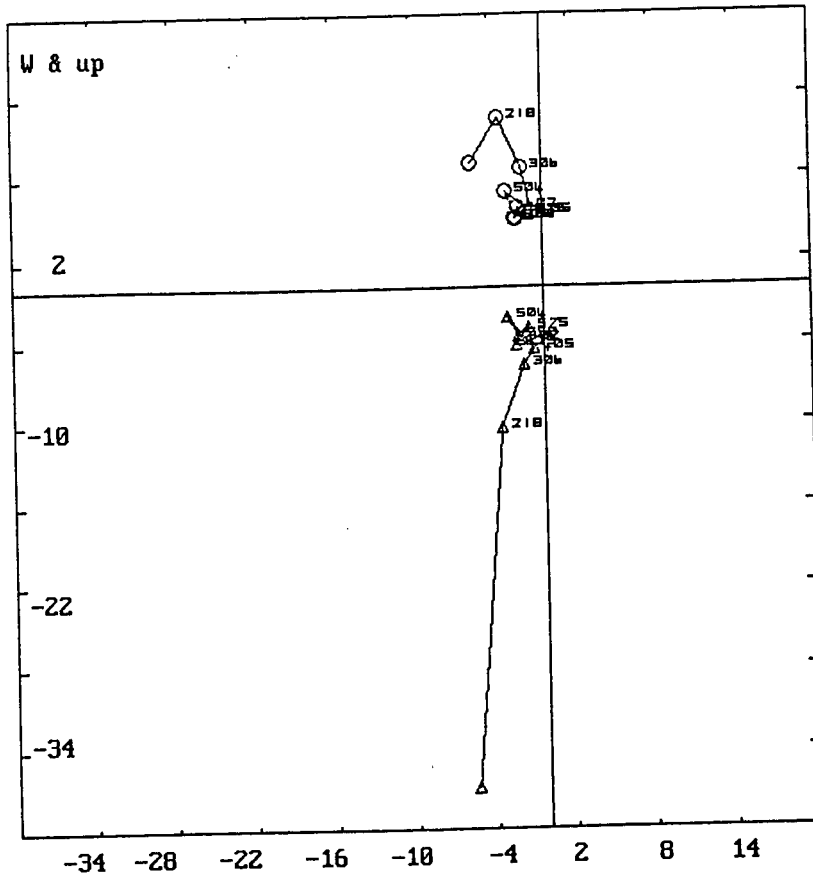 06-08-1994
Vector Diff
Plot: shows
vectors
added in
nature
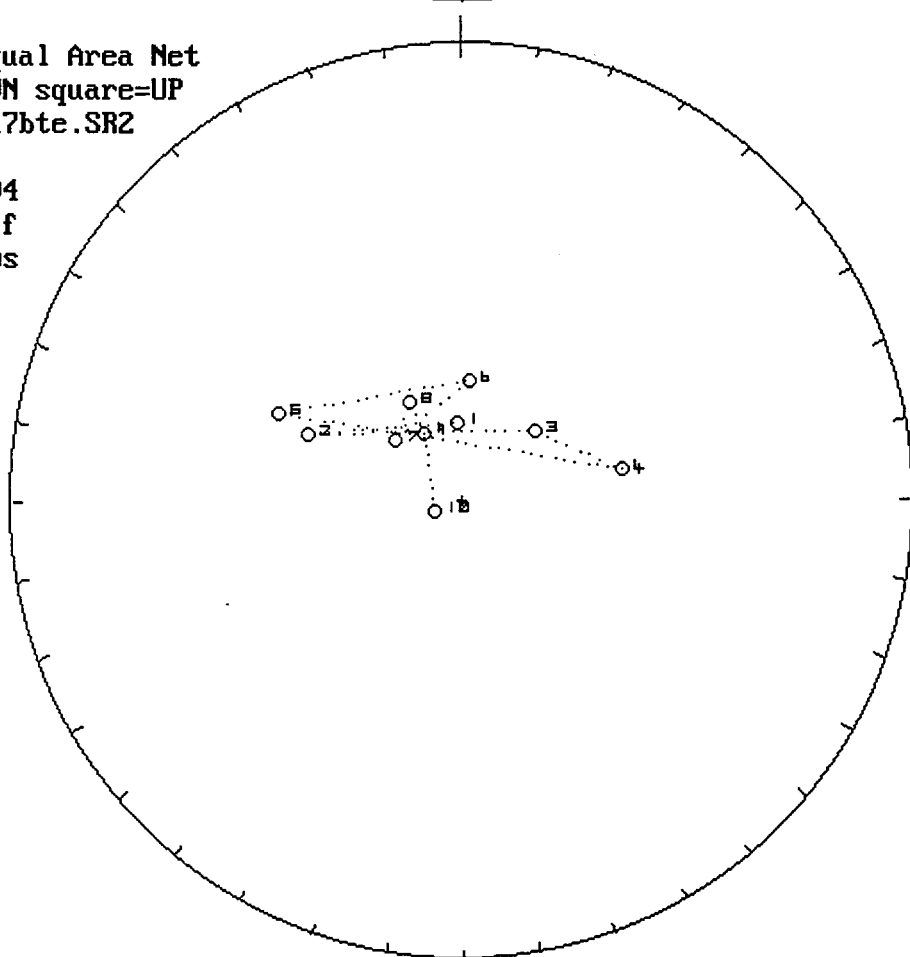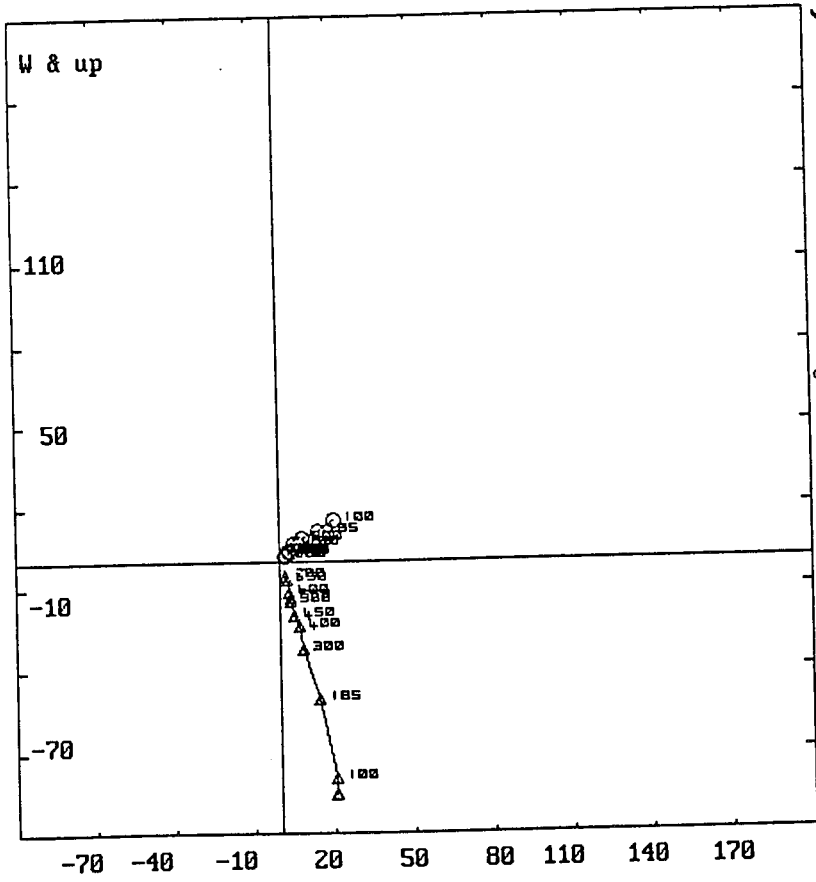
\thermal\sy17bte.SR2
06-08-1994
n = 11
 circle =horiz.plo
 triang. =vert.plot
 units mA/m
PCA decl= 325.5
PCA incl= 73.5
for points 1 to 11
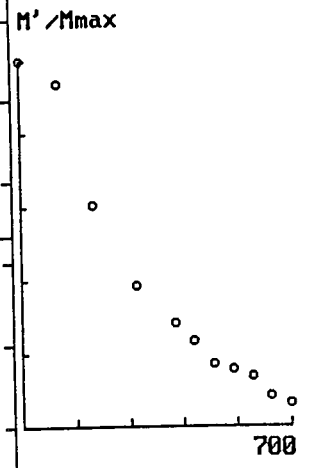
Lwr.Hem.Equal Area Net
circle=DOWN square=UP
 ermal\sy18bte.SR2
 n = 12
 06-08-1994
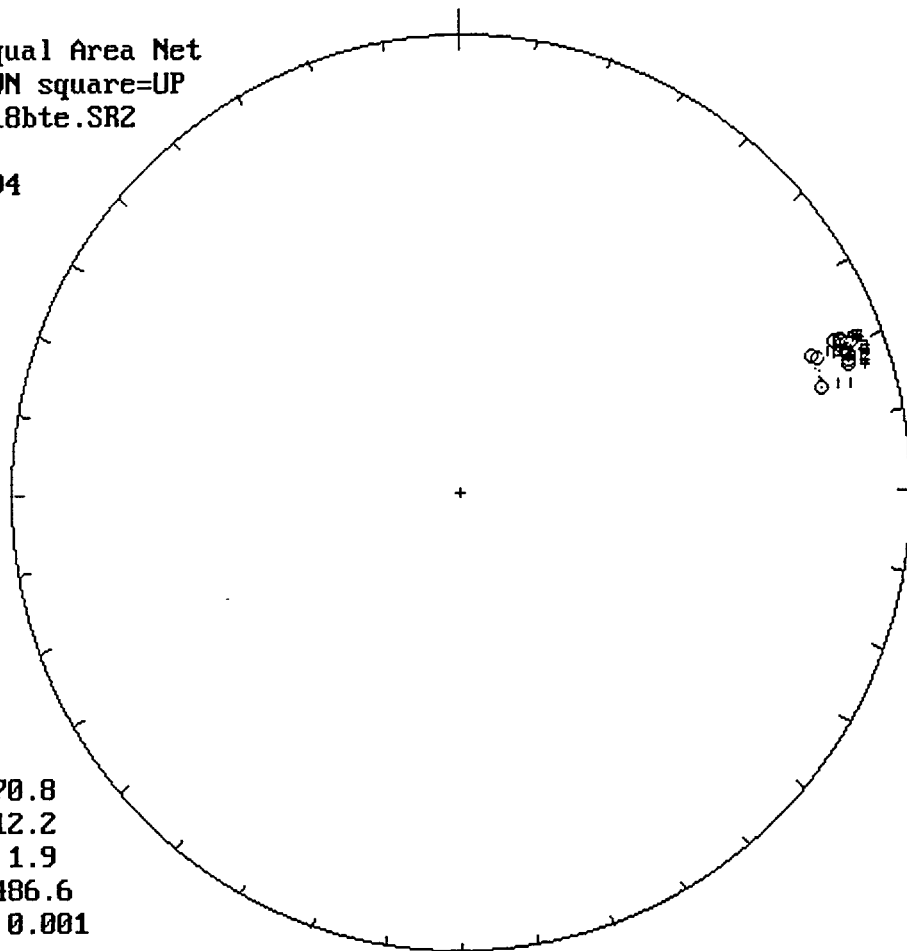
m.dec.= 70.8
m.inc.= 12.2
alpha95= 1.9
Fish. k= 486.6
sp.var.= 0.001

Lwr.Hem.Equal Area Net
circle=DOWN square=UP
 ermal\sy18bte.SR2
 n = 11
 06-08-1994
Vector Diff
Plot: shows
vectors
added in
nature

\thermal\sy18bte.SR2
06-08-1994
n = 12
 circle =horiz.plo
 triang. =vert.plot
 units A/m
PCA decl= 71.0
PCA incl= 9.9
for points 1 to 12

W & up

0.2
1.0
2.2
3.4

-3.4 -2.8 -2.2 -1.6 -1.0 -0.4 0.2 0.8 1.4 S to N

M'/Mmax

700
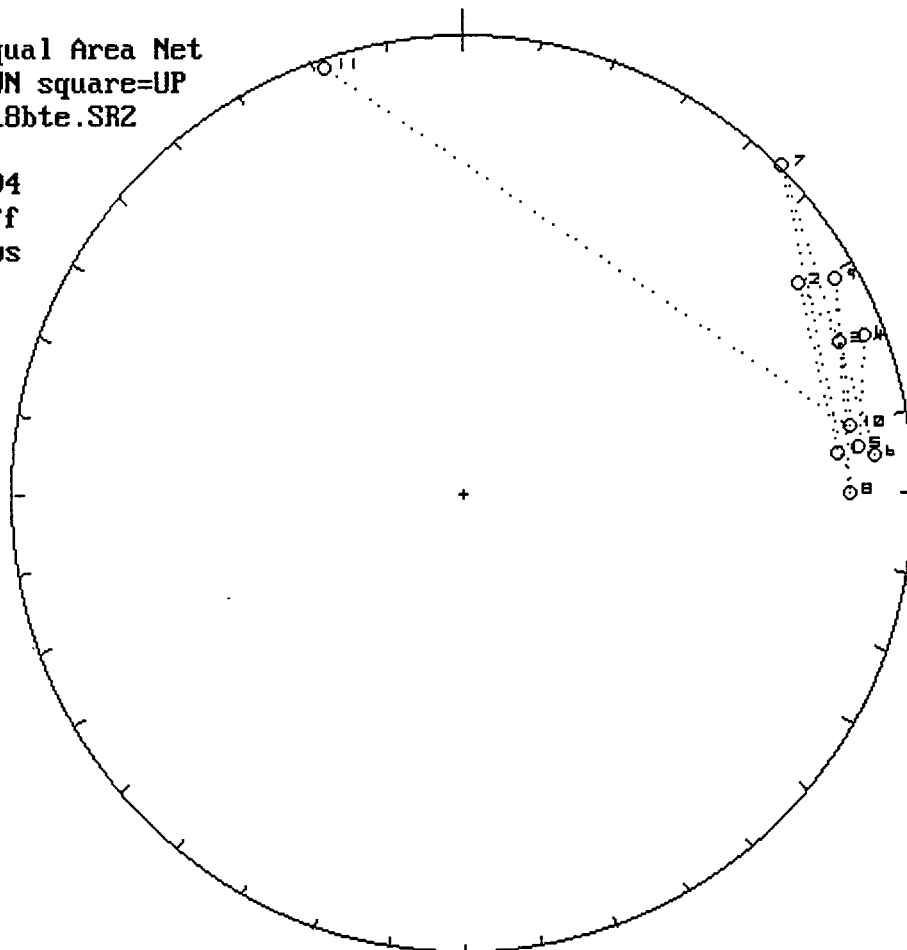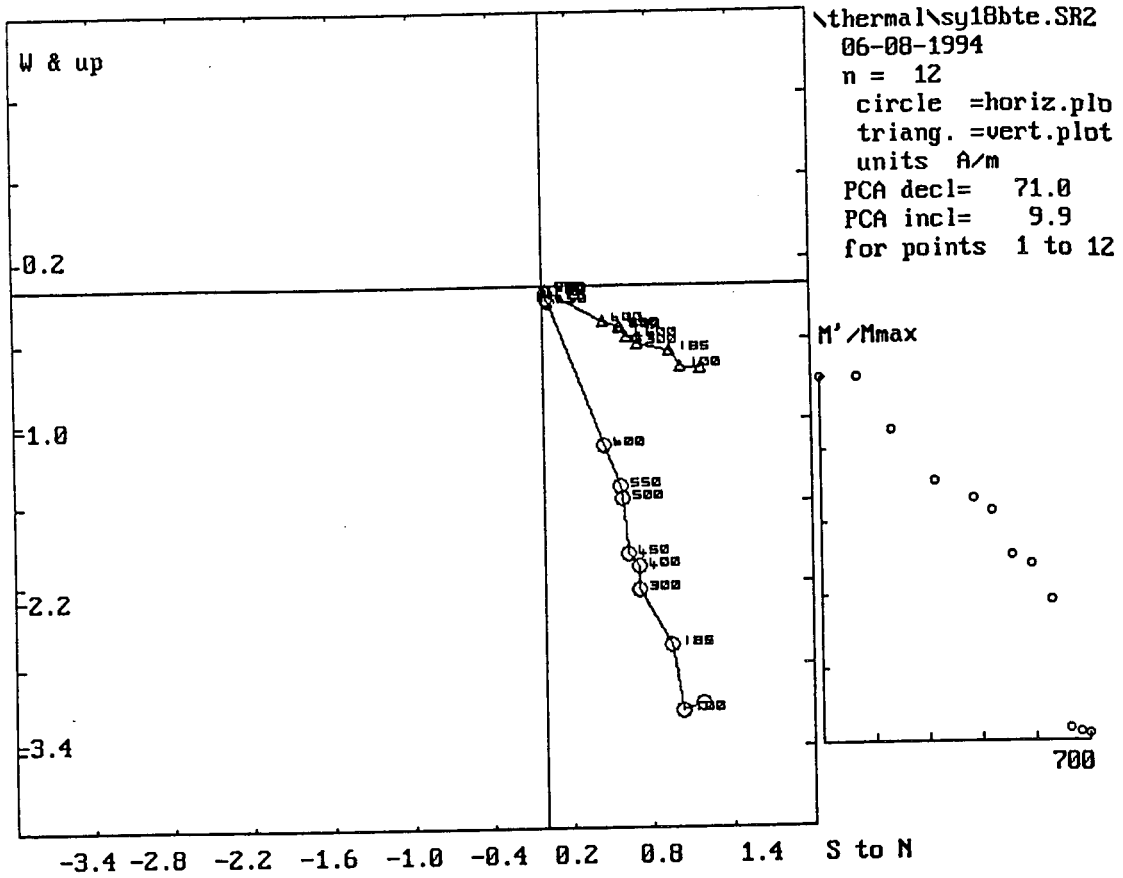
Lwr.Hem.Equal Area Net
circle=DOWN square=UP
 ermal\sy24bte.SR2
 n = 9
 06-08-1994
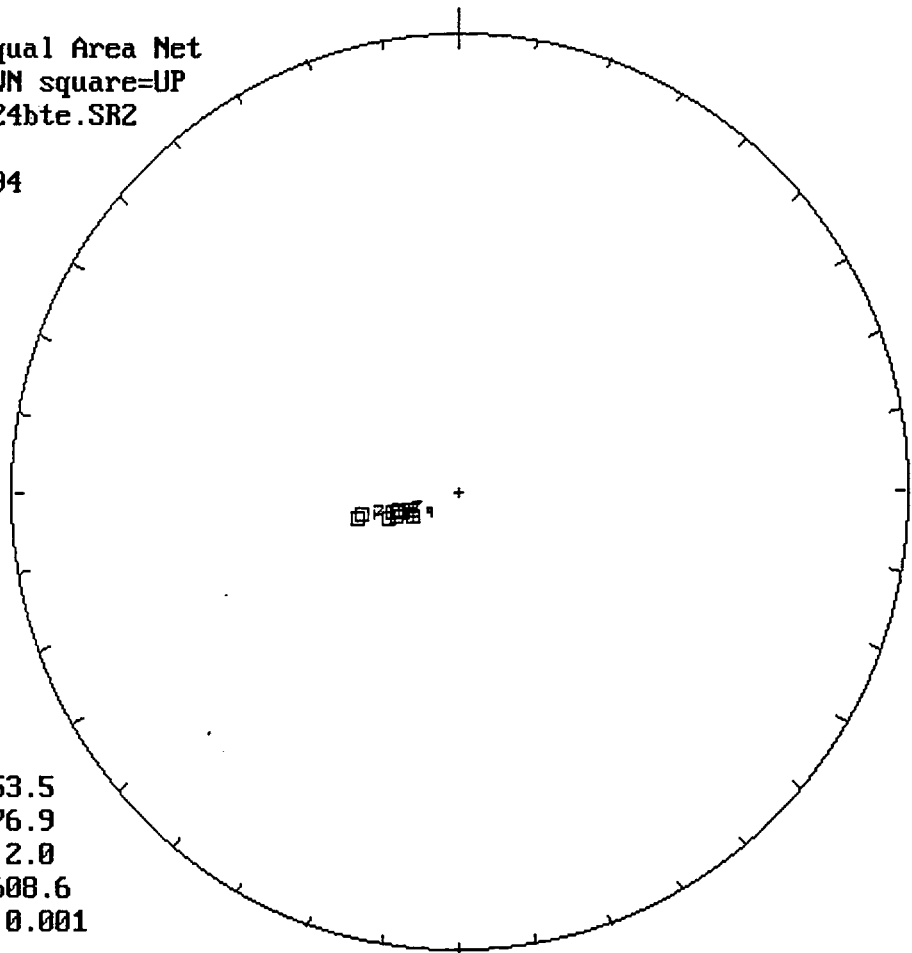
m.dec.= 253.5
m.inc.= -76.9
alpha95= 2.0
Fish. k= 608.6
sp.var.= 0.001

Lwr.Hem.Equal Area Net
circle=DOWN square=UP
 ermal\sy24bte.SR2
 n = 8
 06-08-1994
Vector Diff
Plot: shows
vectors
added in
nature

W & up

11

5

-1

-7

-7   -4   -1   2   5   8   11   14   17   S to N
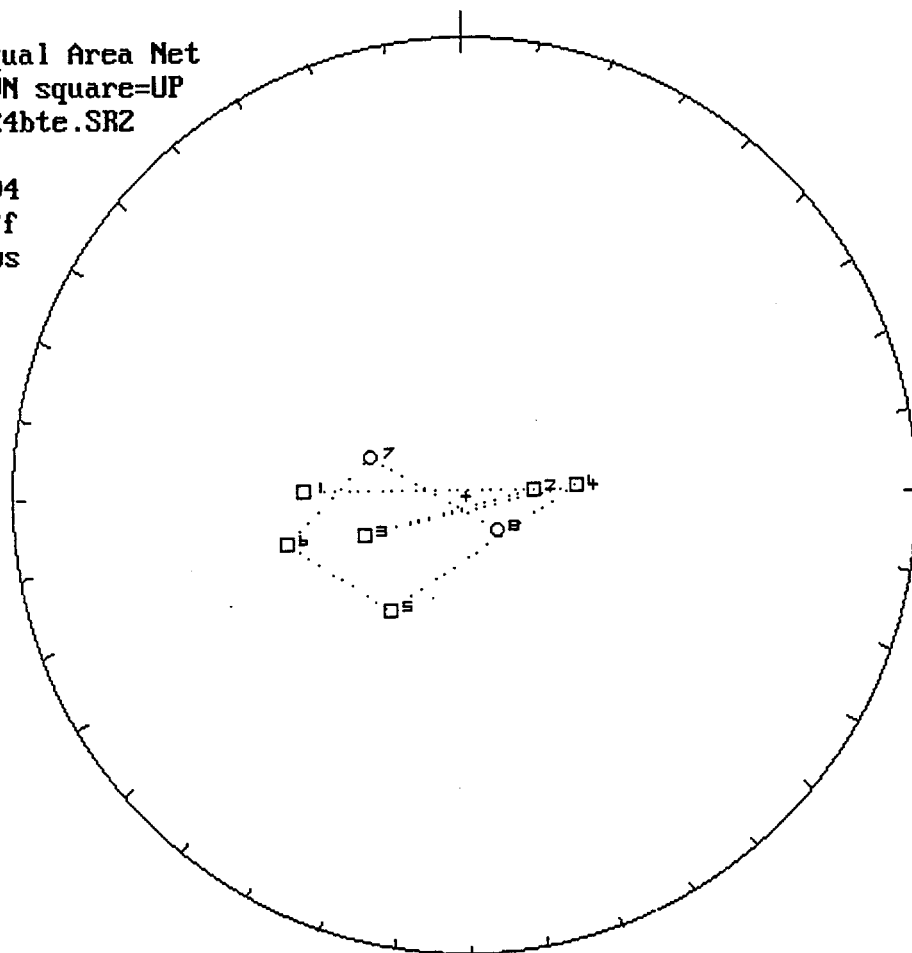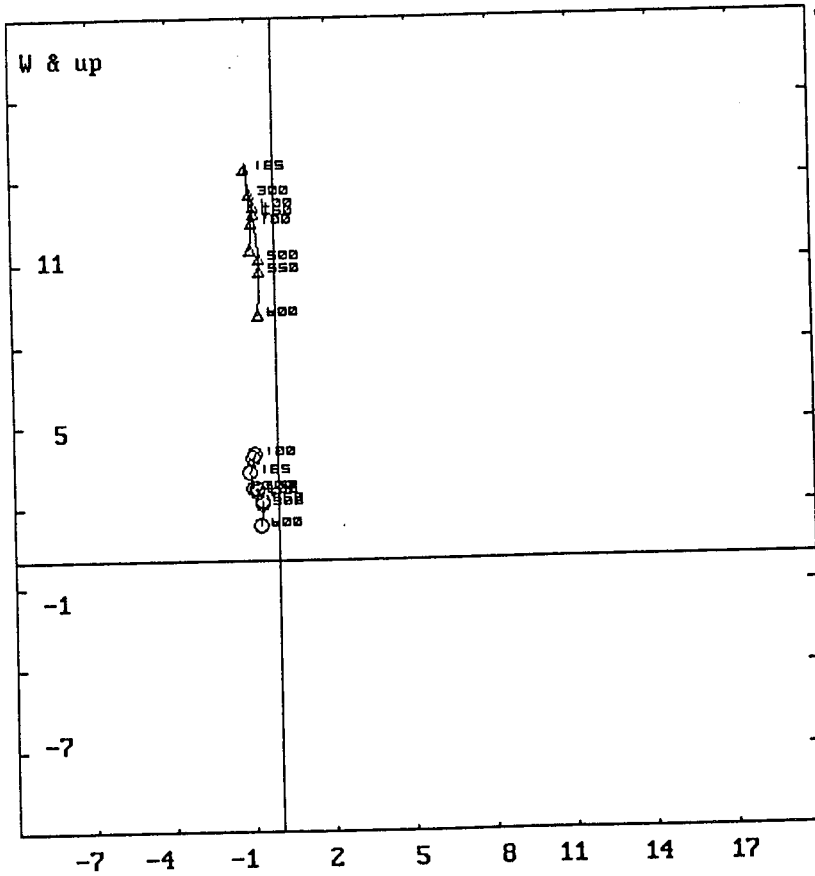
\thermal\sy24bte.SR2
06-08-1994
n = 9
 circle =horiz.plo
 triang. =vert.plot
 units mA/m
PCA decl= 256.2
PCA incl= -70.1
for points 1 to 9

M'/Mmax

600
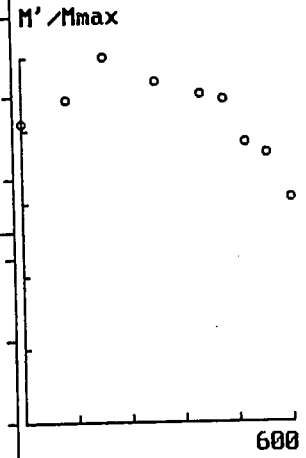
Lwr.Hem.Equal Area Net
circle=DOWN square=UP
 ermal\sy25bte.SR2
 n = 9
 06-08-1994
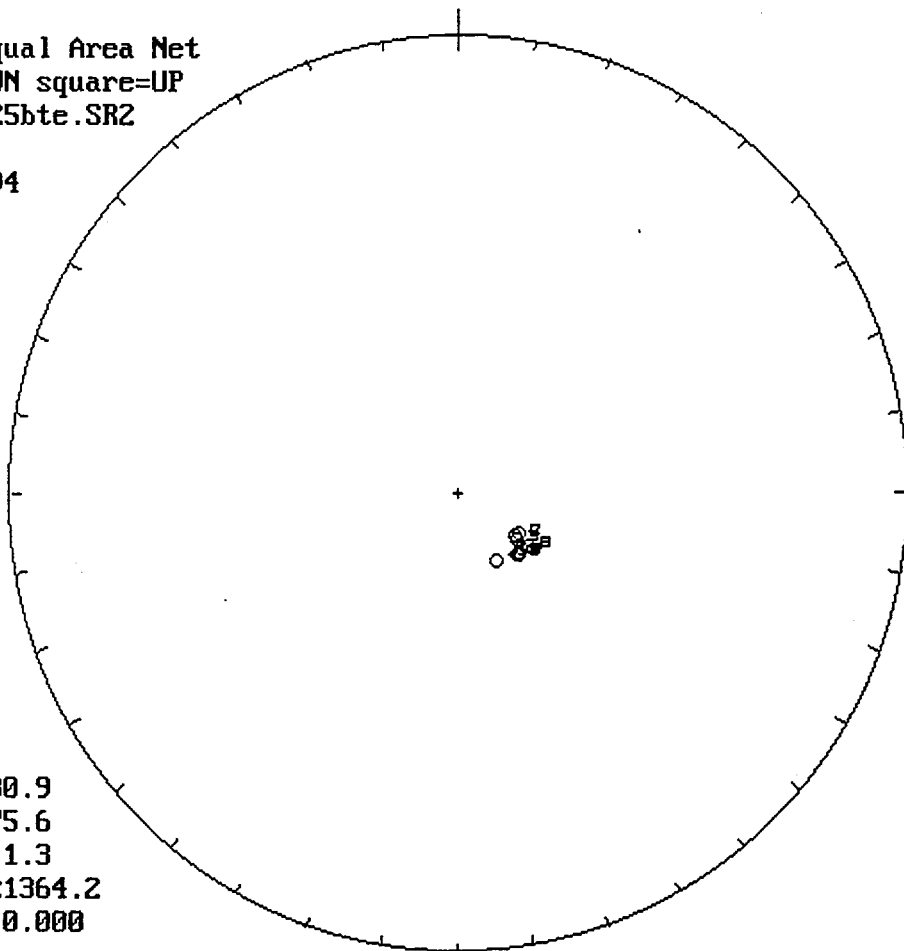
m.dec.= 130.9
m.inc.= 75.6
alpha95= 1.3
Fish. k= ⁒1364.2
sp.var.= 0.000

Lwr.Hem.Equal Area Net
circle=DOWN square=UP
 ermal\sy25bte.SR2
 n = 8
 06-08-1994
Vector Diff
Plot: shows
vectors
added in
nature

W & up

-80

-200

-320

-440

-440 -380 -320 -260 -200 -140 -80 -20 40   S to N

\thermal\sy25bte.SR2
  06-08-1994
  n = 9
   circle =horiz.plo
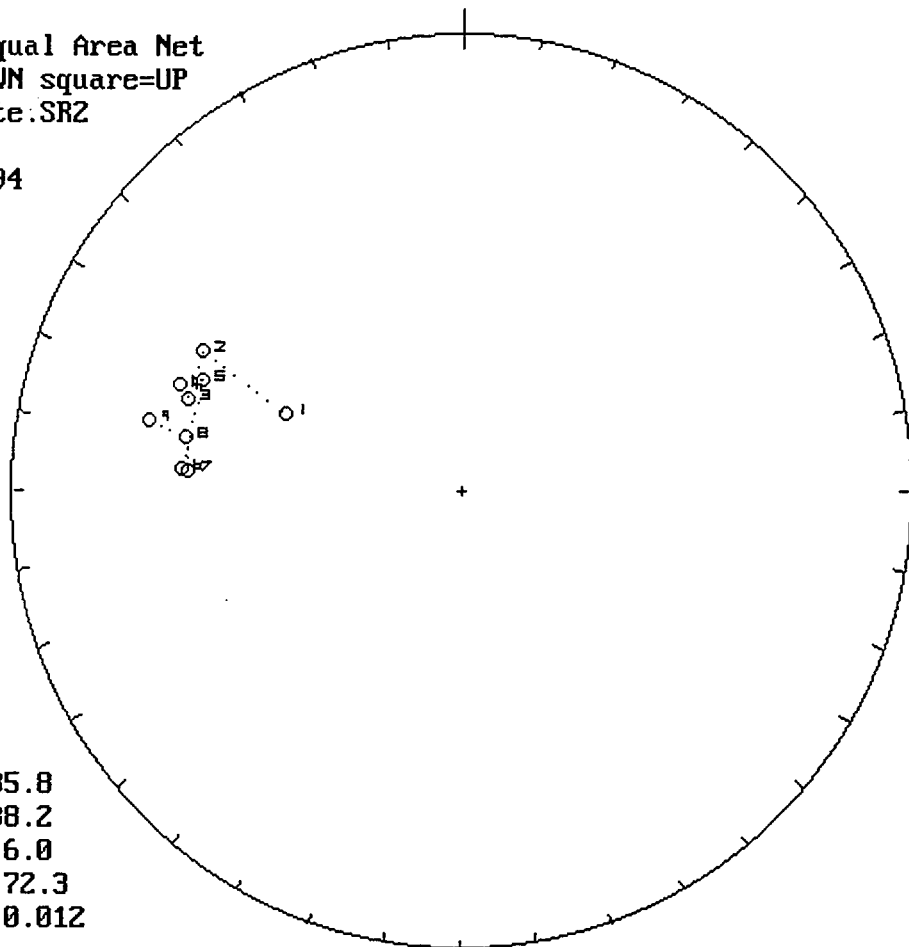   triang. =vert.plot
   units mA/m
  PCA decl= 121.4
 PCA incl=   77.4
  for points 1 to 9

M'/Mmax

600
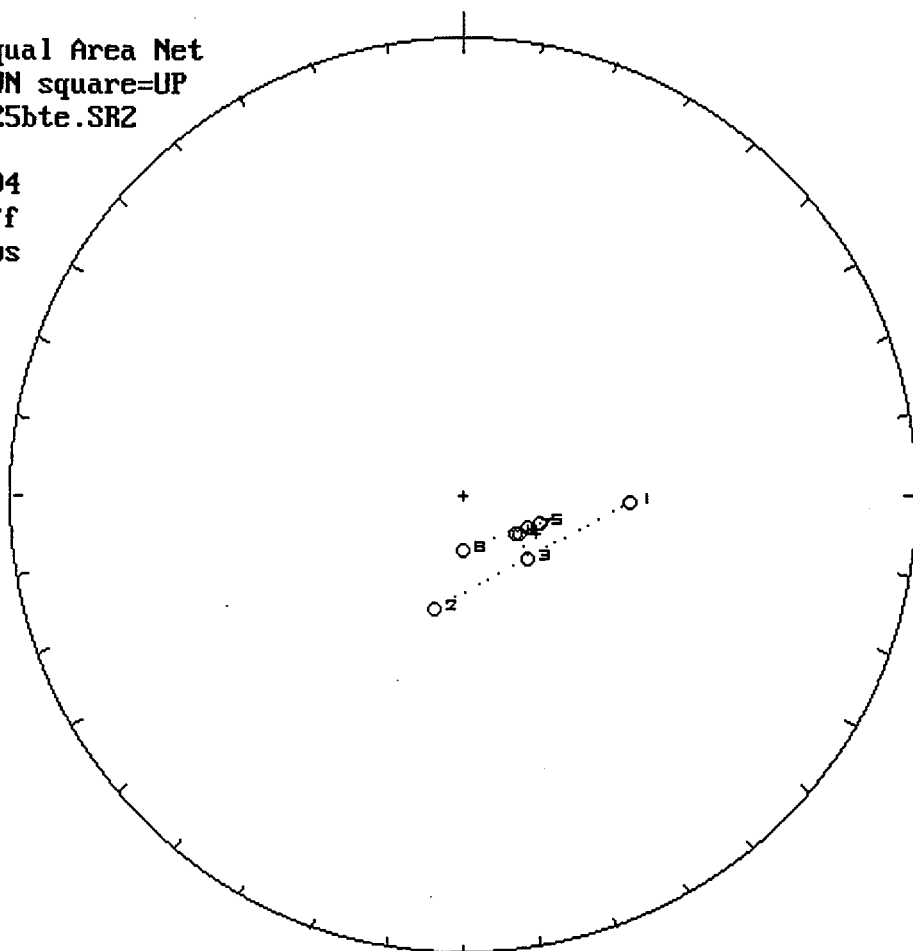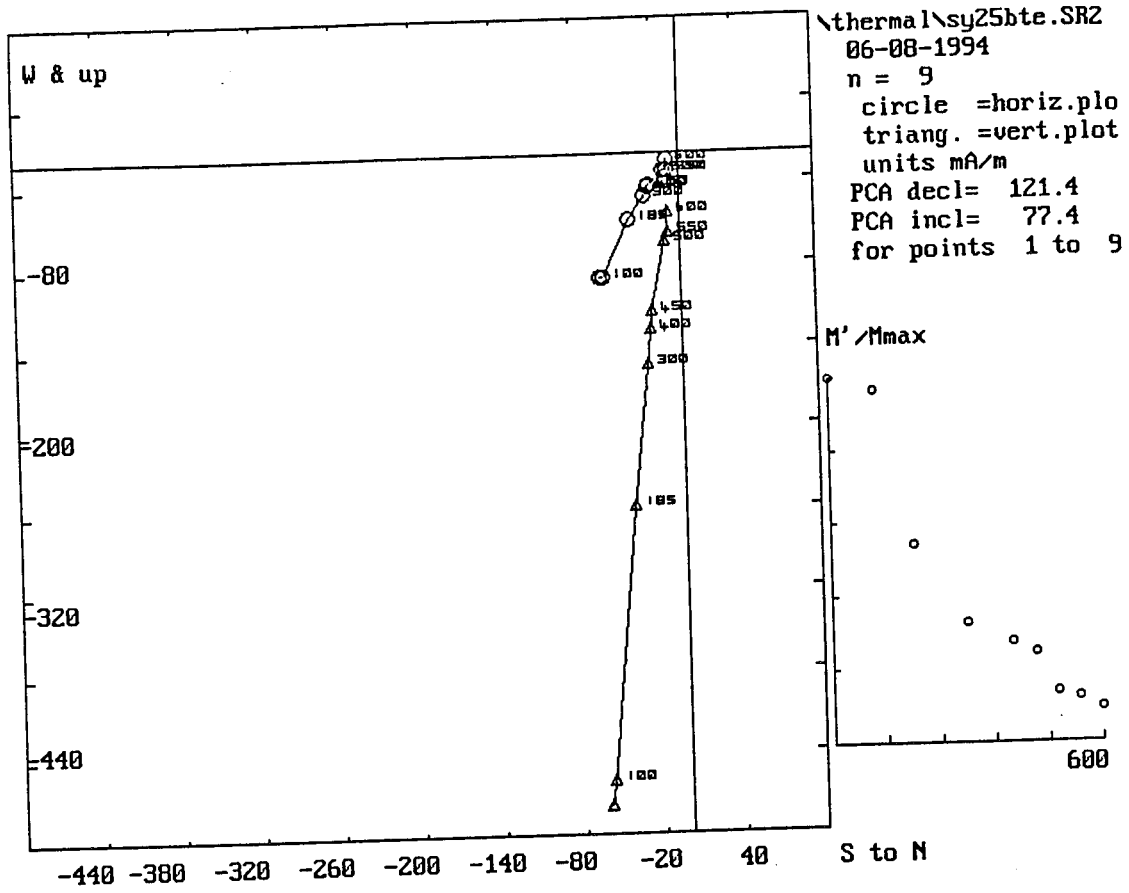
Lwr.Hem.Equal Area Net
circle=DOWN square=UP
 ermal\sy28bte.SR2
 n = 9
 06-08-1994
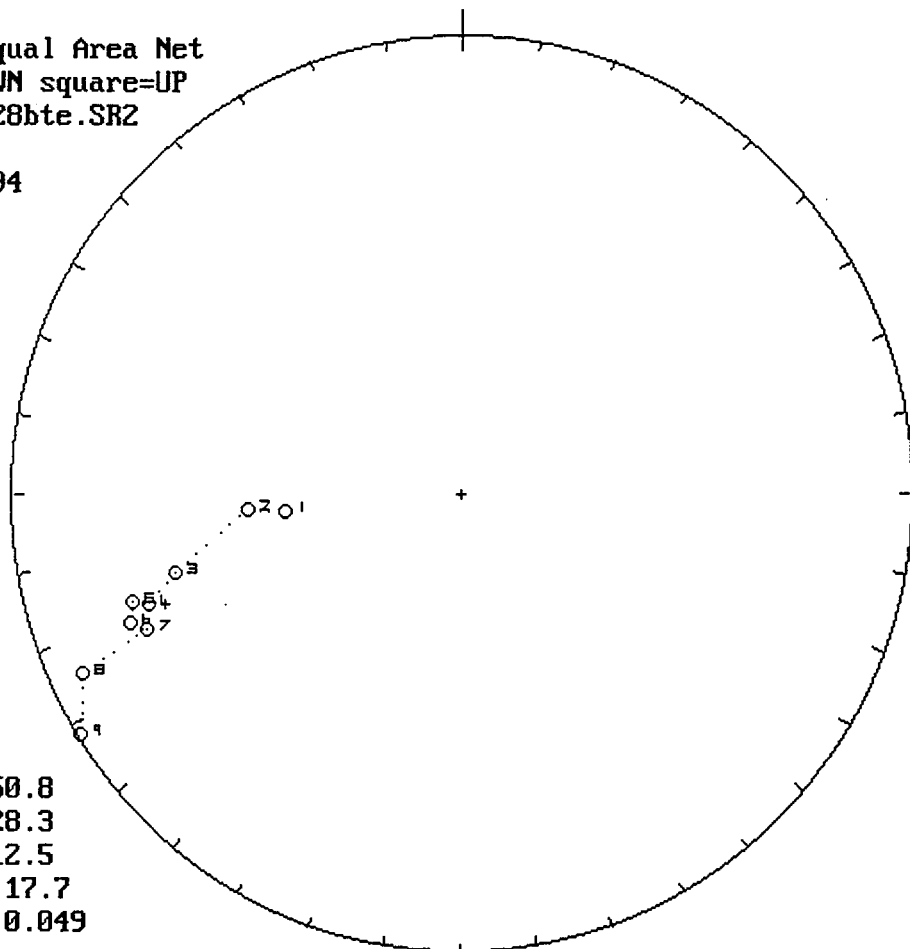
m.dec.= 250.8
m.inc.= 28.3
alpha95= 12.5
Fish. k= 17.7
sp.var.= 0.049

Lwr.Hem.Equal Area Net
circle=DOWN square=UP
 ermal\sy28bte.SR2
 n = 8
 06-08-1994
Vector Diff
Plot: shows
vectors
added in
nature
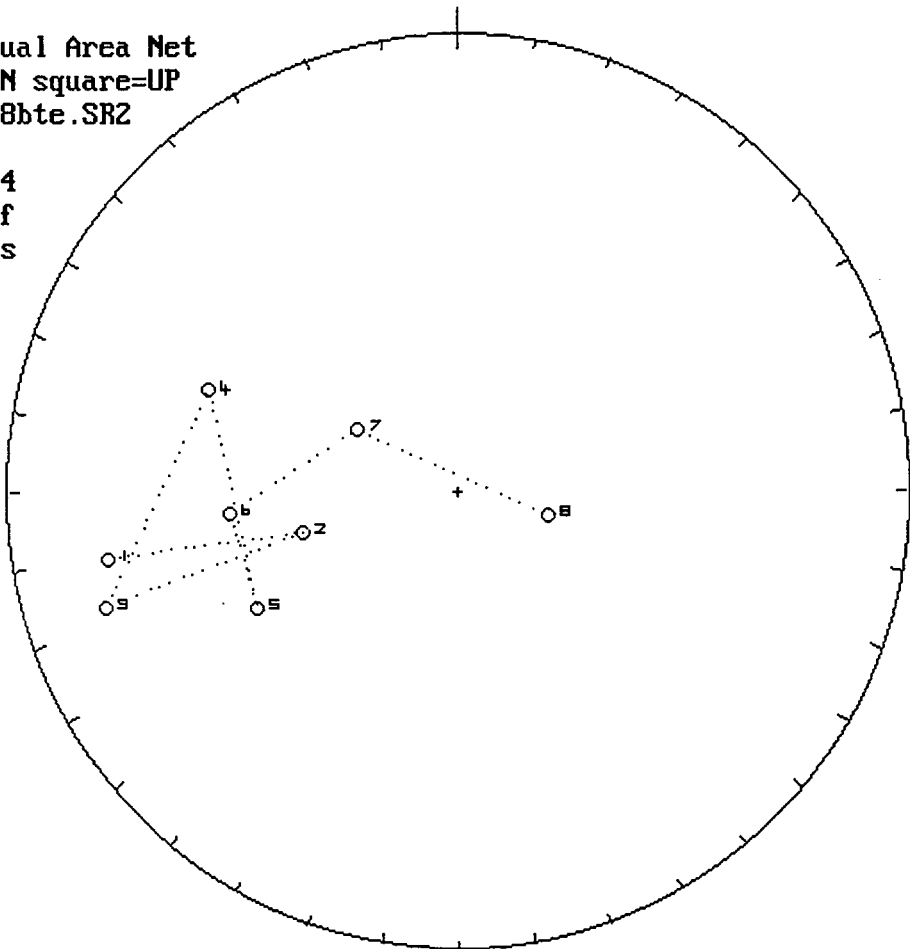
\thermal\sy28bte.SR2
06-08-1994
n = 9
 circle =horiz.plo
 triang. =vert.plot
 units mA/m
PCA decl=   99.8
PCA incl= -61.5
for points 2 to 6

W & up

M'/Mmax

-240 -180 -120 -60   0   60 120 180 240   S to N

\thermal\sy28bte.SR2
06-08-1994
n = 9
 circle =horiz.plo
 triang. =vert.plot
 units mA/m
PCA decl= 253.9
PCA incl=   31.1
for points 6 to 9

W & up

M'/Mmax

-240 -180 -120 -60   0   60 120 180 240   S to N
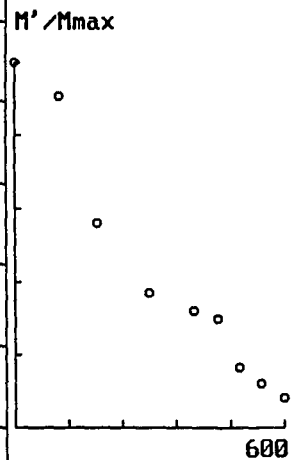
Lwr.Hem.Equal Area Net
circle=DOWN square=UP
 b:\sy31bte.SR2
 n = 9
 08-09-1994
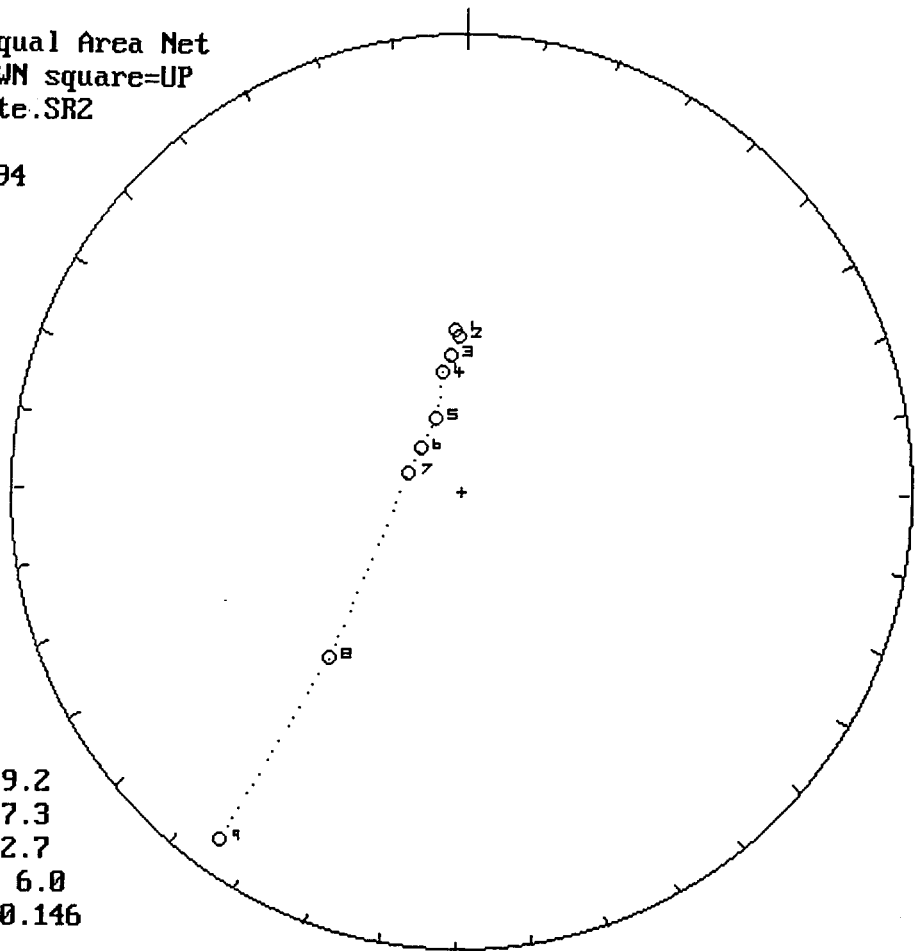
m.dec.= 299.2
m.inc.= 77.3
alpha95= 22.7
Fish. k=   6.0
sp.var.= 0.146

Lwr.Hem.Equal Area Net
circle=DOWN square=UP
 b:\sy31bte.SR2
 n = 8
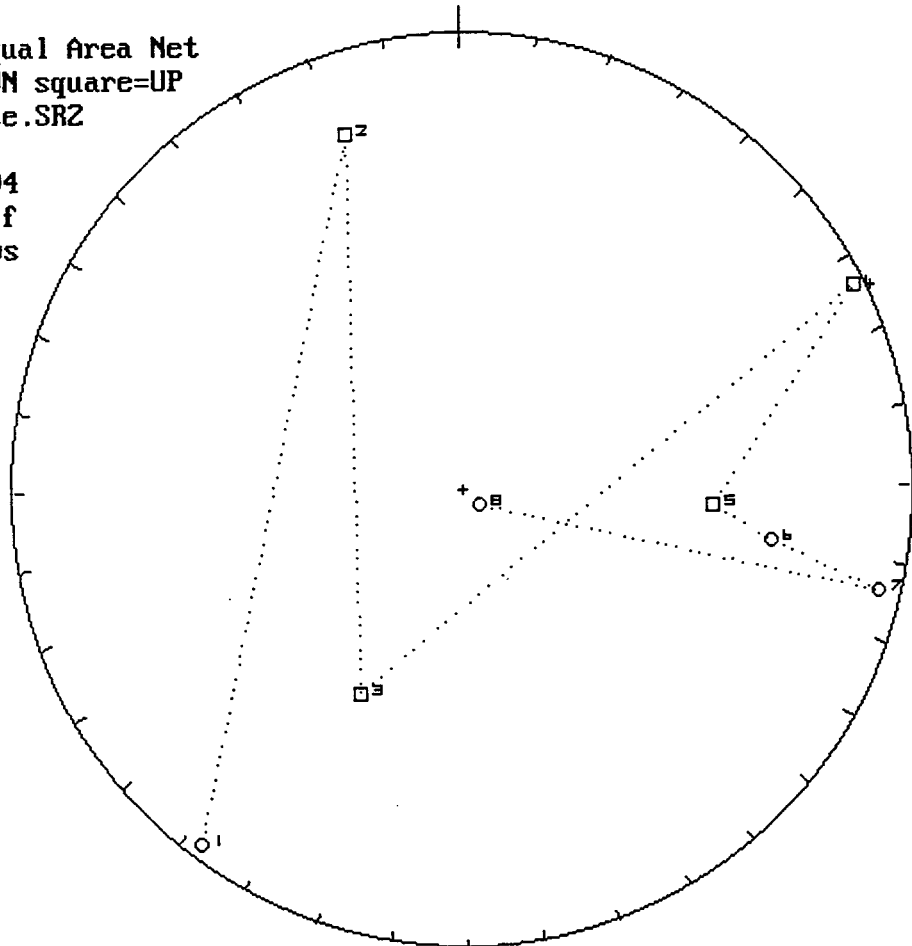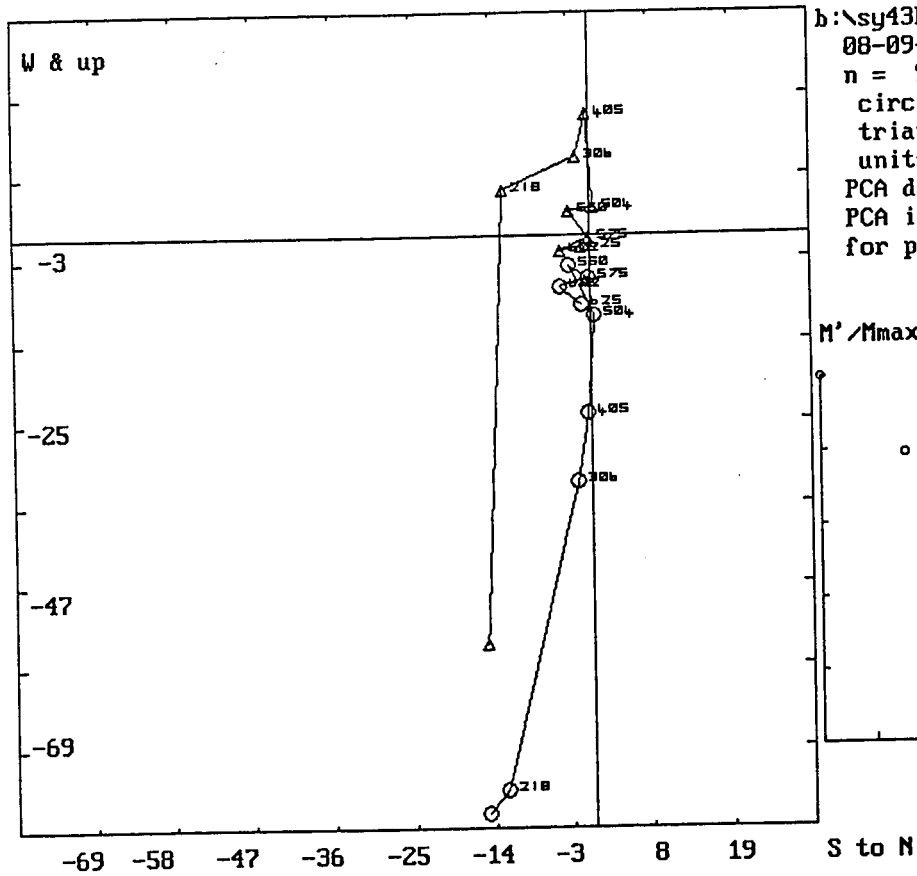 08-09-1994
Vector Diff
Plot: shows
vectors
added in
nature
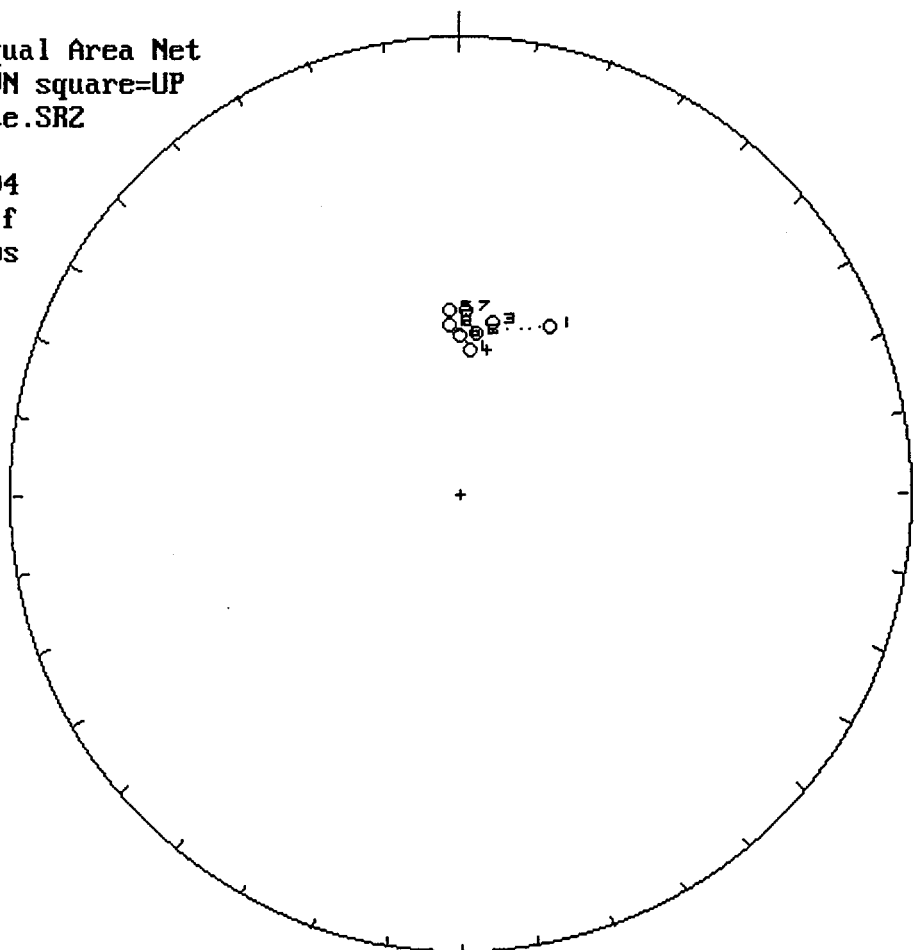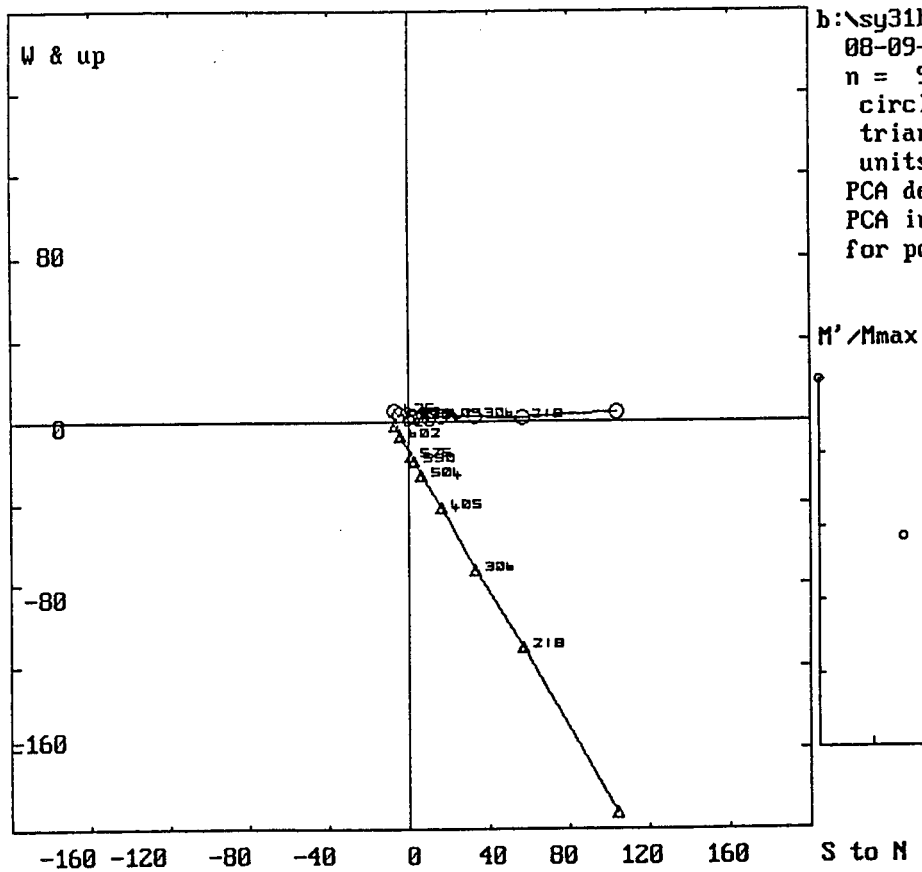
Lwr.Hem.Equal Area Net
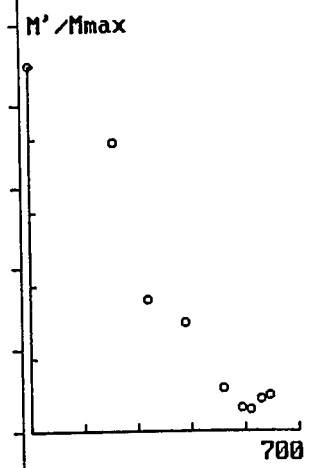circle=DOWN square=UP
 b:\sy34bte.SR2
 n = 9
 08-09-1994

m.dec.= 189.1
m.inc.=   5.3
alpha95= 29.7
Fish. k=   3.9
sp.var.= 0.225

Lwr.Hem.Equal Area Net
circle=DOWN square=UP
 b:\sy34bte.SR2
 n = 8
 08-09-1994
Vector Diff
Plot: shows
vectors
added in
nature

W & up

b:\sy34bte.SR2
08-09-1994
n = 9
circle =horiz.plo
triang. =vert.plot
units mA/m
PCA decl= 102.5
PCA incl= 85.8
for points 1 to 9

M'/Mmax

S to N

Lwr.Hem.Equal Area Net
circle=DOWN square=UP
 b:\sy37bte.SR2
 n = 9
 08-09-1994

m.dec.= 252.8
m.inc.= 37.3
alpha95= 10.4
Fish. k= 25.4
sp.var.= 0.034

Lwr.Hem.Equal Area Net
circle=DOWN square=UP
 b:\sy37bte.SR2
 n = 8
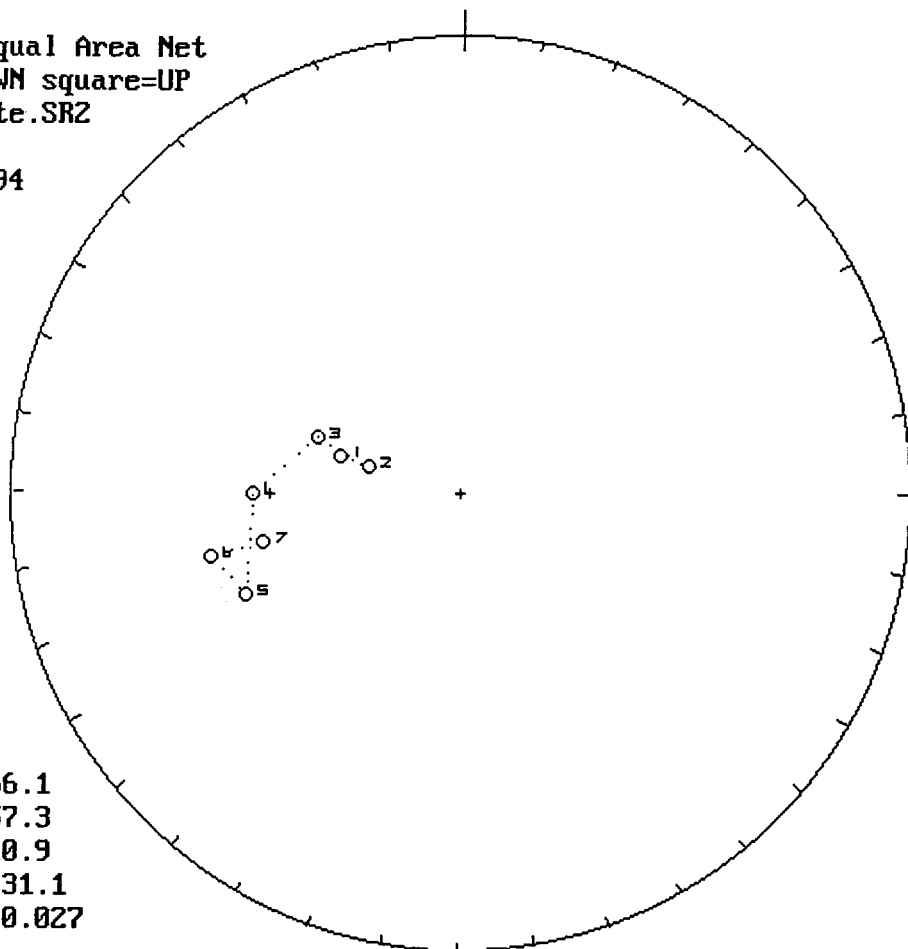 08-09-1994
Vector Diff
Plot: shows
vectors
added in
nature

W & up

b:\sy37bte.SR2
 08-09-1994
 n = 9
  circle =horiz.plo
  triang. =vert.plot
  units mA/m
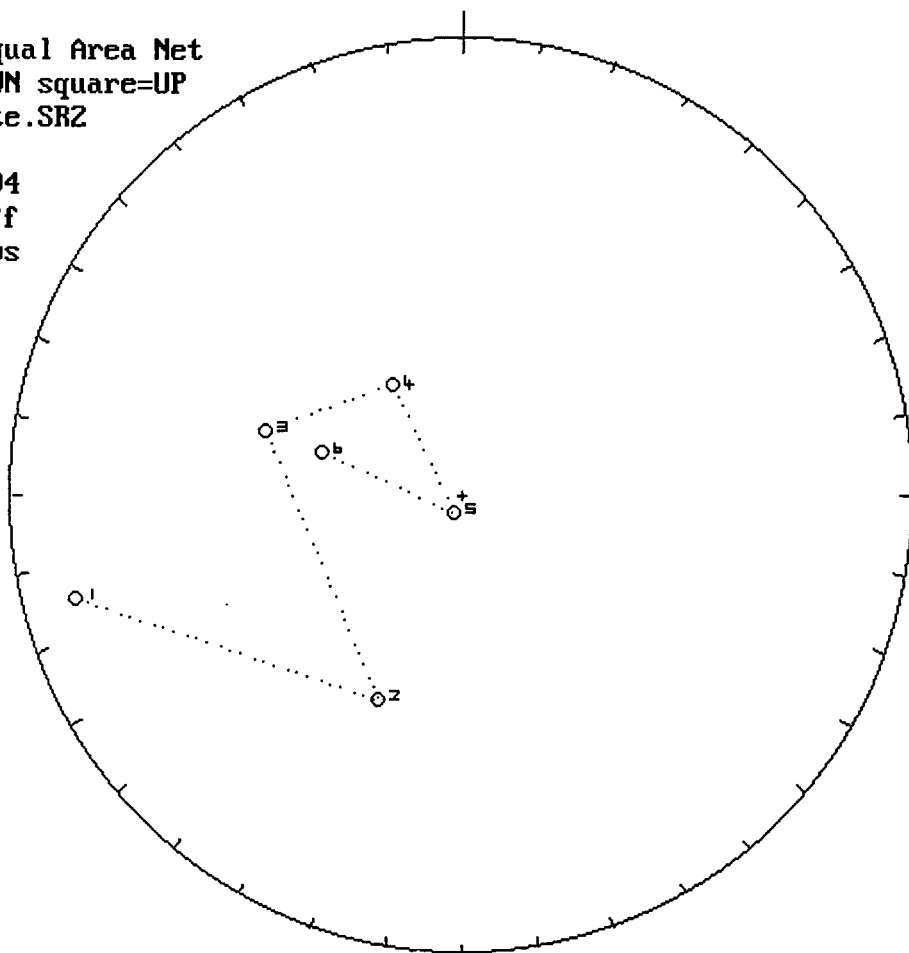PCA decl= 224.8
PCA incl= 81.0
 for points 1 to 9

M'/Mmax

700

S to N
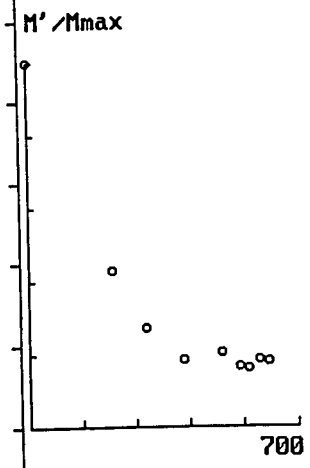
Lwr.Hem.Equal Area Net
circle=DOWN square=UP
 b:\sy38bte.SR2
 n = 9
 08-09-1994
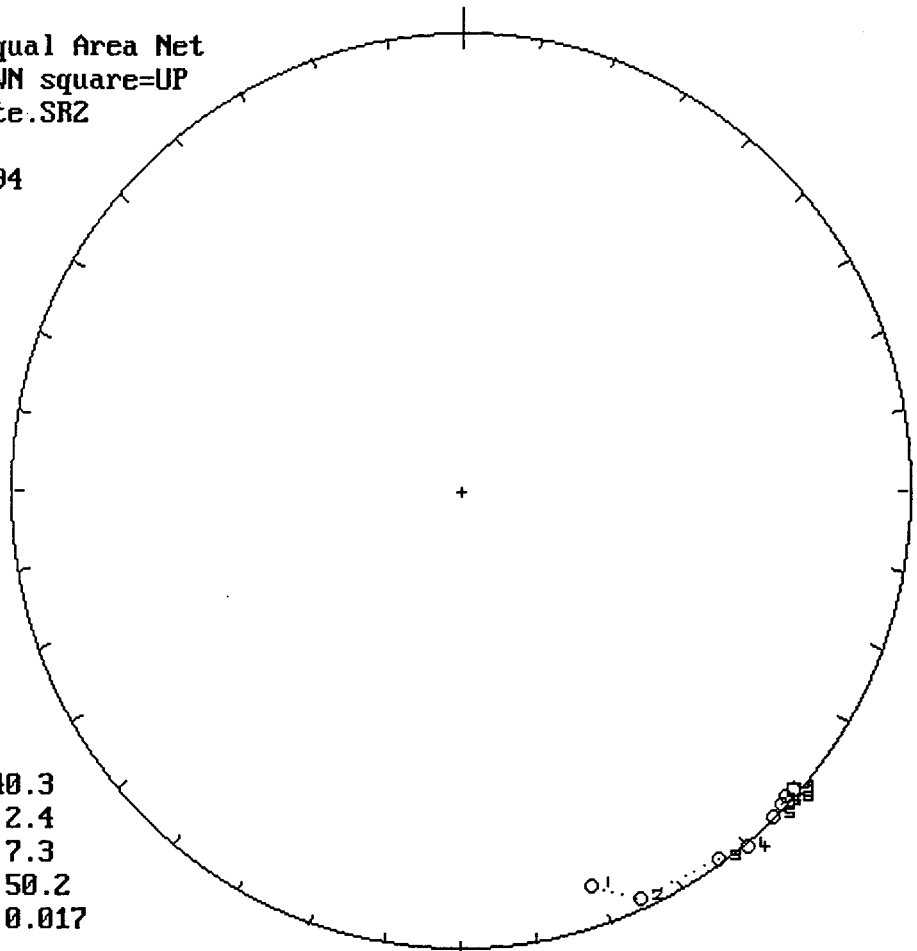
m.dec.= 140.3
m.inc.=   2.4
alpha95= 7.3
Fish. k= 50.2
sp.var.= 0.017

Lwr.Hem.Equal Area Net
circle=DOWN square=UP
 b:\sy38bte.SR2
 n = 8
 08-09-1994
Vector Diff
Plot: shows
vectors
added in
nature
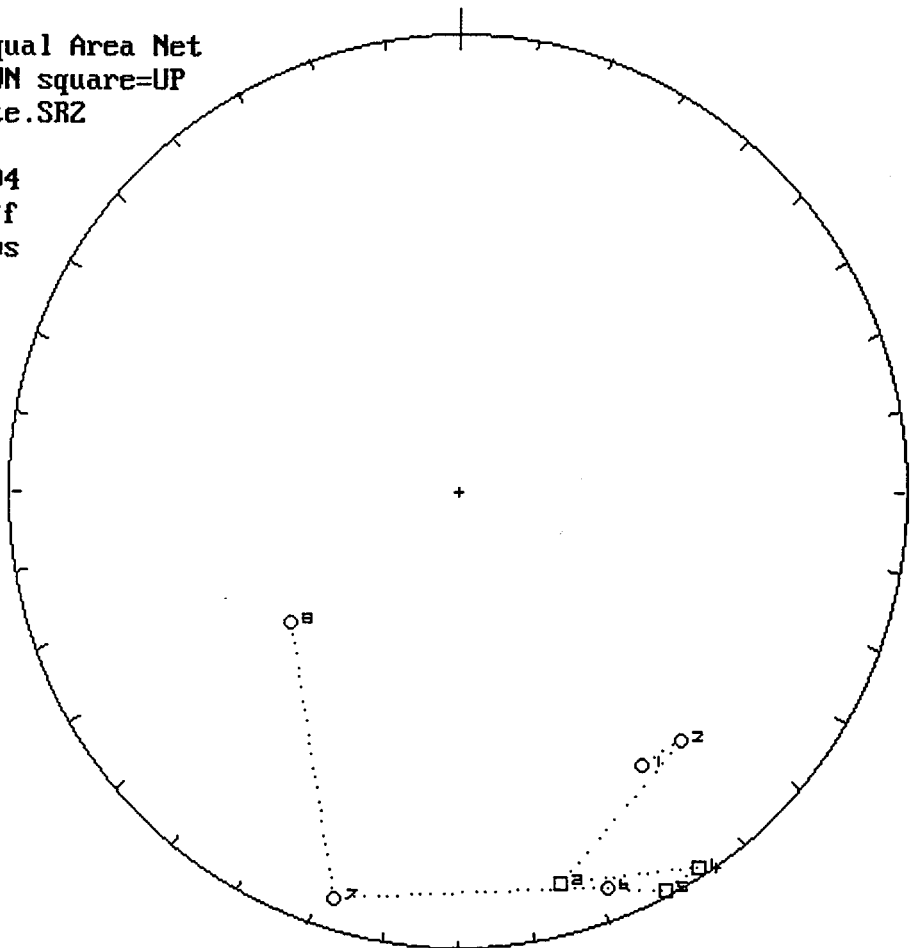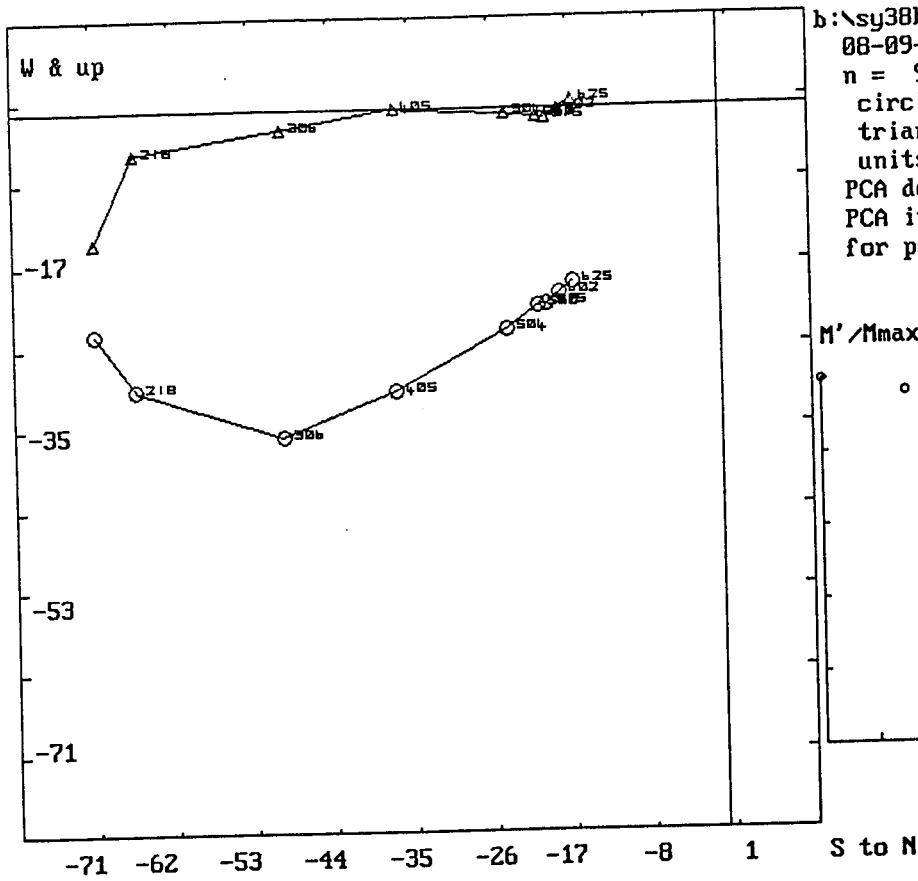
b:\sy38bte.SR2
08-09-1994
n = 9
circle = horiz.plo
triang. = vert.plot
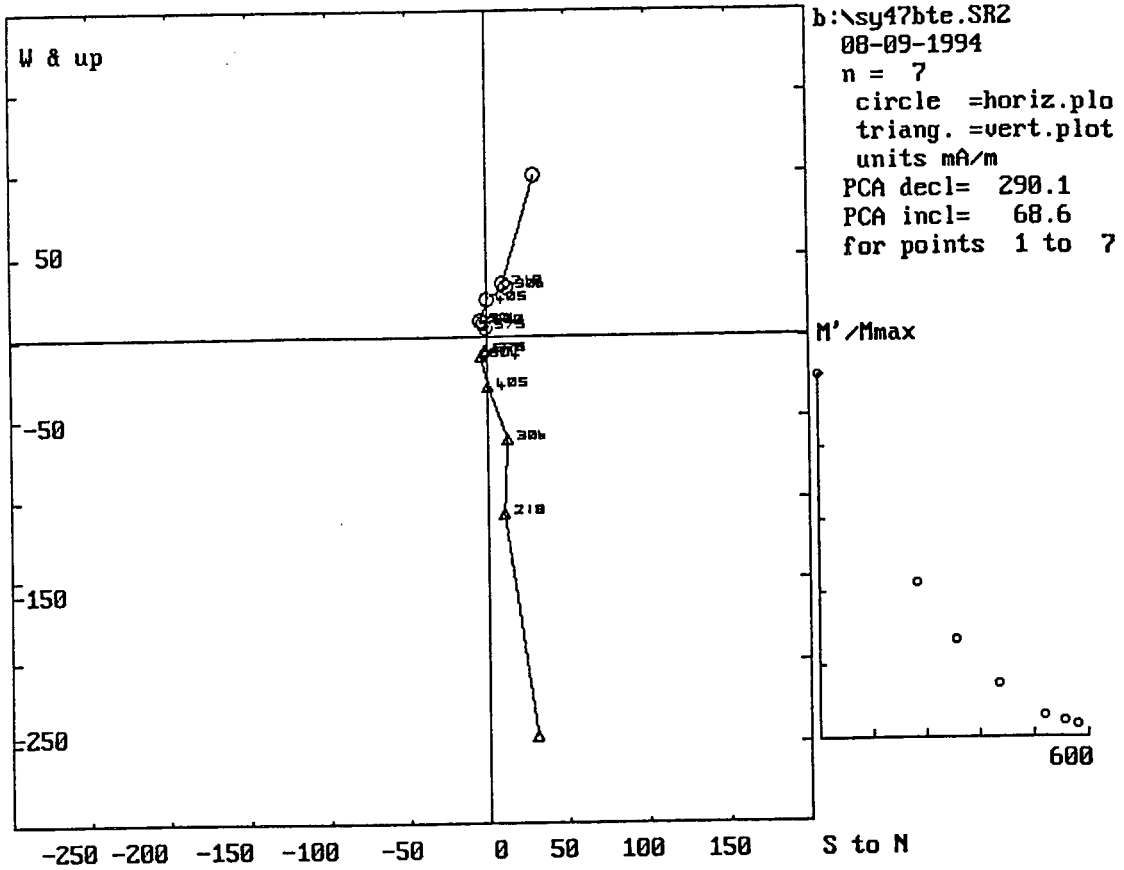units mA/m
PCA decl= 170.2
PCA incl= 10.0
for points 1 to 9
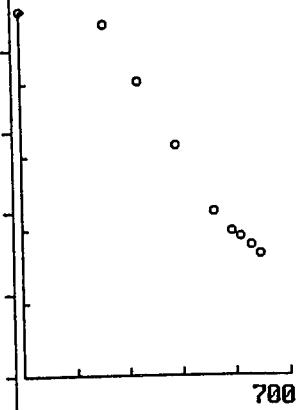
Lwr.Hem.Equal Area Net
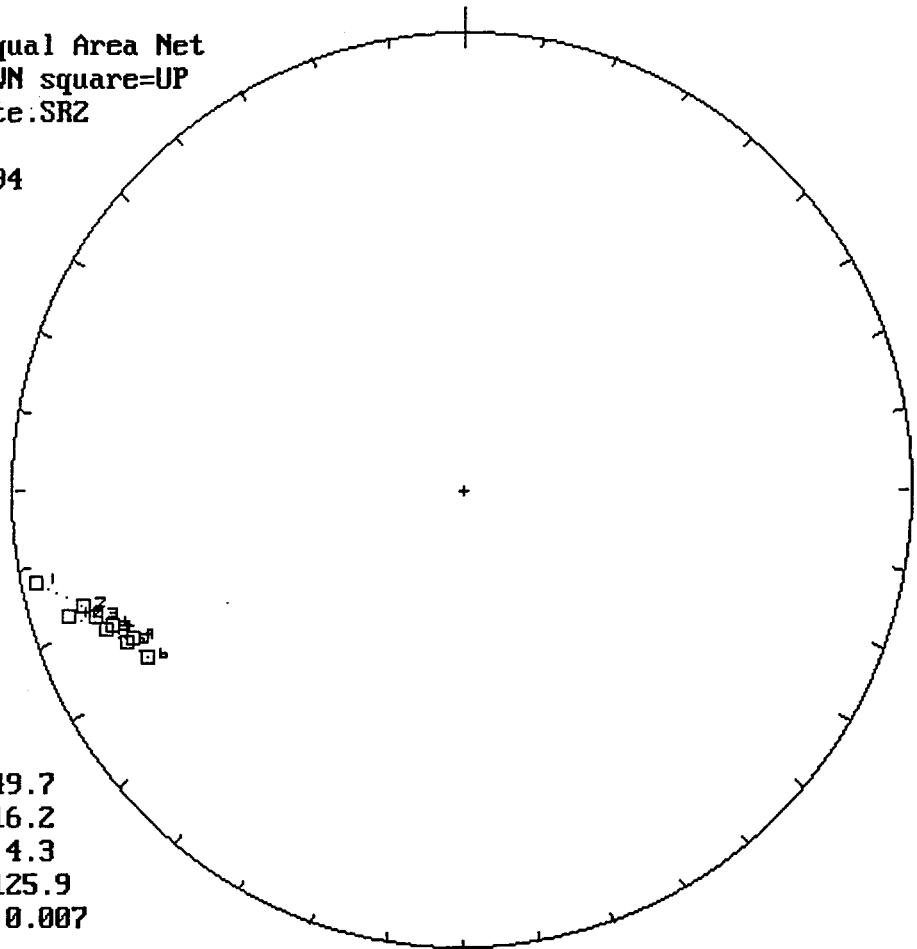circle=DOWN square=UP
 b:\sy42bte.SR2
 n = 9
 08-09-1994

m.dec.= 285.8
m.inc.= 38.2
alpha95= 6.0
Fish. k= 72.3
sp.var.= 0.012

Lwr.Hem.Equal Area Net
circle=DOWN square=UP
 b:\sy42bte.SR2
 n = 8
 08-09-1994
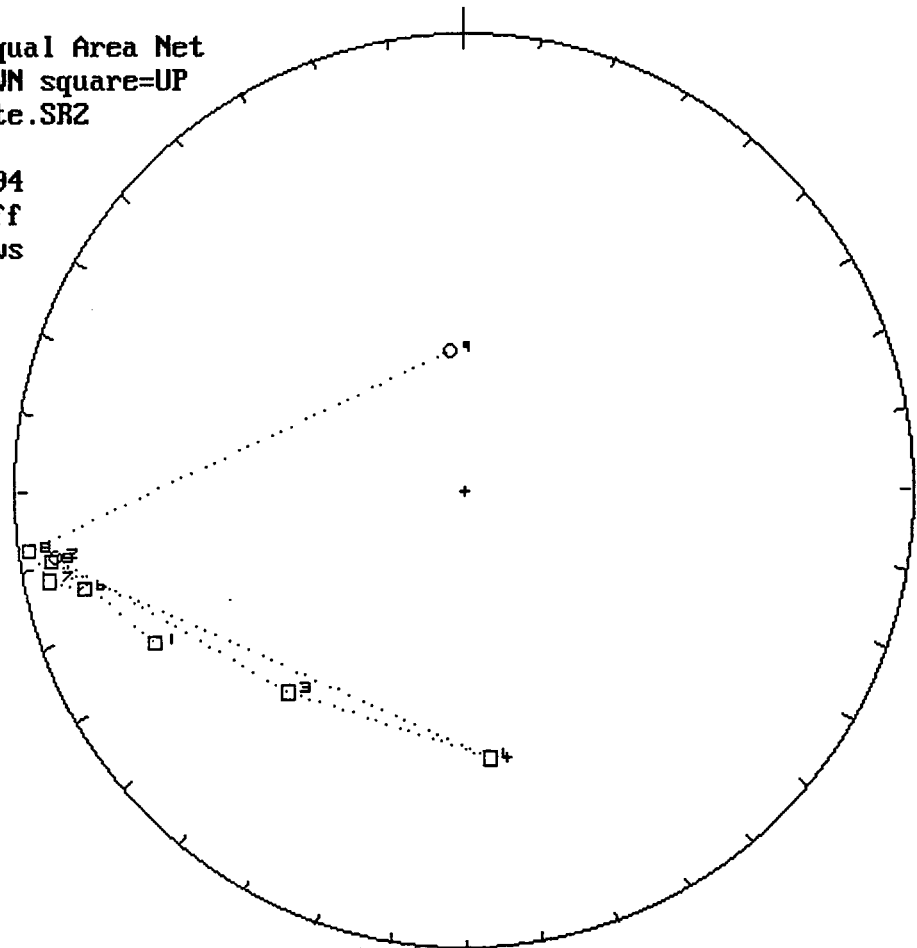Vector Diff
Plot: shows
vectors
added in
nature

b:\sy42bte.SR2
08-09-1994
n = 9
circle =horiz.plo
triang. =vert.plot
units mA/m
PCA decl= 299.1
PCA incl= 50.9
for points 1 to 9
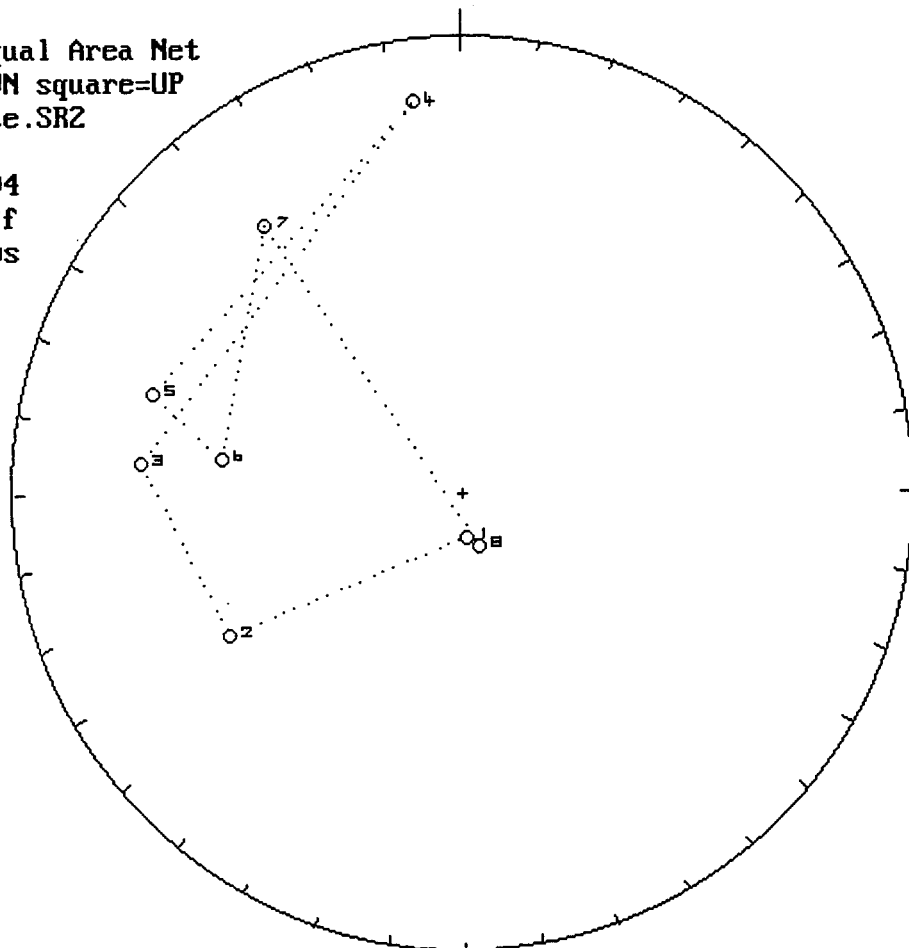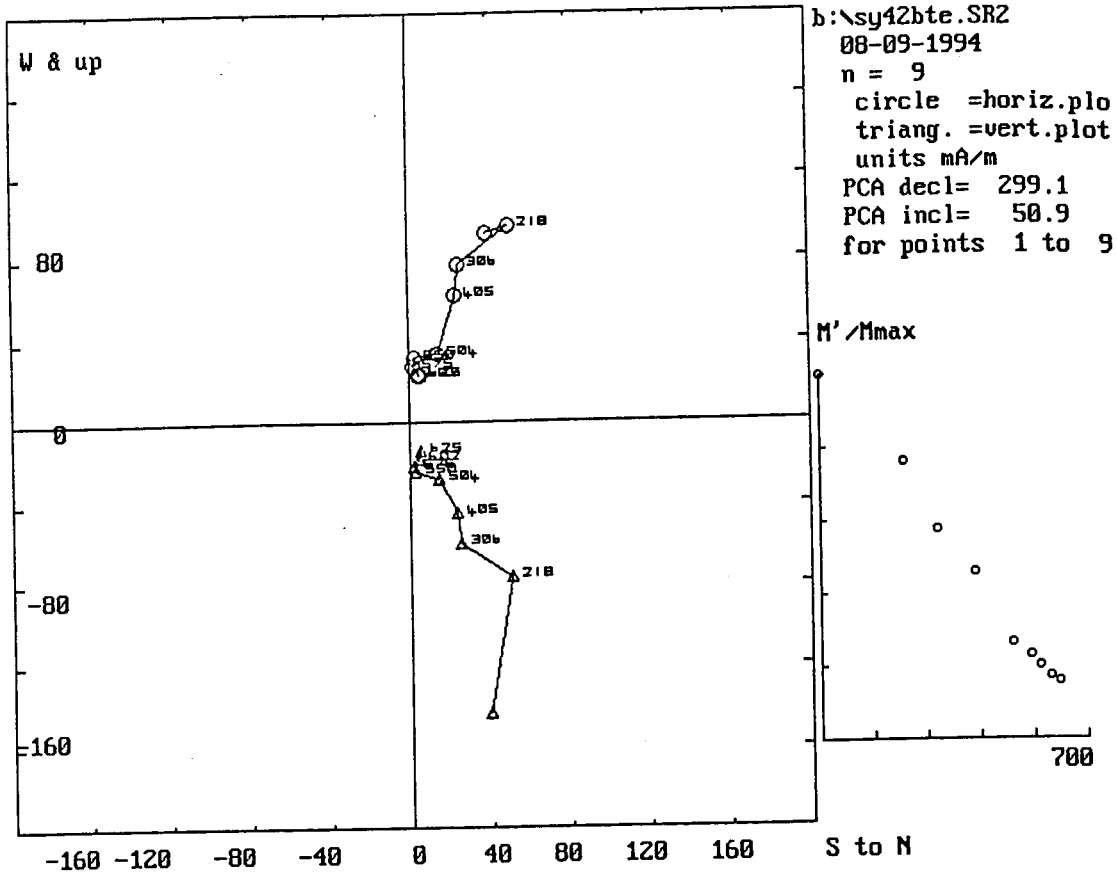
Lwr.Hem.Equal Area Net
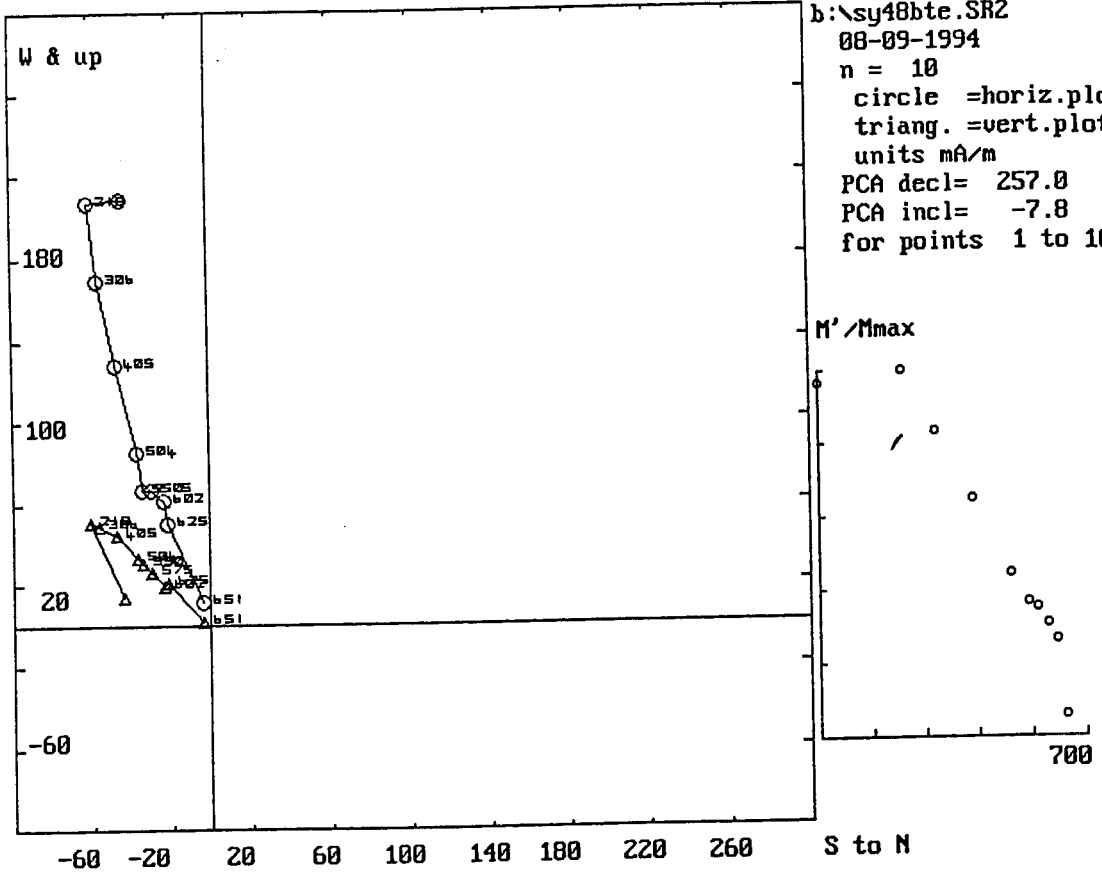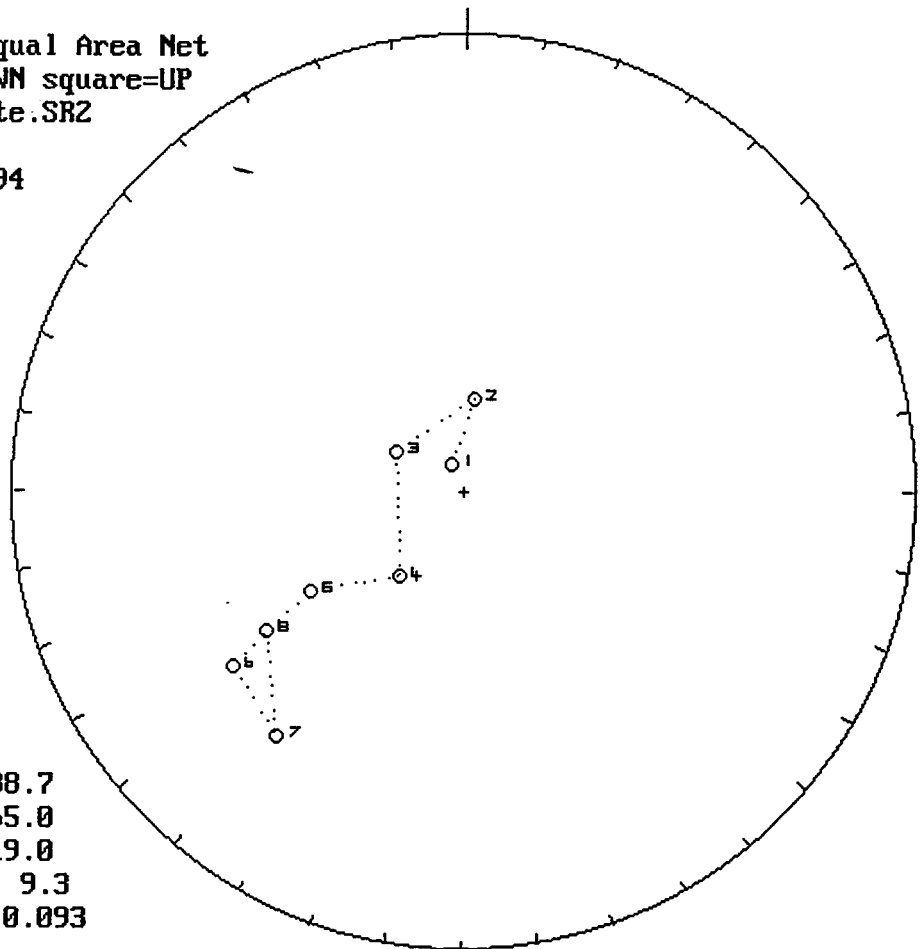circle=DOWN square=UP
 b:\sy43bte.SR2
 n = 9
 08-09-1994
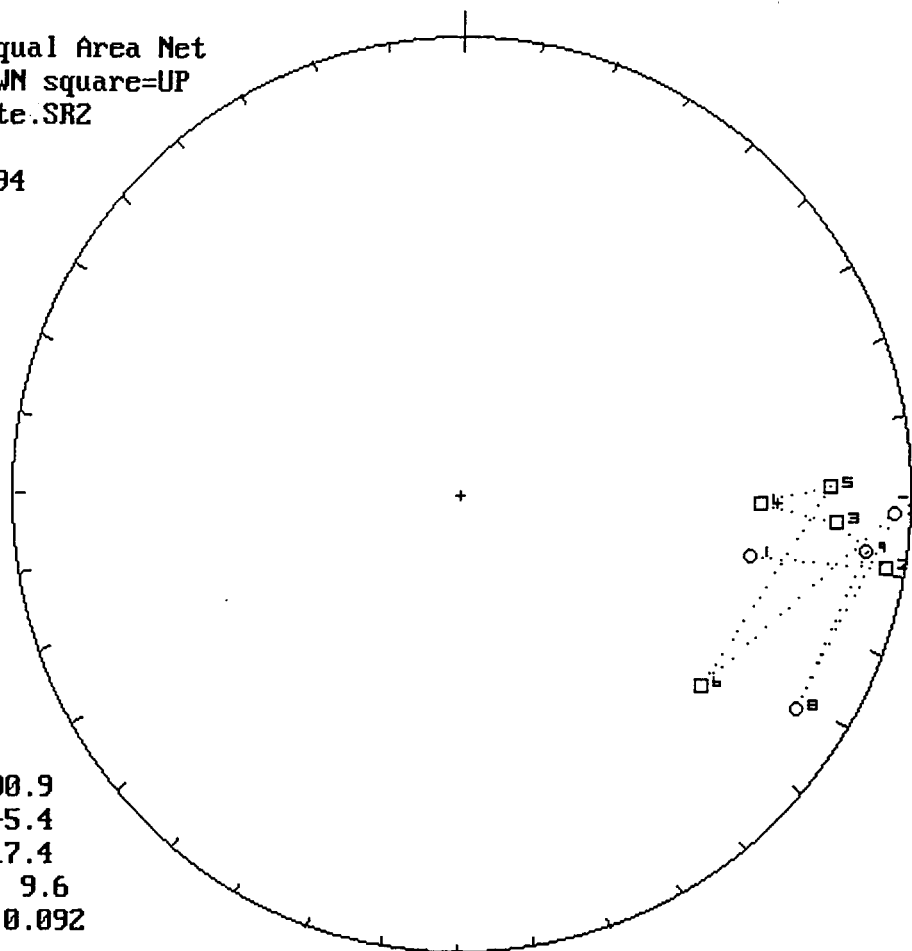
m.dec.= 100.9
m.inc.= -5.4
alpha95= 17.4
Fish. k=   9.6
sp.var.= 0.092

Lwr.Hem.Equal Area Net
circle=DOWN square=UP
 b:\sy43bte.SR2
 n = 8
 08-09-1994
Vector Diff
Plot: shows
vectors
added in
nature

W & up

b:\sy43bte.SR2
08-09-1994
n = 9
 circle =horiz.plo
 triang. =vert.plot
 units mA/m
PCA decl= 100.5
PCA incl=   27.5
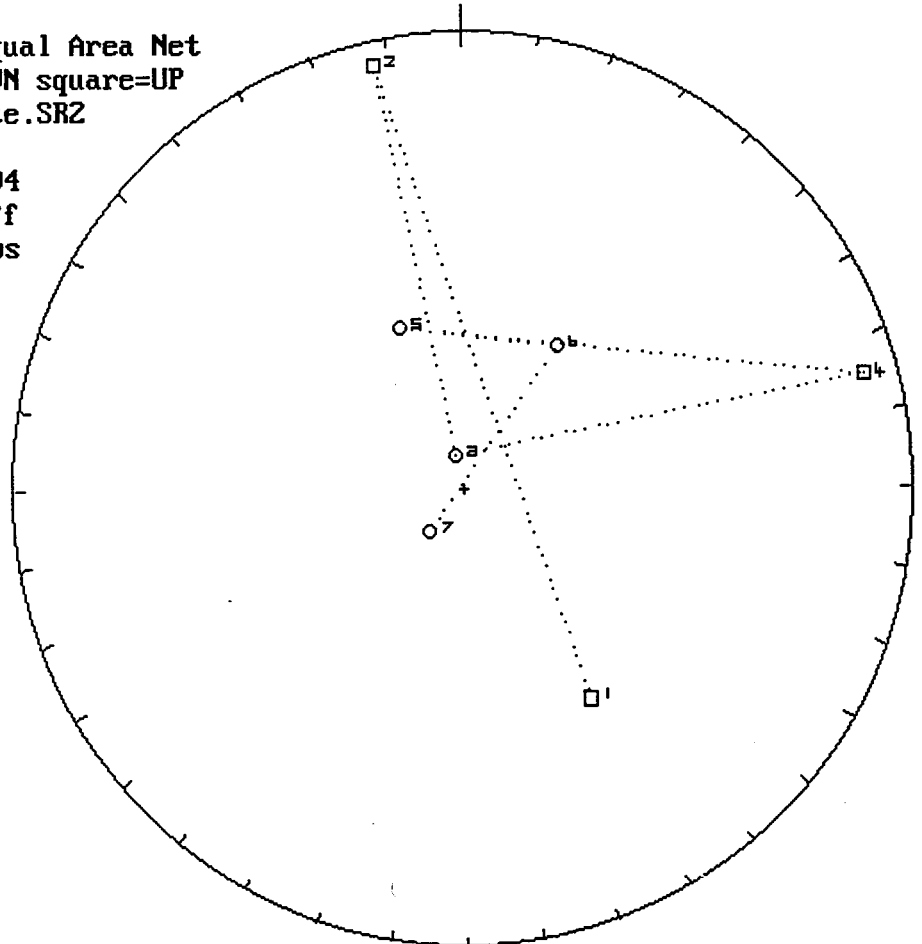for points 1 to 9

M'/Mmax

700

S to N

Lwr.Hem.Equal Area Net
circle=DOWN square=UP
 b:\sy47bte.SR2
 n = 7
 08-09-1994

m.dec.= 266.1
m.inc.= 57.3
alpha95= 10.9
Fish. k= 31.1
sp.var.= 0.027

Lwr.Hem.Equal Area Net
circle=DOWN square=UP
 b:\sy47bte.SR2
 n = 6
 08-09-1994
Vector Diff
Plot: shows
vectors
added in
nature

W & up

b:\sy47bte.SR2
08-09-1994
n = 7
 circle =horiz.plo
 triang. =vert.plot
 units mA/m
PCA decl= 290.1
PCA incl= 68.6
for points 1 to 7

M'/Mmax

50

-50

150

250

-250 -200 -150 -100 -50 0 50 100 150

S to N

600

Lwr.Hem.Equal Area Net
circle=DOWN square=UP
 b:\sy48bte.SR2
 n = 10
 08-09-1994

m.dec.= 249.7
m.inc.= -16.2
alpha95= 4.3
Fish. k= 125.9
sp.var.= 0.007

Lwr.Hem.Equal Area Net
circle=DOWN square=UP
 b:\sy48bte.SR2
 n = 9
 08-09-1994
Vector Diff
Plot: shows
vectors
added in
nature

b:\sy48bte.SR2
08-09-1994
n = 10
 circle =horiz.plo
 triang. =vert.plot
 units mA/m
PCA decl= 257.0
PCA incl= -7.8
for points 1 to 10

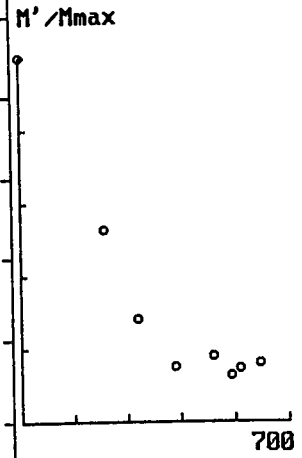Lwr.Hem.Equal Area Net
circle=DOWN square=UP
 b:\sy49bte.SR2
 n = 8
 08-09-1994

m.dec.= 238.7
m.inc.= 65.0
alpha95= 19.0
Fish. k=   9.3
sp.var.= 0.093

Lwr.Hem.Equal Area Net
circle=DOWN square=UP
 b:\sy49bte.SR2
 n = 7
 08-09-1994
Vector Diff
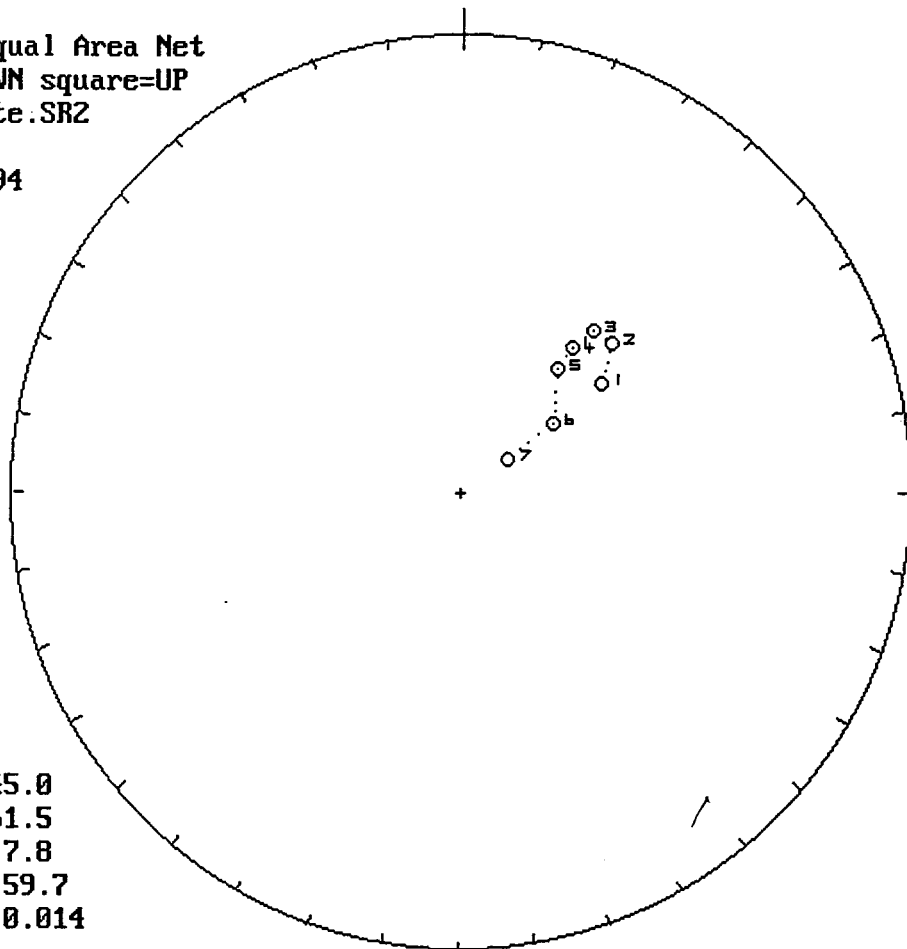Plot: shows
vectors
added in
nature

W & up

8

0

-8

-16

-16 -12 -8 -4 0 4 8 12 16 S to N
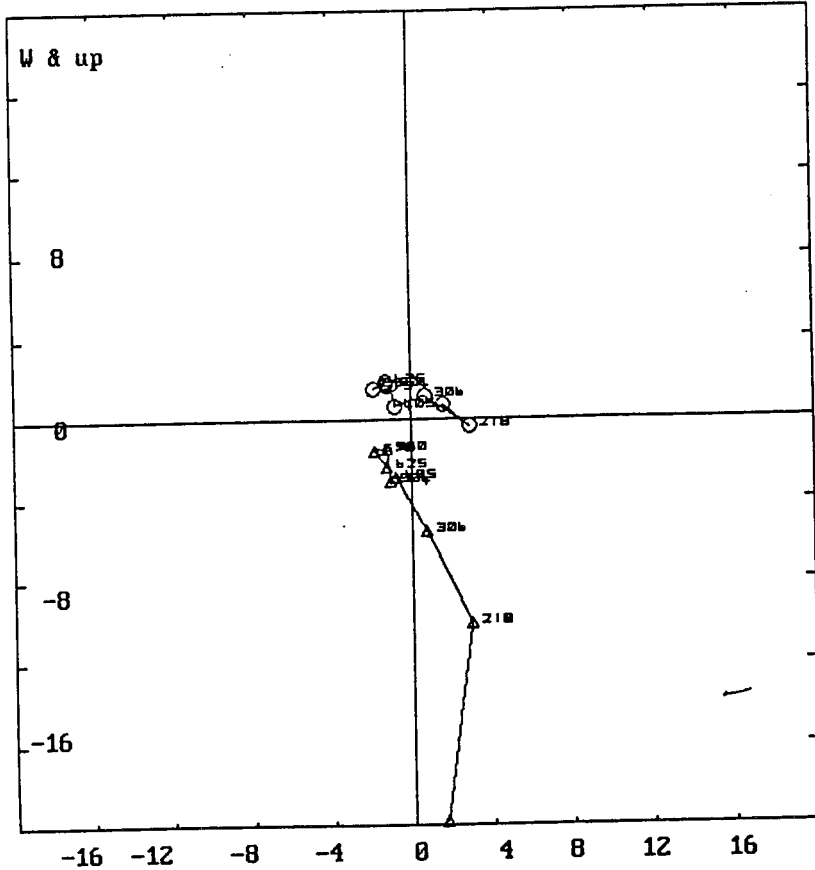
b:\sy49bte.SR2
08-09-1994
n = 8
 circle =horiz.plo
 triang. =vert.plot
 units mA/m
PCA decl= 197.5
PCA incl= -77.4
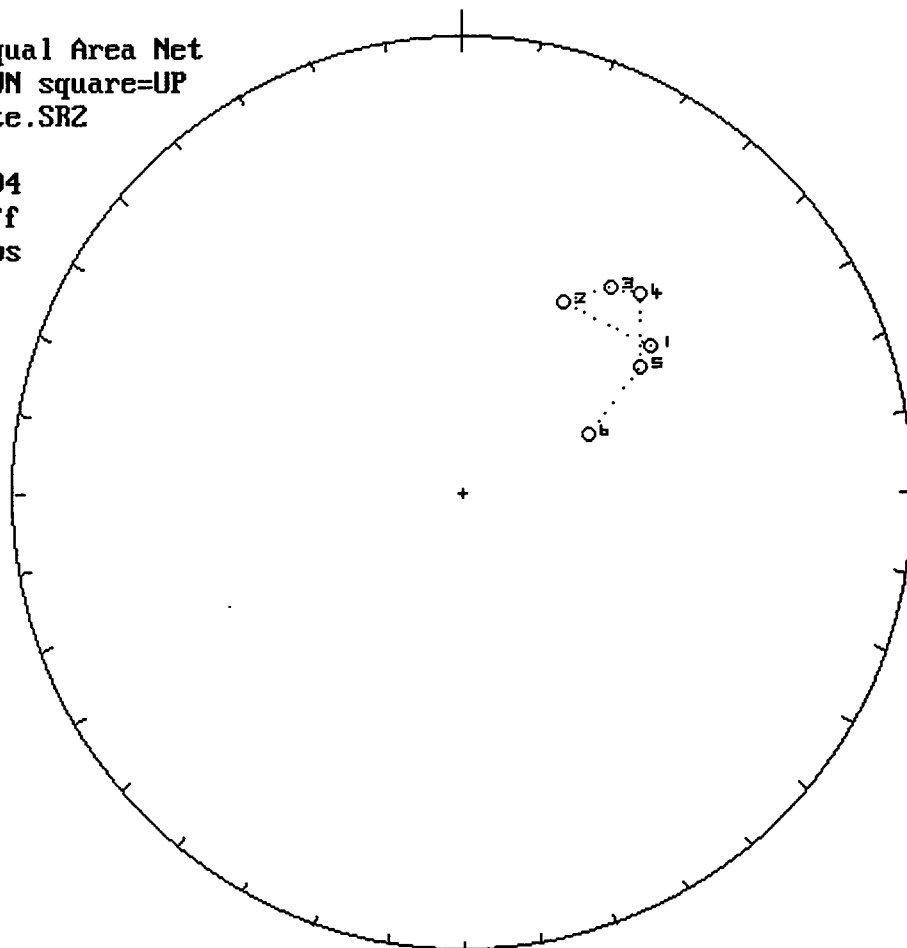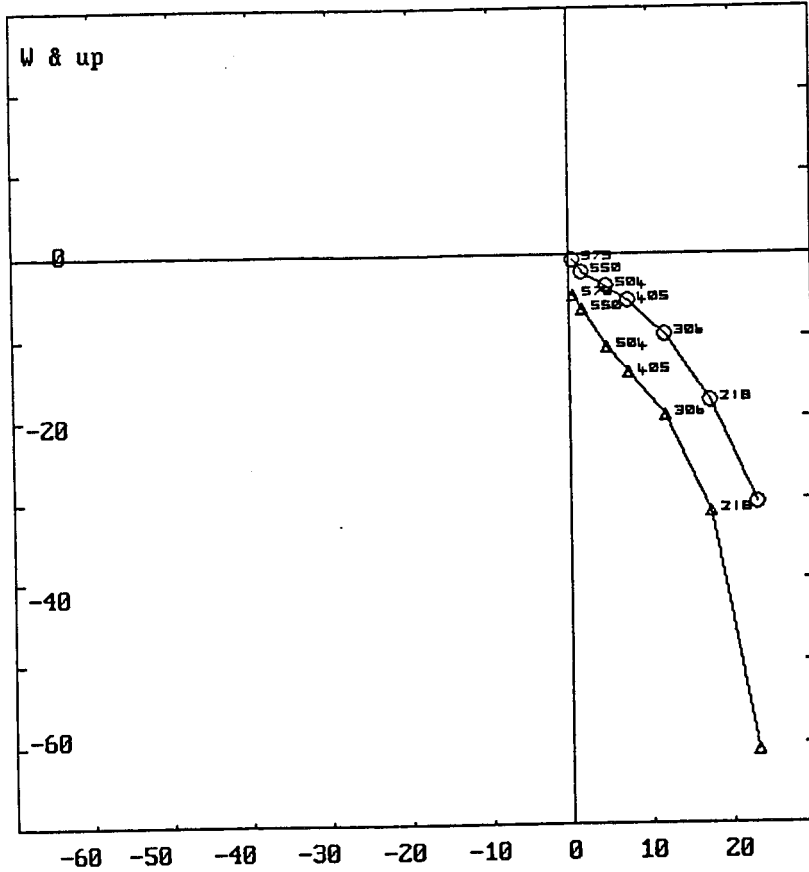for points 1 to 8

M'/Mmax

700

Lwr.Hem.Equal Area Net
circle=DOWN square=UP
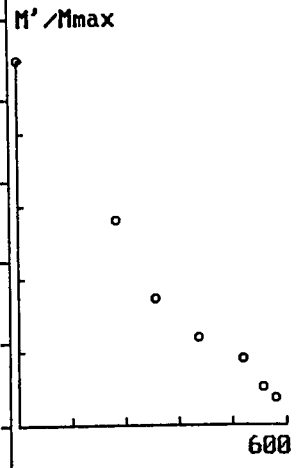 b:\sy52bte.SR2
 n = 7
 08-09-1994

m.dec.= 45.0
m.inc.= 61.5
alpha95= 7.8
Fish. k= 59.7
sp.var.= 0.014

Lwr.Hem.Equal Area Net
circle=DOWN square=UP
 b:\sy52bte.SR2
 n = 6
 08-09-1994
Vector Diff
Plot: shows
vectors
added in
nature

W & up

0

-20

-40

-60

-60 -50 -40 -30 -20 -10 0 10 20 S to N

b:\sy52bte.SR2
08-09-1994
n = 7
 circle =horiz.plo
 triang. =vert.plot
 units mA/m
PCA decl=   52.7
PCA incl=   55.6
for points 1 to 7

M'/Mmax

600

APPENDIX F

THERMAL DEMAGNETIZATION
"TRANSITIONAL SAMPLES"
(DATA, STEREOGRAPHIC PROJECTIONS, PCAs)

thermal demagnetization transitional samples

sample	date	time	declination	inclination	mA/m	cm3	temp.C	error %
sy7bt	04-08-199	11:54	176.71	74.1	4.46	11.15	0	1.4
sy7bt	04-08-199	11:54	150.2	47.27	1.509	11.15	100	6
sy7bt	04-08-199	15:43	201.5	27.27	1.061	11.15	500	1.4
sy7bt	04-11-199	09:05	137.26	-40.36	1.081	11.15	550	1.9
sy7bt	04-11-199	11:45	89.75	40.78	0.764	11.15	600	2.8
sy7bt	04-11-199	14:34	131.64	-27.68	0.689	11.15	650	2.6
sy7bt	04-11-199	17:26	31.32	-31.29	1.604	11.15	675	6.9
sy7bt	04-12-199	10:23	75.15	-7.07	0.983	11.15	700	2
sy30bt	06-10-199	11:49	40.38	57.14	199	11.15	0	0.8
sy30bt	06-14-199	10:01	32.8	31.4	74.9	11.15	218	1
sy30bt	06-14-199	14:04	29.11	26.77	40.5	11.15	306	0.9
sy30bt	06-14-199	19:27	23.8	19.76	19.4	11.15	405	0.9
sy30bt	06-14-199	23:45	8.89	-38.4	10.4	11.15	504	2.9
sy30bt	06-15-199	20:51	135.49	-69.87	3.88	11.15	550	1.6
sy30bt	06-16-199	00:39	63.11	41.53	3.23	11.15	575	2.3
sy30bt	06-16-199	19:21	246.12	-44.71	12.8	11.15	602	1.2
sy30bt	06-16-199	23:24	236.79	-3.9	9.05	11.15	625	1.6
sy30bt	06-19-199	19:56	268.92	-12.43	6.94	11.15	651	1
sy30bt	06-20-199	21:56	237.37	-7.76	4.29	11.15	680	1.1
sy30bt	06-21-199	01:39	228.55	3.94	9.14	11.15	690	0.9
sy36bt	06-10-199	11:59	245.83	78.85	70.9	11.15	0	0.4
sy36bt	06-14-199	10:05	184.3	57.37	23	11.15	218	1
sy36bt	06-14-199	14:09	185.6	33.99	12.85	11.15	306	0.5
sy36bt	06-14-199	19:32	122.04	46.69	4.85	11.15	405	1.9
sy36bt	06-14-199	23:52	152.33	-23.47	2.64	11.15	504	4.8
sy36bt	06-15-199	20:56	173.18	15.64	3.44	11.15	550	3.6
sy36bt	06-16-199	00:44	168.42	32.54	5.85	11.15	575	2.5
sy36bt	06-16-199	19:25	178.87	35.64	6.57	11.15	602	1.5
sy36bt	06-16-199	23:28	197.09	29.14	9.22	11.15	625	1.1
sy36bt	06-19-199	20:01	344.98	-41.15	5.48	11.15	651	1
sy36bt	06-20-199	22:00	225.73	-26.02	5.53	11.15	680	1.5
sy36bt	06-21-199	01:44	258.39	8.69	4.06	11.15	690	1.7
sy41bt	06-10-199	12:04	353.64	74.65	34.3	11.15	0	0.7
sy41bt	06-14-199	10:11	188.32	82.67	11.2	11.15	218	0.9

thermal demagnetization transitional samples

sample	date	time	declination	inclination	mA/m	cm3	temp.C	error %
sy41bt	06-14-199	14:14	297.82	52.73	4.7	11.15	306	1.2
sy41bt	06-14-199	19:37	300.68	-8.9	2.68	11.15	405	1.3
sy41bt	06-14-199	23:57	43.91	64.9	2.42	11.15	504	2.9
sy41bt	06-15-199	21:01	91.77	33.51	2.61	11.15	550	1.5
sy41bt	06-16-199	00:48	86.24	14.35	4.22	11.15	575	2.5
sy41bt	06-16-199	19:29	103.8	-9.6	3.92	11.15	602	2.1
sy41bt	06-16-199	23:32	119.69	13.52	2.21	11.15	625	3.2
sy41bt	06-19-199	20:06	238.64	38.23	3.85	11.15	651	1.1
sy41bt	06-20-199	22:05	239.01	26.8	1.512	11.15	680	2.3
sy41bt	06-21-199	01:49	245.85	4.79	2.3	11.15	690	1.4
sy44bt	06-10-199	12:18	271.55	78.12	205	11.15	0	0.3
sy44bt	06-14-199	10:16	335.55	61.13	90	11.15	218	0.2
sy44bt	06-14-199	14:18	283.63	54.84	48.6	11.15	306	0.4
sy44bt	06-14-199	19:41	299.11	56.68	31	11.15	405	0.6
sy44bt	06-15-199	00:01	283.7	33.39	21	11.15	504	1.4
sy44bt	06-15-199	21:05	252.52	27.88	20.7	11.15	550	1.7
sy44bt	06-16-199	00:52	232.79	29.26	18.6	11.15	575	3.2
sy44bt	06-16-199	19:33	229.37	33.32	15.88	11.15	602	2.9
sy44bt	06-16-199	23:36	264.47	4.88	15.3	11.15	625	2.2
sy44bt	06-19-199	20:11	238.2	-6.39	8.54	11.15	651	2.8
sy44bt	06-20-199	22:10	228.59	-31.39	6.48	11.15	680	4.6
sy46bt	06-10-199	12:08	45.39	82.47	70.9	11.15	0	0.5
sy46bt	06-14-199	10:17	58.42	77.01	37	11.15	218	0.4
sy46bt	06-14-199	14:20	60.02	81.81	24.8	11.15	306	0.7
sy46bt	06-14-199	19:42	186.6	71.53	7.54	11.15	405	0.6
sy46bt	06-15-199	00:02	194.2	39.96	8.64	11.15	504	1
sy46bt	06-15-199	21:06	204.3	33.34	7.06	11.15	550	1
sy46bt	06-16-199	00:54	186.59	15.9	6.11	11.15	575	2.2
sy46bt	06-16-199	19:35	325.83	-72.71	5.39	11.15	602	2.8
sy46bt	06-16-199	23:38	161.98	10.22	1.86	11.15	625	3
sy46bt	06-19-199	20:12	249.12	-8.09	4.62	11.15	651	1.2
sy46bt	06-20-199	22:13	216.57	-37	5.4	11.15	680	1.5
sy46bt	06-21-199	01:56	258.51	15.29	5.36	11.15	690	1.4

transitional thermal orientations

sample			declination	inclination
sy7bt			206.1	82.7
sy7bt			7.9	-35.4
sy30bt			43.5	60.6
sy30bt			244.5	-26.6
sy36bt			259.6	78.7
sy36bt			185.8	34.3
sy44bt			81.8	-82.5
sy44bt			246.1	51
sy46bt			31.1	83.7
sy46bt			170.4	63.7

Lwr.Hem.Equal Area Net
circle=DOWN square=UP
 hermal\sy7bte.SR2
 n = 8
 06-07-1994
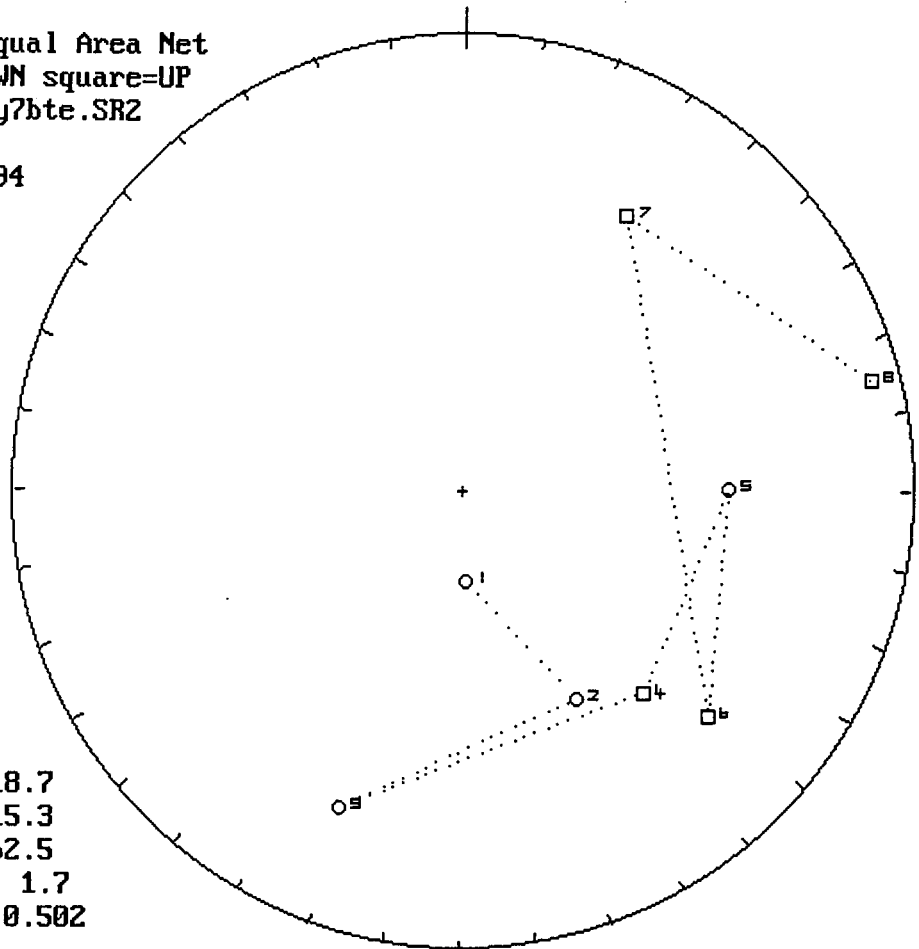
m.dec.= 118.7
m.inc.= 15.3
alpha95= 62.5
Fish. k= 1.7
sp.var.= 0.502

Lwr.Hem.Equal Area Net
circle=DOWN square=UP
 hermal\sy7bte.SR2
 n = 7
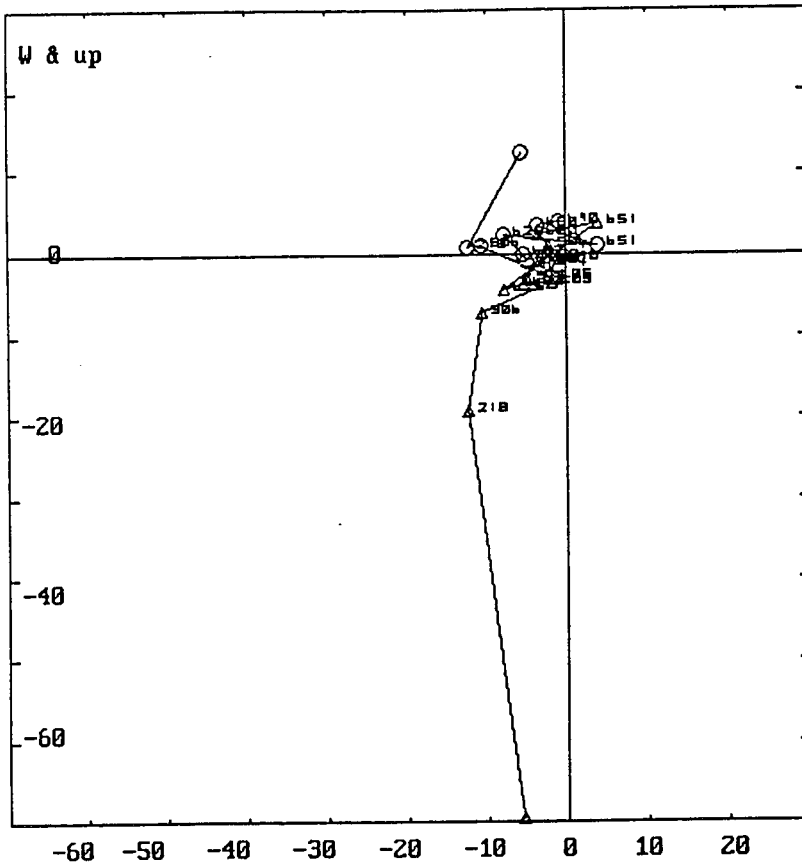 06-07-1994
Vector Diff
Plot: shows
vectors
added in
nature

W & up

:\thermal\sy7bte.SR2
06-07-1994
n = 8
 circle =horiz.plo
 triang. =vert.plot
 units mA/m
PCA decl= 200.5
PCA incl= 40.2
for points 2 to 8

M'/Mmax

700

=0.1

=1.5

=2.9

=4.3

-4.3 -3.6 -2.9 -2.2 -1.5 -0.8 -0.1 0.6 1.3 S to N
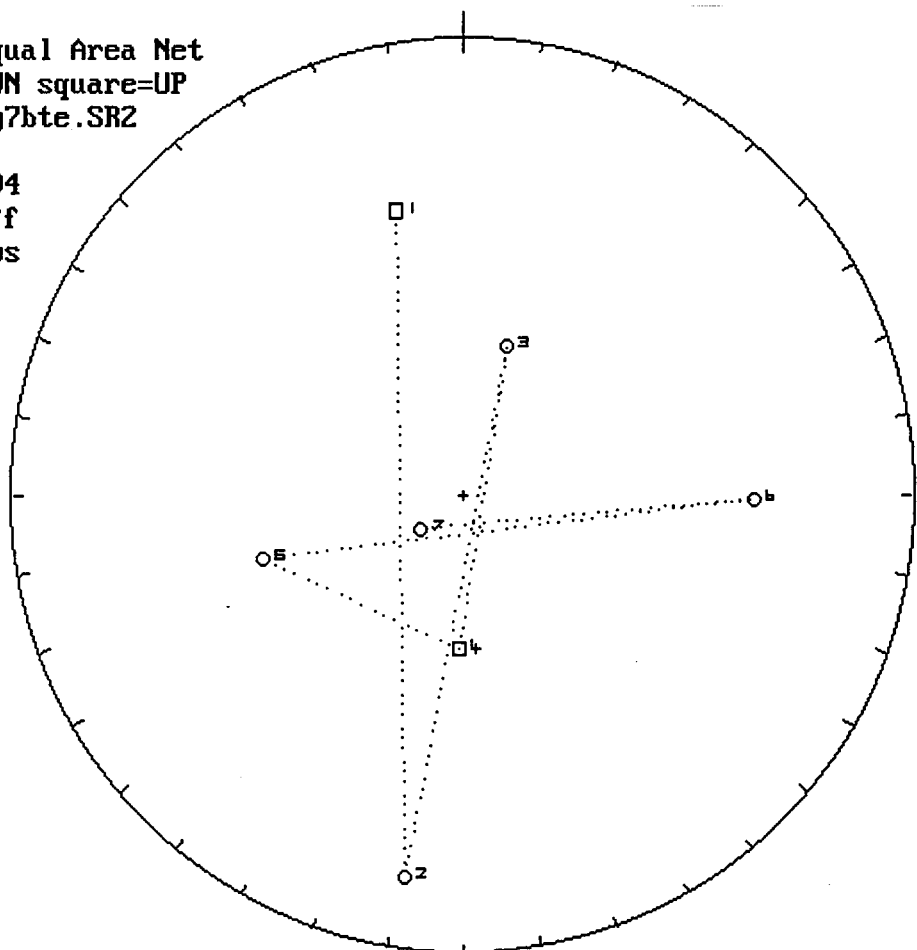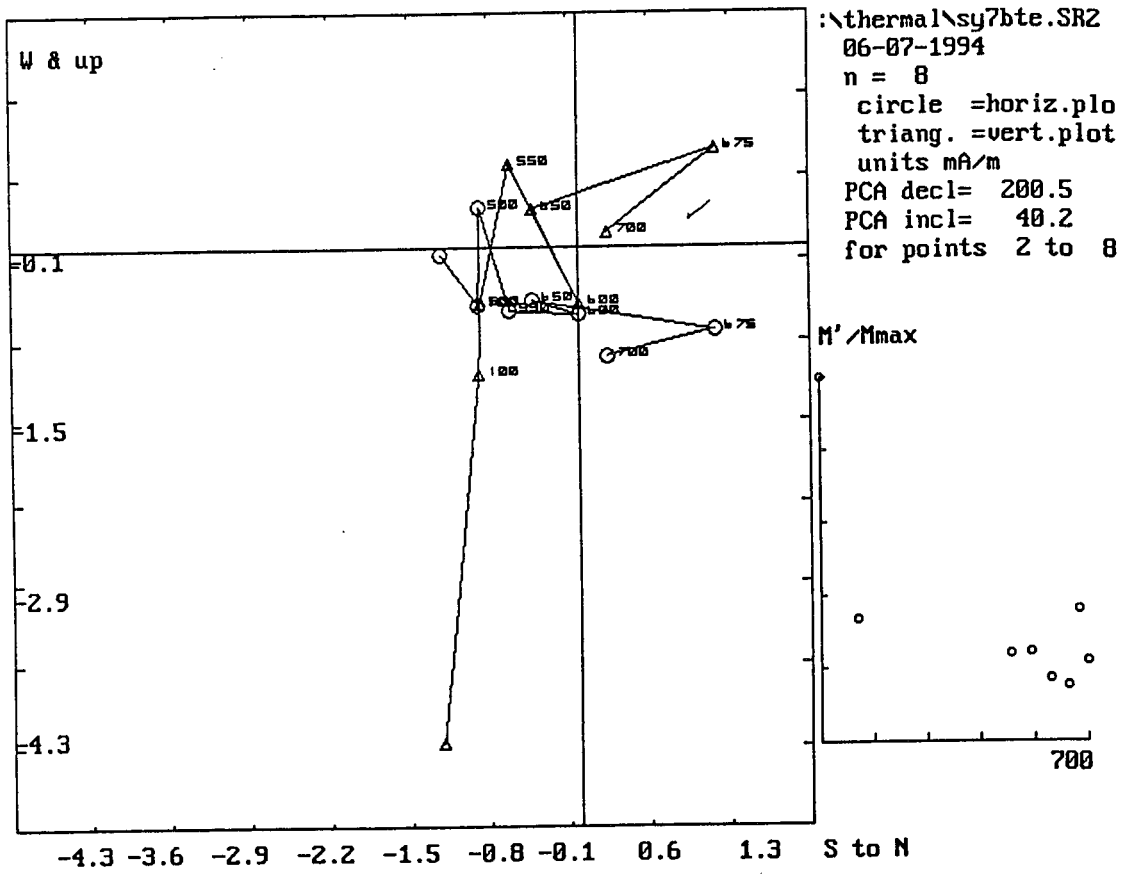
Lwr.Hem.Equal Area Net
circle=DOWN square=UP
 b:\sy30bte.SR2
 n = 12
 08-09-1994
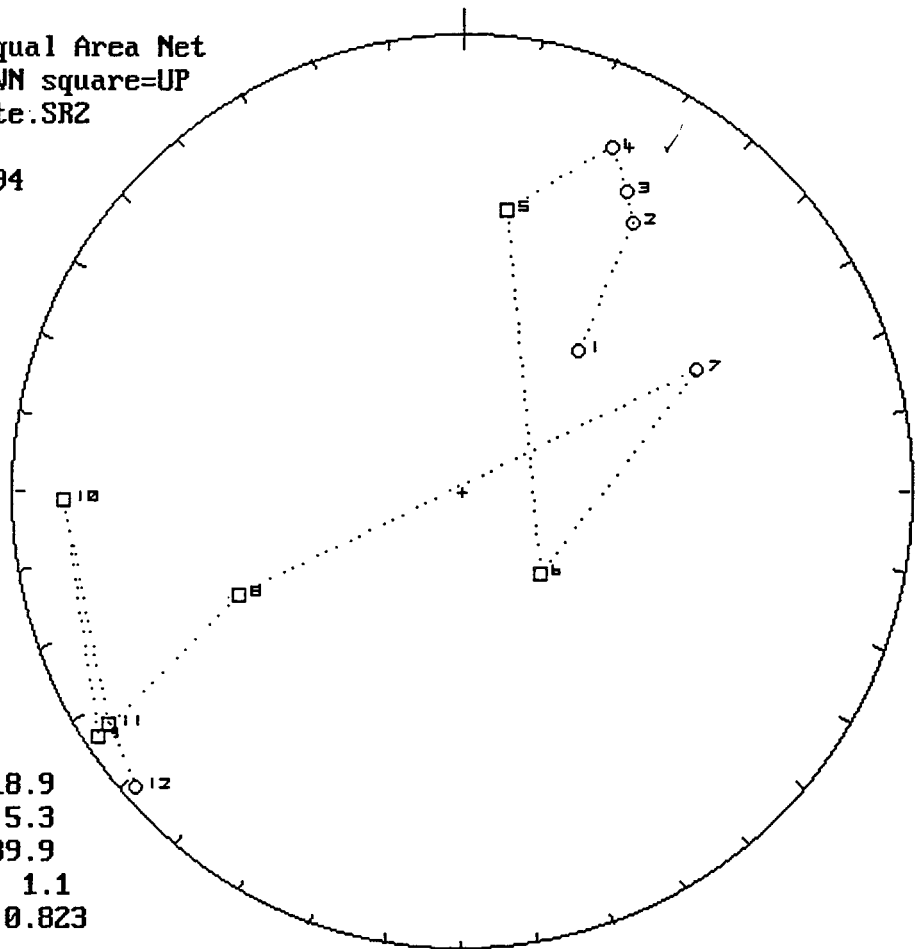
m.dec.= 318.9
m.inc.=   5.3
alpha95= 89.9
Fish. k=   1.1
sp.var.= 0.823

Lwr.Hem.Equal Area Net
circle=DOWN square=UP
 b:\sy30bte.SR2
 n = 11
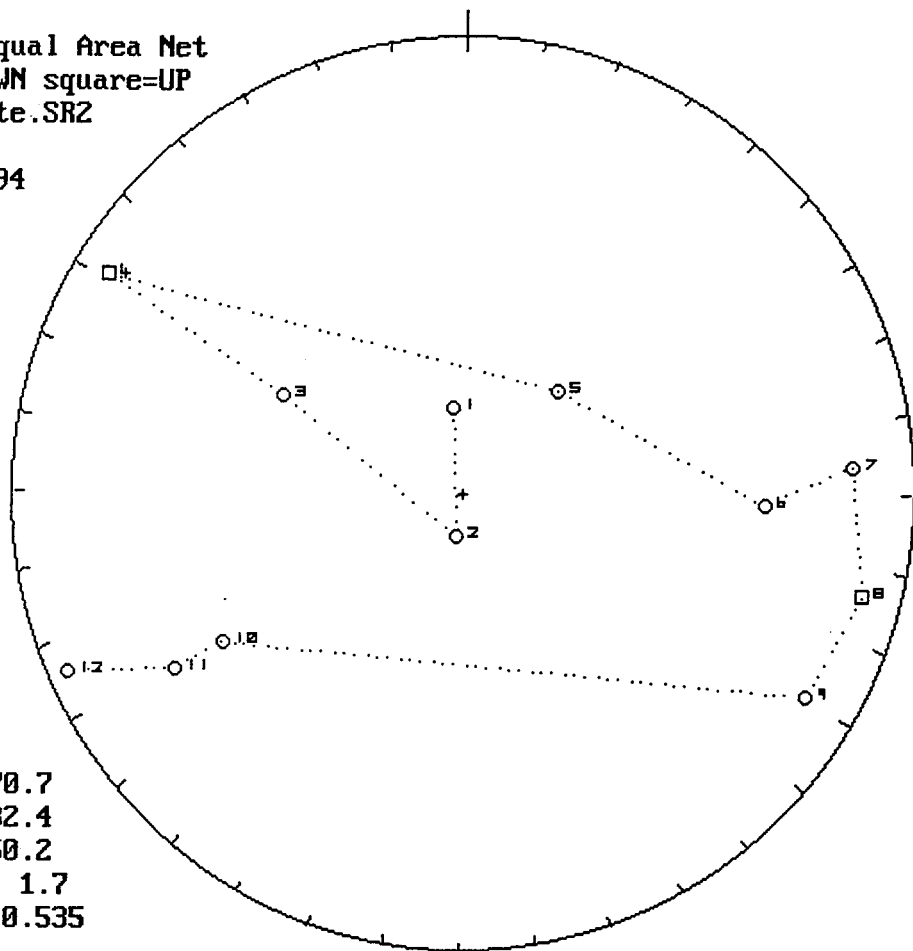 08-09-1994
Vector Diff
Plot: shows
vectors
added in
nature

W & up

b:\sy30bte.SR2
08-09-1994
n = 12
circle =horiz.plo
triang. =vert.plot
units mA/m
PCA decl= 40.6
PCA incl= 54.3
for points 1 to 12

M'/Mmax

S to N

700

80

0

-80

-160

-160 -120 -80 -40 0 40 80 120 160
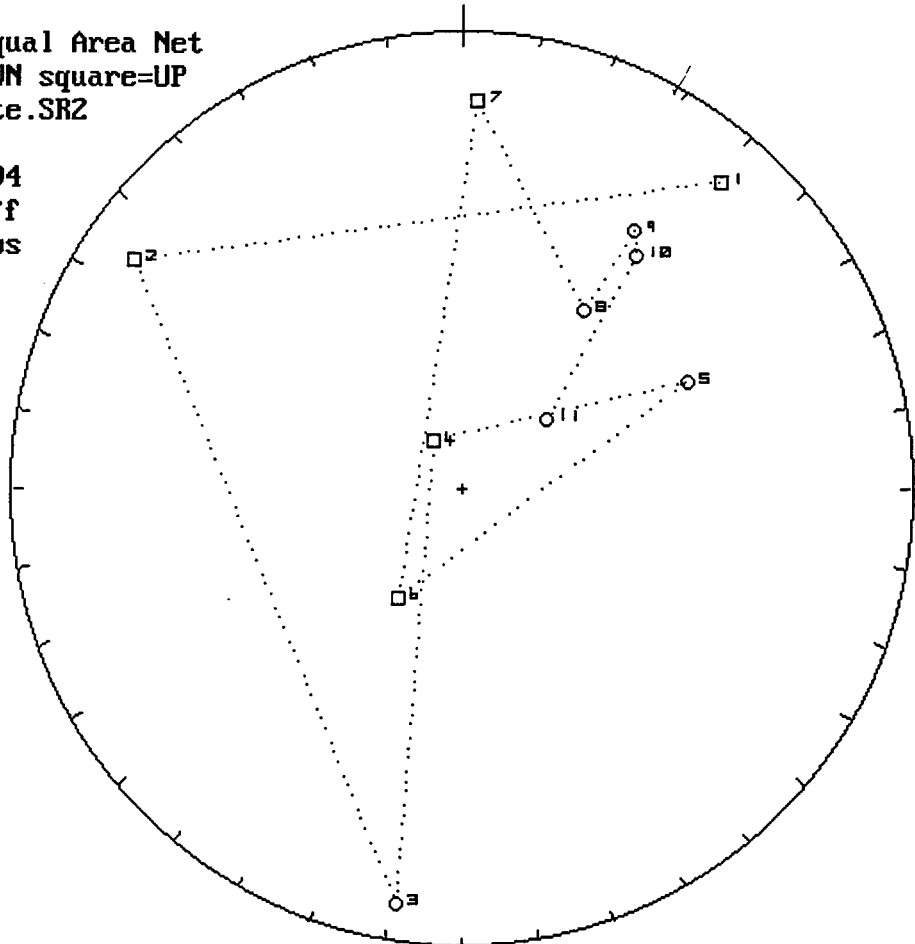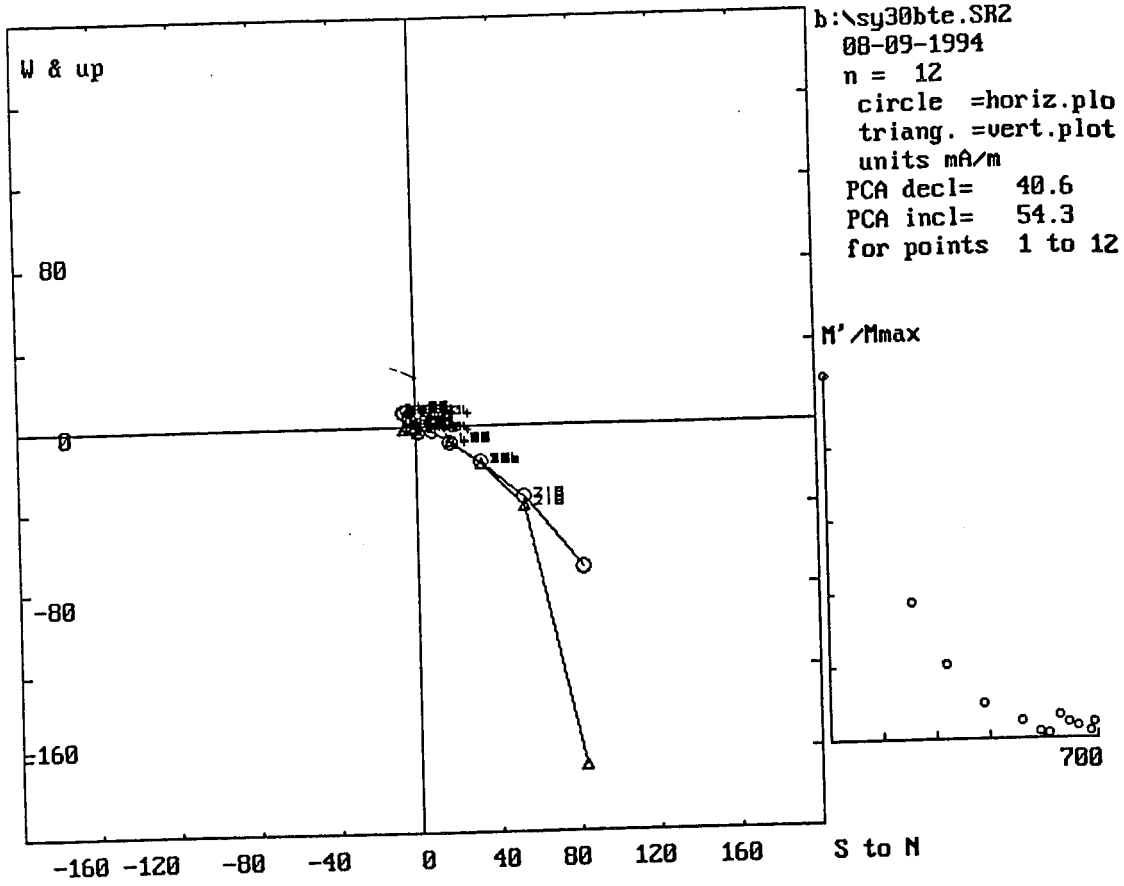
Lwr.Hem.Equal Area Net
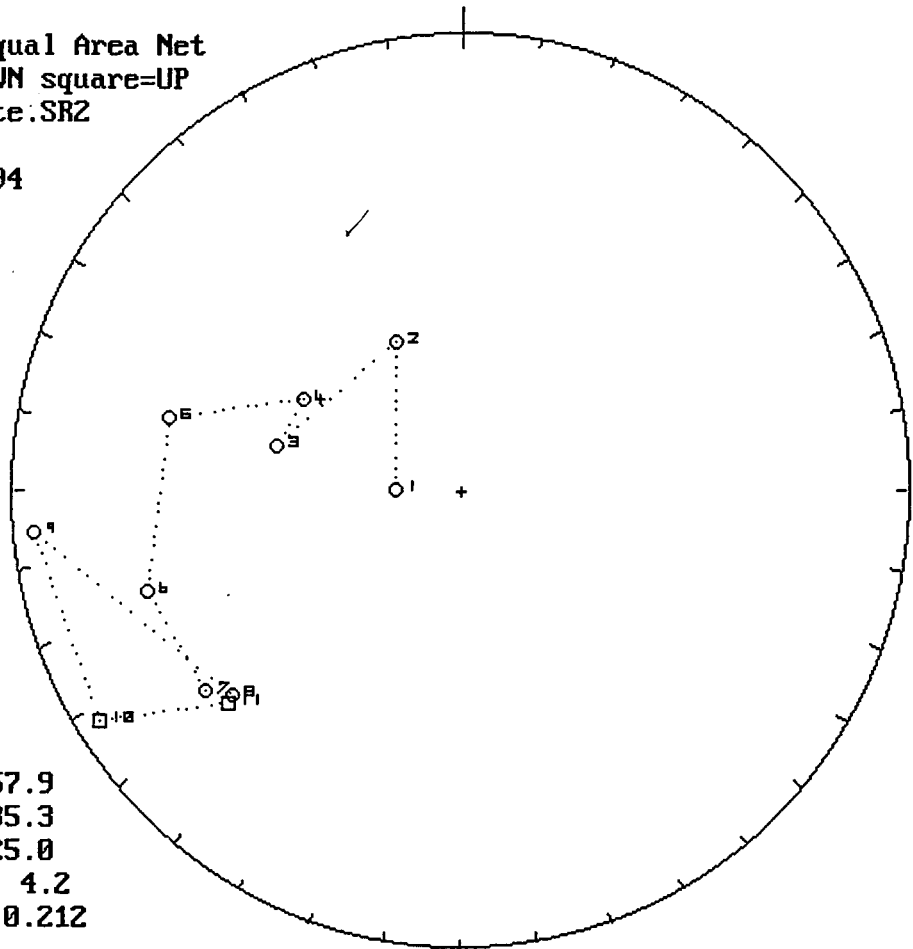circle=DOWN square=UP
 b:\sy36bte.SR2
 n = 12
 08-09-1994
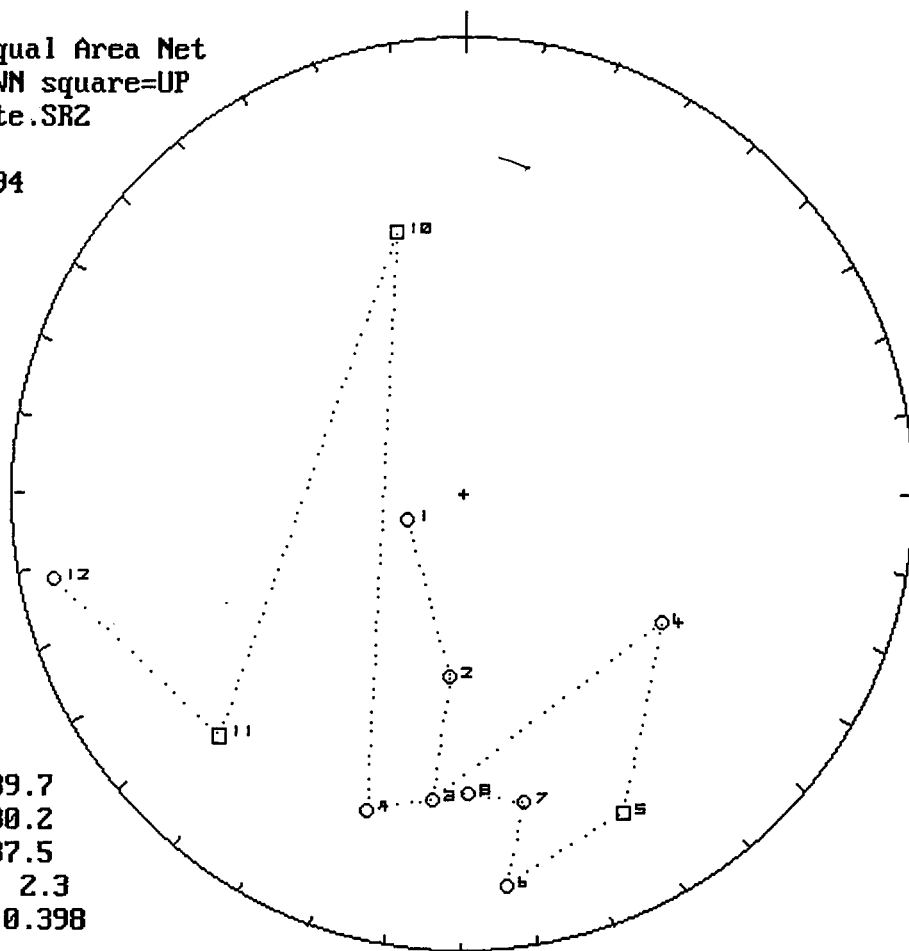
m.dec.= 189.7
m.inc.= 30.2
alpha95= 37.5
Fish. k=   2.3
sp.var.= 0.398

Lwr.Hem.Equal Area Net
circle=DOWN square=UP
 b:\sy36bte.SR2
 n = 11
 08-09-1994
Vector Diff
Plot: shows
vectors
added in
nature

W & up
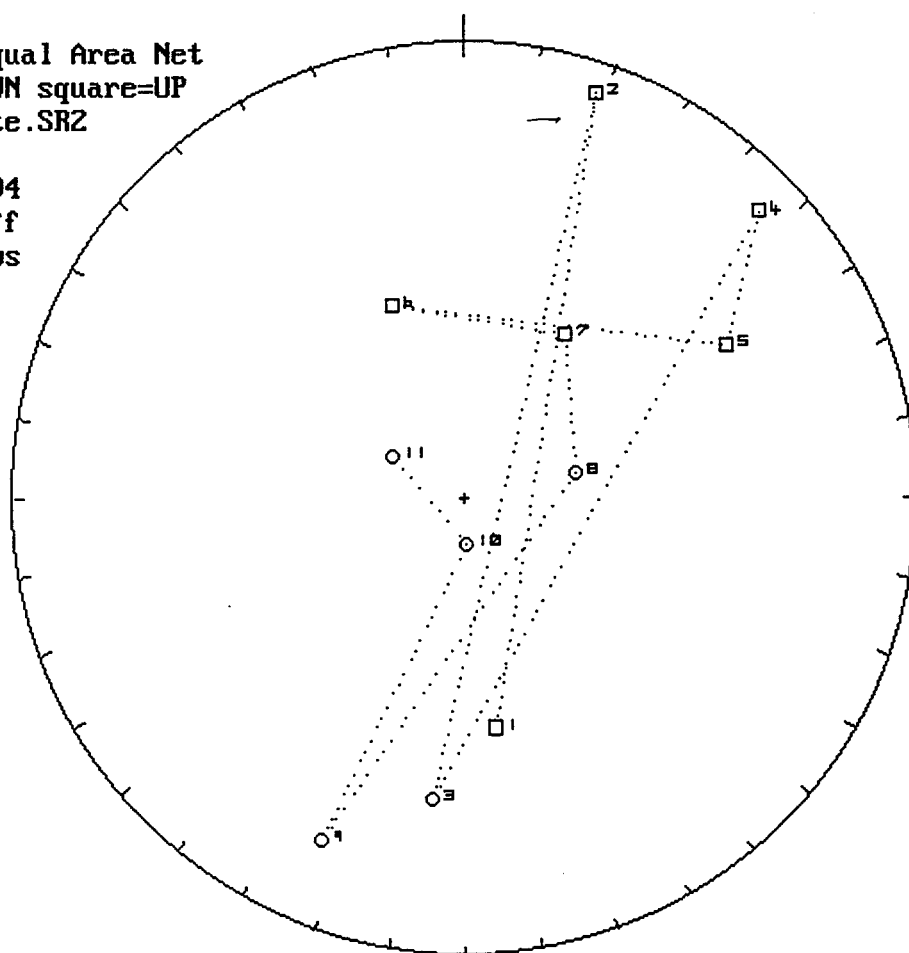
b:\sy36bte.SR2
08-09-1994
n = 12
 circle =horiz.plo
 triang. =vert.plot
 units mA/m
PCA decl= 245.6
PCA incl= 79.9
for points 1 to 12

M'/Mmax

700

S to N
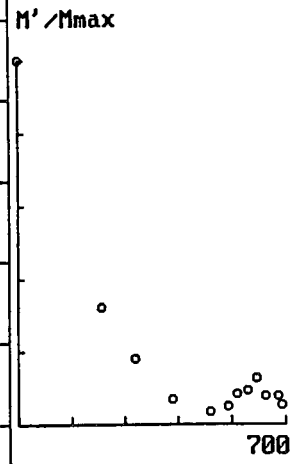
Lwr.Hem.Equal Area Net
circle=DOWN square=UP
 b:\sy41bte.SR2
 n = 12
 08-09-1994

m.dec.= 170.7
m.inc.= 82.4
alpha95= 50.2
Fish. k=   1.7
sp.var.= 0.535

Lwr.Hem.Equal Area Net
circle=DOWN square=UP
 b:\sy41bte.SR2
 n = 11
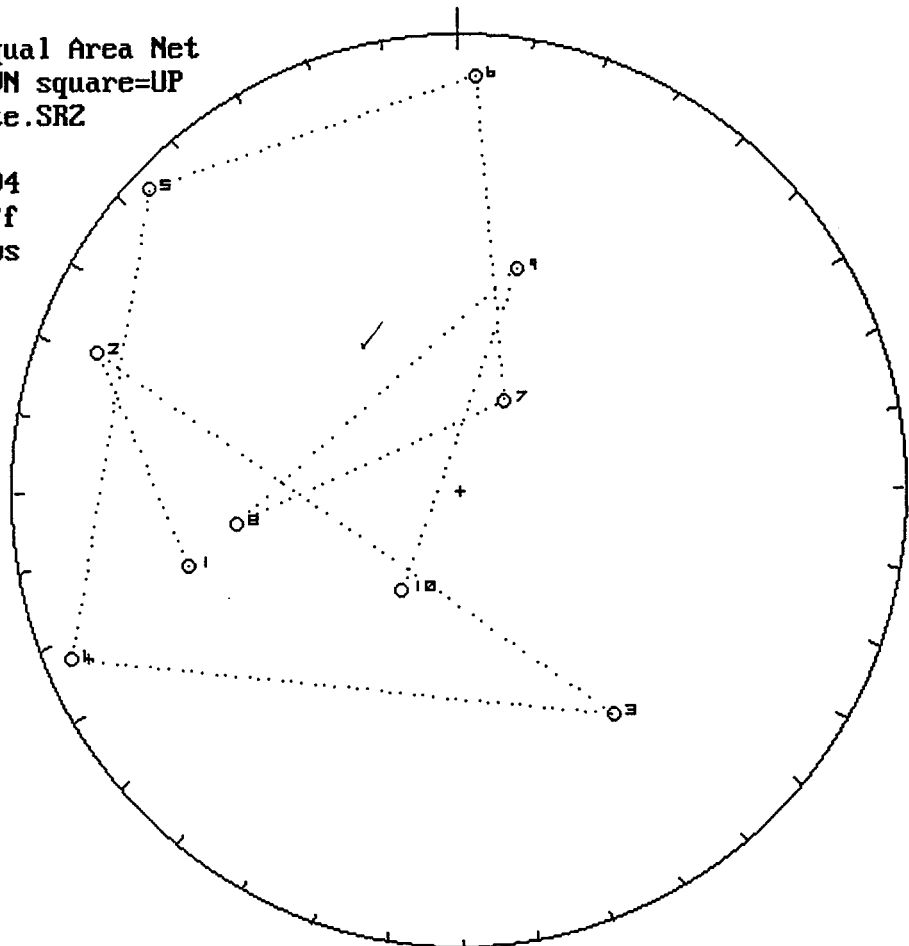 08-09-1994
Vector Diff
Plot: shows
vectors
added in
nature

b:\sy41bte.SR2
08-09-1994
n = 12
 circle =horiz.plo
 triang. =vert.plot
 units mA/m
PCA decl= 349.1
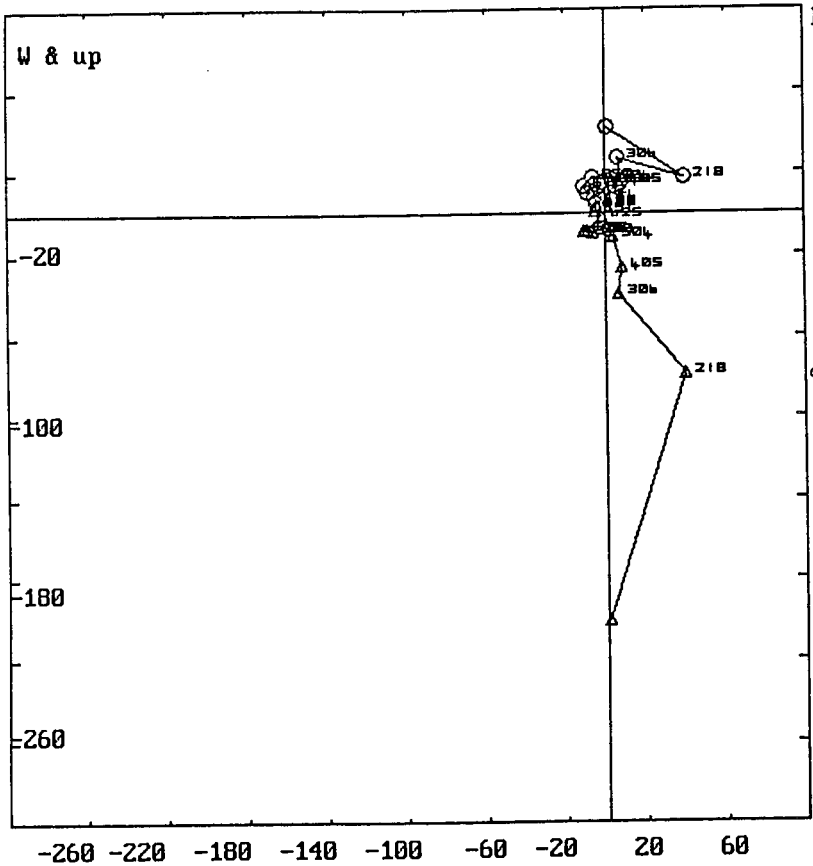PCA incl= 74.9
for points 1 to 12
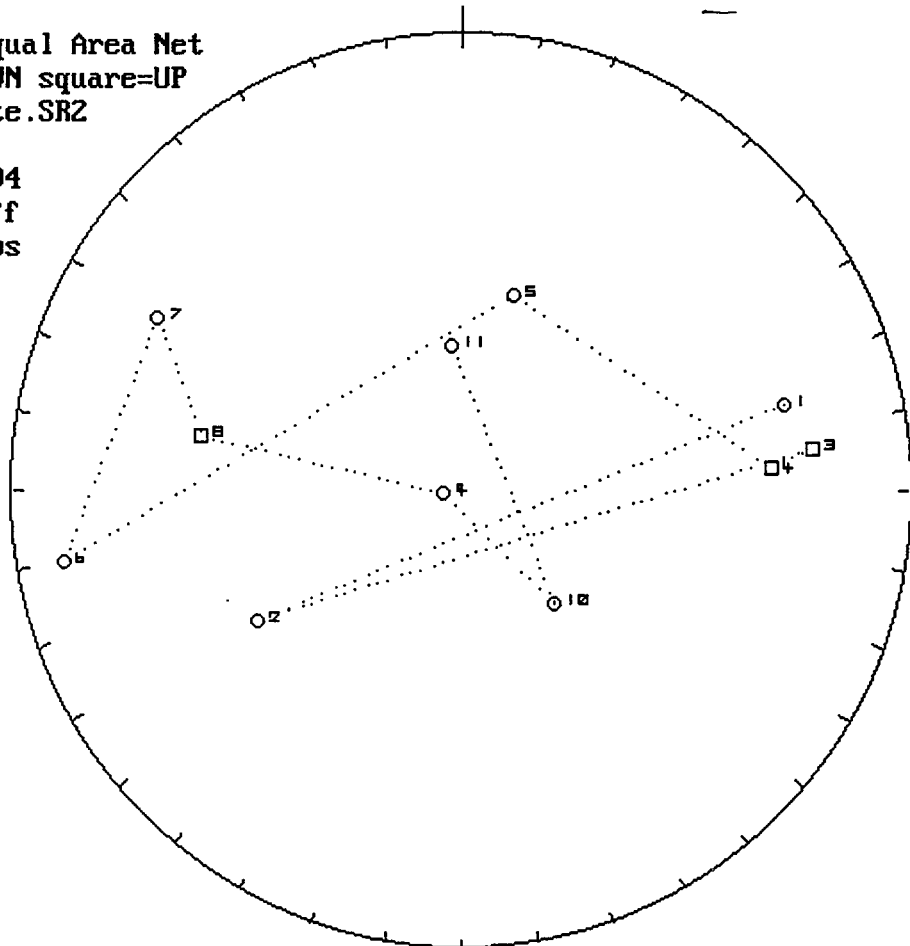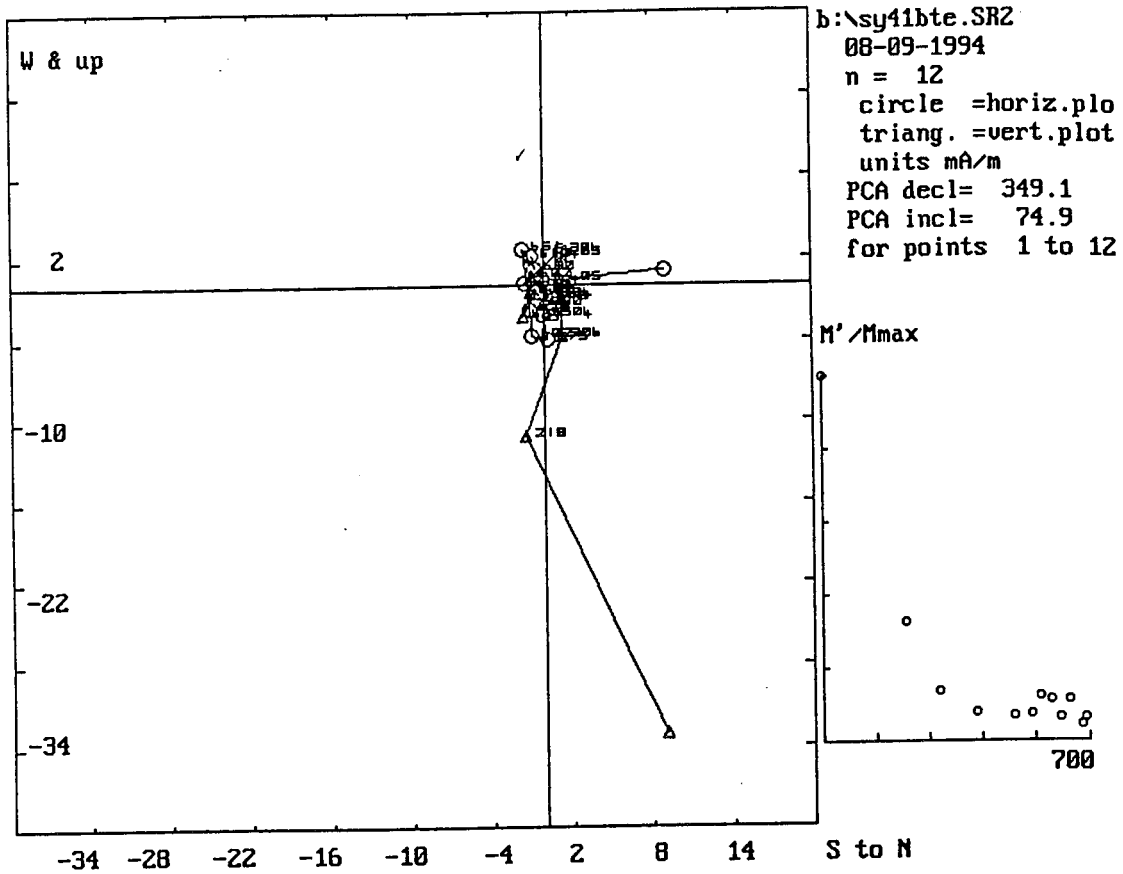
Lwr.Hem.Equal Area Net
circle=DOWN square=UP
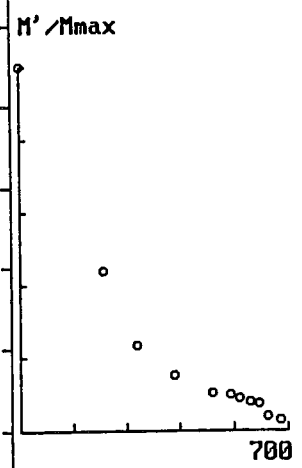 b:\sy44bte.SR2
 n = 11
 08-10-1994

m.dec.= 257.9
m.inc.= 35.3
alpha95= 25.0
Fish. k=   4.2
sp.var.= 0.212

Lwr.Hem.Equal Area Net
circle=DOWN square=UP
 b:\sy44bte.SR2
 n = 10
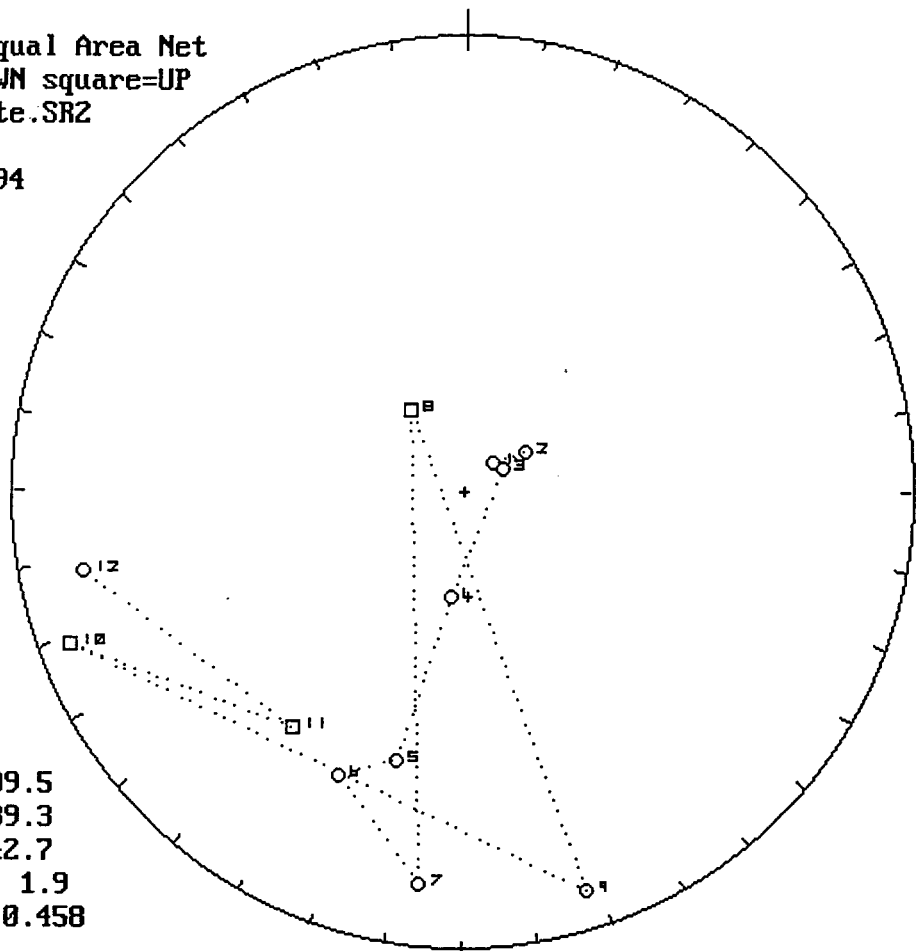 08-10-1994
Vector Diff
Plot: shows
vectors
added in
nature

W & up

-20

-100

-180

-260

-260 -220 -180 -140 -100 -60 -20   20   60   S to N

b:\sy44bte.SR2
08-10-1994
n = 11
circle = horiz.plo
triang. = vert.plot
units mA/m
PCA decl= 297.6
PCA incl= 80.2
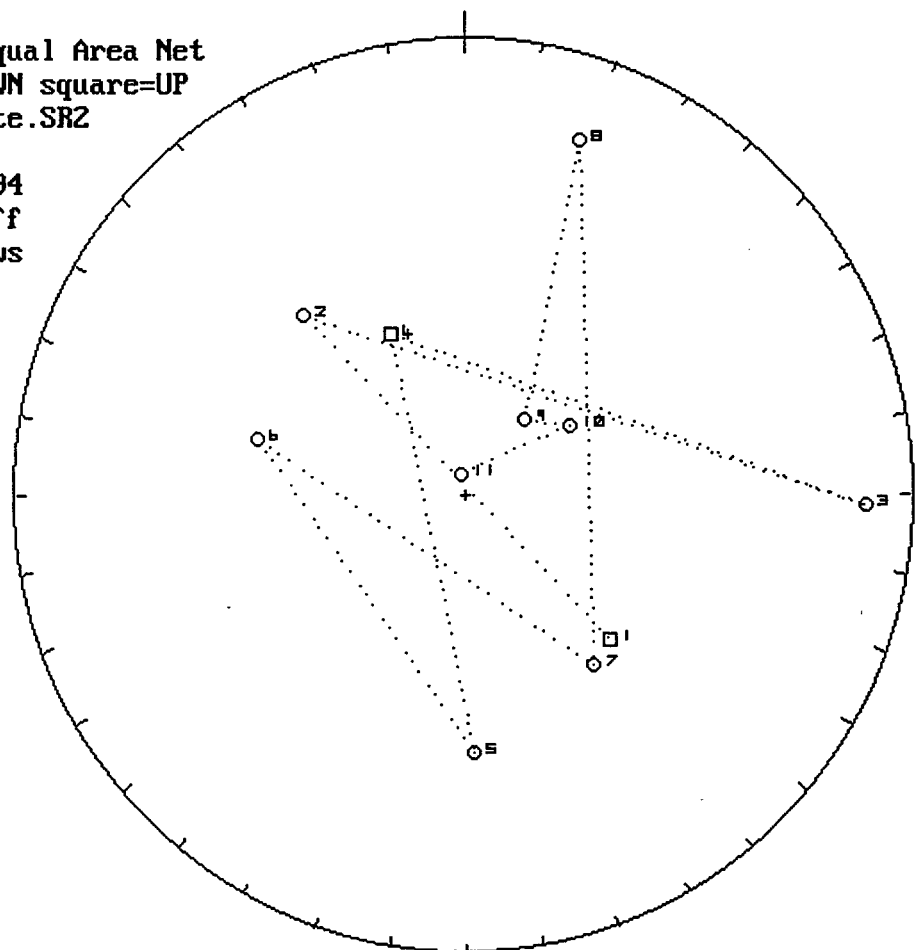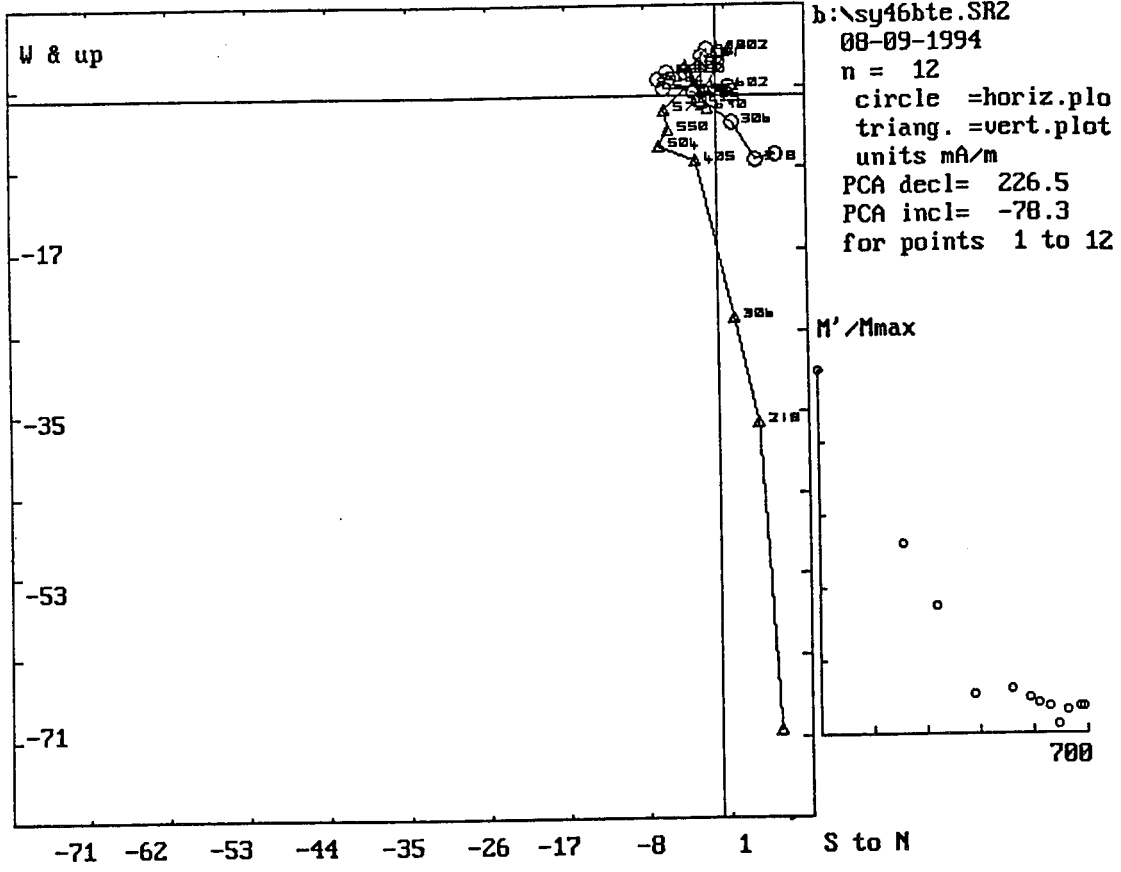for points 1 to 11

M'/Mmax

700

Lwr.Hem.Equal Area Net
circle=DOWN square=UP
 b:\sy46bte.SR2
 n = 12
 08-09-1994

m.dec.= 209.5
m.inc.= 39.3
alpha95= 42.7
Fish. k=   1.9
sp.var.= 0.458

Lwr.Hem.Equal Area Net
circle=DOWN square=UP
 b:\sy46bte.SR2
 n = 11
 08-09-1994
Vector Diff
Plot: shows
vectors
added in
nature

W & up

b:\sy46bte.SR2
08-09-1994
n = 12
circle =horiz.plo
triang. =vert.plot
units mA/m
PCA decl= 226.5
PCA incl= -78.3
for points 1 to 12

-17

-35

-53

-71

M'/Mmax

700

-71 -62 -53 -44 -35 -26 -17 -8 1 S to N

APPENDIX G

COMBINED A.F. DEMAGNETIZATION AND THERMAL DEMAGNETIZATION
(DATA, STEREOGRAPHIC PROJECTIONS, PCAs)

Alternating field demagnetization followed by thermal demagnetization

| sample	date	time	declination	inclination	mA/m	cm3	temp. C	error %
sy1bnt	05-25-199	12:14	18.89	-2.49	1.372	11.15	555	0.9
sy1bnt	05-26-199	09:40	2.12	-24.08	2.15	11.15	585	12.9
sy1bnt	05-30-199	10:23	6.59	-30.04	1.95	11.15	617	9.5
sy1bnt	05-30-199	13:49	342.35	-29.59	1.612	11.15	645	6.6
sy1bnt	05-31-199	09:51	1.11	-8.25	1.65	11.15	675	7.3
sy1bnt	05-31-199	13:54	258.17	-81.75	0.611	11.15	700	6
sy2bnt	05-25-199	12:16	187.81	-23.96	3.9	11.15	555	2.9
sy2bnt	05-26-199	09:42	211.5	-64.61	6.53	11.15	585	1.2
sy2bnt	05-30-199	10:25	229.04	-56.71	6.66	11.15	617	0.7
sy2bnt	05-30-199	13:51	133.71	-34.9	3.84	11.15	645	3.5
sy2bnt	05-31-199	09:53	302.29	-18.43	5.94	11.15	675	0.6
sy2bnt	05-31-199	13:56	274.45	-36.33	4.95	11.15	700	1.6
sy3bnt	05-25-199	12:17	21.51	-40.92	17	11.15	555	1.2
sy3bnt	05-26-199	09:44	18.8	-40.6	18	11.15	585	1.3
sy3bnt	05-30-199	10:27	23.41	-36.09	16.11	11.15	617	1.1
sy3bnt	05-30-199	13:52	22.53	-34.65	15.16	11.15	645	0.3
sy3bnt	05-31-199	09:59	19.95	-23.82	12.57	11.15	675	1.3
sy3bnt	05-31-199	13:58	274.9	7.74	4.26	11.15	700	2.6
sy9bnt	05-25-199	12:23	285.18	81.66	1.039	11.15	555	3.8
sy9bnt	05-26-199	09:47	237.61	14.34	4.46	11.15	585	1.4
sy9bnt	05-30-199	10:30	238.26	8.11	7.04	11.15	617	0.9
sy9bnt	05-30-199	13:54	242.95	-2.71	9.63	11.15	645	1.3
sy9bnt	05-31-199	10:01	265	0.95	4.63	11.15	675	1.3
sy9bnt	05-31-199	13:59	235.53	24.41	4.94	11.15	700	2.4
sy10bnt	05-25-199	12:26	12.49	53.02	1.226	11.15	555	1.4
sy10bnt	05-26-199	09:49	333.81	40.6	1.147	11.15	585	0.6
sy10bnt	05-30-199	10:33	304.64	61.22	1.458	11.15	617	1.9
sy10bnt	05-30-199	13:56	288.94	50.83	1.214	11.15	645	1.1
sy10bnt	05-31-199	10:03	294.99	48.39	0.887	11.15	675	1.4
sy10bnt	05-31-199	14:01	305.56	-39.76	0.74	11.15	700	0.3
sy15bnt	05-25-199	12:33	184.41	60.57	4.7	11.15	555	28.5
sy15bnt	05-26-199	09:52	107.09	54.24	0.879	11.15	585	4.9

Alternating field demagnetization followed by thermal demagnetization

sample	date	time	declination	inclination	mA/m	cm3	temp. C	error %
sy15bnt	05-30-199	10:34	228.64	14.56	5.86	11.15	617	0.8
sy15bnt	05-30-199	13:58	256.18	17.63	3.15	11.15	645	1.6
sy15bnt	05-31-199	10:05	281.07	11.71	5.62	11.15	675	2.3
sy15bnt	05-31-199	14:04	220.92	5.38	1.23	11.15	700	4.1
sy16bnt	05-25-199	12:34	297.58	-12.04	8.36	11.15	555	0.6
sy16bnt	05-26-199	09:54	278.82	6.9	6.64	11.15	585	1.3
sy16bnt	05-30-199	10:36	229.91	-3.73	5.99	11.15	617	1.3
sy16bnt	05-30-199	13:59	298.21	-8.89	3.85	11.15	645	1.4
sy16bnt	05-31-199	10:06	294.25	-14.83	5.45	11.15	675	1.2
sy16bnt	05-31-199	14:05	260.75	36.45	5.95	11.15	700	3.1
sy19bnt	05-25-199	12:36	24.59	-1.05	2.96	11.15	555	1.4
sy19bnt	05-26-199	09:56	350.73	-22.06	3.61	11.15	585	2.3
sy19bnt	05-30-199	10:39	273.82	24.6	3.19	11.15	617	1.3
sy19bnt	05-30-199	14:02	239.01	-18	4.75	11.15	645	1.9
sy19bnt	05-31-199	10:08	305.16	-1.48	3.49	11.15	675	2
sy19bnt	05-31-199	14:07	265.69	-13.18	2.74	11.15	700	2.6
sy20bnt	05-25-199	12:39	300.29	38.71	1.657	11.15	555	5.4
sy20bnt	05-26-199	09:58	85.71	78.16	1.012	11.15	585	1
sy20bnt	05-30-199	10:42	250.06	-21.11	0.88	11.15	617	0.9
sy20bnt	05-30-199	14:05	299.16	23.94	1.393	11.15	645	0.8
sy20bnt	05-31-199	10:11	317.28	15.35	0.947	11.15	675	0.3
sy20bnt	05-31-199	14:09	148.97	-41.58	0.996	11.15	700	1
sy21bnt	05-25-199	12:40	231	-7.41	7.01	11.15	555	1.8
sy21bnt	05-26-199	10:00	237.64	21.1	9.98	11.15	585	2.6
sy21bnt	05-30-199	10:44	248.25	6.54	10.05	11.15	617	1.9
sy21bnt	05-30-199	14:06	278.7	21.6	11.47	11.15	645	1.1
sy21bnt	05-31-199	10:12	273.86	26.15	7.93	11.15	675	2.5
sy21bnt	05-31-199	14:11	249.94	2.65	7.88	11.15	700	2.9
sy22bnt	05-25-199	12:42	270.47	-10.97	38.9	11.15	555	1.7
sy22bnt	05-26-199	10:01	283.15	10.19	41	11.15	585	1.4
sy22bnt	05-30-199	10:45	271.5	-3.96	63.7	11.15	617	1.4
sy22bnt	05-30-199	14:07	259.74	-1.62	44.6	11.15	645	2.3

Alternating field demagnetization followed by thermal demagnetization

sample	date	time	declination	inclination	mA/m	cm3	temp. C	error %
sy22bnt	05-31-199	10:14	263.2	-7.14	29.1	11.15	675	1.8
sy22bnt	05-31-199	14:12	265.08	1.68	24	11.15	700	3.6
sy23bnt	05-25-199	12:44	346.2	17.83	6.87	11.15	555	1.7
sy23bnt	05-26-199	10:04	116.25	43.78	4.5	11.15	585	1.5
sy23bnt	05-30-199	10:47	288.29	-1.46	8.28	11.15	617	1
sy23bnt	05-30-199	14:09	258.82	16.27	14.78	11.15	645	2.6
sy23bnt	05-31-199	10:15	246.92	-18.02	7.64	11.15	675	1.4
sy23bnt	05-31-199	14:14	310.4	-52.19	21.9	11.15	700	0.3
sy26bnt	05-25-199	12:46	323.61	72.07	5.92	11.15	555	3
sy26bnt	05-26-199	10:05	294.87	43.83	4.2	11.15	585	1.5
sy26bnt	05-30-199	10:49	265.12	-25.24	2.66	11.15	617	1.1
sy26bnt	05-30-199	14:10	253.77	15.81	4.47	11.15	645	3.2
sy26bnt	05-31-199	10:18	343.34	25.25	1.149	11.15	675	0.7
sy26bnt	05-31-199	14:15	283.2	-3.97	11.85	11.15	700	0.6
sy27bnt	05-25-199	12:49	318.81	-45.1	3.38	11.15	555	2.9
sy27bnt	05-26-199	10:07	283.95	43.86	5.89	11.15	585	2.4
sy27bnt	05-30-199	10:51	219.82	21.63	4.89	11.15	617	1.3
sy27bnt	05-30-199	14:14	295.73	15.97	3.78	11.15	645	6.7
sy27bnt	05-31-199	10:20	143.73	64.23	11.29	11.15	675	2.1
sy27bnt	05-31-199	14:20	260.21	-34.74	5.97	11.15	700	2.7

Principal component analyses for alternating field
demagnetization followed by thermal demagnetization

sample		declination	inclination
sy1bnt		5.6	-5.8
sy2bnt		133.4	-4.5
sy3bnt		37	-37.3
sy9bnt		240.7	-8.1
sy10bnt		28.9	83.3
sy15bnt		98.9	10.3
sy16bnt		345.2	-25
sy19bnt		41.1	1.6
sy20bnt		315.7	38.1
sy21bnt		152.7	-31.5
sy22bnt		94.7	4.6
sy23bnt		322.4	-60.1
sy26bnt		278	-20.9
sy27bnt		126.2	59.2

Lwr.Hem.Equal Area Net
circle=DOWN square=UP
 hermal\sy1bnt.SR2
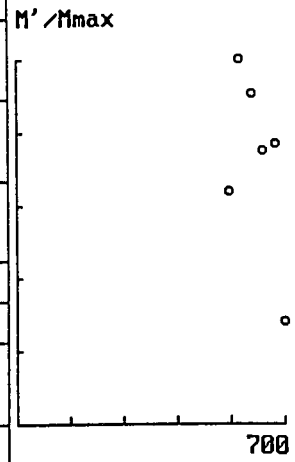 n = 6
 06-01-1994
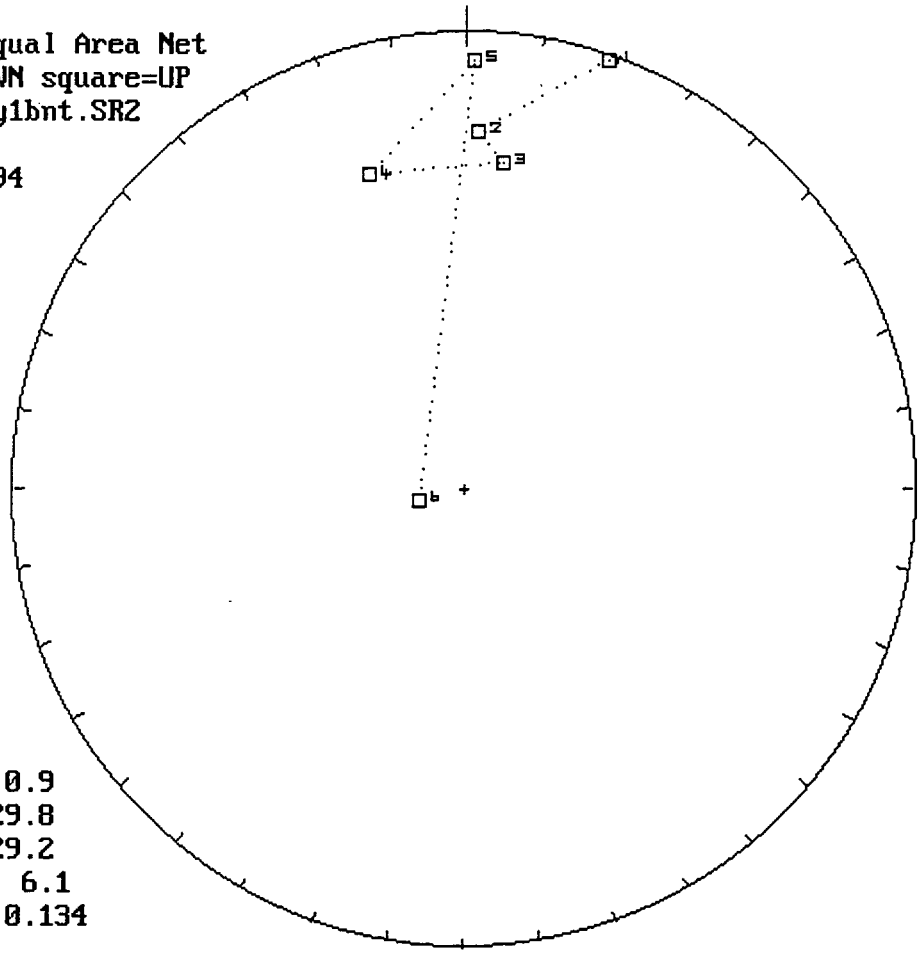
m.dec.=   0.9
m.inc.= -29.8
alpha95= 29.2
Fish. k=   6.1
sp.var.=   0.134

Lwr.Hem.Equal Area Net
circle=DOWN square=UP
 hermal\sy1bnt.SR2
 n = 5
 06-01-1994
Vector Diff
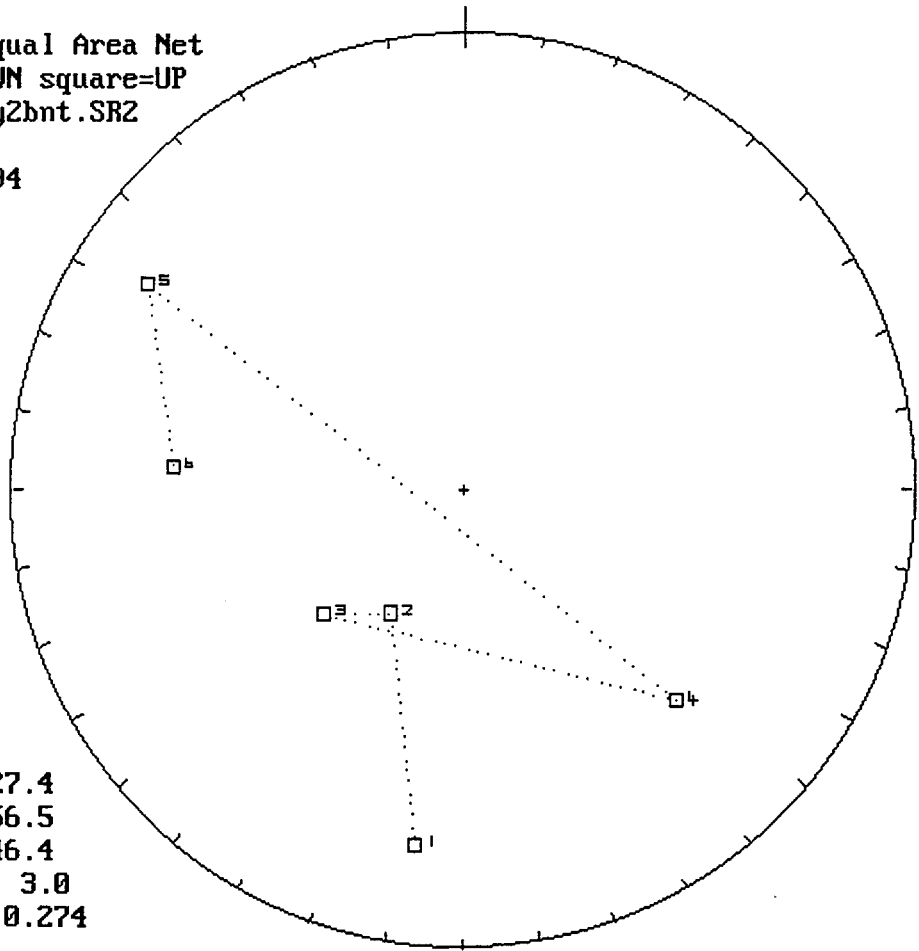Plot: shows
vectors
removed by
demag.
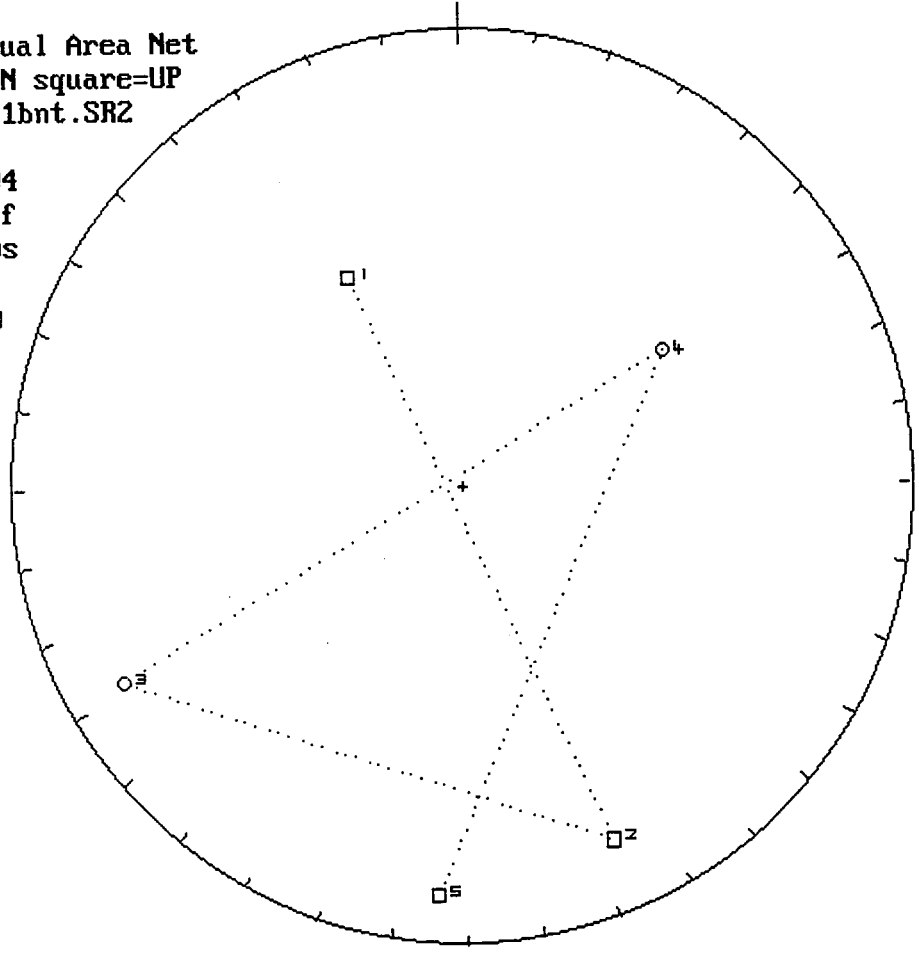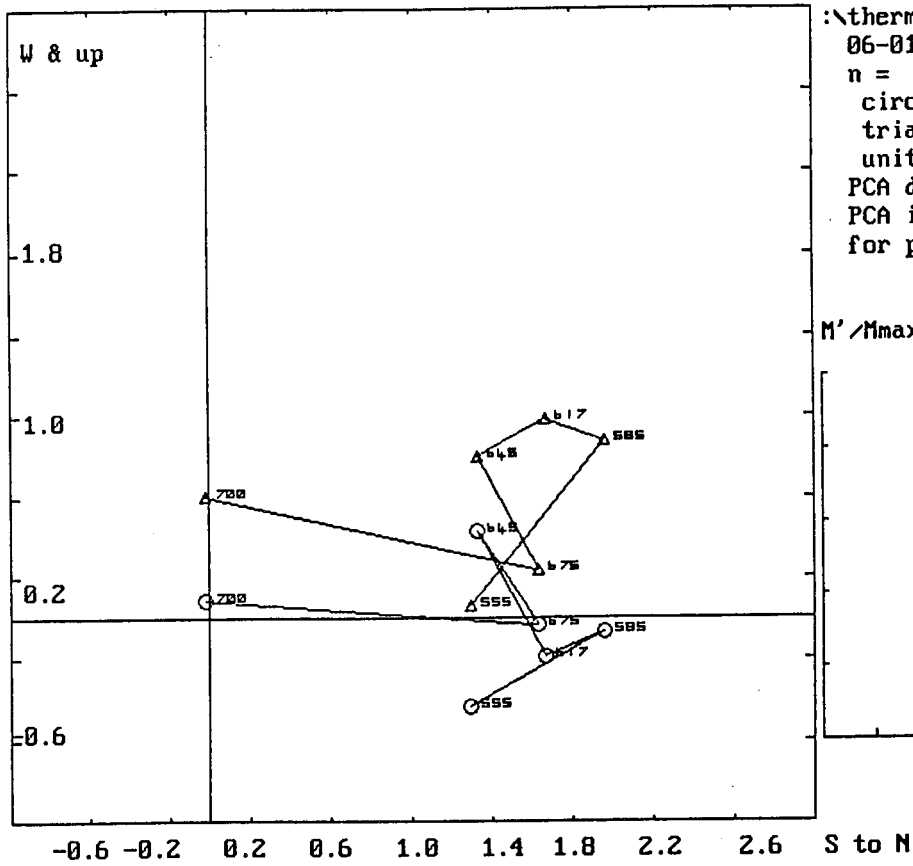
:\thermal\sy1bnt.SR2
06-01-1994
n = 6
  circle =horiz.pl
  triang. =vert.plo
  units mA/m
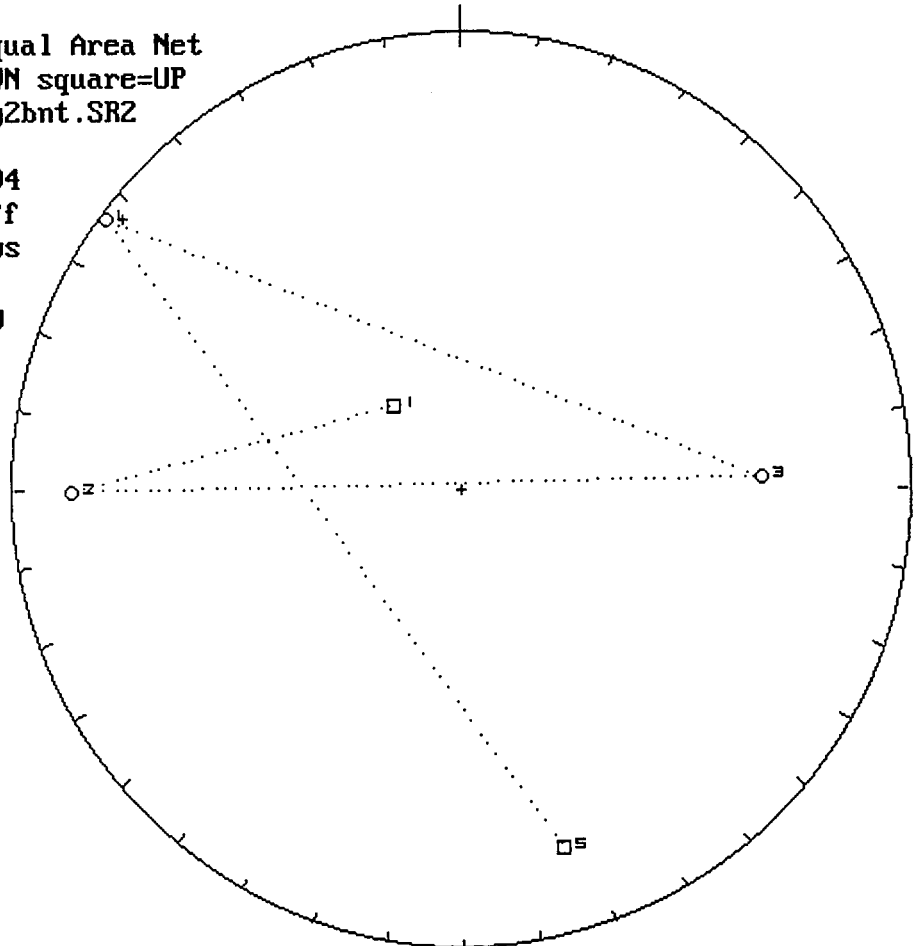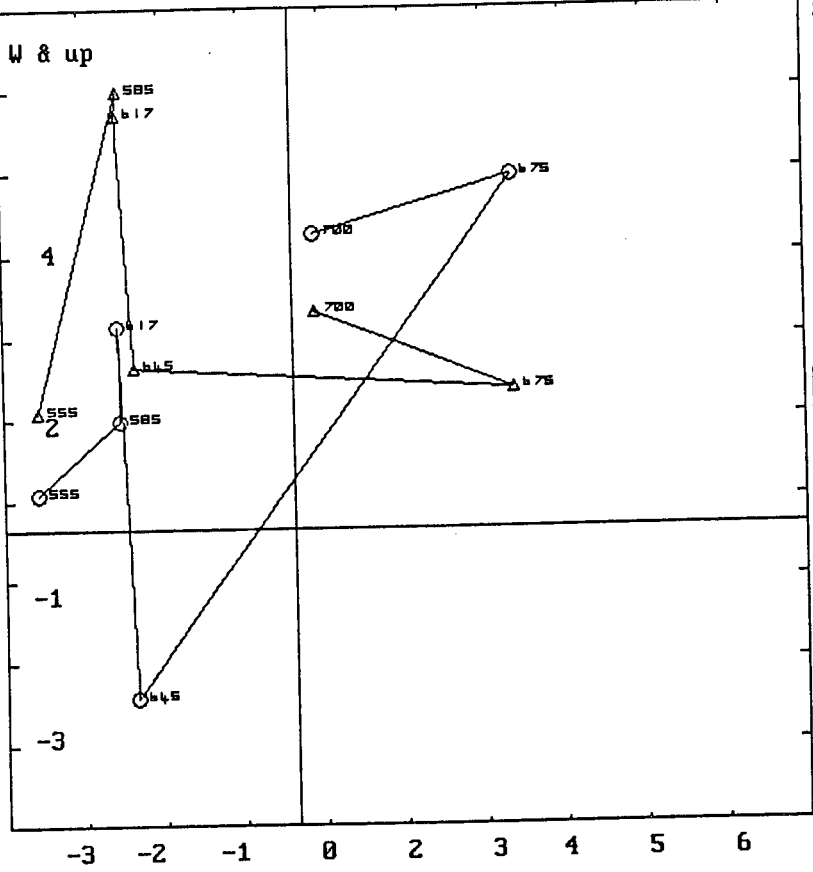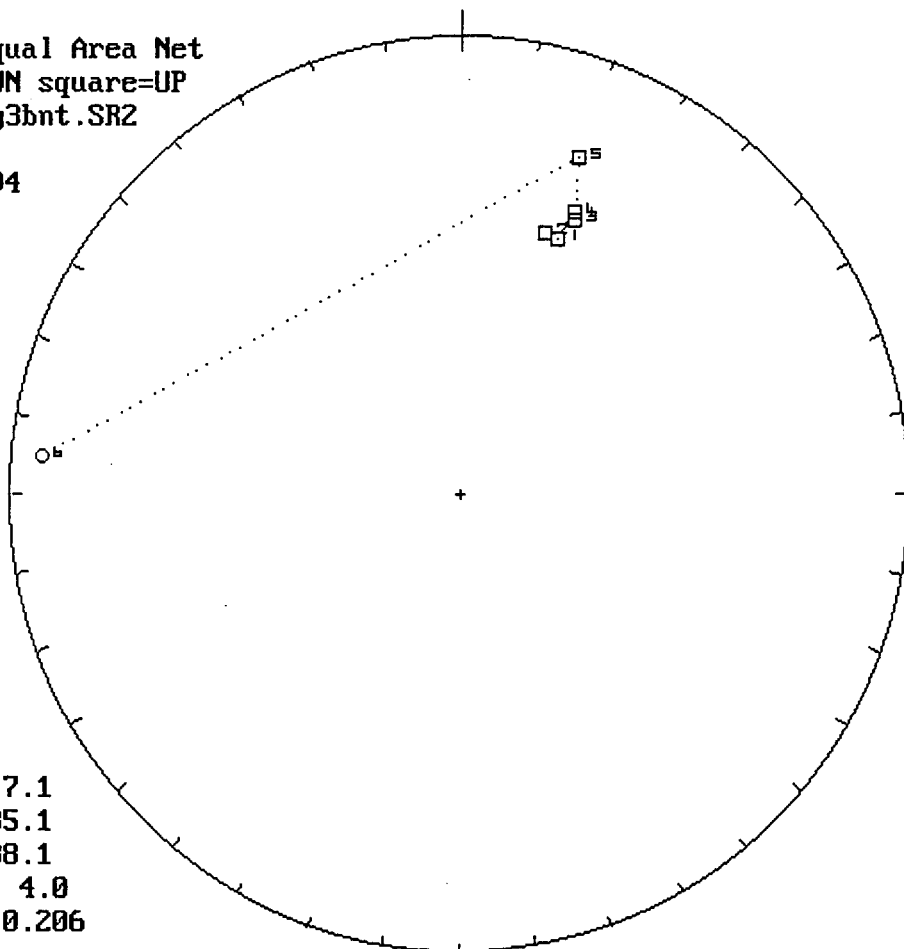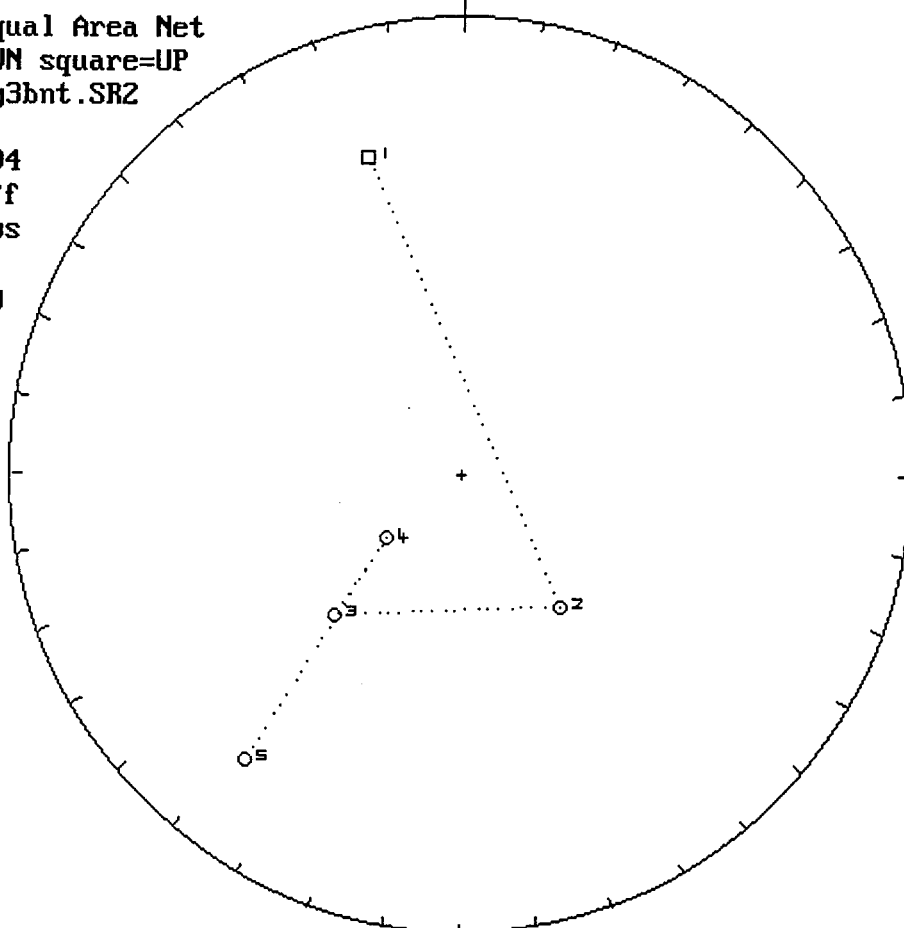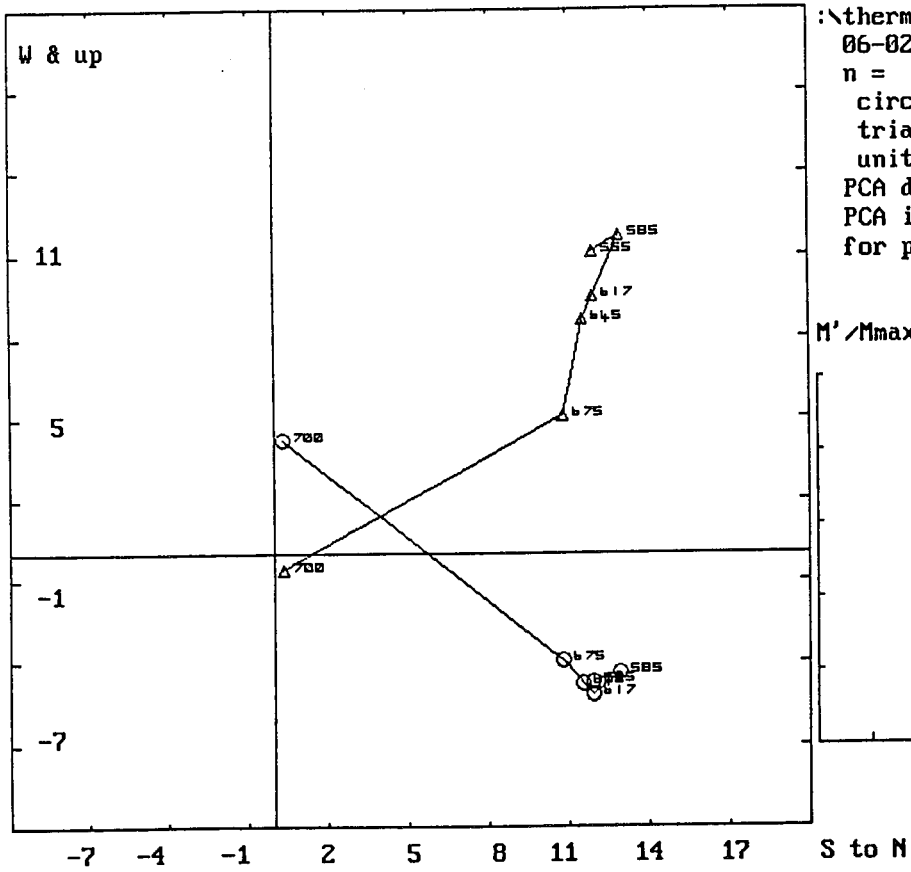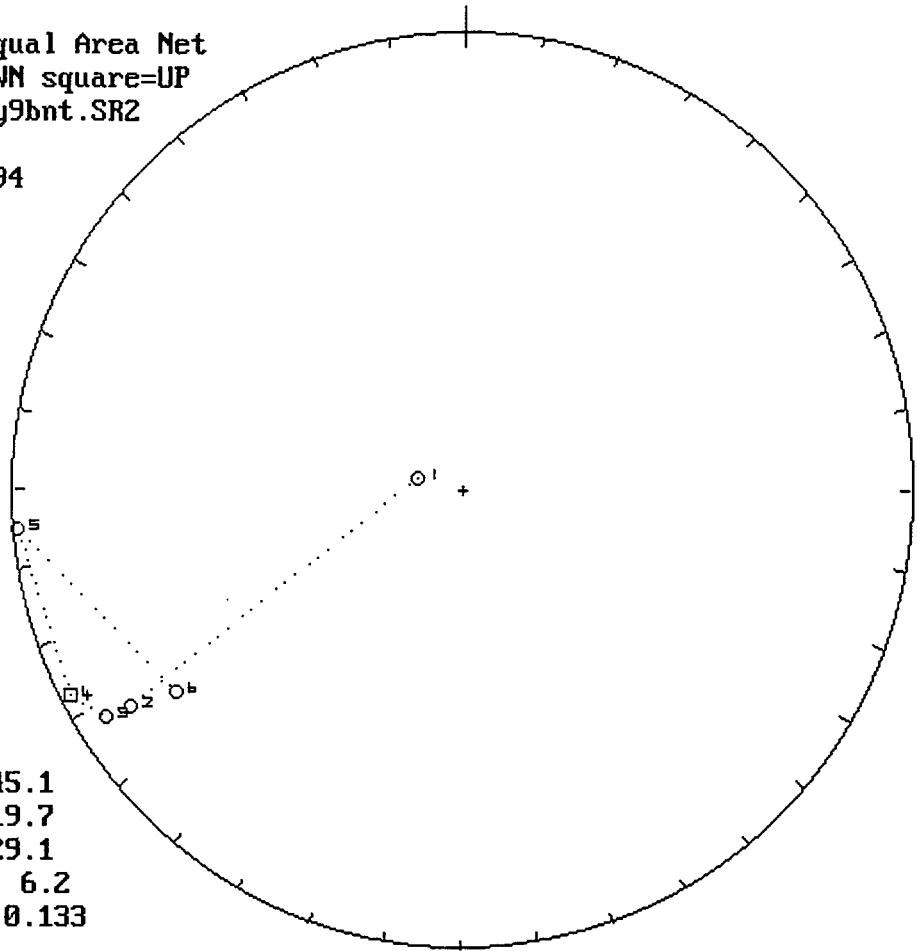PCA decl=   5.6
PCA incl=   -5.8
for points 1 to
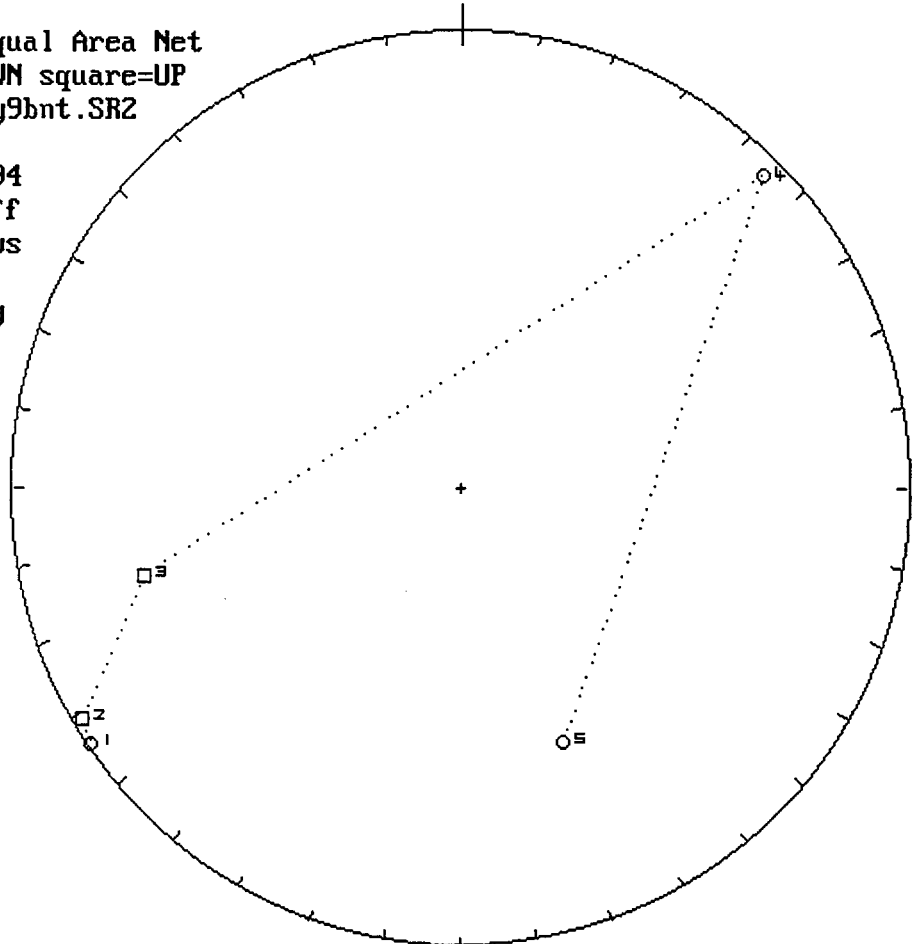
Lwr.Hem.Equal Area Net
circle=DOWN square=UP
 hermal\sy2bnt.SR2
 n = 6
 06-01-1994

m.dec.= 227.4
m.inc.= -56.5
alpha95= 46.4
Fish. k=   3.0
sp.var.= 0.274

Lwr.Hem.Equal Area Net
circle=DOWN square=UP
 hermal\sy2bnt.SR2
 n = 5
 06-01-1994
Vector Diff
Plot: shows
vectors
removed by
demag.

:\thermal\sy2bnt.SR2
06-01-1994
n = 6
  circle =horiz.plo
  triang. =vert.plot
  units mA/m
PCA decl= 133.4
PCA incl= -4.5
for points 1 to 6
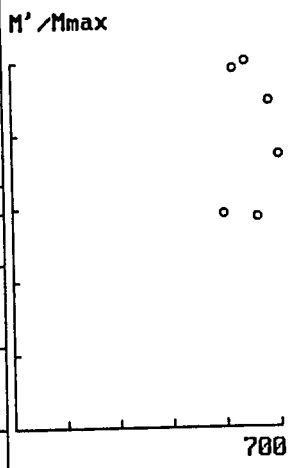
Lwr.Hem.Equal Area Net
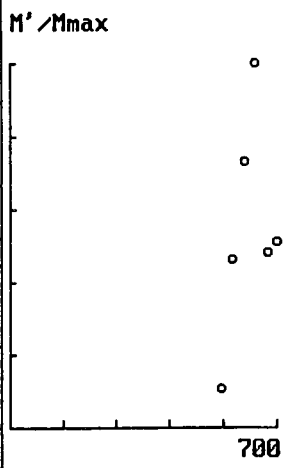circle=DOWN square=UP
 hermal\sy3bnt.SR2
 n = 6
 06-02-1994

□s
□₄
□₃
□₁
○⁶

m.dec.=   7.1
m.inc.= -35.1
alpha95= 38.1
Fish. k=   4.0
sp.var.= 0.206

Lwr.Hem.Equal Area Net
circle=DOWN square=UP
 hermal\sy3bnt.SR2
 n = 5
 06-02-1994
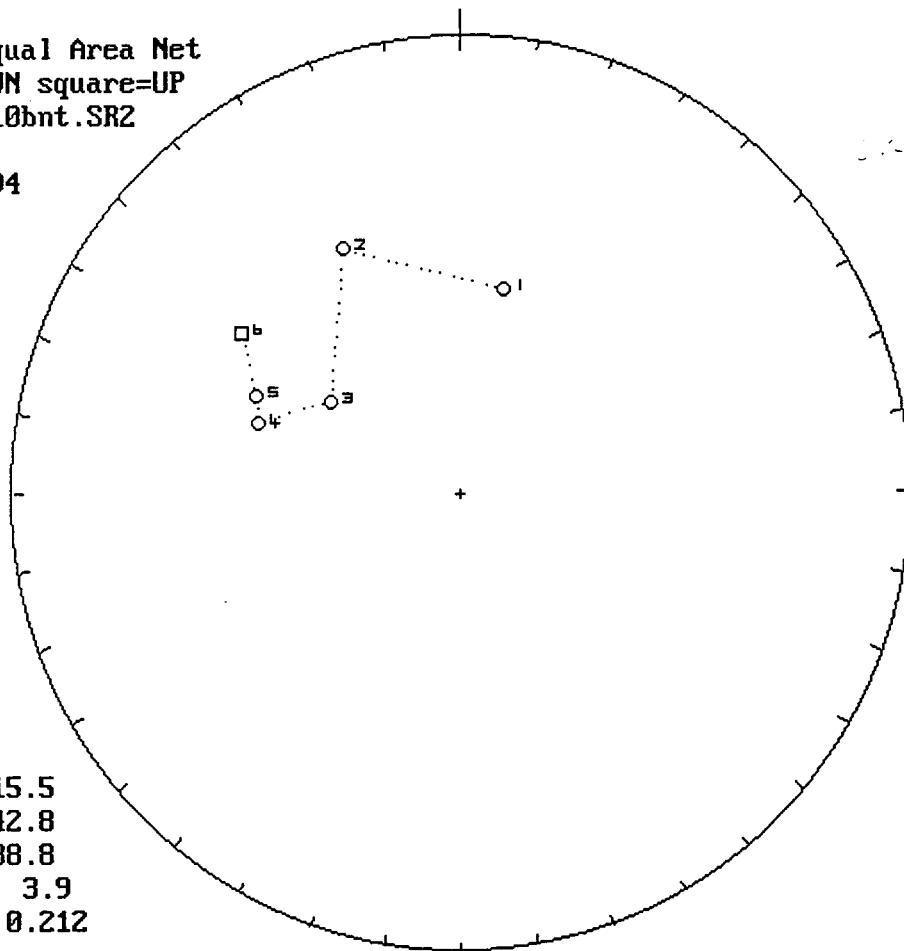Vector Diff
Plot: shows
vectors
removed by
demag.

□¹
○⁴
○³
○z
○⁵

:\thermal\sy3bnt.SR2
06-02-1994
n = 6
 circle =horiz.plo
 triang. =vert.plot
 units mA/m
PCA decl= 37.0
PCA incl= -37.3
for points 1 to 6
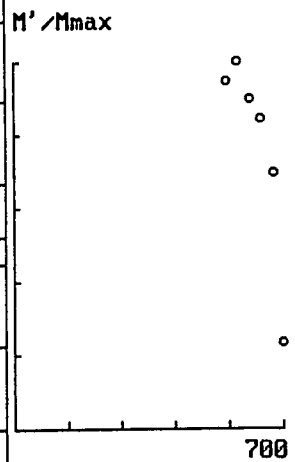
Lwr.Hem.Equal Area Net
circle=DOWN square=UP
 hermal\sy9bnt.SR2
 n = 6
 06-02-1994

m.dec.= 245.1
m.inc.= 19.7
alpha95= 29.1
Fish. k=   6.2
sp.var.= 0.133

Lwr.Hem.Equal Area Net
circle=DOWN square=UP
 hermal\sy9bnt.SR2
 n = 5
 06-02-1994
Vector Diff
Plot: shows
vectors
removed by
demag.

W & up
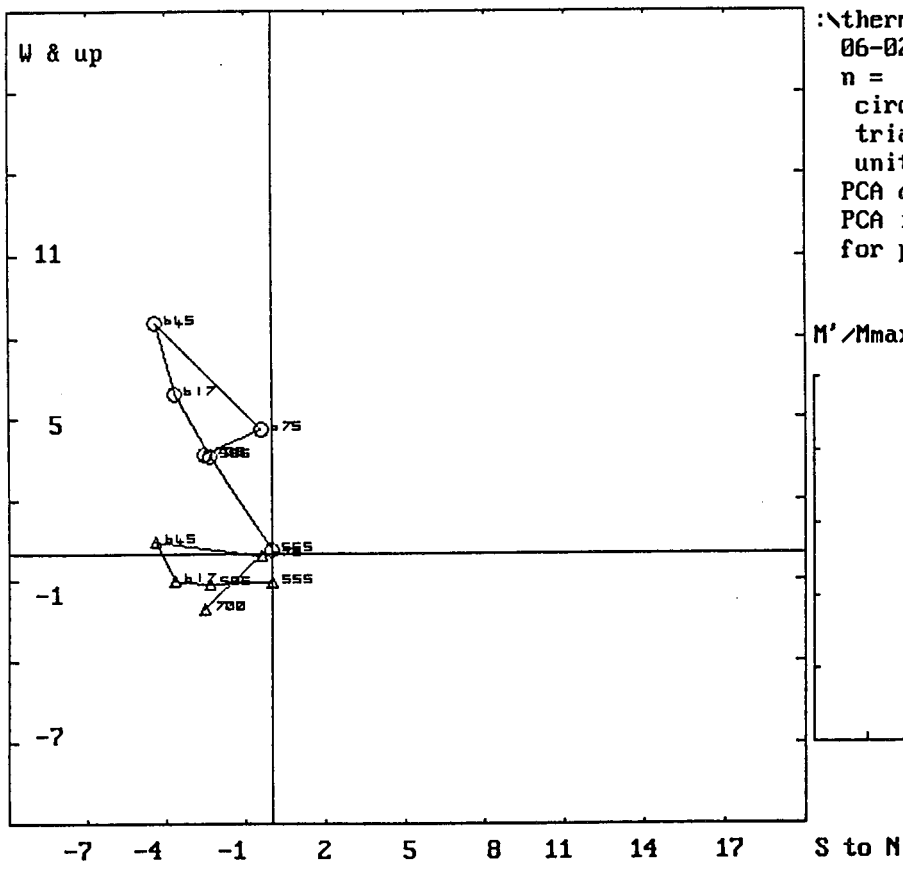
:\thermal\sy9bnt.SR2
06-02-1994
n = 6
 circle =horiz.plo
 triang. =vert.plot
 units mA/m
PCA decl= 240.7
PCA incl= −8.1
for points 1 to 6

M'/Mmax

700

S to N

Lwr.Hem.Equal Area Net
circle=DOWN square=UP
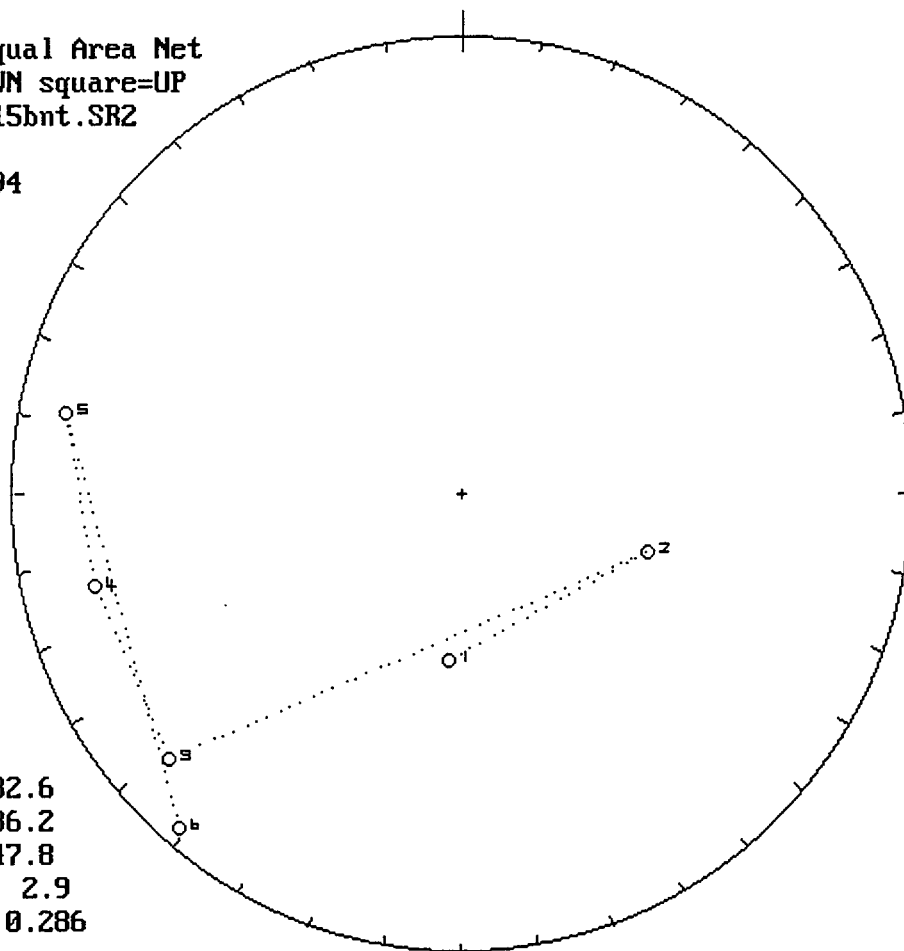 ermal\sy10bnt.SR2
 n = 6
 06-02-1994

m.dec.= 315.5
m.inc.= 42.8
alpha95= 38.8
Fish. k=   3.9
sp.var.= 0.212

Lwr.Hem.Equal Area Net
circle=DOWN square=UP
 ermal\sy10bnt.SR2
 n = 5
 06-02-1994
Vector Diff
Plot: shows
vectors
removed by
demag.

W & up

0.8

0.0

0.8

1.6

-1.6 -1.2 -0.8 -0.4 -0.0 0.4 0.8 1.2 1.6   S to N

\thermal\sy10bnt.SR2
06-02-1994
n = 6
 circle =horiz.plo
 triang. =vert.plot
 units mA/m
PCA decl= 28.9
PCA incl= 83.3
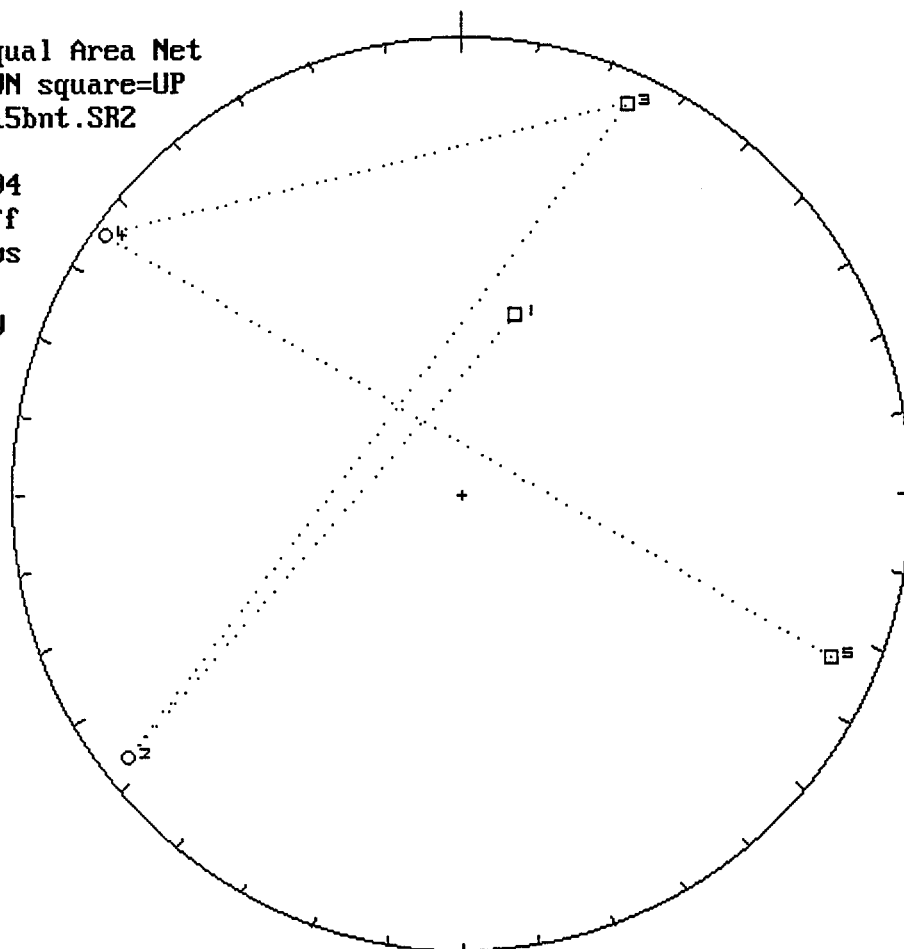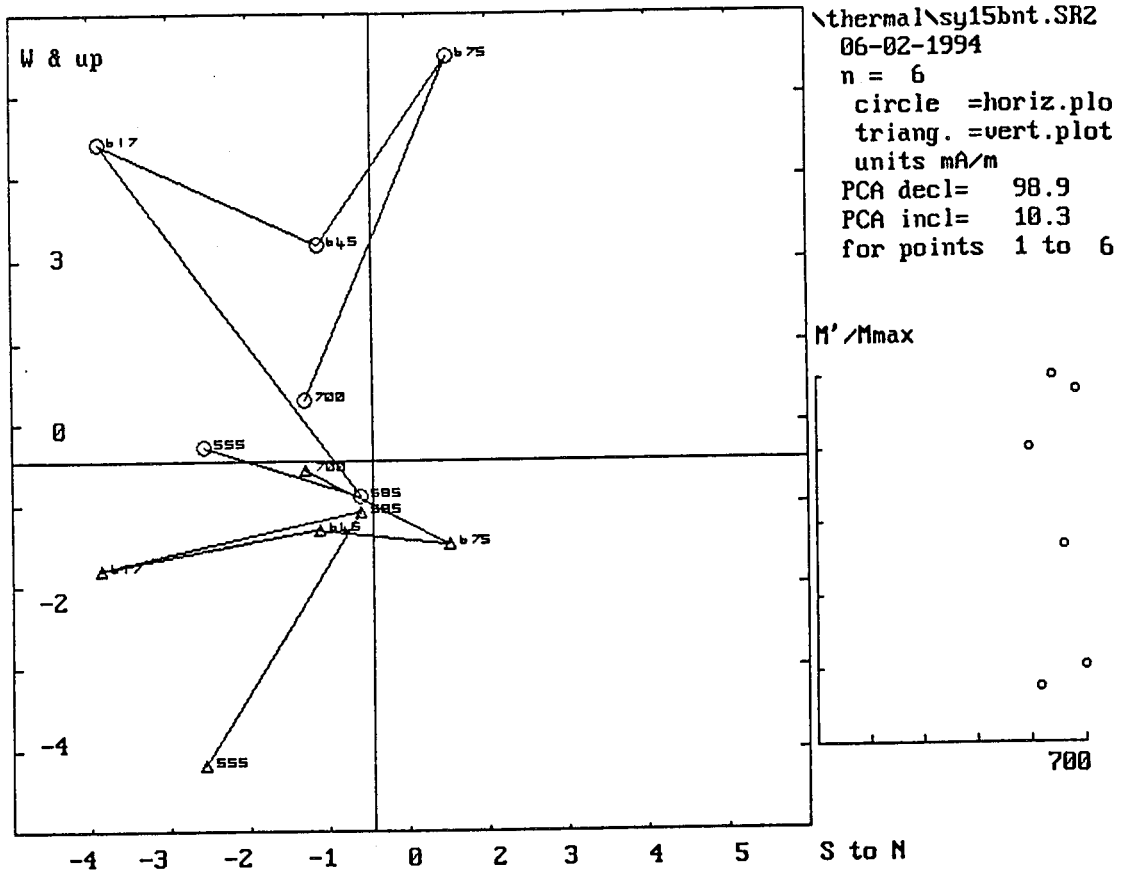for points 1 to 6

M'/Mmax

700
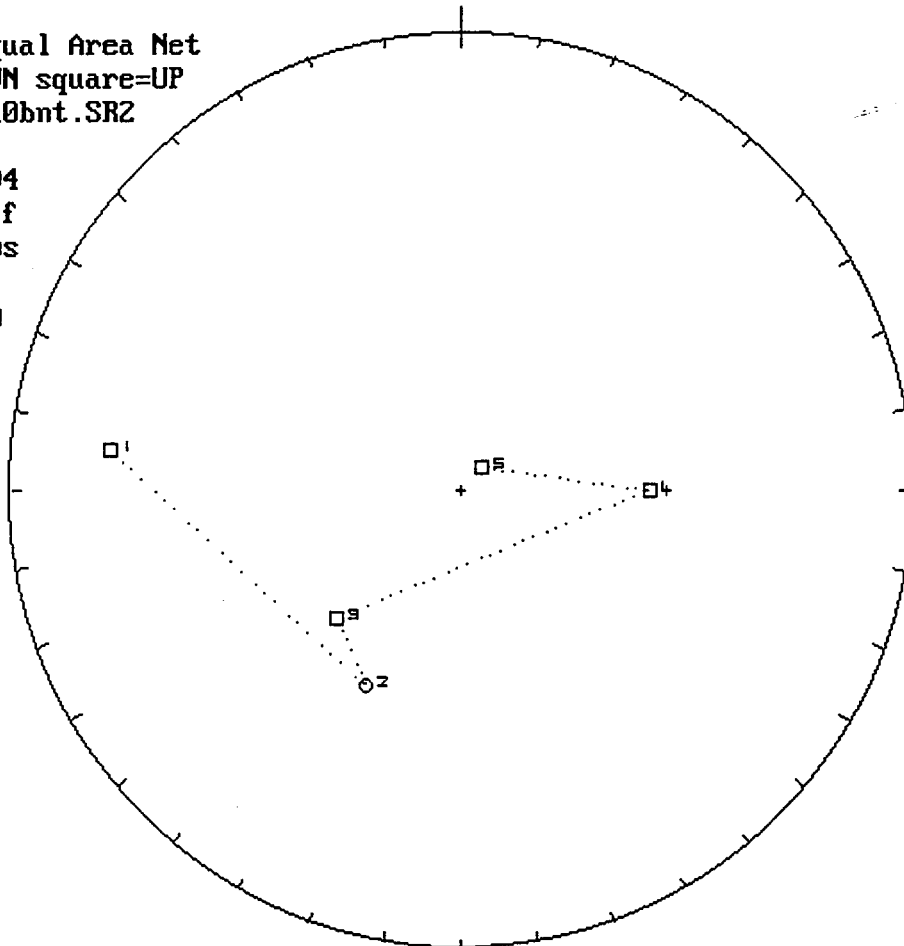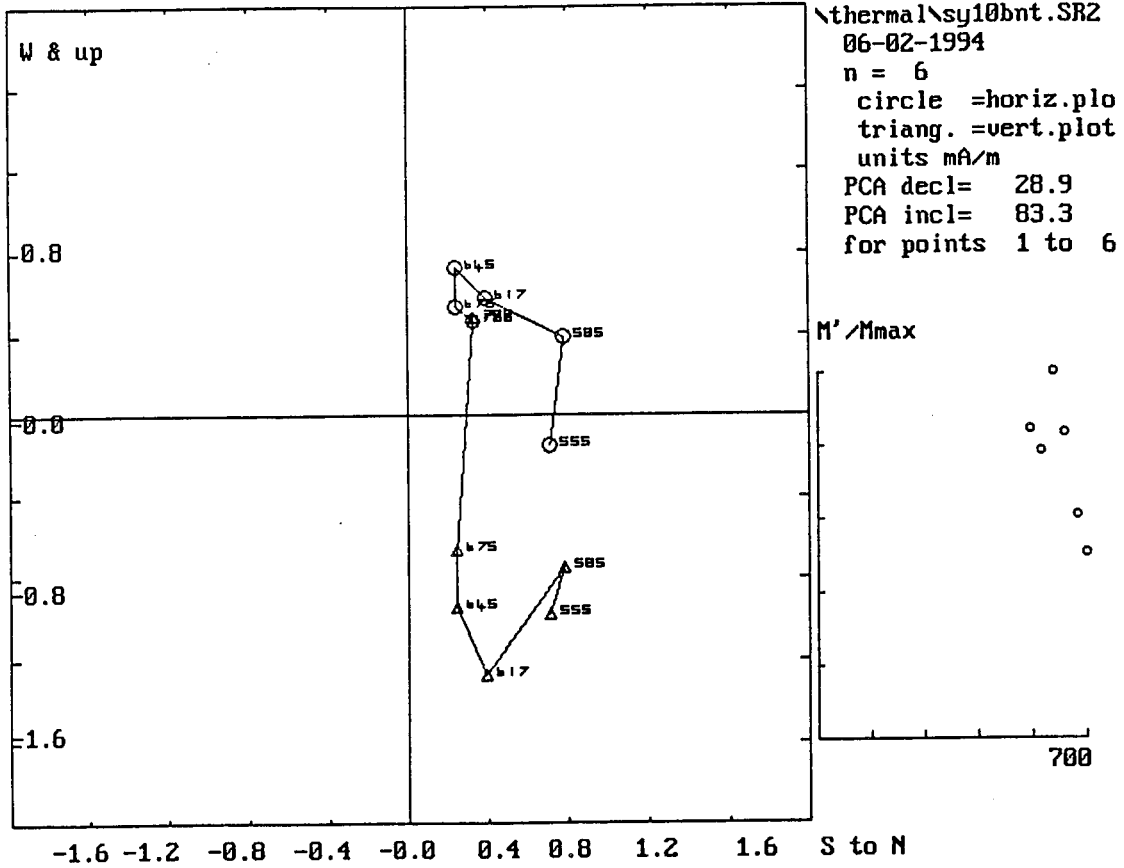
Lwr.Hem.Equal Area Net
circle=DOWN square=UP
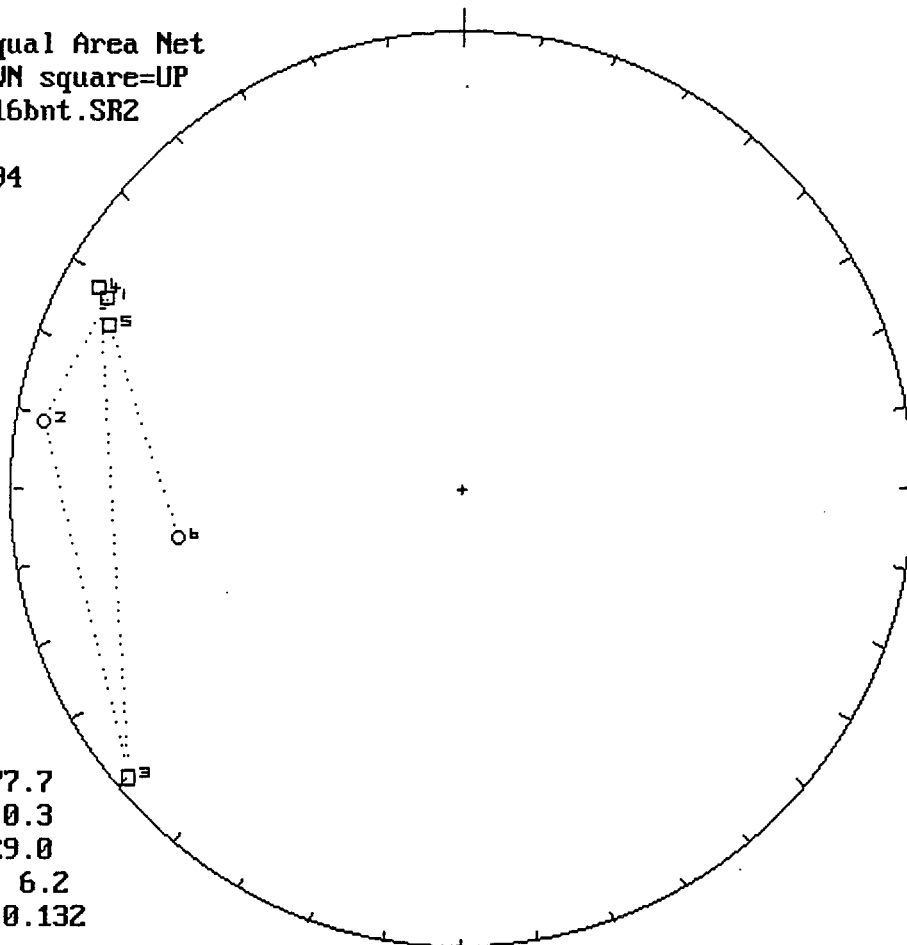 ermal\sy15bnt.SR2
 n = 6
 06-02-1994

m.dec.= 232.6
m.inc.= 36.2
alpha95= 47.8
Fish. k=   2.9
sp.var.= 0.286

Lwr.Hem.Equal Area Net
circle=DOWN square=UP
 ermal\sy15bnt.SR2
 n = 5
 06-02-1994
Vector Diff
Plot: shows
vectors
removed by
demag.

W & up

\thermal\sy15bnt.SR2
06-02-1994
n = 6
circle =horiz.plo
triang. =vert.plot
units mA/m
PCA decl=   98.9
PCA incl=   10.3
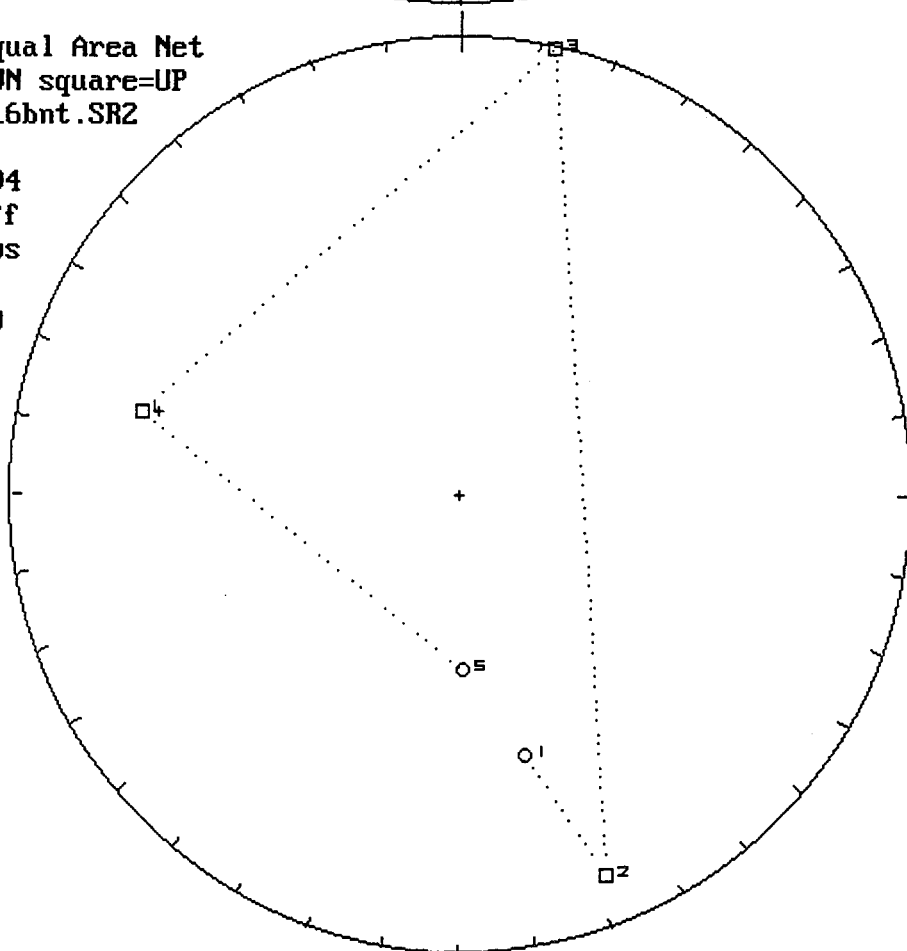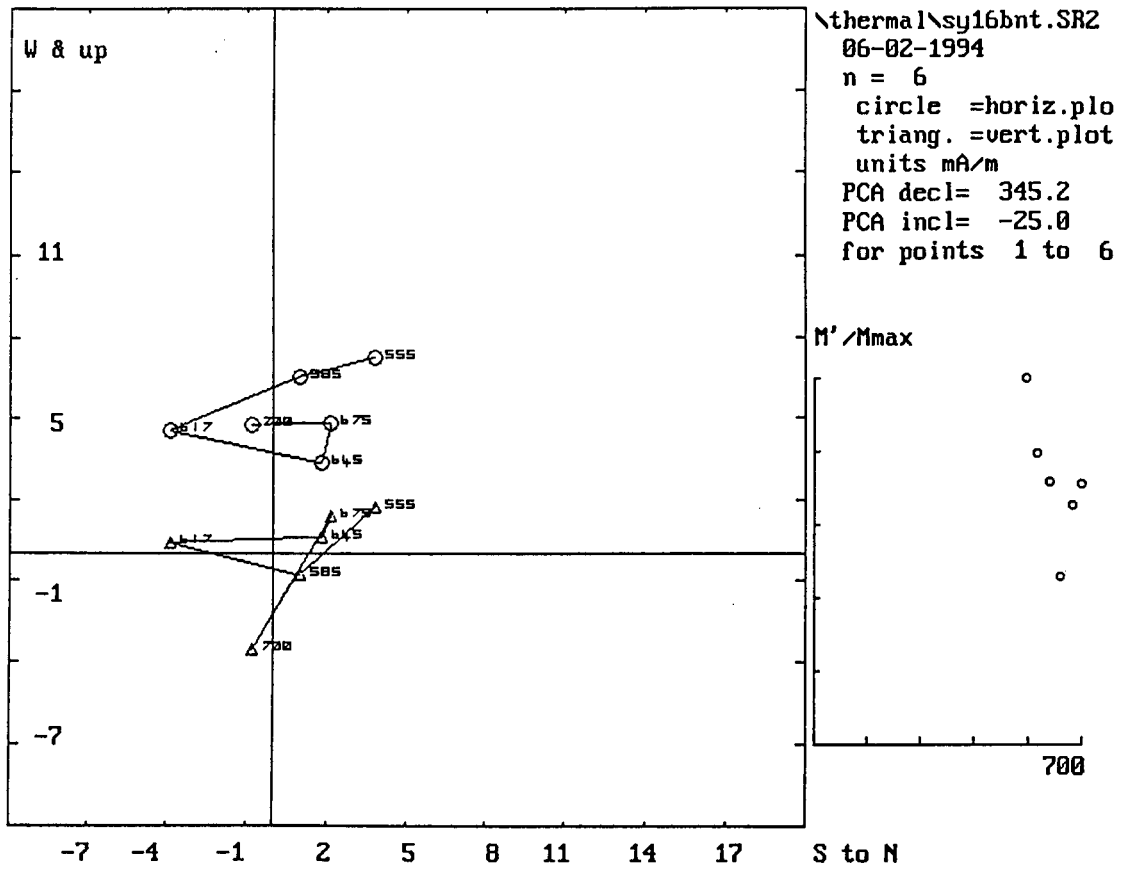for points 1 to 6

M'/Mmax

S to N

700

Lwr.Hem.Equal Area Net
circle=DOWN square=UP
 ermal\sy16bnt.SR2
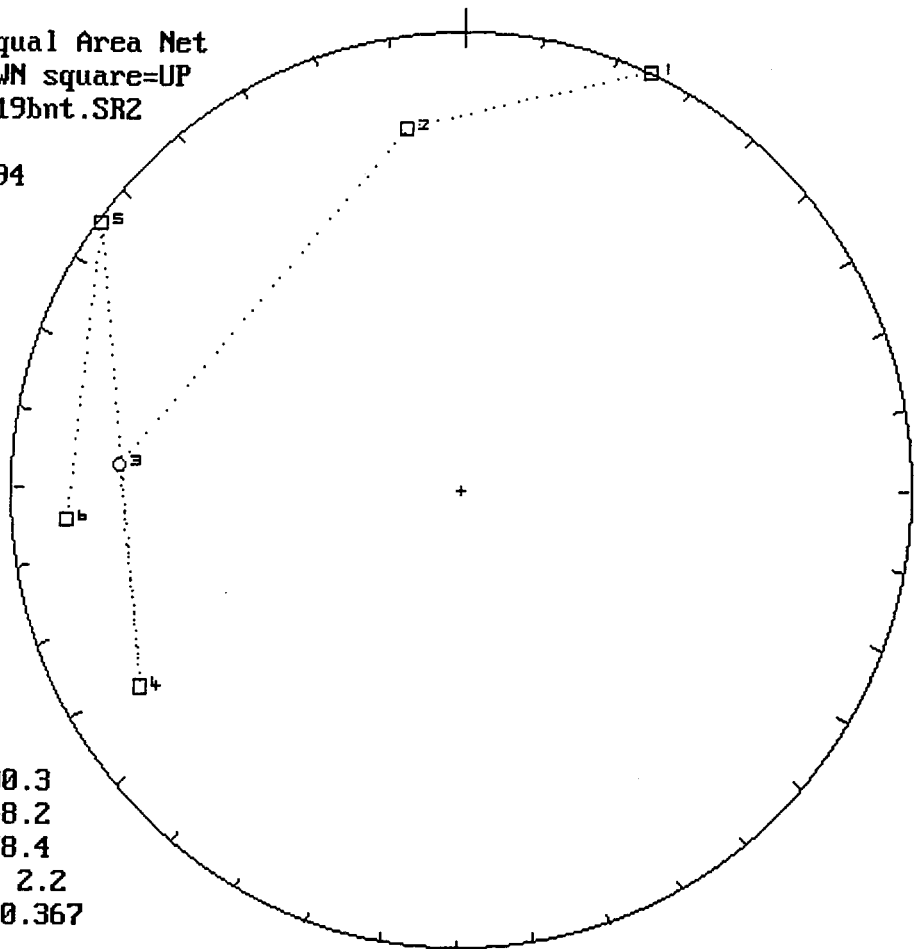 n = 6
 06-02-1994

m.dec.= 277.7
m.inc.=   0.3
alpha95= 29.0
Fish. k=   6.2
sp.var.= 0.132

Lwr.Hem.Equal Area Net
circle=DOWN square=UP
 ermal\sy16bnt.SR2
 n = 5
 06-02-1994
Vector Diff
Plot: shows
vectors
removed by
demag.

\thermal\sy16bnt.SR2
06-02-1994
n = 6
circle =horiz.plo
triang. =vert.plot
units mA/m
PCA decl= 345.2
PCA incl= -25.0
for points 1 to 6

Lwr.Hem.Equal Area Net
circle=DOWN square=UP
 ermal\sy19bnt.SR2
 n = 6
 06-02-1994

m.dec.= 300.3
m.inc.= -8.2
alpha95= 58.4
Fish. k=   2.2
sp.var.= 0.367

Lwr.Hem.Equal Area Net
circle=DOWN square=UP
 ermal\sy19bnt.SR2
 n = 5
 06-02-1994
Vector Diff
Plot: shows
vectors
removed by
demag.

\thermal\sy19bnt.SR2
06-02-1994
n = 6
circle =horiz.plo
triang. =vert.plot
units mA/m
PCA decl= 41.1
PCA incl= 1.6
for points 1 to 6

Lwr.Hem.Equal Area Net
circle=DOWN square=UP
 ermal\sy20bnt.SR2
 n = 6
 06-02-1994

m.dec.= 284.0
m.inc.= 26.6
alpha95= 87.0
Fish. k=   1.5
sp.var.= :0.535

Lwr.Hem.Equal Area Net
circle=DOWN square=UP
 ermal\sy20bnt.SR2
 n = 5
 06-02-1994
Vector Diff
Plot: shows
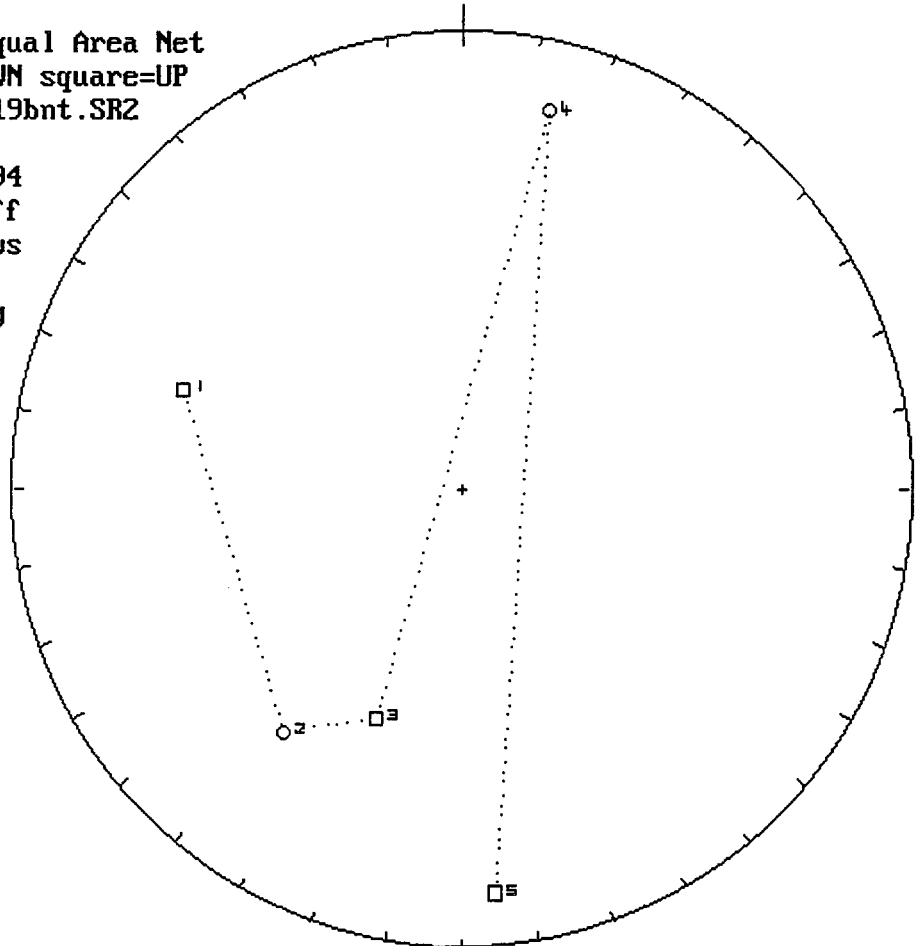vectors
removed by
demag.
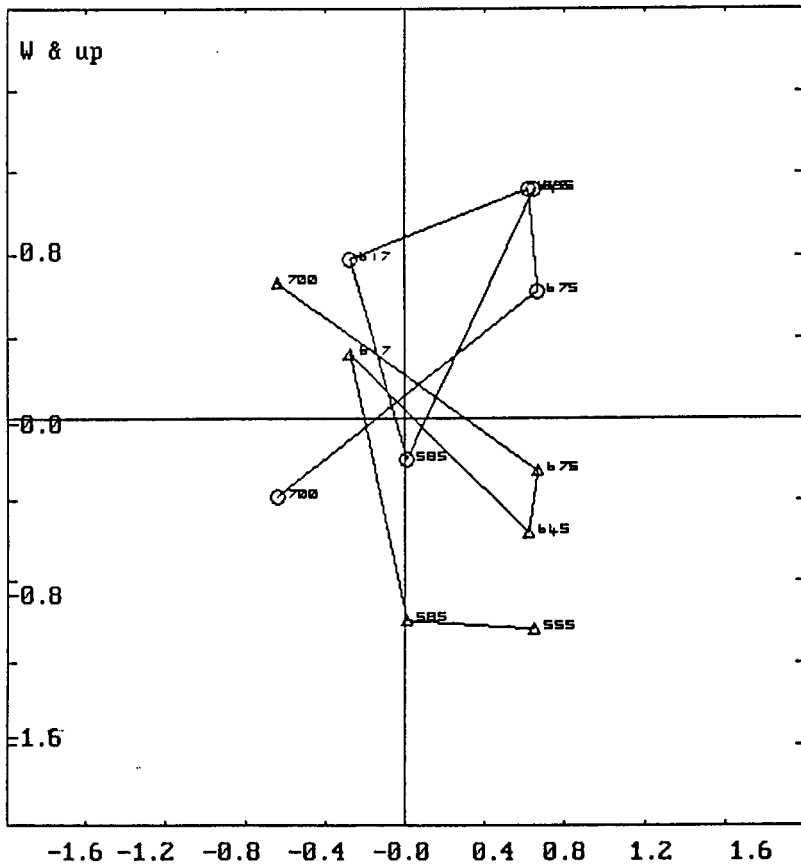
\thermal\sy20bnt.SR2
06-02-1994
n = 6
circle =horiz.plot
triang. =vert.plot
units mA/m
PCA decl= 315.7
PCA incl= 38.1
for points 1 to 6

Lwr.Hem.Equal Area Net
circle=DOWN square=UP
 ermal\sy21bnt.SR2
 n = 6
 06-02-1994

m.dec.= 252.6
m.inc.=   12.3
alpha95= 19.3
Fish. k=   12.9
sp.var.=   0.064

Lwr.Hem.Equal Area Net
circle=DOWN square=UP
 ermal\sy21bnt.SR2
 n = 5
 06-02-1994
Vector Diff
Plot: shows
vectors
removed by
demag.
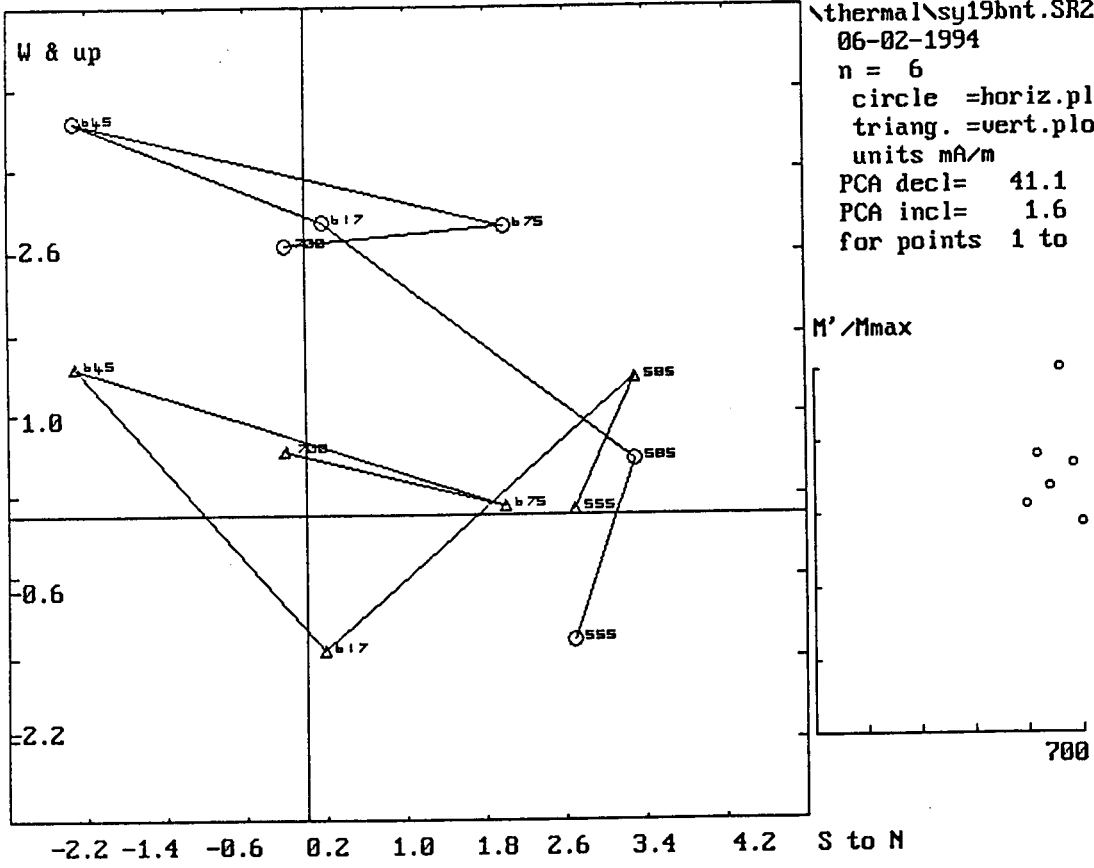
\thermal\sy21bnt.SR2
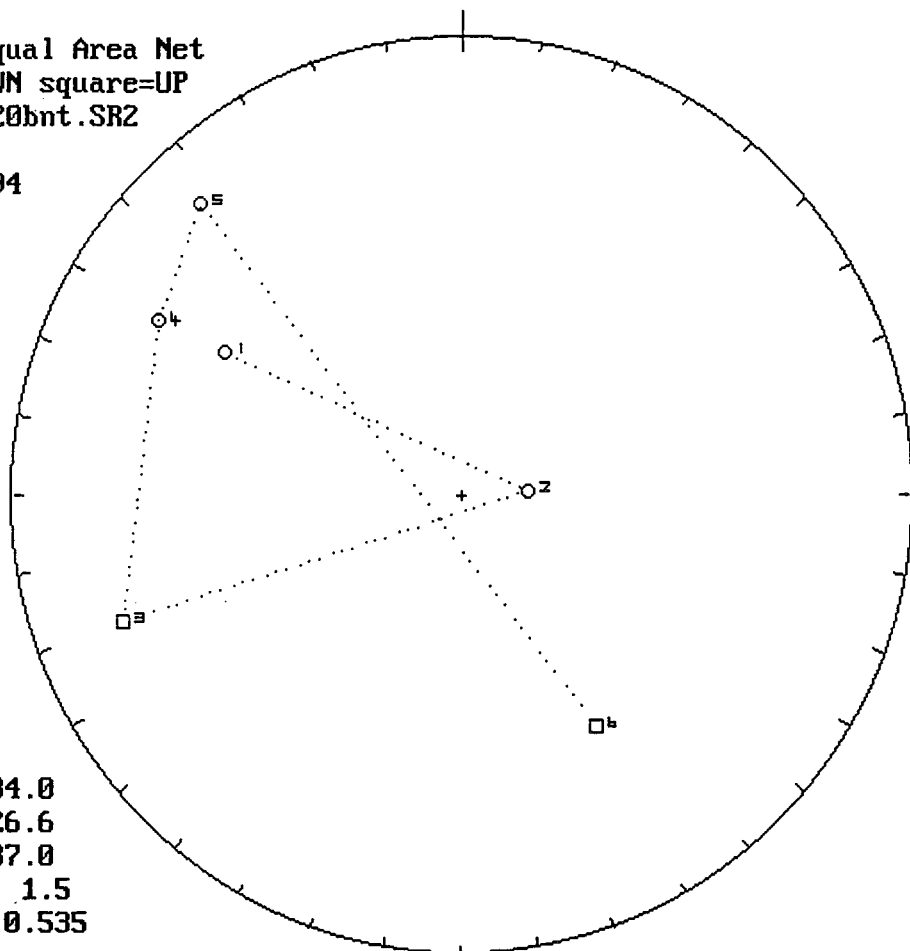06-02-1994
n = 6
circle =horiz.plo
triang. =vert.plot
units mA/m
PCA decl= 152.7
PCA incl= -31.5
for points 1 to 6

M'/Mmax
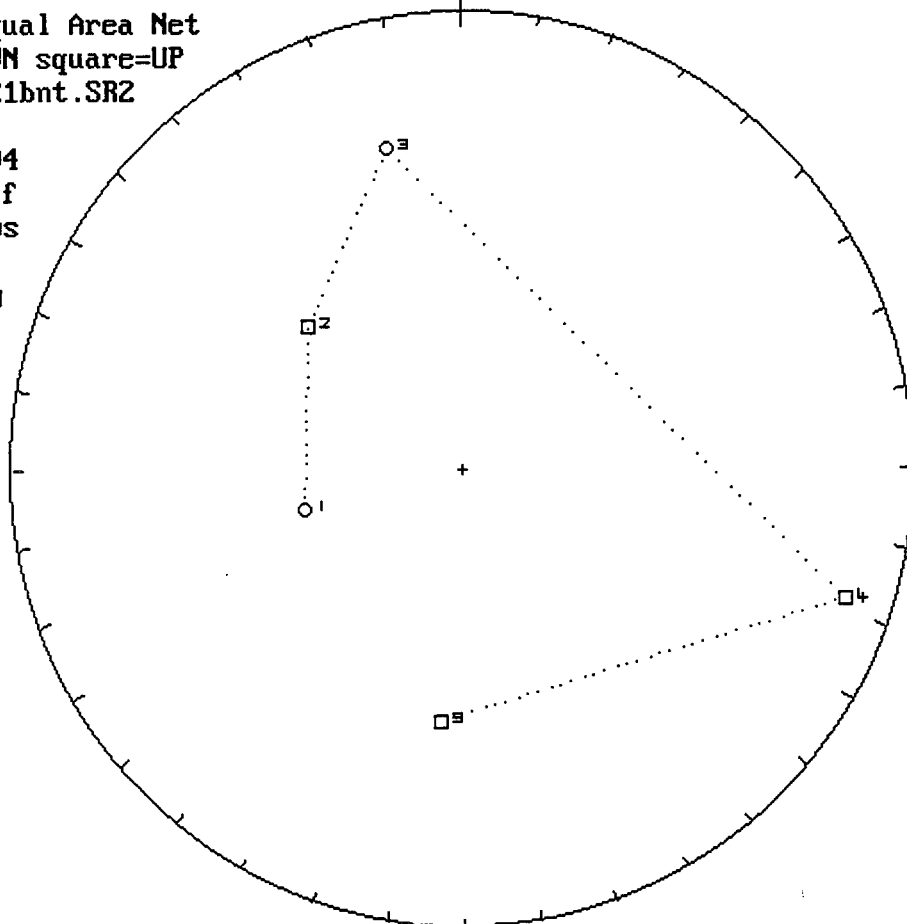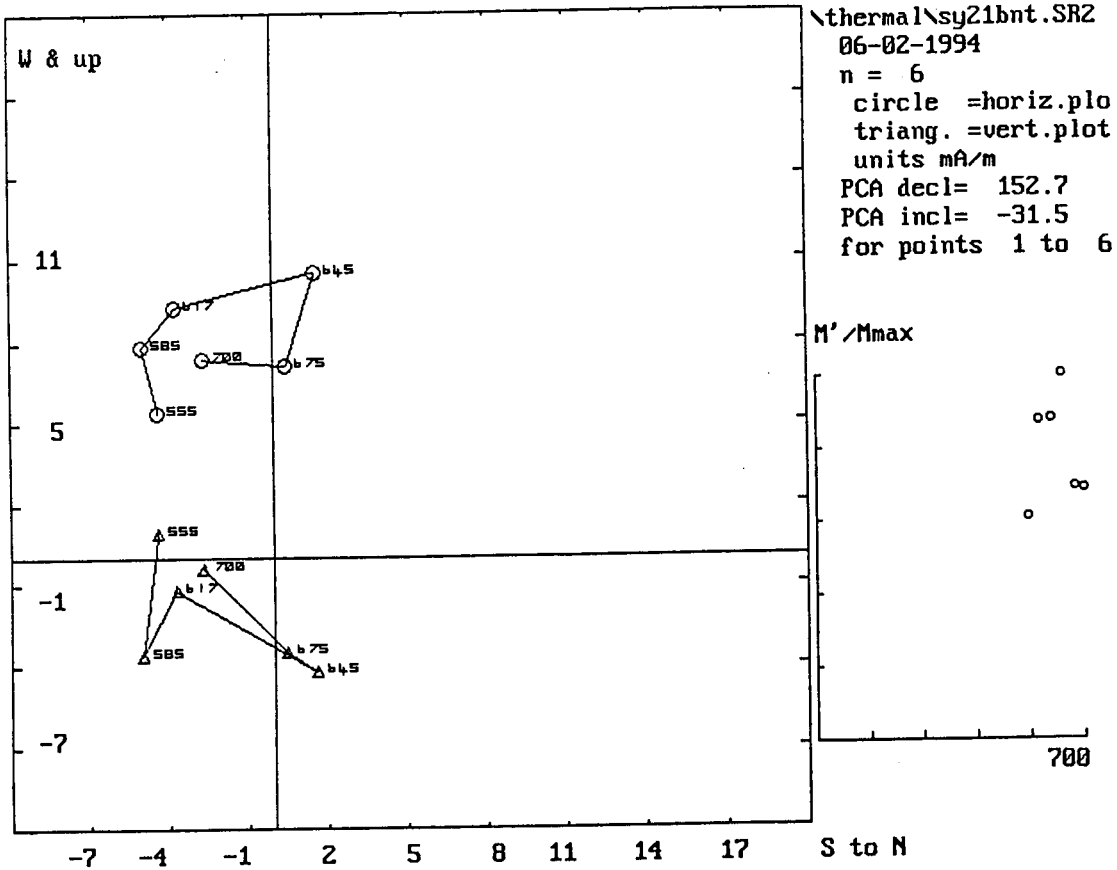
Lwr.Hem.Equal Area Net
circle=DOWN square=UP
 ermal\sy22bnt.SR2
 n = 6
 06-02-1994

m.dec.= 268.8
m.inc.= -2.0
alpha95= 9.2
Fish. k= 53.7
sp.var.= 0.015

Lwr.Hem.Equal Area Net
circle=DOWN square=UP
 ermal\sy22bnt.SR2
 n = 5
 06-02-1994
Vector Diff
Plot: shows
vectors
removed by
demag.

W & up

\thermal\sy22bnt.SR2
06-02-1994
n = 6
 circle =horiz.plo
 triang. =vert.plot
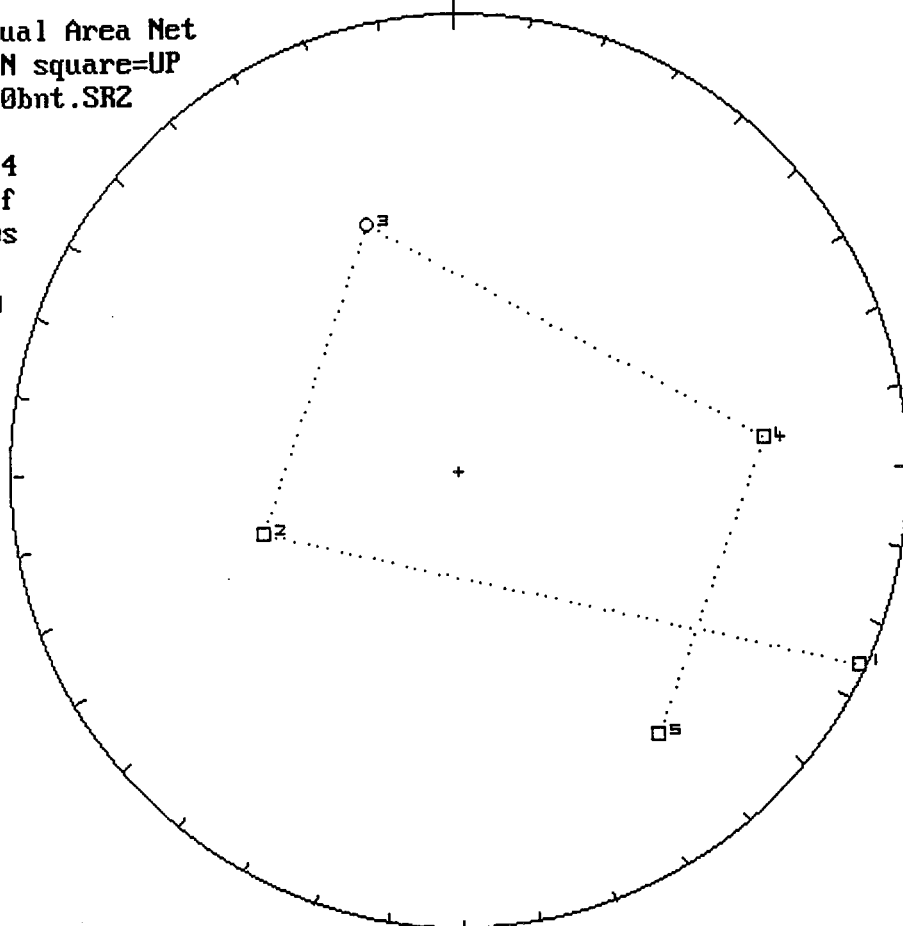 units mA/m
PCA decl=   94.7
PCA incl=   4.6
for points 1 to 6

M'/Mmax

700

53

35

17

1

-1   8   17   26   35   44   53   62   71   S to N

Lwr.Hem.Equal Area Net
circle=DOWN square=UP
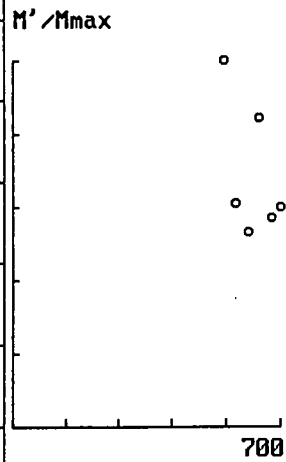 ermal\sy23bnt.SR2
 n = 6
 06-02-1994

m.dec.= 285.0
m.inc.=   3.0
alpha95= 82.3
Fish. k=   1.6
sp.var.= 0.513

Lwr.Hem.Equal Area Net
circle=DOWN square=UP
 ermal\sy23bnt.SR2
 n = 5
 06-02-1994
Vector Diff
Plot: shows
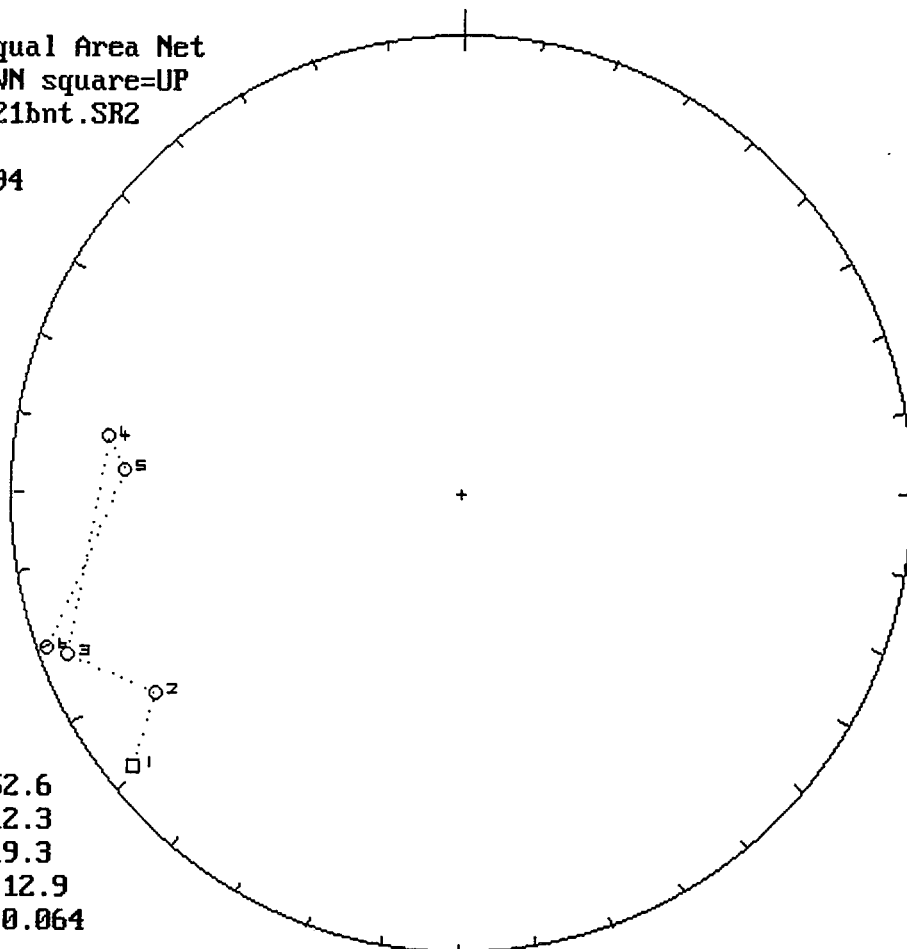vectors
removed by
demag.

\thermal\sy23bnt.SR2
06-02-1994
n = 6
circle =horiz.plo
triang. =vert.plot
units mA/m
PCA decl= 322.4
PCA incl= -60.1
for points 1 to 6
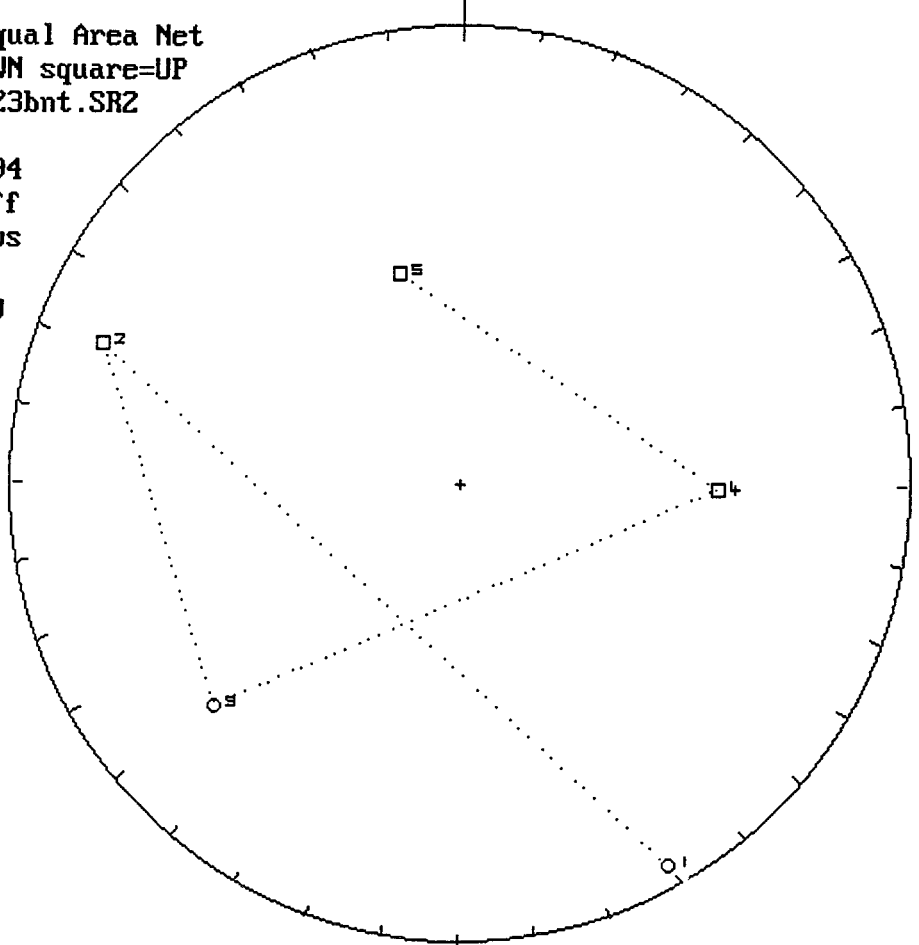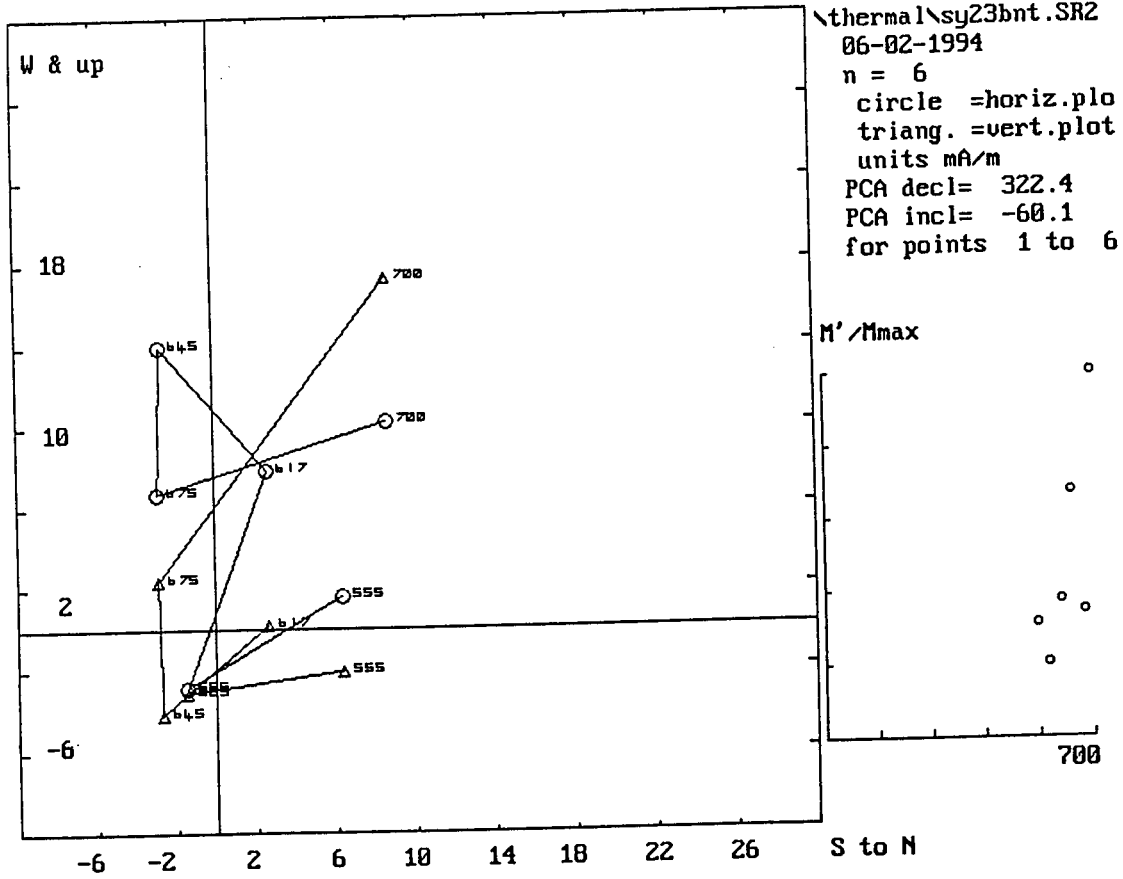
Lwr.Hem.Equal Area Net
circle=DOWN square=UP
 ermal\sy26bnt.SR2
 n = 6
 06-02-1994
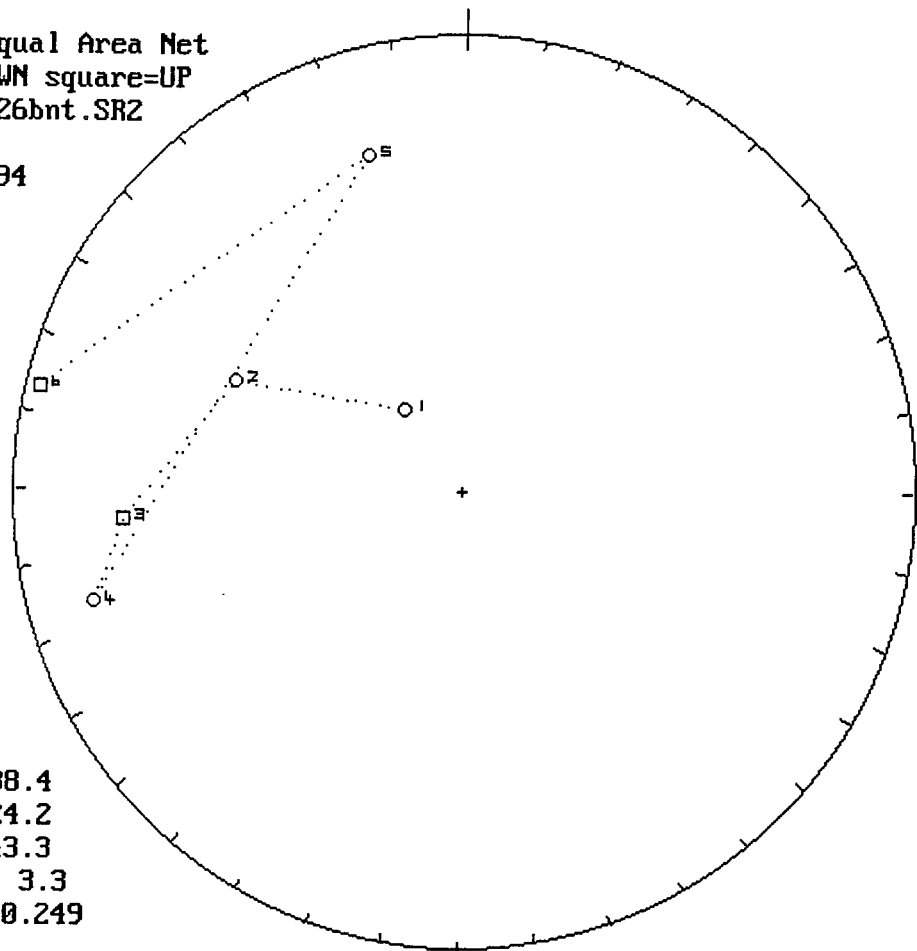
m.dec.= 288.4
m.inc.= 24.2
alpha95= 43.3
Fish. k=   3.3
sp.var.= 0.249

Lwr.Hem.Equal Area Net
circle=DOWN square=UP
 ermal\sy26bnt.SR2
 n = 5
 06-02-1994
Vector Diff
Plot: shows
vectors
removed by
demag.

\thermal\sy26bnt.SR2
06-02-1994
n = 6
 circle =horiz.plo
 triang. =vert.plot
 units mA/m
PCA decl= 278.0
PCA incl= -20.9
for points 1 to 6

Lwr.Hem.Equal Area Net
circle=DOWN square=UP
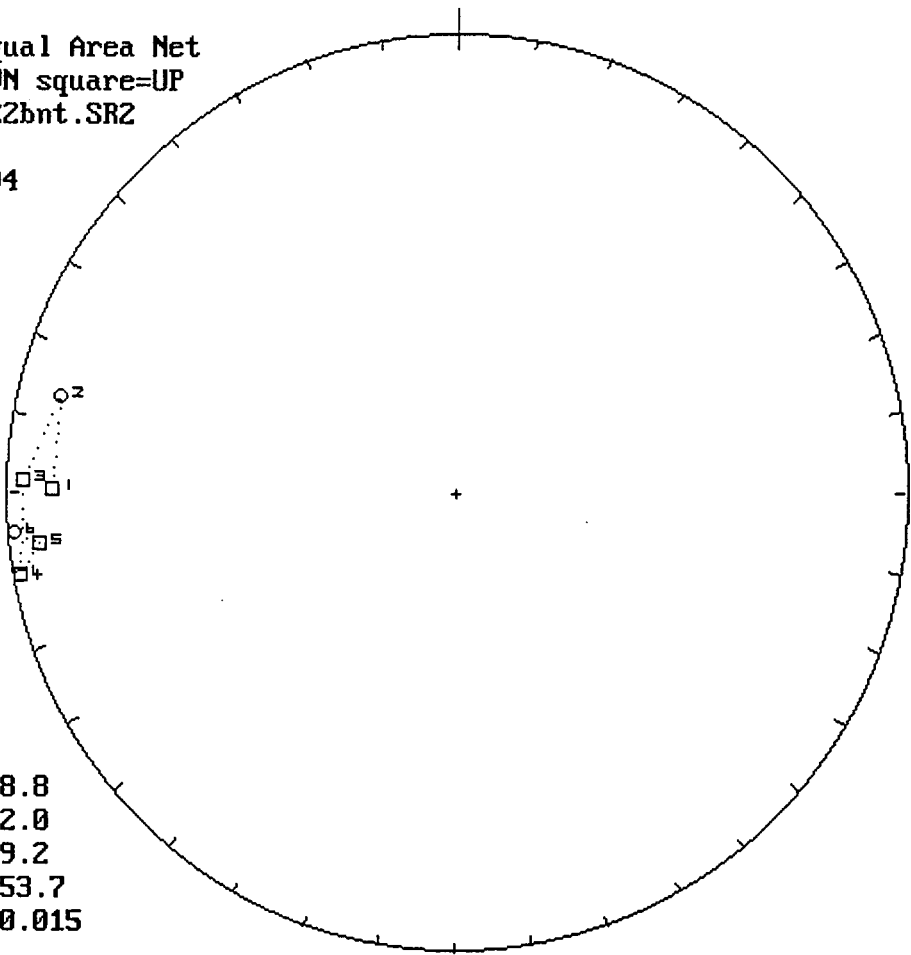 ermal\sy27bnt.SR2
 n = 6
 06-02-1994
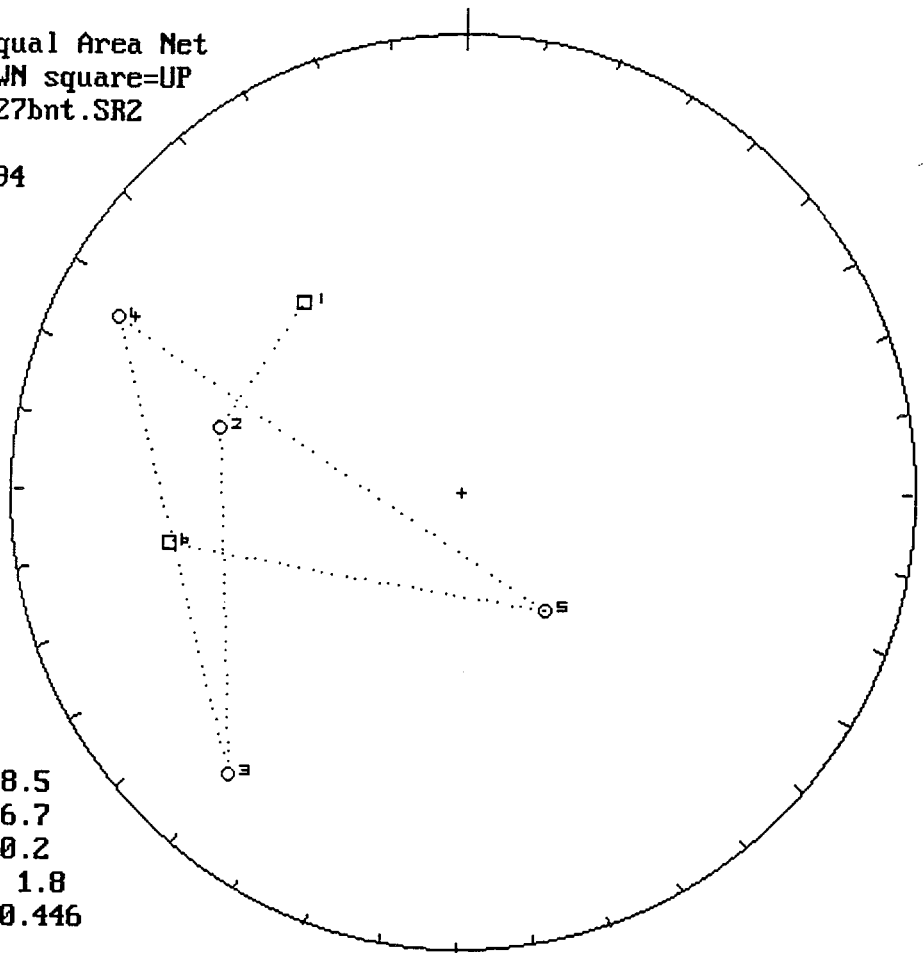
m.dec.= 268.5
m.inc.= 16.7
alpha95= 70.2
Fish. k= 1.8
sp.var.= 0.446

Lwr.Hem.Equal Area Net
circle=DOWN square=UP
 ermal\sy27bnt.SR2
 n = 5
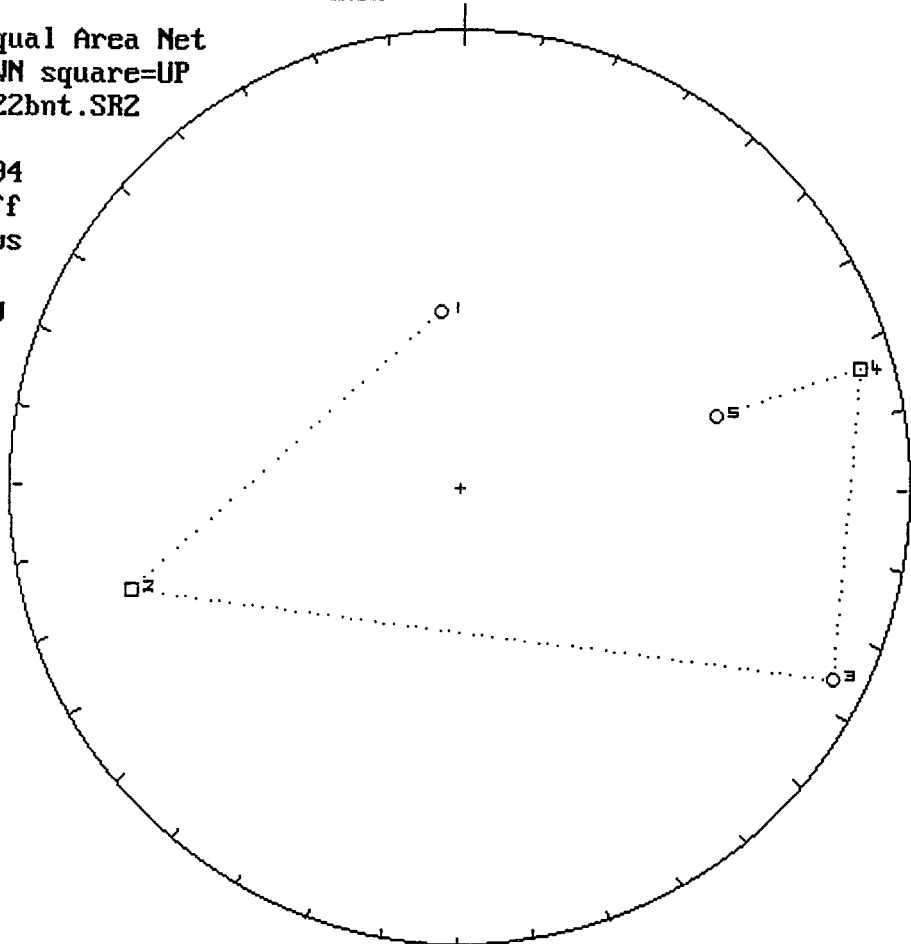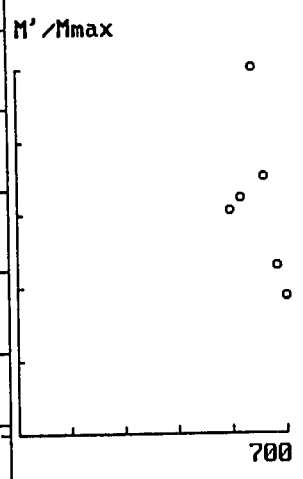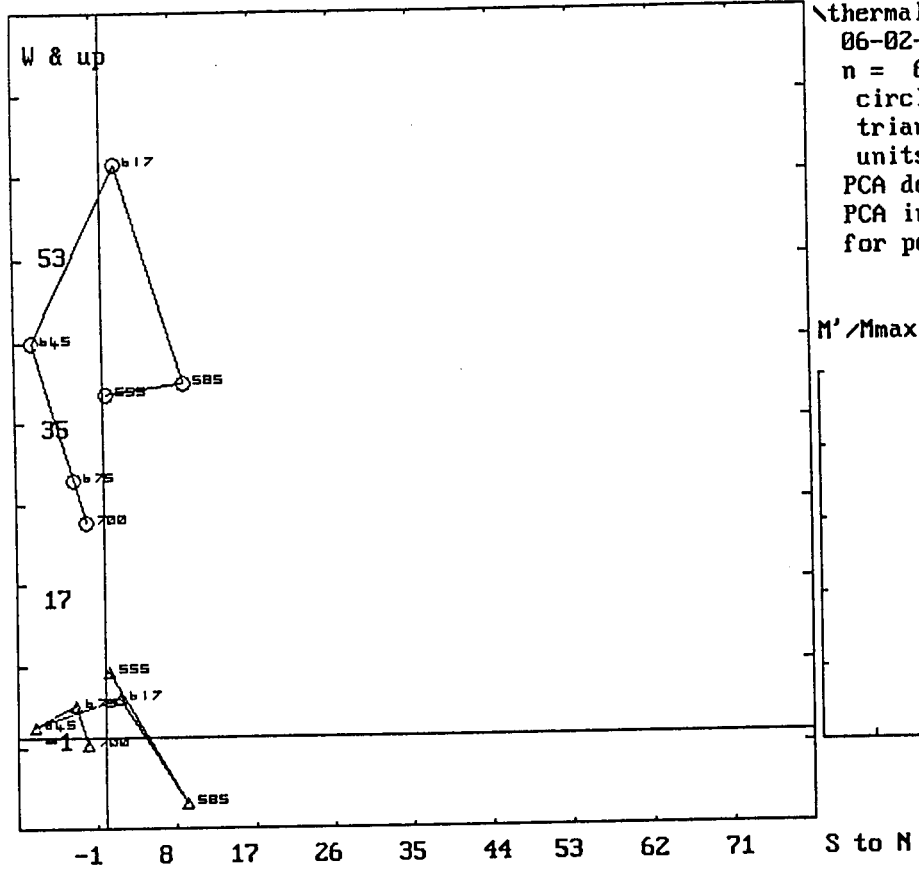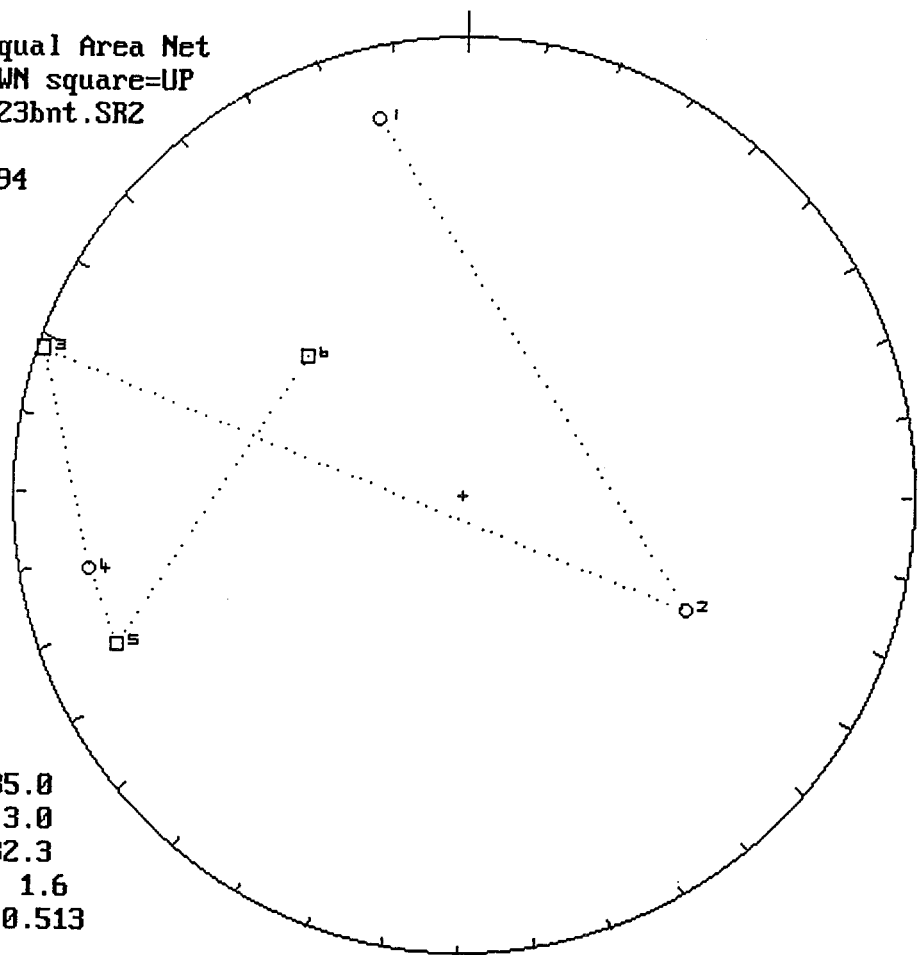 06-02-1994
Vector Diff
Plot: shows
vectors
removed by
demag.
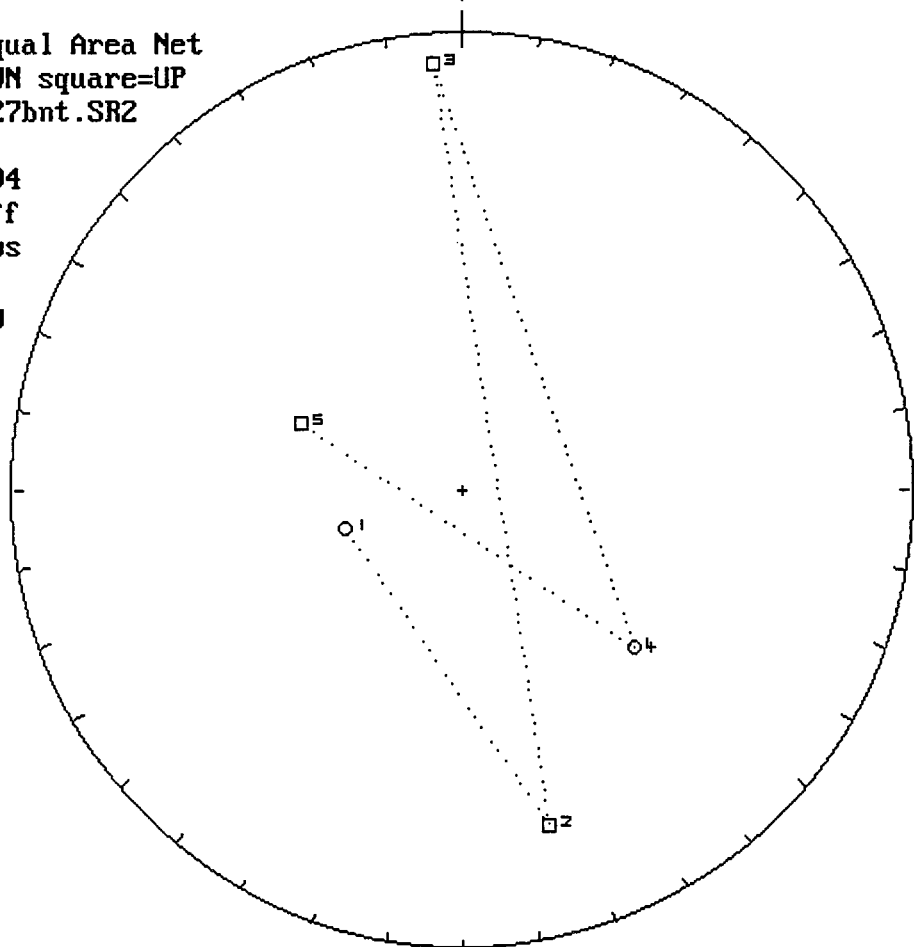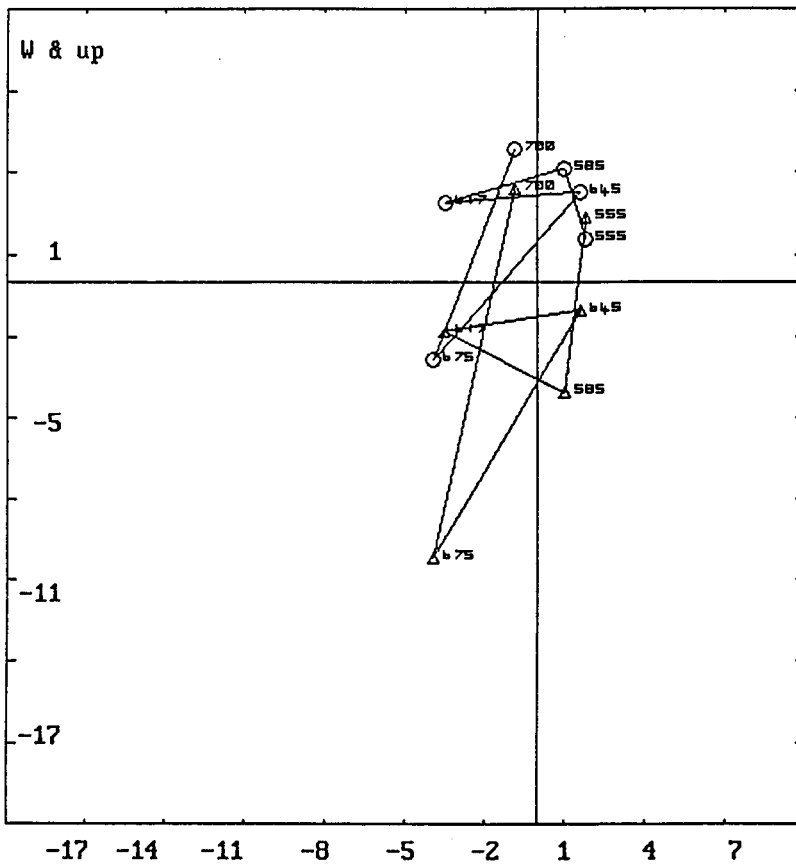
\thermal\sy27bnt.SR2
06-02-1994
n = 6
 circle =horiz.plo
 triang. =vert.plot
 units mA/m
PCA decl= 126.2
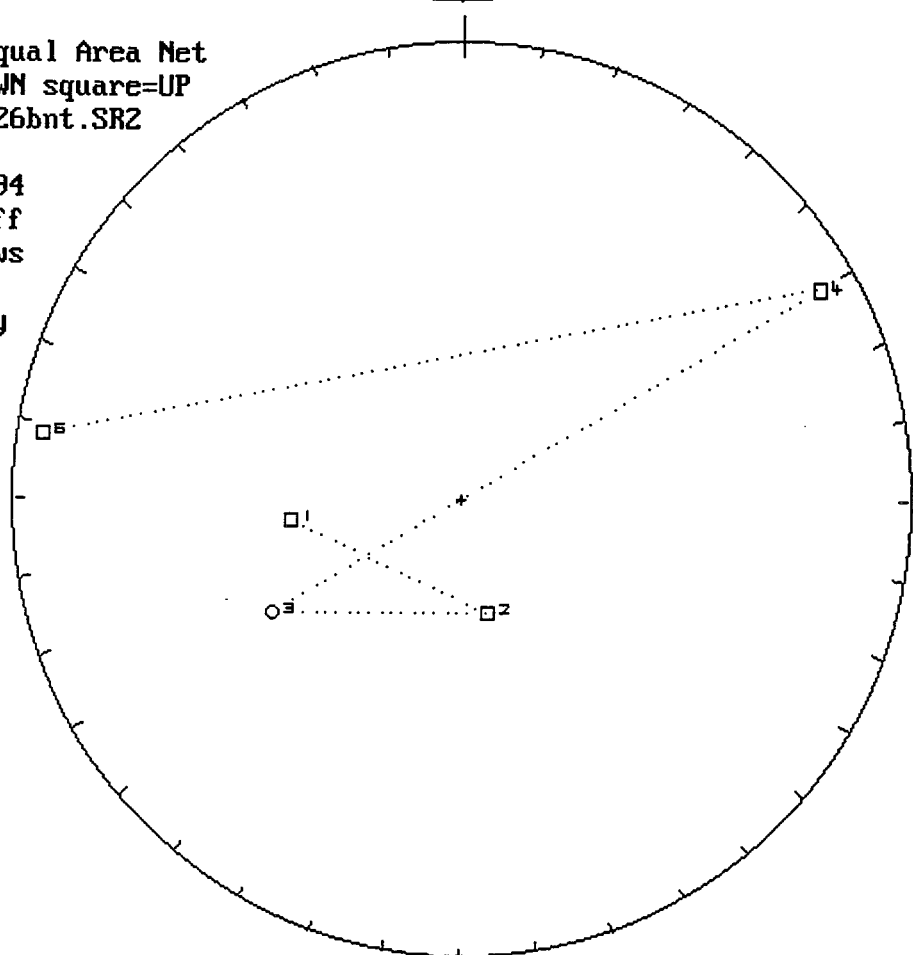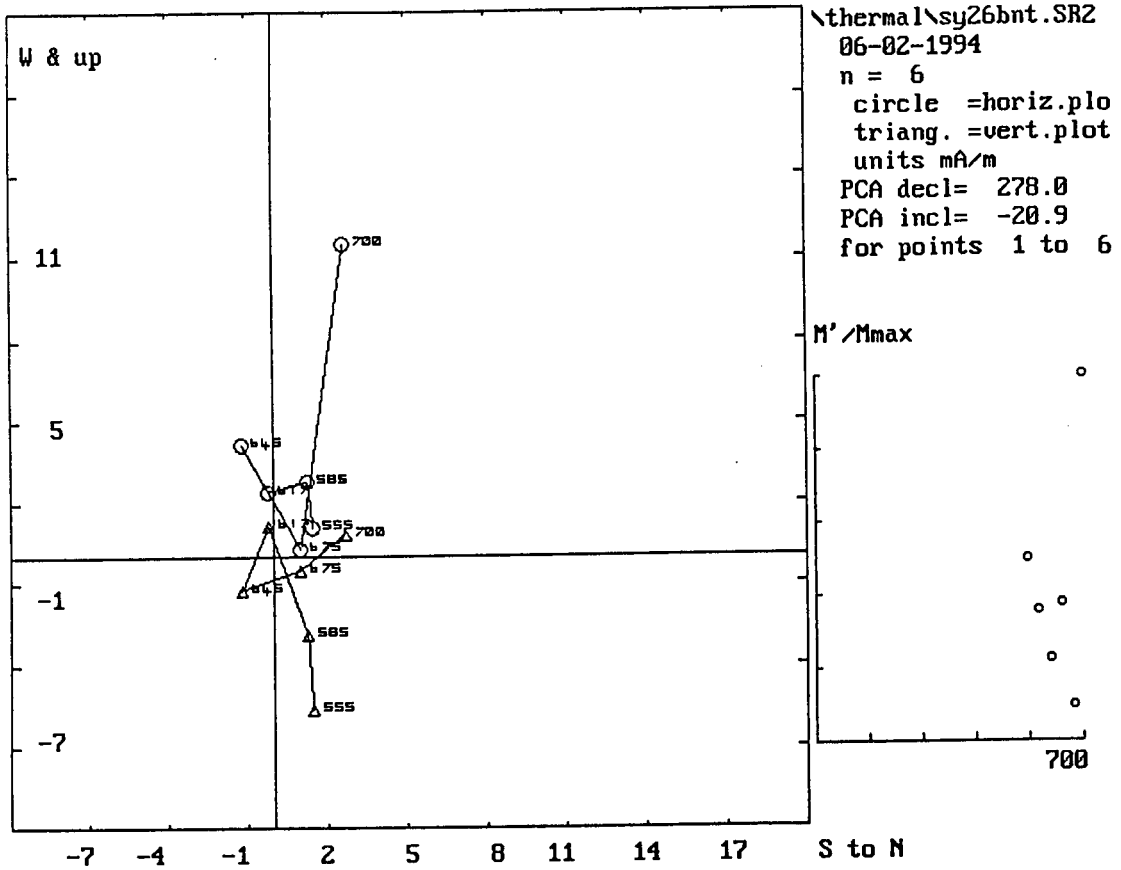PCA incl= 59.2
for points 1 to 6
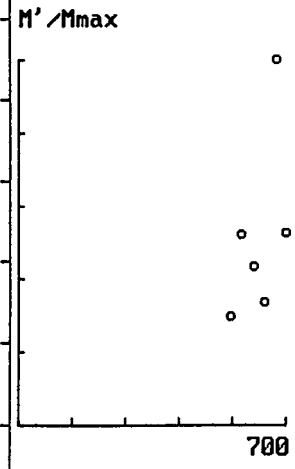
APPENDIX H

AMS DATA

sample	k1/k2	k2/k3	P'	T
sy11a	1.131359	1.183159	1.340796	0.153524
sy11b	1.060178	1.141891	1.216555	0.388491
sy11c	1.068692	1.130632	1.211831	0.297768
sy11d	1.018285	1.089517	1.117368	0.651044
sy18a	1.065896	1.051594	1.121223	-0.11836
sy18b	1.070011	1.039882	1.114124	-0.26749
sy17a	1.040535	1.017265	1.060073	-0.39784
sy17c	1.053282	1.012863	1.070932	-0.60486
sy16a	1.040068	1.067688	1.111703	0.250139
sy16c	1.051148	1.061141	1.115598	0.086621
sy1a	1.064516	1.071185	1.140404	0.047569
sy1b	1.037864	1.092808	1.138184	0.409686
sy3a	1.038289	1.125935	1.177194	0.518852
sy3b	1.03804	1.153334	1.209399	0.585158
sy14a	1.085127	1.037885	1.129378	-0.37442
sy14b	1.060312	1.034254	1.097871	-0.26974
sy25a	1.172848	1.228915	1.44421	0.127741
sy25c	1.18311	1.261158	1.496587	0.159638
sy24b	1.042953	1.114842	1.168453	0.442113
sy24a	1.036522	1.138267	1.19017	0.566198
sy28a	1.014226	1.053093	1.071813	0.571021
sy28b	1.032091	1.012854	1.046731	-0.42413
sy6a	1.00836	1.04446	1.057244	0.678708
sy6b	1.015712	1.046045	1.064971	0.485539
sy8a	1.059792	1.005769	1.073173	-0.81977
sy8b	1.060697	1.004131	1.073099	-0.86922
sy4a	1.039909	1.039633	1.081134	-0.00341
sy4b	1.033922	1.022168	1.057261	-0.20681
sy7b	1.032241	1.040279	1.073978	0.108903
sy13a	1.11076	1.230777	1.375612	0.328126
sy13b	1.105314	1.218715	1.354966	0.327828
sy27a	1.047023	1.096018	1.150504	0.332276
sy27b	1.031574	1.123459	1.16834	0.57849
sy26a	1.048356	1.103209	1.160051	0.350648
sy26b	1.026895	1.177955	1.229159	0.721102
sy23a	1.023944	1.032479	1.057422	0.14923
sy23b	1.007924	1.046247	1.058985	0.70271
sy22a	1.128783	1.201716	1.360176	0.205358

sample	k1/k2	k2/k3	P'	T
sy22b	1.125895	1.271588	1.442865	0.339113
sy21a	1.031045	1.033799	1.065919	0.041801
sy21b	1.033362	1.037742	1.072417	0.060539
sy20b	1.037901	1.00418	1.046611	-0.79835
sy19a	1.012257	1.025263	1.038583	0.34383
sy19b	1.033535	1.030206	1.064789	-0.0514
sy16a	1.043628	1.047365	1.093102	0.040181
sy16b	1.040437	1.056591	1.099795	0.162707
sy15a	1.016534	1.036914	1.055362	0.377049
sy15b	1.012807	1.034651	1.049576	0.456035
sy10b	1.06106	1.054037	1.118503	-0.05936
sy9a	1.24938	1.213014	1.518325	-0.07105
sy9b	1.218029	1.13395	1.385834	-0.22149
sy2a	1.020654	1.057652	1.082442	0.465485
sy2b	1.018128	1.051809	1.073599	0.475294
sy30a	1.185351	1.265744	1.505058	0.161751
sy30b	1.190336	1.276912	1.525221	0.167692
sy31a	1.012669	1.038581	1.053918	0.500865
sy31b	1.010109	1.040197	1.053684	0.593337
sy32a	1.007789	1.0558	1.069971	0.749954
sy32b	1.02289	1.065937	1.093863	0.476637
sy33b	1.078289	1.029478	1.113852	-0.4436
sy34a	1.062092	1.076414	1.143562	0.100044
sy34b	1.064961	1.106579	1.180325	0.233443
sy35a	1.052521	1.108967	1.170711	0.337869
sy35b	1.060437	1.067431	1.132054	0.053037
sy36a	1.023252	1.033881	1.058259	0.183517
sy36b	1.013452	1.053519	1.071678	0.591992
sy37a	1.111226	1.175498	1.309333	0.210468
sy37b	1.09272	1.130177	1.236315	0.159705
sy38a	1.00851	1.012339	1.021071	0.182763
sy38b	1.006462	1.011598	1.018379	0.283243
sy39a	1.29173	1.244788	1.612309	-0.07794
sy39b	1.02614	1.089112	1.123439	0.535757
sy40a	1.100337	1.059957	1.16816	-0.24302
sy40b	1.010921	1.057756	1.07459	0.675832
sy41a	1.009525	1.05941	1.075453	0.717838
sy41b	1.041197	1.078785	1.125278	0.305184

sample	k1/k2	k2/k3	P'	T
sy42a	1.022915	1.109301	1.144338	0.641462
sy42b	1.046768	1.106472	1.162304	0.377635
sy43a	1.032881	1.062005	1.098461	0.300565
sy43b	1.091902	1.076035	1.175289	-0.0908
sy44a	1.009269	1.028313	1.039441	0.503209
sy44b	1.011413	1.029638	1.042736	0.440389
sy45b	1.023987	1.02419	1.04876	0.004137
sy46a	1.040386	1.050277	1.092893	0.106722
sy46b	1.051567	1.086037	1.143583	0.242847
sy47a	1.049571	1.082603	1.137736	0.242567
sy47b	1.05703	1.08939	1.152819	0.213744
sy48a	1.015316	1.014604	1.030147	-0.0236
sy48b	1.01891	1.005922	1.026061	-0.52065
sy49a	1.019736	1.029444	1.050086	0.195106
sy49b	1.018636	1.055715	1.078495	0.491914
sy50a	1.053541	1.044	1.100075	-0.09554
sy50b	1.016079	1.064579	1.086573	0.593758
sy51a	1.111285	1.234043	1.380189	0.331773
sy52a	1.142807	1.124908	1.286192	-0.06285
sy52b	1.111341	1.215516	1.35761	0.297938
sy56	1.028848	1.039313	1.069574	0.151052
sy56b	1.025239	1.03054	1.056639	0.09374
sy55a	1.015017	1.048272	1.06693	0.519566
sy55b	1.00761	1.029316	1.039248	0.584292
sy54a	1.022172	1.064091	1.091125	0.478181
sy54b	1.042876	1.06905	1.115963	0.227939
sy53a	1.037027	1.021131	1.059675	-0.26974
sy53b	1.038741	1.035939	1.076099	-0.03685

sample	Kmax	Kint	Kmin	K(bulk)a
sy11a	1.148367	1.015035	0.857904	1671.533
sy11b	1.086743	1.025058	0.897686	726.9333
sy11c	1.088951	1.018958	0.90123	1153.6
sy11d	1.041496	1.022794	0.93876	1204.3
sy18a	1.061106	0.995507	0.946666	11051.77
sy18b	1.059872	0.990525	0.952536	9148.333
sy17a	1.032719	0.992489	0.975645	7232.867
sy17c	1.039632	0.987042	0.974506	5267.2
sy16a	1.049194	1.008775	0.944823	11505.13
sy16c	1.054468	1.003159	0.945359	5489.833
sy1a	1.066734	1.002084	0.935491	1288.767
sy1b	1.055864	1.017344	0.930946	1102.233
sy3a	1.066718	1.027381	0.912471	3069.933
sy3b	1.075129	1.035731	0.898033	2550.767
sy14a	1.069145	0.985272	0.949308	18432.7
sy14b	1.051553	0.99174	0.958894	18402.1
sy25a	1.191244	1.015687	0.826493	8445.233
sy25c	1.208572	1.021523	0.80999	8658.366
sy24b	1.066385	1.022467	0.917142	527.0333
sy24a	1.069383	1.031704	0.906383	726.3333
sy28a	1.02702	1.012614	0.961562	25611.37
sy28b	1.025638	0.993748	0.981137	32166.07
sy6a	1.020252	1.011794	0.968725	17525.07
sy6b	1.025724	1.009857	0.965405	17608.87
sy8a	1.041469	0.982711	0.977075	15158.2
sy8b	1.041496	0.981898	0.977859	14216.07
sy4a	1.039816	0.999912	0.961794	1007.9
sy4b	1.029989	0.996196	0.974592	1551
sy7b	1.034913	1.002589	0.96377	1355.567
sy13a	1.149404	1.034792	0.840765	35581.67
sy13b	1.141889	1.033092	0.847691	42233.67
sy27a	1.063106	1.015361	0.92641	21859.63
sy27b	1.061335	1.02885	0.915789	15915.77
sy26a	1.066329	1.017145	0.921989	5833.567
sy26b	1.074962	1.046809	0.888668	8016.167
sy23a	1.026781	1.002771	0.971227	20896.63
sy23b	1.02054	1.012516	0.967761	20507.67
sy22a	1.152587	1.021089	0.849694	83714.66

sample	Kmax	Kint	Kmin	K(bulk)a
sy22b	1.172502	1.041396	0.818975	61039.17
sy21a	1.031962	1.000889	0.968167	18491.83
sy21b	1.034819	1.001411	0.96499	18697.33
sy20b	1.026536	0.989051	0.984934	923.1667
sy19a	1.016574	1.004265	0.979519	9416.967
sy19b	1.032424	0.998925	0.969636	8316.367
sy16a	1.044872	1.001192	0.955916	11218.43
sy16b	1.045794	1.005149	0.951313	15014.23
sy15a	1.023282	1.006639	0.970803	10126.23
sy15b	1.020036	1.007138	0.973409	9809.4
sy10b	1.058713	0.997789	0.946636	1485.333
sy9a	1.237136	0.990202	0.816317	10409.43
sy9b	1.18933	0.97644	0.861097	6979.533
sy2a	1.03284	1.01194	0.95678	20641.5
sy2b	1.029233	1.010908	0.961114	20498.67
sy30a	1.211562	1.022115	0.807523	19303.5
sy30b	1.218519	1.023679	0.801685	18761.83
sy31a	1.021234	1.008457	0.970996	2192.067
sy31b	1.02004	1.009832	0.970809	3370.533
sy32a	1.023545	1.015634	0.961957	708.2
sy32b	1.037042	1.013835	0.951122	883.9667
sy33b	1.061766	0.984677	0.956483	280.4667
sy34a	1.066844	1.004475	0.933169	5849.7
sy34b	1.078656	1.01286	0.915309	8035.433
sy35a	1.071009	1.017566	0.917581	2439.333
sy35b	1.062763	1.002193	0.938884	1023.267
sy36a	1.026783	1.00345	0.970567	18348.4
sy36b	1.026635	1.013008	0.961548	19344.63
sy37a	1.132248	1.018919	0.866799	8495.8
sy37b	1.105064	1.011298	0.894815	9791.334
sy38a	1.009784	1.001264	0.98906	3990.6
sy38b	1.008171	1.001698	0.990213	4449.367
sy39a	1.275886	0.987737	0.7935	4324.033
sy39b	1.046714	1.020051	0.936591	2740.867
sy40a	1.086708	0.987615	0.93175	150.6667
sy40b	1.026297	1.01521	0.959778	252.6667
sy41a	1.025887	1.016207	0.95922	6428.767
sy41b	1.053578	1.011891	0.937993	5261.867

sample	Kmax	Kint	Kmin	K(bulk)a
sy42a	1.050935	1.027393	0.926163	16854.1
sy42b	1.066302	1.018662	0.92064	15789.13
sy43a	1.042499	1.009312	0.950384	6006.6
sy43b	1.086586	0.995133	0.924815	13835.87
sy44a	1.015577	1.006251	0.978546	45574.83
sy44b	1.017452	1.005971	0.977014	45446.4
sy45b	1.024055	1.000066	0.976446	1084.033
sy46a	1.043672	1.003159	0.955138	4371.767
sy46b	1.062933	1.010809	0.930733	10039
sy47a	1.060468	1.010382	0.933291	28628.43
sy47b	1.067708	1.010102	0.927219	28515.13
sy48a	1.015078	0.999766	0.985376	12043.5
sy48b	1.014562	0.995733	0.989871	16087.43
sy49a	1.022961	1.003163	0.974471	4228.467
sy49b	1.030849	1.011989	0.958582	2397.8
sy50a	1.05035	0.996972	0.954955	1109.9
sy50b	1.031995	1.015664	0.954053	1078.333
sy51a	1.150782	1.035543	0.839149	62.13334
sy52a	1.136808	0.994752	0.884297	2016.833
sy52b	1.145033	1.030317	0.847639	2974.233
sy56	1.032324	1.003379	0.965426	12248.33
sy56b	1.027003	1.00172	0.972035	9427.767
sy55a	1.025982	1.010804	0.964258	16937.47
sy55b	1.014794	1.00713	0.978446	16519.97
sy54a	1.035958	1.013487	0.952444	13666.1
sy54b	1.051528	1.008297	0.943172	9358.967
sy53a	1.0317	0.994864	0.974277	39618.63
sy53b	1.037805	0.9991	0.96444	26959.03

Map 2203
Tilly Lake Sheet
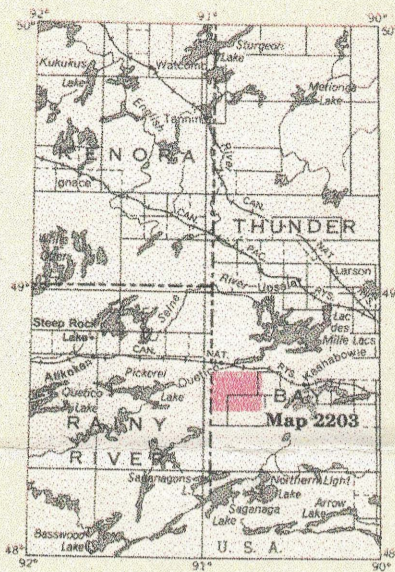
Scale, 1 inch to 50 miles

N.T.S. reference 52 B/10

LEGEND

SYMBOLS

CENOZOIC[a]

RECENT

Swamp and stream deposits.

PLEISTOCENE

Sand, clay, till.

UNCONFORMITY

PRECAMBRIAN[b]

INTRUSIVE ROCKS
LATE MAFIC INTRUSIVE ROCKS

8a Lamprophyre (dikes).
8b Diabase (dikes).

INTRUSIVE CONTACT
LATE FELSIC AND INTERMEDIATE
INTRUSIVE ROCKS

7 Quartz-feldspar porphyry (sills),
granite and syenite (dikes, sills), da-
cite porphyry (sill).

RELATIONS UNKNOWN
SYENITE AND RELATED ROCKS

6a Hornblende syenite, biotite syenite,
minor quartz syenite.
6b Syenite porphyry ?
6c Albite syenodiorite, hornblendite.

RELATIONS UNKNOWN
GRANITE AND RELATED ROCKS

5a Biotite granite, hornblende granite.
5b Pegmatite.
5c Migmatite.
5d Granodiorite, quartz monzonite ?

INTRUSIVE CONTACT
MAFIC, ULTRAMAFIC, AND INTER-
MEDIATE INTRUSIVE ROCKS

4a Peridotite.
4b Diorite, quartz diorite, gabbro, an-
orthosite.
4c Basalt porphyry ?
4d Andesite porphyry, dacite porphyry).

INTRUSIVE CONTACT

METAVOLCANICS AND
METASEDIMENTS[c]
MAFIC TO INTERMEDIATE META-
VOLCANICS

3a Massive lava.
3b Tuff, agglomerate.
3c Pillow lava.
3d Vesicular and amygdaloidal lava.
3e Foliated lava, chlorite schist.
3f Plagioclase-hornblende schist.
3g Diabase (flows).
3h Intermediate metavolcanics with
minor amounts of 3.

INTERCALATED IN PART
FELSIC TO INTERMEDIATE META-
VOLCANICS

7a Massive rhyolite.
7b Porphyritic rhyolite.
7c Banded rhyolite.
2d Tuff, agglomerate, breccia.
2e Sericite schist.
2f Intermediate metavolcanics with
minor amounts of 3

INTERCALATED IN PART
METASEDIMENTS

1 Greywacke, biotite quartz-feldspar
paraschist.

Q Quartz
S Sulphide mineralization

Glacial striae.
Esker.
Small bedrock outcrop.
Area of bedrock outcrop.
Bedding, top unknown; (inclined, verti-
cal).
Bedding, top (arrow) from grain grada-
tion; (inclined, vertical, overturned).
Lava flow; top in direction of arrow.
Schistosity; (horizontal, inclined, verti-
cal).
Gneissosity; (horizontal, inclined, verti-
cal).
Foliation; (horizontal, inclined, vertical).
Lineation with plunge.
Geological boundary, observed.
Geological boundary, position interpre-
ted.
Fault; (observed, assumed). Arrows in-
dicate horizontal movement.
Lineament.
Jointing; (horizontal, inclined, vertical).
Drag folds with plunge.
Drill hole; (vertical, inclined).
Vein. Width in inches.
Muskeg or swamp.
Motor road. Provincial highway number
encircled where applicable.
Other road.
Trail, portage, winter road.
Building.
District boundary.
Township boundary, approximate posi-
tion only.
Property boundary, approximate position
only.
Surveyed line, approximate position only.
Location of mining property, surveyed.
See List of Properties.

[a] Unconsolidated deposits. Cenozoic deposits are rep-
resented by the lighter coloured parts of the map.

[b] Bedrock geology. Outcrops and inferred extensions
of each rock map unit are shown respectively in deep
and light tones of the same colour. Where in places a
formation is too narrow to show colour and must be
represented in black, a short black bar appears in the
appropriate black.

[c] Relative ages unknown.

[c] These rocks are mapped on companion sheet Map
2204, Powell Lake Sheet.

SOURCES OF INFORMATION

Geology by F. R. Harris and assistants, 1967
Geology is not tied to surveyed lines.

G.S.C.-O.D.M. Aeromagnetic maps 1111G, 1112G.

Preliminary maps P.391 Moss Lake Area (South Part),
issued 1967, P.451 Moss Lake Area (North Part) issued
1968. Scale 1 inch to ¼ mile.

THUNDER BAY DISTRICT

Scale 1:31,680 or 1 Inch to ½ Mile

Metres

Feet
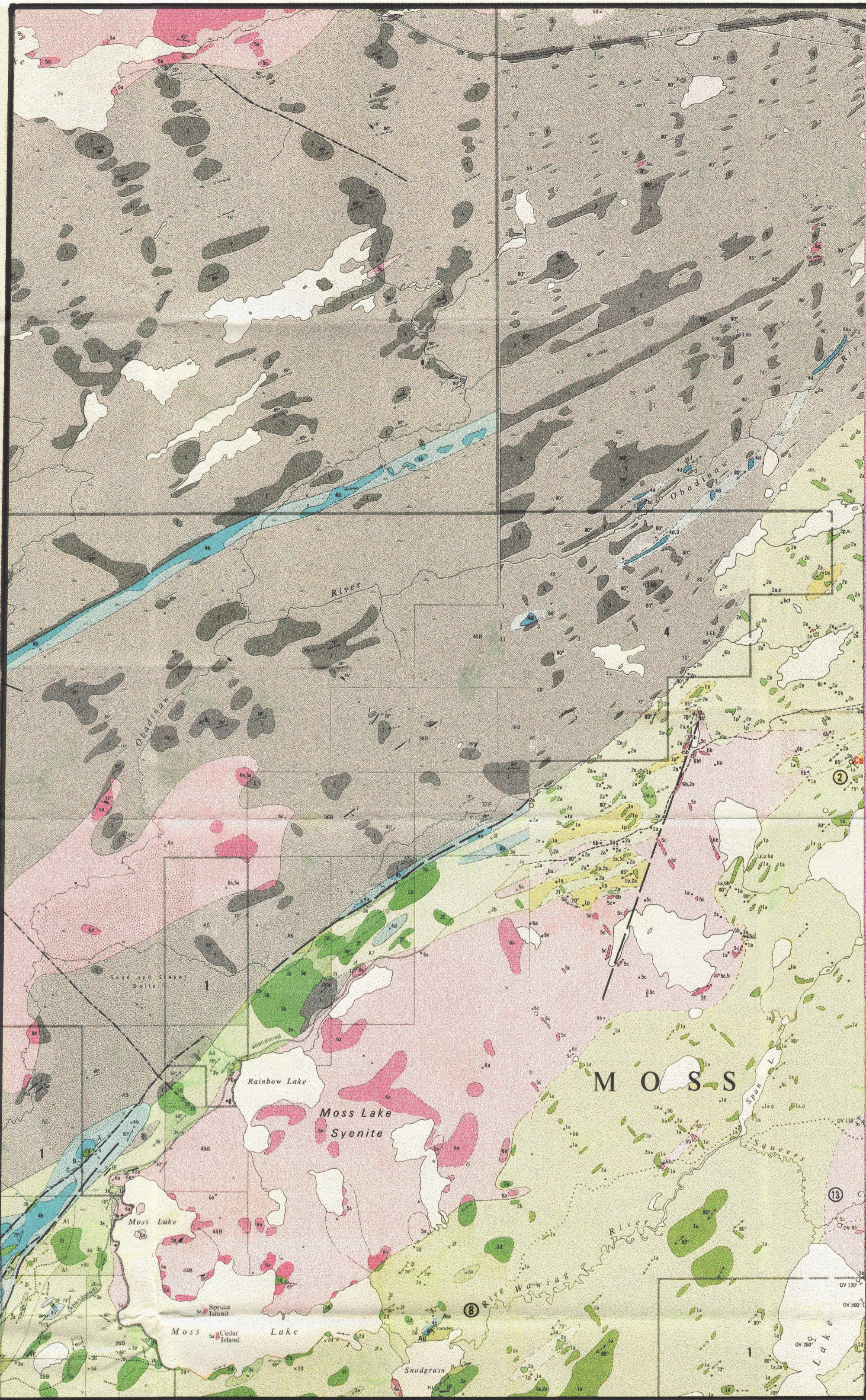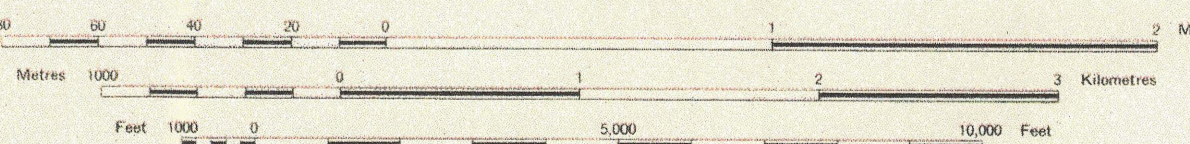
MAP "A": GEOLOGY OF THE THESIS AREA

This map is compiled from Ontario Mines and Northern Affairs
maps #2203 (Tilly Lake Sheet), #2204 (Powell Lake Area) and #2036
(Burchell Lake Area), Thunder Bay District. The thesis study area
is outlined. The Moss Lake stock is labelled as "Moss Lake syenite"
on the map. The Snodgrass Lake fault is the fault shown cutting the
Moss Lake stock. The different numbers of rock types have no
stratigraphic significance.
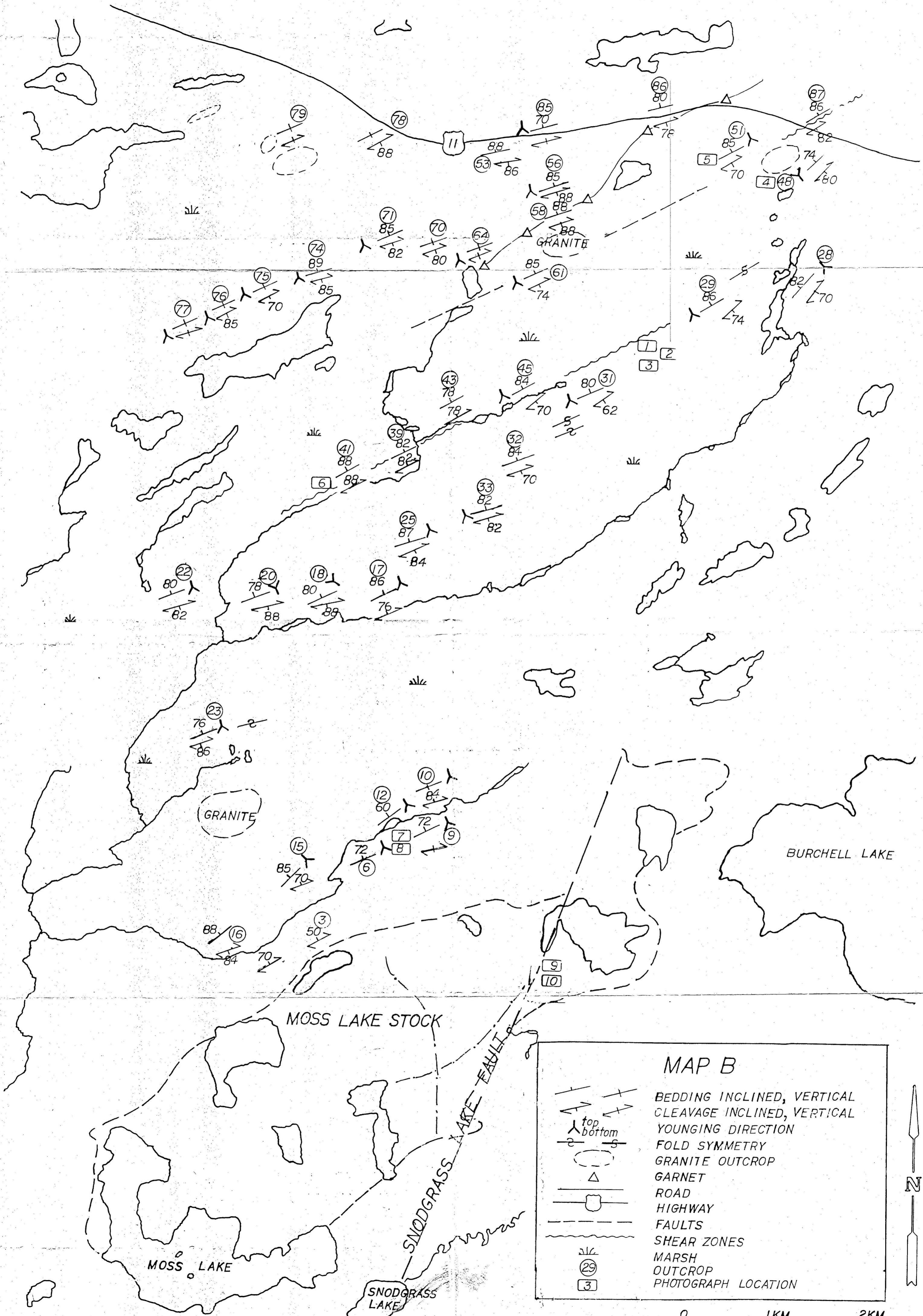
MAP B

BEDDING INCLINED, VERTICAL
CLEAVAGE INCLINED, VERTICAL
YOUNGING DIRECTION
top
bottom
FOLD SYMMETRY
GRANITE OUTCROP
GARNET
ROAD
HIGHWAY
FAULTS
SHEAR ZONES
MARSH
OUTCROP
PHOTOGRAPH LOCATION

SCALE   0   1KM   2KM

N

BURCHELL LAKE

MOSS LAKE STOCK

SNODGRASS LAKE FAULT

MOSS LAKE

SNODGRASS LAKE

GRANITE